DE GRUYTER

REVIEWS in MINERALOGY

Volume 9A

AMPHIBOLES and OTHER HYDROUS PYRIBOLES - MINERALOGY

DAVID R. VEBLEN, Editor

CONTENTS

THIS VOLUME (9A)

CRYSTAL CHEMISTRY of the AMPHIBOLES	F. C. Hawthorne
AMPHIBOLE SPECTROSCOPY	F. C. Hawthorne
An INTRODUCTION to the MINERALOGY and PETROLOGY of the BIOPYRIBOLES	J. B. Thompson, Jr.
NON-CLASSICAL PYRIBOLES and POLYSOMATIC REACTIONS in BIOPYRIBOLES	D. R. Veblen
AMPHIBOLE ASBESTOS MINERALOGY	Tibor Zoltai
The GEOLOGIC OCCURRENCES and HEALTH HAZARDS of AMPHIBOLE and SERPENTINE ASBESTOS	Malcolm Ross
SUBSOLIDUS REACTIONS and MICROSTRUCTURES in AMPHIBOLES	Subrata Ghose

CONTENTS of VOLUME 9B

PHASE RELATIONS of METAMORPHIC AMPHIBOLES: NATURAL OCCURRENCE and THEORY	Peter Robinson, F. S. Spear, J. C. Schumacher, Jo Laird, Cornelis Klein, B. W. Evans & B. L. Doolan
EXPERIMENTAL STUDIES of AMPHIBOLE STABILITY	M. C. Gilbert, R. T. Helz, R. K. Popp & F. S. Spear
AMPHIBOLES in the IGNEOUS ENVIRONMENT	D. R. Wones & M. C. Gilbert

Series Editor: Paul H. Ribbe

MINERALOGICAL SOCIETY OF AMERICA

REVIEWS in MINERALOGY

Volume 9A

AMPHIBOLES and OTHER HYDROUS PYRIBOLES - MINERALOGY

DAVID R. VEBLEN, Editor

The Authors

Subrata Ghose
Dept. of Geological Sciences
University of Washington
Seattle, WA 98195

Frank C. Hawthorne
Dept. of Earth Sciences
University of Manitoba
Winnipeg, Manitoba R3T 2N2 Canada

Malcolm Ross
U.S. Geological Survey
959 National Center
Reston, VA 22092

James B. Thompson, Jr.
Dept. of Geological Sciences
Harvard University
Cambridge, MA 02138

David R. Veblen
Dept. of Earth and Planetary Sciences
The Johns Hopkins University
Baltimore, MD 21218

Tibor Zoltai
Dept. of Geology and Geophysics
University of Minnesota
Minneapolis, MN 55455

Series Editor Paul H. Ribbe

Department of Geological Sciences
Virginia Polytechnic Institute and State University
Blacksburg, Virginia 24061

MINERALOGICAL SOCIETY OF AMERICA

PRINTED BY

BookCrafters, Inc.
Chelsea, Michigan 48118

REVIEWS IN MINERALOGY

(Formerly: SHORT COURSE NOTES)

ISSN 0275-0279

VOLUME 9A: AMPHIBOLES and Other Hydrous Pyriboles - Mineralogy

ISBN 0-939950-09-X
0-939950-10-3

ADDITIONAL COPIES

Additional copies of this volume as well as those listed below may be obtained at moderate cost from

Mineralogical Society of America
2000 Florida Avenue, NW
Washington, D.C. 20009

Vol. 1:	SULFIDE MINERALOGY, P.H. Ribbe, Editor (1974)	284 p.
Vol. 2:	FELDSPAR MINERALOGY, P.H. Ribbe, Editor (1975; revised 1981)	∿300 p.
Vol. 3:	OXIDE MINERALS, Douglas Rumble III, Editor (1976)	502 p.
Vol. 4:	MINERALOGY and GEOLOGY of NATURAL ZEOLITES, F.A. Mumpton, Editor (1977)	232 p.
Vol. 5:	ORTHOSILICATES, P.H. Ribbe, Editor (1980)	381 p.
Vol. 6:	MARINE MINERALS, Roger G. Burns, Editor (1979)	380 p.
Vol. 7:	PYROXENES, C.T. Prewitt, Editor (1980)	525 p.
Vol. 8:	KINETICS of GEOCHEMICAL PROCESSES, A.C. Lasaga and R.J. Kirkpatrick, Editors (1981)	391 p.
Vol. 9A:	AMPHIBOLES and Other Hydrous Pyriboles - Mineralogy, D.R. Veblen, Editor (1981)	372 p.
Vol. 9B:	AMPHIBOLES: Petrology and Experimental Phase Relations, D.R. Veblen and P.H. Ribbe, Editors (1981)	∿375 p.

REVIEWS in MINERALOGY

FOREWORD

It was immediately preceding the annual meetings of the Geological Societ of America in 1965 that the first mineralogical "short course" was sponsored b the American Geological Institute. That course on feldspars was convened by J.V. Smith of the University of Chicago; approximately one hundred geologists participated in the lectures, discussions and workshops. The notes for that course were exactly that: skeletal outlines with a few hand drawn figures int spersed. They were duplicated on *Ditto* machines and assembled in small 3-ring binders. The thirty to forty pages of notes have long since faded to unreadability. I recall David Stewart once saying that that would be an appropriate fate for all geological literature. But such is not to be, for mineralogical short courses have become institutionalized.

The Mineralogical Society of America revived the short course "movement" in 1974 with lectures and workshops on sulfides in Miami. It was attended by approximately one hundred geologists. Volume 1 of "Short Course Notes," *Sulfide Mineralogy*, was 284 pages long and represented contributions from six authors. It is in its third printing. This year (1981), participants in the course on amphiboles at Erlanger, Kentucky, convened by David Veblen, will number approximately one hundred geologists, but the published "notes" may threaten many of them with excess baggage charges on their return flights. No less than two (2) volumes totalling 750 pages were prepared for this event by no less than seventeen (17) authors. The first press run will total 2 × 450 copies (up from 1 × 1500 copies in 1974), with the first 1450 copies of volume 9A and 9B being sent to all of M.S.A.'s institutional and library subscribers. Furthermore, the ink is unfading and the covers are plastic-coated!

Paul H. Ribbe
Series Editor
Blacksburg, VA

N.B. - Additional copies of this and other volumes now published by the Mineralogical Society of America under the title "Reviews in Mineralogy" are available at a moderate cost (about 2¢ per page). See details on page *ii*.

PREFACE and ACKNOWLEDGMENTS

This volume of "Reviews in Mineralogy" was prepared in conjunction with the Mineralogical Society of America Short Course on *Amphiboles and Other Hydrous Pyriboles*, Fall, 1981. Had it not been split into two volumes, 9A and 9B, it would have resembled in some respects the Manhattan telephone directory (it is hoped, however, that the content is more readable and relevant to the geological sciences). The length of this collection of papers appears to result from a combination of phenomena. The amphiboles themselves must accept most of the blame: their structural complexity and resulting chemical variability and diversity of petrologic behavior preclude brief description. In addition, while some of these papers are relatively brief summaries of the published literature that easily and quickly can be consumed by students, others are exhaustive (and lengthy) discourses that may not be digestible in one sitting by even the most dedicated amphibole researcher. Finally, it appears that some geologists, probably with justification, love amphiboles so much that they would never have stopped writing had there been no publication deadline.

The extremely short time between the preparation of papers and publication of "Reviews in Mineralogy" and the authors' intimate knowledge of their fields ensure that the papers reflect the very latest in research results. The rapid production of the "Reviews," however, inevitably results in a few errors that might be caught in a more leisurely publication process; the editors apologize for any such errors that are included in this volume. In addition, the sequence of presentation of papers reflects not only the editors' notions of order in the amphibole universe, but also somewhat the order in which papers were received.

Although a collection of reviews of this sort cannot claim to give exhaustive coverage to all aspects of a topic, it is hoped that the papers presented here do review most of the important areas of active amphibole research. The papers have been split in a somewhat arbitrary fashion into Volume 9A, *Amphiboles and Other Hydrous Pyriboles - Mineralogy*, and Volume 9B, *Amphiboles: Petrology and Experimental Phase Relations*. Everyone is encouraged to purchase *both* volumes, however, because there is a hefty dose of petrology in 9A (witness the paper by Thompson, for example) and not a little mineralogy in 9B.

Colleagues too numerous to mention assisted in the preparation of these volumes of "Reviews in Mineralogy" through their advice and encouragement. Institutional support was provided by Arizona State University, The Johns Hopkins University, and Virginia Polytechnic Institute and State University. I thank the authors for producing readable copy, especially those who submitted their papers by the first (of many) deadlines! Above all, I thank Paul Ribbe for being of invaluable assistance during all phases of this endeavor and most obviously for producing the camera-ready copy from which these volumes were reproduced. Finally, I thank Sarah Veblen for proofreading and for maintaining a much-needed sense of humor throughout. Margie Strickler, Ramonda Haycocks, and Rachel Elliott of Blacksburg, Virginia, were responsible for typing the final manuscripts. John Grover provided invaluable assistance as local organizer for the Short Course itself.

David Veblen
Baltimore, MD
September 1981

VOLUME 9A

AMPHIBOLES and Other Hydrous Pyriboles—Mineralogy

TABLE of CONTENTS

	Page
Copyright and Additional Copies	ii
Foreword	iii
Preface and Acknowledgments	iv
CHAPTER 1. CRYSTAL CHEMISTRY OF THE AMPHIBOLES Frank C. Hawthorne	
INTRODUCTION	1
CLASSIFICATION AND NOMENCLATURE	1
The four principal amphibole groups	3
Fe-Mg-Mn amphiboles	3
Calcic amphiboles	7
Sodic-calcic amphiboles	7
Alkali amphiboles	7
General considerations	9
THE AMPHIBOLE CRYSTAL STRUCTURES	9
Choice of axes	11
Principal structure types	12
Site nomenclature in amphiboles	13
The C2/m amphibole structure	14
The $P2_1/m$ amphibole structure	17
The P2/a amphibole structure	18
The Pnma amphibole structure	20
The Pnmn amphibole structure	21
Amphiboles as layer structures	22
Space group variations in amphiboles	24
THE TETRAHEDRAL DOUBLE CHAIN	25
The C2/m amphiboles	26
Covalent bonding model	26
Bond-valence model	29
The $P2_1/m$ amphiboles	34
The P2/a amphiboles	34
The Pnma amphiboles	34
The Pnmn amphiboles	36
Ordering of tetrahedrally-coordinated Al	38
THE OCTAHEDRAL STRIP	42
The C2/m amphiboles	42
The $P2_1/m$ amphiboles	50
The P2/a amphiboles	51
The Pnma amphiboles	52
The Pnmn amphiboles	56

Page

THE M(4) SITE 56

The C2/m amphiboles 57
The $P2_1/m$ amphiboles 58
The P2/a amphiboles 58
The Pnma amphiboles 58
The Pnmn amphiboles 59
General considerations 59

THE A-SITE 63

The C2/m amphiboles 63
The $P2_1/m$ amphiboles 64
The P2/a amphiboles 64
The Pnma amphiboles 65
The Pnmn amphiboles 66

THE O(3) SITE 66

CATION DISTRIBUTIONS IN AMPHIBOLES 69

Aluminum 71
Ferric iron 72
Titanium 73
Ferrous iron 73
Fe-Mg-Mn amphiboles 73
Calcic amphiboles 75
Sodic-calcic amphiboles 75
Alkali amphiboles 75
Magnesium 76
Manganese 77
Lithium 77
Calcium 78
Sodium 78
Potassium 78
Beryllium 79
Boron 79
Cobalt 79
Nickel 79
Chromium 79
Zinc 79
Germanium 80

FACTORS AFFECTING CATION ORDERING IN AMPHIBOLES 80

Structure energy 80
Bond-valence 81
Miscellaneous factors 81
Ionic size 82
Strongly polarizing cations 82
Relief of Si-O-Si bond strain 82
Steric considerations 82
Crystal field stabilization energy 83
General considerations 84

Page

OXIDATION-DEHYDROXYLATION IN AMPHIBOLES. 85

HIGH-TEMPERATURE CRYSTAL STRUCTURE STUDIES 86

CELL DIMENSIONS. 91

CONCLUSIONS AND SUGGESTIONS FOR FUTURE WORK. 91

ACKNOWLEDGMENTS. 93

TABLE A-1. CRYSTAL STRUCTURE REFINEMENTS OF AMPHIBOLES. 94

CHAPTER 1 REFERENCES 95

CHAPTER 2. AMPHIBOLE SPECTROSCOPY Frank C. Hawthorne

INTRODUCTION 103

MÖSSBAUER SPECTROSCOPY 103

Site-occupancy characterization 106
Amphibole spectra 107
Fe-Mg-Mn amphiboles 107
Alkali amphiboles 113
Sodic-calcic amphiboles 113
Calcic amphiboles 115
General considerations 116

VIBRATIONAL SPECTROSCOPY 117

The hydroxyl stretching region 119

ELECTRONIC ABSORPTION SPECTROSCOPY 126

Amphibole spectra 128
Fe-Mg-Mn amphiboles 128
Calcic amphiboles 130
Sodic-calcic amphiboles 130
Alkali amphiboles 132
Other transition metals 133

OTHER TYPES OF SPECTROSCOPIC INVESTIGATION 135

CONCLUSIONS AND SUGGESTIONS FOR FUTURE WORK. 135

ACKNOWLEDGMENTS. 136

CHAPTER 2 REFERENCES 137

Page

CHAPTER 3. AN INTRODUCTION TO THE MINERALOGY AND PETROLOGY OF THE BIOPYRIBOLES James B. Thompson, Jr.

INTRODUCTION 141

PYRIBOLE POLYSOMES 141

PYRIBOLE POLYTYPES 145

UNIT CELLS AND SPACE GROUPS. 147

POLYSOME STABILITY 151

POLYTYPE STABILITY 156

THE CHEMICAL DESCRIPTION OF COMPLEX MINERALS 158

CONDENSED COMPOSITION SPACES, PYROXENES AND MICAS. 162

CONDENSED AMPHIBOLE SPACE. 166

CONDENSED BIOPYRIBOLE SPACE. 170

BIOPYRIBOLES AND OTHER ROCK MINERALS 176

SUGGESTIONS FOR FURTHER WORK 184

ACKNOWLEDGMENTS. 185

CHAPTER 3 REFERENCES 186

CHAPTER 4. NON-CLASSICAL PYRIBOLES AND POLYSOMATIC REACTIONS IN BIOPYRIBOLES David R. Veblen

INTRODUCTION 189

BIOPYRIBOLE NOMENCLATURE 190

ORDERED NON-CLASSICAL BIOPYRIBOLES 191

Pyribole structures, unit cells, and symmetries 194
Crystal-chemical details of ordered non-classical pyriboles 197
Polyhedral geometries 197
Structural control of chemistry 202
Electron microscopic observations of ordered wide-chain biopyriboles 204
Known structure types observed with HRTEM 204
New pyribole structure types discovered with HRTEM 207

CHAIN-WIDTH DISORDER IN PYRIBOLES. 208

Chain-width disorder in amphiboles 208
Amphibole asbestos 208
Nephrite (actinolite jade) 210
Acicular and massive amphiboles 210

Page

CHAIN-WIDTH DISORDER IN PYRIBOLES, continued

Chain-width disorder in wide-chain pyriboles 211
Chain-width disorder in pyroxenes 213

TERMINATION DEFECTS. 214

Chain terminations 214
Zipper terminations 217
Termination rules 220
Rule #1 (the "subchain rule") 220
Rule #2 (the "odd-even rule") 222

POLYSOMATIC REACTIONS IN BIOPYRIBOLES. 223

Mechanisms of polysomatic reactions 223
Kinetics of polysomatic reactions 228
Distinguishing primary growth microstructures from reaction microstructures 231

CONCLUSION AND SUGGESTIONS FOR FUTURE WORK 233

ACKNOWLEDGMENTS. 234

CHAPTER 4 REFERENCES 235

CHAPTER 5. AMPHIBOLE ASBESTOS MINERALOGY Tibor Zoltai

INTRODUCTION 237

FIBROUS AND ASBESTIFORM HABITS 238

The columnar growth habit 238
The reticulated growth habit 240
The radiated growth habit 242
The massive-fibrous growth habit 242
Isolated fiber growth habit 244
Synthetic asbestos and whiskers 245

THE UNIQUE STRUCTURE OF AMPHIBOLE ASBESTOS 246

Structural defects in amphibole asbestos 249

THE SURFACE STRUCTURE OF FIBERS. 254

Fiber length and strength 263
Fibers, crystals and fragments 265
Polycrystalline wires and aggregates 265

ORIGIN OF ASBESTOS AND WHISKER FIBERS. 267

Whisker growth 267
Origin of asbestos 269

CONCLUSIONS. 271

CHAPTER 5 REFERENCES 274

Page

CHAPTER 6. THE GEOLOGIC OCCURRENCES AND HEALTH HAZARDS OF AMPHIBOLE AND SERPENTINE ASBESTOS Malcolm Ross

INTRODUCTION 279

The problem 279
The dilemma 280

THE ASBESTOS MINERALS. 281

Amphibole asbestos 281
Chrysotile asbestos 283

ASBESTOS IN THE WORLD ECONOMY. 284

Early beginnings 284
The modern industry 286
Modern asbestos uses 287

MAJOR GEOLOGICAL OCCURRENCES OF AMPHIBOLE ASBESTOS 287

Amosite and crocidolite in ironstones of South Africa 288
Transvaal asbestos field 288
Cape asbestos field 290
Formation of banded ironstones 290
Crocidolite in ironstones of Western Australia 291
Anthophyllite in Alpine-type ultramafic rocks of East Finland 292

MINOR GEOLOGICAL OCCURRENCES OF AMPHIBOLE ASBESTOS 294

Anthophyllite asbestos 294
Tremolite asbestos 295
Actinolite, amosite, and crocidolite asbestos 296

MAJOR OCCURRENCES OF CHRYSOTILE ASBESTOS 296

Type I deposits 296
Type II deposits of southern Africa 299
South Africa and Swaziland 299
Zimbabwe 300
Type III deposits 300

HEALTH HAZARDS OF ASBESTOS 301

Diseases related to asbestos exposure 301
Epidemiology 304
Asbestos trades workers 305
Asbestos miners and millers 308
Mortality comparisons, trades vs mines 310
Crocidolite exposure 314

SUMMARY. 316

Production 316
Geology 317
Asbestos and health 317

Page

CHAPTER 6, continued

ACKNOWLEDGMENTS 319

CHAPTER 6 REFERENCES 320

CHAPTER 7. SUBSOLIDUS REACTIONS AND MICROSTRUCTURES IN AMPHIBOLES Subrata Ghose

INTRODUCTION 325

THERMODYNAMICS AND KINETICS OF THE Fe^{2+}-Mg^{2+} ORDER-DISORDER REACTION IN FERROMAGNESIAN AMPHIBOLES. 325

Mg-Fe in cummingtonite and actinolite 325
Mg-Fe in anthophyllite and the cooling rate of rocks 332
Mg-Fe in sodic amphiboles 337

PHASE TRANSITIONS IN FERROMAGNESIAN AMPHIBOLES. 338

The *P2₁/m → C2/m* phase transition in magnesium-rich cummingtonite 338
Nature of the structural changes 338
Possible anti-phase domains in cummingtonite 339
Anthophyllite-cummingtonite phase relations 340

MISCIBILITY GAPS AND EXSOLUTION TEXTURES IN AMPHIBOLES 341

Introduction 341
Actinolite-hornblende 344
Hornblende-anthophyllite 345
Actinolite (tremolite)-anthophyllite 346
Hornblende-cummingtonite 346
(Tremolite) actinolite-cummingtonite 350
Tremolite (actinolite)-riebeckite 352
Actinolite-glaucophane 352
Hornblende-glaucophane 353
Glaucophane-riebeckite 353
Richterite-magnesio-riebeckite 354
Anthophyllite-gedrite 357
Arfvedsonite-cummingtonite 360
Tremolite-richterite 362
Conclusions 363

THE THERMAL DECOMPOSITION OF AMPHIBOLES INTO PYROXENES AND OTHER PHASES. 364

Crocidolite and sodic amphiboles 364
Tremolite 365
Grunerite (and amosite) 366

ACKNOWLEDGMENTS. 368

CHAPTER 7 REFERENCES 369

For contents of Volume 9B, "AMPHIBOLES: Petrology and Experimental Phase Relations," see front cover.

Chapter 1

CRYSTAL CHEMISTRY of the AMPHIBOLES

Frank C. Hawthorne

INTRODUCTION

An appreciation of the crystal chemistry of a mineral group is fundamental to our perception of the role of such minerals in petrologic processes. This premise has particular validity when considering the amphiboles. Few other mineral groups show such a wide range of parageneses and none show as wide a range in chemistry. Consequently, our understanding of the amphiboles has not progressed quite as rapidly as for the less complex silicate minerals. Schaller (1916) was first to derive the formula of tremolite when he recognized that hydroxyl is an essential constituent of that mineral. It had long been recognized that there was a strong relationship between the chemistry, physical properties and paragenesis of the pyroxenes and the amphiboles. Warren (1929) and Warren and Modell (1930a) showed that this relationship also extended to the unit cell dimensions and diffraction patterns, and solved the structures of tremolite and anthophyllite by analogy with the known structures of diopside (Warren and Bragg, 1928) and enstatite (Warren and Modell, 1930b). Warren (1930) and Kunitz (1930) showed the structural and chemical homology of the amphiboles, emphasizing the importance of both homovalent and heterovalent substitutions to the chemistry of this group.

Since 1965 there have been significant technological advances in the fields of x-ray diffraction, electron microprobe analysis and resonance spectroscopy. The resulting proliferation of structural and chemical data has led to a substantial increase in our understanding of the amphiboles. A synthesis of this information is presented here.

CLASSIFICATION AND NOMENCLATURE

A standard amphibole formula may be written

$$A_{0-1}B_2C_5T_8O_{22}(OH,F,Cl)_2$$

A = Na,K

B = Na,Li,Ca,Mn,Fe^{2+},Mg

C = Mg,Fe^{2+},Mn,Al,Fe^{3+},Ti

T = Si,Al

Table 1. Prefixes and Adjectival Modifiers for the Amphiboles

	Prefixes
alumino-	see Tables 2, 3 and 4, also text
chlor-	when Cl ⩾ 1.00 (∿4% Cl)
chromium-	when Cr ⩾ 1.00 (∿9% Cr_2O_3)
ferri-	when Fe^3 ⩾ 1.00 (∿9% Fe_2O_3) except in alkali amphiboles and hastingsite
ferro-	see Tables 2, 3 and 4, also text
fluor-	when F ⩾ 1.00 (∿2% F)
hydro-	when OH ⩾ 3.00 (∿3% H_2O)
manganese-	when Mn ⩾ 1.00 (∿10% MnO) except in end-members containing Mn
magnesio-	see Tables 2, 3 and 4, also text
oxy-	when (OH+F+Cl) is confirmed as <1.00
potassium-	when K ⩾ 0.50 (∿2.7% K_2O)
sodium-	see Table 2
titanium-	when Ti ⩾ 1.00 (∿10% TiO_2) except in kaersutite
zinc-	when Zn ⩾ 1.00 (∿5% ZnO)
	Adjectival modifiers
calcian	see Tables 2 and 5
chromian	when Cr = 0.25-0.99 (∿2.3-9% Cr_2O_3)
ferrian	when Fe^3 = 0.75-0.99 (∿6.8-9% Fe_2O_3) except in alkali amphiboles and hastingsite
ferroan	see Figure 2 (only with pargasite and pargasitic hornblende)
lithian	when Li ⩾ 0.25 (∿0.4% Li_2O) except in alkali amphiboles when lithian is used for Li ⩾ 0.50 (∿0.8% Li_2O). Not used with holmquistite and clinoholmquistite
magnesian	see Figure 2 (only with hastingsite and hastingsitic hornblende)
manganoan	when Mn = 0.25-0.99 (∿2.5-10% MnO) except in end-members containing Mn
plumbian	when Pb ⩾ 0.08 (∿1.1% PbO)
potassian	when K = 0.25-0.49 (∿1.3-2.7% K_2O)
silicic	see Figure 2 and Table 3
subcalcic	see Table 3
subsilicic	see Table 3
titanian	when Ti = 0.25-0.99 (∿2.5-10% TiO_2)
zincian	when Zn = 0.25-0.99 (∿1.2-5% ZnO)

The complexity of the amphiboles has given rise to a proliferation of mineral names that has no systematic basis. The need for a precise nomenclature that is sufficiently flexible to encompass the chemical variations within the group has long been apparent (Leake, 1968). The report of the I.M.A. Subcommittee on Amphiboles (Leake, 1978) provides such a nomenclature. This classification is based largely on crystal chemistry, having as its foundation the chemical contents of the formula unit calculated to 24 (O,OH,F,Cl) where possible. The basic philosophy of the scheme is to denote principal stoichiometries by generally

well-established names, with prefixes and adjectival modifiers to indicate the presence of substantial substitutions that are not essential constituents of the end members. Prefixes are an inseparable part of the name and should be attached by a hyphen. Consequently, an amphibole should be indexed under (the initial letter of) the prefix, with perhaps a cross-reference under the species name. Adjectival modifiers are not an essential part of the amphibole name, but are simple adjectives ending in -ian or -oan according to the valency of the substituting ion. They denote minor substitutions and are not an essential part of the amphibole name; consequently, they are not used in the first stage of indexing and the amphibole should be indexed under its species name. Prefixes and adjectival modifiers of general application are listed in Table 1, together with the limits and restrictions on their use. Additional adjectives may be approved as needed (e.g., nickeloan, cuprian). A few prefixes must be defined differently in the different amphibole groups; these will be given later. The prefixes magnesio-, ferro-, alumino- and ferri- are often used with names that refer to part of a series. Alternate names are often so widely used for ends of some series that they are preferable to the ideal names (e.g., tremolite instead of magnesio-actinolite; tschermakite instead of alumino-tschermakite). The prefix "pure" *may* be used to indicate a theoretical end-member formula.

The amphiboles are divided into four principal groups on the basis of the B group cation occupancy:

$(Ca+Na)_B < 1.34$	Iron-magnesium-manganese group
$(Ca+Na)_B \geq 1.34$ $Na_B < 0.67$	Calcic amphibole group
$(Ca+Na)_B \geq 1.34$ $0.67 \leq Na_B < 1.34$	Sodic-calcic amphibole group
$Na_B \geq 1.34$	Alkali amphibole group

General formulae, end-member formulae and limits on the use of end-member names for each of these groups are given in Tables 2-5 and Figures 1-4.

Fe-Mg-Mn amphiboles: This group naturally divides into two subgroups, the orthorhombic and the monoclinic groups.

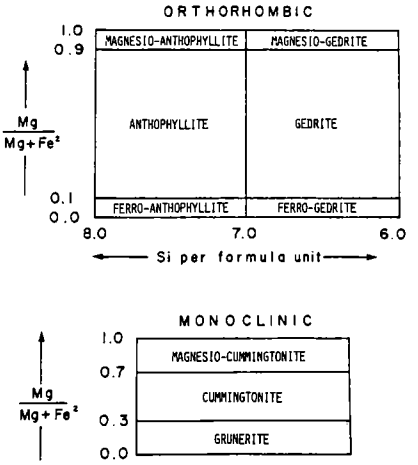

Figure 1. The nomenclature of the iron-magnesium-manganese amphiboles for which Li is < 1.0 atoms p.f.u. From Leake (1978).

Figure 2 appears on the facing page.

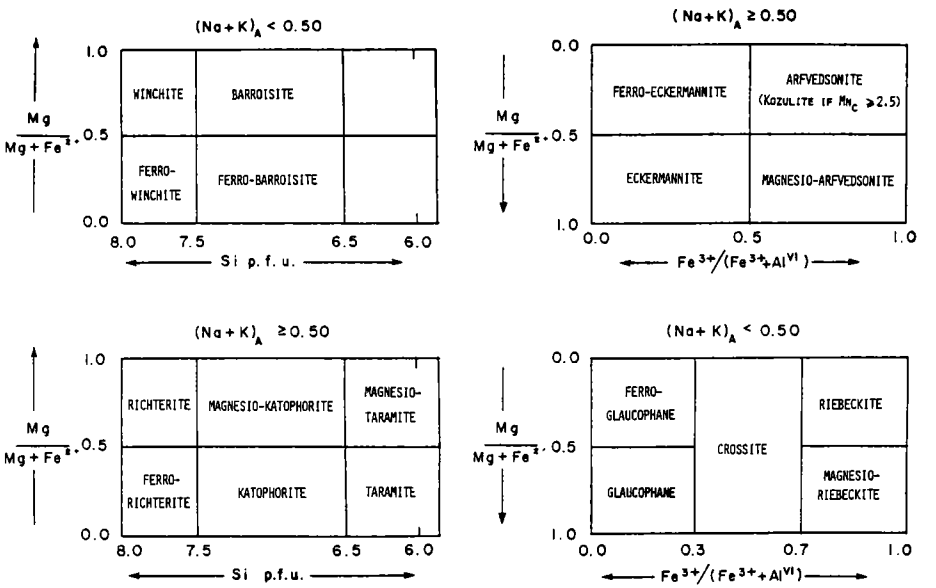

Figure 3. The nomenclature of the sodic-calcic amphiboles. From Leake (1978).

Figure 4. The nomenclature of the alkali amphiboles. Modified from Leake (1978).

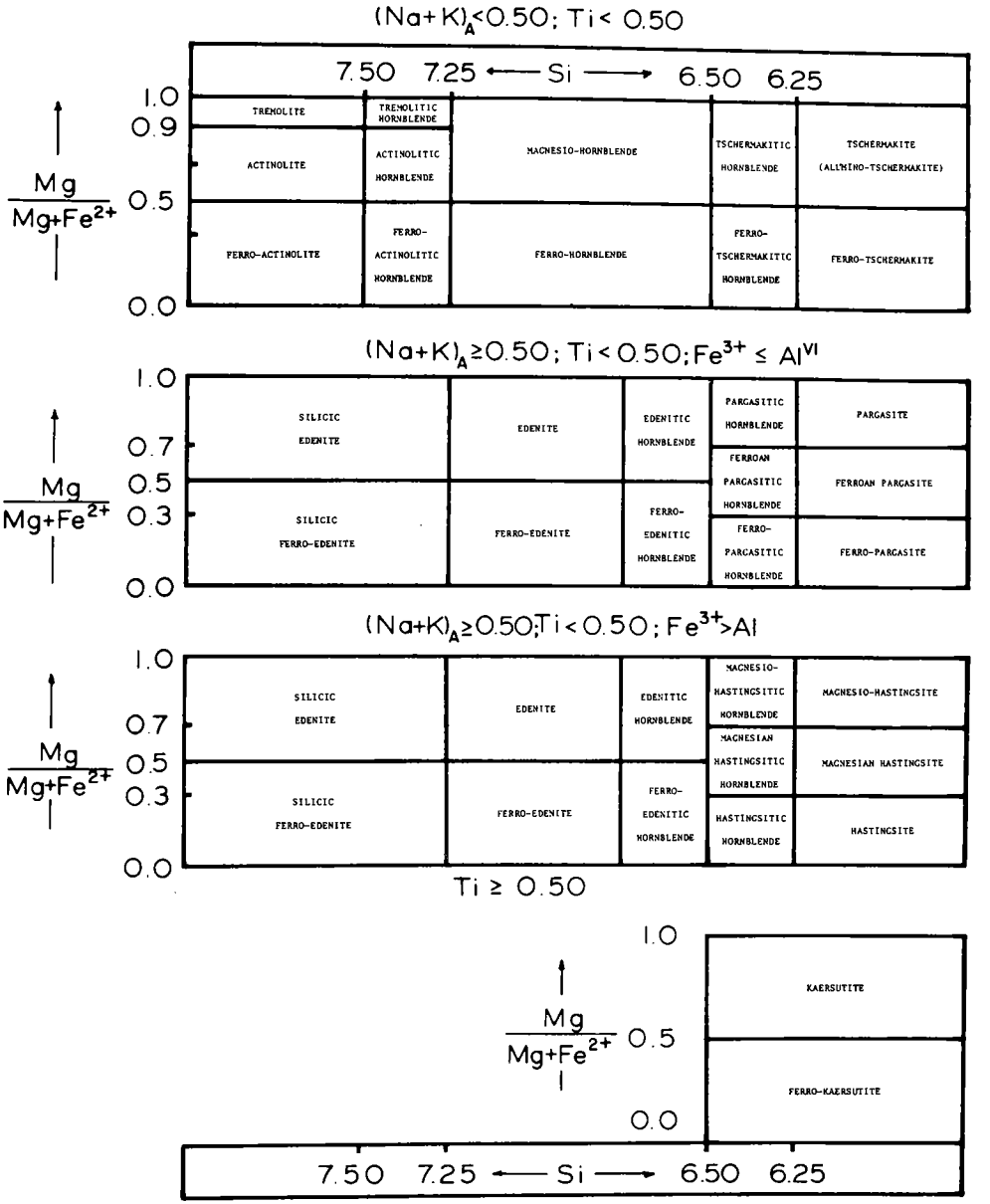

Figure 2. The nomenclature of the calcic amphiboles. Modified from Leake (1978).

Table 2. The Iron-Magnesium-Manganese Amphiboles: General Formulae, End Member Names and End Member Formulae

Orthorhombic forms

Anthophyllite $Na_x(Mg,Mn,Fe^{2})_{7-y}Al_y(Al_{x+y}Si_{8-x-y})O_{22}(OH,F,Cl)_2$ $x+y < 1.00$

End member	Formula
Magnesio-anthophyllite	$Mg_7Si_8O_{22}(OH)_2$
Ferro-anthophyllite	$Fe^{2}_7Si_8O_{22}(OH)_2$
Sodium-anthophyllite	$Na(Mg,Fe^{2})_7AlSi_7O_{22}(OH)_2$

Gedrite $Na_x(Mg,Mn,Fe^{2})_{7-y}Al_y(Al_{x+y}Si_{8-x-y})O_{22}(OH,F,Cl)_2$ $x+y \geq 1.00$

End member	Formula
Magnesio-gedrite	$Mg_5Al_2Si_6Al_2O_{22}(OH)_2$
Ferro-gedrite	$Fe^{2}_5Al_2Si_6Al_2O_{22}(OH)_2$
Sodium-gedrite	$Na(Mg,Fe^{2})_6AlSi_6Al_2O_{22}(OH)_2$

Holmquistite $Li_2(Mg,Fe^{2})_3(Fe^{3},Al)_2Si_8O_{22}(OH,F,Cl)_2$

End member	Formula
Magnesio-holmquistite	$Li_2Mg_3Al_2Si_8O_{22}(OH)_2$
Ferro-holmquistite	$Li_2Fe^{2}_3Al_2Si_8O_{22}(OH)_2$

Monoclinic forms

Cummingtonite series $(Mg,Fe^{2},Mn)_7Si_8O_{22}(OH)_2$

End member	Formula
Magnesio-cummingtonite	$Mg_7Si_8O_{22}(OH)_2$
Grunerite	$Fe^{2}_7Si_8O_{22}(OH)_2$
Tirodite	$Mn_2Mg_5Si_8O_{22}(OH)_2$
Dannemorite	$Mn_2Fe^{2}_5Si_8O_{22}(OH)_2$

Clinoholmquistite $Li_2(Mg,Fe^{2},Mn)_3(Fe^{3},Al)_2Si_8O_{22}(OH,F,Cl)_2$

End member	Formula
Magnesio-clinoholmquistite	$Li_2Mg_3Al_2Si_8O_{22}(OH)_2$
Ferro-clinoholmquistite	$Li_2Fe^{2}_3Al_2Si_8O_{22}(OH)_2$

Prefixes and adjectival modifiers specific to Fe-Mg-Mn amphiboles

Anthophyllite	Alumino-	$Al^{VI} \geq 0.50$
Gedrite	Sodium-	$Na \geq 0.75$
Cummingtonite series	Sodian	$Na \geq 0.25$
Fe-Mg-Mn group	Calcian	$Ca \geq 0.50$

Table 3. The Calcic Amphiboles: End Member Names and End Member Formulae

End member	Formula
Tremolite	$Ca_2Mg_5Si_8O_{22}(OH)_2$
Ferro-actinolite	$Ca_2Fe^{2}_5Si_8O_{22}(OH)_2$
Edenite	$NaCa_2Mg_5Si_7AlO_{22}(OH)_2$
Ferro-edenite	$NaCa_2Fe^{2}_5Si_7AlO_{22}(OH)_2$
Pargasite	$NaCa_2Mg_4AlSi_6Al_2O_{22}(OH)_2$
Ferro-pargasite	$NaCa_2Fe^{2}_4AlSi_6Al_2O_{22}(OH)_2$
Hastingsite	$NaCa_2Fe^{2}_4Fe^{3}Si_6Al_2O_{22}(OH)_2$
Magnesio-hastingsite	$NaCa_2Mg_4Fe^{3}Si_6Al_2O_{22}(OH)_2$
Alumino-tschermakite	$Ca_2Mg_3Al_2Si_6Al_2O_{22}(OH)_2$
Ferro-alumino-tschermakite	$Ca_2Fe^{2}_3Al_2Si_6Al_2O_{22}(OH)_2$
Ferri-tschermakite	$Ca_2Mg_3Fe^{3}_2Si_6Al_2O_{22}(OH)_2$
Ferri-ferro-tschermakite	$Ca_2Fe^{2}_3Fe^{3}_2Si_6Al_2O_{22}(OH)_2$
Alumino-magnesio-hornblende	$Ca_2Mg_4AlSi_7AlO_{22}(OH)_2$
Alumino-ferro-hornblende	$Ca_2Fe^{2}_4AlSi_7AlO_{22}(OH)_2$
Kaersutite	$NaCa_2Mg_4TiSi_6Al_2(O+OH)_{24}$
Ferro-kaersutite	$NaCa_2Fe^{2}_4TiSi_6Al_2(O+OH)_{24}$

Prefixes specific to calcic amphiboles

Alumino-	$Al^{VI} \geq 1.00$
Sodian	$Na \geq 1.00$ ($\sim$3.5% Na_2O)
Subcalcic	$Ca < 1.50$ ($\sim$9.5% CaO)
Silicic	$Si > 7.25$ $(Na+K)^{A} \geq 0.50$
Subsilicic	$5.75 > Si \geq 5.50$

Calcic amphiboles: With tschermakite, tschermakitic hornblende, ferro-tschermakite and ferro-tschermakitic hornblende, the prefixes alumino- and ferri- immediately precede the word tschermakite; otherwise, the order in which prefixes are used is not fixed. Neither ferri- nor ferrian should be used with hastingsite, as hastingsite implies high Fe^{3+}.

Sodic-calcic amphiboles: As with the calcic amphiboles, the prefixes alumino- and ferri- immediately precede the fundamental amphibole name; otherwise, the order in which the prefixes are used is not fixed.

Alkali amphiboles: Optic orientation may be indicated by prefixing the symbol G, C, O or R for the four possible orientations (Borg, 1967b).

Table 4. The Sodic-Calcic Amphiboles: End Member Names and End Member Formulae

End member	Formula
Richterite	$NaCaNaMg_5Si_8O_{22}(OH)_2$
Ferro-richterite	$NaCaNaFe^{2}_5Si_8O_{22}(OH)_2$
Ferri-winchite	$CaNaMg_4Fe^{3}Si_8O_{22}(OH)_2$
Alumino-winchite	$CaNaMg_4AlSi_8O_{22}(OH)_2$
Ferro-alumino-winchite	$CaNaFe^{2}_4AlSi_8O_{22}(OH)_2$
Ferro-ferri-winchite	$CaNaFe^{2}_4Fe^{3}Si_8O_{22}(OH)_2$
Alumino-barroisite	$CaNaMg_3Al_2Si_7AlO_{22}(OH)_2$
Ferro-alumino-barroisite	$CaNaFe^{2}_3Al_2Si_7AlO_{22}(OH)_4$
Ferri-barroisite	$CaNaMg_3Fe^{3}_2Si_7AlO_{22}(OH)_2$
Ferro-ferri-barroisite	$CaNaFe^{2}_3Fe^{3}_2Si_7AlO_{22}(OH)_2$
Magnesio-ferri-katophorite	$NaCaNaMg_4Fe^{3}Si_7AlO_{22}(OH)_2$
Magnesio-alumino-katophorite	$NaCaNaMg_4AlSi_7AlO_{22}(OH)_2$
Ferri-katophorite	$NaCaNaFe^{2}_4Fe^{3}Si_7AlO_{22}(OH)_2$
Alumino-katophorite	$NaCaNaFe^{2}_4AlSi_7AlO_{22}(OH)_2$
Ferri-taramite	$NaCaNaFe^{2}_3Fe^{3}_2Si_6Al_2O_{22}(OH)_2$
Magnesio-ferri-taramite	$NaCaNaMg_3Fe^{3}_2Si_6Al_2O_{22}(OH)_2$
Alumino-taramite	$NaCaNaFe^{2}_3Al_2Si_6Al_2O_{22}(OH)_2$
Magnesio-alumino-taramite	$NaCaNaMg_3Al_2Si_6Al_2O_{22}(OH)_2$
Prefixes specific to sodic-calcic amphiboles	
Alumino-	$Al^{VI} \geq 1.00$

Table 5. The Alkali Amphiboles: End Member Names and End Member Formulae

End member	Formula
Glaucophane	$Na_2Mg_3Al_2Si_8O_{22}(OH)_2$
Ferro-glaucophane	$Na_2Fe^{2}_3Al_2Si_8O_{22}(OH)_2$
Magnesio-riebeckite	$Na_2Mg_3Fe^{3}_2Si_8O_{22}(OH)_2$
Riebeckite	$Na_2Fe^{2}_3Fe^{3}_2Si_8O_{22}(OH)_2$
Eckermannite	$NaNa_2Mg_4AlSi_8O_{22}(OH)_2$
Ferro-eckermannite	$NaNa_2Fe^{2}_4AlSi_8O_{22}(OH)_2$
Magnesio-arfvedsonite	$NaNa_2Mg_4Fe^{3}Si_8O_{22}(OH)_2$
Arfvedsonite	$NaNa_2Fe^{2}_4Fe^{3}Si_8O_{22}(OH)_2$
Kozulite	$NaNa_2Mn_4(Fe^{3},Al)Si_8O_{22}(OH)_2$
Prefixes specific to alkali amphiboles	
Calcian	$Ca \geq 0.50$ ($\sim$3% CaO)
Lithian	$Li \geq 0.50$ ($\sim$1% Li_2O)

General considerations

For amphiboles that are not precisely characterized (e.g., identified from optical properties without chemical analysis), it is not possible to allocate a precise name. In this case, the assigned amphibole name should be made into an adjective followed by the word amphibole, thus, tremolitic amphibole, pargasitic amphibole. Similarly, hornblende is to be used for calcic amphiboles identified by physical and/or optical properties and not confidently identifiable as near to an end member.

For the various asbestiform amphiboles, mineralogical usage should involve the precise mineral name followed by -asbestos; thus, anthophyllite-asbestos, actinolite-asbestos (see chapter by Zoltai, this volume). Where the nature of the mineral is not known, asbestos alone may be appropriate. When the approximate nature of the mineral is known but not its precise composition, the assigned amphibole name should be made into an adjective followed by the word asbestos; thus, anthophyllitic asbestos. For this purpose, crocidolite is used to cover alkali amphibole asbestos in general, whereas the above recommendations are to be followed when the precise composition is known.

A large number of amphibole names have been formally abandoned (Leake, 1978) and should not be used; this included barkevikite, basaltic hornblende, ferrohastingsite and carinthine. This nomenclature is fairly simple considering the complexity of the amphibole group and should result in rapid and unambiguous naming of amphiboles.

THE AMPHIBOLE CRYSTAL STRUCTURES

The essential feature of the amphibole structure is a double chain of corner-linked tetrahedra that extends infinitely in one direction and has the general stoichiometry $(T_4O_{11})_\infty$. The direction of infinite polymerization of the double-chain unit defines the Z-axis of the amphibole cell in the normal orientation. The actual value of the repeat distance in the Z-direction is the c-dimension of the unit cell and is dependent on such factors as the occupancy of the tetrahedrally-coordinated cation sites and the stereochemistry of the tetrahedra; however, these factors produce only minor perturbations from the ideal value of $\sim$5.3 Å for an $(Si_4O_{11})_\infty$ chain. It is convenient to recognize two different types of

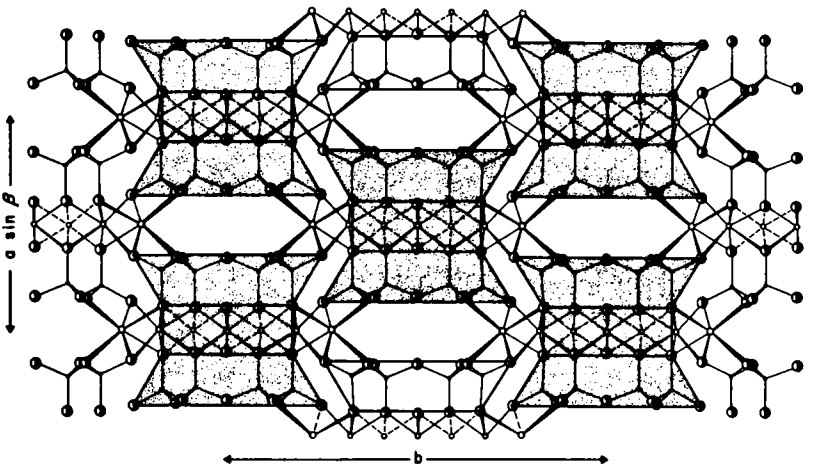

Figure 5. The crystal structure of C2/m amphibole projected down [001]. Shaded areas show the I-beam units of the structure. From Cameron and Papike (1978).

oxygen anions in this double-chain element. The oxygens lie in two planes parallel to the chain direction. All oxygens lying in the plane containing the linkages between adjacent tetrahedra are called *basal oxygens*, while the oxygens lying in the other plane are called *apical oxygens*. Oxygens bonded to two tetrahedrally-coordinated cations are called *bridging* (linking two TO_4 tetrahedra together) and here are denoted as O(br), while oxygens bonded to one tetrahedrally-coordinated cation are called *non-bridging* and here are denoted as O(nbr).

The $(T_4O_{11})_\infty$ chains are linked by medium-sized (ionic radius 0.53-0.83 Å) divalent and trivalent cations that bond to the O(nbr) anions of the chains. Two types of inter-chain linkage may be recognized. First, a strip of divalent and trivalent cations are intercalated between two layers of apical oxygens belonging to double chains that adjoin each other orthogonally to the plane of the basal oxygens. The adjacent double chains are staggered in the Z-direction so that the apical oxygens of adjacent chains assume a pseudo-octahedral arrangement around each of the linking divalent and trivalent cations. In order to complete the coordination of the cations in the center of this strip, it is necessary to add another anion to the plane of the apical oxygens; this is the monovalent anion in the amphibole formula. Thus, these adjacent double chains are tightly bonded together and form a modular unit, an I-beam, that plays an important

role in model amphibole structures (Thompson, 1970; Papike and Ross, 1970; see chapters by Thompson and Veblen, this volume).

The second type of inter-chain linkage joins these modular units together in a three-dimensional array (Fig. 5). The divalent and trivalent cations at the edges of an I-beam unit link laterally to the non-bridging basal oxygens of adjacent I-beams. These divalent and trivalent cations, together with their coordinating anions, define a strip of edge-sharing octahedra that extends infinitely in the Z-direction. Thus, an I-beam may also be thought of as a strip of edge-sharing octahedra sandwiched between two double chains of corner-sharing tetrahedra.

As described thus far, the structure consists of C- and T-type cations. Further linkage between the modular units is provided by the A and B cations. The B cations are situated at the margins of the octahedral strips, where they provide additional linkage both within individual I-beams and between adjacent I-beams. The inter-chain linkage provided by the B-type cations differs from the second type of inter-chain linkage described above. The C-type cations all bond to non-bridging anions whereas the B-type cations bond with the non-bridging and bridging anions. The B cations are surrounded by eight anions, not all of which are necessarily bonded to the central cation. These anions are arranged in a distorted square antiprism, the exact configuration of which is a function of the central cation and local structural requirements. Between the back-to-back double chains is a large cavity that is surrounded by 12 bridging oxygens. The A cations are situated within this cavity; the actual position assumed by the A-type cations and the number and configuration of the surrounding anions to which it is bonded are a function of local stereochemical requirements, and vary with the chemistry of the amphibole. The A cations thus provide additional linkage between adjacent double chains orthogonal to the plane of the double chain. The complete structure is one of great elegance; schematic projections are shown in Figures 5 and 7.

Choice of axes

The original crystal structure determination for tremolite by Warren (1929) was referred to an I-centered cell and conformed to the early morphological convention of defining β as the acute angle between the X and

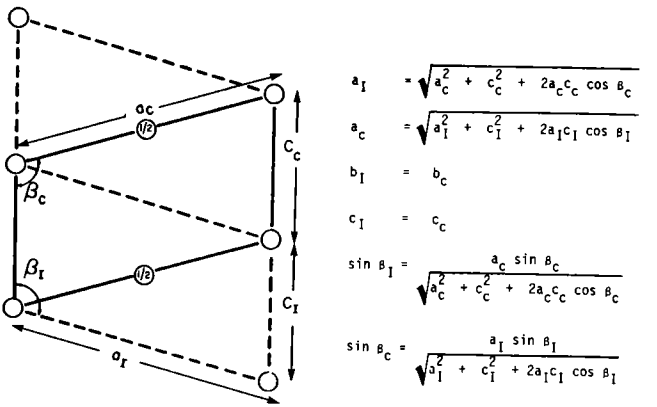

Figure 6. The geometrical relationships between the *I*- and *C*-centered cells of the clinoamphiboles. Modified from Whittaker and Zussman (1961).

the *Z* axes. Some confusion subsequently arose concerning this point (Whittaker and Zussman, 1961). Warren's work was done before the introduction of the Hermann-Mauguin symbols and the space group was reported as 2Ci-3 using the Wyckoff notation. This was translated into the standard form C2/m by later workers, but the unit-cell parameters were still given in the I-centered orientation. Current crystallographic convention for the monoclinic crystal system defines β as the obtuse angle between the *X* and *Z* crystallographic axes. Several later studies (Zussman, 1955; Heritsch *et al.*, 1960; Heritsch and Kahler, 1960; Heritsch and Reichert, 1960) report atomic coordinates in an I-centered cell with β obtuse; in these studies, the signs of the *z* coordinates should be reversed.

Here, all crystallographic information has been standardized to a C-centered cell with β obtuse. Maintaining a right-handed set of crystallographic axes with β obtuse, Figure 6 summarizes the relationships between the I- and C-centered cells.

Principal structure types

The extensive morphological investigations of the 19th century had shown that amphiboles occur in both monoclinic and orthorhombic varieties, and Warren's studies showed that these were related structures with space group symmetries C2/m and Pnma, respectively. More detailed work during the past 20 years has unearthed three more structural variants with different space groups. Gibbs *et al.* (1960) reported the synthesis of

Table 6. Site-Nomenclature Scheme for Amphibole Structure Types

	C2/m	$P2_1/m$		P2/a		Pnma		Pnmn
tetrahedrally coordinated sites	T(1)	T(1A)	T(1B)	T(1)A	T(1)B	T1A	T1B	T1
	T(2)	T(2A)	T(2B)	T(2)A	T(2)B	T2A	T2B	T2
octahedrally coordinated sites	M(1)	M(1)		M(1)A	M(1)B	M1		M1
	M(2)	M(2)		M(2)A	M(2)B	M2		M2
	M(3)	M(3)		M(3)		M3		M3
cubic antiprismatic sites	M(4)	M(4)		M(4)A	M(4)B	M4		M4
[12] cavity*	A	A		A(2)		A		A
non-bridging anion sites	O(1)	O(1A)	O(1B)	O(1)A	O(1)B	O1A	O1B	O1
	O(2)	O(2A)	O(2B)	O(2)A	O(2)B	O2A	O2B	O2
	O(3)	O(3A)	O(3B)	O(3)		O3A	O3B	O3
	O(4)	O(4A)	O(4B)	O(4)A	O(4)B	O4A	O4B	O4
bridging anion sites	O(5)	O(5A)	O(5B)	O(5)A	O(5)B	O5A	O5B	O5
	O(6)	O(6A)	O(6B)	O(6)A	O(6)B	O6A	O6B	O6
	O(7)	O(7A)	O(7B)	O(7)		O7A	O7B	O7

*the more complex nomenclature used to describe the positional disorder of cations occupying this site is described in the section on the A-site.

protoamphibole, a new orthorhombic amphibole with space group symmetry Pnmn; Gibbs (1964, 1969) subsequently refined the protoamphibole structure. Deer *et al.* (1963) postulated the existence of a magnesium-rich Fe-Mg-Mn amphibole with $P2_1/m$ symmetry. Bown (1966) subsequently reported such an amphibole, and the structure of a tirodite $P2_1/m$ was refined by Papike *et al.* (1969). Moore (1968a,b) reported the existence of a peculiar amphibole-like mineral from Långban, Sweden. The unit-cell dimensions and space group (P2/a) were compatible with an amphibole-type structure but the chemical analysis was not. Subsequent solution and refinement of the structure of this mineral (joesmithite) showed it to be a *bona fide* amphibole with a beryllo-silicate double chain (Moore, 1969).

Site nomenclature in amphiboles

In order to facilitate inter-structure comparison of structural features in the amphiboles, it is desirable to have a site-nomenclature that differentiates between structure types but maintains some sort of congruence between analogous sites in different structures. A completely general site-nomenclature that would satisfy these restrictions for all possible structures would have the same type of basis as the nomenclature schemes that have been derived for the pyroxenes (Burnham *et al.*, 1967) and the feldspars (Megaw, 1956). Such a scheme would also be extremely

cumbersome and is not really necessary unless numerous additional structural varieties are discovered. The scheme developed here is not as systematic as those for pyroxenes and feldspars, but is convenient (Table 6). The site-nomenclature used by Robinson *et al.* (1973) and Hawthorne and Grundy (1973a,b) is adopted here for the C2/m amphibole structure type. The site-nomenclatures for the other structural variants can be derived from this nomenclature by changes that correspond to the space group differences of the structures involved. The difference between the monoclinic and orthorhombic amphiboles may be indicated by the presence or absence of parentheses in the site symbols. This is consistent with the current nomenclature of the Pnma amphiboles (Finger, 1970; Papike and Ross, 1970) which is thus adopted in the current scheme. The site-nomenclature of the Pnmn structure (Gibbs, 1969) is changed; the parentheses are not used and the Si(1) and Si(2) sites become the T1 and T2 sites. For the $P2_1/m$ structure type, parentheses were added to the nomenclature scheme of Papike *et al.* (1969, Fig. 2). The site-nomenclature scheme for the P2/a structure (Moore, 1969) does not resemble that of the other amphiboles and was completely revised. The site numbering was adjusted to correspond with numbering in the other amphibole structures. For the "pseudo-mirror equivalent" pairs of atoms, those with the smaller value of the y-coordinate were labelled by addition of a suffix A while those with the larger value of the y-coordinate were labelled with the suffix B. Parentheses are used because this structure type is monoclinic; however, in order to distinguish sites in this structure type from similar sites in the $P2_1/m$ structure type, the parentheses enclose the numbers only in the P2/a structure type. The sites of all the various structure types are summarized in Table 6.

The C2/m amphibole structure

This is the most common of the amphibole structure types, suggesting that this must be the most flexible, or chemically compliant, of these structures. A schematic polyhedral representation of this structure type is shown in Figure 7. There are three non-bridging atoms: O(1), O(2) and O(4); of these, O(1) and O(2) are apical oxygens and O(4) is a basal oxygen. There are three bridging anions: O(5), O(6) and O(7); all of these are basal oxygens, and O(5) and O(6) bridge along the length

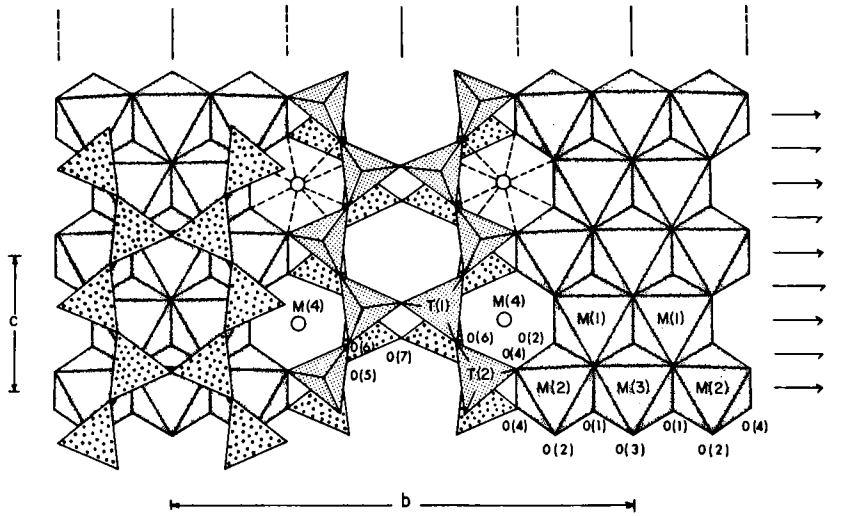

Figure 7. The C2/m amphibole structure projected onto (100); the space group symmetry elements are shown. From Hawthorne (1982).

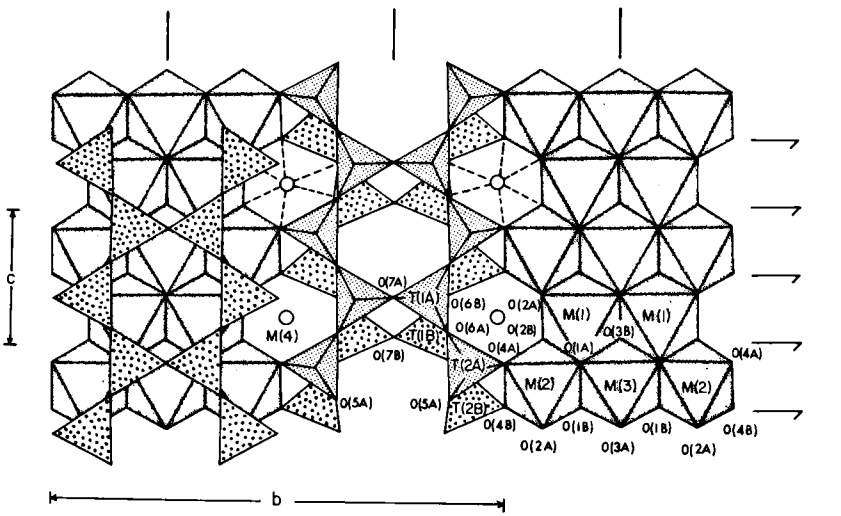

Figure 8. The $P2_1/m$ amphibole structure projected onto (100); the space group symmetry elements are shown. From Hawthorne (1982).

of the $(T_4O_{11})_\infty$ double chain while O(7) is the anion that links the two pyroxene-like components of the double chains together. In addition, there is the O(3) anion that is bonded to three octahedrally-coordinated cations; the O(3) site may be occupied wholly or in part by OH, F, Cl or O^{2-}. The anions are arranged in layers parallel to the (100) plane. These layers are not close-packed but bear a simple relationship to both cubic and hexagonal close-packed arrangements.

There are two unique cation sites with pseudo-tetrahedral coordination, the T(1) and T(2) sites, both of which have point symmetry 1. The T(1) site is coordinated by three bridging and one non-bridging anions, whereas the T(2) site is coordinated by two bridging and two non-bridging anions. T(1) and T(2) tetrahedra alternate along the chain; thus, all linkages $\|Z$ are of the type T(1)-T(2). Cross-linkages $\|Y$ are of the type T(1)-T(1), as required by the symmetry of the chain. All tetrahedral chains in this structure type are identical.

There are three unique sites with pseudo-octahedral coordination, the M(1), M(2) and M(3) sites; the point symmetry of the M(1) and M(2) sites is 2 and the point symmetry of the M(3) site is 2/m. Both the M(1) and M(3) sites are coordinated by four oxygens and two O(3) anions; around the M(1) site, the O(3) anions are in a *cis* arrangement whereas around the M(3) site they are in a *trans* arrangement. The M(2) site is coordinated by six oxygens and is situated at the margins of the octahedral strip. These three sites differ significantly in next-nearest-neighbor configuration, and thus afford great opportunity for differential ordering of C-type cations in this structure type.

There is one unique cation site surrounded by eight anions, the M(4) site with point symmetry 2. The anions are arranged in a distorted square antiprism, but the actual cation coordination may vary with cation occupancy. The M(4) site is situated at the periphery of the octahedral strip and is occupied by the B-type cations of the standard formula. Between the back-to-back chains is a large cavity surrounded by 12 anions, at the center of which is the A-site with point symmetry 2/m. This site may or may not be occupied depending on the chemical composition of the amphibole. Detailed studies have shown that the cation occupying this cavity is postionally disordered off the center of symmetry.

The $P2_1/m$ amphibole structure

A schematic polyhedral representation of this structure type is shown in Figure 8. There are six non-bridging anions: O(1A), O(2A), O(4A), O(1B), O(2B) and O(4B); of these, O(4A) and O(4B) are basal oxygens and the remainder are apical oxygens. There are six bridging anions: O(5A), O(6A), O(7A), O(5B), O(6B) and O(7B); all of these are basal oxygens, with O(7A) and O(7B) cross-linking the double chains and the remainder bridging along the length of the $(T_4O_{11})_\infty$ double chains. In addition, there are two anion positions, O(3A) and O(3B) that are coordinated to three octahedrally-coordinated cations; these positions are generally occupied by OH in this structure type.

There are four unique cation sites with pseudo-tetrahedral coordination, the T(1A), T(2A), T(1B) and T(2B) sites, all of which have point symmetry 1. The topological details of their coordination are similar to the coordination of the corresponding sites in the C2/m structure type, with the restriction that cation sites labelled A always bond to anions labelled A, and likewise for the B-labelled cations. The double chains in this structure still have mirror symmetry and retain the same linkage configurations as the C2/m structure in regard to the labelling of the atoms of the chains. However, the back-to-back double chains are crystallographically non-equivalent, and are designated the A- and B-chains. The B-chain shows a much greater deviation from an extended chain configuration than does the A-chain, with the average chain kinking being similar to that found in structures of similar composition with C2/m symmetry.

There are three unique sites with pseudo-octahedral coordination, the M(1), M(2) and M(3) sites; the point symmetry of the M(1) and M(2) sites is 1 and the point symmetry of the M(3) site is m. The relative configuration of these sites and their coordinating anions is similar to the corresponding sites in the C2/m structure; note that the anions on one side of the octahedral strip are A-type anions while the anions on the other side of the octahedral strip are B-type anions. Whereas there are two types of tetrahedral double chain in this structure type, there is only one type of octahedral strip.

At the margins of the octahedral strip is the M(4) site, with point symmetry 1, surrounded by eight anions arranged in a very distorted square antiprism. The cations occupying the M(4) site may not bond to all of the

surrounding anions; indeed, the existence of this structure type seems to hinge on the bonding requirements of the M(4) cation(s). Between the back-to-back A- and B-chains is the A-site, with point symmetry m and two degrees of positional freedom. This site is identified by analogy with other structure types, as it is unoccupied in all $P2_1/m$ structures examined thus far.

The P2/a amphibole structure

Only one representative of this structure type has so far been discovered. Joesmithite is a beryllo-silicate amphibole whose unusual structure can be directly related to its unusual chemical composition. A schematic polyhedral representation of joesmithite is shown in Figure 9. Note that the site nomenclature is different from that used by Moore (1969). There are six non-bridging anions: O(1)A, O(2)A, O(4)A, O(1)B, O(2)B and O(4)B; of these, O(4)A and O(4)B are basal oxygens and the remainder are apical oxygens. There are five bridging anions: O(5)A, O(6)A, O(5)B, O(6)B and O(7); all of these are basal oxygens, with O(7) cross-linking the double chain and the rest bridging along the length of the double chain. In addition, there is the O(3) anion position that is coordinated to three octahedrally-coordinated cations and is occupied by OH.

There are four unique cation sites with pseudo-tetrahedral coordination, the T(1)A, T(2)A, T(1)B and T(2)B sites, all of which have point symmetry 1. The topological details of their coordination is similar to the coordination of the corresponding sites in the $P2_1/m$ structure type. Whereas in the $P2_1/m$ and Pnma structures the four unique tetrahedrally-coordinated sites occur in two distinct tetrahedral double chains, in the P2/a structure the four unique tetrahedra are all found in just one double chain, and all double chains in this structure type are identical.

There are five unique sites with pseudo-octahedral coordination, the M(1)A, M(2)A, M(1)B, M(2)B and M(3) sites, all of which have point symmetry 2. The relative configurations of these sites and their coordinating anions are similar to the analogous sites in the C2/m structure. Cations denoted by A and B bond to A- and B-type anions, respectively. There is only one type of octahedral strip. At the margins of the octahedral strip are the M(4)A and M(4)B sites, both of which have point symmetry 2. The anions surrounding each site are arranged in a distorted

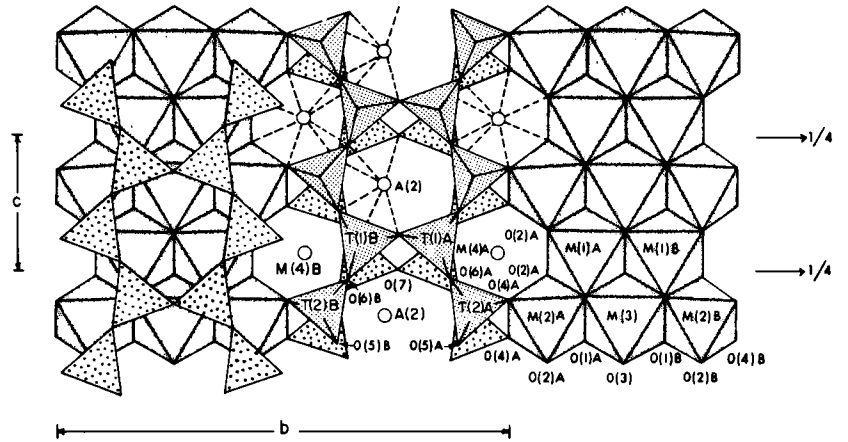

Figure 9. The P2/a amphibole structure projected onto (100); the space group symmetry elements are shown. From Hawthorne (1982).

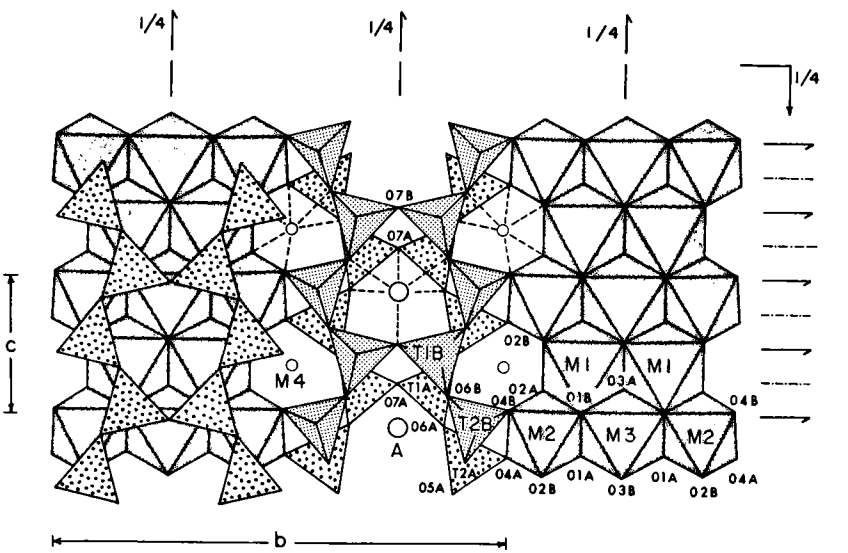

Figure 10. The Pnma amphibole structure projected onto (100); the space group symmetry elements are shown. From Hawthorne (1982).

square antiprism, with all the anions bonded to the central cation in joesmithite itself. Sandwiched between the back-to-back double chains is the A-site cavity, surrounded by 12 anions. In joesmithite, this cavity is fully occupied by divalent cations that assume an ordered off-center position, the A(2) site. This displacement is along the two-fold axis towards the T(1)B site that contains Be.

The Pnma amphibole structure

This is the only structure type found thus far for naturally-occurring orthorhombic amphiboles. A schematic polyhedral representation of this structure type is shown in Figure 10. There are six non-bridging anions: O1A, O2A, O4A, O1B, O2B and O4B; of these, O4A and O4B are basal oxygens and the rest are apical oxygens. There are six bridging anions: O5A, O6A, O7A, O5B, O6B and O7B; all of these are basal oxygens, with O7A and O7B bridging across the chains and the rest bridging along the length of the chains. In addition, there are the O3A and O3B anion positions, both of which are coordinated to three octahedrally-coordinated cations and are occupied by OH, F, Cl or O^{2-}.

There are four unique cation sites with pseudo-tetrahedral coordination, the T1A, T2A, T1B and T2B sites, all of which have point symmetry 1. The T1A and T1B sites are coordinated by three bridging and one non-bridging anions and the T2A and T2B sites are coordinated by two bridging and two non-bridging anions. Sites designated A and B are coordinated respectively to A- and B-type anions only. There are two crystallographically distinct double chains, the A-chain and the B-chain, that are constituted from A- and B-type atoms, respectively. Both A- and B-chains have mirror symmetry and all of the intra-chain linkages are analogous to those in the C2/m structure type. There is generally a significant decrease in the degree of ditrigonal rotation of each chain, the B-chain being more kinked than the A-chain.

There are three unique sites with pseudo-octahedral coordination, the M1, M2 and M3 sites, with point symmetries 1, 1 and m, respectively. Apart from the differences in point symmetry, the coordination of these sites is similar to the corresponding sites in the C2/m structure. The anions on one side of the octahedral strip are A-type anions and on the other side are B-type anions. There is only one type of octahedral strip in this structure type.

At the edges of the octahedral strip is the M4 site, with point symmetry 1, surrounded by eight anions. The actual coordination number almost certainly varies with cation occupancy of this site and is possibly one of the more important factors in the occurrence of this structure type. The cations occupying this site may bond to bridging anions of both the A and B tetrahedral double chains. Thus, the cations occupying this site have great flexibility with regard to the possible coordination geometry they assume. Between the back-to-back A and B double chains is the A-site, point symmetry m, that is coordinated by six bridging anions. This site may or may not be occupied depending on the chemical composition of the amphibole. Unlike the C2/m amphibole structure, there seems to be no significant positional disorder of the cations occupying this position in amphiboles of the Pnma structure type.

The Pnmn amphibole structure

No naturally-occurring amphiboles with this structure type have yet been found. Protoamphibole (Gibbs *et al.*, 1960) is a synthetic amphibole with orthorhombic symmetry and the only representative of this structure type known. A schematic polyhedral representation of this structure type is shown in Figure 11. There are three non-bridging anions: O1, O2 and O4; the latter is a basal oxygen and the other two are apical oxygens. There are three bridging anions: O5, O6 and O7; all of these are basal oxygens with O7 bridging across and O5 and O6 bridging along the tetrahedral double chain. In addition, there is the O3 anion position which is coordinated to three octahedrally-coordinated cations and is occupied by F in protoamphibole. There are two unique cation sites with pseudo-tetrahedral coordination, the T1 and T2 sites with point symmetry 1. The T1 site is coordinated by three bridging and one non-bridging anions and the T2 site is coordinated by two bridging and two non-bridging anions. There is only one symmetrically distinct tetrahedral double chain in this structure type.

There are three unique sites with pseudo-octahedral coordination, the M1, M2 and M3 sites, with point symmetry 2, 2 and 2/m, respectively. The coordination of these sites is similar to the analogous sites in the C2/m amphibole structure, and there is only one symmetrically distinct octahedral strip. At the edge of the octahedral strip is the M4 site, with

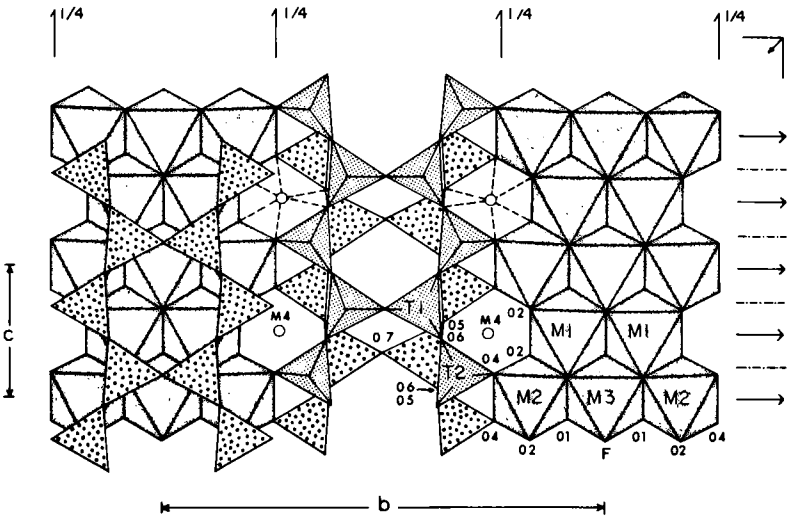

Figure 11. The Pnmm amphibole structure projected onto (100); the space group symmetry elements are shown. From Hawthorne (1982).

point symmetry 2, surrounded by eight anions only six of which are bonded to the central M4 cation. Although only coordinated by six anions, the M4 site still differs significantly from the pseudo-octahedrally coordinated M1, M2 and M3 cation sites of the octahedral strip in that its central cation bonds both to non-bridging and bridging anions. Between the back-to-back double chains is a large cavity surrounded by 12 anions, in the center of which is the A-site with point symmetry 2/m. According to the chemical analysis of protoamphibole, this site should be almost completely occupied by Li; however, Gibbs (1969) could not locate the position of Li (a very weak x-ray scatterer) in the structure refinement and suggested that it is positionally disordered within this cavity.

Amphiboles as layer structures

Amphiboles may be considered as ordered stacking sequences along X of alternate layers of octahedra and tetrahedra (Figs. 5 and 12). Because the apical oxygens of the tetrahedral layers provide the octahedral coordination of the octahedral layers, there is a stagger of approximately $\pm c/3$ between adjacent tetrahedral layers. For the C2/m, $P2_1/m$ and P2/a structure types, this stagger is always in the same direction. The orthorhombic amphiboles require a regular reversal of this stagger in order

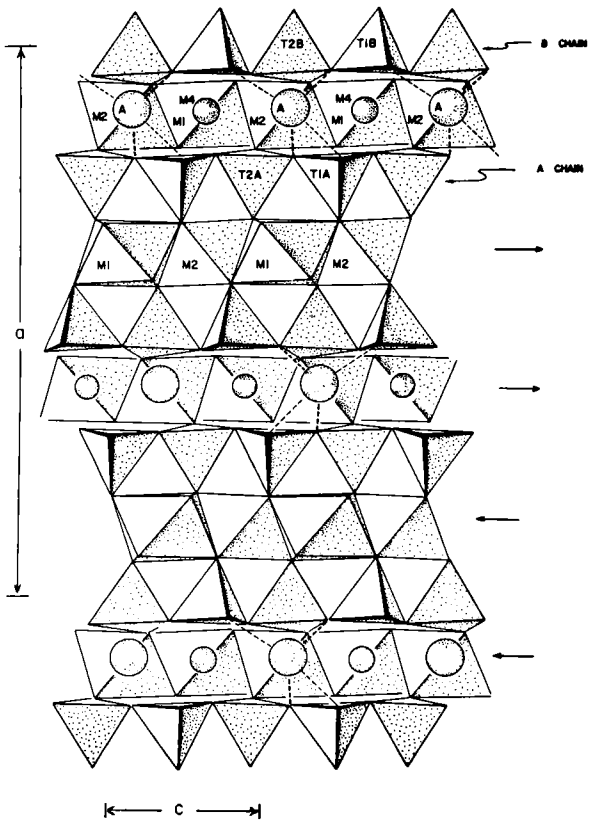

Figure 12. The Pnma amphibole structure projected onto (010); the arrows indicate the direction of stagger of the octahedral layers. From Papike and Ross (1970).

Table 7. Observed Amphibole Space Groups and Representative Structures

$C2/m$[1]	calcic amphiboles, sodic-calcic amphiboles alkali amphiboles, monoclinic Fe-Mg-Mn amphiboles
$P2_1/m$[2]	magnesio-cummingtonite
P2/a	joesmithite
Pnma	orthorhombic Fe-Mg-Mn amphiboles, holmquistite
Pnmn	protoamphibole

[1] Ginzburg (1965) reports clinoholmquistite with P2/m symmetry; however, Litvin et al. (1975a) have refined the structure of clinoholmquistite in the space group C2/m.

[2] Woensdregt and Hartman (1969) report a hornblende with $P2_1/m$ symmetry.

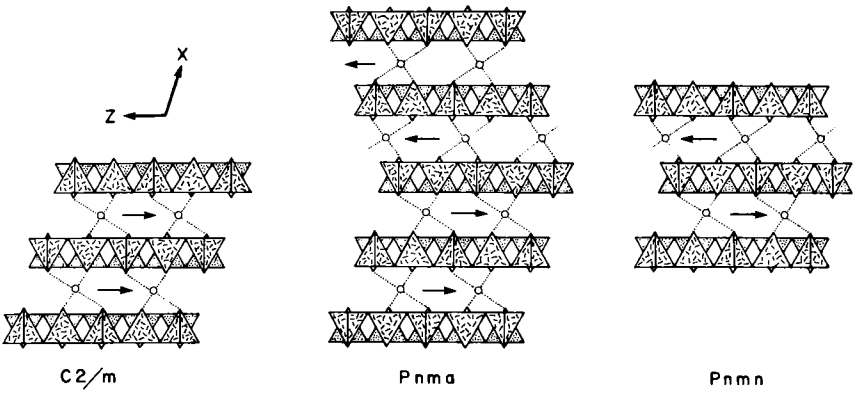

Figure 13. Schematic representation of the layer stacking sequences projected down Y for the various amphibole structure types. Modified from Gibbs (1966). The $P2_1/m$ and P2/a sequences are the same as for the C2/m structure type, and are not depicted here.

that the resulting structures conform to the requirements of orthorhombic symmetry. For the Pnma structure type, the stagger between adjacent tetrahedral layers is $+c3,+c/3,-c/3,-c/3$ (or simply ++--), while for the Pnmn structure type, the stacking sequence stagger is $+c/3$, $-c/3$, $+c/3$, $-c/3$ (or +-+-). This is summarized in Figure 13.

Space group variations in amphiboles

There are at present five known structural variants of amphiboles, details of which are given above. The amphiboles known to occur with these structure types are listed in Table 7. In regard to the existence of other possible structure types, it is instructive to consider the P2/a and $P2_1/m$ structures. The P2/a structure has the same topological arrangement as the C2/m structure, but a different topochemical arrangement. It is the difference in cation ordering that leads to the different space group; note that there is no major change in the shape or size of the unit cell and that the space group P2/a is a subgroup of the space group C2/m. The $P2_1/m$ structure has the same topochemical arrangement as the C2/m structure. Whether or not the topological arrangement is the same is a moot point. However, we can understand the difference in symmetry between these two structure types as a relaxation of symmetry constraints to allow local relaxation in the structure; there is no major topological change in the structure type, such as a change in stacking sequence. Again, the space group $P2_1/m$ is a subgroup of the space group C2/m. Thus, we can identify the C2/m, Pnma and Pnmn structures as

principal structure types in the amphiboles, as none of these can be considered as simple subgroup derivatives of the other(s). All possible space groups for amphibole structures derivative from the C2/m, Pnma and Pnmn structures without a change in shape or size of the unit cell are subgroups of these space groups. The possible supergroups of these three space groups are not consistent with the amphibole structure without a change in shape and size of the unit cell, and thus all possible space groups may be derived from C2/m, Pnma and Pnmn by group reduction (for an introduction to group theory and symmetry, see Yale, 1968).

A space group G may be written as G = P·Q, where P is the primitive lattice group and Q is the factor group (Zachariasen, 1945). Thus, all space groups that are subgroups of G may be formed by taking the semi-direct product of P and all subgroups of Q. For each of the space groups under consideration, the rank of Q is 8; thus, the ranks of all relevant subgroups of Q are 4, 2 and 1. In each case, all elements of Q are binary and thus all subgroups, H, of Q with rank 2 are (I·e) where e is a non-identity element of Q. All subgroups, F, of Q with rank 4 may then be derived from the relation H·F = Q.

Subgroups of C2/m, Pnma and Pnmn derived in this manner are listed in Table 8. The two $P\bar{1}$ space groups listed as subgroups of C2/m are structurally distinct as there are two symmetrically distinct centers of symmetry in C2/m. This situation does not arise for $C\bar{1}$ as both centers of symmetry are elements of this space group. Other amphibole structure types in addition to the ones examined here are possible. However, they involve a change in the shape and size of the unit cell or a change in the stacking sequence along the *X* axis.

THE TETRAHEDRAL DOUBLE CHAIN

There are at least two unique sites with pseudo-tetrahedral coordination in each of the amphibole structure types. Considerable variation in local environment from structure to structure causes significant stereochemical differences among the tetrahedra. This in turn has promoted studies of these variations in relation to bonding models. In addition to being of intrinsic interest, such studies have considerable implication in regard to cation ordering and constraints on chemical substitutions in amphiboles.

Table 8. Subgroups of C2/m, Pnma and Pnmn

*C2/m	*Pnma	*Pnmn
Monoclinic (y)	Orthorhombic	Orthorhombic
$P2_1/a$	$Pn2_1a$	Pn2n
*$P2_1/m$	$Pnm2_1$	$Pnm2_1$
*P2/a	$P2_1ma$	$P2_1mn$
P2/m	$P2_12_12_1$	$P2_12_12_1$
Cm	Monoclinic (x)	Monoclinic (x)
C2	$P2_1/n$	$P2_1/n$
$P2_1$	$P2_1$	$P2_1$
P2	Pn	Pn
Pa	Monoclinic (y)	Monoclinic (y)
Pm	$P2_1/m$	P2/m
Triclinic	$P2_1$	P2
$C\bar{1}$	Pm	Pm
C1	Monoclinic (z)	Monoclinic (z)
$P\bar{1}$	$P2_1/a$	$P2_1/n$
$P\bar{1}$	$P2_1$	$P2_1$
P1	Pa	Pn
	Triclinic	Triclinic
	$P\bar{1}$	$P\bar{1}$
	P1	P1

*reported as amphibole space groups

The C2/m amphiboles

Individual Si-O bond lengths range from 1.572 to 1.704 Å and there have been several attempts to rationalize these variations in terms of particular bonding models. Two models for the Si-O bond have been considered.

Covalent bonding model. Pauling (1939) suggested the formation of a double bond involving the 3d orbitals (in addition to the 3s and 3p orbitals) for silicon tetrahedrally coordinated by oxygen. This idea was extended by Cruickshank (1961) who used simple group theory arguments to show that only two strong d-p-π bonds will be formed (by the e_g orbitals on silicon combining with the $2p\pi$ and $2p\pi'$ orbitals on oxygen) in polymerized tetrahedra of T_d symmetry. Assuming these arguments can be extended to tetrahedra showing some deviation from T_d symmetry, several predictions can be made concerning the stereochemistry of polymerized tetrahedra (Cruickshank, 1961; Brown *et al.*, 1969):

(i) Si-O(nbr) bonds are usually shorter than Si-O(br) bonds, providing the Si-O(br)-Si angle is not wide and $\bar{\chi}$ (the mean electronegativity of the non-tetrahedral cations) is not large;

(ii) the shorter Si-O(br) bonds are usually associated with the wider Si-O(br)-Si angles;

(iii) tetrahedral angles usually decrease in the order O(nbr)-Si-O(nbr) > O(nbr)-Si-O(br) > O(br)-Si-O(br).

Brown and Gibbs (1969, 1970) examined the steric details in the double chains of four C2/m amphiboles and showed that they conform to the above predictions. In addition, they correlated individual Si-O bond lengths with $\bar{\chi}$ (the mean electronegativity of the non-tetrahedral cations). This approach was developed further by Mitchell *et al.* (1971) who presented equations relating the T-O(nbr) bond lengths to <T-O(br)-T> and $\bar{\chi}$:

$$T(1)\text{-}O(1) = 1.137 + 0.0029 \langle T\text{-}O(5,6,7)\text{-}T \rangle + 0.051\ \bar{\chi}_{O(1)}$$

$$T(2)\text{-}O(2) = 1.211 + 0.0029 \langle T\text{-}O(5,6)\text{-}T \rangle + 0.007\ \bar{\chi}_{O(2)}$$

$$T(2)\text{-}O(4) = 1.213 + 0.0026 \langle T\text{-}O(5,6)\text{-}T \rangle + 0.009\ \bar{\chi}_{O(4)}$$

An equation relating bond length to bond order was deduced by Robinson (1963) and applied to Si-O, P-O and S-O bonds by Gillespie and Robinson (1963, 1964). For Si-O bonds:

$$Si\text{-}O = 1.83 - 0.32/(1 + 0.6[(2-n)/(n-1]) ,$$

where n is the bond order. As the second derivative of this curve is positive, an increase in some bond lengths in a polyhedron must be accompanied by a decrease of lesser magnitude in the remaining bonds if the mean bond order is to remain constant at $\sim$1.5. Consequently, irregular tetrahedra that are characterized by large differences between their individual Si-O bond lengths will have a larger <Si-O> bond length than more regular tetrahedra (Fig. 14).

A considerable amount of work has been done on Extended Hückel Molecular Orbital (EHMO) calculations in silicates (Gibbs *et al.*, 1972; Louisnathan and Gibbs, 1972a,b,c), and further stereochemical relationships have come to light as a result of these studies:

(i) Si-O(br) is not a linear function of Si-O(br)-Si but an inverse function of cos(Si-O(br)-Si);

Figure 14 (to the right). Variation in mean bond length as a function of polyhedral distortion parameter Δ for C2/m amphiboles with little or no tetrahedrally coordinated Al.

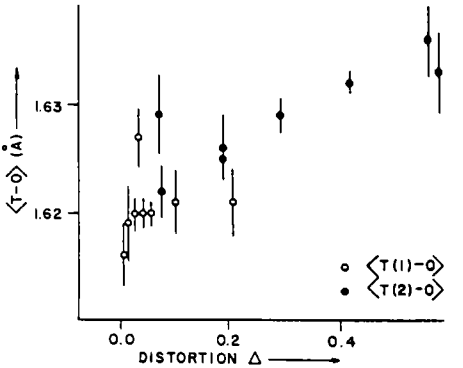

Figure 15 (below, center). Variation in grand <T-O(br)> as a function of grand <T-O(br)-T> for the C2/m amphiboles with little or no tetrahedrally coordinated Al. The variation in <T-O(br)-T> angle is not sufficient to show the non-linearity inherent in the graph to the right.

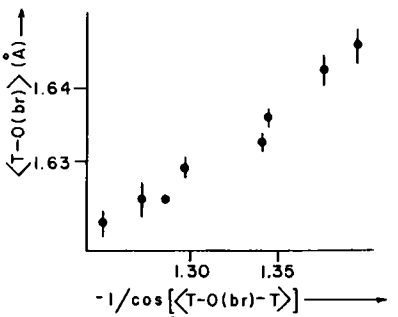

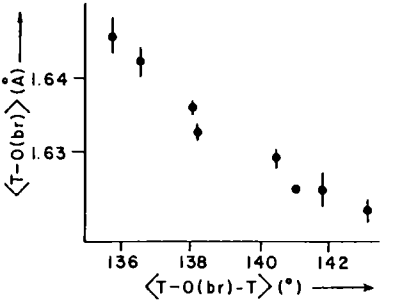

Figure 16 (to the left, below). Variation in individual Si-O bond lengths as a function of the mean value of the three O-Si-O angles involved in that bond for the C2/m amphiboles with little or no tetrahedrally coordinated Al.

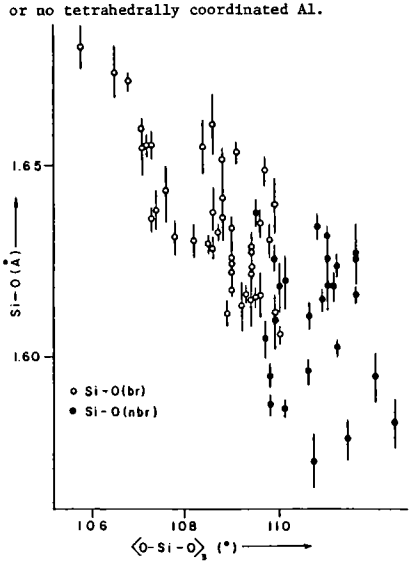

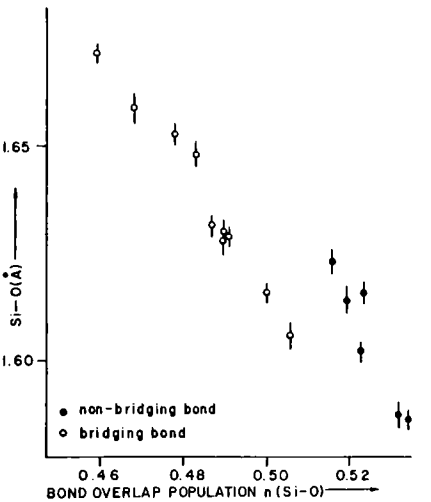

Figure 17 (to the right, above). Variation in observed Si-O bond lengths for tremolite (30) and fluor-tremolite (36) as a function of bond overlap population calculated using extended Hückel molecular orbital theory.

(ii) Si-O bond lengths are a function of the O-Si-O angles in which they are involved.

These predictions are examined for the C2/m amphiboles in Figures 15 and 16, where it can be seen that the results support the above contentions.

Cameron and Gibbs (1973) performed EHMO calculations for tremolite (30)* and fluor-tremolite(36), and noted that the observed bond lengths are inversely correlated with the Si-O bond overlap populations (Fig. 17). Although a valence basis set was used for these calculations, the Si-O(br) and Si-O(nbr) seem to form two separate populations (*cf.* Gibbs *et al.*, 1972). In a series of calculations for idealized orthosilicic acid molecules, Louisnathan and Gibbs (1972c) found that bond overlap population is non-linearly correlated with O-Si-O angles involved in the bond. This correlation varies with differing molecular orbital environments along the basal-apical bond directions and can be rationalized in terms of changes in the non-equivalent hybridization characteristics of the central Si atom. Thus, the presence of two ordered populations in Figure 17 is not inconsistent with the conclusion of Gibbs *et al.* (1972) that at least part of the Si-O bond length variations observed in silicates can be rationalized in terms of a covalent bonding model.

Bond-valence model. The utility of the ionic model in understanding the chemical bond in solids has long been recognized (Bent, 1968). Bragg (1924, 1926) extended the hard sphere model of atoms originally developed by Barlow and developed the idea of ionic radius (Bragg and West, 1927). Pauling (1929, 1960) extended previous work and produced a set of empirical rules to predict stable configurations in inorganic crystals and to rationalize observed distortions in terms of ion-ion interactions. These rules have been tested extensively in minerals and synthetic inorganic oxides and have been found to be quite successful. Of particular interest is Pauling's second rule: "In a stable ionic structure, the valence of each anion, with the sign changed, is equal to the sum of the strengths of the electrostatic bonds to it from the adjacent cations," where the electrostatic bond strength is defined

*Numbers in parentheses following amphibole names refer to structure refinements in Table A-1 at the end of the chapter.

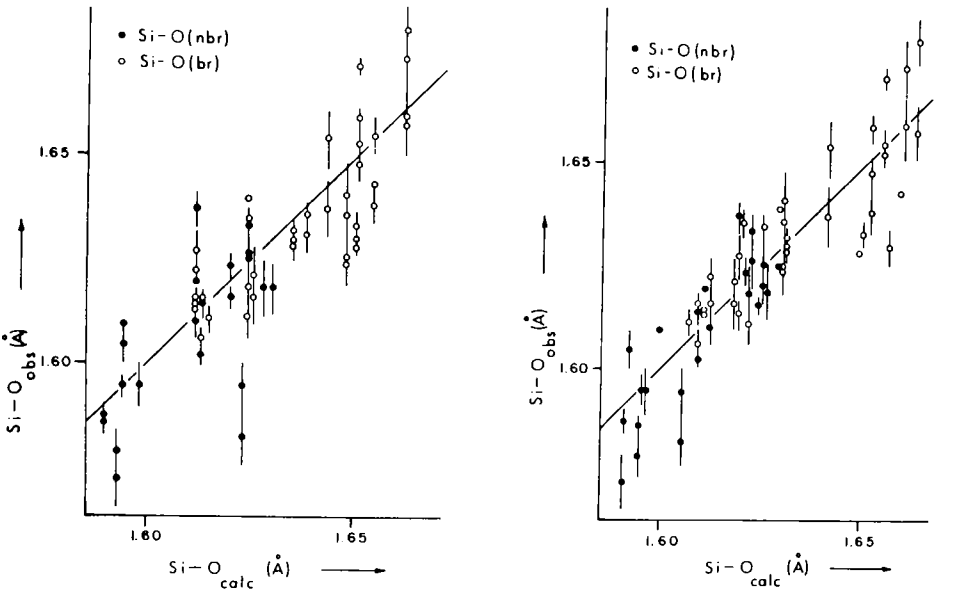

Figure 18. Comparison of observed Si-O bond lengths in C2/m amphiboles (with little or no tetrahedrally coordinated Al) with values calculated according to the methods of Baur (1970, 1971). The left-hand graph shows values calculated using predicted <Si-O> distances and the right-hand graph shows values calculated using observed <Si-O> distances.

as the formal valence of the cation divided by its coordination number. Deviations of up to 40% from this rule are encountered in mineral structures and these deviations are accompanied by antipathetic variations in cation-anion distances. Several schemes that relate bond lengths to bond strengths have been developed; of these, the schemes of Baur (1970, 1971) and Brown and Shannon (1973) are the most general.

Baur (1971) has derived an equation relating Si-O bond length to the total Pauling bond strength received by the oxygen anion. This equation may be used both to predict individual bond lengths absolutely from a forecast mean bond length, or it may be used in conjunction with the observed mean bond length to predict deviations from that mean. A graphical comparison of the observed and calculated bond lengths is given in Figure 18. The agreement with the observed values is much the same for each method, with a grand mean deviation of 0.01 Å. This indicates that the amphiboles obey the extended electrostatic valence rule (Baur, 1970) quite well, and the predictive nature of this scheme promises to be useful in structure modelling by distance least-squares methods (DLS; Meier and Villiger, 1969).

Brown and Shannon (1973) have derived curves relating bond length to bond valence. Although they are not immediately predictive as is the scheme of Baur (1970, 1971), they recognize weak bonding interactions that are either ignored or overemphasized in the previous method. Additional bond-strength curves, including some for the fluorine anion, have been presented by Brown and Wu (1976) and Brown (1978). Table 9 shows the results of a complete bond-valence analysis on eight clinoamphiboles containing little or no tetrahedral Al, where the results are compared with the bond-strength sums calculated from the formal Pauling scheme. It is apparent that the bond length variations observed in the refined structures tend to minimize the deviations from ideality in the bond-valence sums around the anions. This is of particular significance with respect to cations coordinating the O(4) anion, all of which show extremely short bonds to O(4). Thus in the clinoamphiboles, generally T(2)-O(4) $\leqslant$ 1.60 Å regardless of other variations in chemistry and/or structure. In order to maintain a mean bond length in accord with the size of its constituent cation (Si), there is a concomitant lengthening of the other bonds. As a result of this, T(2) is generally the more distorted of the two tetrahedra.

Brown and Shannon (1973) and Shannon (1975, 1976) have shown that mean bond lengths are significantly correlated with polyhedral distortion

$$\Delta \equiv \{ \sum_{i=1}^{n} [(l_i - l_m)/l_m]^2/n \} \times 10^4 ,$$

where l_i = bond length, l_m = mean bond length, n = coordination number. In the non-Al^{IV} amphiboles, <T(2)-O> varies between 1.622 and 1.636 Å, and Hawthorne (1976) showed that this variation correlates with Δ. Figure 14 shows the relation between mean bond length and Δ for C2/m amphibole tetrahedra containing little or no Al. Although the correlation is well developed, its significance is not clear as the factors affecting mean bond lengths in tetrahedral oxyanions are not clear. Calculation of the ideal relationship from the Si-O bond strength curve of Brown and Shannon (1973) suggests that any relationship between mean bond length and distortion should be obscured by random error in the observed values. Baur (1974) has shown that $\langle P\text{-}O \rangle^{IV}$ is significantly correlated with tetrahedral distortion. Conversely, Baur (1978) showed that <Si-O> in a large number (314) of silicate tetrahedra was not significantly

Table 9. Empirical Bond-Valence (v.u.) Tables for Selected Non-aluminous C2/m Amphiboles.

	M(1)	M(2)	M(3)	M(4)	A	T(1)	T(2)	Σ	Σ^P
Cummingtonite (21): r.m.s. deviations are 3.2% and 9.6% respectively									
O(1)	0.375	0.312	0.346 ↓x2			1.008		2.041	2.000
O(2)	0.325	0.347		0.333			0.992	1.997	2.000
O(3)	0.353 →x2		0.367					1.073	1.000
O(4)		0.386		0.480			1.035	1.901	1.667
O(5)				(0.045)		1.021	0.956	1.977	2.000
O(6)				0.107		0.984	0.946	2.037	2.333
O(7)						1.024 →x2		2.048	2.000
Σ	2.106	2.090	2.160	1.840		4.037	3.929		
Glaucophane (26): r.m.s. deviations are 4.2% and 9.2% respectively									
O(1)	0.355	0.384	0.343 ↓x2			1.011		2.093	2.167
O(2)	0.352	0.474		0.185			1.011	2.022	1.958
O(3)	0.338 →x2		0.364					1.040	1.000
O(4)		0.591		0.212			1.078	1.881	1.625
O(5)				0.097		1.016	0.961	2.074	2.125
O(6)				0.173		1.003	0.920	2.096	2.125
O(7)						1.030 →x2		2.060	2.000
Σ	2.090	2.898	2.100	1.334		4.060	3.970		
Tremolite (30): r.m.s. deviations are 4.4% and 11.3% respectively									
O(1)	0.356	0.309	0.351 ↓x2			1.055		2.071	2.000
O(2)	0.345	0.342		0.287			1.016	1.990	1.917
O(3)	0.342 →x2		0.361					1.064	1.000
O(4)		0.395		0.341			1.101	1.837	1.583
O(5)				0.133		0.974	0.922	2.029	2.250
O(6)				0.211		0.982	0.878	2.071	2.250
O(7)						1.016 →x2		2.032	2.000
Σ	2.086	2.092	2.146	1.944		4.027	3.917		
Fluor-tremolite (36): r.m.s. deviations are 6.8% and 11.3% respectively									
O(1)	0.359	0.301	0.362 ↓x2			1.021		2.043	2.000
O(2)	0.363	0.346		0.291			0.997	1.997	1.917
O(3)	0.282 →x2		0.311					0.818	1.000
O(4)		0.387		0.359			1.098	1.844	1.583
O(5)				0.138		0.984	0.934	2.056	2.250
O(6)				0.226		0.979	0.908	2.113	2.250
O(7)						1.043 →x2		2.086	2.000
Σ	1.980	2.068	2.012	2.028		4.027	3.937		

	M(1)	M(2)	M(3)	M(4)	A	T(1)	T(2)	Σ	Σ^P
Grunerite (22): r.m.s. deviations are 1.6% and 9.6% respectively									
O(1)	0.393	0.319	0.361 ↓x2			0.961		2.034	2.000
O(2)	0.322	0.346		0.350			0.971	1.989	2.000
O(3)	0.334 →x2		0.353					1.021	1.000
O(4)		0.395		0.516			1.049	1.960	1.667
O(5)				(0.033)		0.987	1.030	2.017	2.000
O(6)				0.086		0.979	0.959	2.024	2.333
O(7)						1.024 →x2		2.048	2.000
Σ	2.098	2.120	2.150	1.904		3.951	4.009		
Tirodite (28): r.m.s. deviations are 3.4% and 9.6% respectively									
O(1)	0.371	0.308	0.347 ↓x2			1.032		2.058	2.000
O(2)	0.330	0.346		0.327			1.011	2.014	2.000
O(3)	0.354 →x2		0.367					1.075	1.000
O(4)		0.402		0.419			1.078	1.899	1.667
O(5)				(0.050)		1.000	0.969	1.969	2.000
O(6)				0.134		0.971	0.917	2.022	2.333
O(7)						1.016 →x2		2.032	2.000
Σ	2.110	2.112	2.122	1.760		4.019	3.975		
Fluor-richterite (34): r.m.s. deviations are 6.8% and 12.9% respectively									
O(1)	0.359	0.278	0.351 ↓x2			1.113		2.101	2.000
O(2)	0.381	0.359		0.236			0.992	1.968	1.854
O(3)	0.276 →x2		0.300					0.852	1.000
O(4)		0.398		0.273			1.125	1.796	1.521
O(5)				0.103	0.087 ↓x2	0.992	0.910	2.092	2.271
O(6)				0.166	0.061 ↓x2	0.951	0.858	2.036	2.271
O(7)					0.182	0.964 →x2		2.110	2.200
Σ	2.032	2.070	2.004	1.556	0.956	4.020	3.885		
Ferro-glaucophane(69): r.m.s. deviations are 4.1% and 9.2% respectively									
O(1)	0.367	0.396	0.339 ↓x2			0.992		2.094	2.167
O(2)	0.361	0.476		0.193			0.977	1.947	1.958
O(3)	0.341 →x2		0.382					1.064	1.000
O(4)		0.605		0.220			1.072	1.897	1.625
O(5)				0.094		1.019	0.927	2.040	2.125
O(6)				0.175		0.997	0.917	2.089	2.125
O(7)						1.013 ←x2		2.026	2.000
Σ	2.138	2.954	2.120	1.364		4.021	3.893		

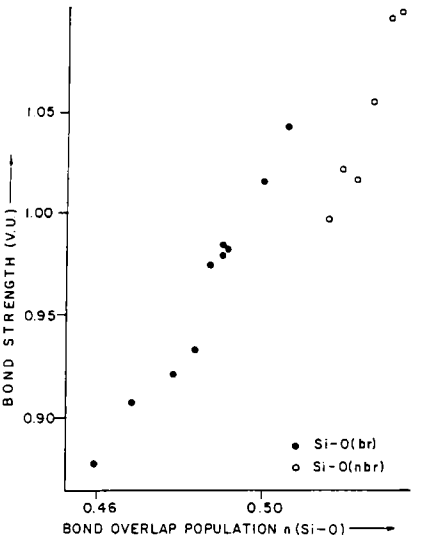

Figure 19. Variation in bond strength, calculated from the equations of Brown and Shannon (1973), with bond overlap population calculated from extended Hückel molecular orbital theory (Cameron and Gibbs, 1973).

correlated with tetrahedral distortion but was a linear function of the number of O(br) anions per tetrahedron and the mean coordination number of all O atoms within the tetrahedron. This would suggest that the correlation of Figure 14 is spurious, while the phosphate study (Baur, 1974) could be taken as supporting this correlation. As indicated earlier, an argument based on the covalent model for the Si-O bond has been put forward (Mitchell *et al.*, 1971) to rationalize the same trend. However, Figure 14 has considerable implications concerning the derivation of Al/Si site-occupancies (Hawthorne, 1976) and is perhaps best considered as an empirical correlation at present.

The arguments presented above indicate that the steric variations in the tetrahedral double chain of the C2/m amphiboles may be rationalized by both covalent and bond-strength models of the chemical bond. That both models may be used to rationalize the same features does not invalidate either of them; indeed, in this context they may not be mutually incompatible. With regard to the amphibole structure, Figure 19 shows the relationship between the bond-valence of the Si-O bonds in tremolite(30) and fluor-tremolite(36), calculated from the curves of Brown and Shannon (1973), and the corresponding bond overlap populations calculated using EHMO theory (Cameron and Gibbs, 1973). Both bond valence and bond overlap population are a measure of the strength of a bond, and the extremely well-developed correlation between them suggests a certain compatibility between the two models. This correlation is also in accord with the discussion of Brown and Shannon (1973) where they suggest that the covalence of an individual bond is a function of its bond length.

The $P2_1/m$ amphiboles

Papike *et al.* (1969) showed the "average structure" of $P2_1/m$ cummingtonite(27) to be very similar to tirodite(28) and hence this amphibole will behave as tirodite in all correlations involving average parameters (see previous section on C2/m amphiboles). With regard to individual bond lengths, Si-O(br) tend to be longer than Si-O(nbr), although there is some overlap of the values. Similarly, there is a *tendency* for the bond angles to order themselves in the sequence O(nbr)-Si-O(nbr) > O(br)-Si-O(nbr) > O(br)-Si-O(br), although some discrepancies do occur. Thus, the observed stereochemistry shows qualitative agreement with predictions made from d-p-π bonding theory (Cruickshank, 1961). Examination of the bond-valence distributions in the tetrahedral part of the structure (Table 10) shows that the tetrahedral bond-length variations may be adequately rationalized using a bond-valence model. As with other amphibole types, the O(4A) and O(4B) anions play a major role in controlling bond-length variations. In the A-chain T(2A)-O(4A) is very short and the T(2A)-O(br) bonds are long in order to compensate for this. This effect is less important in the B-chain, where the M(4) cation(s) contributes a much greater bond valence than in the A-chain. Accordingly, T(2B)-O(4B) > T(2A)-O(4A), and hence the T(2B) tetrahedron is far less distorted than the T(2A) tetrahedron.

The P2/a amphiboles

The joesmithite structure (Moore, 1969) shows reasonable correspondence with the predictions (cited above) of a covalent bonding model. Si-O(br) is usually larger than Si-O(nbr) although some overlap between the two populations does occur. Also, the O-Si-O angles tend to order in the sequence O(nbr)-Si-O(nbr) > O(br)-Si-O(nbr) > O(br)-Si-O(br), although some overlap does occur. A bond-valence table for joesmithite is shown in Table 11. As with all other amphibole types, the bond-valence requirements of the O(4)A and O(4)B anions are a major factor in the control of the tetrahedral bond-length variations. Superimposed upon this is the effect of Be occupying the T(1)B site, together with the occupancy of the A(2) site by a divalent cation.

The Pnma amphiboles

Let us first examine the tetrahedral chains using the covalent model for the Si-O bond. Although Si-O(br) bonds (grand mean value = 1.628 Å),

Table 10. Bond-Valence Table for Cummingtonite $P2_1/m$ (27)

	M(1)	M(2)	M(3)	M(4)	T(1A)	T(2A)	T(1B)	T(2B)	Σ
O(1A)	0.352	0.308	$0.337^{\downarrow x2}$		1.089				2.086
O(2A)	0.315	0.362		0.337		0.995			2.009
O(3A)	$0.346^{\rightarrow x2}$		0.372						1.064
O(4A)		0.395		0.386		1.134			1.915
O(5A)				(0.048)	1.041	0.961			2.002 (2.050)
O(6A)				0.168	1.016	0.869			2.053
O(7A)					$0.984^{\rightarrow x2}$				1.968
O(1B)	0.368	0.303	$0.351^{\downarrow x2}$				1.003		2.025
O(2B)	0.335	0.326		0.327				1.035	2.023
O(3B)	$0.348^{\rightarrow x2}$		0.347						1.043
O(4B)		0.396		0.454				1.032	1.882
O(5B)				(0.075)			0.969	0.966	1.935 (2.010)
O(6B)				0.127			0.964	0.966	2.057
O(7B)							$1.052^{\rightarrow x2}$		2.104
Σ	2.064	2.090	2.095	1.799^{VI} 1.874^{VII} 1.922^{VIII}	4.130	3.959	3.988	3.999	
Ideal Charge	2.00	2.00	2.00	2.00	4.00	4.00	4.00	4.00	

Table 11. Empirical Bond-Valence Table for Joesmithite(25)

	M(1)A	M(2)A	M(1)B	M(2)B	M(3)	M(4)A	M(4)B	A(2)	T(1)A	T(2)A	T(1)B	T(2)B	Σ
O(1)A	0.368	0.348			0.315				1.107				2.138
O(2)A	0.362	0.367				0.277				1.016			2.022
O(1)B			0.471	0.484	0.392						0.500		1.847
O(2)B			0.385	0.461			0.219					0.956	2.021
O(3)	0.352		0.393		0.386								1.131
O(4)A		0.399				0.351				1.075			1.825
O(5)A						0.166			0.977	0.896			2.039
O(6)A						0.184			0.977	0.922			2.083
O(4)B				0.551			0.328					1.128	2.007
O(5)B							0.226	$0.242^{\downarrow x2}$			0.458	0.924	1.850
O(6)B							0.214	$0.220^{\downarrow x2}$			0.453	0.944	1.831
O(7)								$0.235^{\downarrow x2}$	1.113		0.604		1.952
Σ*	2.164	2.228	2.498	2.992	2.186	1.956	1.974	$(1.394)^{VI}$	4.174	3.909	2.015	3.592	
Ideal Charge	2.15	2.26	2.68	3.00	2.00	2.00	2.00	2.00	4.00	4.00	2.00	4.00	

*all M-site bond strengths (v.u.) have a multiplicity of 2 in the cation sum.

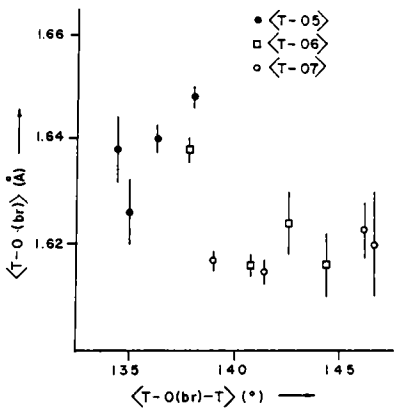

Figure 20. Variation in individual <T-O(br)> as a function of individual <T-O(br)-T> for the Pnma amphiboles with little or no tetrahedrally coordinated Al.

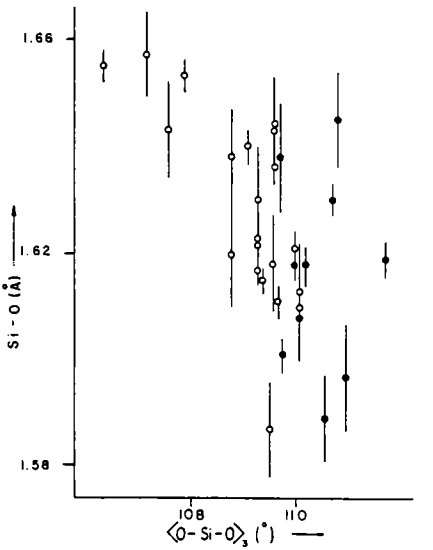

Figure 21. Variation in individual Si-O bond lengths as a function of the mean value of the three O-Si-O angles involved in that bond for the Pnma amphiboles with little or no tetrahedrally coordinated Al.

tend to be larger than Si-O(nbr) bonds (grand mean value = 1.618 Å), there is considerable overlap between the two different populations. There is some tendency for shorter Si-O(br) bonds to be associated with wider Si-O (br)-Si angles (Fig. 20), but as with the C2/m amphiboles, the correlation is not well developed. The O-Si-O angles do tend to decrease in the forecast order, but again there is considerable overlap among the different populations. Figure 21 shows the variation in Si-O with $\langle O\text{-}Si\text{-}O\rangle_3$ for the non-Al^{IV} orthoamphiboles. As with the C2/m clinoamphiboles, the correlation is significant, indicating that at least part of the variation in Si-O distances can be rationalized in terms of a covalent bonding model.

An examination of tetrahedral bond-length variations in terms of bond valence is shown in Table 12. The results are very similar to those for the other amphibole types, confirming the importance of anion bond-strength requirements in controlling bond lengths and emphasizing the role of the O4A and O4B anions in this regard.

The Pnmn amphiboles

Gibbs (1969) has discussed in detail the stereochemical variations in protoamphibole and has shown that these variations are consistent with

Table 12. Empirical Bond-Valence (v.u.) Table for Selected Pnma Amphiboles.

	M1	M2	M3	M4	T1A	T1B	T2A	T2B	Σ	Σ^P
Anthophyllite [23] : r.m.s. deviations are 4.4% and 8.0% respectively										
01A	0.365	0.304	0.354 $\overset{x2}{\downarrow}$		1.011				2.034	1.995
01B	0.373	0.317	0.350 $\overset{x2}{\downarrow}$			1.011			2.051	2.000
02A	0.324	0.360		0.318			1.008		2.010	2.061
02B	0.308	0.348		0.341				0.979	1.976	2.066
03A	0.348 $\overset{x2}{\rightarrow}$		0.371						1.067	1.000
03B	0.365 $\overset{x2}{\leftarrow}$		0.368						1.098	1.000
04A		0.415		0.422			1.057		1.894	1.728
04B		0.388		0.479				1.038	1.905	1.733
05A				0.185	0.954		0.917		2.056	2.390
05B				(0.070)		0.964		0.946	1.910	2.000
06A				(0.025)	1.030		1.003		2.033	1.990
06B				(0.070)		1.000		0.922	1.922	2.000
07A					1.019 $\overset{x2}{\rightleftarrows}$				2.038	1.990
07B						1.013 $\overset{x2}{\rightleftarrows}$			2.206	2.000
Σ	2.083	2.132	2.147	1.745	4.014	3.988	3.985	3.885		

	M1	M2	M3	M4	A	T1A	T1B	T2A	T2B	Σ	Σ^P
Gedrite [32] : r.m.s. deviations are 4.4% and 7.5% respectively											
01A	0.361	0.387	0.369 $\overset{x2}{\downarrow}$			0.927				2.044	2.041
01B	0.372	0.407	0.338 $\overset{x2}{\downarrow}$				0.893			2.010	2.034
02A	0.316	0.425		0.275				0.966		1.982	2.105
02B	0.298	0.393		0.356					0.934	1.981	2.073
03A	0.353 $\overset{x2}{\rightarrow}$		0.401							1.107	1.000
03B	0.366 $\overset{x2}{\leftarrow}$		0.396							1.128	1.000
04A		0.487		0.339				1.122		1.948	1.772
04B		0.458		0.438					0.979	1.875	1.740
05A				0.272				0.959		2.107	2.267
05B				0.181			0.910		0.882	2.015	2.228
06A				(0.020)	0.041 $\overset{x2}{\downarrow}$	0.966		1.041		2.048	1.992
06B				(0.073)	0.041 $\overset{x2}{\downarrow}$		0.920		0.951	1.912	1.953
07A					0.062	0.954 $\overset{x2}{\rightleftarrows}$				1.970	1.927
07B					0.076		0.946 $\overset{x2}{\rightleftarrows}$			1.968	1.913
Σ	2.066	2.557	2.211	1.861	0.304	3.723	3.669	4.088	3.746		

	M1	M2	M3	M4	T1A	T1B	T2A	T2B	Σ	Σ^P
Holmquistite [31] : r.m.s. deviations are 4.3% and 5.0% respectively										
01A	0.363	0.403	0.357 $\overset{x2}{\downarrow}$		0.959				2.082	2.155
01B	0.369	0.389	0.352 $\overset{x2}{\downarrow}$			0.979			2.089	2.166
02A	0.333	0.473		0.180			0.979		1.965	2.037
02B	0.333	0.476		0.193				0.941	1.943	2.037
03A	0.356 $\overset{x2}{\rightarrow}$		0.380						1.092	1.000
03B	0.356 $\overset{x2}{\leftarrow}$		0.387						1.099	1.000
04A		0.617		0.170			1.092		1.879	1.704
04B		0.598		0.211				1.069	1.878	1.704
05A				0.127	1.011		0.912		2.050	2.193
05B				(0.052)		1.024		0.959	1.983	2.000
06A				(0.024)	1.098		0.944		2.042	1.989
06B				(0.065)		1.032		0.946	1.978	2.000
07A					0.997 $\overset{x2}{\rightleftarrows}$				1.994	1.978
07B						1.005 $\overset{x2}{\rightleftarrows}$			2.010	2.000
Σ	2.110	2.956	2.185	0.881	4.065	4.040	3.927	3.915		

	M1	M2	M3	M4	A	T1A	T1B	T2A	T2B	Σ	Σ^P
Gedrite [33] : r.m.s. deviations are 4.5% and 7.6% respectively											
01A	0.382	0.401	0.345 $\overset{x2}{\downarrow}$			0.922				2.050	2.061
01B	0.384	0.413	0.336 $\overset{x2}{\downarrow}$				0.862			1.995	2.018
02A	0.301	0.423		0.257				1.024		2.005	2.122
02B	0.307	0.423		0.352					0.854	1.936	2.055
03A	0.347 $\overset{x2}{\rightarrow}$		0.378							1.072	1.000
03B	0.374 $\overset{x2}{\leftarrow}$		0.384							1.132	1.000
04A		0.500		0.345				1.046		1.891	1.789
04B		0.470		0.453					0.954	1.877	1.722
05A				0.262		0.905		0.915		2.082	2.260
05B				0.190			0.867		0.862	1.919	2.150
06A				(0.016)	0.064 $\overset{x2}{\downarrow}$	0.951		0.977		1.992	1.937
06B				(0.066)	0.064 $\overset{x2}{\downarrow}$		0.887		0.905	1.856	1.827
07A					0.097	0.932 $\overset{x2}{\rightleftarrows}$				1.961	1.875
07B					0.106		0.892 $\overset{x2}{\rightleftarrows}$			1.890	1.789
Σ	2.095	2.630	2.124	1.859	0.459	3.710	3.508	3.962	3.575		

the d-p-π bonding model of Cruickshank (1961). Si-O(br) bonds are longer than Si-O(nbr) bonds, and the angles of the T1 tetrahedron decrease in the sequence O(nbr)-Si-O(nbr) > O(br)-Si-O(nbr) > O(br)-Si-O(br). The angles of the T2 tetrahedron deviate somewhat from this sequence due to perturbing electrostatic and geometrical factors. Possibly as a result of this, the Si-O bond lengths do not show good correlation with the $\langle O\text{-}Si\text{-}O\rangle_3$ angles. The T2 tetrahedron shows a far greater range of O-Si-O angles than the T1 tetrahedron, presumably the result of relaxation due to cation-cation repulsion across the shared edge between the T2 and M4 polyhedra. As is the case for most non-Al^{IV} amphiboles, <T2-O> is larger than <T1-O>, a feature that Gibbs (1969) ascribes to the difference in mean anion coordination numbers for the two tetrahedra.

An examination of tetrahedral bond-length variations in terms of a bond-valence model is shown in Table 13. It is immediately apparent that the observed bond-length variations tend to minimize the deviations from ideality in the bond-valence sums around the anions. This is of particular importance with regard to the cations coordinating the O4 anion, all of which show extremely short bonds to O4. Thus, the other bonds involving these cations have to lengthen in order to maintain ideal bond-valence sums at the cations. M2-O1 lengthens and T1-O1 accordingly shortens to maintain the required bond-valence sum around O1. Similarly, M4-O6 lengthens and the T-O6 bond lengths presumably compensate for this. It is interesting to note that the expected decrease in T-O6 bond valence because of the presence of the M4-O6 bond occurs entirely in the T2-O6 bond where it compensates for the increase in the T2-O4 bond strength. The way in which T1 compensates for the increase in the T1-O1 bond valence is not apparent.

Ordering of tetrahedrally-coordinated Al

The Al content of the tetrahedral sites in the amphiboles varies between 0.0 and $\sim$3.0 atoms p.f.u., although it should be noted that amphiboles in which tetrahedral Al exceeds $\sim$2.0 atoms p.f.u. are rather uncommon (Appleyard, 1975; Bunch and Okrusch, 1973). The Al will be distributed over the crystallographically distinct tetrahedral sites in the double-chain element of the structure. Because the x-ray scattering factors of Al and Si are very similar, determination of site populations by direct refinement of single-crystal x-ray data is not a practical proposition.

Table 13. Empirical Bond-Valence Table (v.u.) for Protoamphibole [20]

	M 1	M 2	M 3	M 4	A	T 1	T 2	Σ
O 1	0.350	0.282	0.357 ↓x2			1.083		2.072
O 2	0.334	0.341		0.289			1.046	2.010
O 3	0.291 →x2		0.305					0.887
O 4		0.417		0.339			1.083	1.839
O 5					-	1.016	0.989	2.005
O 6				0.151	-	0.997	0.917	2.065
O 7					-	0.995 →x2		1.990
Σ	1.950	2.080	2.038	1.558[1]	-	4.091	4.035	

[1] ideal sum is 1.75 v.u. All M-site bond-valences have a multiplicity of 2 in the cation sum.

Consequently, tetrahedral site occupancies must be derived from mean bond-length considerations.

Papike *et al.* (1969) proposed that the Al be assigned to the T(1) and T(2) sites in the C2/m amphiboles by comparison of the mean bond lengths with those of tremolite(30). Using data for five clinoamphiboles and a series of pyroxenes, Robinson *et al.* (1973) developed separate equations for predicting Al occupancy of T(1) and T(2) in C-centered clinoamphiboles by plotting the <T(1)-O> and <T(2)-O> distances against the refined Al site occupancies

$$Al_{T(1)} = 760(77)\langle T(1)\text{-}O\rangle - 1230(4) \quad R = 0.98$$

$$Al_{T(2)} = 766(54)\langle T(2)\text{-}O\rangle - 1248(2) \quad R = 0.98 \ .$$

Bocchio *et al.* (1978) proposed the following equation relating total Al^{IV} per formula unit to the <T(1)-O> distance:

$$Al^{IV}(p.f.u.) = (\langle T(1)\text{-}O\rangle - 1.620) \times 37.7 \ .$$

Here, it is assumed that there is no Al^{IV} at the T(2) site (except in obvious examples such as subsilicic titanian magnesian hastingsite(58)). Hawthorne (1976) and Ungaretti (1980) suggest that variations in both individual and mean bond lengths occur as a result of other cation substitutions in the structure (Fig. 14); Ungaretti (1980) suggests that much of the variation in <T(2)-O> in aluminous amphiboles is due to these other factors rather than substitution of Al^{IV}. This may well be the case.

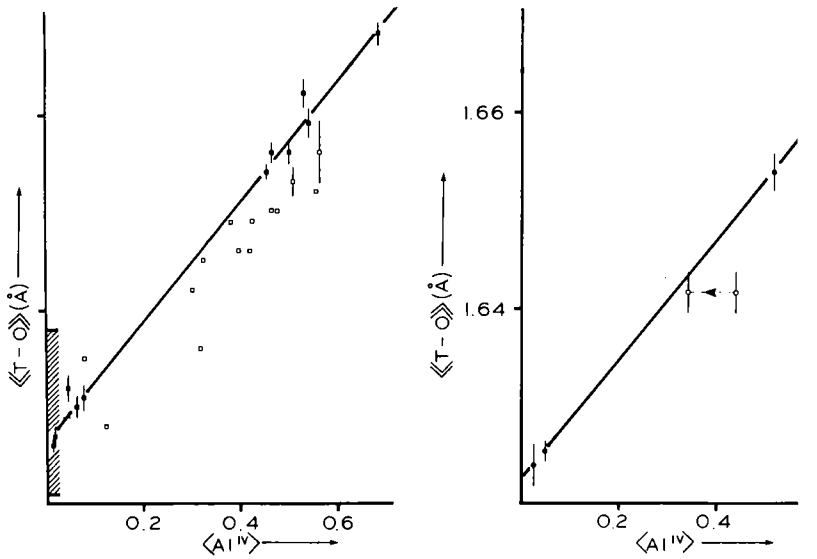

Figure 22. Variation in grand <T-O> distance with total Al^{IV} per T(1)+T(2) site in the C2/m amphiboles (left) and Pnma amphiboles (right). For the C2/m amphiboles, the hatched region shows the range of <<T-O>> values observed for amphiboles with $Al^{IV} \sim 0.0$ (see Fig. 14); the variation in this region correlates with polyhedron distortion. The solid line and solid squares are from Hawthorne and Grundy (1977a); the hollow squares are additional data, much of which is of lower accuracy. For the Pnma amphiboles, the full line is drawn parallel to the trend for the C2/m amphiboles, through the three data points shown; the point for gedrite [32] was modified as indicated by Hawthorne (1982).

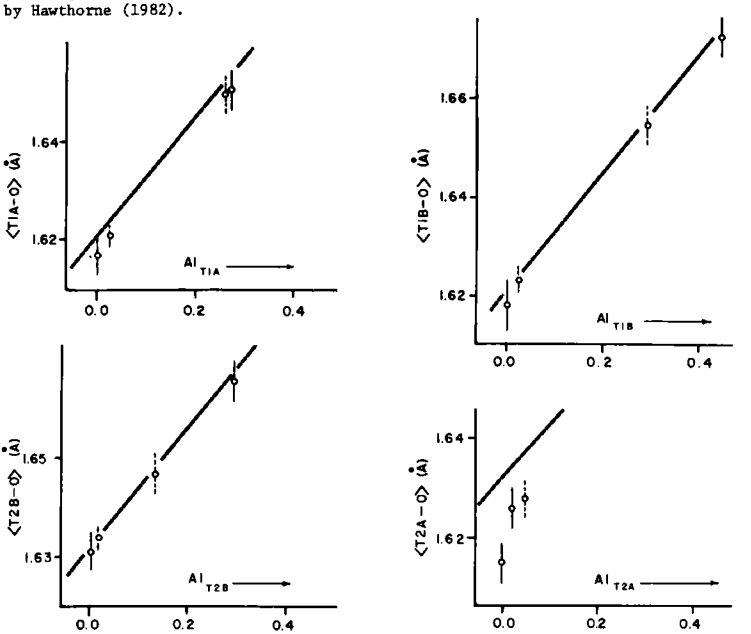

Figure 23. Variation in individual <T-O> distances with constituent Al site occupancies in the Pnma amphiboles; the broken lines are the individual relationships for the T(1) and T(2) sites in the C2/m amphiboles (Hawthorne and Grundy, 1977a).

Hawthorne and Grundy (1977a) showed that the grand <T-O> distance in a series of 10 clinoamphiboles was linearly related to the total amount of tetrahedral Al per T(1)+T(2) site (i.e., Al^{IV} p.f.u./4.0) by the equation

$$Al_{TET} = 16.252\langle T\text{-}O\rangle - 26.434 \qquad R = 0.997 \ .$$

With the assumption that the slopes of the individual relationships for the T(1) and T(2) tetrahedra were the same, the following two equations relating <T(1)-O> and <T(2)-O> to the Al occupancies were derived:

$$Al_{T(1)} = 8.126\langle T(1)\text{-}O\rangle - 13.170 \ ; \quad Al_{T(2)} = 8.126\langle T(2)\text{-}O\rangle - 13.262 \ .$$

As indicated above, the second equation may not be very reliable at small Al occupancies, but it should indicate where significant Al^{IV} occupancy of T(2) does occur. Figure 22 shows a comparison between the total Al^{IV} p.f.u. and some of the equations given above. No matter which curve is considered, some scatter is encountered; this is presumably the perturbing effect of non-tetrahedrally coordinated cations (or unrepresentative chemical analyses).

The primitive clinoamphiboles and the Pnmn orthoamphiboles contain little or no tetrahedral Al and thus the question of tetrahedral Al ordering does not arise.

The natural orthorhombic (Pnma) amphiboles may contain up to ∿2.25 tetrahedral Al p.f.u., and this is distributed over the four unique tetrahedral sites in the structure. Figure 22 shows the variation in grand <T-O> distance with the amount of tetrahedral Al per unique tetrahedral site in the structure; the trend is distinctly nonlinear. However, comparison with the analogous relationship for the monoclinic amphiboles (Hawthorne and Grundy, 1977a) shows three of the four data points to be collinear, defining a trend parallel to that of the monoclinic amphiboles but displaced downwards by 0.004 Å. The deviant value for gedrite[32] is probably wrong; an estimate of 1.36 Al^{IV} p.f.u. (Hawthorne, 1982) agrees with the trend of the other data. Assignment of Al to the four individual sites is taken from Hawthorne (1982); the resulting bond length *vs.* site-occupancy curves are shown in Figure 23; the curves shown are the C2/m amphibole curves shifted down by 0.004 Å, as there is insufficient data available to warrant the development of independent Pnma predictive curves.

THE OCTAHEDRAL STRIP

There are at least three unique sites with pseudo-octahedral coordination in each of the different amphibole structure types. The wide difference in ligancy ensures considerable and complex cation ordering at these sites, a detailed knowledge of which is essential to understand amphibole crystal chemistry, phase relations and physical properties. Thus, considerable effort has been expended in the characterization of cation ordering at these sites. The steric details of this part of the structure are of primary importance both in the interpretation of ordering patterns and frequently in the actual derivation of complete site-ordering patterns in the more complex chemical variants.

The C2/m amphiboles

There are three unique sites with pseudo-octahedral coordination in this structure type, the M(1), M(2) and M(3) sites. The M(1) site has point symmetry 2 and is coordinated by four oxygens and two O(3) anions that may be OH^-, F^-, Cl^- or O^{2-}, with the O(3) anions arranged in a *cis* configuration. The M(1) octahedron shares five edges with the surrounding octahedra and one edge with the M(4) polyhedron. The M(2) site has point symmetry 2 and is coordinated by six oxygens; the M(2) octahedron shares three edges with neighboring octahedra and one edge with each of the two adjacent M(4) polyhedra. The M(3) site has point symmetry 2/m and is coordinated by four oxygens and two O(3) anions, the latter being arranged in a *trans* configuration. The M(3) octahedron shares six edges with the adjacent octahedra.

The variation in grand mean bond length as a function of grand mean ionic radius for the M(1), M(2) and M(3) sites is shown in Figure 24. A linear relationship is reasonably well developed, being described by the equation

$$\langle M\text{-}O \rangle = 1.527 + 0.764(17)\langle r \rangle \ .$$

Some of the scatter is due to chemical variation at the O(3) anion position, as the data for the fluor-amphiboles indicates [$r(F^{III}) = 1.30$ Å; $r(OH^{III}) = 1.34$ Å]. However, some of the scatter seems to be due to bad or unrepresentative chemical analyses (Fig. 24); hence, this relationship should be a useful check on the compositional data for

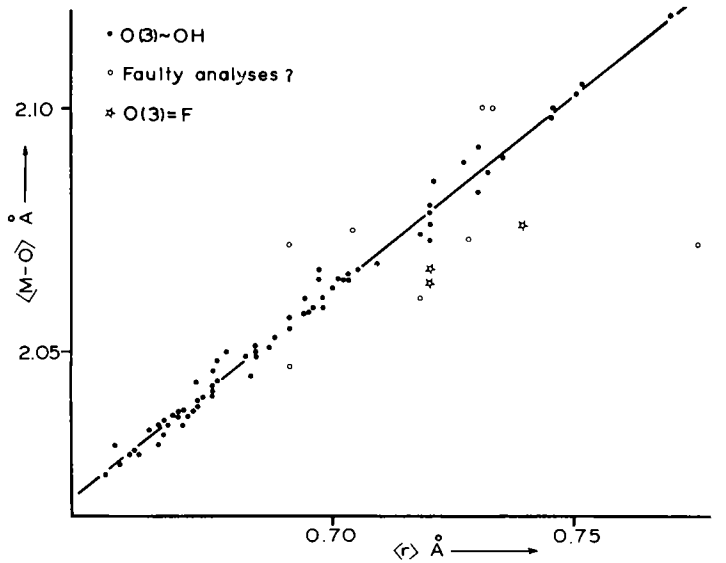

Figure 24. Variation in grand <M-O> with mean ionic radius of the constituent cations for the C2/m amphiboles. The regression line was calculated for hydroxyamphiboles only, using data where the e.s.d. of the individual bond lengths <0.01 Å; data deviating significantly from the line were omitted from the regression analysis as their chemical composition is suspect.

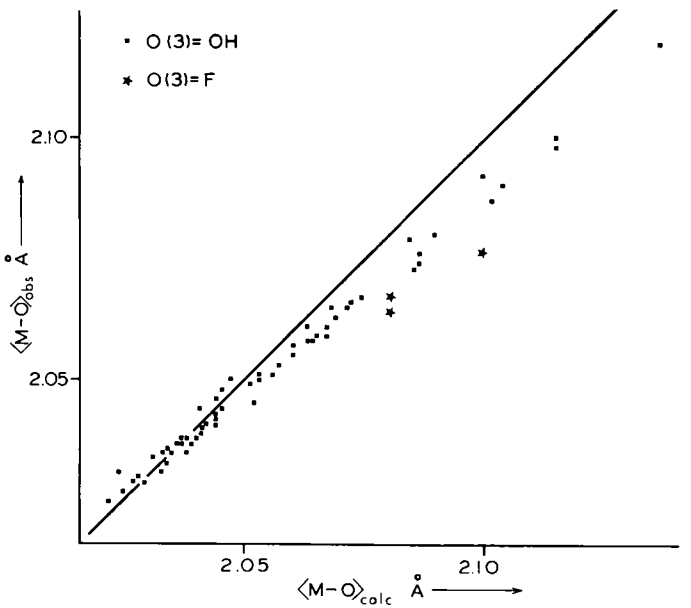

Figure 25. Comparison of the grand <M-O> with the corresponding sum of the constituent cation and anion radii for the C2/m amphiboles.

the crystal. Inclusion of the ionic radius of the O(3) anion into the above equation gives the relation

$$\langle M\text{-}O\rangle = 1.017 + 0.817(13)\langle r\rangle + 0.354(37)r_{O(3)} \ .$$

The grand <M-O> bond length can also be calculated by summing the relevant cation and anion radii; a comparison of the values obtained with the observed data is given in Figure 25. There is a systematic deviation from the ideal hard sphere model; the calculated values are less than the ideal values at larger ionic radii, but the reason for this is not clear. The fluor-amphiboles also deviate from the general trend of Figure 25; the reason for this is also not apparent.

Where mean bond length-ionic radius relationships are well characterized, they are extremely useful in deriving complete site occupancies when the results of site-occupancy refinement do not give a unique solution. As the ligancy and local environment of the three octahedrally-coordinated M sites differ considerably among themselves, it is best to examine such relationships separately for each site. This was originally done by Hawthorne for a series of 19 C2/m amphiboles and has been extended here for the much larger data set now available. Figure 26 shows the mean bond length-ionic radius relationships for approximately 70 amphibole structures; the less precise structures from Table A1 were not used. The relationship for the M(2) site is well developed and is similar to those developed in previous studies. For the M(1) and M(3) sites, there is considerable scatter in these relationships; much of this stems from the variable occupancy of the O(3) site by OH^-, F^-, Cl^- and/or O^{2-}. Inclusion of the mean ionic radius of the O(3) anion as an independent variable in a stepwise linear regression analysis indicates that this factor contributes significantly to variations in the mean bond lengths at the M(1) and M(3) sites; the results of this analysis are summarized in Table 14, and a comparison of the observed and calculated mean bond lengths is given in Figure 26. As is apparent in Figure 26, significant scatter still exists, particularly in the relationship for the M(3) site. Coordination polyhedron distortion does not significantly contribute to mean bond-length variations in amphiboles (Hawthorne, 1978a). However, the results of Ungaretti *et al.* (1981) suggest some kind of inductive effect of other cations on the <M-O> bond lengths. Figure 27 suggests that this

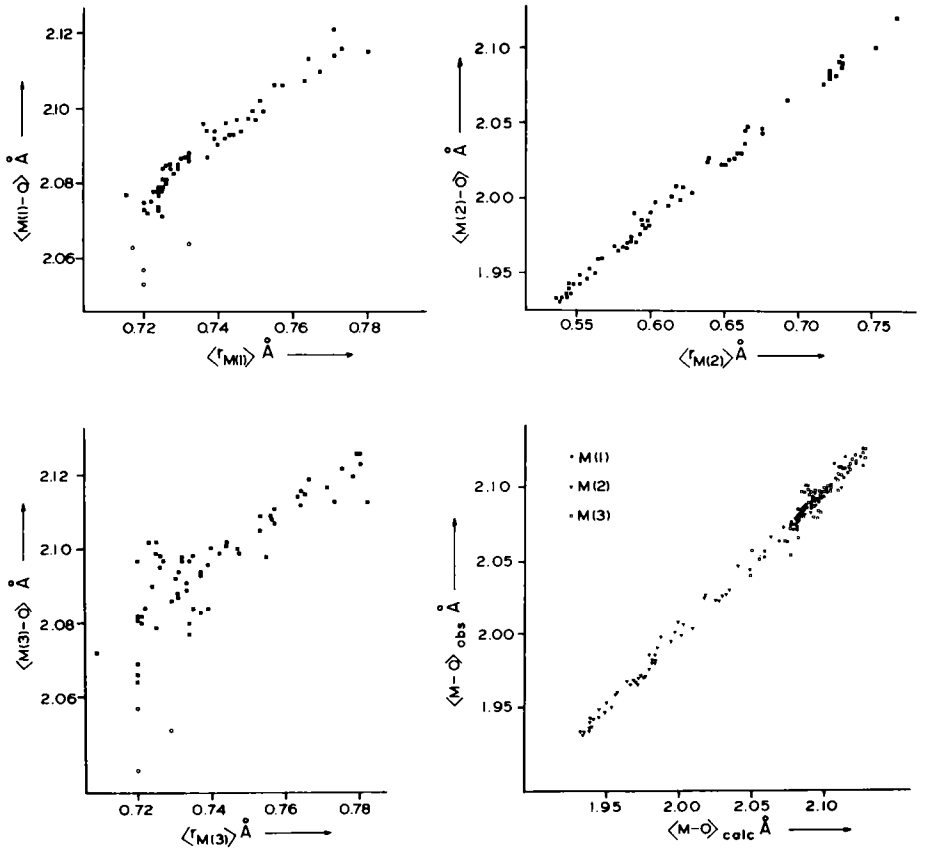

Figure 26 (above). Variation in individual <M-O> with mean ionic radius of the constituent cations for the C2/m amphiboles. Modified after Hawthorne (1978a). Also shown is a comparison of the observed mean bond lengths at the octahedrally coordinated M sites with the corresponding values calculated from the regression equations of Table 14.

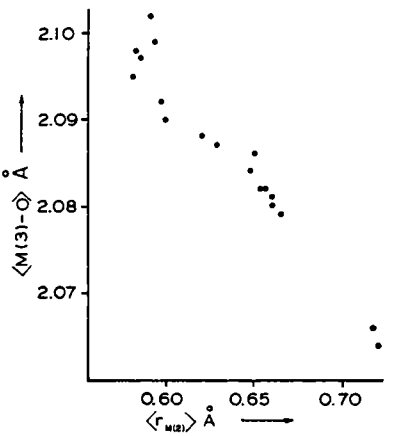

Figure 27. Variation in <M(3)-O> as a function of the mean ionic radius of the constituent M(2) cations for values of $r_{M(3)}$ in the range 0.72-0.73 Å.

Table 14. Regression Analysis Results for C2/m Amphiboles

Dependent variable	Independent variable	c	m	R	σ	|t|[1]
<M(1)-O>	$r_{M(1)}$	0.877	0.82(3)	0.961	0.004	26.39
	$r_{O(3)}$		0.46(5)			8.50
<M(2)-O>	$r_{M(2)}$	1.488	0.827(8)	0.997	0.004	97.08
<M(3)-O>	$r_{M(3)}$	0.387	0.73(4)	0.925	0.007	16.34
	$r_{O(3)}$		0.87(9)			9.08
<M-O>	<r>	1.527	0.76(2)	0.983	0.004	43.68
<M-O>	<r>	1.017	0.82(1)	0.993	0.002	64.40
	$r_{O(3)}$		0.35(4)			9.46
<M(3)-O>	$r_{M(3)}$	0.773	0.69(4)	0.949	0.006	18.08
	$r_{O(3)}$		0.64(9)			7.06
	$r_{M(2)}$		-0.07(1)			5.43

[1] |t|-values are calculated for the null hypothesis H_o: m = 0.0

is the case, <M(3)-O> being significantly affected by the mean size of the constituent M(2) cation. Multiple regression analysis (Table 14) shows <M(3)-O> to be significantly affected by $\langle r \rangle_{M(2)}$. However, <M(1)-O> and <M(2)-O> are dependent only on their constituent cation and anion radii.

A somewhat different approach has been taken by Litvin *et al.* (1972a) and Ungaretti *et al.* (1978), who proposed ideal mean bond lengths for complete occupancy of an octahedral site by a specific cation. These values (Table 15) were subsequently used together with other structure

Table 15. Ideal <M-O> Distances (Å) for Complete Occupancy of M(1,2,3) Sites by a Single Cation

	1	2			3		
	M(1,2,3)	M(1)	M(2)	M(3)	M(1)	M(2)	M(3)
Al	1.90	-	1.929	-	1.924	1.931	1.947
Fe^{3+}	2.03	-	2.031	-	2.014	2.022	2.027
Ti^{4+}	-	-	1.960	-	1.982	1.989	1.998
Ti^{3+}	-	-	-	-	2.035	2.043	2.045
Mg	2.07	2.078	2.078	2.083	2.075	2.084	2.082
Fe^{2+}	2.14	2.119	2.119	2.125	2.124	2.134	2.126
Mn^{2+}	-	-	-	-	2.165	2.175	2.163
Li	-	-	-	-	2.109	2.117	2.112

[1] Litvin (1973); [2] Ungaretti et al. (1981); [3] calculated from the curves of Table 14 with O(3) = OH.

refinement results for cation occupancy assignment in amphiboles. Ungaretti *et al.* (1981) have developed a scheme for deriving both cation occupancies *and* cell contents from structure refinement using charge balance and the mean bond length-cation occupancy relationship at the M(2) site:

(i) Al^{IV} is estimated from <T(1)-O>;

(ii) total charge at A+M(4) is estimated from site-occupancy refinements, Na (+K when available from chemical analysis) at the A-site and Ca+Na+Fe^{2+} at M(4) (Fe^{2+} being included only when indicated by difference Fourier maps);

(iii) total charge of C-type cations = total charge of $(Si,Al)_8O_{22}(OH)_2$ minus total charge at A+M(4);

(iv) the M(2) site populations are calculated from the refined electron density at M(2) and the observed mean bond length using the mean bond lengths of Table 15. If the Ti content is available from chemical analysis, it can be incorporated into the procedure at this stage; otherwise, M(2) is assumed to be occupied only by Al, Mg and Fe^{3+} at this stage;

(v) the residual charge (Q) to be neutralized by the M(1) and M(3) cations can now be calculated; in general, this will be equal to 6. If $Q < 6$, M(1)+M(3) is assumed to be occupied by divalent cations only and sufficient Fe^{2+} is introduced into M(2) to make $Q = 6$ and satisfy the corresponding electron density and distance equations. If $Q > 6$, trivalent cations are introduced into M(1) and/or M(3), substituting Fe^{3+} for Fe^{2+} and estimating the amount of Mg, Fe^{2+} and Fe^{3+} from mean bond lengths;

(vi) if the total charge imbalance ≤ 0.07, Al^{IV} is modified to obtain a neutral chemical formula. If the total charge imbalance >0.07, the A and M(4) compositions are adjusted by considering the occupancy of A by K, and then the occupancy of M(4) by Ca, Na and Fe^{2+}.

Ungaretti *et al.* (1981) get excellent agreement between amphibole compositions determined in this fashion and by electron microprobe analysis. Compositions determined by x-ray methods are closer to the wavelength-dispersive spectrometer analyses than are the energy-dispersive

spectrometer analyses. It will be interesting to see how well this method works for a wide variety of amphiboles.

Amphiboles exhibit considerable deviations from Pauling's second rule (Pauling, 1960) for a formal bond-valence model, and thus bond-valence requirements should have an extremely strong effect on bond-length variations in amphiboles. Table 9 shows empirical bond-valence tables for C2/m amphiboles, in which it can be seen that the bond-length variations observed tend to minimize the deviations from ideality in the bond-valence sums around the anions. As we saw when examining the tetrahedral double chain, this is particularly significant with respect to cations coordinating the O(4) anion, all of which show extremely short bonds to O(4). In order to maintain mean bond lengths in accord with the size of the constituent cations, there is a concomitant lengthening of the other bonds to these cations, resulting in extremely distorted cation sites. This is evident from Table 16 which lists some distortional parameters for the cation polyhedra in selected amphibole structures. Also in accord with this argument is the correlation between the dispersion of the M(2)-O bond lengths and the mean charge of the M(4) cations (Fig. 28).

Table 16. Polyhedron Distortion Parameters in Selected C2/m Amphiboles

	T(1)		T(2)		M(1)		M(2)		M(3)	
	Δ	σ^2	Δ	σ^2	Δ	σ^2	Δ	σ^2	Δ	σ^2
Grunerite(22)	0.29	0.8	0.78	15.8	2.25	36.0	2.79	43.2	0.11	60.9
Glaucophane(26)	0.05	0.6	1.88	17.4	0.21	69.5	15.77	35.0	0.34	85.0
Tremolite(30)	0.54	5.0	4.14	19.9	0.15	35.6	5.52	22.9	0.09	43.6
Fluor-richterite(34)	2.06	14.3	5.60	22.4	0.62	43.1	12.54	33.1	0.97	43.3
Fluor-tremolite(36)	0.38	6.2	3.45	19.3	0.01	46.9	5.76	21.9	1.03	47.9
Potassian pargasite(38)	0.59	6.6	1.42	19.1	1.25	50.5	5.98	24.3	0.01	75.7
Ferro-tschermakite(54)	0.63	4.8	0.61	17.0	4.00	57.3	5.00	19.6	0.33	106.0
Potassian oxy-kaersutite(55)	0.29	5.8	1.16	18.9	14.35	47.9	7.06	31.2	0.05	56.8
Potassian ferri-taramite(59)	0.25	3.6	1.53	13.8	2.45	45.8	8.53	28.7	0.08	82.3
Potassium-arfvedsonite(67)	1.05	11.4	5.54	21.4	0.51	44.6	17.27	44.5	0.60	67.6
Fluor-riebeckite(68)	0.02	4.4	2.02	12.7	0.29	47.9	15.48	39.1	0.26	68.7
Ferro-glaucophane(69)	0.06	0.7	2.04	14.8	0.39	70.5	14.36	31.9	1.14	97.4

$\Delta = \{ \sum_{i=1}^{n} [(\ell_i - \ell_m)/\ell_m]^2/n \} \times 10^4$, where ℓ_i = individual bond length, ℓ_m = mean bond length, n = number of bond in coordination polyhedron; $\sigma^2 = \sum_{i=1}^{n} (\theta_i - \theta_m)^2/(n-1)$, where θ_i = individual bond angle, θ_m = ideal bond angl

n = number of bond angles in coordination polyhedron.

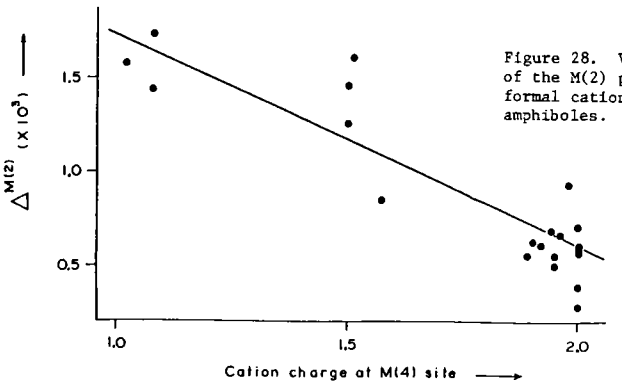

Figure 28. Variation in polyhedral distortion Δ of the M(2) polyhedron as a function of the mean formal cation charge at the M(4) site in the C2/m amphiboles. After Hawthorne (1976).

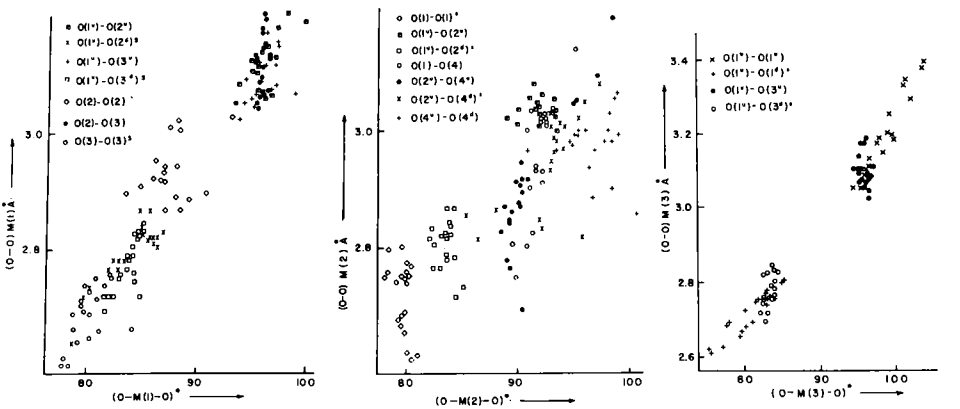

Figure 29. Variation in octahedral edge lengths with the corresponding angles subtended at the cation for the octahedrally coordinated M sites in a variety of C2/m amphiboles.

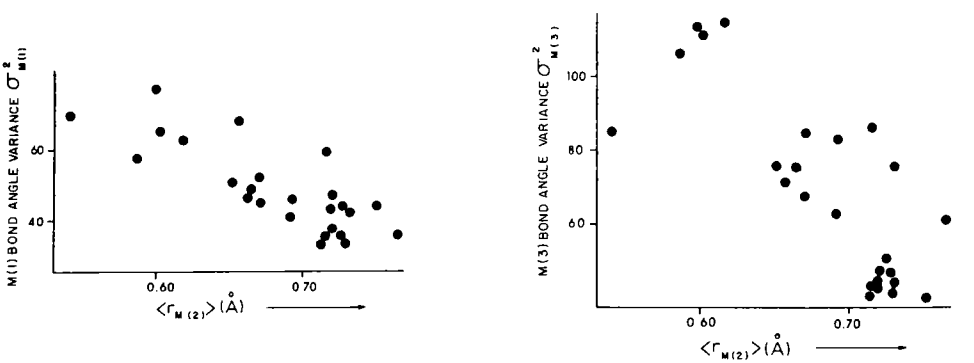

Figure 30. Variation in octahedral angle variance, σ^2, for M(1) and M(3) with the mean ionic radius of the constituent M(2) cations for the C2/m amphiboles. After Hawthorne (1978a).

It has been suggested (Pauling, 1960) that cation-cation repulsive interactions are much stronger than anion-anion repulsive interactions and that as a result, edges shared between polyhedra are shorter and subtend smaller angles at the cation than unshared edges. In the octahedral strip of the clinoamphibole structure, the M(1), M(2) and M(3) octahedra share six, five and six edges, respectively, with adjacent cation polyhedra, suggesting that cation-cation repulsion should play an important role in bond angle distortion. As indicated in Figure 29, this appears to be the case. For the M(1) and M(3) octahedra, the separation of the edges and angles into two populations corresponding to shared and unshared elements together with the marked linear correlations exhibited *suggests* that cation-cation repulsion is of prime importance. For the M(2) octahedron, although there is a tendency for the data to separate out into two populations corresponding to shared and unshared elements, considerable overlap occurs and the linear correlation is far less marked than for the M(1) and M(3) octahedra.

There is considerable variation in the sizes of the octahedra in the clinoamphiboles with variation in cation occupancy. As polyhedral elements are shared between octahedra of disparate size, shared elements must adjust accordingly. Prominent in this respect is the mean size of the cations occupying the M(2) site, and the octahedral angle variance of both the M(1) and M(3) sites is negatively correlated with mean ionic radius of the constituent M(2) cations (Fig. 30), a feature that could have a significant effect on site occupancies at the M(1) and M(3) sites.

The $P2_1/m$ amphiboles

There are three unique sites with pseudo-octahedral coordination in this structure type, the M(1), M(2) and M(3) sites. Both the octahedra and the way they link together are similar to the corresponding octahedra in the C2/m amphiboles. However, the point symmetry of the M(1), M(2) and M(3) sites is 1, 1 and m, respectively. Our understanding of this structure type suggests that it should be of magnesian cummingtonite compositions. In agreement with this, nearly all $P2_1/m$ amphiboles reported are restricted to this compositional range (Ross *et al.*, 1968; Kisch, 1969; Rice *et al.*, 1974; Yakovleva *et al.*, 1978). This being the case, the octahedral sites will show virtually complete occupancy by Mg, and the

only octahedral bond-length variations expected in this structure type will be due to inductive effects of the M(4) cation(s). Thus, the octahedral strip element of $P2_1/m$ tirodite(27) should be fairly representative of all compositional variations in this structure type.

In $P2_1/m$ tirodite(27), the octahedral sites are completely occupied by Mg, and the mean bond lengths are not significantly different from those in tremolite(30). The bonding radii of Mg and Fe are much smaller than that of Ca, and thus the interaction between the M(4) cation(s) and the chain-bridging anions will be much weaker in Fe-Mg-Mn amphiboles. In order to satisfy the bond-valence requirements of the M(4) cation(s), the bonding to the non-bridging anions O(2) and O(4) will have to be stronger in $P2_1/m$ tirodite(27) than in tremolite(30). In order to accommodate this, the M(1)-O(2) bonds are longer in tirodite. Examination of the differences between the M-O(A) and M-O(B) bonds (Table 10) shows that the only significant differences occur for the O(2A) and O(2B) anions. This reinforces the above conclusion that the inductive effect of the M(4) cation affects the octahedral strip through the O(2A) and O(2B) anions.

All edges shared between adjacent octahedra are shorter than all unshared elements, indicating the influence of cation-cation repulsion. In addition, this amphibole agrees with the correlations developed for the C2/m amphiboles (Hawthorne, 1978a), indicating that packing considerations and bond-strength requirements significantly affect inter-bond angles and the amount of structural relaxation due to cation-cation repulsion.

The P2/a amphiboles

There are five unique sites with pseudo-octahedral coordination in this structure type, the M(1)A, M(1)B, M(2)A, M(2)B, and M(3) sites. The M(1)A and M(1)B sites have point symmetry 2 and are coordinated by four oxygens and two O(3) anions that are OH in the only representative of this structure type yet found (Moore, 1968a,b, 1969); the O(3) anions are arranged in a *cis* configuration. The M(2)A and M(2)B sites have point symmetry 2 and are coordinated by six oxygens. The M(3) site has point symmetry 2 and is coordinated by four oxygens and two O(3) anions arranged in a *trans* configuration. The edge-sharing characteristics of these octahedra are similar to those found in the C2/m amphibole structure.

Joesmithite (Moore, 1969) is the only amphibole of this structure type that is known. Polyhedral distortions, aside from effects of local electroneutrality, result largely from cation-cation repulsion effects. Shared edges between octahedra are the shortest distances for each of the polyhedra and subtend the smallest angles at the central cation.

The Pnma amphiboles

There are four unique sites with pseudo-octahedral coordination in this structure type, the M1, M2, M3 and M4 sites. However, the M4 site will not be regarded as part of the octahedral strip and discussion of it will be deferred until later. The M1 site has point symmetry 1 and is coordinated by four oxygens and two O3 anions that may be OH^-, F^-, or O^{2-}, with the O3 anions arranged in a *cis* configuration. The M1 octahedron shares five edges with the surrounding strip octahedra and one edge with the M4 octahedron. The M2 site has point symmetry 1 and is coordinated by six oxygens; the M2 octahedron shares three edges with neighboring strip octahedra and two edges with the adjacent M4 octahedra. The M3 site has point symmetry m and is coordinated by four oxygens and two O3 anions, the latter being arranged in a *trans* configuration. The M3 octahedron shares six edges with the adjacent strip octahedra. For the octahedral strip derived from the cations of the asymmetric unit, anions with $x > 0$ are B-type anions while anions with $x < 0$ are A-type anions (note correspondence with u-d nomenclature of the monoclinic amphiboles).

The variation in grand mean bond length as a function of grand mean ionic radius for the M1, M2 and M3 sites is shown in Figure 31. The trend is linear and is similar to the corresponding trend in the C2/m amphiboles, the regression curve from which is shown in this figure. Analogous relationships for the individual sites are shown in Figure 32. Consider first the relationship for the M2 site. The minimum value for holmquistite[31], the maximum value for gedrite[33] and anthophyllite[23] are collinear. The values for gedrite[32] assigned from the site occupancy of Papike and Ross (1970) straddle this trend. For the M1 and M3 sites, the values for anthophyllite are well defined and as a starting approximation, the curves were assumed to pass through the values for anthophyllite with a slope of 1.0. The values for each site consistent

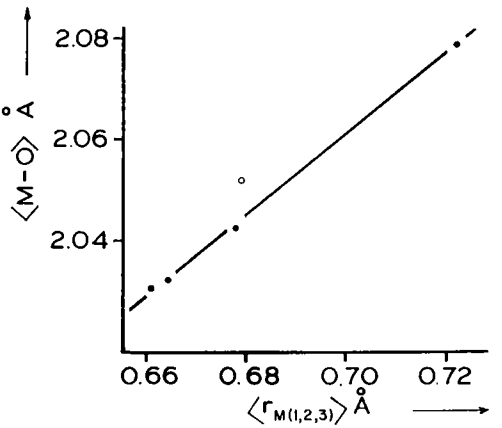

Figure 31 (above). Variation in grand mean M-O bond lengths with mean ionic radius of the constituent cations for the Pnma amphiboles; gedrite [32] was omitted from the regression analysis. See Hawthorne (1982).

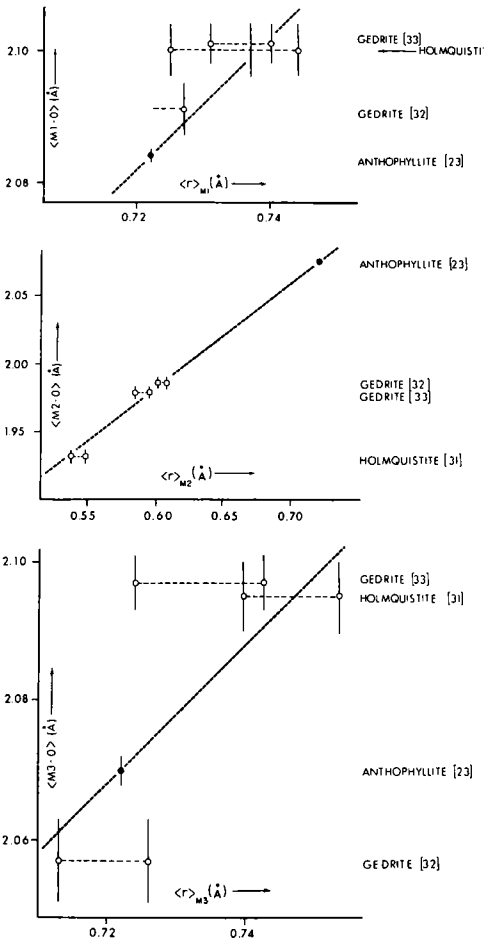

Figure 32 (right). Variation in individual <M-O> with mean ionic radius of the constituent cations for the Pnma amphiboles. The possible ranges of constituent mean ionic radius at each site consonant with the diffraction and chemical analysis results are shown. The relationship shown in each graph was derived to obtain the best fit for all three sites, together with the constraint that these relationships should be fairly similar to the analogous ones for the C2/m amphiboles.

with the overall stoichiometry of each amphibole are marked on each of the graphs (Fig. 32). The paucity of the data does not warrant linear regression analysis at the present time.

The Pnma orthoamphiboles show considerable deviations from Pauling's second rule (Pauling, 1960) for a formal bond-strength model, and thus bond-strenth requirements should have an extremely strong effect on bond-length variations in orthoamphiboles. Table 12 shows bond-valence tables together with the formal bond-strength sums around the anions. Inspection of this table shows that the bond-length variations observed tend to minimize the deviations from ideality in the bond-valence sums around the anions. As with the C2/m amphiboles, this accounts for the cations showing

Table 17. Comparison of M-O Bond Lengths in Four Amphiboles Where the Octahedral Sites are Occupied by Magnesium

	Protoamphibole [20]	Fluor-tremolite (36)	Tremolite (30)	Fluor-richterite (34)
M(1)-O(1)	2.072(4)	2.059(3)	2.064(2)	2.060(6)
M(1)-O(2)	2.094(4)	2.054(4)	2.078(2)	2.031(6)
M(1)-O(3)	2.043(4)	2.057(3)	2.083(2)	2.069(5)
<M(1)-O,F>	2.070	2.057	2.075	2.053
M(2)-O(1)	2.179(4)	2.146(4)	2.133(2)	2.186(6)
M(2)-O(2)	2.084(4)	2.077(3)	2.083(2)	2.059(6)
M(2)-O(4)	1.986(4)	2.024(4)	2.014(2)	2.011(6)
<M(2)-O>	2.084	2.082	2.077	2.085
M(3)-O(1)	2.062(4)	2.055(3)	2.070(2)	2.071(5)
M(3)-O(3)	2.021(4)	2.011(4)	2.057(3)	2.028(6)
<M(3)-O,F>	2.048	2.040	2.066	2.057

short bonds to the O4A and O4B anions. In addition, when M4 is occupied by a monovalent cation (Li^+), the M2 octahedron is much more distorted than when M4 is occupied by a divalent cation. Examination of the orthorhombic amphiboles using the scheme of Baur (1970, 1971) parallels the results given for the C2/m amphiboles. Bond lengths calculated for the M1 and M3 octahedra are generally larger than the observed values, whereas the deviation between the observed and calculated bond lengths for the M2 octahedron is correlated with the mean ionic radius of the constituent M2 cation.

The distortion of the three octahedra in terms of shared and unshared elements is examined in Figure 33. The results are similar to those of the C2/m amphiboles. For the M1 and M3 octahedra, the data separate into two populations corresponding to shared and unshared elements. For the M2 octahedron, there is some overlap between the two populations and the linear correlation is far less marked than for the M1 and M3 octahedra. The arguments put forward by Hawthorne (1978a) for the C2/m amphiboles should be directly applicable to the Pnma amphiboles. Thus, the angular distortion of the M1 and M3 octahedra should be a function of the mean ionic radius of the constituent M2 cations, and Figure 34 shows this to be the case. Similarly, the O4A and O4B bond-strength requirements should considerably affect the angular distortion of the M2 octahedron.

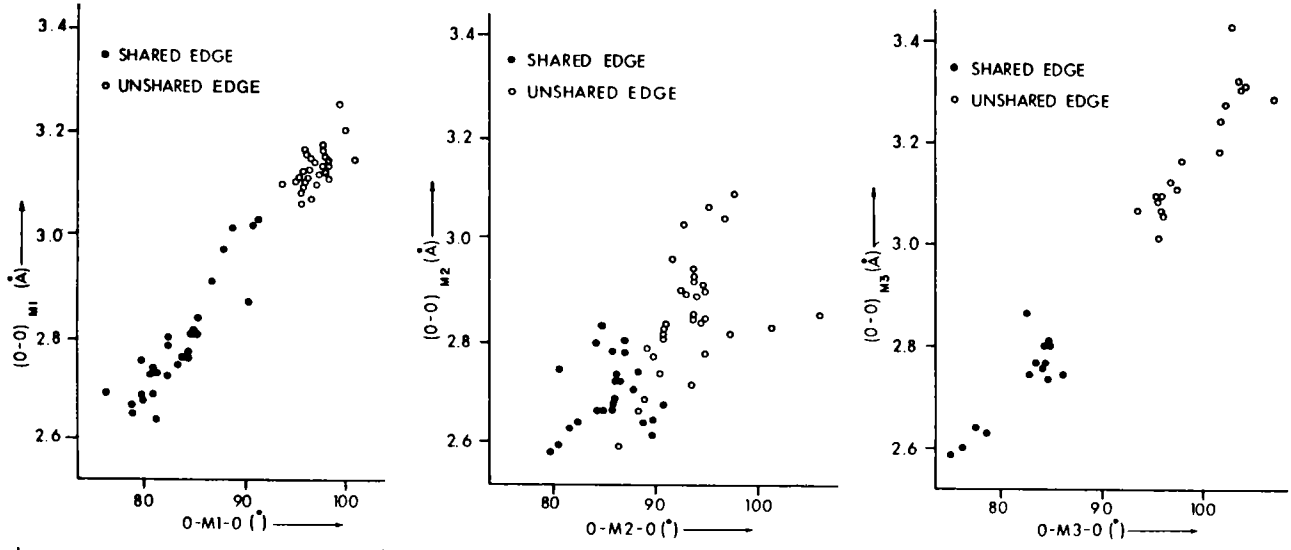

Figure 33. Variation in octahedral edge lengths with the corresponding angles subtended at the central cation for the M1, M2 and M3 sites in the Pnma amphiboles.

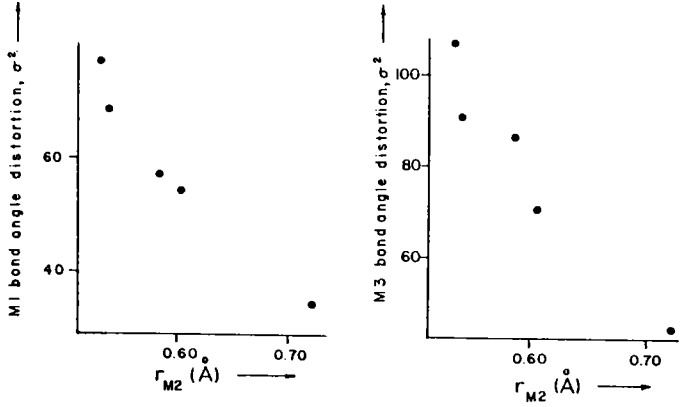

Figure 34. Variation in octahedral angle variance, σ^2, for M1 and M3 with the mean ionic radius of the constituent M2 cations.

The Pnmn amphiboles

There are three unique sites with pseudo-octahedral coordination in this structure type, the M1, M2 and M3 sites; these are similar to the analogous sites in the C2/m amphiboles. It should be noted that the M4 site is also probably [6]-coordinate, but this polyhedron will be considered in the section on the M(4) site. Only one example of this structure type has been reported (Gibbs, 1962, 1969; Gibbs *et al.*, 1960); this was called "protoamphibole" as it appears to bear the same relationship to tremolite and anthophyllite as protoenstatite (Smith, 1969) does to diopside and enstatite. In protoamphibole, the M1, M2 and M3 sites are completely occupied by Mg. Table 17 compares the octahedral bond lengths in protoamphibole[20] with those in tremolite(30), fluor-richterite(34) and fluor-tremolite(36). The <M1-O> in protoamphibole[20] is significantly greater than the corresponding distances in fluor-richterite(34) and fluor-tremolite(36), being almost as large as <M(1)-O> in tremolite(30). However, <M3-O> for protoamphibole[20] is intermediate between the values for fluor-richterite(34) and fluor-tremolite(36), and it is difficult to explain the large <M1-O> distance. <M(2)-O> is statistically identical in all three fluor-amphibole structures and is equal to the corresponding distance in tremolite(30).

Inspection of the empirical bond-valence table for protoamphibole[20] (Table 13) shows that the bond-length variations tend to minimize the deviations of the bond-valence sums from their ideal values. As is evident from Tables 13 and 9, the M2 octahedron is far more distorted than the corresponding octahedra in tremolite(30) and fluor-tremolite(36), as expected for an amphibole with a high M4 occupancy of monovalent cations. Polyhedral elements shared between adjacent polyhedra are generally shorter than the unshared elements, presumably as a result of cation-cation repulsion (Gibbs, 1969). The steric effects of the O4 bond-valence requirements significantly affect the interbond angles of the M3 octahedron, as has been shown for the C2/m amphiboles.

THE M(4) SITE

In all amphibole structure types, the M(4) site is situated at the junction of the octahedral strip and the tetrahedral chain. The importance

Table 18. Comparison of the M(4) Polyhedra in Tirodite $P2_1/m(27)$ and Tirodite(28)

	Tirodite $P2_1/m(27)$		Mean($2\bar{7}$)	Tirodite(28)
	A-set	B-set	<A+B>	-
M(4)-O(2)	2.195(6)	2.208(6)	2.202	2.204(3)
M(4)-O(4)	2.139(8)	2.074(8)	2.107	2.109(4)
M(4)-O(5)	3.209(6)	2.932(6)	3.071	3.101(3)
M(4)-O(6)	2.511(8)	2.650(8)	2.581	2.592(4)
<M(4)-O>[8]	2.490		2.490	2.502
<M(4)-O>[6]	2.296		2.296	2.302

Table 19. Bond Lengths (Å) and Bond-Valences* (v.u.) around the M(4) Site in Tirodite(28), Tirodite $P2_1/m(27)$, Average Tirodite $P2_1/m(\bar{27})$, Anthophyllite[23] and Gedrite[33].

	(28)	(27)	($\bar{27}$)	[23]	[33]
M(4)-O(2)A	2.204(3)	2.195(6)	2.202	2.156(3)	2.254(8)
M(4)-O(2)B		2.208(6)		2.128(3)	2.121(8)
M(4)-O(4)A	2.109(4)	2.139(8)	2.107	2.044(3)	2.129(8)
M(4)-O(4)B		2.074(8)		1.996(3)	2.019(8)
M(4)-O(5)A	3.101(3)	3.209(6)	3.071	2.387(3)	2.246(7)
M(4)-O(5)B		2.932(6)		2.867(3)	2.391(8)
M(4)-O(6)A	2.592(4)	2.511(8)	2.581	3.481(3)	3.911
M(4)-O(6)B		2.650(8)		2.865(3)	2.951
M(4)-O(2)A	0.322	0.324	0.320	0.321	0.256
M(4)-O(2)B		0.316		0.342	0.350
M(4)-O(4)A	0.401	0.366	0.395	0.418	0.343
M(4)-O(4)B		0.424		0.469	0.451
M(4)-O(5)A	0.058	0.054	0.068	0.195	0.261
M(4)-O(5)B		0.082		0.080	0.190
M(4)-O(6)A	0.144	0.172	0.152	0.031	0.017
M(4)-O(6)B		0.132		0.081	0.065
Σ^{VIII}	1.850	1.870	1.870	1.937	1.933
Σ^{VI}	1.734	1.734	1.734	$(1.745)^V$	1.851

*calculated from the curves of Brown and Wu (1976).

of this site and its influence on the structure type of amphibole resulting from a given bulk chemistry has long been known (Warren, 1930) and has been reemphasized by recent studies.

The C2/m amphiboles

The M(4) site has point symmetry 2 and is *surrounded* by eight oxygens, not all of which are necessarily bonded to the cation(s) occupying the M(4) site. If the eight nearest-neighbor anions are included, the coordination polyhedron is a distorted cubic or tetragonal antiprism. The antiprism shares seven edges with adjacent polyhedra, four with the tetrahedra and three with the octahedra.

There has been some discussion as to the actual coordination number of the M(4) site in the ferromagnesian amphiboles, although for the calcic and sodic amphiboles the coordination number [8] is generally accepted (Hawthorne and Grundy, 1977b). The coordination number [6] seems most likely for Fe-Mg-Mn amphiboles.

The $P2_1/m$ amphiboles

The M(4) site has point symmetry 1 and is *surrounded* by eight oxygens, not all of which are necessarily bonded to the central cation(s). Comparison of the individual bond lengths with those in tirodite(28) (Table 18) show the effect of the relaxation in symmetry constraints. The most noticeable differences involve the bridging oxygens of the tetrahedral chains; the differential kinking of the two symmetrically distinct chains in the $P2_1/m$ structure causes large changes in the bond lengths to bridging anions in each chain.

The P2/a amphiboles

The M(4)A and M(4)B sites have point symmetry 2 and are surrounded by eight oxygens arranged in a distorted cubic antiprism. All eight oxygens around each site bond to the central cation, and the overall arrangement around each site is very similar to that in tremolite. Each site shares three edges with adjacent octahedra, four edges with adjacent tetrahedra and two edges with the rather irregular A(2) polyhedron.

The Pnma amphiboles

The M4 site has point symmetry 1 and is surrounded by eight oxygen atoms, not all of which bond to the central cation. The M4 cation coordination may differ somewhat with change in amphibole type. Finger (1967, 1970) suggests that the M4 cation has [7]-fold coordination in anthophyllite, Papike and Ross (1970) suggest [6]-fold coordination in gedrite, and Irusteta and Whittaker (1975) note that the M4 site in homlquistite has five close neighbors. However, no quantitative justification was given for these assignments. Table 19 shows selected bond-valence sums in these structures. In general, the best agreement with ideal bond-valence sums occurs for a coordination number of [8]; however, the difference between the coordination numbers [8] and [7] is definitely not significant and thus [7] is to be preferred to [8]. The bond-valence

sums around M4 for a coordination number of [5] are significantly less than their ideal values, suggesting that the preferred M4 coordination number is greater than [5]. If this is the case, the M4 coordination number is [7] in anthophyllite and holmquistite as the sixth and seventh strongest bonds (M4-O5B and M4-O6B) are of approximately equal strength. For the gedrites, bond-valence considerations indicate that an M4 coordination number of [7] is to be preferred, although geometrical considerations suggest a coordination number of [6]. As with the monoclinic amphiboles, the question of M4 coordination number is far from clearcut when this site is occupied by Fe^{2+} and Mg.

The Pnmn amphiboles

The M4 site has point symmetry 2 and is surrounded by eight anions, only six of which appear to be bonded to the central cation. These six oxygens are arranged in a very distorted octahedron. The M4 octahedron shares three edges with octahedra of the octahedral strip, one edge with the T2 tetrahedron, and one corner with the T1 tetrahedron. Examination of the bond valences in the protoamphibole structure (Table 13) shows that the actual sum around the M4 cation (1.56 v.u.) is considerably less than the ideal value (1.75 v.u.); inclusion of the two next-nearest anions does not significantly improve the bond-valence sum (1.63 v.u.).

General considerations

The cation occupancy of the M(4) site is the primary feature upon which the current nomenclature scheme of the amphiboles is based and is a major factor in the crystal chemistry of the amphiboles. This was recognized in earlier studies (Warren, 1930; Kunitz, 1930; Sundius, 1946) and in the work of Whittaker (1960) who emphasized the importance of the M(4) site to the structure and chemistry of the whole group. Whittaker (1960) treated the amphiboles as a packing of silicate double chains, with the β-angle of the unit cell controlled by the inter-chain contacts, the most important of which involve the M(4) polyhedron and the relative arrangement of the O(5) and O(6) anions in adjacent chains. Variation in β is strongly correlated with the mean ionic radius of the cations occupying the M(4) site (see also Gibbs, 1966). Note that here we use the C-centered orientation whereas Whittaker (1960) used the I-centered orientation. Decreasing β results in a closer packing of the tetrahedral

chains because the increasing stagger in the arrangement of the O(5) and O(6) anions in adjacent chains allows closer approach without decreasing inter-chain anion-anion contacts. In the orthorhombic amphiboles, the staggering of adjacent silicate double chains is almost complete, permitting a closer packing of the chains than does the monoclinic structure; according to the data of Finger (1967), the molar volume of pure anthophyllite and the extrapolated value of monoclinic $Mg_7Si_8O_{22}(OH)_2$ are equal, but with Fe^{2+} substitution in anthophyllite, the molar volume curve deviates strongly from the extrapolated curve of the monoclinic amphiboles. This argument is a persuasive one but more recent data would suggest that other factors are also of importance. The importance of Mg occupancy of M4 in anthophyllite led Whittaker (1960) to suggest that Fe^{2+} should order preferentially at the M1 and M3 positions in order to avoid perturbing the "edge-wise" packing of the chains. X-ray and Mössbauer studies of anthophyllites show this not to be the case. Fe^{2+} is always strongly ordered at the M4 site, although the M4 site always contains significant Mg. Conversely, Whittaker (1960) indicated that a larger cation than Mg should not occur at M4 unless a smaller cation substitutes at M2. In line with this, the data of Seifert (1977) indicate an increase in Al^{VI} (and Al^{IV}) with increasing Fe/Fe+Mg and X^{M4}_{Fe2+} in anthophyllites.

Ross *et al.* (1968, 1969) and Papike *et al.* (1969) emphasize the importance of the M(4) cation occupancy on the phase relations of the Fe-Mg-Mn and calcic amphiboles. At high temperatures, the divalent cations Ca, Mn, Fe and Mg can substitute readily at the M(4) site and there is complete solid solution, as suggested by both natural assemblages (e.g., Klein, 1968) and phase studies (Cameron, 1975). At lower temperatures, amphiboles intermediate between the Fe-Mg-Mn and calcic series are unstable because the difference in size (and bonding characteristics?) between Ca and Mn/Fe^{2+} is not compensated by large amplitudes of thermal vibration as occurs at higher temperatures. The M(4) site of the C2/m Fe-Mg-Mn amphiboles often contains up to ~0.40 Ca p.f.u., and the M(4) site of tremolite-actinolites can contain significant Fe^{2+} (Goldman and Rossman, 1977; Hawthorne *et al.*, 1980). Whether these small amounts of cations are distributed uniformly throughout the structure or are segregated to form G.P. zones or incipient exsolution lamellae must await

transmission electron microscopy studies. When the M(4) site of a monoclinic Fe-Mg-Mn amphibole is partially occupied by Mg, the symmetry may be $P2_1/m$ rather than C2/m. Papike *et al.* (1969) suggest that cummingtonite $P2_1/m$ occurs because the increase in positional degrees of freedom of the atoms at and around the M(4) site can allow the necessary coordination for the *joint* Ca/Mg occupancy of the M(4) site. This infers that the occurrence of Ca at M(4) is also a controlling factor in the existence of the $P2_1/m$ structure. As cummingtonite $P2_1/m$ can occur with down to ∿0.06 Ca p.f.u. (Rice *et al.*, 1974) and cummingtonite C2/m frequently contains up to ∿0.40 Ca p.f.u., the importance of Ca in this regard is somewhat questionable. In principle, this question may be examined using synthesis methods along the $Mg_7Si_8O_{22}(OH)_2$-$Fe^{2+}_7Si_8O_{22}(OH)_2$ join. Popp (1975) and Popp *et al.* (1976) have synthesized amphiboles along this join but they are orthorhombic and of unknown structure; whether or not this further complication to the situation reflects the complete absence of Ca from the system is not clear. Yakovleva *et al.* (1978) have determined the transition composition between the C2/m and $P2_1/m$ structures as 71% $Mg_7Si_8O_{22}(OH)_2$. This is approximately the boundary between cummingtonite and magnesiocummingtonite and is exactly the composition $Fe_2Mg_5Si_8O_{22}(OH)_2$ at which Mg *must* begin to enter M(4) for the cummingtonite to be any more magnesian. This is not to say that the slightest amount of Mg at M(4) causes the C2/m → $P2_1/m$ transition. Mössbauer experiments (Hafner and Ghose, 1971; Ghose and Weidner, 1972) have shown that Fe^{2+} occurs at the M(1,2,3) sites in the most magnesian cummingtonite known (Kisch, 1969), from which we may draw the inference that Mg partially occupies M(4) at compositions less magnesian than $Fe_2Mg_5Si_8O_{22}(OH)_2$. If a K_d [= $X^{Fe}_{M(1,2,3)}(1-X^{Fe}_{M(4)})/X^{Fe}_{M(4)}(1-X^{Fe}_{M(1,2,3)})$] value of 0.03 is assumed (*cf.* Ghose and Weidner, 1972) as an average value for the composition $Fe_2Mg_5Si_8O_{22}(OH)_2$, the site occupancy $X^{Mg}_{M(4)}$ = 0.23 is obtained. Although this value for the $P2_1/m$ → C2/m transition is highly speculative and may vary with Mn, Fe^{2+} and Ca contents of the M(4) site, it is in accord with the known occupancy values for $P2_1/m$ magnesio-cummingtonites and tirodites (Papike *et al.*, 1969; Ghose and Weidner, 1972) and values for C2/m cummingtonites if allowance is made for Ca and Mn occupancies of M(4).

The C2/m → $P2_1/m$ transition has been very well characterized experimentally, and the qualitative explanation that the transition occurs to

provide the necessary coordination around Mg at M(4) appears satisfactory. However, attempts to provide a more quantitative rationalization in terms of bonding around the M(4) site are not as yet adequate. Bond lengths and bond valences around the M(4) site cations in tirodite(28), $P2_1/m$ tirodite(27), anthophyllite[23] and gedrite[33] are shown in Table 19. Comparision of the bond valences in tirodite(28), $P2_1/m$ tirodite(27) and the average values for $P2_1/m$ tirodite($\overline{27}$) show there to be no apparent significant difference among the three sets of values. Thus, an empirical bond-valence analysis of the $C2/m \rightarrow P2_1/m$ transition does not seem to bear out the qualitative explanation given above. However, it should be noted that the bond-valence sums around M(4) are not satisfactory for coordination numbers of [6] or [8], except perhaps for [8]-coordination in anthophyllite[23] and gedrite [33] where these coordination numbers do not appear to be reasonable. It should be noted that very irregular coordination polyhedra (such as M(4) in amphiboles and M2 in pyroxenes) are not amenable to close examination using bond-valence models. If the entry of Mg into the M(4) polyhedron requires a tighter coordination about the M(4) site, this could be achieved in the C2/m structure by S-rotation of the silicate double-chain element (see Thompson, 1970; Papike and Ross, 1970, for chain rotation nomenclature). The reasons why this does not occur are not clear, but may involve cation-cation repulsion between the M(4) and T(2) cations.

Klein (1968, 1969), Himmelberg and Papike (1969), Dobretsov *et al.* (1971), Miller (1977) and Raith *et al.* (1977) have documented the coexistence of calcic and alkali amphibole pairs, and the problem of miscibility between calcic and sodic amphiboles has been reviewed by Robinson and Ghose, this volume. As with the Fe-Mg-Mn and calcic amphiboles, the stability of these amphibole pairs seems to hinge upon the occupancy of the M(4) site. However, unlike the Fe-Mg-Mn and calcic amphiboles, amphiboles intermediate to calcic and alkali amphiboles occur; in fact, amphiboles of this type constitute the sodic-calcic group (Leake, 1978). Inspection of the available analyses suggests that the immiscibility involves glaucophane only as there appear to be no well-documented accounts of amphiboles of the magnesio-riebeckite riebeckite series coexisting with calcic amphiboles, whereas intermediate amphiboles of this composition do occur (Katagas, 1974). This is in accord with the conclusions of Ernst

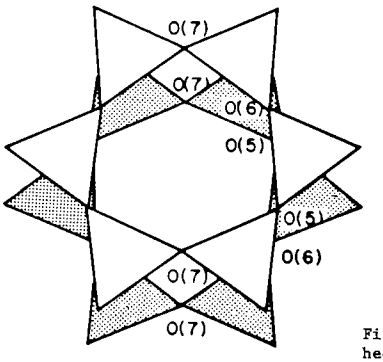

Figure 35. The configuration of the tetrahedral chains around the A-site in the C2/m amphibole structure, projected onto (100).

Table 20. A-Site Nomenclature in C2/m Amphiboles

Site	Wyckoff symbol	Coordinates
A(2/m)	2b	0, 1/2, 0
A(2)	4g	0, y, 0
A(m)	4i	x, 1/2, z
A(1)	8j	x, y, z

(1979) who discussed the occurrence of alkali and calcic amphibole pairs in high-pressure metamorphic belts. Although the evidence is far from conclusive, coexisting amphibole pairs of this type are favored by low temperatures and relatively high pressures, consistent with the stability of glaucophane (Maresch, 1977).

No study has yet addressed the question as to why a miscibility gap appears between glaucophane and the calcic amphiboles at high pressures. Crystal structure refinements at high pressure may help to solve this problem.

THE A-SITE

The A-site is a large cavity situated between the back-to-back tetrahedral chains of the amphibole structures, surrounded by an irregular array of 12 chain-bridging anions (Fig. 35). Warren (1929) noted that this site is empty in tremolite, but proposed (Warren, 1930) that it was occupied by alkali cations in hornblende; this was later confirmed by Heritsch *et al.* (1957, 1960).

The C2/m amphiboles

Early 3-D structure refinements showed the presence of highly anisotropic electron density at the A-site in several C2/m amphiboles. This has been interpreted as positional disorder of the A-site cation about the ideal site at the center of the cavity. The site nomenclature and positional relationships are shown in Table 20.

In general, there are three species (Na, K and vacancy) to be distributed over more than one site, and thus it is possible to obtain only the electron density at each site and not the actual cation site populations. Various reasons have been suggested for the positional disorder of the A-site cations, including the type of O(3) anions, the type of A-site cation and the presence of tetrahedral Al. The A-site disorder patterns in potassium-magnesio-katophorite(29), potassium-arfvedsonite(67) and potassium-fluor-richterite (Cameron *et al.*, 1973a) suggest that the identity of the O(3) anion is not the major factor in the cation disorder. Cation bond-valence requirements suggest that K will order at the A(m) site and Na will order at the A(2) site (Hawthorne and Grundy, 1978). Observed electron densities at the A(2) and A(m) sites are approximately compatible with this scheme but do not prove it. Even if the A-site cation identity is the most important factor, variable occupancy of T(1), T(2), M(4) and O(3) could still exert a secondary effect.

Hawthorne and Grundy (1978) have examined the possibility of interaction between the A-site cation and the H atom in hydroxy-amphiboles. They concluded that Na could occupy the A(2) site without any appreciable bonding interaction with the H atom. However, K could not occupy the A(m) site in a disordered configuration without the formation of a hydride bond between K and H, and the H atom may be positionally disordered in potassium-hydroxy-amphiboles if K occupies the A(m) site. In natural potassium amphiboles, this could be alleviated by a coupled association between occupancy of the one disordered configuration adjacent to O(3) with occupancy of O(3) by F or O^{2-}. This would account for the anomalously weak high frequency principal OH band observed in natural clinoamphiboles (Rowbotham and Farmer, 1973).

The $P2_1/m$ amphiboles

As this structure type is restricted to very magnesium-rich cummingtonite compositions, the A-site is empty (or perhaps has a very low cation occupancy). The geometry of the cavity is very similar to that exhibited by the C2/m cummingtonites.

The P2/a amphiboles

In joesmithite(25), the A-site cations occupy the A(2) site that is displaced ∿0.6 Å along the two-fold axis away from the central A position;

Table 21. Bond-Valences (v.u.) around Selected Anions in the Joesmithite(25) Structure

	M(4)B	A(2)	T(1)B	T(2)B	T(1)A	Σ^1	Σ^2	Σ^3
O(5)B	0.23	0.26	0.45	0.94		1.62	1.73	1.88
O(6)B	0.21	0.24	0.44	0.97		1.62	1.73	1.86
O(7)		0.26	0.47		1.08	1.55	1.66	1.81

[1]Bond strength sums without A-site cation contribution.

[2]Sums with contribution from central A-site cation.

[3]Sums with contribution from A(2) site cation.

the A(2) site is analogous to the A(2) site in the C2/m amphiboles. However, in joesmithite this displacement is ordered, with the A-site cation displaced towards the T(1)B site that is occupied by Be. It is probably this coupled ordered arrangement that results in the unusual space group of this amphibole. Joesmithite is also unique in that it is the only amphibole to have the A-site occupied by divalent cations, although Pb-bearing pargasite (Gillberg, 1959) may have small amounts of Pb at the A-site. Certainly, the joesmithite A-site content of (0.6 Ca + 0.4 Pb) is unusual, although the occurrence of Pb is probably fortuitous (Moore, 1969) and any large divalent cation could possibly occupy this site.

There is little doubt that the coupled relationship between (Ca+Pb) and Be is the result of local bond-valence requirements. As Be contributes only about half the bond valence that Si does, the anions coordinating Be would be extremely undersaturated if the central A-site were occupied instead of the A(2) site (Moore, 1969). This is illustrated in Table 21 which shows the bond valence contributed to the anions coordinating Be in the joesmithite structure. Although the bond-valence sums deviate considerably from their ideal value of 2.0, the values with the A(2) site cation contribution are significantly closer to ideality than the values calculated assuming the A-site cations occupy the central A-site position. However, there is no convincing argument for why the structure adopts an ordered rather than a disordered configuration.

The Pnma amphiboles

The A-site cations in this structure type are much more tightly coordinated than the A-site atoms in the C2/m amphiboles. This is the result of the different configurations of the tetrahedral chains

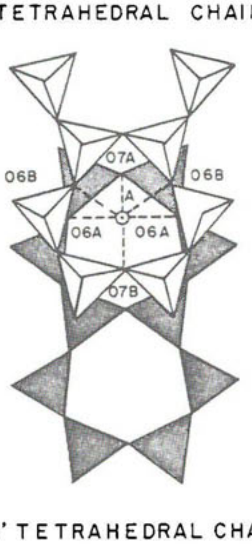

Figure 36. The configuration of the tetrahedral chains around the A-site in the Pnma amphibole structure, projected onto (100).

adjacent to the site in the two structure types (Fig. 36). In the C2/m amphiboles, the ditrigonal distortions of the tetrahedral chains above and below the site are oppositely directed, and the coordination number of cations at the A(2/m) site is [12] or [10], with no obvious cutoff in the cation-anion distances to signify a definite coordination number. In the Pnma amphiboles, the tetrahedral chains above and below the A-site are identically directed (Fig. 36). This results in six short A-O distances and six long A-O distances, suggesting that the A-site cations in gedrite are [6]-coordinate with the anions in a distorted octahedral arrangement.

The Pnmn amphiboles

The A-site in protoamphibole is occupied by Li, according to the unit-cell contents derived from the chemical analysis. However, Gibbs (1969) noted that difference maps of the A-site cavity did not show any significant concentration of electron density that could be attributed to Li, and suggested that Li was randomly distributed around the periphery of the cavity, being particularly close to the short O5-O7 edge of the T1 tetrahedron.

THE O(3) SITE

Warren (1929) used Pauling's second rule (Pauling, 1929) to indicate that the O(3) position in tremolite is predominantly occupied by OH. In a general examination of the chemistry of the monoclinic amphiboles, Warren (1930) also assigned F to the O(3) position. Chemical analysis (Warren, 1929) showed that O(3) could be completely occupied by OH. Synthesis of fluor-amphiboles was accomplished by Bowen and Schairer

Table 22. The H Environment in Tremolite(56)

x	0.2088(6)
y	0
z	0.7628(14)
O(3) - H	0.960(6) Å
H-O(7)	2.764(7)
O(3)-O(7)	3.305(3)
O(3)-H-O(7)	116.4(2)°
O(3)'-O(3)-H	90.4(2)°

(1935), and chemical analysis of synthetic fluor-tremolite (Comeforo and Kohn, 1954) showed that the O(3) position could be completely occupied by F. Chemical analysis of natural amphiboles (Geijer, 1959; Leelanandam, 1969a,b; Fominykh, 1974) shows that Cl also occurs in amphiboles, apparently substituting for OH at the O(3) site; Leake (1968) records an analysis (673) with O(3) completely occupied by Cl, although no end-member Cl amphiboles have yet been synthesized.

The first information concerning the attitude of the OH^- anion was derived from infrared spectroscopic studies. Hanisch (1966) showed that the three-dimensional absorption figure for the OH-stretching frequency in riebeckite is a lemniscate, rotated around its longer axis which coincides with X^*; the O-H bond is thus parallel with X^*. A similar result was also found by Burns and Strens (1966); the absence of bands in the first overtone region of the polarized β spectrum show the O-H bond to be confined to the (010) mirror plane, while from the relative overtone absorbances in the polarized α and γ spectra, calculations showed the O-H bond to make an angle of 85(8)° with the Z-axis. Papike *et al.* (1969) and Hawthorne and Grundy (1973a) approximately located the position of the hydrogen atom in tremolite(30) and ferro-tschermakite(54) using x-ray diffraction; these results were in agreement with the infrared results concerning the orientation of the O-H bond. More precise data were provided by the neutron diffraction study of tremolite(56b) (Hawthorne and Grundy, 1976), as summarized in Table 22. The O(3)-H bond length of 0.960(6) Å is fairly typical for an hydroxyl ion and shows that little or no hydrogen bonding with the chain-bridging anions occurs; the infrared spectrum of this amphibole showed a single narrow band at 3684 cm^{-1}. The occurrence of the fundamental O-H band in amphiboles between 3600-3700 cm^{-1} is also indicative of little or no hydrogen bonding, in agreement with the crystal structure results.

The O(3) position may also be occupied by O^{2-} in oxy-amphiboles, but the origin and role of O^{2-} in this position are not well understood. Extensive studies on dehydroxylation and oxidation of both natural and

synthetic amphiboles have shown that these are cooperative processes in iron-rich amphiboles, and hence the amount of O^{2-} at O(3) produced by dehydroxylation in the solid state should correlate with the amount of Fe^{3+} produced by the accompanying oxidation. No general correlation of this sort is apparent in natural amphiboles, and the question arises as to whether this correlation is obscured by cation substitutions involving Fe^{3+}, or whether post-crystallization oxidation is not an important process in producing dehydroxylated amphiboles, except in certain high pO_2 environments. Certainly an alternate possibility is that amphiboles may crystallize hydroxyl deficient, with the $O^{2-} \rightleftarrows OH^-$ substitution balanced by a polyvalent cation substitution. This possibility has been suggested by Leake (1968), with Ti being involved in the substitution. Kitamura *et al.* (1975) have shown that Ti preferentially occupies the M(1) site in potassian oxykaersutite(40), a feature they interpreted as resulting from cation disorder accompanying oxidation-dehydroxylation. Presumably, the strong ordering of Ti at M(1) occurs as a result of local bond-valence requirements upon loss of the hydrogen atom. This is certainly in line with the negative correlation between (OH+F+Cl) and Ti shown by Leake (1968) for the Engel and Engel (1962) data, although the paragenesis of these amphiboles suggests that the hydroxyl deficiency may have originated during crystallization rather than by post-crystallization oxidation. However, the general significance of this is not clear. Other sets of good quality analyses with fairly variable (OH+F+Cl) contents give different correlations or no correlations at all (e.g., Binns, 1965; Appleyard, 1976). Certainly it appears that O^{2-} substituting for monovalent anions at the O(3) position may be coupled with polyvalent cation substitutions as an integral part of amphibole chemistry as well as being involved in oxidation-dehydroxylation reactions.

A question of some uncertainty is the role of "excess" OH in the amphibole structure. This has been documented in both natural (Leake, 1968) and synthetic (Witte *et al.*, 1969; Maresch and Langer, 1976) amphiboles. However, the structural details of the substitution and its general significance in natural amphiboles are unknown.

Table 23. Normal Cation Site-Assignments in Amphiboles

Cation	A	M(4)	M(1), M(2), M(3)	T(1), T(2)
Si				———
Al			———	———
Fe^{3+}			———	
Ti			———	
Fe^{2+}		——	———	
Mn		——	———	
Mg		——	———	
Li	——	——	———	
Ca		——		
Na	——	——		
K	——			

CATION DISTRIBUTIONS IN AMPHIBOLES

The wide variety of cation coordinations in the amphiboles, together with the large structural compliance of some of the sites results in considerable chemical complexity in these minerals. A knowledge of the site occupancies and order-disorder relationships in the amphiboles is essential to a better understanding of their crystal chemistry, phase relations, optical and electrical properties and oxidation-dehydroxylation mechanisms. Consequently, the amphiboles more than any other mineral group have been studied from the viewpoint of site-population characterization. However, before examination of the results of the various techniques used to study this problem, a few preliminary considerations are in order.

Most of the spectroscopic techniques used for site-population characterization are sensitive only to one or two cations in the structure while the remaining techniques, although in principle sensitive to all (or most) cation species in all (or most) sites, cannot practically distinguish between some cation species in all possible arrangements. Thus, it is necessary to assign certain cations or groups of cations to certain sites or groups of sites in the structure. Based on knowledge of the general chemical variations in amphiboles, certain assignments may be made with a fair degree of confidence (Table 23). However, these assignments are strongly dependent on the accuracy of the chemical analysis, errors in which may not be immediately apparent from the general criteria of a "good" amphibole analysis (Leake, 1968; Papike *et al.*, 1974).

The O(3) position in the amphiboles may be occupied by OH^-, F^-, Cl^- and/or O^{2-}. Although it is not generally considerdd as an important constituent, Cl does occur in considerable amounts in amphiboles according to Geijer (1959) and Leelanandam (1969a,b); thus, it is necessary to analyze for H_2O, F and Cl unless it can be demonstrated that O(3) is occupied completely by one or two of these species. Cameron (1970) has suggested that Fe^{2+} may prefer sites coordinated by OH and avoid sites coordinated by F. Obviously, the interpretation of ordering patterns in natural amphiboles, where O(3) may be partially occupied by both OH and F, is contingent upon accurate knowledge of the monovalent anion contents of the unit cell if this is the case. We have seen that the mean bond lengths at the M(1) and M(3) sites are partially a function of the anion occupancy of O(3). If relationships of this sort are to be further developed, and used for site-population characterization of cations that are resistant to direct experimental examination, a knowledge of the anion occupancy of O(3) is essential.

Another problem concerns the occurrence of certain elements in the amphiboles that have a variable valence state. By far the most important is Fe, which may occur in both divalent and trivalent states. As the role of Fe in the structure is strongly dependent on its valence state, it is extremely important to know the amounts of Fe^{2+} and Fe^{3+} in the cell as accurately as possible. For example, many studies are concerned with the site-ordering of Mg and Fe^{2+}; if the Fe^{3+}/Fe^{2+} ratio of the unit cell contents is not known, the problems in characterizing exact site-populations become more intractable. In addition to problems such as this, the calculation of the cell contents from the chemical analysis will be in error if the Fe^{3+}/Fe^{2+} ratio is unknown. The relative amounts of FeO and Fe_2O_3 may be measured by wet-chemical techniques or by Mössbauer spectroscopy, so that this should not constitute a major problem. However, increasing numbers of mineral analyses are now obtained using the electron microprobe, which cannot distinguish valence states; although various schemes have been devised to determine Fe^{3+}/Fe^{2+} ratios from microprobe data (Papike *et al.*, 1974; Vieten and Hamm, 1971), these assume various stoichiometric requirements of the mineral concerned that may or may not be valid and will also be greatly affected by error in the data. The only answer to this problem would appear to be a combination

of microprobe and wet-chemical techniques or Mössbauer spectroscopy in the event that a clean separation of the amphibole can be achieved.

The valence states of Ti and Mn are not well characterized in amphiboles. There has been much speculation on the valence state of Ti in silicates. Traditionally, it has been assumed that Ti is quadrivalent in silicates. However, there has been recent support for the idea that trivalent Ti can occur in pyroxenes. The similarity of the coordination polyhedra in the pyroxenes and the amphiboles suggests that what is a possibility in one structure is a possibility in the other, and thus amphiboles could contain both Ti^{3+} and/or Ti^{4+}. A similar situation occurs for Mn. In general, it has been assumed that Mn is divalent in amphiboles, and the stoichiometry of Mn-rich amphiboles supports this (Tirodite....Dannemorite - $Mn_2^{2+}(Mg,Fe^{2+})_5Si_8O_{22}(OH)_2$; natural and synthetic Mn-rich tremolites and actinolites). However, electronic absorption spectra of some Mn-bearing tremolites show the presence of some Mn^{3+} (Goldman, 1977). Electron spin resonance studies of Mn-bearing tremolites of similar composition (but different geographic location) show the Mn to be divalent (Bershov *et al.*, 1966; Manoogian, 1978). Thus, amphiboles can feasibly contain both Mn^{2+} and/or Mn^{3+}. These problems of mixed valences are compounded for Ti and Mn by the fact that we do not have a convenient characterization technique for oxidation ratio as is the case for Fe by Mössbauer resonance. In view of this situation, it is perhaps fortunate that Ti and Mn are minor constituents in most amphiboles.

The ordering pattern of Table 23 is essentially due to Warren (1930). Whittaker (1949) showed a non-random distribution of group C cations over the M(1), M(2) and M(3) sites in magnesio-riebeckite(3), and Papike and Clark (1967) showed a non-random distribution of group T cations over the T(1) and T(2) sites in potassian titanian magnesio-hastingsite(24). In the last 15 years, considerable effort has gone into the characterization of cation ordering in amphiboles; a summary of the current knowledge follows.

Aluminum

Al is both a C-group and a T-group cation, occurring in both octahedral and/or tetrahedral coordination. In the monoclinic (C2/m) amphiboles, Al shows the site-preference T(1) >> T(2); subsilicic amphiboles

definitely have Al at the T(2) site, but the presence of Al at T(2) in amphiboles where Si $\geq$ 6.0 atoms p.f.u. is somewhat questionable (Ungaretti, 1980). In the orthorhombic (Pnma) amphiboles, Al shows the site-preference T1B $\geq$ T1A $\geq$ T2B > T2A; as indicated in Figure 23, the T2B site shows considerable Al occupancy in the gedrites.

When Al is a C-group cation, it is very strongly ordered at the M(2) site. This result was derived from mean bond length-ionic radius relationships that are not sufficiently accurate to tell whether or not this ordering is complete. Bancroft and Burns (1969) have assigned weak peaks in the infrared spectra of glaucophanes to cation arrangements involving Al at the M(1) or M(3) sites. Because of the problems associated with the derivation of site-occupancies from infrared spectra, this cannot be considered as good evidence for occupancy of M(1) or M(3) sites. In support of this view, Strens (1974) reports that of 15 glaucophanes examined by this method, none showed minor bands. In a detailed crystallographic analysis of 26 blue amphiboles, Ungaretti *et al.* (1978) used mean bond-length and charge-balance arguments to show complete order of Al at M(2). Thus, there is no direct evidence of Al occurring at the M(1) and M(3) sites, the current evidence favoring complete order at the M(2) site (except perhaps for oxy-amphiboles?).

Ferric iron

Fe^{3+} is a C-group cation; there is no convincing evidence for tetrahedrally-coordinated Fe^{3+} as is the case in the pyroxenes (Hafner and Huckenholz, 1971; Virgo, 1972). Although it has long been surmised that Fe^{3+} is strongly ordered at the M(2) site, it was not until the structure refinements of potassian ferri-taramites(51) and (59) that there was convincing crystallographic evidence for this. A considerable number of more recent refinements have confirmed this. Detailed analysis of mean bond lengths and charge requirements indicates complete Fe^{3+} order at M(2) in some cases (Ungaretti *et al.*, 1978) and the occurrence of small amounts of Fe^{3+} at the M(1) and/or M(3) sites in other cases (Ungaretti *et al.*, 1981; Hawthorne and Grundy, 1977a); it is not clear if the latter represents the equilibrium crystallization configuration or is the result of post-equilibration oxidation by dehydroxylation.

Unequal doublet half-widths in Fe Mössbauer spectra have been taken as evidence for Fe^{3+} at the M(1) and/or M(3) sites in amphiboles.

This cannot be considered as significant because the larger Fe^{3+} half-width may be an artifact of the fitting procedure (Hawthorne, 1981) and/or the result of subtitutional broadening (Dowty and Lindsley, 1973; Dollase and Gustafson, 1977). Similarly, minor peaks in the infrared spectra have been assigned to Fe^{3+} at M(1) and/or M(3); it has been suggested that these are not valid peaks (Strens, 1974).

Titanium

Ti is generally considered as a C-group cation, although some authors do assign Ti^{4+} to the T group when Si+Al < 8.0. There is no direct evidence for tetrahedrally-coordinated Ti in amphiboles. In most x-ray studies, Ti has been assigned to the M(2) site together with all the other trivalent cations in the formula unit. However, there is no direct evidence for this assignment of Ti. The only experimental evidence for Ti ordering in amphiboles is the neutron refinement of potassian oxy-kaersutite(40) by Kitamura *et al.* (1975). They showed that Ti is strongly ordered at the M(1) site. Whether this is an equilibrium crystallization feature or whether it is associated with post-crystallization disorder during oxidation-dehydroxylation is not known.

Ferrous iron

Fe^{2+} is generally assigned to the B and C groups of the amphibole formula and can occupy the M(1), M(2), M(3) and/or M(4) sites. As the character of the ordering patterns exhibited by Fe^{2+} changes with the amphibole type, it is convenient to consider each principal amphibole group separately (see Table 24).

Fe-Mg-Mn amphiboles. In the amphiboles of the magnesio-cummingtonite...grunerite series, extensive site-occupancy studies by structure refinement, Mössbauer, infrared and electronic absorption spectroscopies have shown that Fe^{2+} is very strongly ordered at the M(4) site. The relative ordering of Fe^{2+} between the M(4) and M(1,2,3) sites is a function of equilibration temperature (Ghose and Weidner, 1972). The relative ordering of Fe^{2+} over the M(1), M(2) and M(3) sites is less well characterized, as Mössbauer measurements do not give this information. Structure refinements indicate the ordering scheme M(3) $\geq$ M(1) > M(2); this is also compatible with the results of combined Mössbauer and infrared experiments (Bancroft *et al.*, 1967a).

Table 24. Fe^{2+} Site Occupances from Crystal Structure Refinements

	M(1)	M(2)+	M(3)	M(4)	
			Iron-magnesium-manganese group		
(21)	0.29	0.05	0.29	0.76	M(4) >>M(1) ~ M(3) > M(2)
(22)	0.85	0.77	0.89	0.99	M(4) > M(3) > M(1) > M(2)
(28)	0.03	0.16	-	0.09	M(2) > M(4) > M(1) > M(3)
(57)	-	0.17	-	0.05	M(2) > M(4) > M(1) ~ M(3)
(61)	0.25	-	0.30	-	M(3) > M(1) >>M(2) ~ M(4)
[23]	0.03	0.02	0.03	0.51	M(4) > M(1) ~ M(2) ~ M(3)
[31]	0.40	-	0.56	-	M(3) > M(1) >>M(2) ~ M(4)
[32]	0.12	(0.04)	0.10	0.42	M(4) > M(1) ~ M(3) > M(2)
[33]	0.33	(0.09)	0.39	0.65	M(4) > M(3) ≥ M(1) >>M(2)
			Calcic group		
(24)	0.35	(0.11)	0.35	-	M(1) ~ M(3) > M(2) ≥ M(4)
(37)*	0.61	0.46	0.58	-	M(1) ≥ M(3) > M(2) >>M(4)
(38)	0.23	(0.20)	0.24	-	M(1) ~ M(3) > M(2) ≥ M(4)
(39)	0.32	(0.17)	0.32	-	M(1) ~ M(3) > M(2) ≥ M(4)
(42)	0.29	-	-	-	M(1) >>M(2) ~ M(3) ~ M(4)
(44)	1.00	0.59	0.59	-	M(1) > M(2) ~ M(3) >>M(4)
(45)	0.46	0.35	0.48	-	M(1) ~ M(3) > M(2) >>M(4)
(46)	0.49	0.42	0.27	-	M(1) > M(2) > M(3) >>M(4)
(48)	0.52	-	0.52	-	M(1) ~ M(3) >>M(2) ~ M(4)
(49)	0.7	-	0.6	-	M(1) > M(3) >>M(2) ~ M(4)
(50)	0.6	-	0.4	-	M(1) > M(3) >>M(2) ~ M(4)
(54)	0.61	0.05	0.78	-	M(3) > M(1) >>M(2) ≥ M(4)
(58)**	(0.69)	(0.31)	(0.84)	0.07	M(3) > M(1) >>M(4) ≥ M(2)
(60)	0.36	0.18	0.45	-	M(3) > M(1) > M(2) >>M(4)
(61)	0.30	0.07	0.24	-	M(1) > M(3) >>M(2) > M(4)
(70)**	0.17	(0.15)	0.22	0.03	M(3) > M(1) >>M(4) > M(2)
(71)**	0.19	(0.15)	0.28	0.03	M(3) > M(1) >>M(4) > M(2)
(72)**	0.17	(0.16)	0.29	0.04	M(3) > M(1) >>M(4) > M(2)
(73)	0.32	(0.21)	0.45	0.17	M(3) > M(1) > M(4) >>M(2)
			Sodic calcic group		
(35)	0.20	0.52	0.15	0.04	M(2) > M(1) > M(3) > M(4)
(51)	0.85	0.18	0.85	-	M(1) ~ M(3) >>M(2) > M(4)
(59)	0.73	0.13	0.71(0.85)	-	M(3) ≥ M(1) >>M(2) > M(4)
			Alkali group		
(26)	0.16	-	0.29	-	M(3) > M(1) >>M(2) ~ M(4)
(64)	1.00	-	0.67	-	M(1) > M(3) >>M(2) ~ M(4)
(65)	0.93	0.34	0.88	-	M(1) > M(3) >>M(2) > M(4)
(66)	0.75	-	-	-	M(1) >>M(1) ~ M(2) ~ M(3)
(67)*	1.00	0.42	0.76(0.89)	-	M(1) > M(3) > M(2) >>M(4)
(68)*	0.93	-	0.48(0.64)	-	M(1) > M(3) >>M(2) ~ M(4)
(69)	0.59	-	0.80	-	M(3) > M(1) >>M(2) ~ M(4)

+values given in parentheses for the M(2) site are predominantly Fe^{3+}.
*considerable Mn is included in the site occupancies given; where an estimate of Mn site occupancies has been made, individual estimated Fe^{2+} site occupancies are given with the combined Fe+Mn occupancy in parentheses.
**results suggest significant Fe^{3+} at the M(1) and/or M(3) sites.

In the amphiboles of the tirodite-dannemorite series, Mn^{2+} is strongly ordered at M(4); however, Mössbauer measurements show this ordering is not complete and Fe^{2+} also occurs at M(4). Combined Mössbauer and infrared measurements (Bancroft *et al.*, 1967a) show Fe^{2+} to be strongly ordered at M(2) relative to M(1) and M(3) in tirodite.

The Fe^{2+} distribution in holmquistite is very different from that exhibited by the other Fe-Mg-Mn amphiboles. Crystal structure refinement shows the Fe^{2+} site preference M3 > M1 >> M2 ∿ M4 ∿ 0.0, and this is confirmed by Mossbauer (Law, 1973) and infrared spectroscopy (Wilkins *et al.*, 1970).

Anthophyllites show strong ordering of Fe^{2+} at M4; this ordering is temperature dependent (Seifert, 1978). Gedrites show the same site-preference, but the degree of ordering is not as great. In addition, the M2 site in gedrite is occupied by Al, whereas Fe^{2+} is approximately equally distributed among the M1, M2 and M3 sites in anthophyllite.

Calcic amphiboles. The calcic amphibole group shows an extremely complex variation in Fe^{2+} ordering. The results of crystal structure refinements are summarized in Table 24 where it can be seen that no exact overall pattern is apparent. However, the predominant Fe^{2+} ordering pattern seems to be M(1) ⩾ M(3) > M(2) ⩾ M(4). Obviously, the Fe^{2+} ordering pattern is strongly dependent on bulk composition, and it may not be reasonable to look for an overall pattern. Thus, the Fe^{2+} content of M(2) is affected by the trivalent cation content of that site. Goldman and Rossman (1977) have shown that low Fe^{2+} tremolite may show the ordering scheme M(4) > M(1,2,3), whereas actinolites show M(1,2,3) > M(4), a result of the fact that M(4) is predominantly occupied by Ca in tremolite. More subtle inductive effects may also be present, but these will need more adequate experimental data to characterize with any certainty.

Sodic-calcic amphiboles. The hydroxy-amphiboles of this group so far examined tend to show the site-occupancy pattern M(3) ⩾ M(1) >> M(2) ⩾ M(4). All of these amphiboles show significant trivalent cation occupancy of M(2); a different pattern is expected for the richterites. In fluor-richterite, Fe^{2+} shows the ordering scheme M(2) > M(1) > M(3) > M(4); this pattern presumably results from the well-known antipathy of Fe^{2+} for F-coordinated sites in minerals.

Alkali amphiboles. Metamorphic amphiboles of the glaucophane...ferro-glaucophane...magnesio-riebeckite...riebeckite series show a regular Fe^{2+} distribution (Fig. 37) with the ordering pattern M(3) > M(1). This may be perturbed by the presence of Li, which preferentially orders

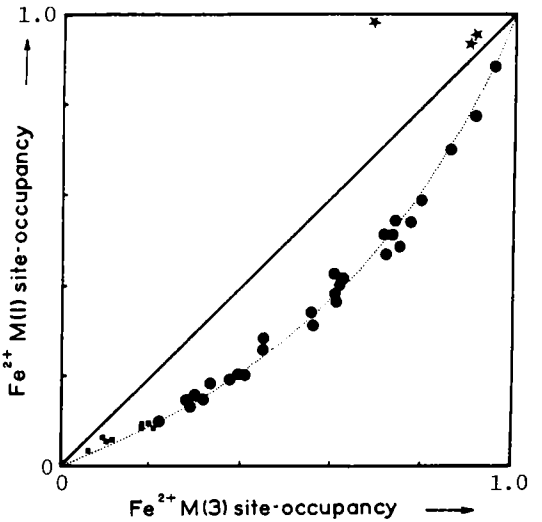

Figure 37. The distribution of Fe^{2+} over the M(1) and M(3) sites in glaucophane... ferro-glaucophane...magnesio-riebeckite... riebeckite amphiboles (●) and nyboites (■); from Ungaretti *et al.* (1978). The * indicates riebeckites of igneous origin that contain significant Li.

at M(3) and can lead to a reversal of the Fe^{2+} ordering pattern. Fe^{2+} ordering in nyboites is somewhat irregular. Generally, these show M(3) > M(1), but Fe^{2+} may be strongly ordered into M(2) or completely avoid M(2); this could be clarified by examination of less magnesium-rich varieties.

Magnesium

The behavior of Mg in amphiboles is generally antipathetic to that of Fe^{2+} and will be considered only where it is of particular crystal-chemical interest. In C-centered amphiboles of the magnesio-cummingtonite...grunerite series, Mg seems to be virtually excluded from the M(4) site. In studies where the derived Fe^{2+} occupancy of M(4) is less than 1.0, the balance may be assigned to the small amount of Ca generally present. Any significant M(4) occupancy by Mg occurs only in $P2_1/m$ tirodite(27) and is thought to be the cause of this particular structure variant (Papike *et al.*, 1968, 1969). The orthorhombic Fe-Mg-Mn amphiboles anthophyllite[23] and gedrites[32] and [33] show considerable occupancy of M4 by Mg, as does protoamphibole[20] and synthetic (Li, □)$(Li,Mg)_2Mg_5Si_8O_{21+x}(OH)_{3-x}$ (Maresch and Langer, 1976). The only other amphibole of note with regard to unusual Mg site-occupancy is the synthetic monoclinic Fe-Mg-Mn amphibole $NaMgNaMg_5Si_8O_{22}(OH)_2$ prepared by Witte *et al.* (1969), in which the M(4) site is presumably occupied by Mg and Na in equal proportions.

Manganese

In Fe-Mg-Mn amphiboles, Mn is strongly ordered at the M(4) site (Bancroft *et al.*, 1967a; Hawthorne and Grundy, 1977b). For the remaining amphibole groups, there is little information on the distribution of Mn. When the C-group cation sum exceeds 5.0, some studies have assigned the excess cations to the B-group in the order Mn > (Fe,Mg); there is no direct proof of this, although it is consistent with the behavior of Mn in the Fe-Mg-Mn amphiboles. Some studies (Hawthorne, 1976; Hawthorne and Grundy, 1978) have attempted to derive Mn site-preference in sodic-calcic and alkali amphiboles on the basis of mean bond lengths at the M(1), M(2) and M(3) sites; the preference M(3) > M(1) $\sim$ M(2) was observed in both studies, although these results are highly speculative. When Mn is present in the trivalent state, ordering at the M(2) site is to be expected by analogy with the behavior of Al and Fe^{3+}.

Lithium

Li occurs in significant quantities only in certain amphibole types, although it is capable of occupying a wide variety of sites in amphiboles. In the Fe-Mg-Mn amphiboles, only holmquistite and clinoholmquistite show significant Li. Crystal structure refinements show Li to be virtually completely ordered at the M(4) site. This agrees with the infrared results of Wilkins *et al.* (1970), which show that no significant Li occurs at the M1 + M3 sites in holmquistite. Li also occurs in protoamphibole [20] and $(Li,\square)(Li,Mg)_2Mg_5Si_8O_{21+x}(OH)_{3-x}$ (Maresch and Langer, 1976), both the M4 site (together with Mg) and at the A-site.

Analyses of calcic amphibole coexisting with holmquistite (Knorring and Hornung, 1961; Wilkins *et al.*, 1970) show only small amounts of Li ($\sim$0.16 atoms p.f.u.), and there is no evidence where the Li occurs in the structure. Conversely, Li can be an important constituent of alkali amphiboles, and stoichiometric considerations (Sundius, 1946; Borley, 1963) suggest that Li is a C-group cation in these amphiboles. On the basis of infrared spectroscopy, Addison and White (1968) proposed that Li occurs at the M(1) + M(3) sites in riebeckite. Subsequent crystal structure refinement of a fluor-riebeckite(68) containing significant Li showed Li to be almost completely ordered at the M(3) site. However, it should be stressed that this ordering pattern is for a fluor-amphibole

[O(3) ∿ 0.6F + 0.4OH] and the ordering may be different in a hydroxy-amphibole, although high Li contents are generally associated with high F contents in alkali amphiboles (Lyons, 1976).

Calcium

Ca is virtually always assigned to the B-group in the unit formula, and all x-ray studies of calcic and sodic-calcic amphiboles appear to be compatible with this assignment, Ca occupying the M(4) site in all structures so far examined. It is not certain whether Ca is ever significantly in excess of that required to fill the B-group in the unit formula. Hawthorne (1976) has suggested that some alkali amphiboles may have small amounts of Ca at the M(1,2,3) sites or that many of these amphiboles contain significant amounts of minor components (e.g., Li) that have been ignored during analysis but would show significant C-group occupancy. In the Fe-Mg-Mn amphiboles, the small amounts of Ca are assumed to occupy the M(4) site; whether this occupancy is real or whether these amphiboles contain incipient calcic amphibole lamellae must await detailed transmission electron microscopy studies. Certainly in coexisting Fe-Mg-Mn and calcic amphibole assemblages, exsolution of calcic amphibole by the Fe-Mg-Mn amphibole is widespread. In the rare amphibole joesmithite, Ca occupies the two M(4) sites and the A(2) site; this is the only recorded amphibole where the A-cavity is occupied by a divalent cation.

Sodium

Na is assigned to the A- and B-groups of the unit formula. Warren (1929, 1930) proposed that Na would occupy the M(4) and A-sites in the amphibole structure, and this was confirmed by Whittaker (1949) and Heritsch *et al.* (1957) by crystal-structure refinement. All subsequent crystal-structure work has confirmed these results.

Potassium

K is always assigned to the A-group in the amphibole formula unit, and all experimental work so far published is in agreement with this (Papike *et al.*, 1969; Cameron *et al.*, 1973b; Hawthorne, 1976). The positional disorder of Na and K observed in crystal structure studies is discussed in detail in the section on the A-site.

Beryllium

Joesmithite is a remarkable amphibole in which Be^{2+} occupies the T(1)B site, apparently showing no disorder with Si over the four distinct tetrahedral sites.

Boron

Kohn and Comeforo (1955) report the synthesis of a calcic fluor-amphibole containing considerable B^{3+}. The chemical analysis indicates 1.12 B^{IV} and 0.33 B^{VI} p.f.u.; as B^{3+} has not been recorded in octahedral coordination in an oxide environment, additional evidence is needed before this result can be accepted.

Cobalt

Co^{2+} occupies the M(1), M(2), M(3) and M(4) sites in the structure of "$Na_2H_2Co_5Si_8O_{22}(OH)_2$" (Prewitt, 1963; Gibbs and Prewitt, 1968), which apparently deviates somewhat from its ideal composition. Similar results are apparent from the chemical analysis of fibrous cobalt amphibole synthesized by Nesterchuk *et al.* (1968). On the basis of optical absorption spectra, Chigareva *et al.* (1969) proposed that Co^{2+} occurs in both octahedral and [8]-fold coordination in synthetic cobalt fluor-richterite.

Nickel

Chemical analysis of synthetic nickel richterite (Fedoseev *et al.*, 1968) shows Ni to occupy the M(1), M(2), M(3) and M(4) sites.

Chromium

On the basis of optical absorption spectra, Chigareva *et al.* (1969) propose that Cr^{3+} occurs in [8]-fold coordination in "chromium fluor-amphibole."

Conversely, Goldman (1977) presents electronic absorption spectra for Cr^{3+}-bearing actinolites that indicate Cr^{3+} to be in [6]-coordination.

Zinc

Klein and Ito (1968) report chemical analyses and physical data for several zinc-bearing amphiboles from Franklin, New Jersey. The chemical analyses suggest that Zn occurs at the M(1,2,3) sites.

Germanium

Sipovskii *et al.* (1972) and Grebenshchikov *et al.* (1974) report the synthesis and characterization of a fibrous amphibole, $Na_2Mg_6Ge_8O_{22}(OH)_2$ where Si is entirely replaced by Ge.

FACTORS AFFECTING CATION ORDERING IN AMPHIBOLES

Several studies have examined the factors affecting cation ordering in amphiboles (Ghose, 1965, 1977; Litvin, 1966; Hawthorne, 1978b), but as yet the problem is far from being resolved.

Structure energy

In a refinement of the crystal structure of magnesio-riebeckite(3), Whittaker (1949) found that the monovalent cations were ordered at the M(4) site and the trivalent cations were ordered at the M(2) site. The preferential occupancy of M(2) by trivalent cations was explained as arising from the lower electrostatic potential at M(2) that results from the occupancy of the adjacent M(4) site by a monovalent cation. As indicated by Whittaker (1971), this does not completely explain the situation, because the question then arises as to why the monovalent cation occupies the M(4) site. In the case of riebeckite, this may be assumed to result from the large size of the Na atom. However, for holmquistite and clinoholmquistite, which show a similar cation charge arrangement, this argument cannot apply as Li is small enough to occupy the M(1), M(2) and/or M(3) sites, and has been shown to do so in Li-bearing riebeckite (Hawthorne, 1978c). Ghose (1965) has also cited this factor as affecting cation-ordering in amphiboles and further suggested that Fe^{3+} and Ti^{4+} may occupy the M(1) and M(3) sites in oxy-amphiboles. The effect of relative electrostatic potentials at different sites in the amphibole structures has been considered in more detail by Whittaker (1971), who made the following predictions:

(i) Richterite has Na at A and NaCa at M(4); this is the case for fluor-richterites(34) and (35).

(ii) Clinoholmquistite has Li_2 at M(4); this is true for clinoholmquistite(62).

(iii) $LiNaMg_6Si_8O_{22}F_2$ has Na at A, Mg at M(4) and Li at M(3).

(iv) Oxy-amphiboles have a preference for trivalent or quadrivalent cations at M(1); this is the case for potassian oxykaersutite(40).

(v) All amphiboles (except oxy-amphiboles) have trivalent C-type cations strongly ordered at M(2); this is generally the case.

(vi) In magnesio-hornblende and tschermakite, Al is preferentially ordered at T(2); this is not the case for magnesio-hornblende (45) and ferro-tschermakite(54).

(vii) In edenite, katophorite and taramite, T(1) should be preferentially occupied by Al; this is the case for potassian ferri-taramite(59).

Bond-valence

The effect of local charge balance around the bridging anions in amphiboles with occupied A-sites has been examined by Ghose (1965) who concluded that tetrahedral Al should order into the T(1) site. Hawthorne (1978b) has considered the effect of local bond-valence requirements on the cation ordering patterns in amphiboles. Recent work has shown the importance of local bond-valence requirements and their relationships to variation in bond length, suggesting that the same mechanism should exert stringent controls on cation ordering. Calculation of the mean square (R.M.S.) deviation from exact agreement with Pauling's second rule (Pauling, 1960) for all possible charge arrangements consonant with a particular amphibole stoichiometry shows the arrangement with the smallest R.M.S. deviation to be the preferred cation arrangement for that specific stoichiometry.

Miscellaneous factors

Although reasonable success has been achieved in the rationalization of cation ordering in amphiboles by energy and bond-valence methods, these only apply to the relative ordering of cation species with different formal valences. They do not apply (at least at the present level of sophistication) to Al/Fe^{3+} and $Mg/Fe^{2+}/Mn$ ordering, and an appeal to other criteria must be made. Ghose (1977) has reviewed several factors that may influence ordering in amphiboles:

Ionic size. Ghose (1965) suggested that this factor plays a role in the site-occupancy of the M(4) site. The large [8]-fold site in the monoclinic amphiboles can accept Ca and Na, whereas the smaller [6]-fold site in the orthorhombic amphiboles can accept only Fe^{2+}, Mg and smaller cations. Papike and Ross (1970) suggest that size plays a role in the distribution of tetrahedral Al in gedrites.

Strongly polarizing cations. Strongly polarizing cations like Fe^{2+} tend to form more covalent bonds with oxygen and hence will prefer the M(4) site (Ghose, 1961, 1962). Strongly polarizing cations will tend to avoid each other. In addition, strongly polarizing cations will tend to distort the octahedral sheet and hence will be repelled from the M(1) and M(3) sites, in accord with the fact that in orthopyroxene-cummingtonite assemblages, orthopyroxenes are more Fe^{2+} rich than the coexisting cummingtonite.

Relief of Si-O-Si bond strain. Devore (1957) suggested that tetrahedral Al is more likely to order into the T(1) site, as the occupation of this position by Al causes fewer Si^{4+} cations to share more than two anions with other Si^{4+} cations, hence relieving the Si-O-Si bond strain.

Steric considerations. When M(4) is occupied by Ca or Na, Ghose (1965) proposed that the O(4) atoms recoil away from the M(4) site causing an anticlockwise rotation of the T(2) tetrahedron; substitution of Al into T(1) will cause T(1) to rotate clockwise to compensate for this rotation.

Certain remarks are in order concerning some of the mechanisms proposed above. Firstly, the use of ionic size to forecast site-ordering patterns is of use only in exaggerated cases where gross differences in cation radius (e.g., Ca and Mg) occur. In general, the coordination polyhedron of a cation adjusts to accommodate its constituent cation, and its size is irrelevant to the possible occupancy of other cations with the exception that the normal radius ratio rules will probably apply. With regard to the possible effect of highly polarizing cations, Fe^{2+} does prefer the M(4) site in the Fe-Mg-Mn amphiboles (Ghose, 1961; Finger, 1967, 1969, 1970) and in tremolite (Goldman and Rossman, 1977). However, Mn^{2+} has an even higher preference for the M(4) site (Bancroft *et al.*,

1967b; Hawthorne and Grundy, 1977b) that is not in accord with this mechanism. In addition, if strongly polarizing cations tend to avoid each other, then there should be a lack of clustering of Fe^{2+} cations in the structure. Except for the cummingtonite-grunerite series, this is not in accord with the infrared results of Strens (1966) which indicate significant clustering of Fe^{2+} (and Mg) in holmquistite, glaucophane, riebeckite, tremolite and anthophyllite.

Crystal field stabilization energy

In the free ion or in a spherically-symmetric potential field, the 3d-orbitals are energetically degenerate. Application of a potential field of lower symmetry removes the complete degeneracy of the orbital energy levels as the reducible representation spanned by these orbitals must contain the irreducible representations of the symmetry group. High-spin Fe^{2+} has a d^6 configuration, and thus the lowest energy 3d-orbital is occupied by two electrons. As the average energy of the five orbitals is equal to the energy of the degenerate levels in a corresponding spherically-symmetric crystal field, the difference between this value and the energy of the lowest energy 3d-orbital thus enhances the stability of the undegenerate configuration and is known as the crystal field stabilization energy (C.F.S.E.). Thus, the greater the orbital energy level splitting, the greater the C.F.S.E. term, and hence Fe^{2+} will tend to occupy the site with the largest C.F.S.E. term.

Several studies have attempted to correlate C.F.S.E. with nearest-neighbor configuration on the assumption that the bonded anions reflect the strength and symmetry of the crystal field. According to this argument, increased distortion will produce a greater splitting of the energy levels and enhance the C.F.S.E., providing that the "bond type" is identical in each coordination polyhedron. The agreement is not particularly good; Fe^{2+} is often enriched at the M(1) and M(3) sites as compared with the predicted enrichment at the M(2) site. There are several factors that are pertinent to the use of this criteron. Firstly, the effects of polyhedron distortion on the C.F.S.E. are not well understood. Variation in individual bond lengths *and* variation in bond angles affect the magnitude of the orbital splitting. Some studies have examined the effect of varying bond angles in a simple systematic way (Krishnamurthy

and Schaap, 1970; Garner and Mabbs, 1970) with constant bond length; the relative orbital energy levels are considerably affected by this. The effect of variation in individual bond lengths (with a constant mean bond length) is not well characterized. Thus, deciding which of two irregular pseudo-octahedral coordinations is the more irregular with regard to estimating the larger C.F.S.E. is extremely difficult unless gross differences occur. Another factor that may influence the magnitude of the C.F.S.E. is the effect of next-nearest neighbor ions. This factor has been examined by Jager and Perthel (1967, 1970), who concluded that non-coordination ions have a considerable effect on orbital splitting in an octahedral environment. Thirdly, the C.F.S.E. is dependent on the *local* environment in the crystal, not on the average environment as characterized by crystallographic studies, and this may also significantly affect the orbital splitting (Das, 1965). Thus, using the average configuration of the coordination polyhedra in a structure is not strictly applicable unless that structure is an Fe^{2+} end member.

Ribbe and Gibbs (1971) have suggested that the C.F.S.E. may also be a function of anion type, noting that Dq (a measure of the orbital splitting in an octahedral crystal field) decreases along the spectrochemical series for octahedrally-coordinated $Fe^{2+}X_6$ groups. Consequently, Fe^{2+} will tend to avoid sites coordinated by F, as suggested by the site-populations exhibited by the fluor-richterites(34) and (35). This argument is supported by data for micas (Rosenburg and Foit, 1977) and humites (Ribbe and Gibbs, 1971).

The C.F.S.E. method, as with the Madelung energy and site-potential methods, predicts ordering on the basis of part of the total structure energy, with the assumption that the remainder of the structure energy terms remain constant and thus do not contribute to the ordering process.

General considerations

The ordering pattern assumed by a specific cation can be strongly affected by other cations in the structure. Thus in cummingtonite, Fe^{2+} shows a site-occupancy arrangement M(4) > M(1,2,3). In tirodite, Fe^{2+} shows a site-occupancy arrangement M(1,2,3) > M(4); the presence of Mn^{2+} has strongly affected the ordering pattern of Fe^{2+}. In extreme cases, this effect is automatically acknowledged by the use of separate amphibole names; for example, glaucophane does not show the same Fe^{2+} ordering

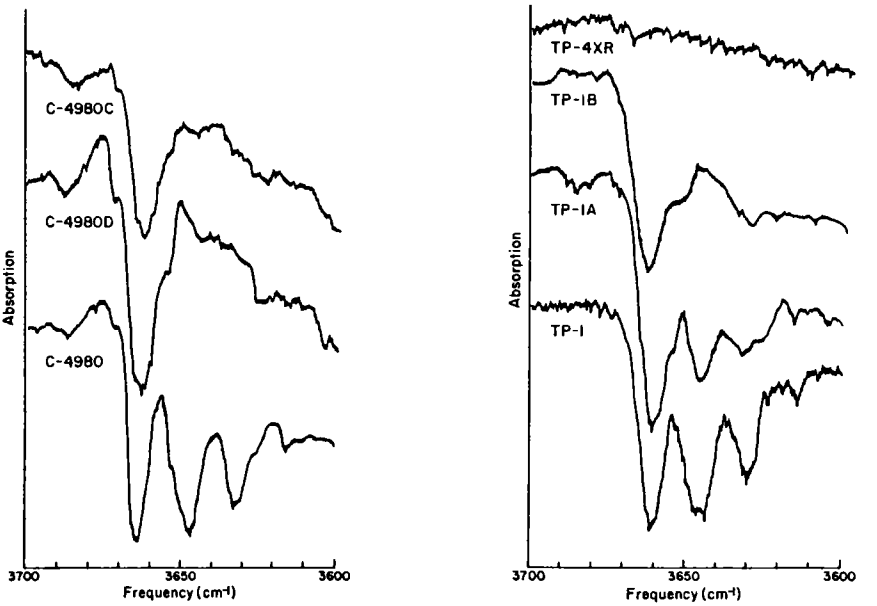

Figure 38. Infrared spectra of natural and heated magnesio-riebeckite (C-4980) and glaucophane (TP-1). From Ernst and Wai (1970). C-4980D and TP-1A were heated at one atmosphere, $fO_2 = 10^{-0.3}$, T = 705°C for one hour; C-4980C and TP-1B were heated at one atmosphere, T = 705°C for 94 hours. TP-4XR was hydrothermally treated at 2 kbar P_{fluid}, $fO_2 \sim 10^{-22}$, T = 513 (±10)°C for 15,667 hours. Note the rapid loss of bands due to configurations involving Fe^{2+}.

pattern as cummingtonite, because the M(2) site is blocked by Al and the M(4) site is blocked by Na. This effect is much more subtle in such cation combinations as (Mg,Fe^{2+},Mn) or (Mg,Fe^{2+},Li), and yet can still have a considerable effect on the Fe^{2+} site-occupancy pattern observed.

OXIDATION-DEHYDROXYLATION IN AMPHIBOLES

The behavior of amphiboles on heating has been the subject of a large number of studies over the past century. Early studies were prompted by the similarity of heated hornblende to "basaltic hornblende," combined with the controversy concerning the origin of the peculiar optical properties of "basaltic hornblende."

Dehydrogenation occurs rapidly at high temperatures in amphiboles that contain Fe^{2+}. Infrared spectra (Fig. 38) show that all OH groups coordinated to Fe^{2+} are lost, with only the [MgMgMg]OH configuration being unaffected by heating (Patterson and O'Connor, 1966; Ernst and Wai, 1970). This provides good evidence for oxidation-dehydroxylation proceeding by the reaction

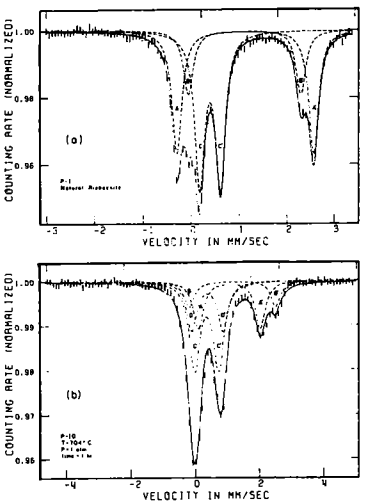

Figure 39. Mössbauer spectra of natural (top) and heat-treated (bottom) riebeckite. From Ernst and Wai (1970).

$$Fe^{2+} + OH \rightarrow Fe^{3+} + O^{2-} + \tfrac{1}{2}H_2$$

as suggested by Barnes (1930). Mössbauer spectra of the heated products indicate that dehydroxylation is accompanied by oxidation, with extra Fe^{3+} doublets in the spectra being assigned to Fe^{3+} at the M(1) and M(3) sites. In crocidolite, there is a 1:1 correlation between the FeO content and the loss of OH from the sample (measured as the sum of the integrated absorbances of the OH bands), indicating that while OH is present, oxidation proceeds by dehydrogenation (Rouxhet *et al.*, 1972). In fibrous grunerite, there is a 3:2 correlation between FeO content and OH content, indicating that dehydrogenation and oxidation occur together (Addision *et al.*, 1962; Hodgson *et al.*, 1965; Ernst and Wai, 1970). Oxidation is accompanied by a loss of tensile strength of the fibers (e.g., Aveston, 1969). Examination of the Mössbauer spectra of natural and heat-treated magnesio-riebeckite (Fig. 39) shows a drastic change in the ratio of Fe at the various sites upon heating, suggesting that considerable cation disorder has also accompanied oxidation. This has been substantiated by structure refinement of natural and heat-treated crystals (Ungaretti, 1980).

HIGH-TEMPERATURE CRYSTAL STRUCTURE STUDIES

Although heating studies on amphiboles have been carried out for several decades, these have been concerned mainly with oxidation-

dehydroxylation relationships. It is only recently that high-temperature crystal structure studies have been carried out on amphiboles. The first studies involved cummingtonite and the possibility of a high-temperature phase transition. Ross *et al.* (1968, 1969) pointed out that cummingtonite $P2_1/m$ (Bown, 1966) is the amphibole analog of pigeonite, suggesting that cummingtonite $P2_1/m$ would invert to a C2/m phase at high temperatures. This was demonstrated by Prewitt *et al.* (1970) who showed that a $P2_1/m \rightarrow C2/m$ transition occurred at ∿45°C for a cummingtonite of composition $(Ca_{0.36}Na_{0.06}Mn_{0.96}Mg_{0.57})Mg_5Si_8O_{22}(OH)_2$. Sueno *et al.* (1972) showed that a tirodite $P2_1/m$ inverted to C2/m symmetry at ∿100°C, and refined the crystal structure of the C2/m phase at 270°C [tirodite(41)]. The high-temperature structure is very similar to that of tirodite(28). Perhaps the most significant aspect of the primitive- to high-cummingtonite transition concerns the degree of kinking of the tetrahedral double chains. At room temperature, the O(5)-O(6)-O(5) angles are 166.2(4) and 178.4(4)° for the B and A chains, respectively. As the temperatures increases, the A chain becomes more kinked and the B chain straightens until they become equivalent at the transition. Sueno *et al.* (1972) suggest that differential expansion of octahedra and tetrahedra is an important factor in this transition. Octahedra expand more rapidly than tetrahedra, and hence increasing temperature affects the structure in the same way as substitution of larger cations into the structure. Perhaps of more significance is the attitude of the chain-bridging anions in the neighborhood of the M(4) site and the relative position of the M(4) cation with respect to the adjacent non-bridging anions. Associated with this is the anomalously low increase in the isotropic temperature factor for the M(4) site cations; Sueno *et al.* (1972) suggest that this results from a decrease in positional disorder at the M(4) site, which offsets the effect of increased thermal vibration.

Other structures that have been refined with high-temperature x-ray data are tremolite(53), fluor-richterite (Cameron *et al.*, 1973a) and potassium-fluor-richterite (Cameron *et al.*, 1973b). These three amphiboles are notable in that they all have the same octahedral strip and tetrahedral chain chemical components. The thermal expansion data for these structures are shown in Figure 40. The a and c dimensions show the largest and smallest mean thermal expansion coefficients, respectively.

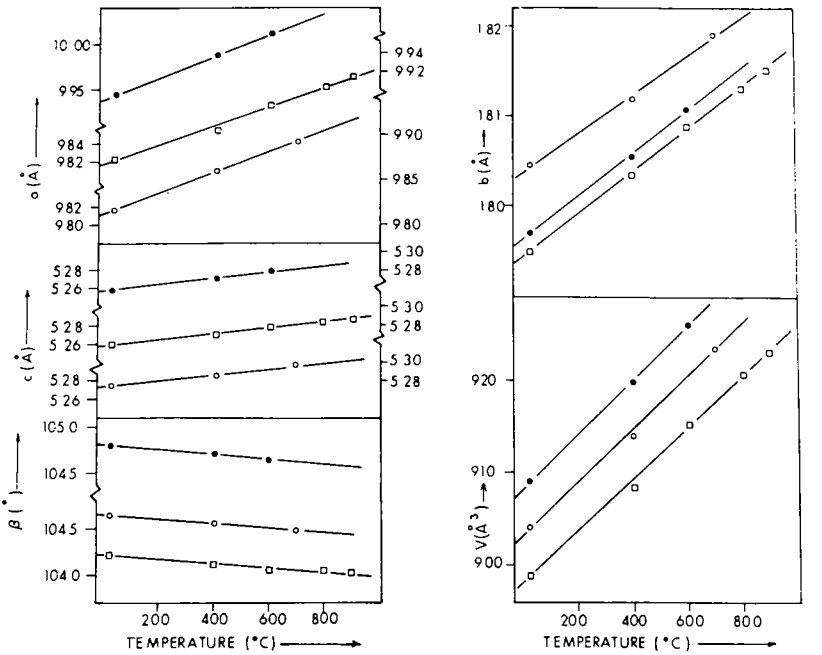

Figure 40. Variation of cell dimensions as a function of temperature for tremolite (O), fluor-richterite (■) and potassium fluor-richterite (●). After Cameron and Papike (1978).

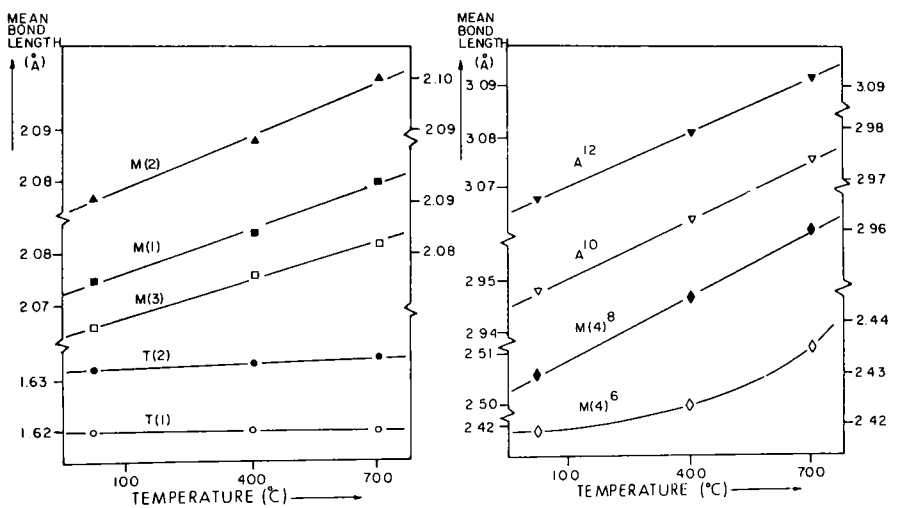

Figure 41. Variation in mean bond lengths as a function of temperature for tremolites (30), (53a) and (53b).

Sueno *et al.* (1973) contrast the thermal expansion behavior of tremolite with that of diopside, where the *b* dimension has the largest mean thermal expansion coefficient; in tremolite(53), the A-site has a large mean thermal expansion coefficient, resulting in the large value of this parameter along *X*. Expansion along *Z* is controlled in part by the straightening of the double chains of relatively inert silicon tetrahedra. The small amount of chain straightening coupled with the negligible increase in size or distortion of the tetrahedra result in a "clamping effect" on expansion of the octahedral strip in the *Z* direction. Similar arguments may be applied to the parallel behavior of the richterites (Fig. 40). The relative displacement of the back-to-back tetrahedral chains strongly affects the anion arrangement about the M(4) site; increasing temperature increases this displacement while increasing M(4) cation size decreases this displacement. Sueno *et al.* (1973) showed that chain displacement is positively correlated with the "coordination coefficient" of M(4), a measure of the dispersion of the M(4)-O distances. Thus, the M(4) cation tends to become more six-coordinated with increasing temperature.

The high-temperature structure refinements for tirodite(41) and tremolite(53a) and (53b) show marked differential polyhedral expansion with increasing temperature, a feature that is also exhibited by the two fluor-richterites (Cameron and Papike, 1979). The silicate tetrahedra are virtually unaffected by increasing temperature with no significant increases in either mean bond length or bond angles. However, the remaining polyhedra show significant increases in mean bond lengths that are linear with temperature (Fig. 41), although bond angles are only slightly changed except where affected by differential polyhedral expansion. Thus with increasing temperature, the octahedral strip module shows considerable thermal expansion as a result of expansion of the individual octahedra, an effect that is not present in the double-chain element. This produces a potential misfit between the two modules that is accommodated by a straightening of the tetrahedral double chain, together with a tilting of the tetrahedra (Fig. 42). The effects involved here are *similar* to those involved in accommodation of the two structure modules with variable chemical composition.

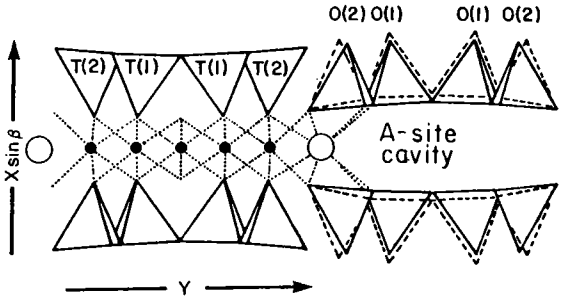

Figure 42. The room temperature structure of tremolite projected down [001]. The dashed lines associated with the tetrahedral chains show their movement (highly exaggerated) with increasing temperature. After Sueno *et al.* (1973).

Figure 43. The variation in $a\sin\beta$ as a function of β for C2/m amphiboles. Modified from Gibbs (1966).

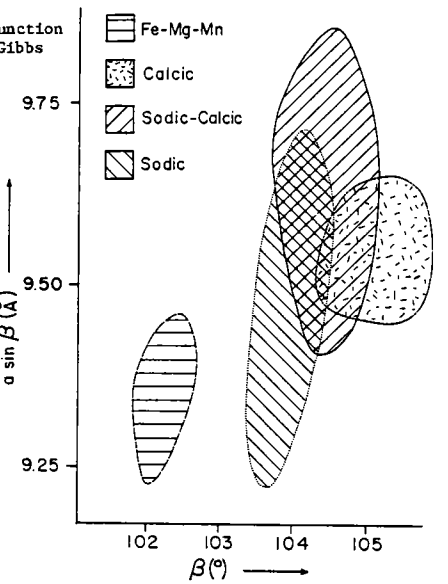

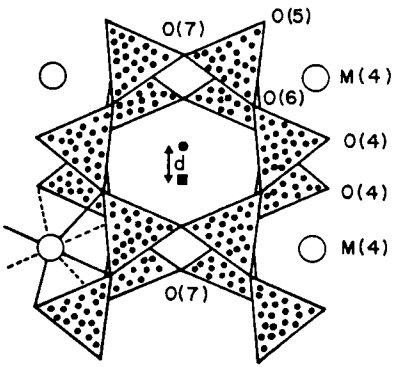

Figure 44. The back-to-back double-chains in the C2/m amphibole structure, showing the centers of the tetrahedral rings (● and ■) and the chain displacement (d) projected onto (100); from Sueno *et al.* (1973).

CELL DIMENSIONS

Variations in cell dimensions of amphiboles show gross correlation with bulk compositional variations. This is well illustrated by the $a\sin\beta$ versus β plot of Figure 43. The amphiboles tend to separate out into fields corresponding to the four principal groups based on M(4) cation occupancy. Hence, M(4) cation type is an important factor affecting the β angle (Whittaker, 1960). This is a result of the interrelationship between the tetrahedral chain displacement and the configuration of the chain-bridging anions around the M(4) site. The tetrahedral chain displacement is defined as the distance between the centers of two opposing six-member rings, projected on to (100) as shown in Figure 44. As is apparent from this figure, increasing this chain displacement increases the length of the M(4)-O(5) bond. The relationships between chain displacement, M(4)-O(5) bond valence and the β-angle are shown in Figure 45. Increased bond valence requirements of O(5) correlate with decreasing chain displacement and increasing β angle.

Considering the amphibole structure as a combination of tetrahedral double chain and octahedral strip, Figure 46 shows the relative contributions of these two modules to the b parameter in the C2/m amphiboles. The chain width is $\sim 9.0 \pm 0.11$ Å, wider chains being associated with Al^{IV}-rich amphiboles. The octahedral strip width shows a much greater variation (8.6-9.5 Å) that correlates strongly with the b parameter. As the width of the octahedral strip is a function of the mean ionic radius of the C-type cations, this is the main control on the b parameter.

There have been several studies concerned with cell parameter variation as a function of amphibole composition; these are summarized in Table 25.

CONCLUSIONS AND SUGGESTIONS FOR FUTURE WORK

The structures of most amphiboles have now been refined, and the general outlines of amphibole crystal chemistry are in place. There is much interesting work to be done concerning cation ordering as a function of crystal composition (to say nothing of T, fO_2 and P), work that is fairly tractable with current experimental techniques. Of some importance is the role of monovalent anions (OH+F+Cl) in the structure: Is

Table 25. Studies (post 1960) Concerning Cell-Dimension Variations in Amphiboles

Composition	Reference
Anthophyllites	Finger (1967)
Fe-Mg orthoamphiboles	Popp et al. (1976)
Fe-Mg-Mn clinoamphiboles	Klein (1964)
	Viswanathan and Ghose (1965)
	Finger (1967)
Edenite...potassium-edenite	Hinrichsen and Schurmann (1977)
Pargasite...potassium-pargasite	Hinrichsen and Schurmann (1977)
Pargasite...ferro-pargasite	Charles (1980)
Natural hornblendes	Wenk (1971)
Pargasite...richterite	Braue and Seck (1977)
Richterite...potassium-richterite	Huebner and Papike (1970)
Richterite...ferro-richterite	Charles (1974a,b)
Glaucophane...riebeckite	Borg (1967b)
Magnesio-riebeckite...ferro-glaucophane	Borg (1967b)
Arfvedsonite...eckermannite	Kempe (1969)
All amphiboles	Colville et al. (1966)

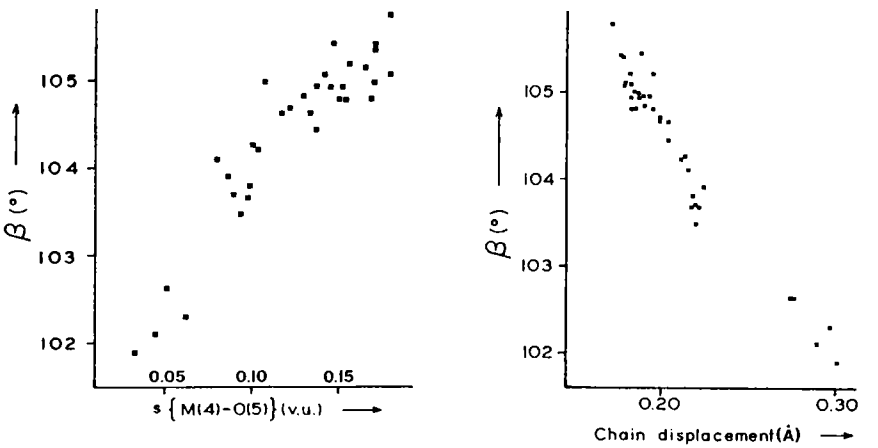

Figure 45. The variation in β-angle as a function of M(4)-O(5) bond-valence (left) and tetrahedral chain displacement (right) for a selection of C2/m amphiboles.

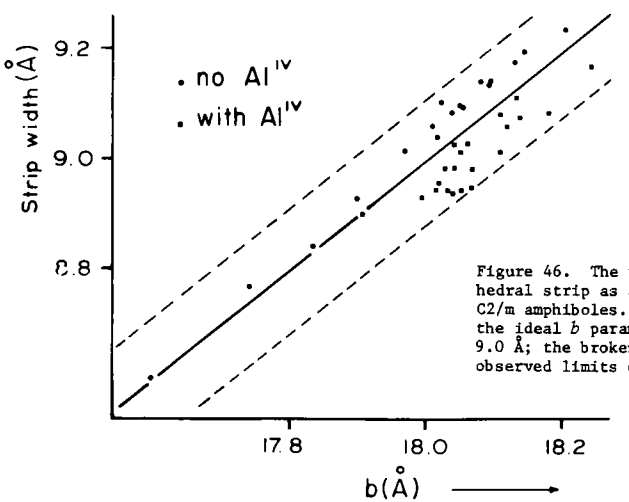

Figure 46. The variation in width of the octahedral strip as a function of the *b* parameter in C2/m amphiboles. The heavy central line denotes the ideal *b* parameter for a tetrahedral chain of 9.0 Å; the broken lines denote the maximum observed limits of variation in chain width.

O(3) completely occupied by (OH+F+Cl) upon *crystallization* (with all O^{2-} occupancy of O(3) caused by post-crystallization oxidation-dehydroxylation), or does the amphibole structure during crystallization admit chemical substitutions of the form

$$M^{n+} + (OH,F)^{-} \rightleftarrows M^{(n+1)+} + O^{2-} \ ?$$

Whether or not such substitutions are possible and evaluation of their importance in natural amphiboles is one remaining major uncertainty in amphibole chemistry.

The following topics are of particular interest:

(i) systematic characterization of Mg/Fe^{2+} cation ordering along pseudo-binary joins;

(ii) characterization of minor element (Mn^{2+},Cr^{3+},Ti^{3+},Ti^{4+}) ordering, particularly Mn^{2+} in calcic amphiboles;

(iii) neutron structure refinement and infrared spectroscopic examination of amphibole with definite "excess H_2O";

(iv) characterization and comparison of cation ordering patterns in associated ferromagnesian minerals (pyroxenes, amphiboles, micas) from natural assemblages.

ACKNOWLEDGMENTS

I thank David R. Veblen, Johns Hopkins University, for his comments on this manuscript. Financial support was provided by a research fellowship and grant to the author from the Natural Sciences and Engineering Research Council of Canada.

TABLE A-1. CRYSTAL STRUCTURE REFINEMENTS OF AMPHIBOLES

EARLY STRUCTURE DATA

(1)	Tremolite	Warren (1929)
[2]	Anthophyllite	Warren and Modell (1930)
(3)	Magnesio-riebeckite	Whittaker (1949)
[4]	Anthophyllite	Ito and Morimoto (1951)
(5)	Magnesio-hornblende	Zussman (1955)
(6)	Pargasitic hornblende	Heritsch et al. (1957)
(7)	Edenitic hornblende	Heritsch et al. (1957)
(8)	Tremolite	Zussman (1959)
(9)	Cummingtonite	Ghose and Hellner (1959)
(10)	Tschermakitic hornblende	Heritsch and Kahler (1960)
(11)	Alumino-pargasitic hornblende	Heritsch and Kahler (1960)
(12)	Potassian titanian magnesio-hastingsite	Heritsch and Riechert (1960)
(13)	Potassian titanian magnesio-hastingsite	Heritsch et al. (1960)
(14)	Potassian arfvedsonite	Kawahara (1963)
(15)	$Na_2H_2Co_5Si_8O_{22}(OH)_2$	Prewitt (1963), Gibbs and Prewitt (1968)
(16)	$Na_2H_2Mg_5Si_8O_{22}F_2$	Prewitt (1963), Gibbs and Prewitt (1968)
(17)	Riebeckite	Colville and Gibbs (1964)
[18]	Anthophyllite	Lindeman (1964)
(19)	Pargasitic hornblende	Trojer and Walitzi (1965)

MODERN ORTHORHOMBIC (Pnma) STRUCTURES

[23]	Anthophyllite	Finger (1967, 1970)
[31]	Holmquistite	Whittaker (1969), Irusteta and Whittaker (1975)
[32]	Gedrite	Papike and Ross (1970)
[33]	Gedrite	Papike and Ross (1970)
[47]	Holmquistite	Litvin et al. (1973a)

MODERN VARIETIES

[20]	Protoamphibole	Gibbs et al. (1960); Gibbs (1962, 1964, 1969)
(25)	Joesmithite	Moore (1968b, 1969)
(27)	Tirodite $P2_1/m$	Papike et al. (1968, 1969)

MODERN MONOCLINIC (C2/m) STRUCTURES

(21)	Cummingtonite	Ghose (1961); Fischer (1966); Mitchell et al. (1971)
(22)	Grunerite	Finger (1967, 1969); Finger and Zoltai (1967)
(24)	Potassian titanian magnesio-hastingsite	Papike and Clark (1967); Papike et al. (1969); Robinson (1971); Robinson et al. (1973)
(26)	Glaucophane	Papike and Clark (1968)
(28)	Tirodite	Papike et al. (1969)
(29)	Potassium-magnesio-katophorite	Papike et al. (1969); Cameron (1970)
(30)	Tremolite	Papike et al. (1969)

MODERN MONOCLINIC (C2/m) STRUCTURES, continued

(34)	Fluor-richterite	Cameron (1970); Cameron and Gibbs (1971)
(35)	Fluor-richterite	Cameron (1970); Cameron and Gibbs (1971)
(36)	Fluor-tremolite	Cameron (1970); Cameron and Gibbs (1973)
(37)	Manganoan ferro-actinolite	Mitchell et al. (1971)
(38)	Potassian pargasite	Robinson et al. (1970,1973); Robinson (1971)
(39)	Potassian titanian pargasite	Robinson (1971); Robinson et al. (1973)
(40)	Potassian oxy-kaersutite	Kitamura and Tokonami (1971); Kitamura et al. (1975)
(41)	Tirodite	Sueno et al. (1972)
(42)	Magnesio-hornblende	Litvin et al. (1971)
(43)	Tremolite	Litvin et al. (1972a); Litvin (1973)
(44)	Hastingsite	Litvin et al. (1972a); Litvin (1973)
(45)	Magnesio-hornblende	Litvin et al. (1971a, 1972b); Litvin (1973)
(46)	Magnesio-hornblende	Litvin et al. (1972b); Litvin (1973)
(48)	Tschermakite	Litvin (1973)
(49)	Ferro-tschermakitic hornblende	Litvin et al. (1973b)
(50)	Tschermakitic hornblende	Litvin et al. (1973b)
(51)	Potassian ferri-taramite	Litvin et al. (1973c)
(52)	Potassian ferri-tschermakitic hornblende	Kawahara et al. (1972)
(53)	Tremolite	Sueno et al. (1972b, 1973)
(54)	Ferro-tschermakite	Hawthorne (1973); Hawthorne and Grundy (1973a)
(55)	Potassian oxy-kaersutite	Hawthorne (1973); Hawthorne and Grundy (1973b)
(56)	Tremolite	Hawthorne (1973); Hawthorne and Grundy (1976)
(57)	Zincian tirodite	Hawthorne (1973); Hawthorne and Grundy (1973c,1977b)
(58)	Subsilic titanian magnesian hastingsite	Hawthorne (1973); Hawthorne and Grundy (1977a)
(59)	Potassian ferri-taramite	Hawthorne (1973); Hawthorne and Grundy (1978)
(60)	Potassian tschermakite	Litvin et al. (1974a)
(61)	Pargasite	Litvin et al. (1974b)
(62)	Sodian fluor-clinoholmquistite	Litvin et al. (1975a)
(63)	Pargasitic hornblende	Litvin et al. (1975b)
(64)	Arfvedsonite	Litvin et al. (1976)
(65)	Potassium-arfvedsonite	Litvin et al. (1976)
(66)	Potassium-arfvedsonite	Litvin et al. (1976)
(67)	Potassium-arfvedsonite	Hawthorne (1976)
(68)	Fluor-riebeckite	Hawthorne (1978b)
(69)	Ferro-glaucophane	Hawthorne (1979)
(70)	Pargasitic hornblende	Bocchio et al. (1978)
(71)	Pargasite	Bocchio et al. (1978)
(72)	Magnesio-hastingsite	Bocchio et al. (1978)
(73)	Ferroan pargasitic hornblende	Hawthorne et al. (1980)
(74)	.....	Ungaretti et al. (1978, 1981), Ungaretti (1980)

Addison, C. C., Addison, W. E., Neal, G. H. and Sharp, J. H. (1962) Amphiboles. Part I. The oxidation of crocidolite. J. Chem. Soc. 1962, 1468-1471.

Addison, W. E. and White, A. D. (1968) Spectroscopic evidence for the siting of lithium ions in a riebeckite. Mineral. Mag. 36, 743-745.

Appleyard, E. C. (1975) Silica-poor hastingsitic amphiboles from the metasomatic alkaline gneisses at Wolfe, Eastern Ontario. Canadian Mineral. 13, 342-351.

Aveston, J. (1969) Mechanical properties of asbestos. J. Mater. Sci. 4, 625-633.

Bancroft, G. M. and Burns, R. G. (1969) Mössbauer and absorption spectral study of alkali amphiboles. Mineral. Soc. Amer. Spec. Paper 2, 137-148.

———, ———, and Maddock, A. G. (1967a) Determination of the cation distribution in the cummingtonite-grunerite series by Mössbauer spectroscopy. Amer. Mineral. 52, 1009-1026.

_____ , Maddock, A. G. and Burns, R. G. (1967b) Applications of the Mössbauer effect to silicate mineralogy - I. Iron silicates of known crystal structure. Geochim. Cosmochim. Acta 31, 2219-2246.

Barnes, V. E. (1930) Changes in hornblende at about 800°C. Amer. Mineral. 15, 393-417.

Baur, W. H. (1970) Bond length variation and distorted coordination polyhedra in inorganic crystals. Amer. Crystallogr. Assoc. Trans. 6, 129-155.

_____ (1971) The prediction of bond-length variations in silicon-oxygen bonds. Amer. Mineral. 56, 1573-1599.

_____ (1974) The geometry of polyhedral distortions. Predictive relationships for the phosphate group. Acta Crystallogr. B30, 1195-1215.

_____ (1978) Variation of mean Si-O bond lengths in silicon-oxygen tetrahedra. Acta Crystallogr. B34, 1751-1756.

Bent, H. A. (1968) Tangent-sphere models of molecules. VI. Ion-packing models of covalent compounds. J. Chem. Ed. 45, 768-777.

Bershov, L. V., Marfunin, A. S. and Mineyeva, R. M. (1966) Electron paramagnetic resonance of Mn^{2+} in tremolite. Geochem. Intern. 1966, 352-355.

Binns, R. A. (1965) The mineralogy of metamorphosed basic rocks from the Willyama complex, Broken Hill district, New South Wales, Part I. Hornblendes. Mineral. Mag. 35, 306-326.

Bocchio, R., Ungaretti, L. and Rossi, G. (1978) Crystal chemical study of eclogitic amphiboles from Alpe Arami, Lepontine Alps, Southern Switzerland. Rend. Soc. Ital. Mineral. Petr. 34, 453-470.

Borg, I. Y. (1967a) On conventional calculations of amphibole formulae from chemical analyses with inaccurate $H_2O(+)$ and F determinations. Mineral. Mag. 36, 583-590.

_____ (1967b) Optical properties and cell parameters in the glaucophane-riebeckite series. Contrib. Mineral. Petrol. 15, 67-92.

Borley, G. D. (1963) Amphiboles from the younger granites of Nigeria. Part I. Chemical classification. Mineral. Mag. 33, 358-376.

Bowen, N. L. and Schairer, J. F. (1935) Grunerite from Rockport, Mass., and a series of synthetic fluor-amphiboles. Amer. Mineral. 20, 543-552.

Bown, G. M. (1966) A new amphibole polymorph in intergrowth with tremolite: clino-anthophyllite? (abstr.). Amer. Mineral. 51, 259-260.

Bragg, W. H. (1924) *X-rays and Crystal Structure*. G. Bell & Sons, London.

Bragg, W. L. (1926) Interatomic distances in crystals. Phil. Mag. 2, 258-266.

_____ and West, J. (1927) Structure of certain silicates. Proc. Roy. Soc. London 114A, 450-473.

Braue, W. and Seck, H. A. (1977) Stability of pargasite-richterite solid solutions at 1 kb water vapour pressure. Neues Jahrbuch Mineral. Abh. 130, 19-32.

Brown, G. E., and Gibbs, G. V. (1969) Oxygen coordination and the Si-O bond. Amer. Mineral 54, 1528-1539.

_____ and _____ (1970) Stereochemistry and ordering in the tetrahedral portion of silicates. Amer. Mineral. 55, 1587-1607.

_____, _____ and Ribbe, P. H. (1969) The nature and the variation in length of the Si-O and Al-O bonds in framework silicates. Amer. Mineral. 54, 1044-1061.

Brown, I. D. and Shannon, R. D. (1973) Empirical bond length-bond strength curves for oxides. Acta Crystallogr. A29, 266-282.

_____ and Wu, K. K. (1976) Empirical parameters for calculating cation-oxygen bond valences. Acta Crystallogr. B32, 1957-1959.

_____ (1978) Bond valences - a simple structural model for inorganic chemistry. Chem. Soc. Rev. 7, 359-376.

Bunch, T. E. and Okrusch, M. (1973) Al-rich pargasite. Amer. Mineral. 58, 721-726.

Burnham, C. W., Clark, J. R., Papike, J. J. and Prewitt, C. T. (1967) A proposed crystallographic nomenclature for clinopyroxene structures. Z. Kristallogr. 125, 1-6.

Burns, R. G. and Strens, R. G. J. (1966) Infrared study of the hydroxyl bands in clinoamphiboles. Science 153, 890-892.

Cameron, K. L. (1975) An experimental study of the actinolite-cummingtonite phase relations with notes on the synthesis of Fe-rich anthophyllite. Amer. Mineral. 60, 375-391.

Cameron, M. (1970) *The Crystal Chemistry of Tremolite and Richterite. A Study of Selected Anion and Cation Substitutions.* Ph.D. Dissertation, Virginia Polytechnic Institute and State University, Blacksburg, VA.

_____ and Gibbs, G. V. (1971) Refinement of the crystal structure of two synthetic fluor-richterites. Carnegie Inst. Wash. Yearbook 70, 150-153.

_____ and _____ (1973) The crystal structure and bonding of fluor-tremolite: a comparison with hydroxyl tremolite. Amer. Mineral. 58, 878-888.

_____, Sueno, S., Prewitt, C. T. and Papike, J. J. (1973a) High-temperature crystal chemistry of K-fluor-richterite (abstr.). Trans. Amer. Geophys. Union 54, 497-498.

_____, _____, _____ and _____ (1973b) High-temperature crystal chemistry of Na-fluor-richterite (abstr.). Trans. Amer. Geophys. Union 54, 1230.

_____ and Papike, J. J. (1979) Amphibole crystal chemistry: a review: Fortschr. Mineral. 57, 28-67.

Charles, R. W. (1974a) Physical properties of synthetic richterites. Carnegie Inst. Wash. Yearbook 73, 510-513.

_____ (1974b) The physical properties of the Mg-Fe richterites. Amer. Mineral 59, 518-528.

_____ (1980) Amphiboles on the join pargasite-ferropargasite. Amer. Mineral 65, 996-1001.

Chigareva, O. G., Grum-Grzhimailo, S. V. and Fedoseev, A. D. (1969) Spectrophotometric study of synthetic fibrous fluor-amphiboles. Zap. Vses. Mineral. Obschchest. 98, 96-101.

Colville, A. A. and Gibbs, G. V. (1964) Refinement of crystal structure of riebeckite (abstr.). Geol. Soc. Amer. Spec. Paper 82, 31.

Colville, P. A., Ernst, W. G. and Gilbert, M. C. (1966) Relationships between cell parameters and chemical compositions of monoclinic amphiboles. Amer. Mineral. 51, 1727-1754.

Comeforo, J. E. and Kohn, J. A. (1954) Synthetic asbestos investigations, I: Study of synthetic fluor-tremolite. Amer. Mineral. 39, 537-548.

Cruickshank, D. W. J. (1961) The role of 3d-orbitals in π-bonds between (A) silicon, phosphorus, sulphur or chlorine and (B) oxygen or nitrogen. J. Chem. Soc. 1077, 5486-5504.

Das, T. P. (1965) Theory of crystalline fields of iron-group ions in solid solutions. Phys. Rev. 140, A1957-A1965.

Deer, W. A., Howie, R. A. and Zussman, J. (1963) *Rock-Forming Minerals. Vol. 2, Chain Silicates.* Longmans, Green and Co., London.

Devore, G. W. (1957) The association of strongly polarizing cations with weakly polarizing cations as a major influence in element distribution, mineral composition, and crystal growth. J. Geol. 65, 178-195.

Dobretsov, N. L., Kostyuk, Yu. A., Lavrent'yev, Yu.G., Ponomareva, L. G., Pospelova, L. N. and Sobolev, V. S. (1971) Immiscibility in the sodium-calcium amphibole series and its classification. Dokl. Akad. Nauk. SSSR 199, 677-680.

Dollase, W. A. and Gustafson, W. I. (1977) Mössbauer spectral analysis of mixed-valence clinopyroxenes. Geol. Soc. Amer. Abstr. with Prog. 9, 951-952.

Dowty, E. and Lindsley, D. H. (1973) Mössbauer spectra of synthetic hedenbergite-ferrosilite pyroxenes. Amer. Mineral 58, 850-868.

Engel, A. E. J. and Engel, C. E. (1962) Hornblendes formed during progressive metamorphism of amphibolites. Northwest Adirondack Mountain, New York. Geol. Soc. Amer. Bull 73, 1499-1515.

Ernst, W. G. (1979) Coexisting sodic and calcic amphiboles from high-pressure metamorphic belts and the stability of barroisitic amphibole. Mineral. Mag. 43, 269-278.

_____ and Wai, C. M. (1970) Infrared, X-ray and optical study of cation ordering and dehyrogenation in natural and heat-treated sodic amphiboles. Amer. Mineral. 55, 1226-1258.

Fedoseev, A. D., Makarova, T. A., Nesterchuk, N. I. and Sipovskii, D. P. (1968) Hydrothermal synthesis of fibrous amphiboles and study of some of their properties. Krist. Tech. 3, 95-100.

Finger, L. W. (1967) *The Crystal Structures and Crystal Chemistry of Ferromagnesian Amphiboles.* Ph.D. Thesis, University of Minnesota, Minneapolis, Minnesota.

_____ (1969) The crystal structure and cation distribution of a grunerite. Mineral. Soc. Amer. Spec. Paper 2, 95-100.

_____ (1970) Refinement of the crystal structure of an anthophyllite. Carnegie Inst. Wash. Yearbook 68, 283-288.

Fischer, K. F. (1966) A further refinement of the crystal structure of cummingtonite, $(Mg,Fe)_7(Si_8O_{22})(OH)_2$. Amer. Mineral. 51, 814-818.

Fominykh, V. G. (1974) Fluorine and chlorine in the coexisting apatites and amphiboles in the rocks and ores of the titanomagnetite deposits of the Urals. Geochem. Int. 1974, 354-356.

Garner, C. D. and Mabbs, F. E. (1970) Studies in eight-co-ordination. Part I. Crystal-field energies in the D_{2d} point-group. J. Chem. Soc. 1970A, 1711-1716.

Geijer, P. (1959) The distribution of halogens in skarn amphiboles in central Sweden. Arkiv. Min. Geol. 2, 481-503.

Ghose, S. (1961) The crystal structure of cummingtonite. Acta Crystallogr. 14, 622-627.

_____ (1962) The nature of Mg^{2+}-Fe^{2+} distribution in some ferromagnesian silicate minerals. Amer. Mineral. 47, 388-394.

_____ (1965) A scheme of cation distribution in the amphiboles. Mineral. Mag. 35, 46-54.

_____ (1977) Cation distribution and subsolidus phase relations in amphiboles: A review. Ind. J. Earth Sci. 1977, 171-185.

_____ and Hellner, E. (1959) The crystal structure of grunerite and observations on the Mg-Fe distribution. J. Geol. 67, 691-701.

_____ and Weidner, J. R. (1972) Mg^{2+}-Fe^{2+} order-disorder in cummingtonite, $(Mg,Fe)_7(Si_8O_{22})(OH)_2$: a new geothermometer. Earth Planet. Sci. Lett. 16, 346-354.

Gibbs, G. V. (1962) *The Crystal Structure of Protoamphibole.* Ph.D. Dissertation. The Pennsylvania State University, University Park, PA.

_____ (1964) Crystal structure of protoamphibole (abstr.). Geol. Soc. Amer. Spec. Paper 82, 71.

_____ (1966) Untitled article. In *AGI Short Course Lecture Notes on Chain Silicates,* 1-23.

_____ (1969) The crystal structure of protoamphibole. Mineral. Soc. Amer. Spec. Paper 2, 101-110.

_____ and Prewitt, C. T. (1968) Amphibole cation site disorder (abstr.). Int. Mineral. Assoc. Pap. Proc. 5th Gen. Meet., Mineral. Soc. London, 334-335.

_____, Bloss, F. D. and Shell, H. R. (1960) Protoamphibole, a new polytype. Amer. Mineral. 45, 974-989.

_____, Hamil, M. M., Louisnathan, S. J., Bartell, L. S. and Yow, H. (1972) Correlation between Si-O bond length, Si-O-Si angle and bond overlap populations calculated using extended Huckel molecular orbital theory. Amer. Mineral. 57, 1578-1613.

Gillberg, M. (1959) A lead-bearing variety of pargasite from Langban, Sweden. Arkiv. Mineral. Geol. 34, 425-430.

Gillespie, R. J. and Robinson, E. A. (1963) The sulphur-oxygen bond in sulphuryl and thionyl compounds. Correlation of stretching frequencies and force constants with bond lengths, bond angles, and bond orders. Canadian J. Chem. 41, 2074-2085.

_____ and _____ (1964) Characteristic vibrational frequencies of compounds containing Si-O-Si, P-O-P, and Cl-O-Cl bridging groups. Canadian J. Chem. 42, 2496-2503.

Ginzburg, I. V. (1965) Holmquistite and its structural variety clinoholmquistite. Trudy. Mineral. Muz. Akad. Nauk. SSSR 16, 73-89.

Goldman, D. A. (1977) *Crystal-field and Mössbauer Applications to the Study of Site Distribution and Electronic Properties of Ferrous Iron in Minerals with Emphasis on Calcic Amphiboles, Orthopyroxene and Cordierite.* Ph.D. Dissertation, California Institute of Technology, Pasadena, CA.

_____ and Rossman, G. R. (1977) The identification of Fe^{2+} in the M(4) site of calcic amphiboles. Amer. Mineral. 62, 205-216.

Grebenshchikov, R. G., Romanov, D. P., Sipovskii, D. P. and Kosulina, G. I. (1974) Structure of a germanate hydroxyamphibole. Zhur. Prikl. Khimii 47, 1905-1910.

Hafner, S. S. and Ghose, S. (1971) Iron and magnesium distribution in cummingtonites, $(Fe,Mg)_7Si_8O_{22}(OH)_2$. Z. Kristallogr. 133, 301-326.

_____ and Huckenholz, H. G. (1971) Mössbauer spectrum of synthetic ferridiopside. Nature 233, 9-11.

Hanisch, K. (1966) Messung des Ultrarot-Pleochroismus von Mineralen. VI. Der Pleochroismus der OH-Streckfrequenz in Riebeckit. Neues Jahrb. Mineral. Monatsch. 1966, 109-112.

Hawthorne, F. C. (1973) *The Crystal Chemistry of the Clinoamphiboles.* Ph.D. Dissertation, McMaster University, Hamilton, Ontario.

_____ (1976) The crystal chemistry of the amphiboles. V. The structure and chemistry of arfvedsonite. Canadian Mineral. 14, 346-356.

_____ (1978a) The crystal chemistry of the amphiboles. VI. The stereochemistry of the octahedral strip. Canadian Mineral. 16, 37-52.

_____ (1978b) The crystal chemistry of the amphiboles. VIII. The crystal structure and site chemistry of fluor-riebeckite. Canadian Mineral. 16, 187-194.

_____ (1978c) The crystal chemistry of the amphiboles. IX. Polyvalent-cation ordering in clinoamphiboles. Canadian Mineral. 16, 521-525.

_____ (1979) The crystal chemistry of the amphiboles. X. Refinement of the crystal structure of ferroglaucophane and an ideal polyhedral model for clinoamphiboles. Canadian Mineral. 17, 1-10.

_____ (1981) The quantitative characterization of cation ordering in minerals. A review. Amer. Mineral. (submitted).

_____ (1982) The crystal chemistry of the amphiboles: a review. Canadian Mineral. (submitted).

_____ and Grundy, H. D. (1972) Positional disorder in the A-site of clinoamphiboles. Nature 235, 72-73.

_____ and _____ (1973a) The crystal chemistry of the amphiboles I. Refinement of the crystal structure of ferrotschermakite. Mineral. Mag. 39, 36-48.

_____ and _____ (1973b) The crystal chemistry of the amphiboles. II. Refinement of the crystal structure of oxy-kaersutite. Mineral. Mag. 39, 390-400.

_____ and _____ (1973c) The crystal structure and site chemistry of a zinc manganese cummingtonite by least-squares refinement of single crystal X-ray and Mössbauer data (abstr.). Amer. Mineral. 58, 1103.

_____ and _____ (1976) The crystal chemistry of the amphiboles. IV. X-ray and neutron refinements of the crystal structure of tremolite. Canadian Mineral. 14, 334-345.

_____ and _____ (1977a) The crystal chemistry of the amphiboles. III. Refinement of the crystal structure of a sub-silicic hastingsite. Mineral. Mag. 41, 43-50.

_____ and _____ (1977b) The crystal structure and site-chemistry of a zincian tirodite by least-squares refinement of X-ray and Mössbauer data. Canadian Mineral. 15, 309-320.

_____ and _____ (1978) The crystal chemistry of the amphiboles. VII. The crystal structure and site-chemistry of potassian ferri-taramite. Canadian Mineral. 16, 53-62.

_____, Griep, J. L. and Curtis ,L. (1980) A three-amphibole assemblage from the Tallan Lake Sill, Peterborough County, Ontario. Canadian Mineral. 18, 275-284.

Heritsch, H. and Kahler, E. (1960) Strukturuntersuchung an zwei Kluftkarinthinen, ein Beitrag zur Karinthinfrage. Tscher. Mineral. Petrog. Mitt. 7, 218-234.

_____ and Riechert, L. (1960) Strukturuntersuchung an einer basaltischen Hornblende von Cernosin, CSR. Tscher. Mineral. Petrog. Mitt. 7, 235-245.

_____, Bertoldi, G. and Walitzi, E. M. (1960) Strukturuntersuchung in einer basaltischen Hornblende von Kuruzzenkogel, sudlich Fehring, Steirmark. Tscher. Mineral. Petrog. Mitt. 7, 210-217.

_____, Paulitsch, P. and Walitzi., E. M. (1957) Die Struktur von Karinthin und einer barroisitschen Hornblende. Tscher. Mineral. Petrog. Mitt. 6, 215-225.

Himmelberg, G. R. and Papike, J. J. (1969) Coexisting amphiboles from blueschist facies metamorphic rocks. J. Petrol. 10, 102-114.

Hinrichsen, Th. and Schürmann, K. (1977) Experimental investigations on the Na/K substitution in edenites and pargasites. Neues Jahrb. Mineral. Abh. 130, 12-13.

Hodgeson, A. A., Freeman, A. G. and Taylor, H. F. W. (1965) The thermal decomposition of crocidolite from Koegas, South Africa. Mineral. Mag. 35, 5-30.

Huebner, J. S. and Papike, J. J. (1970) Synthesis and crystal chemistry of sodium-potassium richterite, $(Na,K)NaCaMg_5Si_8O_{22}(OH,F)_2$: a model for amphiboles. Amer. Mineral. 55, 1973-1992.

Irusteta, M. C. and Whittaker, E. J. W. (1975) A three-dimensional refinement of the structure of holmquisite. Acta Crystallogr. B31, 145-150.

Ito, T. and Morimoto, N. (1951) Anthophyllite. In *X-ray Studies on Polymorphism*. Maruzen Co. Ltd., Tokyo, 42-49.

Jager, E. and Perthel, R. (1967) The crystal field theory of spinel lattices. Phys. Stat. Sol. 20, 433-441.

_____ and _____ (1970) About the crystal field theory of tetrahedral sites in spinel lattices. Phys. Stat. Sol. 38, 735-746.

Katagas, C. (1974) Alkali amphiboles intermediate in composition between actinolite and riebeckite. Contrib. Mineral. Petrol. 46, 257-264.

Kawahara, A. (1963) X-ray studies on some alkaline amphiboles. Mineral.J. (Japan) 4, 30-40.

_____, Ohno, M. and Takano, Y. (1972) Structural study of the amphibole in volcanic tuff. Sci. Paper Col. Gen. Educ. Univ. Tokyo 22, 67-78.

Kempe, D. R. C. (1969) The cell parameters of the arfvedsonite-eckermannite series, with observations on the MgO and total iron content of amphiboles. Mineral. Mag. 37, 317-332.

Kisch, H. J. (1969) Magnesiocummingtonite - $P2_1/m$: a Ca- and Mn-poor clinoamphibole from New South Wales. Contrib. Mineral. Petrol. 21, 319-331.

Kitamura, M. and Tokonami, M. (1971) The crystal structure of kaersutite. Sci. Rep. Tohoku Univ. Ser. 3, 11, 125-141.

_____, _____ and Morimoto, N. (1975) Distribution of titanium atoms in oxy-kaersutite. Contrib. Mineral. Petrol. 51, 167-172.

Klein, C., Jr. (1964) Cummingtonite-grunerite series: a chemical, optical and X-ray study. Amer. Mineral. 49, 963-982.

_____ (1968) Coexisting amphiboles. J. Petrol. 9, 281-330.

_____ (1969) Two-amphibole assemblages in the system actinolite-hornblende-glaucophane. Amer. Mineral. 54, 212-237.

_____ and Ito, J. (1968) Zincian and manganoan amphiboles from Franklin, New Jersey. Amer. Mineral. 53, 1264-1275.

Knorring, O. von and Hornung, G. (1961) On the lithium amphibole holmquisite, from Benson pegmatite mine, Mtoko, Southern Rhodesia. Mineral. Mag. 32, 731-735.

Kohn, J. A. and Comeforo, J. E. (1955) Synthetic asbestos investigations, II: X-ray and other data on synthetic fluor-richterite, -edenite, and -boron edenite. Amer. Mineral. 40, 410-421.

Krishnamurty, R. and Schaap, W. B. (1970) Computing ligand field potentials and relative energies of d orbitals. J. Chem. Ed. 47, 433-446.

Kunitz, W. (1930) Die Isomorphieverhoiltnisse in der Hornblende-gruppe. Neues Jahrb. Mineral. Abh. 60, 171-250.

Law, A. D. (1973) Critical evaluation of 'statistical best fits' to Mössbauer spectra. Amer. Mineral. 58, 128-131.

Leake, B. E. (1968) A catalogue of analyzed calciferous and subcalciferous amphiboles together with their nomenclature and associated minerals. Geol. Soc. Amer. Spec. Paper 98.

_____ (1978) Nomenclature of amphiboles. Canadian Mineral. 16, 501-520.

Leelanandam, C. (1969a) Electron microprobe analyses of chlorine in hornblendes and biotites from the charnockitic rocks of Kondapalli, India. Mineral. Mag. 37, 362-365.

_____ (1969b) Fluorine and chlorine in the charnockitic hornblendes and biotites from the charnockitic rocks of Kondapalli, India. Mineral. Mag. 37, 362-365.

_____ (1969b) Fluorine and chlorine in the charnockitic hornblendes from Kondapalli, India. Neues Jahrb. Mineral. Monatsh. 8, 379-383.

Lindeman, W. (1964) Beitrag zur Struktur des Anthophyllits (abstr.). Forts. Mineral. 42, 205.

Litvin, A. L. (1966) Factors regulating isomorphous substitution in the calcian amphibole group. Mineral. Sb. 20, 437-440.

_____ (1973) *Calcic Amphiboles (Structure, Cation Distribution, Unit Cell Dimensions).* Naukova Dumka, Kiev.

_____, Egorova, L. N. and Tepikin, V. E. (1971a) Structure and distribution of the $Mg\text{-}Fe^{2+}$ in the hornblendes of gneisses from the Ros River (Ukrainian Shield). Constitution and Properties of Minerals 5, 3-8.

_____, Udovkina, N. G., Egorova, L. N. and Tepikin, V. E. (1971b) Karinthine: structure refinement and distribution of cations. Izv. Acad. Sci. USSR Geol. Ser. 11, 83-92.

_____, Egorova, L. N. , Michnik, T. L., Ostapenko, S. S. and Tepikin, V. E. (1972a) The structural refinements of actinolite and high-ferrous hornblende. Mineral. Sbornik, Lvov State Univ. 26, 341-350.

_____, _____, Ostapenko, S. S. and Tepikin, V. E. (1972b) A comparison of structural characteristics of hornblendes from amphibolite and granulite metamorphic facies (Ukrainian Shield). Constitution and Properties of Minerals 6, 3-14.

_____, Ginzburg, I. V., Egorova, L. N. and Ostapenko, S. S. (1973a) On the crystal structure of holmquistite. Constitution and Properties of Minerals 7, 18-31.

_____, Egorova, L. N., Michnik, T. L., Moskovchenko, N. I., Ostapenko, S. S. and Turchenko, S. I. (1973b) On cation distribution in two aluminous hornblendes from X-ray data. Constitution and Properties of Minerals 7, 31-34.

_____, Michnik, T. L., Ostapenko, S. S. and Polshin, E. V. (1973c) X-ray diffraction and Mössbauer investigation of cation distribution in kataphorite (taramite). Geol. Zhurnal Kiev 33, 49-56.

_____, Egorova, L. N. and Petrunina, A. A. (1974a) Refinement of the structure of hornblende from garnet amphibolite from the central Bug region (Ukrainian Shield). Constitution and Properties of Minerals 8, 6-8.

_____, Ginzburg, I. V., Egorova, L. N. and Petrunina, A. A. (1975a) On the crystal structure of clinoholmquistite. Constitution and Properties of Minerals 9, 3-6.

_____, Egorova, L. N., Michnik, T. L., Petrunina, A. A. and Udovkina, N. G. (1975b) Comparative characteristics of the structures of smaragdite and carinthine. Constitution and Properties of Minerals 9, 7-10.

_____, Michnik, T. L., Petrunina, A. A., Pol'shin, E. V., Seimov, A. F. and Kovalenko, V. I. (1976) Structure and some characteristics of the crystal chemistry of three alkali amphiboles. Constitution and Properties of Minerals 10, 3-9.

Louisnathan, S. J. and Gibbs, G. V. (1972a) The effect of tetrahedral angles on Si-O bond overlap populations for isolated tetrahedra. Amer. Mineral. 57, 1614-1642.

_____ and _____ (1972b) Variation in Si-O distances in olivines, sodamelilite and sodium metasilicate as predicted by semi-empirical molecular orbital calculations. Amer. Mineral. 57, 1643-1663.

_____ and _____ (1972c) Bond length variations in oxyanions of the third row elements, T = Al, Si, P, S and Cl. Mater. Res. Bull. 7, 1281-1292.

Lyons, P. C. (1976) The chemistry of riebeckite of Massachusetts and Rhode Island. Mineral. Mag. 40, 474-479.

Manoogian, A. (1968) The electron spin resonance of Mn^{2+} in tremolite. Canadian J. Phys. 46, 129-133.

Maresch, W. V. (1977) Experimental studies on glaucophane. An analysis of present knowledge. Tectonophysics 43, 109-125.

_____ and Langer, K. (1976) Synthesis, lattice constants and OH-valence vibrations of an orthorhombic amphibole with excess OH in the system Li_2O-MgO-SiO_2-H_2O. Contrib. Mineral. Petrol. 56, 27-34.

Megaw. H. D. (1956) Notation for feldspar structures. Acta Crystallogr. 9, 56-60.

Meier, W. M. and Villiger, H. (1969) Die Methode der Abstandsverfeinerung zur Bestimmung der Atomkoordinaten idealisierter Geruststrukturen. Z. Kristallogr. 129, 411-423.

Miller, C. (1977) Chemismus und Phasenpetrologische Untersuchungen der Gesteine aus Eklogitzone des Tauernfensters, Osterreich. Tscher. Mineral. Petrogr. Mitt. 24, 221-277.

Mitchell, J. T., Bloss, F. D. and Gibbs, G. V. (1971) Examination of the actinolite structure and four other C2/m amphiboles in terms of double bonding. Z. Kristallogr. 133, 273-300.

Moore, P. B. (1968a) Joesmithite, a new amphibole-like mineral from Langban. Arkiv. Mineral. Geol. 28, 487-492.

_____ (1968b) The crystal structure of joesmithite: a preliminary note. Mineral. Mag. 36, 876-879.

_____ (1969) Joesmithite: a novel amphibole crystal chemistry. Mineral. Soc. Amer. Spec. Paper 2, 111-115.

Nesterchuk, N. I., Makarova, T. A. and Fedoseev, A. D. (1968) Hydrothermal synthesis of fibrous sodium-cobalt amphibole. Dokl. Akad. Nauk SSSR 179, 106-107.

Papike, J. J. and Clark, J. R. (1967) Crystal-chemical role of potassium and aluminum in a hornblende of proposed mantle origin (abstr.). Geol. Soc. Amer. Spec. Paper 115, 171.

_____ and _____ (1968) The crystal structure and cation distribution of glaucophane. Amer. Mineral. 53, 1156-1173.

_____ and Ross, M. (1970) Gedrites: crystal structures and intracrystalline cation distributions. Amer. Mineral. 55, 1945-1972.

_____, _____ and Clark, J. R. (1968) Crystal-chemical and petrologic significance of the $P2_1/m$ amphibole analog of pigeonite (abstr.). Trans. Amer. Geophys. Union 49, 340-341.

_____, _____ and _____ (1969) Crystal chemical characterization of clinoamphiboles based on five new structure refinements. Mineral. Soc. Amer. Spec. Paper 2, 117-136.

_____, Cameron, K. L. and Baldwin, K. (1974) Amphiboles and pyroxenes: characterization of other than quadrilateral components and estimates of ferric iron from microprobe data (abstr.). Geol. Soc. Amer. Abstracts with Programs 6, 1053-1054.

Patterson, J. H. and O'Connor, D. J. (1966) Chemical studies of amphibole asbestos I. Structural changes of heat-treated crocidolite, amosite and tremolite from infrared absorption studies. Australian J. Chem. 19, 1155-1164.

Pauling, L. (1929) The principles determining the structure of complex ionic crystals. J. Amer. Chem. Soc. 51, 1010-1026.

_____ (1939) *The Nature of the Chemical Bond.* 1st Ed., Cornell University Press, Ithaca, New York.

_____ (1960) *The Nature of the Chemical Bond.* 3rd Ed., Cornell University Press, Ithaca, New York.

Popp, R. K. (1975) *Iron-Magnesium Amphiboles: Synthesis and Stability with respect to Temperature, Pressure, Oxygen Fugacity and Sulphur Fugacity.* Ph.D. Dissertation, Virginia Polytechnic Institute and State University, Blacksburg, VA.

_____, Gilbert, M. C. and Craig, J. R. (1976) Synthesis and X-ray properties of Fe-Mg orthoamphiboles. Amer. Mineral. 61, 1267-1279.

Prewitt, C. T. (1963) Crystal structures of two synthetic amphiboles. Geol. Soc. Amer. Ann. Meet. Prog., New York, 132A-133A.

_____, Papike, J. J. and Ross, M. (1970) Cummingtonite. A reversible, non-quenchable transition from $P2_1/m$ to C2/m symmetry. Earth Planet. Sci. Lett. 8, 448-450.

Raith, M., Hormann, P. K. and Abraham, K. (1977) Petrology and metamorphic evolution of the Penninic ophiolites in the western Tauern window (Austria). Schweiz. Mineral. Petrog. Mitt. 57, 187-232.

Ribbe, P. H. and Gibbs, G. V. (1971) Crystal structures of the humite minerals. III. Mg/Fe ordering in humite and its relation to other ferromagnesian silicates. Amer. Mineral. 56, 1155-1173.

Rice, J. M., Evans, B. W. and Trommsdorff, V. (1974) Widespread occurrence of magnesio-cummingtonite in ultramafic schists, Cima di Gagnone, Ticino, Switzerland. Contrib. Mineral. Petrol. 43, 245-251.

Robinson, E. A. (1963) Characteristic vibrational frequencies of oxygen compounds of silicon, phosphorus and chlorine. Correlation of stretching frequencies and force constants with bond lengths and bond orders. Canadian J. Chem. 41, 3021-3033.

Robinson, K. (1971) *The Crystal Structures of Zircon, Clinohumite and the Hornblendes. A Determination of Polyhedral Distortion and Order-Disorder.* Ph.D. Dissertation, Virginia Polytechnic Institute and State University, Blacksburg, VA.

_____, Gibbs, G. V. and Ribbe, P. H. (1970) A refinement of the crystal structure of pargasite (abstr.). Amer. Mineral. 55, 307.

_____, _____, _____, and Hall, M. R. (1973) Cation distribution in three hornblendes. Amer. J. Sci. 273A, 522-535.

Ross, M., Papike, J. J. and Weiblen, P. W. (1968) Exsolution in clinoamphiboles. Science 159, 1099-1102.

_____, Papike, J. J. and Shaw, K. W. (1969) Exsolution textures in amphiboles as indicators of subsolidus thermal histories. Mineral. Soc. Amer. Spec. Paper 2, 275-299.

Rosenburg, P. E. and Foit, F. F. (1977) Fe^{2+}-F avoidance in silicates. Geochim. Cosmochim. Acta 41, 345-346.

Rouxhet, P. G., Gillard, J. L. and Fripiat, J. J. (1972) Thermal decomposition of amosite, crocidolite and biotite. Mineral. Mag. 38, 583-592.

Rowbotham, G. and Farmer, V. C. (1973) The effect of "A" site occupancy on the hydroxyl stretching frequency in clinoamphiboles. Contrib. Mineral. Petrol. 38, 147-149.

Schaller, W. T. (1916) The chemical composition of tremolite. U.S. Geol. Surv. Bull. 610, 133-136.

Seifert, F. (1977) Compositional dependence of the hyperfine interaction of ^{57}Fe in anthophyllite. Phys. Chem. Minerals 1, 43-52.

_____ (1978) Equilibrium Mg-Fe^{2+} cation distribution in anthophyllite. Am. J. Sci. 278, 1323-1333.

Shannon, R. D. (1975) Systematic studies of interatomic distances in oxides. In *Petrophysics.* R. G. J. Strens, ed., John Wiley and Sons, New York.

_____ (1976) Revised effective ionic radii and systematic studies of interatomic distances in halides and chalcogenides. Acta Crystallogr. A32, 751-757.

Sipovskii, D. P., Grebenshchikov, R. G. and Makarova, T. A. (1972) New chemical compound fibrous amphibole-like germanate. Dokl. Akad. Nauk. SSSR 205, 404-406.

Smith, J. V. (1969) Crystal structure and stability of the $MgSiO_3$ polymorphs; physical properties and phase relationships of Mg,Fe pyroxenes. Min. Soc. Amer. Spec. Paper, 2, 3-29.

Strens, R. G. J. (1966) Infrared study of cation ordering and clustering in some (Fe,Mg) amphibole solid solutions. Chem. Comm. 15, 519-520.

_____ (1974) The common chain, ribbon and ring silicates. In *The Infrared Spectra of Minerals.* Mineralogical Society, London, 305-330.

Sueno, S., Papike, J. J., Prewitt, C. T. and Brown, G. E. (1972) Crystal structure of high cummingtonite. J. Geophys. Res. 77, 5767-5777.

_____, _____, _____ and _____ (1973) The high temperature crystal chemistry of tremolite. Amer. Mineral. 58, 649-664.

Sundius. N. (1946) The classification of the hornblendes and the solid solution relations in the amphibole group. Arsbok Sver. Geol. Undersok. 40, No. 4.

Thompson, J. B. (1970) Geometrical possibilities for amphibole structures. Model biopyriboles (abstr.). Amer. Mineral. 55, 292-293.

Trojer, F. and Walitzi, E. M. (1965) Strukturuntersuchung an einer Hornblende aus dem eklogitischen Gestein von Stramez, sudliche Koralpe. Tscher. Mineral. Petrog. Mitt. 10, 233-240.

Ungaretti, L. (1980) Recent developments in X-ray single crystal diffractometry applied to the crystal-chemical study of amphiboles. 15th Conf. Yugoslav Centre Crystallogr., Bor, Yugoslavia.

_____, Mazzi, F., Rossi, G. and Dal Negro, A. (1978) Crystal-chemical characterization of blue amphiboles. Proc. Internat. Mineral. Assoc., Novosibirsk (in press).

_____, Smith, D. C. and Rossi, G. (1981) Crystal-chemistry by X-ray structure refinement and electron microprobe analysis of a series of sodic-calcic to alkali amphiboles from Nybö eclogite pod, Norway. To be published.

Vieten, K. and Hamm, H.-M. (1971) Zur Berechnung der kristallchemischen Formel und des Fe^{3+}-Gehaltes von Klinopyroxenen aus Elektronenstrahl-Microanalysen. Neues Jahrb. Mineral. Mh. 1971, 310-314.

Virgo, D. (1972) ^{57}Fe Mössbauer analysis of Fe^{3+} clinopyroxenes. Carnegie Inst. Wash. Yearbook 71, 534-538.

Viswanathan, K. and Ghose, S. (1965) The effect of Mg^{2+} substitution on the cell dimensions of cummingtonites. Amer. Mineral. 50, 1106-1112.

Warren, B. E. (1929) The structure of tremolite. Z. Kristallogr. 72, 42-57.

_____ (1930) The crystal structure and chemical composition of the monoclinic amphiboles. Z. Kristallogr. 72, 493-517.

_____ and Bragg, W. L. (1928) The structure of diopside, $CaMg(SiO_3)_2$. Z. Kristallogr. 69, 168-193.

_____ and Modell, D. I. (1930a) The structure of enstatite. Z. Kristallogr. 75, 1-16.

_____ and _____ (1930b) The structure of anthophyllite. Z. Kristallogr. 75, 161-178.

Wenk, H-R. (1971) Variations of lattice constants in clinoamphiboles. Z. Kristallogr. 133, 341-363.

Whittaker, E. J. W. (1949) The structure of Bolivian crocidolite. Acta Crystallogr. 2, 312-317.

_____ (1960) The crystal chemistry of the amphiboles. Acta. Crystallogr. 13, 291-298.

_____ (1969) The structure of the orthorhombic amphibole holmquistite. Acta Crystallogr. B25, 394-397.

_____ (1971) Madelung energies and site-preferences in amphiboles. I. Amer. Mineral. 56, 980-996.

_____ and Zussman, J. (1961) The choice of axes in amphiboles. Acta Crystallogr. 14, 54-55.

Wilkins, R. W. T., Davidson, L. R. and Ross, J. R. (1970) Occurrence and infrared spectra of holmquistite and hornblende from Mt. Marion, near Kalgoorlie, Western Australia. Contrib. Mineral. Petrol. 28, 280-287.

Witte, P., Langer, K., Seifert, F. and Schreyer, W. (1969) Synthetische Amphibole mit Oh-Uberschuss im System Na_2O-MgO-SiO_2-H_2O. Naturwissenschaften 56, 414-415.

Woensdregt, C. F. and Hartman, P. (1969) Regular intergrowth of cummingtonite and hornblende, both with space group $P2_1/m$. Neues Jahrb. Mineral. Monatsh. 12, 558-563.

Yakovleva, A. K., Yegorova, K. N. and Litvin, A. L. (1978) Magnesiocummingtonite with primitive cell $P2_1/m$. Int'l Geol. Rev. 20, 1357-1562.

Yale, P. B. (1968) *Geometry and Symmetry*. Holden-Day, San Francisco.

Zachariasen, W. H. (1945) *Theory of X-ray Diffraction in Crystals*. John Wiley and Sons, New York.

Zussman, J. (1955) The crystal structure of actinolite. Acta Crystallogr. 8, 301-308.

_____ (1959) A re-examination of the structure of tremolite. Acta Crystallogr. 12, 309-312.

Chapter 2

AMPHIBOLE SPECTROSCOPY

Frank C. Hawthorne

INTRODUCTION

The diversity of cation coordinations and chemical compositions in the amphiboles has encouraged the use of a wide variety of spectroscopic techniques on these minerals. Much of the early work was concerned with the oxidation and dehydroxylation characteristics of fibrous and asbestiform amphiboles; although this was only qualitative, it showed the potential of these techniques for amphiboles. A considerable amount of work has been done in the past 15 years, particularly in the area of site-population characterization. Most studies have used three types of spectroscopy: Mössbauer resonance, vibrational and electronic (optical) absorption. Brief descriptions of each method are given here. More detailed reviews with a bent towards mineralogy can be found as follows: Mössbauer spectroscopy -- Bancroft (1973); vibrational spectroscopy -- Lazarev (1972), Farmer, (1974), Karr (1975); electronic absorption spectroscopy -- Burns (1970).

In what follows, we will concentrate on understanding the spectroscopic characteristics of amphiboles and determining what crystal-chemical information we can or cannot derive from experiments. We will not dwell on the use of such crystal-chemical information in a petrologic context, because this is covered in subsequent chapters.

MÖSSBAUER SPECTROSCOPY

The Mössbauer effect is the recoil-free emission and absorption of γ-rays by a specific atomic nucleus. The emission of a γ-ray during a nuclear transition causes a recoil of the emitting atom; this recoil energy dissipates by transfer to the phonon spectrum of the structure. As the phonon spectrum is quantized, this transfer must occur in integral multiples of the phonon energy and the probability exists that no energy is transferred. The effective line-width of the zero-phonon (recoil-free) process is that of the γ-ray; this is extremely small (Wertheim, 1964) in relation to the characteristic energies of interaction between the nucleus and its surrounding electrons. If the zero-phonon γ-ray encounters

another nucleus, its energy may be absorbed by raising that nucleus to an excited state, provided that the transition energies of the emission and absorption events are equal to within the line-width of the γ-ray. As the line-width of the γ-ray is much smaller than the characteristic interaction energies between nuclei and electrons, a change in structural environment is generally sufficient to bring the two nuclei out of resonance. However, the energy of the γ-ray may be modulated by applying a doppler shift to bring the system into resonance. In this way, nuclear transition energies may be compared in different environments.

A change in the s-electron density at the nucleus of an atom will result in a shift in the nuclear energy levels. Where such a variation occurs between emitter and absorber, the processes are separated in the energy spectrum by an amount known as the *Isomer Shift* (I.S.) or *Chemical Shift* (C.S.). This quantity is thus a measure of the relative s-electron density at the nucleus. Two factors are principally responsible for variations in isomer shift. Screening of s-electrons from the nucleus by valence electrons is strongly affected by valence state and degree of covalent bonding. Thus isomer shift may be used to characterize valence state and coordination number. If the nucleus does not have a uniform charge density, a quadrupole moment arises which can interact with the *electric field gradient* (E.F.G.) at the nucleus to lift the degeneracy of the nuclear state. This gives rise to a doublet in the energy spectrum; the separation of the two components is known as the *Quadrupole Splitting* (Q.S.) and is thus a measure of the E.F.G. at the nucleus. Principal factors affecting the E.F.G. at the nucleus are the non-spherical electron distribution in the atom itself, a function of valence state, and the non-spherical component of the crystal field. Thus quadrupole splitting may be used to characterize valence state and variations in structural environment.

There are 30 or isotopes that are sensitive to the Mössbauer effect; of these, only ^{57}Fe is of use in amphibole studies. However, the almost ubiquitous occurrence of Fe^{2+} and Fe^{3+} has resulted in application of this technique to a wide variety of amphiboles. The hyperfine parameters of amphiboles show significant variation with changes in coordination, site-occupancy and compositional type of amphibole. The systematics of these variations are of interest both with regard to peak

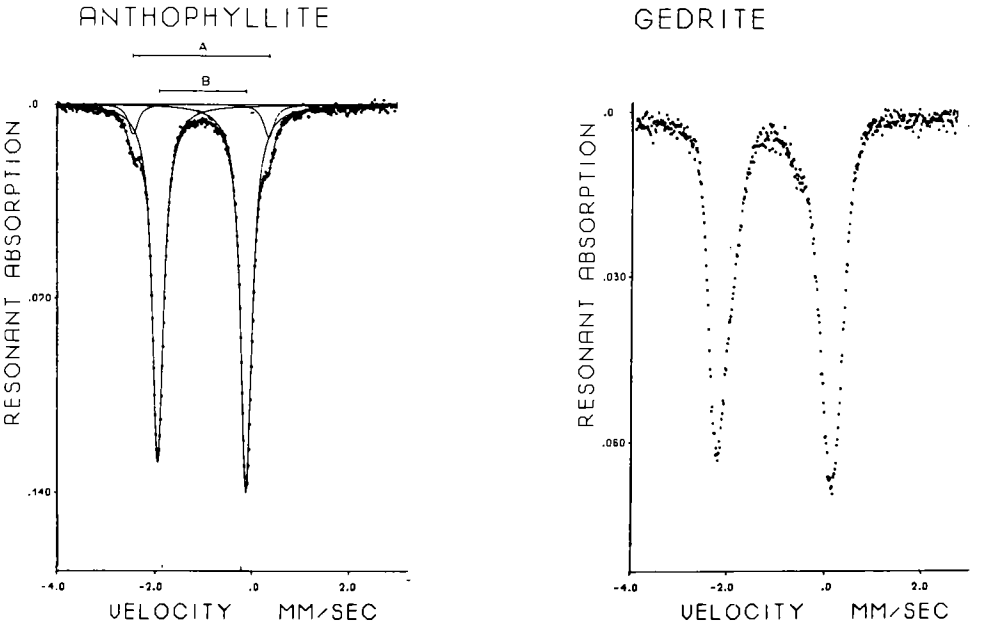

Figure 1. Room-temperature Mössbauer spectra of anthophyllite (left) and gedrite (right). From Seifert (1977). In the anthophyllite spectrum, the more intense inner doublet is due to Fe^{2+} at M4 and the weaker outer doublet is due to Fe^{2+} at M1,2,3.

assignment in Mössbauer spectra and the crystal-chemical systematics of the amphiboles themselves. Some of the general conclusions of Ingalls (1964) concerning the behavior of the quadrupole splitting of high spin Fe^{2+} with changes in ligand environment are pertinent. In particular, Fe^{2+} in a cubic field has no quadrupole splitting; slight distortion of the field from cubic symmetry produces a large quadrupole splitting ($\sim$3.7 mm/sec), with increasing distortion of the ligand environment producing a gradual decrease in the quadrupole splitting. The crystal field contribution to the quadrupole splitting contains both distance and angular terms and hence is sensitive to distortion of the coordination polyhedron with regard to both bond lengths and bond angles. Consequently, the criterion by which distortion is measured should encompass both these factors, and failure to do so has led to some confusion in discussions relating Mössbauer parameters to crystal structure. Next-nearest-neighbor cations will also have a significant effect on the quadrupole splitting. This is of particular importance in the amphiboles

where coupled polyvalent cation substitutions at the M(2), M(4), T(1), T(2) and A sites are particularly common.

Site-occupancy characterization

In a typical experimental set-up, the γ-ray source is repeatedly swept through a range of velocities at constant acceleration. This energy-modulated γ-ray beam passes through a randomly-oriented powdered sample where absorption occurs. The resultant beam is recorded in a multi-channel analyzer, in which each channel accumulates the counts recorded while the γ-ray source was moving in a specific velocity interval. Two experimental Mössbauer spectra are shown in Figure 1. Each data point represents the number of counts recorded over that particular source velocity interval. The counts at the margins of the spectra represent the background counts and are approximately constant; the average background value is termed the off-resonance count. Towards the center of the spectra, the counts decrease. This is due to the resonant absorption of γ-rays of this specific energy by the sample. The ideal shape of a single absorption peak (line) in a Mössbauer spectrum is Lorentzian. Thus, the observed spectra consist of a series of Lorentzian peaks, the number and characteristics of which are a function of the structural type and chemical composition of the amphibole. Deconvolution of an observed envelope into its component peaks is done using least-squares refinement techniques. This is a non-trivial process, and the problems associated with it are discussed in detail by Hawthorne (1981).

Bancroft *et al.* (1967a) have considered the assumptions inherent in using the Mössbauer effect for site-population characterization of iron in silicates when two distinct quadrupole split doublets occur in the spectrum. We may generalize this to r quadrupole split doublets in the spectrum. The area under a peak is given by (Bancroft *et al.*, 1967a)

$$A_i = \frac{\Pi}{2} f_i f_e \sigma_o \tau_i G(n_i, f_i, \sigma_o) n_i$$

where f_i is the recoil-free fraction of the absorber
f_e is the recoil-free fraction of the emitter
σ_o is the maximum resonant absorption cross-section
τ_i is the half-width of the peak (peak width at half-height)

$G(n_i, f_i, \sigma_o)$ is the saturation correction,

n_i is the number of atoms per formula unit.

Expressing the area of the *jth* doublet as a function of the total absorption,

$$A_j / \sum_{i=1}^{r} A_i = n_j / \sum_{i=1}^{r} C_i n_i \ ,$$

where $C_i = \frac{f_i}{f_j} \frac{\tau_i}{\tau_j} \frac{G_i(n_i, f_i, \sigma_o)}{G_j(n_j, f_j, \sigma_o)}$.

In most studies, C_i is assumed to be unity. Considering the individual terms in the above expression for C_i, this generally seems to be a reasonable assumption. Saturation corrections approach unity for thin absorbers, and deviations from this value should be self-cancelling providing that the n_i values are not radically different from each other. Extensive experimental evidence has confirmed that half-widths of *single peaks* are approximately equal; in principal, the recoil-free fractions can be determined, but this has rarely been done. Some studies have derived C values different from unity but such results have often been somewhat controversial. Thus, site occupancies, n_j, can be derived from area ratios, $A_j / \sum_{i=1}^{r} A_i$, in minerals.

Amphibole spectra

The general appearance of amphibole Mössbauer spectra varies considerably with amphibole type, and the peak assignment in such spectra is frequently not straightforward. Consequently, we will look at a variety of amphibole spectra and consider the systematics of the Mössbauer parameters.

Fe-Mg-Mn amphiboles. Spectra for the orthorhombic Fe-Mg-Mn amphiboles are shown in Figure 1. The anthophyllite spectrum consists of two doublets; the outer doublet is attributable to Fe^{2+} at the M1, M2 and M3 sites, with the inner doublet due to Fe^{2+} at the M4 site. This contrasts with the gedrite spectrum, where only a single wide doublet occurs. The reason for this is apparent in the systematics of the quadrupole splittings for these amphiboles as shown in Figure 2. Extrapolation of the quadrupole splitting values for the M4 and M1+M2+M3 (≡ M1,2,3) peaks in

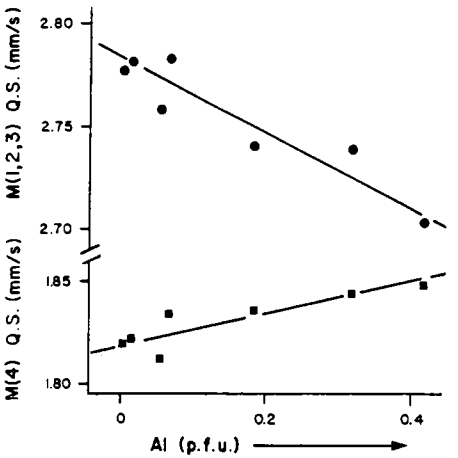

Figure 2. Quadrupole splitting (at room temperature) as a function of Al p.f.u. in orthorhombic amphiboles. After Seifert (1977).

the anthophyllite spectra to Al values typical of gedrite shows that the Q.S. values overlap, with a concommitant lack of resolution in the gedrite spectra.

The spectrum of holmquistite (Fig. 3) has three doublets that may be assigned to Fe^{3+} at the M2 site (D1D2) and Fe^{2+} at the M1(A1A2) and M3(C1C2) sites. It is unlike any other Fe-Mg-Mn amphibole spectra, because of the differences in next-nearest-neighbor cation configurations. In holmquistite, these are similar to those in the glaucophane-riebeckite amphiboles, the spectra of which bear a strong similarity to that of holmquistite.

Typical Mössbauer spectra for the monoclinic Fe-Mg-Mn amphiboles are shown in Figure 4; note the slightly greater resolution attained in low-temperature spectra, a feature also exhibited by anthophyllite spectra. The spectra are similar to the anthophyllite spectra, with the outer and inner doublets assigned to Fe^{2+} at the M(1)+M(2)+M(3) and M(4) sites, respectively.

Perhaps the most notable feature of the Fe-Mg-Mn amphibole spectra is the complete overlap of doublets due to Fe^{2+} at the M(1), M(2) and M(3) sites. At first sight, this appears to be incompatible with the fact that these amphiboles show considerable differences in nearest- and next-nearest-neighbor configurations among these three sites. However, closer examination shows an inverse relationship between the distance (Δ) and angle (σ^2) distortion parameters (Fig. 5). One may thus surmise that the differences in angular distortion at the M(1), M(2), and M(3) sites are compensated for by the differences in bond length variations, with the result that the quadrupole splittings at the various sites are similar. This similarity is enhanced by the occupancy of the four M sites by Mg + Fe^{2+} + Mn only, leading to as similar

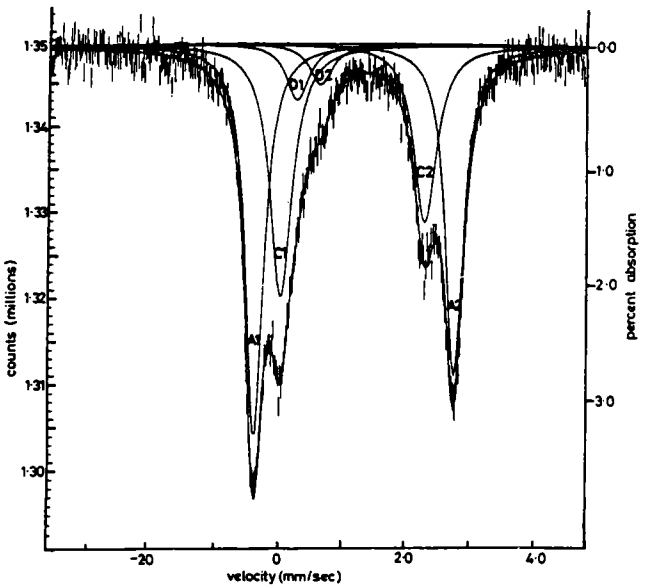

Figure 3. Room-temperature Mössbauer spectrum of holmquistite; from Law (1973). The doublets are assigned as follows: $A1A2\text{-}Fe^{2+}$ at M1; $C1C2\text{-}Fe^{2+}$ at M3, $D1D2$ Fe^{3+} at M2.

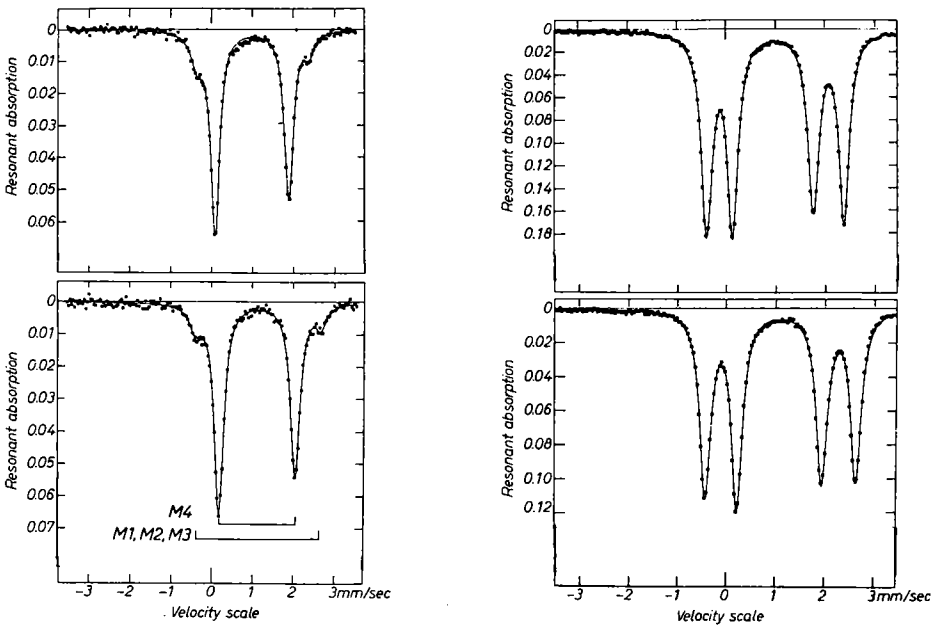

Figure 4. Room-temperature (upper) and liquid-nitrogen temperature (lower) Mössbauer spectra of magnesio-cummingtonite (left) and grunerite (right). From Hafner and Ghose (1971).

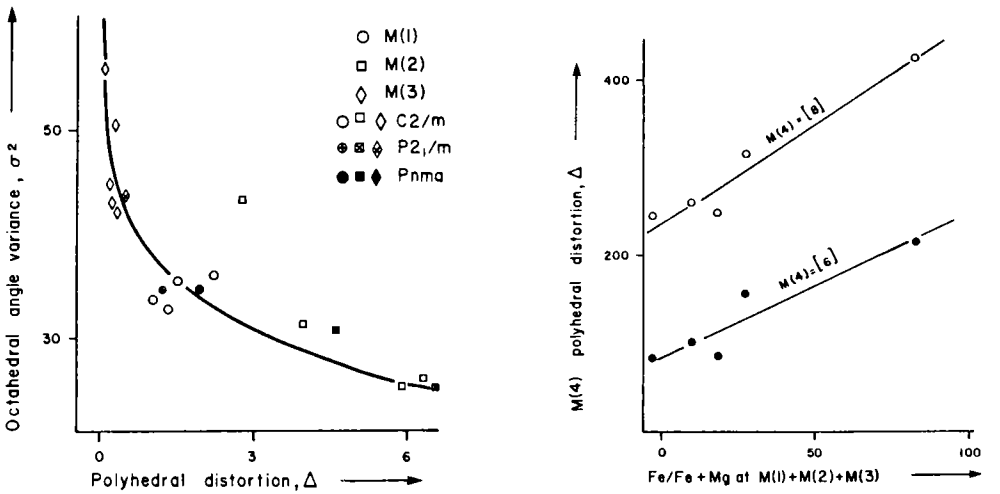

Figure 5. Left: octahedral angle variance as a function of polyhedral distortion for the M(1), M(2) and M(3) sites in the Fe-Mg-Mn amphiboles. Right: M(4) polyhedral distortion as a function of composition for the monoclinic Fe-Mg-Mn amphiboles.

a next-nearest-neighbor environment for the M(1), M(2) and M(3) sites as is possible in the amphibole structure.

The quadrupole splitting of Fe^{2+} at M(4) is significantly less than that of Fe^{2+} at M(1),(2),(3). This is in agreement with Ingalls (1964) model, the M(4) site having the more distorted environment. Further systematic variations of Mössbauer parameters have been characterized in several studies (Bancroft *et al.*, 1967a,b; Barabanov and Tomilov, 1973; Seifert, 1977; Goldman, 1979). As shown in Figure 6, the quadrupole splitting of Fe^{2+} at M(4) is negatively correlated with the Fe/(Fe+Mg) ratio of the amphibole, a slight non-linearity in the relationship being apparent, particularly at low Fe/(Fe+Mg) ratios when the orthorhombic amphiboles are included in the correlation. The correlation is perhaps improved slightly if the M(4) Fe^{2+} quadrupole splitting is plotted against the mean Fe/(Fe+Mg) content of the M(1), M(2), and M(3) sites. This is in line with the suggestion of Hafner and Ghose (1971) that the octahedral distortions and thence the quadrupole splittings are dictated not by the site-occupancy of the specific site but by the linkage between the octahedral and tetrahedral parts of the structure. Certainly the geometry of the M(4) site in the monoclinic amphiboles is consonant with this suggestion. Figure 5 shows the variation in M(4) polyhedral distortion Δ with the mean Fe/(Fe+Mg) content

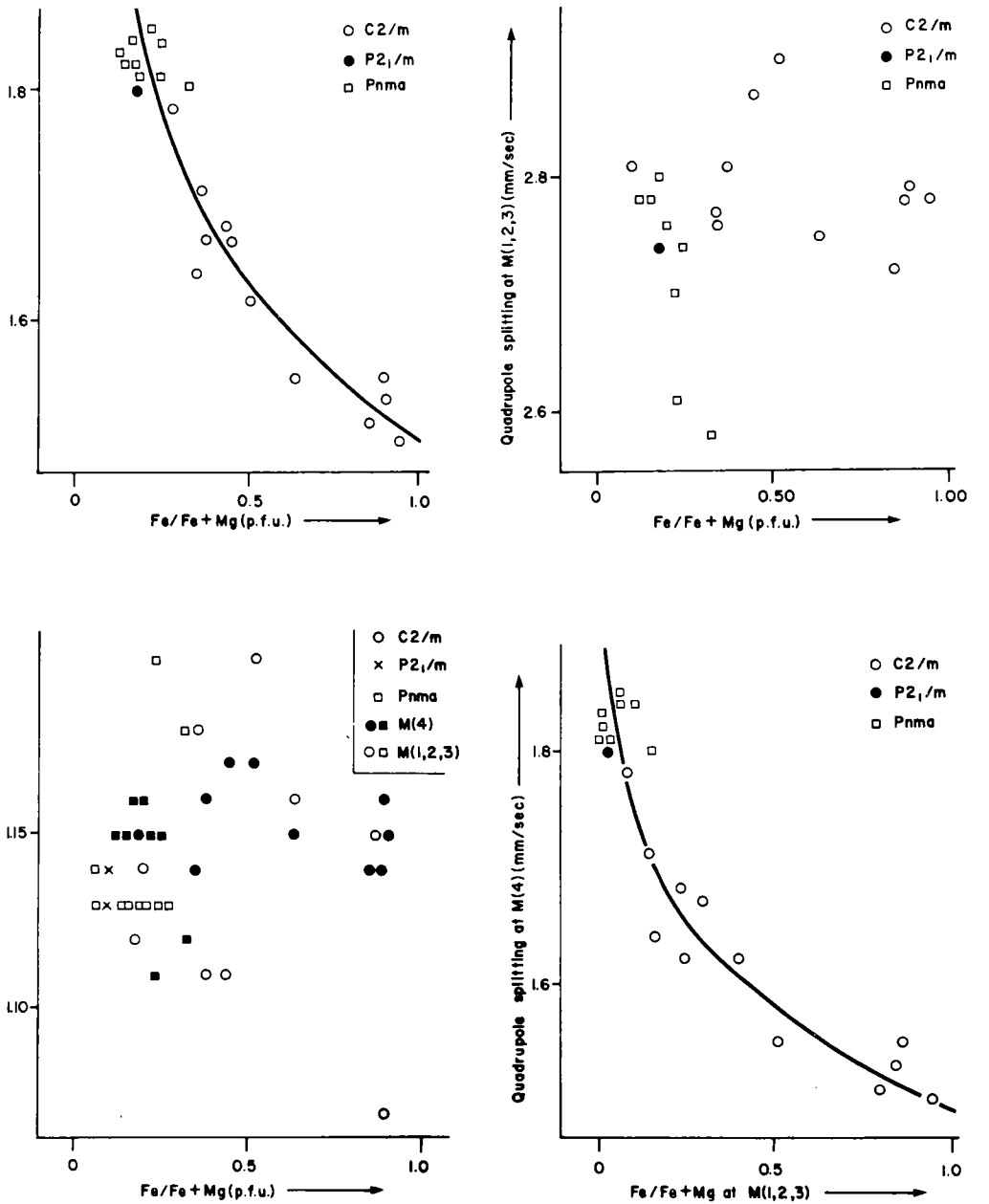

Figure 6. Compositional systematics of the Mössbauer parameters in the Fe-Mg-Mn amphiboles.

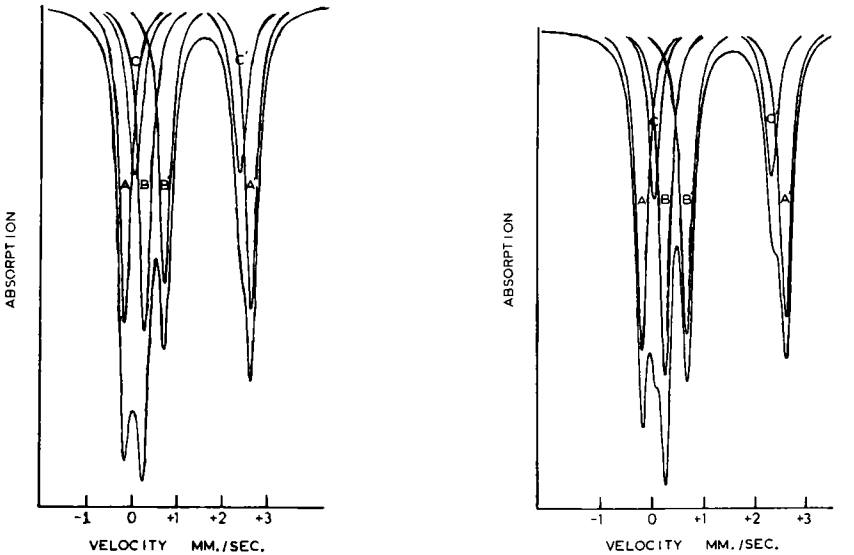

Figure 7. Room-temperature Mössbauer spectra of glaucophane (left) and magnesioriebeckite (right). From Bancroft and Burns (1969). The doublets are assigned as follows: AA'-Fe^{2+} at M(1); CC'-Fe^{2+} at M(3); BB'-Fe^{3+}, predominantly at M(2).

of the M(1), M(2) and M(3) sites; the regular increase in distortion with increasing Fe/(Fe+Mg) correlates with the decreasing quadrupole splitting of Fe^{2+} at M(4), in agreement with the conclusions of Ingalls (1964).

For the orthorhombic amphiboles, the increasing quadrupole splitting of Fe^{2+} at M4 with increase in the gedrite content correlates with

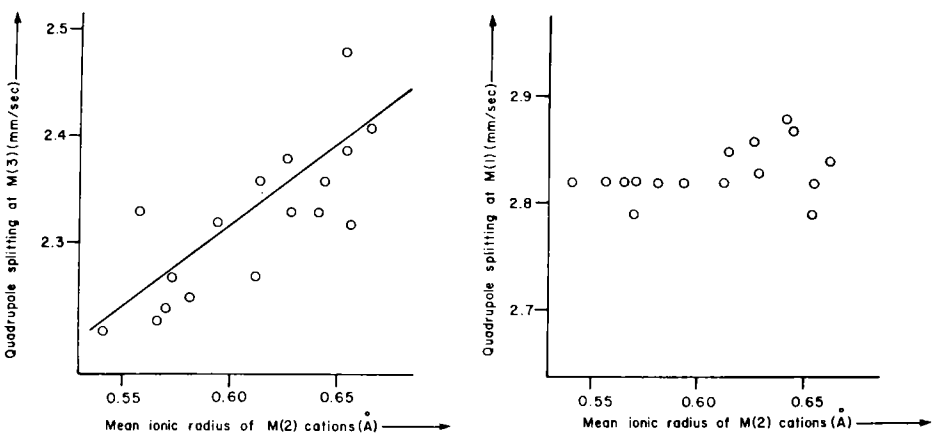

Figure 8. Compositional systematics of the Mössbauer parameters in the alkali amphiboles.

the fact that the M4 polyhedron is far more regular in gedrite than in anthophyllite.

Alkali amphiboles. Spectra for alkali amphiboles are shown in Figure 7. The glaucophane spectrum consists of three doublets, one of which is assigned to Fe^{3+} at M(2)(BB') and two of which are assigned to Fe^{2+} at M(1)(AA') and M(3)(CC'), respectively. The magnesio-riebeckite spectrum is fairly similar, except the Fe^{3+} doublet is stronger than in the glaucophane spectrum. Substitution of an actinolite and/or arfvedsonite component into riebeckite can give rise to a third Fe^{2+} doublet due to a contribution from Fe^{2+} at M(2). The arfvedsonite spectrum consists of four doublets, one due to Fe^{3+} at M(2) and three due to Fe^{2+} at M(1), M(2) and M(3), respectively.

The systematics of the hyperfine parameters are shown in Figure 8. The quadrupole splitting of Fe^{2+} at M(1) is fairly constant at $\sim$2.80 mm/sec, but has greater scatter at larger values of the M(2) cation radius; there does not seem to be any correlation with the M(4) site-occupancy. The quadrupole splitting of Fe^{2+} at M(3) shows a positive correlation with the mean ionic radius of the M(2) cations. In this particular case, the effect of next-nearest-neighbor cation charge variation is minimized, as the M(2) cations are mainly trivalent and the only variable at this site is cation size, and the M(3) site is remote from the M(4) site, where some variation in cation charge does occur. Thus, the change in quadrupole splitting of Fe^{2+} at M(3) is due to a change in M(3) polyhedral distortion and/or a change in the next-nearest-neighbor cation distances. As was shown in the previous chapter, the angular distortions of the M(1) and M(3) polyhedra are strongly dependent on the M(2) site-occupancy. Thus, increasing M(2) cation size causes decreased angular distortion of the M(3) octahedron, which results in increased quadrupole splitting of Fe^{2+} at M(3), in agreement with the deductions of Ingalls (1964). The reason why the quadrupole splitting of Fe^{2+} at M(1) does not exhibit analogous behavior is not clear. There seems to be no systematic variation of isomer shift with composition for Fe^{2+} at M(1) or M(3) in the alkali amphiboles.

Sodic-calcic amphiboles. Little has been done on the amphiboles of this group; the one available spectrum is shown in Figure 9. The spectrum

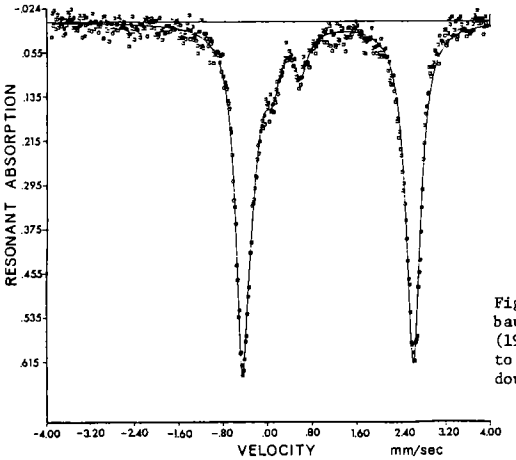

Figure 9. Liquid-nitrogen temperature Mössbauer spectrum of richterite. From Virgo (1974). The intense outer doublet is due to Fe^{2+} at M(1,2,3) and the weaker inner doublet is due to Fe^{3+}.

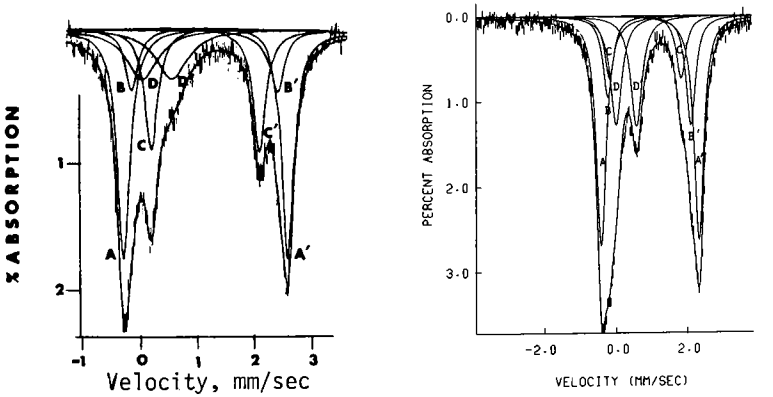

Figure 10. Room-temperature Mössbauer spectra of actinolite (left) and magnesio-hornblende (right). From Burns and Greaves (1971) and Bancroft and Brown (1975), respectively. The doublets are assigned as follows: AA'-Fe^{2+} at M(1); BB'-Fe^{2+} at M(3); CC'-Fe^{2+} at M(2); DD'-Fe^{3+} predominantly at M(2).

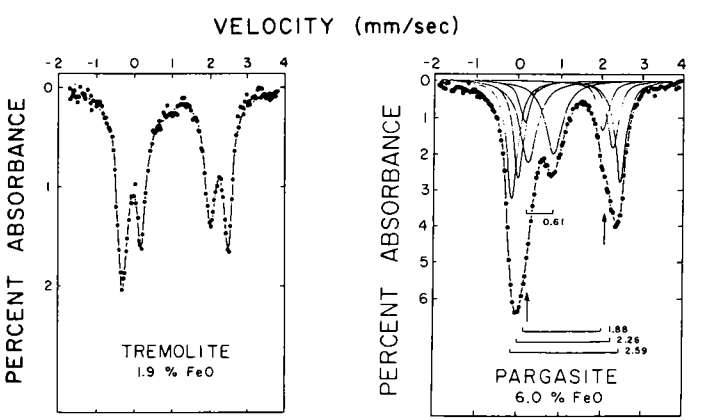

Figure 11. Room-temperature Mössbauer spectra of tremolite (left) and pargasite (right). From Goldman and Rossman (1977) and Goldman (1979), respectively. The doublets are assigned as follows: tremolite - outer doublet - Fe^{2+} at M(1,2,3); inner doublet - Fe^{2+} at M(4); plus a weak Fe^{3+} doublet. Pargasite -- the doublet quadrupole splitting parameters (mm/s) are shown and were assigned as follows: 2.59 - Fe^{2+} at M(1,3); 2.26 - Fe^{2+} at M(2); 1.88 - Fe^{2+} at M(4); 0.61 - Fe^{3+} predominantly at M(2).

of ferro-richterite consists of two resolvable doublets due to Fe^{2+} and Fe^{3+}; the Fe^{2+} doublets consist of three closely overlapping quadrupole split doublets from Fe^{2+} at M(1),(2),(3).

Calcic amphiboles. Interpretation of calcic amphibole spectra is not straightforward and peak assignments differ from study to study. Typical spectra are shown in Figures 10 and 11. Burns and Greaves (1971) have resolved actinolite spectra into four quadrupole-split doublets assigned to Fe^{3+}(DD') and Fe^{2+} at M(1)(AA'), M(2)(CC') and M(3)(BB'), respectively. Bancroft and Brown (1975) have resolved the spectra of a series of "hornblendes" in a similar fashion, except that the assignment of the C and D peaks was reversed. Goldman and Rossman (1977) presented the Mössbauer spectrum of a tremolite with one Fe^{3+} doublet (CC') and two resolvable Fe^{2+} doublets (Fig. 11); they advance persuasive evidence in the form of electron absorption spectra (see following sections) that the two Fe^{2+} doublets represent Fe^{2+} at M(4)(BB') and M(1),(2),(3)(AA'), respectively. As Fe^{2+} contents of M(4) in tremolite-actinolite amphiboles are low, any doublet due to Fe^{2+} at M(4) should be swamped out in ferro-actinolites by greatly increased response from Fe^{2+} at M(1),(2),(3); Goldman (1979) shows that this is indeed the case.

Goldman (1979) proposed that the Fe^{2+} peak assignments in previous studies of actinolites be altered as follows: AA' = M(1)+M(3), BB' = M(2), CC' = M(4); in some cases, this is backed up by electronic absorption spectral evidence. This argument is based on:

(i) the Q.S. value for the CC' doublet (∿1.8 mm/sec) is similar to M(4) doublet values in the Mg-Fe-Mn amphiboles,

(ii) comparison of amphibole spectra with corresponding pyroxene spectra,

(iii) stoichiometric indications that C-type cations must occur at the M(4) site in the calcic amphiboles examined,

(iv) systematics of the hyperfine parameters in amphiboles.

Examination of Figure 8 shows that in the sodic amphiboles, the resolution of the M(1) and M(3) Fe^{2+} doublets decreases with increasing mean ionic radius of the M(2) cation. This would suggest that in amphiboles with large divalent cations at M(2), the resolution between the Fe^{2+} M(1) and M(3) doublets is much less than in the sodic amphiboles.

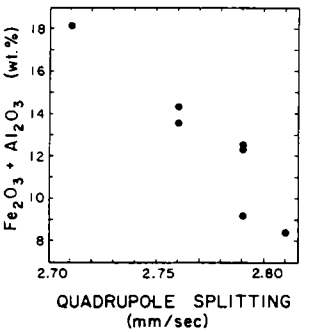

Figure 12. Variation in quadrupole splitting of the outer Fe^{2+} doublet (AA' in Fig. 10 right) as a function of the Al_2O_3 contents in the calcic amphiboles of Bancroft and Brown (1975). From Goldman (1979).

Goldman (1979) has documented a similar systematic variation in Q.S. values for a series of hornblendes (Fig. 12).

Further complications may be illustrated by examining the spectrum of pargasite (Fig. 11). This has been resolved into a doublet due to Fe^{3+} at M(2) and three doublets due to Fe^{2+} at M(1)+M(3), M(2) and M(4), respectively. Comparison with the spectrum of magnesio-hornblende (Fig. 10) shows them to be very similar, suggesting that it will be difficult to recognize either an M(4) or an M(2) Fe^{2+} doublet when *both* are present.

General considerations

A general summary of the variation in Fe^{2+} quadrupole splitting with cation site and amphibole type is given in Figure 13; this should aid peak assignment in the examination of as yet uncharacterized amphibole types. As is apparent from the above discussion, the refinement and assignment of calcic amphibole spectra is not always straightforward; however, some of the problems can be circumvented by use of a combination of experimental techniques.

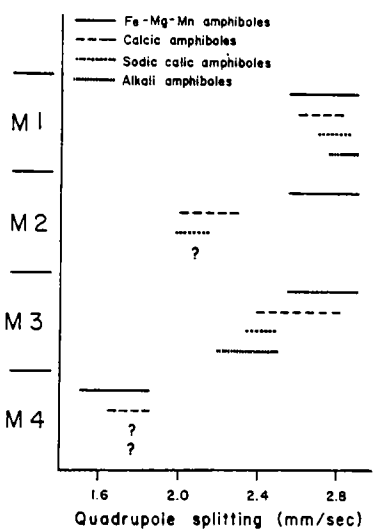

Figure 13. Ranges of quadrupole splitting for Fe^{2+} at the M(1), M(2), M(3) and M(4) sites in amphiboles.

The magnetic behavior of amphiboles has been investigated by Mössbauer spectroscopy, and low-temperature experiments have shown the presence of magnetic ordering (Buckley and Wilkins, 1971; Borg *et al.*, 1974;

Borg and Borg, 1974, 1980; Eisenstein *et al.*, 1975). The ordering has an overall antiferromagnetic character, and the ordering temperature varies with the site occupied by Fe^{2+} (Eisenstein *et al.*, 1975).

VIBRATIONAL SPECTROSCOPY

Vibrational spectroscopy involves the interaction between electromagnetic radiation and the vibrational modes of a crystal. A vibrational mode in a crystal will absorb electromagnetic radiation if the frequencies of the vibration and the radiation are coincident and if the excited vibration changes the dipole moment of the crystal; this effect gives rise to *infrared absorption spectroscopy*. Electromagnetic radiation may be elastically scattered by a crystal (Rayleigh scattering). Scattering may also occur inelastically. In this case, the scattering episode is accompanied by a vibrational transition in the crystal, where energy is absorbed from or imparted to the scattered radiation; this is the Raman effect and gives rise to *Raman spectroscopy*.

Most vibrational spectroscopic work on the amphiboles has been concerned with infrared examination of the hydroxyl stretching region. However, some work has been done in the higher wavelength regions. Figure 14 summarizes infrared spectra for a variety of calcic amphiboles. There have been suggestions that such spectra be used for identification purposes, but this has not met with general acceptance. However, correlations of band frequency with chemical composition (Fig. 14) may be of use.

There has been little Raman spectroscopic work on amphiboles. The Raman effect requires exact translational symmetry over several unit cells in order to produce a sharp spectrum. Perturbation of this symmetry by disorder causes rapid peak broadening and loss of detail in the Raman spectrum. Experimental evidence to this effect can be seen by comparing the Raman spectra for actinolite and tremolite (Fig. 15). Tremolite is fairly well ordered and produces a detailed spectrum, whereas actinolite has significant cation disorder and gives a smeared weak spectrum. These features are independent of the different techniques used to record the spectra.

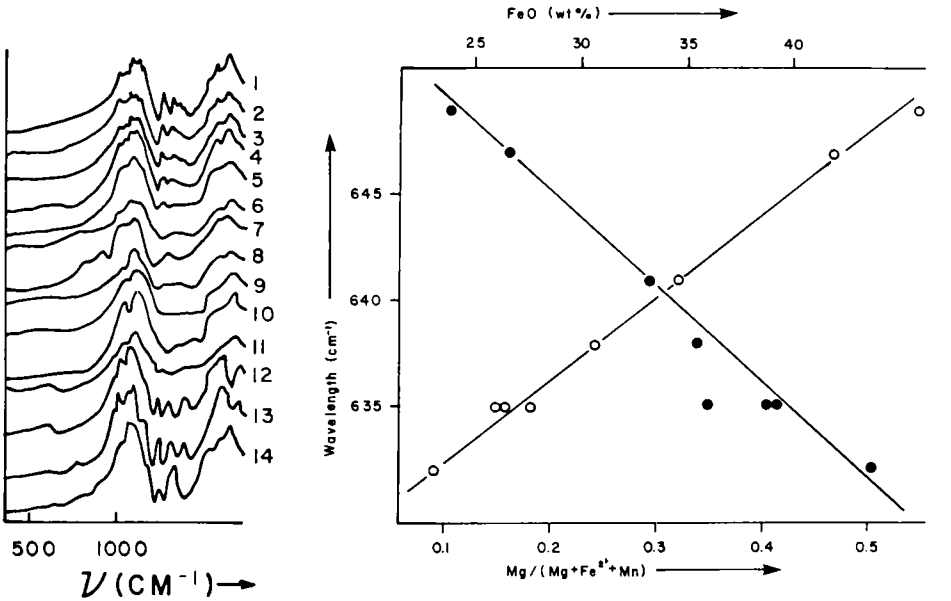

Figure 14. Left: infrared spectra for calcic amphiboles, numbered 1 to 14. After Kukovskii and Litvin (1970). Right: correlation between band frequency and chemical composition in the monoclinic Fe-Mg-Mn amphiboles. Solid circles show the variation of the frequency of the ∿640 band as a function of FeO content in wt %; empty circles show the same band variation as a function of $Mg/(Mg+Fe^{2+}+Mn)$ in the amphibole. After Barabanov *et al.* (1974).

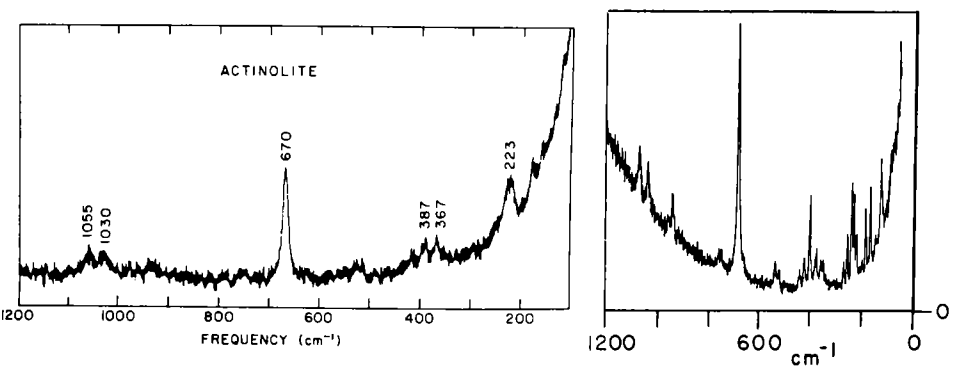

Figure 15. Left: powder Raman spectrum of actinolite. Right: laser Raman spectrum of a crystal of tremolite. From White (1975) and Blaha and Rosasco (1978).

The hydroxyl stretching region

The fundamental band of the O-H stretching vibration occurs from 1500-3800 cm^{-1}. The exact position of this band in the infrared region is a function of the strength of the hydrogen-oxygen bond. Strong bonds are associated with higher frequencies, the lower end of the range being characteristic of symmetrical hydrogen bonds. In the spectra of amphiboles, the fundamental band occurs from 3600-3700 cm^{-1}, indicative of a strong hydroxyl bond and little or no hydrogen bonding; this is compatible with the O(3)-H distance of $\sim$1.0 Å found in crystallographic studies. End-member amphiboles show a single sharp hydroxyl stretching band in this region. However, the principal stretching band in intermediate amphiboles shows considerable fine structure (Fig. 16) that has been attributed to cation substitution effects at those cation sites coordinated by the hydroxyl ion. This is a result of the fact that the frequency of the stretching band varies with the actual cations bonded to the hydroxyl ion. It is instructive to consider the case where the C-type cations are Mg and Fe^{2+} only. There are eight possible ways of distributing two types of cations over the three M sites coordinating a single hydroxyl (Table 1). However, the three M sites coordinating the hydroxyl are in a pseudo-trigonal arrangement that introduces an accidental degeneracy to some bands, reducing the overall number of resolvable bands to four. The cation distribution can be partially derived from the intensities of these peaks. Using the nomenclature of Table 2, the total Fe^{2+} content of the M(1) and M(3) sites in a binary (Mg,Fe^{2+}) amphibole solid solution is given by

$$T_f = B_o + 2C_o + 3D_o \ .$$

If the total Fe content of the amphibole is known from the chemical analysis, the Fe content of the M(2) and M(4) sites may be derived by difference. Where Mg and Fe are confined to the M(1) and M(3) sites, amphibole compositions may be derived. Strens (1966) proposed that the ratio ρ be used to indicate Mg/Fe ordering over the M(1) and M(3) sites, with ρ values greater than unity indicating preferential ordering of Fe^{2+} at the M(3) site.

Such band intensity considerations have been used to derive site-occupancies in Fe-Mg-Mn amphiboles (Burns and Strens, 1966; Strens, 1966;

Table 1. Possible cation arrangements and hydroxyl stretching band assignments in amphiboles with M(1,2,3) completely occupied by Mg and Fe^{2+}

M(1)	M(1)	M(3)	M(1)≠M(3)[1]	M(1)=M(3)[2]
Mg	Mg	Mg_{2+}	A	A
Mg	Mg_{2+}	Fe	B'	B
Mg_{2+}	Fe	Mg	B"	B
Fe_{2+}	Mg_{2+}	Mg	B"	B
Fe_{2+}	Fe	Mg_{2+}	C'	C
Fe	Mg_{2+}	Fe_{2+}	C"	C
Mg_{2+}	Fe_{2+}	Fe_{2+}	C"	C
Fe	Fe	Fe	D	D

[1] ideal band assignment for crystallographically distinct configurations.

[2] band assignments for configurations with accidental degeneracy due to pseudo-trigonal arrangement.

Table 2. Nomenclature of Law (1976) used in the discussion of cation ordering and band intensities in infrared spectra

T_f	total Fe^{2+} at M(1) and M(3) sites
μ_I, ϕ_I	site-occupancies of Mg and Fe^{2+} at M(I)
A_o	normalized observed intensity of peak A
A_r	intensity of peak A for random distribution
A_c	calculated value of intensity of peak A
ρ	$(B_o/B_r)/(C_o/C_r)$
ρ_c	$(B_c/B_r)/(C_c/C_r)$

Table 3. Frequency shift of principal OH band relative to the A band for various cation configurations[1]

Band	Configuration	Displacement (cm^{-1})
A	MgMgMg	0
B	$MgMgFe^{2+}$	-14
C	$MgFe^{2+}Fe^{2+}$	-29
D	$Fe^{2+}Fe^{2+}Fe^{2+}$	-47
E	$MgMgFe^{3+}$	-22
F	$MgFe^{2+}Fe^{3+}$	-36
G	$MgFe^{3+}Fe^{3+}$	-44
H	$Fe^{2+}Fe^{2+}Fe^{3+}$	-51
I	$Fe^{2+}Fe^{3+}Fe^{3+}$	-58
J	$Fe^{3+}Fe^{3+}Fe^{3+}$	-66
K	MgMgAl	-9
L	$MgFe^{2+}Al$	-22
M	$Fe^{2+}Fe^{2+}Al$	-38
N	MgAlAl	-
O	$Fe^{2+}AlAl$	-38
P	$MgFe^{3+}Al$	-
Q	$Fe^{2+}Fe^{3+}Al$	-
-	$LiFe^{2+}Fe^{2+}$	-27
-	$LiFe^{2+}Fe^{3+}$	-34
-	$LiMgFe^{3+}$	-20
-	Na at A	+24
-	K at A	+31
-	Al for Si	-75
-	Ti at M(1,2,3)	-87, -99
-	Ca at M(4)	+2n, 0<n<4

[1] data taken mainly from Strens (1974) and Bancroft & Burns (1969): band nomenclature slightly modified. Configurations R,S and T of Bancroft & Burns (1969) not included. Bands E-Q should not be considered as definitely established. Each specific band configuration is permutable.

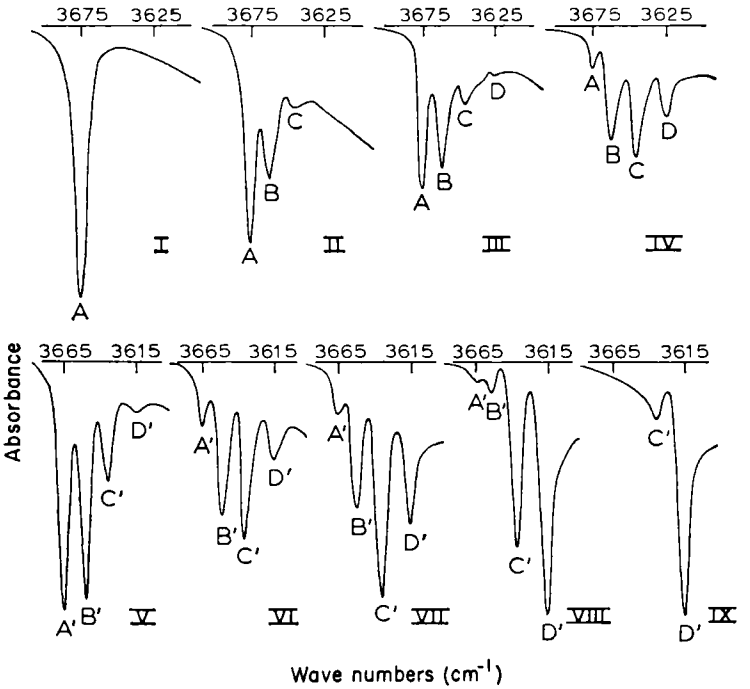

Figure 16. Fine-structure in the fundamental OH stretching band in amphiboles of the magnesio-cummingtonite --- grunerite series (lower) and the tremolite --- ferro-actinolite series (upper); from Burns and Strens (1966). The band nomenclature is that of Table 3. The compositions of the samples, expressed as $Fe^{2+}/(Mg+Fe^{2+})$, is as follows: I - 0.00; II - 0.15; III - 0.30; IV - 0.48; V - 0.36; VI - 0.53; VII - 0.65; VIII - 0.89, IX - 0.98.

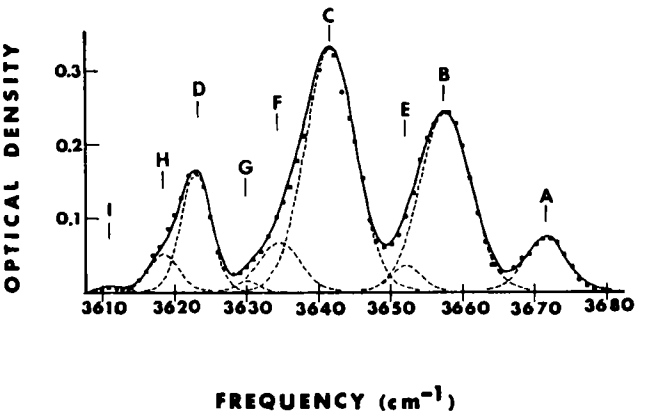

Figure 17. Re-plotted infrared spectrum (OH region) of manganoan ferro-actinolite showing the existence of minor bands when fitting normal gaussian peak shapes. From Burns and Greaves (1971).

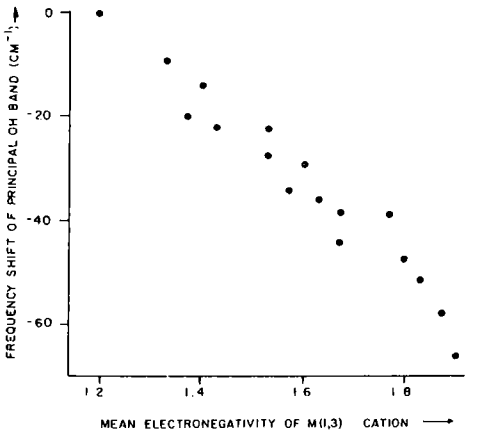

Figure 18. Frequency shift of the principal OH band in C2/m amphiboles as a function of the mean electronegativity of the cations bonded to O(3).

Bancroft *et al.*, 1966, 1967a,b; Buckley and Wilkins, 1971; Burns and Law, 1970; Wilkins *et al.*, 1970), actinolites (Burns and Strens, 1966; Wilkins, 1970; Burns and Greaves, 1971), other calcic amphiboles (Wilkins *et al.*, 1970; Semet, 1973; Nikitina *et al.*, 1973) and alkali amphiboles (Burns and Prentice, 1968; Bancroft and Burns, 1969; Ernst and Wai, 1970; Strens, 1974; Maresch and Langer, 1976). Many of these studies involved amphiboles with other C-type cations present in addition to Mg and Fe^{2+}. It is generally assumed than Mn^{2+} can be grouped with Fe^{2+}, but the presence of any other cations at the M(1) and M(3) sites will give rise to additional bands. Numerous minor bands have been recognized in these studies. Figure 17 gives an example of an actinolite spectrum where minor bands are apparently present; these were assigned to cation configurations involving Fe^{3+}. It is well known that the band frequency is a function of the electronegativity of the cations bonded to the hydroxyl, and this aids in the assignment of these minor bands. Table 3 is a compilation of the bands assigned in previous work, and Figure 18 shows the electronegativity dependence of the frequency shift of these bands. The resolution of these bands in the hydroxyl spectrum is a function of both band width and frequency shift. The intrinsic width of the A and D bands in end-member monoclinic amphiboles is $\sim$5 cm^{-1}, which may be broadened to $\sim$6 cm^{-1} by instrumental and/or minor substitutional effects. Generally, the frequency shift is considerably greater than the band width, ensuring resolution from the A band. Thus, the principal resolution problems arise from accidental overlap of configurations having similar frequency shifts.

Cation substitutions at other sites besides M(1) and M(3) also cause a frequency shift:

(i) Each Ca present in the group of four M(4) positions around each A-site increases the stretching frequency by $\sim$2 cm^{-1}.

(ii) Alkali cations entering the A-site increase the OH stretching frequency considerably: +24 cm^{-1} in riebeckite (Strens, 1974); 30-40 cm^{-1} for hastingsite and pargasite (Semet, 1973), 56 cm^{-1} and 62 cm^{-1}, respectively, for sodium and potassium richterite (Rowbotham and Farmer, 1973).

(iii) The substitution $Fe^{3+} \rightleftarrows Al$ at the M(2) site in alkali amphiboles (Bancroft and Burns, 1969) appears to increase the stretching frequency slightly. Possibly substitution at the tetrahedral sites could also have a slight inductive effect in Al^{IV}-amphiboles.

(iv) In orthorhombic amphiboles, the presence of two nonequivalent hydroxyl groups results in a slight broadening of the band width to $\sim$7 cm^{-1} in anthophyllite (Burns and Law, 1970).

In the more complex amphiboles, such as the hornblendes and the gedrites, the large number of bands together with the considerable band broadening may result in spectra that are too complex to be resolved.

There are several problems associated with the application of this technique to general site-population studies. Problems associated with the curve-fitting procedure are discussed by Hawthorne (1981). One important point has been raised by Strens (1974). In principal, vibrational bands are Lorentzian in form, but Strens (1974) has claimed that line-broadening usually results in a band shape that approximates a skewed Gaussian. If this is the case, use of normal Gaussian curve shape in the spectrum refinement will give rise to spurious bands. Many of the minor bands in previous studies could be of this origin.

The derivation of ordering patterns from band intensities assumes that the band intensity for a specific configuration is related to the frequency of occurrence of that configuration in the same way as all other bands are related to their corresponding configurations. Thus, the transition moment of the OH stretch is assumed to be independent of the type of configuration. Work on micas (Rouxhet, 1970) suggests that this is not the case; however, there is no evidence either way for the amphiboles. The occurrence of weak hydrogen bonding may significantly effect the transition moment of the OH band, whether or not the strength of the

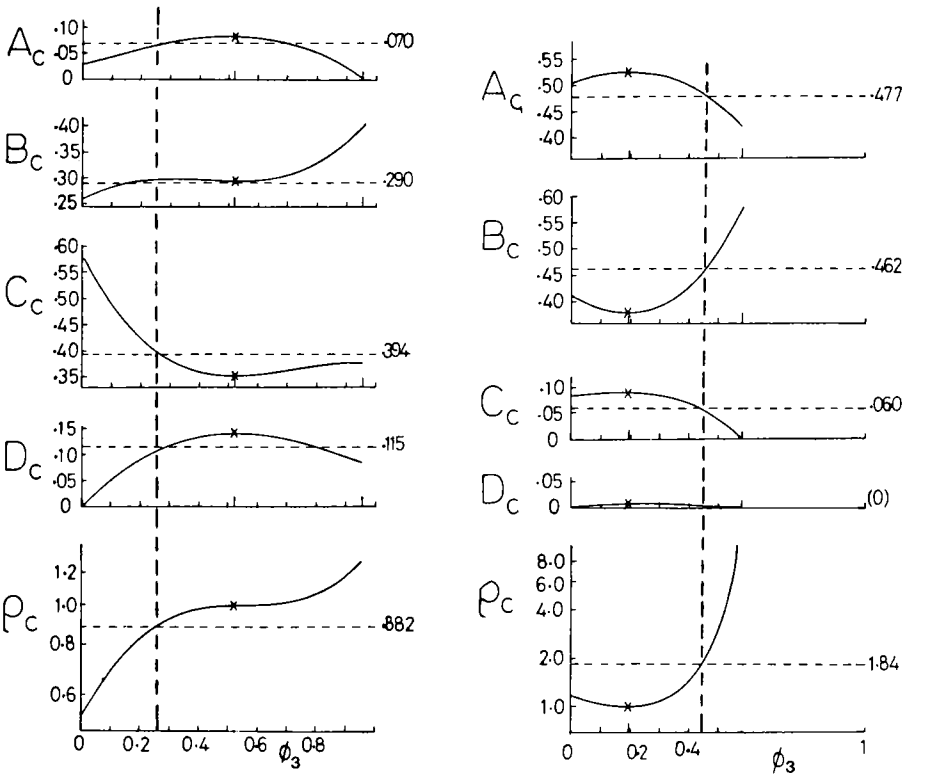

Figure 19. Variation of calculated band intensities as a function of M(3) site population ϕ_3 for two actinolites; observed band intensities are indicated by the horizontal broken lines and the solution for ϕ_3 is indicated by the vertical broken lines. Modified from Law (1976).

hydrogen bonding is related to the cation configuration at the coordinating octahedral sites.

The O(3) position may be occupied by F, O^{2-} and Cl in addition to OH. Thus, in order to derive site-occupancies in OH-deficient amphiboles, it is necessary to assume random mixing of the O(3) anions, with no segregation at specific M(1),(2),(3) cation configurations. Unfortunately, the latter would not appear to be the case, either in F-rich amphiboles, where Fe^{2+} tends to avoid F-coordinated sites (Cameron, 1970; Rosenburg and Foit, 1977), or in oxy-amphiboles where higher-valence cations (Fe^{3+},Ti) are closely associated with O^{2-} at the O(3) position (Kitamura *et al.*, 1975).

Law (1976) has considered the criteria for ordering characterization and has shown them to be misleading. Consider the standard equations

relating peak intensity to mole fraction (see Table 2 for nomenclature):

$$A_c = \mu_1^2 \mu_3 = (1-\phi_1)^2(1-\phi_3)$$
$$B_c = \mu_1^2 \phi_3 + 2\mu_1\phi_1\mu_3 = (1-\phi_1)^2\phi_3 + 2(1-\phi_1)\phi_1(1-\phi_3)$$
$$C_c = \phi_1^2 \mu_3 + 2\mu_1\phi_1\phi_3 = \phi_1^2(1-\phi_3) + 2(1-\phi_1)\phi_1\phi_3$$
$$D_c = \phi_1^2 \phi_3 = \phi_1^2\phi_3$$

Inasmuch as $\phi_1 = \frac{1}{2}(T_f - \phi_3)$, each of the peak intensities can be related to the single variable ϕ_3. The behavior of A_c,B_c,C_c,D_c and ρ_c with varying ϕ_3 is strongly a function of T_f (i.e., the chemical composition of the amphibole). This can be seen in Figure 19, which shows the behavior of these parameters as a function of ϕ_3 (the site-occupancy variable) for amphiboles of different bulk compositions. Site-occupancies may be derived by setting A_c.... equal to A_o.... in the above equations and solving for ϕ_3; four values of ϕ_3 are obtained, and hence where the solution is poorly defined by one or more equations, a fairly precise value is still obtainable from the remaining equations.

Clustering is the tendency for the arrangements [FeFeFe]-OH and [MgMgMg]-OH to occur more often than expected for random mixing. Strens (1966) noted that the infrared technique was sensitive to this effect and suggested that clustering is indicated if the observed intensities of the A and D bands (A_o and D_o) exceed the calculated values assuming random mixing. Law (1976) questions the validity of this criterion for ordering, and Whittaker (1979) has systematically examined the behavior of band intensities with variation in degree of clustering and anti-clustering (the mutual avoidance of like cations). Clustering of Fe increases the intensity of both the A and D bands (although not equally) and anticlustering of Fe has the reverse effect. However, the intensities of the B and C bands are also affected by clustering in a very complex manner that is also a function of bulk composition. If clustering proves to be a common effect in amphiboles, it will almost certainly preclude any widespread use of the infrared method in cation-ordering studies.

ELECTRONIC ABSORPTION SPECTROSCOPY

The 3d orbitals of a transition metal ion are energetically degenerate in a spherically-symmetric potential field. Application of a potential field of lower symmetry removes this degeneracy, as the reducible representation spanned by these orbitals must contain the irreducible representation of the symmetry group. When light passes through a crystal containing a transition metal ion, certain wavelengths are absorbed by excitation of electrons between the nondegenerate 3d-orbital energy levels. As the character and amount of separation of the orbital energy levels is a function of the potential field applied by the crystal, occupancy of different sites in a crystal will produce absorption of different wavelengths of light. The spectra may also be complicated by inter-element electron transitions, i.e., charge transfer bands where the electron transitions take place from cation to anion, anion to cation or cation to cation. These transitions are particularly common when adjacent cations have variable valence states (e.g., Fe^{2+} and Fe^{3+}, Ti^{3+} and Ti^{4+}, Fe^{2+} and Ti^{4+}) and are a major cause of color and pleochroism in amphiboles (Manning and Nickel, 1969; Faye and Nickel, 1970; Strens, 1970). The intensity of this type of band is about two orders of magnitude larger than the intensity of normal d-d transitions. Thus, overlap of these two types of band in an absorption spectrum can obscure the d-d transition bands. The occurrence of more than one type of transition-metal cation in the structure, as is common in most amphiboles, will further complicate the interpretation of the absorption spectra.

The intensity of an absorption band depends on the probability of the transition. The transition probability is governed by the Laporte selection rule (King, 1964) which forbids transitions between 3d orbitals. When a transition-metal cation occupies a site without a center of symmetry, mixing of the 3d and 4p orbitals allows a transition, the intensity of which is a function of the degree of 3d-4p mixing, which is, in turn, related to the deviation of the cation environment from centrosymmetry. Thus, when a transition-metal cation occurs in more than one site in a crystal, the intensities of the d-d bands are a function of both the cation occupancies *and* the deviation of the cation environment from centrosymmetry. In centrosymmetric sites, some 3d-4p orbital mixing

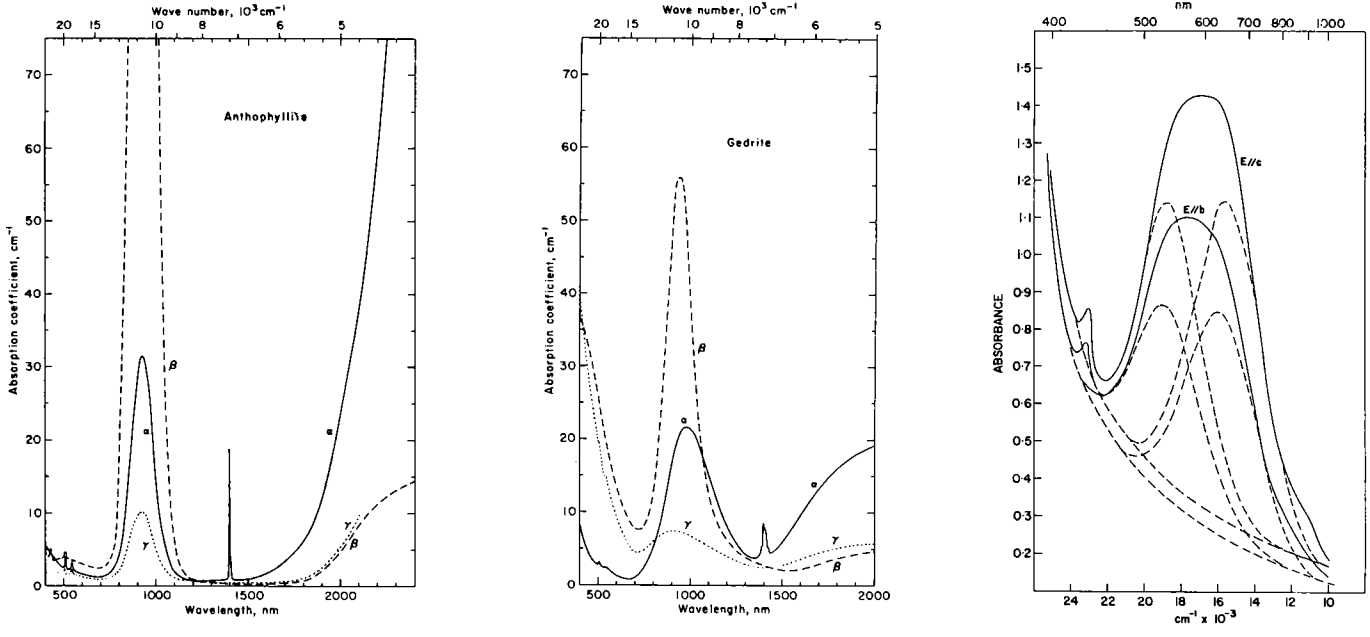

Figure 20. Polarized electronic absorption spectra for anthophyllite (left) and gedrite (center) (from Mao and Seifert, 1974), and holmquisite (right) (from Faye and Nickel, 1970).

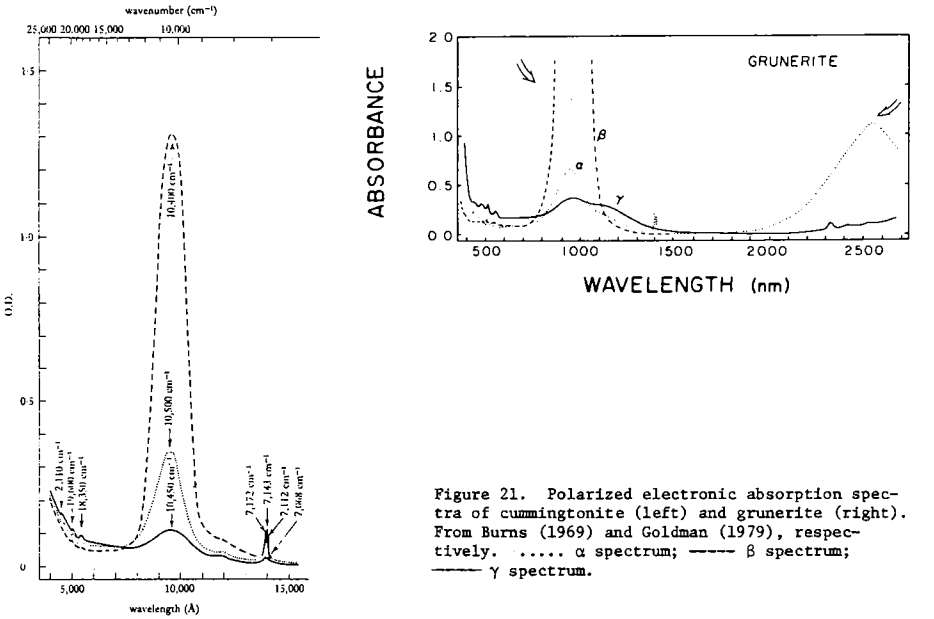

Figure 21. Polarized electronic absorption spectra of cummingtonite (left) and grunerite (right). From Burns (1969) and Goldman (1979), respectively. ..... α spectrum; ----- β spectrum; ——— γ spectrum.

may occur by vibronic coupling and hence very weak bands can result from cations in these sites. Local disorder can also give rise to intensification of d-d bands in solid solutions. Robbins and Strens (1972) have noted this effect in micas and termed it "substitutional intensification." This could lead to nonlinear relationships in Beer's law type plots.

Amphibole spectra

There is considerable variation in spectral appearance with amphibole type, and as with Mössbauer spectra, the interpretation and assignment of spectra is not a trivial matter.

Fe-Mg-Mn amphiboles. Spectra for these amphiboles are shown in Figures 20 and 21. The anthophyllite spectra are dominated by an intense band at ∿10,800 cm^{-1} that is particularly intense in the β spectrum and a broad intense band at ∿4200 cm^{-1} that is particularly intense in the α spectrum. These are assigned to d-d transitions in Fe^{2+} at the M4 site; the predominance of these bands in the spectra is a result of the very noncentrosymmetric configuration about the M4 site that allows violation of the Laporte selection rule. The polarization characteristics of these bands are also compatible with this assignment. The remaining features

of the spectra are much less intense. The sharp spike on the α spectrum at ∿7300 cm^{-1} is an overtone of the principal OH stretch. There are several minor bands in the region 17,000-23,000 cm^{-1}; these are assigned to spin-forbidden transitions in Fe^{2+}. The gedrite spectra are fairly similar to those of anthophyllite. They are also dominated by intense bands at ∿10,800 cm^{-1} in β and ∿4500 cm^{-1} in α that can be assigned to d-d transitions in Fe^{2+} at M4; however, these bands are significantly weaker than in anthophyllite in response to the more regular M4 environment in gedrite. These bands are also broader than in anthophyllite, presumably the result of substitutional broadening. The strong sloping absorption in the gedrite spectra in the region >15,000 cm^{-1} results from the presence of Fe^{3+} in the structure, causing the migration of the metal-ligand charge-transfer band into the visible region. The holmquistite spectrum is shown in Figure 20; it is dominated by an intense charge-transfer band in the 12,000-20,000 cm^{-1} region of the β and γ spectra. There is also a spin-forbidden Fe^{3+} band at ∿22,800 cm^{-1} and a weak spin-allowed Fe^{2+} d-d band at ∿10,800 cm^{-1} in the γ spectrum. Faye and Nickel (1970) chose to deconvolute the major absorption into two bands; discussion of this is deferred until later.

Cummingtonite and grunerite spectra (Fig. 21) show prominent bands at 1000 cm^{-1} (∿1000 nm) in β and 4000 cm^{-1} (∿2450 nm) in α, assigned to d-d transitions in Fe^{2+} at the M(4) site. Also common to both spectra are the sharp but weak spin-forbidden Fe^{2+} bands at 18,000-21,000 cm^{-1} (∿500 nm) and the fine-structure overtones of the principal OH stretch around 7100 cm^{-1}. In the cummingtonite spectra, there is a very weak band at ∿8400 cm^{-1} (∿1200 nm), becoming more prominent in the α and γ spectra of grunerite. Both the compositional dependence of the intensity and the position (by analogy with the orthopyroxene and pigeonite spectra) suggest that this may be assigned to a d-d transition in Fe^{2+} at the M(1), M(2) and M(3) sites. Inasmuch as the environment of M(2) is much more noncentrosymmetric than those of the M(1) and M(3) sites, this should primarily be due to Fe^{2+} at M(2). Comparison with the spectrum of hedenbergite (Rossman, 1980) suggests that other d-d bands due to Fe^{2+} at M(1), M(2) and M(3) may be incorporated into the major absorption bands at ∿10,200 cm^{-1} (∿1000 nm).

Calcic amphiboles. Spectra for these amphiboles are shown in Figure 22. The tremolite and actinolite spectra are dominated by an intense band at ∿9800 cm^{-1} in the β spectrum; also present is a broad absorption at ∿4200 cm^{-1}. Through examination of several amphiboles and heating experiments, Goldman and Rossman (1977) show that the intensity of the 9800 cm^{-1} and 4200 cm^{-1} bands are related, and thus the bands must arise from the same Fe^{2+} cation. Comparison with the Mg-Fe-Mn amphiboles, stoichiometric arguments and band intensity considerations show that these two bands can be assigned to d-d transitions of Fe^{2+} at the M(4) site. Weak spin-forbidden Fe^{2+} and Fe^{3+} transitions occur from ∿18,000-23,000 cm^{-1}, and the overtone of the principal OH stretch is prominent at ∿7300 cm^{-1}. Bands at ∿15,200 cm^{-1} in β and ∿13,800 cm^{-1} in γ may be assigned to Fe^{2+}/Fe^{3+} intervalence charge-transfer (IVCT) bands (in the absence of Cr^{3+}); there is no comparable band in the α spectrum where there is no component of an $^{VI}Fe^{2+}$-$^{VI}Fe^{3+}$ separation parallel to the electric vector. The broad weak bands between 8000 and 12,000 cm^{-1} in the γ spectrum are probably d-d transitions of Fe^{2+} at the M(1), M(2) and M(3) sites, particularly the M(2) site. The fine-structure in the region of ∿4200 cm^{-1} can be attributed to infrared combination modes.

The spectrum of pargasite (Fig. 22) lacks the prominent bands at ∿10,200 cm in β and ∿4200 cm^{-1} in α that are characteristic of Fe^{2+} at M(4); this is in agreement with the stoichiometry of this particular amphibole which indicates no excess of C-type cations at M(4) (Goldman and Rossman, 1977). Weak bands in the 8000-13,000 cm^{-1} region are most probably d-d transitions of Fe^{2+} at M(1),(2),(3), and weak spin-forbidden Fe^{2+} and Fe^{3+} bands occur above ∿20,000 cm^{-1}. In the β and γ spectra are broad bands at ∿15,000 cm^{-1}; their position and polarization dependence suggest that they are Fe^{3+}/Fe^{2+} IVCT bands, but they are surprisingly weak compared with corresponding bands in other amphibole spectra. The wing of the ultraviolet charge-transfer band extends well into the visible region in the β and γ spectra, presumably the result of significant Fe^{3+} at the M(2) site.

Sodic-calcic amphiboles. Spectra are shown in Figure 23. The spectra of potassian ferri-taramite are dominated by broad assymetric bands centered on ∿16,000 cm^{-1} and ∿15,000 cm^{-1} in the β and γ spectra, respectively. The polarization dependence, position and intensity show

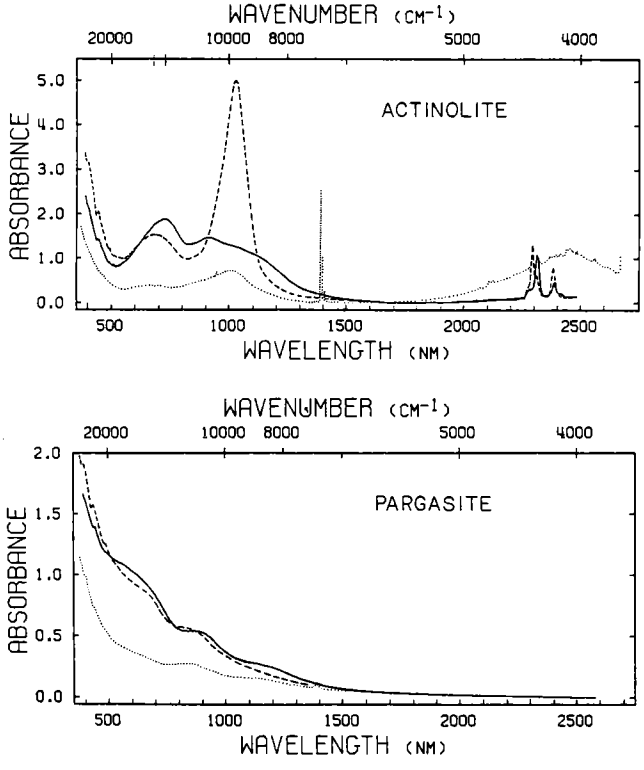

Figure 22. Polarized electronic absorption spectra of actinolite (top) and pargasite (bottom). From Goldman and Rossman (1977). ..... α spectrum; ------ β spectrum; ——— γ spectrum.

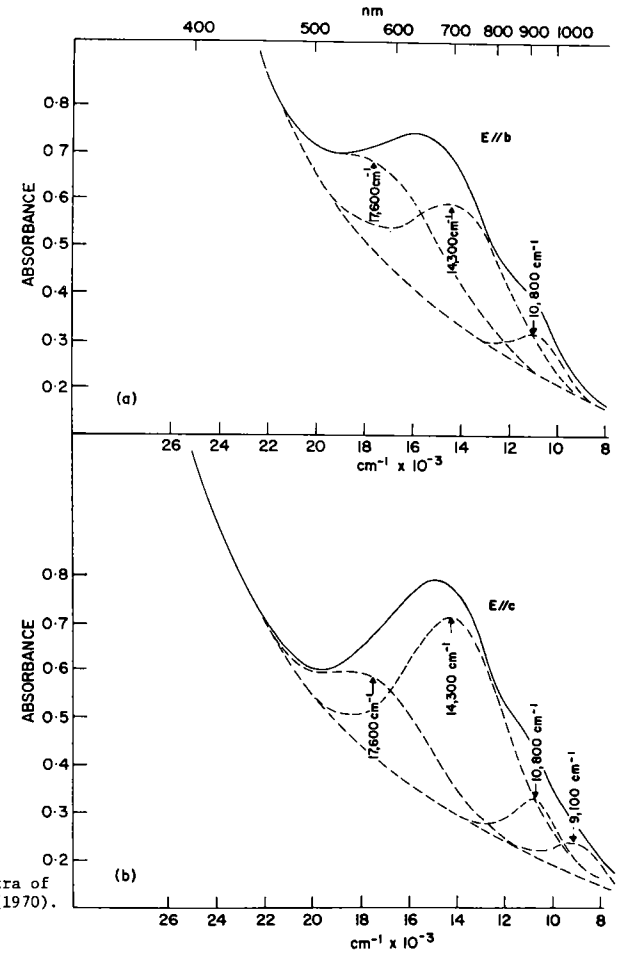

Figure 23. Polarized electronic absorption spectra of potassian ferri-taramite. From Faye and Nickel (1970).

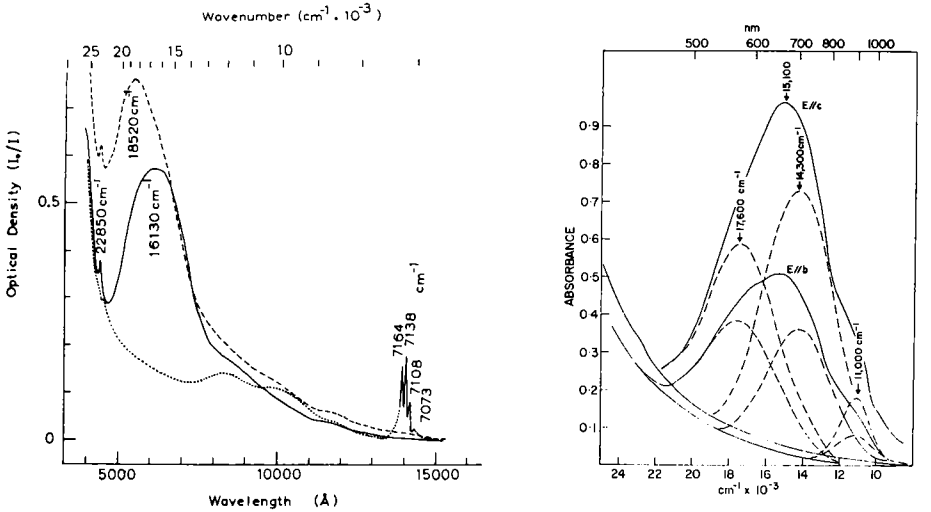

Figure 24. Polarized electronic absorption spectra of glaucophane (left) and riebeckite (right). From Bancroft and Burns (1969) and Faye and Nickel (1970). For glaucophane; ..... α spectrum; ----- β spectrum; ——— γ spectrum.

this to be an intervalence charge-transfer band. There is a prominent shoulder at ∿10,800 cm^{-1} in both the β and the γ spectra, with possibly a secondary shoulder in the γ spectrum at ∿9100 cm^{-1}. These may be assigned to d-d transitions of Fe^{2+}; without the α spectrum at lower wavelengths, it would be premature to assign these to Fe^{2+} at any specific site. Faye and Nickel (1970) deconvoluted the IVCT band into two component bands at ∿17,600 cm^{-1} and 14,300 cm^{-1}, assigning these to $Fe^{2+}_{M(1)} \rightarrow Fe^{3+}_{M(3)}$ and $Fe^{2+}_{M(1)} \rightarrow Fe^{3+}_{M(2)}$ interactions, respectively. This assignment is rather unlikely considering the cation arrangement and configuration in this amphibole (Hawthorne and Grundy, 1978). However, these charge-transfer bands should be composite. The β spectrum should have two Fe^{2+}/Fe^{3+} IVCT bands of approximately equal intensity: $Fe^{2+}_{M(3)} \rightarrow Fe^{3+}_{M(2)}$ and $Fe^{2+}_{M(1)} \rightarrow Fe^{3+}_{M(2)}$; the γ spectrum should have a single Fe^{2+}/Fe^{3+} IVCT band approximately equal in intensity to the resultant band in the β spectrum: $Fe^{2+}_{M(1)} \rightarrow Fe^{3+}_{M(2)}$. This amphibole also contains significant Ti and Mn, giving rise to the possiblity of heteronuclear IVCT bands contributing to the major absorption.

Alkali amphiboles. Spectra for alkali amphiboles are shown in Figure 24. The spectra of glaucophane are dominated by intense charge-

transfer bands at ∿18,500 cm^{-1} and ∿16,100 cm^{-1} in β and γ, respectively. The γ band will contain only a component of the $Fe^{2+}_{M(1)} \rightarrow Fe^{3+}_{M(2)}$ interaction, whereas the β band is due to both this and the $Fe^{2+}_{M(1)} \rightarrow Fe^{3+}_{M(2)}$ interaction; the β band is slightly asymmetric, suggesting an $Fe^{2+}_{M(1)} \rightarrow Fe^{3+}_{M(2)}$ component to its total intensity. The relative energies of the $Fe^{2+}_{M(1)} \rightarrow Fe^{3+}_{M(2)}$ and $Fe^{2+}_{M(3)} \rightarrow Fe^{3+}_{M(2)}$ interactions, as expected from their cation distances, are (M(1)-M(2) < M(2)-M(3)). The spin-forbidden Fe^{3+} peak at ∿22,300 cm^{-1} and the OH stretch overtones at ∿7100 cm^{-1} are also present. The remaining weak bands between 8000 and 13,000 cm^{-1} are d-d transitions of Fe^{2+} at M(1) and M(3).

The spectrum of riebeckite (Fig. 24) is similar to that of glaucophane in that it also is dominated by intense charge-transfer bands in the β and γ spectra. The reason for the much greater band width in riebeckite as compared with glaucophane is not clear.

Other transition metals

Thus far we have only considered spectral contributions from Fe^{2+} and Fe^{3+}. Amphiboles are very gregarious and frequently associate with other transition metals, particularly Mn and Ti. When present in significant amounts, these will contribute to the absorption spectrum, primarily through d-d transitions and heteronuclear IVCT transitions. It is necessary to characterize the spectra of these cations in chemically simple amphiboles so that their presence in more complex amphibole spectra can be recognized.

Figure 25 shows the spectra of a tremolite containing significant Mn. The wide bands at 15,000-20,000 cm^{-1} (∿550 nm) have been assigned to d-d transitions in Mn^{3+}, with the sharp bands at ∿22,000 cm^{-1} (∿420 nm) being spin-forbidden Mn^{2+} or Mn^{3+} transitions. Many amphiboles have prominent Fe^{2+}/Fe^{3+} IVCT bands around ∿15,000 cm^{-1} (∿650 nm) in their β and γ spectra that will tend to obscure any Mn bands; however, the Mn bands should still be observable in the α spectra.

Tremolite with significant Cr^{3+} (Fig. 26) shows broad bands at ∿15,400 cm^{-1} (∿650 nm) and ∿22,200 cm^{-1} (∿450 nm) that are (spin allowed) d-d transitions of Cr^{3+}, with sharp bands at ∿14,400 cm^{-1} (∿695 nm) and ∿14,600 cm^{-1} (∿685 nm) being spin-forbidden transitions. Figure 27 shows the spectrum of an actinolite with significant Cr^{3+}. The bands at

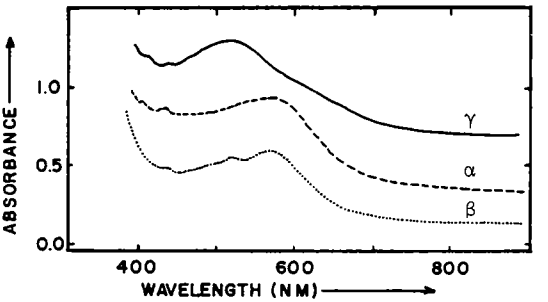

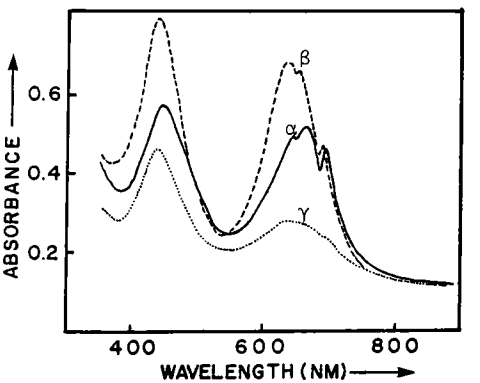

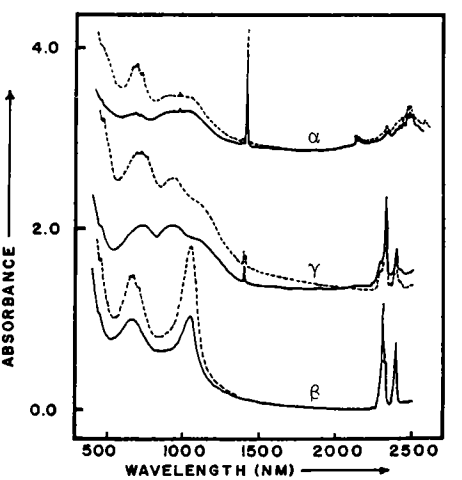

Figure 25 (top). Polarized electronic absorption spectra of Mn-containing tremolite.

Figure 26 (center). Polarized electronic absorption spectra of Cr-bearing tremolite.

Figure 27 (bottom). Polarized electronic absorption spectra of Cr-bearing actinolite.

All three figures from Goldman (1977).

$\sim$15,400 cm^{-1} ($\sim$650 nm) are characteristic, particularly in the α spectrum; without the α spectrum, it is possible that these could be confused with an Fe^{2+}/Fe^{3+} IVCT band. This illustrates the importance of characterizing all transition-metal spectra in amphiboles so that transitions are not overlooked or wrongly assigned.

OTHER TYPES OF SPECTROSCOPIC INVESTIGATION

Other types of spectroscopy have not been extensively applied to the amphiboles, and any studies have been solely exploratory in nature. Kalinichenko *et al.* (1977) used proton magnetic resonance (PMR) to characterize the cation occupancies of the M(1) and M(3) sites; this method is subject to all the drawbacks of the infrared method. X-ray photoelectron spectra of anthophyllite and magnesio-riebeckite are reported by Adams *et al.* (1972); the occurrence of Fe^{2+} and Fe^{3+} in magnesio-riebeckite did not lead to any broadening of the Fe 2p or 3s lines. Bershov *et al.* (1966) and Manoogian (1968) have examined the electron spin resonance (ESR) of Mn^{2+} in tremolite; both studies concluded that Mn^{2+} occupied "one site," and by analogy with the results of Vinokurov *et al.* (1964) on diopside, Bershov *et al.* (1966) suggest that this is the Mg site, i.e., M(1), M(2) and/or M(3). Ghose *et al.* (1968) and Ghose and Schindler (1969) advance a persuasive argument to reverse the site-assignment of the spin Hamiltonian parameters in diopside. Applying the same argument to the results for tremolite indicates that Mn^{2+} occupies the M(4) site. Diffuse reflectance spectra of several amphiboles are presented by Hunt and Salisbury (1970), Adams (1975) and Smith and Strens (1976). These spectra exhibit far less resolution that corresponding polarized transmission spectra.

CONCLUSIONS AND SUGGESTIONS FOR FUTURE WORK

In the decade of the 1970's there has been considerable advance in our understanding and interpretation of the spectroscopy of amphiboles. In many cases, this has involved the discovery of hitherto unrecognized problems in the application of these methods. However, this should be viewed as an important step forward as it leads to a more realistic use of each method. Particularly in minerals as complex as the amphiboles,

it is necessary to regard experimental techniques as complementary rather than competitive or mutually exclusive. The very specific sensitivity of many of the spectroscopic techniques make them a natural counterpart to both diffraction techniques and other spectroscopic methods. The difficulties and ambiguities involved in an experimental method can often be substantially reduced by using a combination of experimental techniques pertinent to the specific problem at hand.

Many of the problems of spectral interpretation could be alleviated by systematic examination of analyzed synthetic amphiboles:

(i) Mössbauer examination of Fe^{2+} and Fe^{3+} *end-member* compositions; because the relative peak intensities are fixed, the correct association of peaks and assignment of doublets will be apparent.

(ii) polarized electronic absorption spectroscopy of synthetic (or possibly natural) amphiboles containing a single transition metal, particularly Ti and Mn.

(iii) polarized electronic absorption spectroscopy of synthetic (or possibly natural) amphiboles containing pairs of transition metals in different valence states; this would allow evaluation of the different IVCT bands which must occur in the more complex natural amphiboles.

(iv) preparation of a series of synthetic amphiboles with M(2) = Al [or Sc] (pargasite/ferro-pargasite, glaucophane/ferro-glaucophane) and their characterization by Mössbauer and infrared spectroscopy and crystal structure refinement. This would allow a practical evaluation of the infrared method under optimum conditions.

ACKNOWLEDGMENTS

I thank Dr. George R. Rossman, California Institute of Technology, for his comments on this manuscript. Financial support was provided by a research fellowship and grant to the author from the Natural Sciences and Engineering Research Council of Canada.

Adams, I., Thomas, J. M. and Bancroft, G. M. (1972) An ESCA study of silicate minerals. Earth Planet. Sci. Lett. 16, 429-439.

Adams, J. B. (1975) Interpretation of reflectance spectra of pyroxenes and other rock-forming minerals. In *Infrared and Raman Spectroscopy of Lunar and Terrestrial Minerals*. Academic Press, New York.

Bancroft, G. M. (1973) *Mössbauer Spectroscopy. An Introduction for Inorganic Chemists and Geochemists*. McGraw-Hill Book Co., Inc., New York.

_____ and Brown, J. R. (1975) A Mössbauer study of coexisting hornblendes and biotites: Quantitative Fe^{3+}/Fe^{2+} ratios. Amer. Mineral. 60, 265-272.

_____ and Burns, R. G. (1969) Mössbauer and absorption spectral study of alkali amphiboles. Mineral Soc. Amer. Spec. Paper 2, 137-148.

_____, _____ and Maddock, A. G. (1967a) Determination of the cation distribution in the cummingtonite-grunerite series by Mössbauer spectroscopy. Amer. Mineral. 52, 1009-1026.

_____, _____, and Strens, R. G. J. (1966) Cation distribution in anthophyllite from Mössbauer and infrared spectroscopy. Nature 212, 913-915.

_____, Maddock, A. G. and Burns, R. G. (1967b) Applications of the Mössbauer effect to silicate mineralogy - I. Iron silicates of known crystal structure. Geochim. Cosmochim. Acta 31, 2219-2246.

Barabanov, A. V. and Tomilov, S. B. (1973) Mössbauer study of the isomorphous series anthophyllite-gedrite and cummingtonite-grunerite. Geochem. Intern. 1973, 1240-1267.

_____, Zorina, M. L. and Sobolev, V. K. (1974) Infrared spectra of amphiboles from metamorphic rocks. Mater. Mineral. Kol'sk. Poluostrova 10, 165-175.

Bershov, L. V., Marfunin, A. S. and Mineyeva, R. M. (1966) Electron paramagnetic resonance of Mn^{2+} in tremolite. Geochem. Intern. 1966, 352-355.

Blaha, J. J. and Rosasco, G. J. (1978) Raman microprobe spectra of individual microcrystals and fibers of talc, tremolite, and related silicate minerals. Anal. Chem. 50, 892-896.

Borg, R. J. and Borg, I. Y. (1974) Magnetic order in certain alkali amphiboles. A Mössbauer investigation. J. Physics (Paris) 6, 553-556.

_____ and _____ (1980) Mössbauer study of behavior of oriented single crystals of riebeckite at low temperatures and their magnetic properties. Phys. Chem. Minerals 5, 219-234.

_____, Szofran, F. R., Burmester, W. L. and Sellmyer, D. J. (1974) Magnetic ordering in several Fe-chain silicate compounds. Proc. 20th Annual Conf. on Magnetism and Magnetic Materials 24, 365-368.

Buckley, A. N. and Wilkins, R. W. T. (1971) Mössbauer and infrared study of a volcanic amphibole. Amer. Mineral. 56, 90-100.

Burns, R. G. (1969) Optical absorption in silicates. In *The Application of Modern Physics to the Earth and Planetary Interiors*. S. K. Runcorn, ed., Wiley Interscience, London.

_____ (1970) *Mineralogical Applications of Crystal Field Theory*. Cambridge University Press, Cambridge, England.

_____ and Greaves, C. J. (1971) Correlations of infrared and Mössbauer site-population measurements of actinolites. Amer. Mineral. 56, 2010-2033.

_____ and Law, A. D. (1970) Hydroxyl stretching frequencies in the infrared spectra of anthophyllites and gedrites. Nature 226, 73-75.

_____ and Prentice, F. J. (1968) Distribution of iron cations in the crocidolite structure. Amer. Mineral. 53, 770-776.

_____ and Strens, R. G. J. (1966) Infrared study of the hydroxyl bands in clinoamphiboles. Science 153, 890-892.

Cameron, M. (1970) *The Crystal Chemistry of Tremolite and Richterite. A Study of Selected Anion and Cation Substitutions*. Ph.D. Dissertation, Virginia Polytechnic Institute and State University, Blacksburg, VA.

Eisenstein, J. C., Taragin, M. F. and Thornton, D. D. (1975) Antiferromagnetic order in amphibole asbestos. AIP Conf. Proc. 24, 357-358.

Ernst, W. G. and Wai, C. M. (1970) Infrared, X-ray and optical absorption study of cation ordering and dehydrogenation in natural and heat-treated sodic amphiboles. Amer. Mineral. 55, 1226-1258.

Farmer, V. C., ed. (1974) *The Infrared Structure of Minerals*. The Mineralogical Society, London.

Faye, G. H. and Nickel, E. H. (1970) The effect of charge-transfer processes on the colour and pleochroism of amphiboles. Canadian Mineral. 10, 616-635.

Ghose, S. and Schindler, P. (1969) Determination of the distribution of trace amounts of Mn^{2+} in diopsides by electron paramagnetic resonance. Mineral Soc. Amer. Spec. Paper 2, 51-58.

_____, _____ and Hafner, S. S. (1968) Mn^{2+} distribution in diopsides by electron spin resonance (abstr.). Trans. Amer. Geophys. Union 49, 340.

Goldman, D. A. (1977) *Crystal Field and Mössbauer Applications to the Study of Site Distribution and Electronic Properties of Ferrous Iron in Minerals with Emphasis on Calcic Amphiboles, Orthopyroxene and Cordierite.* Ph.D. Dissertation, California Institute of Technology, Pasadena, CA.

_____ (1979) A re-evaluation of the Mössbauer spectroscopy of calcic amphiboles. Amer. Mineral. 64, 109-118.

_____ and Rossman, G. R. (1977) The identification of Fe^{2+} in the M(4) site of calcic amphiboles. Amer. Mineral. 62, 205-216.

Hafner, S. S. and Ghose, S. (1971) Iron and magnesium distribution in cummingtonites $(Fe,Mg)_7Si_8O_{22}(OH)_2$. Z. Kristallogr. 133, 301-326.

Hawthorne, F. C. (1981) The quantitative characterization of cation ordering in minerals. A review. Amer. Mineral. (submitted).

_____ (1982) The crystal chemistry of the amphiboles: a review. Canadian Mineral. (submitted).

_____ and Grundy, H. D. (1978) The crystal chemistry of the amphiboles. VII. The crystal structure and site-chemistry of potassian ferri-taramite. Canadian Mineral. 16, 53-62.

Hunt, G. R. and Salisbury, J. W. (1970) Visible and near infrared spectra of minerals and rocks. I. Silicate minerals . Mod. Geol. 1, 283-300.

Ingalls, R. L. (1964) Electric field gradient tensor in ionic compounds. Phys. Rev. 133, A787-A795.

Kalinichenko, A. M., Ranzaraksheev, N. Yu., Matyash, I. V., Litvin, A. L. and Pol'shin, E. V. (1977) Refinement of the structural characteristics of hornblendes by reference to proton-magnetic-resonance data. Sov. Phys. Crystallogr. 22, 225-226.

Karr, C., ed. (1975) *Infrared and Raman Spectroscopy of Lunar and Terrestrial Minerals.* Academic Press, New York.

King, G. W. (1964) *Spectroscopy and Molecular Structure.* Holt, Rinehart and Winston Inc., New York.

Kitamura, M., Tokonami, M. and Morimoto, N. (1975) Distribution of titanium atoms in oxy-kaersutite. Contrib. Mineral. Petrol. 51, 167-172.

Kukovskii, E. G. and Litvin, A. L. (1970) Infrared spectra of amphiboles. Konst. Svoistva. Mineral. 4, 81-85.

Law, A. D. (1973) Critical evaluation of "statistical best fits" to Mössbauer spectra. Amer. Mineral. 58, 128-131.

_____ (1976) A model for the investigation of hydroxyl spectra of amphiboles. In *Physics and Chemistry of Minerals and Rocks,* R. G. J. Strens, ed., NATO Adv. Study Inst. "Petrophysics". Wiley, New York.

Lazarev, A. N. (1972) *Vibrational Spectra and Structure of Silicates.* Consultants Bureau, New York.

Manning, P. G. and Nickel, E. H. (1969) Origin of colour and pleochroism of a titan-augite from Kaiserstuhl and of a riebeckite. Canadian Mineral. 10, 71-83.

Manoogian, A. (1968) The electron spin resonance of Mn^{2+} in tremolite. Canadian J. Phys. 46, 129-133.

Mao, H. K. and Seifert, F. (1974) A study of the crystal-field effects of iron in the amphiboles anthophyllite and gedrite. Carnegie Inst. Wash. Yearbook 73, 500-502.

Maresch, W. V. and Langer, K. (1976) Synthesis, lattice constants and OH-valence vibrations of an orthorhombic amphibole with excess OH in the system Li_2O-MgO-SiO_2-H_2O. Contrib. Mineral. Petrol. 56, 27-34.

Nikitina, L. P., Petkevich, E. Z., Sverdlova, O. V. and Khristoforov, K. K. (1973) Determination of occupancy of octahedral positions in the structures of amphiboles $(Ca,Na,K)_{2-3}(Fe^{2+},Fe^{3+},Mg,Al)_5[(Si,Al)_4O_{11}]_2(OH)_2$ from vibrations of OH^-. Geochim. Int. 1973, 1233-1239.

Robbins, D. W. and Strens, R. G. J. (1972) Charge-transfer in ferromagnesian silicates: the polarized electronic spectra of tri-octahedral micas. Mineral. Mag. 38, 551-563.

Rosenburg, P. E. and Foit, F. F. (1977) Fe^{2+}-F avoidance in silicates. Geochim. Cosmochim. Acta 41, 345-346.

Rossman, G. R. (1980) Structural information from quantitative infrared spectra of minerals. Trans. Amer. Crystallogr. Assn. 15, 77-91.

Rouxhet, P. G. (1970) Kinetics of dehydroxylation and of OH-OD exchange in macrocrystalline micas. Amer. Mineral. 55, 841-853.

Rowbotham, G. and Farmer, V. C. (1973) The effect of "A" site occupancy on the hydroxyl stretching frequency in clinoamphiboles. Contrib. Mineral. Petrol. 38, 147-149.

Seifert, F. (1977) Compositional dependence of the hyperfine interaction of ^{57}Fe in anthophyllite. Phys. Chem. Minerals 1, 43-52.

Semet, M. P. (1973) A crystal-chemical study of synthetic magnesiohastingsite. Amer. Mineral. 58, 480-494.

Smith, G. and Strens, R. G. J. (1976) Intervalence transfer absorption in some silicate, oxide and phosphate minerals. In *Physics and Chemistry of Minerals and Rocks,* R. G. J. Strens, ed., NATO Adv. Study Inst. "Petrophysics". Wiley, New York.

Strens, R. G. J. (1966) Infrared study of cation ordering and clustering in some (Fe,Mg) amphibole solid solutions. Chem. Comm. 15, 519-520.

_____ (1970) Structural interpretation of the infrared absorption spectra and optical properties of glaucophane and related minerals (abstr.). Amer. Mineral. 55, 313.

_____ (1974) The common chain, ribbon, and ring silicates. In *The Infrared Spectra of Minerals.* Mineral. Soc., London, 305-330.

Vinokurov, V. M., Zaripov, M. M. and Stepanov, V. G. (1964) Paramagnetic resonance of Mn^{2+} in diopside crystals. Sov. Phys. Sol. State 6, 870-875.

Virgo, D. (1974) Preliminary fitting of ^{57}Fe Mössbauer spectra of synthetic Mg-Fe richterites. Carnegie Inst. Wash. Yearbook 73, 513-516.

Wertheim, G. K. (1964) *The Mössbauer Effect. Principles and Applications.* Academic Press, New York.

White, W. B. (1975) Structural interpretation of lunar and terrestrial minerals by raman spectroscopy. In *Infrared and Raman Spectroscopy of Lunar and Terrestrial Minerals.* Academic Press Inc., New York.

Whittaker, E. J. W. (1979) Clustering of cations in amphiboles. Phys. Chem. Minerals 4, 1-10.

Wilkins, R. W. T. (1970) Iron-magnesium distribution in the tremolite-actinolite series. Amer. Mineral. 55, 1993-1998.

_____, Davidson, L. R. and Ross, J. R. (1970) Occurrence and infrared spectra of holmquistite and hornblende from Mt. Marion near Kalgoorlie, Western Australia. Contrib. Mineral. Petrol. 228, 280-287.

Chapter 3

An INTRODUCTION to the MINERALOGY and PETROLOGY of the BIOPYRIBOLES

James B. Thompson, Jr.

INTRODUCTION

Although this volume is concerned primarily with amphiboles and other hydrous pyriboles, it is convenient to consider them in this paper as part of a larger mineral supergroup, the biopyriboles, including the pyroxenes (anhydrous pyriboles) at the one extreme and the trioctahedral micas (biotite, talc, etc.) at the other. All hydrous pyriboles may be regarded, at least in an idealized way, as being made of layer modules as in Figures 1 and 2, some of which are pyroxene-like, and some of which are mica-like (see Thompson, 1970, 1978).

The hydrous pyriboles thus have many crystallographic and crystallochemical features in common with either pyroxenes or trioctahedral micas, or both. Because they also have much in common chemically and are often intimately associated in rocks with pyroxenes, micas, or both, it is impossible to consider their phase relations and thermodynamic stability other than in the context of the biopyriboles as a whole.

Hydrous pyriboles have a variety of distinct crystallographic sites that can be occupied, wholly or in part, by all of the major elements found in rocks, as well as many of the minor ones. Indeed, certain common basaltic compositions may, under appropriate conditions (Yoder and Tilley, 1962), be recrystallized wholly to amphibole. Amphiboles play a major role in the metamorphism of mafic rocks and of impure carbonate rocks (Robinson *et al.*, Chapter 8 in the companion volume of this one, Volume 9B). Certain amphiboles, in fact, may be stable well into the Earth's upper mantle.

PYRIBOLE POLYSOMES

The idealization of pyriboles as successive layers (010), along their *b*-axes, of pyroxene and mica modules, leads to their preliminary characterization by means of a stacking formula giving the sequence of mica (M) and pyroxene (P) layers. If the pyribole is an ordered polysome, the sequence is necessarily cyclic, and one cycle is a sufficient characterizatio

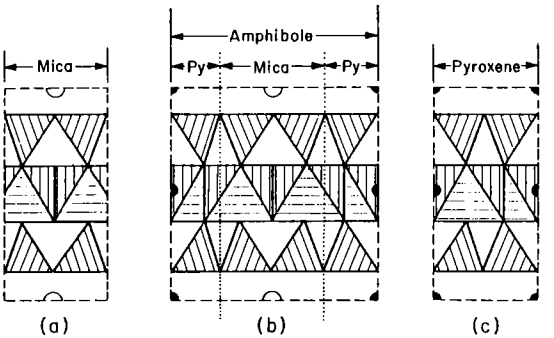

Figure 1. Idealized beam-modules for biopyriboles as seen in cross-section. A sites of amphibole and K sites of micas are shown by open half circles, M4 sites of amphiboles and M2 sites of pyroxenes are shown by solid half circles or quarter circles. All other M sites are idealized as regular octahedra of equal size, and all Si sites are idealized as regular tetrahedra of equal size. The ratio of the tetrahedral edge to the octahedral edge is $\sqrt{3}/2$.

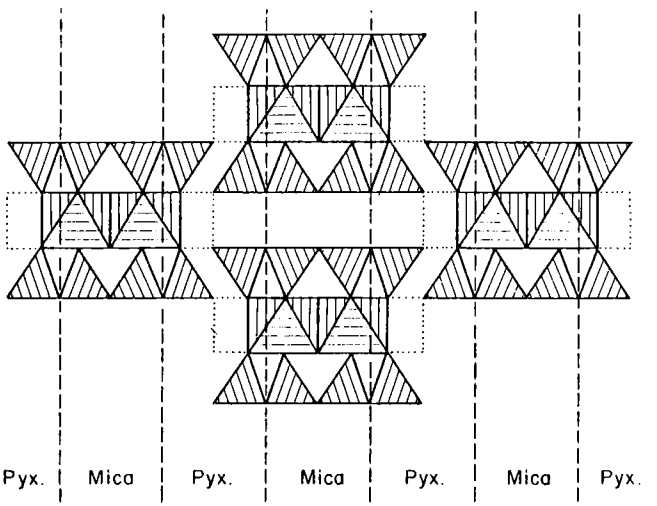

Figure 2. Idealized section $\perp c$ of a $C2/m$ ($I2/m$, if referred to pyroxene axes) amphibole such as tremolite. Dashed vertical lines show (010) cuts that factor it into mica and pyroxene layer modules.

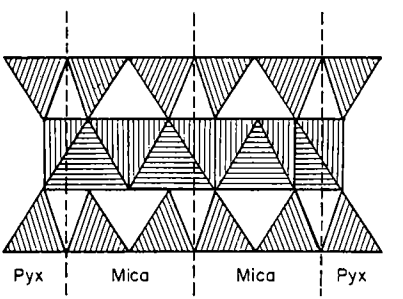

Figure 3. Idealized beam-module found in chesterite and jimthompsonite. Silicon-oxygen strips are of the triple-chain type.

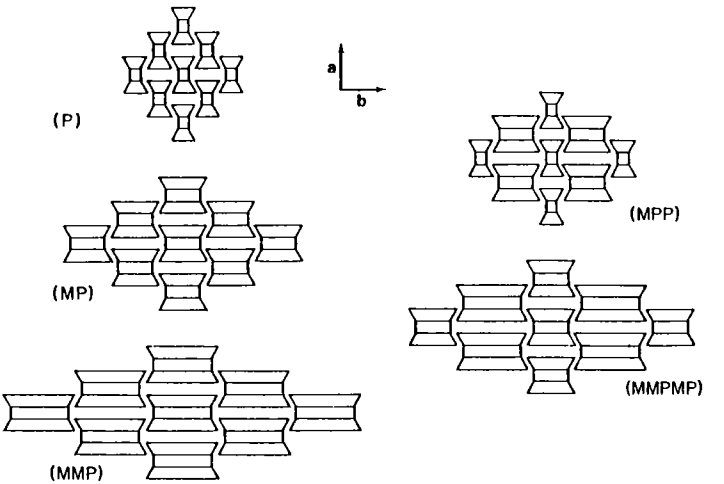

Figure 4. Sections $\perp c$ of some simple pyribole forms. The series on the left ($M_{(n-1)}P$) includes pyroxene, amphibole and jimthompsonite. That on the right ($M_nPM_{(n-1)}P$) includes chesterite (MMPMP). The form (MPP) is a possible form that may yet be found in uralites or smaragdites (amphibole-like alterations of pyroxenes).

Common pyroxenes are thus (P) rather than (PPP---), and common amphiboles are (MP) rather than (MPMPMP-----).

Structurally, the appearance of the sequence ---PP--- in a formula implies the existence of single-chain or pyroxene-like beams parallel to the c-axis, and the sequence ---PMP--- implies the presence of double-chain or amphibole-like beams. Triple-chain beams such as that of Figure 3 are implied by the sequence ---PMMP---, and so forth.

The pyriboles thus far known, at least those that can be isolated as single crystals, fall into two series, as shown in Figure 4. The principal series conforms to the general formula $(M_{(n-1)}P)$ where n is a positive integer giving the number of silicon-oxygen chains in each tetrahedral strip. Thus, if $n = 1$ we have the single-chain pyroxene structure (P) and if $n = 2$ the double-chain amphibole structure (MP). If $n = 3$ we have the triple-chain structure (Veblen and Burnham, 1978a,b) of the jimthompsonite type (MMP).

Although only one member has yet been found as isolated single crystals, it appears that a second series exists conforming to the general formula $M_nPM_{(n-1)}P$. In this series, the tetrahedral strips are of two

types, one containing (n+1)-fold chains and the other n-fold chains. If n = 1, the form MPP would result, yielding a crystal intermediate in both chemical and physical properties between amphibole and pyroxene. It has not yet been isolated as an ordered single crystal, but still might be found, perhaps in an alteration of the uralite or smaragdite type of pyroxenes. The uralites thus far examined, however, are disordered polysomes (approximately amphibole) containing only isolated occurrences of the sequence MPP (Veblen, pers. comm.). If n = 2, we have structures of the chesterite-type (MMPMP), intermediate between amphibole (MP) and jimthompsonite (MMP).

The limit as $n \to \infty$ for both series is talc or a trioctahedral mica (M). Other more complex forms, not belonging to either series, are structurally possible. Of the known, ordered forms, however, it seems probable that only pyroxene, amphibole, and trioctahedral mica occur as other than metastable or "Ostwald" phases. In particular, chesterite and jimthompsonite occur as alteration products of anthophyllite embedded in talc and hence may be metastable relative to anthophyllite-talc (Veblen and Burnham, 1978a,b). Disordered sequences like those in uralites also occur in amphibole-to-talc or amphibole-to-mica alterations. Highly disordered polysomes are at best crystalline in only two dimensions, inasmuch as they are devoid of long-range periodicity along their b-axes (Veblen and Buseck, 1979).

The chemical formulas of ordered polysomes are readily deduced from the polysome stacking formula, if the compositions of the isolated P- and M-layers are known. Thus, if the P-layers are chemically diopside and the M-layers are chemically talc, then each P-layer contributes $Ca_2Mg_2Si_4O_{12}$ and each M-layer contributes $\square Mg_3Si_4O_{10}(OH)_2$. The five simplest pyriboles obtainable by combination of these two modules are then

P $Ca_2Mg_2Si_4O_{12}$ or $CaMgSi_2O_6$ (diopside)

MP $\square Ca_2Mg_5Si_8O_{22}(OH)_2$ (tremolite)

MMP $\square_2Ca_2Mg_8Si_{12}O_{32}(OH)_4$ or $CaMg_4Si_6O_{16}(OH)_2$ (see nephrites in Veblen, this volume)

MPP $\square Ca_4Mg_7Si_{12}O_{34}(OH)_2$ (not yet observed at this composition)

MMPMP $\square_3Ca_4Mg_{13}Si_{20}O_{54}(OH)_6$ (not yet observed at this composition)

All are collinear in composition space with talc and diopside.

PYRIBOLE POLYTYPES

It is apparent from Figure 2 or Figure 4 that pyriboles may also be regarded as made of layer modules parallel to (100). Specifically, layers containing octahedral strips alternate along the a-axes with layers containing tetrahedral strips. The octahedral strips, furthermore, may have two orientations related by a half-rotation about the normal to (100). These two orientations may be characterized by means of a stacking vector parallel to the a-axis. With (100) horizontal, we shall take the stacking vector as positive in the direction in which the ducks (Fig. 5) swim. This corresponds closely to the horizontal projections of the stacking vectors of Smith and Yoder (1956) for characterizing mica polytypes. The orientation of the Smith-Yoder vector, however, is a bit uncomfortable for the bird (Fig. 6); hence, we shall continue with the one defined here.

The key to the major pyribole polytypes is whether or not the stacking vector reverses between two neighboring octahedral layers. We shall therefore assign a dot (•) to the intervening tetrahedral layer if the two adjacent stacking vectors point the same way (parallel) and a cross (×) to the tetrahedral layer if the vectors are opposed (anti-parallel). By making cuts along the median planes of the octahedral layers, we may thus factor any pyribole into a series of layer modules that are either dot or cross modules. With a sequence of dots and crosses, we now have a system of polytype notation that is independent of the accident of initial orientation, unlike the common system using + and - octahedral orientations (see Hawthorne, Chapter 1, and Veblen, this volume). A preliminary characterization of a polytype is then obtained by a stacking formula consisting of a sequence of dots and crosses. If the stacking is an ordered one, the sequence is necessarily cyclic and, again, one cycle is sufficient.

The most frequently encountered polytype, that of the clinopyriboles, is that in which all vectors point the same way (•). Reversal of the vectors at each opportunity yields the protopyriboles (×), and the form (•×) yields the common orthopyriboles. These three simple polytypes are shown schematically in Figure 7. The clino- and protopyriboles contain

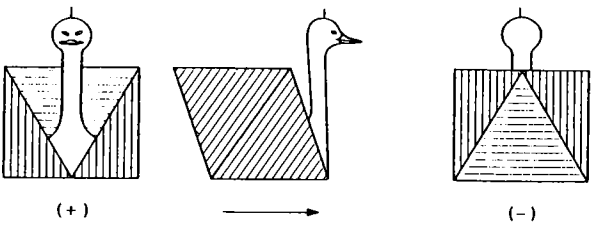

Figure 5. The octahedra in pyriboles are in strips along *c* and are oriented so that symmetry planes of the octahedra are parallel to (010). The stacking vector for a pyribole, with (100) horizontal, is taken as parallel to *c* and its positive direction as that in which the ducks swim.

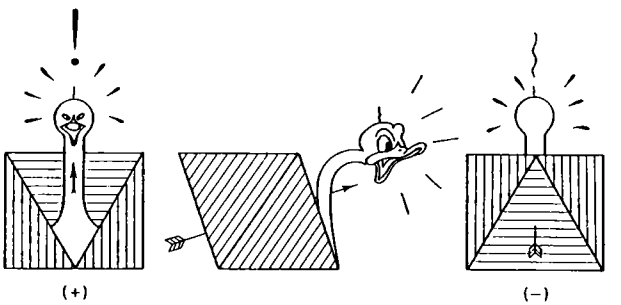

Figure 6. The stacking vector of Figure 5 corresponds to the horizontal projection of the Smith-Yoder (1956) vector for micas. The S-Y vector is distinctly uncomfortable but not necessarily fatal. A real duck so afflicted appeared on television and in the newspapers this past spring. Surgery was successful and the duck has recovered.

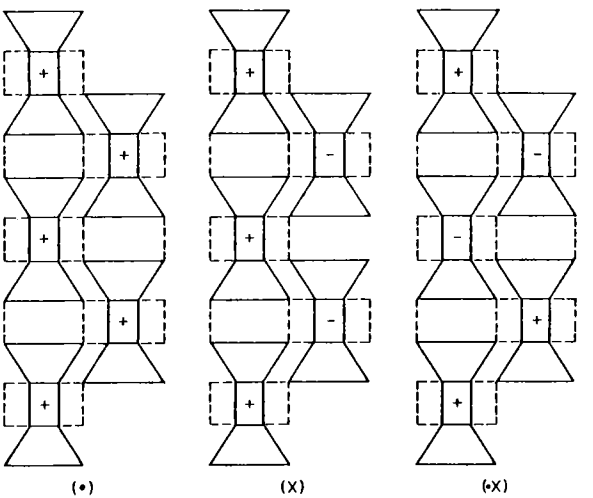

Figure 7. The three simplest pyribole polytypes (shown for pyroxene but applicable to any pyribole). Stacking vectors toward and away from the observer are shown by (+) and (-), respectively. The dot-cross notation discussed in the text is based on whether reversals do not (•) or do (×) occur between successive octahedral layers.

two octahedral layers per unit cell ($a \sin \beta \sim 9.0$ Å), and the orthopyriboles contain four octahedral layers ($a \sim 18.0$ Å). Some exotic forms are known with six or more octahedral layers per cell (Bystrom, 1943; Buseck and Iijima, 1975; Buseck *et al.*, 1980). These exotic forms, however, rarely occur in sufficient volume to be regarded as discrete single crystals. The rarity of pyriboles of exotic polytype suggests that these long-period forms are metastable relative to the three simplest ones: (•), (×), and (•×).

It is also evident from the work of Buseck and Iijima that there are disordered polytypes. As with disordered polysomes, these are truly crystalline in, at most, only two dimensions, inasmuch as there is no periodicity along a. If disordered both polysomatically and polytypically, there can be long-range periodicity in a pyribole only along c.

UNIT CELLS AND SPACE GROUPS[1]

Pyriboles are conventionally described so that the c-axis is parallel to the tetrahedral and octahedral strips (hence parallel to the intersection of the polysomatic and polytypic layers). The b-axis is taken parallel to the polytypic layers, insuring that these are always (100), and the a-axis is taken parallel to the polysomatic layers, insuring that these are always (010). The conventions for mica, however, are different in that (001), mica, corresponds structurally to (100), pyribole.

It is evident that the polysomatic and polytypic formulas are closely analogous in some of their properties. Certain numerical properties of either kind of stacking formula prove useful. In the polysome formula these are n_p, the number of P's per cycle; n_m, the number of M's per cycle; and n_c ($=n_p + n_m$), the number of modular interfaces per cycle. Any two of the three may be odd, or all may be even. This yields a primary distinction between P-C, M-P, and M-C pyriboles, in which n_p and n_c, n_m and n_p, and n_m and n_c, respectively, are odd (the odd-odd combinations); and E-E polysomes (all n's even). The first three may be thought of as pyroxene-like (including the common pyroxenes), amphibole-like (including the common amphiboles), and mica-like, respectively. The corresponding

---

[1]This section is a concentrated dose of material to be presented in extended form in *The Mineralogical Magazine* (1979 Hallimond Lecture).

quantities in the polytype cycle are n_d, the number of dots; n_x, the number of crosses; and n_z ($=n_d + n_x$), the number of modular interfaces (octahedral layers) per cycle. We have then D-Z, D-X, and Z-X polytypes (the odd-odd combinations), and E-E polytypes (all n's even). Here the first three include the common clino-, ortho- and protopyriboles, respectively.

We have selected our layer-modules so that their median planes and the modular interfaces contain the loci of all possible symmetry elements other than (001) glides. Symmetry elements other than (001) glides can occur in a pyribole crystal only if there is a symmetry node (a point from which the forward and backward readings are the same) in the stacking formula. The kinds of possible symmetry nodes, and the nature of (001) glides and of the unit-cell translations with a or b components, can all be deduced from the numerical properties of the stacking formulas. These considerations also permit a more complete classification by type of stacking formula. For the odd-odd formulas, we shall let A-B imply A- and B-nodes and A-Bo imply the same numerical properties but no nodes. For even-even formulas we shall let A-A, B-B, etc. imply A-nodes, B-nodes, etc., and let the symbols S-S and T-T imply E-E polysomes and polytypes, respectively, with no nodes. Our polysome classification is now P-C, P-Co, M-P, M-Po, M-C, M-Co, P-P, M-M, C-C, and S-S; and that for polytypes is D-Z, D-Zo, D-X, D-Xo, Z-X, Z-Xo, D-D, X-X, Z-Z, and T-T.

If we label the beams, as viewed in Figures 2 and 4, so that α-beams are diagonally linked only to β-beams and vice-versa, we find that the octahedral layers (and the modular interfaces they contain) are alternately α and β along the polytype axis (a). Stacks of beams are also alternately α and β along the polysome axis (b). Either the α-beams, collectively, are crystallographically equivalent to the β-beams, collectively, or they are not. If they are equivalent it is because some symmetry operation (including translation) makes them so. The only symmetry operations that do this involve properties of *both* the polysome and the polytype formulas and must meet the following two conditions:

(1) The polysome formula must have either n_p odd, or P-nodes, or both;

(2) the polytype formula must have either n_z odd, or nodes other than Z-nodes, or both.

All combinations of the polysomes that are P-C, M-P, P-Co, M-Po, and P-P with the polytypes that are D-Z, D-X, Z-X, D-Zo, D-D, and X-X meet constraints (1) and (2), and hence have equivalent α- and β-beams or α- and β-octahedral layers (or polytype interfaces). They are thus compatible polysome-polytype pairs, and as such, we shall call pyriboles of this sort Class I pyriboles. No combination of polysomes that are M-C, M-Co, M-M, C-C, or S-S with polytypes that are D-Xo, Z-Z, or T-T meets constraints (1) or (2), but all are compatible polysome-polytype pairs. We shall designate these last as Class II pyriboles.

Because α's and β's are non-equivalent in Class II pyriboles, it is useful to insert Z's in their polytype formulas with subscripts alternately α and β. Class II polytypes that otherwise might be mistaken for D-Z or Z-X forms thus become, for example, $(\cdot\ Z_\alpha\ \cdot\ Z_\beta)$ and $(\times\ Z_\alpha\ \times\ Z_\beta)$, respectively, emphasizing that both are in reality Z-Z polytypes. Conversely, runs of M's and C's that separate P's in the polysome formula may be identified, alternately, by α and β subscripts. $(PC_\alpha PC_\beta)$ is thus a C-C polysome, and $(C_\alpha MC_\beta PC_\alpha MC_\beta P)$ is an M-M polysome. The last can be written more concisely as $(M_\alpha PM_\beta P)$ and still convey the same information; hence, C's are not needed everywhere. Thus, if the polysome is clearly Class II, but the polytype appears to be Class I, we may rectify the situation by inserting Z_α's and Z_β's in the polytype formula. If the polytype formula is clearly Class II, and the polysome formula appears to be Class I, we may insert C_α's and C_β's or, in many instances, simply add subscripts to the M's and again rectify the situation.

The polysome series on the left of Figure 4 is of Class I and alternately P-C and M-P. That on the right of Figure 4 is of Class II and all are M-C. The non-equivalence of the successive octahedral layers or stacks of beams in the latter series is clearly visible.

The notation introduced thus far is sufficient to deduce the unit cell and space group for pyriboles in which the modules and their interfaces permit the same symmetry operations as the idealized forms of Figures 1 through 4. The results, classified first by generalized polysome and then by generalized polytype, are given in Tables 1 and 2. A similar treatment of mica polytypes (Thompson, 1981) may be of interest. All of the space groups of Table 2 are, with the a- and c-axes interchanged, possible space groups for mica polytypes of the fully symmetric type.

TABLE 1. Space groups of Class I Pyriboles.

Polysome	Space Groups[1,2,3]				Remarks
P-C	$C\frac{2}{c}$	$P\frac{2_1}{b}\frac{2_1}{c}\frac{2_1}{a}$	$Pbc2_1$	$P\frac{2_1}{b}\frac{2}{c}\frac{2_1}{n}$	First row represents maximum symmetries of simplest forms.
	Cc	$P\frac{2_1}{c}$		$P2_1cn$	
P-Co	$C2$	$Pb2_1a$	$Pb2n$		May be subgroups of index 2 of corresponding P-C forms.
	Cl	$P2_1$	$Pb--$	$P--n$	
M-P	$I\frac{2}{m}$	$P\frac{2_1}{n}\frac{2_1}{m}\frac{2_1}{a}$	$Pnm2_1$	$P\frac{2_1}{n}\frac{2}{m}\frac{2_1}{n}$	First row represents maximum symmetries of simplest forms.
	Im	$P\frac{2_1}{m}$		$P2_1mn$	
M-Po	$I2$	$Pn2_1a$	$Pn2n$		May be subgroups of index 2 of corresponding M-P forms.
	Il	$P2_1$	$Pn--$	$P--n$	
P-P	$P\frac{2_2}{n}$	$P--\frac{2_1}{a}$	$P\ 2_1\ 2\ \ 2_1$		May be subgroups of index 2 of corresponding P-C or M-P forms.
	Pn	$P\bar{1}$	$P--2_1$	$P2_1--$	

1. *In each two-line array the polytype array follows the scheme:*

		D-Z		Z-X	
	D-Zo		D-X		Z-Xo
		D-D		X-X	

2. *The space groups in the second line of each array may be subgroups of index 2 of the groups diagonally above in the first line.*

3. *To maintain axial correspondence some triclinic groups are referred to unconventional centered cells, and some monoclinic ones to unconventional orientations. In the latter the dashes are place markers.*

Table 2. Space groups of Class II Pyriboles.

Polysome	Space Groups[1,2,3]		Remarks
M-C	$A\frac{2}{m}$	$A2_1ma$	First row represents maximum symmetries of simplest forms.
	Am		
M-Co	$A2$	$A--a$	May be subgroups of index 2 of corresponding M-C forms.
	Al		
C-C	$P\frac{2}{c}$	$P2_1ca$	May be subgroups at index 2 of corresponding M-C or P-C forms. Includes pyroxenes of Class II polytype.
	Pc		
M-M	$P\frac{2}{m}$	$P2_1ma$	May be subgroups of index 2 of corresponding M-C or M-P forms. Includes amphiboles of Class II polytype.
	Pm		
S-S	$P2$	$P--a$	May be subgroups of index 2 of corresponding P-Co, M-Po, P-P, M-M or C-C forms.
	Pl		

1. *In each two-line array the polytype array follows the scheme:*

		Z-Z		D-Xo
			T-T	

2. *The space groups in the second line of each array may be subgroups of Index 2 of the groups diagonally above in the first line.*

3. *To maintain axial correspondence some triclinic groups are referred to unconventional centered cells, and some monoclinic ones to unconventional orientations. In the latter the dashes are place markers.*

Such micas, however, may also have mirrors in the polytype plane, whereas pyriboles may not.

If the modules are less symmetric than the idealized forms, owing to such phenomena as cation ordering or to certain geometric distortions, it is necessary to add additional symbols to the stacking formulas to take this into account. In any case, however, the results lead to space groups that must be subgroups of those in Tables 1 and 2, many of which are already subgroups of each other. The selection of the *a*-axis in D-Z and D-Zo pyriboles is somewhat arbitrary. In Tables 1 and 2 it is oriented so that (010) glides at P-nodes are *n*-glides. This requires the P-C forms to be *C*-centered and the M-P forms to be *I*-centered. If the *a*-axis had been selected so that the P-node glides were *a*-glides, then the *C*- and *I*-centerings would have to be reversed, and the P-P groups *P2/n* and *Pn* would be *P2/a* and *Pa*, respectively. The relation between *C* and *I* cells has been discussed in more detail by Whittaker and Zussmann (1961), Jaffe *et al.* (1968), and Hawthorne (Chapter 1, this volume). A more complete discussion of the foregoing, as well as an extension of the methods to take lowered modular symmetry into account, will soon appear elsewhere (Thompson, in preparation).

POLYSOME STABILITY

Mineral assemblages containing three or more biopyriboles with distinct M-P ratios, such as clinopyroxene-clinoamphibole-biotite, are widespread, both in rocks and in the products of experimental runs. These occurrences imply heterogeneous reactions in which the intermediate form may dissociate or partially dissociate into the extremes (or the corresponding associative reactions if these reactions proceed in the opposite direction). The stoichiometric equations for such reactions, or for their corresponding equilbria, can be written in terms of three biopyribole components, as in Table 3. A sufficient set of stoichiometric relations, however, will also involve certain cation exchanges if the actual phase compositions do not correspond to a set of collinear end members.

All of the equations in Table 3 relate an amphibole component to pyroxene and mica components. Others may be written, as in reactions relating other hydrous pyriboles to pyroxene and mica or to amphibole and

TABLE 3. Biopyribole reactions.

MICA		PYROXENE		AMPHIBOLE	$\Delta\bar{V}^o$ (cm^3/mol amph.)
$Mg_3Si_4O_{10}(OH)_2$ [tc]	+	$Mg_4Si_4O_{12}$ [en]	→	$Mg_7Si_8O_{22}(OH)_2$ [ah]	+ 3.54
$Mg_3Si_4O_{10}(OH)_2$ [tc]	+	$Na_2Al_2Si_4O_{12}$ [jd]	→	$Na_2Mg_3Al_2Si_8O_{22}(OH)_2$ [gl]	+ 3.77
$Mg_3Si_4O_{10}(OH)_2$ [tc]	+	$Ca_2Mg_2Si_4O_{12}$ [di]	→	$Ca_2Mg_5Si_8O_{22}(OH)_2$ [tr]	+ 4.85
$NaMg_3AlSi_3O_{10}(OH)_2$ [np]	+	$Ca_2Mg_2Si_4O_{12}$ [di]	→	$NaCa_2Mg_5AlSi_7O_{22}(OH)_2$ [et]	- 2.42
$KMg_3AlSi_3O_{10}(OH)_2$ [ph]	+	$Ca_2Mg_2Si_4O_{12}$ [di]	→	$KCa_2Mg_5AlSi_7O_{22}(OH)_2$ [k-et]	- 2.88

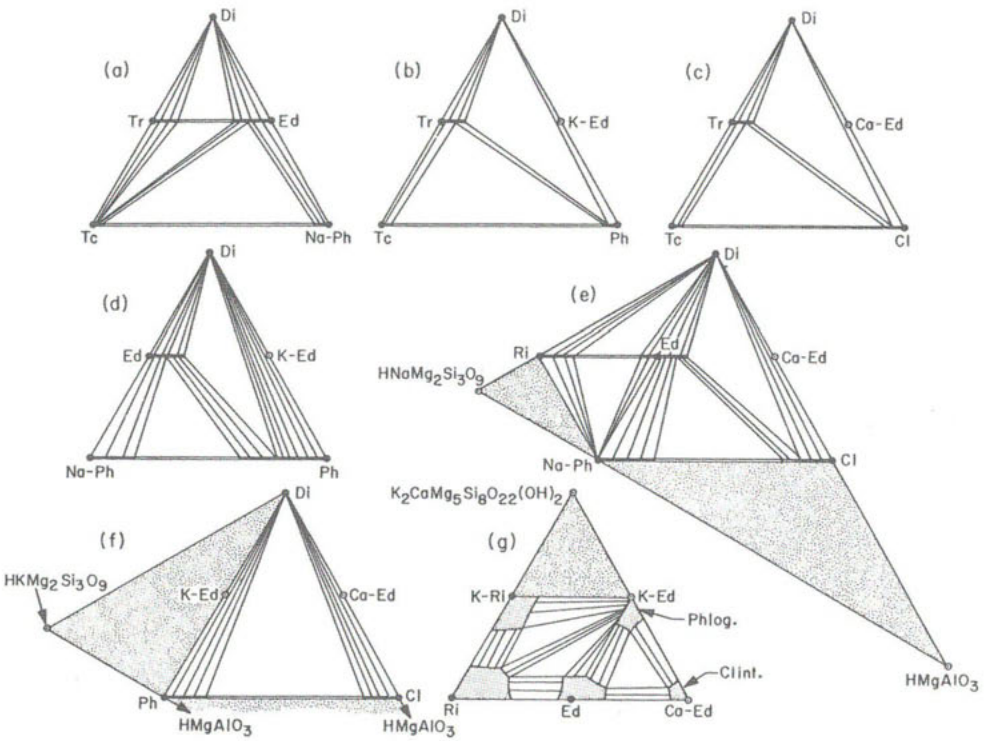

Figure 8. (a) through (f) are composition planes defined by $CaMgSi_2O_6$-(Di) and the mica end-members $Mg_3(Si_4O_{10})(OH)_2$-(Tc), $KMg_3(AlSi_3O_{10})(OH)_2$-(Ph), $NaMg_3(AlSi_3O_{10})(OH)_2$-(Na-Ph), and $CaMg_3(Al_2Si_2O_{10})(OH)_2$-(Cl). These include the stable amphibole end-members $Ca_2Mg_5(Si_8O_{22})(OH)_2$-(Tr), $NaCa_2Mg_5(AlSi_7O_{22})(OH)_2$-(Ed), $Na_2CaMg_5(Si_8O_{22})(OH)_2$-(Ri), and $KNaCaMg_5(Si_8O_{22})(OH)_2$-(K-Ri), and the metastable ones $KCa_2Mg_5(AlSi_7O_{22})(OH)_2$-(K-Ed) and $Ca_3Mg_5(Al_2Si_6O_{22})(OH)_2$-(Ca-Ed). Lightly stippled areas are inaccessible to biopyriboles. (g) shows phases coexisting with diopside in the system that may be defined by Di, Ph, Na-Ph, and Cl. Darker stippling shows fields of amphiboles and micas that coexist with diopside. Micas appear when the amphibole is metastable relative to the mica-pyroxene pair.

either pyroxene or mica, for example. Veblen and Buseck (1979) have considered several reactions relating chesterite and jimthompsonite to anthophyllite and talc. In the absence of clear evidence that either chesterite or jimthompsonite is ever stable relative to anthophyllite or enstatite and talc, however, we are left with equations such as those of Table 3 as the ones of principal interest.

The diagrams of Figure 8 show, schematically, the phase relations in the simple biopyribole systems, as indicated by known natural occurrences. Some readers may be surprised by the inclusion of sodic trioctahedral micas, but these are now known both from natural occurrence (Keusen, 1972; Kulke, 1976; Keusen and Peters, 1980; Schreyer *et al.*, 1980; Spear *et al.*, 1981) and by direct synthesis (Carman, 1974b; Hewitt and Wones, 1975; Franz and Althaus, 1976). Compositions range from Na-phlogopite to a high-alumina form, preiswerkite. The form wonesite has abundant A-site vacancies and is thus chemically intermediate between sodic-biotites (or phlogopites) and talc. Carman (1974b) found that at least some sodic micas form hydrates at low temperatures and high H_2O-activities. This smectitic behavior may occur in weathering or hydrothermal alteration and is probably responsible in part for the rarity of these micas. As pointed out by Carman, many occurrences of sodic vermiculite or montmorillonite may simply be altered sodic micas. Similar materials have also appeared in many attempts at amphibole synthesis (Ernst, 1961, 1968; Carman, 1974a; Greenwood, 1979), commonly with a pyroxene, and may represent sodic micas that hydrated on quenching. Natural occurrences of pyroxenes with biotite or phlogopite and of diopside with clintonite indicate, as shown in Figure 8, that amphiboles with high contents of potassium or calcium in their A-sites are metastable, under normal geologic conditions, relative to the corresponding pyroxene-mica pair. Amphiboles in which the A-site is filled by potassium, however, have been synthesized by Huebner and Papike (1970) and by Hinrichsen and Schürmann (1977), and the unusual beryllium-bearing amphibole, joesmithite, described by Moore (1969) has A-sites occupied by calcium and even some lead!

It is clear from the volume data in Tables 3 and 4 that the total volume of a polysomatic mineral such as amphibole can not be taken as simply the linear sum of the volumes of its isolated component parts,

although the differences are comparatively small relative to those associated with many other heterogeneous reactions. The volumetric strains, and anticipated differences in other thermodynamic properties, can undoubtedly be related to the mismatches at the modular junctions. It is interesting that the ΔV's of dissociation appear to be consistently negative for amphiboles with vacant A-sites and consistently positive for amphiboles with occupied A-sites, at least as measured at room temperature and one atmosphere. This makes crystallochemical sense, in that the volumes

TABLE 4. Unit cell dimensions of biopyriboles.

A. Pyroxenes[1]	$a \sin \beta$	b	c	$-a \cos \beta$	V (Å^3)	Ref.
$4x Mg_4Si_4O_{12}$ [en]	18.236	8.821	5.182	0	833.58	(1)
$2x Na_2Al_2Si_4O_{12}$ [jd]	8.979	8.563	5.211	2.843	400.64	(2)
$2x Ca_2Mg_2Si_4O_{12}$ [di]	9.378	8.931	5.249	2.663	439.62	(3)

B. Micas[2]	$c \sin \beta$	b	a	$c \cos \beta$	V (Å^3)	Ref.
$4x Mg_3Si_4O_{10}(OH)_2$ [tc, 2O]	18.72	9.145	5.252	0	899.17	(1)
$2x Mg_3Si_4O_{10}(OH)_2$ [tc, 1M]	9.36	9.145	5.252	1.751	449.59	(1)
$2x NaMg_3AlSi_3O_{10}(OH)_2$ [np]	9.903	9.203	5.265	1.348	479.82	(4)
$2x KMg_3AlSi_3O_{10}(OH)_2$ [ph]	10.156	9.203	5.317	1.776	496.95	(5)

C. Amphiboles[3]	$a \sin \beta$	b	c	$a \cos \beta$	V (Å^3)	Ref.
$4x Mg_7Si_8O_{22}(OH)_2$ [ah]	18.61	18.01	5.24	0	1756.27	(1)
$2x Na_2Mg_3Al_2Si_8O_{22}(OH)_2$ [gl]	9.23	17.67	5.29	3.040	862.74	(6)
$2x Ca_2Mg_5Si_8O_{22}(OH)_2$ [tr]	9.519	18.054	5.268	2.803	905.33	(7)
$2x NaCa_2Mg_5AlSi_7O_{22}(OH)_2$ [et]	9.562	17.951	5.310	2.701	911.41	(8)
$2x KCa_2Mg_5AlSi_7O_{22}(OH)_2$ [k-et]	-	-	-	-	927.(±)	(8)

1. Monoclinic forms referred to C-centered cells.

2. Molar volume, a and b of talc assumed independent of polytype. c cos β for 1M form assumed to be a/3.

3. Monoclinic forms referred to I-centered cells.

REFERENCES

(1) Greenwood, 1963; (2) Frondel and Klein, 1965; (3) Turnock et al., 1973; (4) Carman, 1974b; (5) Hewitt, 1975 ; (6) Borg, 1967; (7) Colville et al., 1966; (8) Hinrichsen and Schürmann, 1977.

of the A-sites may vary freely in a mica, depending on their occupancy, but are constrained by the cross-linkage between the beams in an amphibole or other hydrous pyribole. Micas also exhibit an unusually high compressibility in the direction normal to the cleavage (Hazen and Finger, 1978); hence, it is probable that at sufficiently high pressures *all* of the ΔV's of dissociation may become negative. These considerations imply that amphibole components with vacant A-sites will be destabilized by increasing pressure, and that other amphibole components will be initially stabilized and subsequently destabilized by increasing pressure.

In the simple systems corresponding to the formulas given, the equations of Table 3 may represent univariant equilibria. The amphiboles glaucophane, tremolite, and anthophyllite all dissociate at high pressures into talc and pyroxene (Greenwood, 1963, 1971; Essene *et al.*, 1970; Gilbert and Popp, 1973; Gilbert and Troll, 1974; Carman, 1974a, as summarized by Maresch, 1977; Chernosky and Autio, 1979; Day and Halbach, 1979; Gilbert *et al.*, Chapter 9, Volume 9B). These dissociations are consistent with the volume data in Table 3. Although all these univariant curves are not yet precisely located, the slopes appear to be positive, indicating that the enthalpy and entropy differences have the same signs as the volume differences (as is usual).

End-member edenite has been reported as synthesized by several authors (Colville *et al.*, 1966; Widmark, 1974; Peto, 1976), but the identification of these amphiboles as true edenites has been questioned by Greenwood (1979), inasmuch as other phases occurred in the run-products. The unit-cell parameters of the edenite of Colville *et al.* (1966), moreover, are suspiciously like those of synthetic tremolites (for which all necessary ingredients were present). An "end-member edenite" with the expected cell-parameters, however, was synthesized by Hinrichsen and Schürmann, who also synthesized a variety of Na-K edenites and pargasites, as well as a (probably metastable) K-edenite. As reported by Greenwood (1979), many of his runs produced diopside and a "soda montmorillonite," indicating that under some conditions end-member edenite may indeed be metastable relative to the diopside and Na-phlogopite.

The decomposition experiments of Hinrichsen and Schürmann (1977, Fig. 1) on two intermediate Na-K edenites invariably yielded diopside and phlogopite among the decomposition products. Also present in some runs

were nepheline, enstatite and forsterite, the dehydration products of Na-phlogopite. Their curves are not equilibrium boundaries, but the presence of edenite, diopside, and phlogopite along them strongly implies that isopleths on the composition of the edenite coexisting with diopside and phlogopite, as in Figure 8d, will have positive slopes, at least in the range 0-5 kbar, such that increasingly K-rich edenites will be stabilized by increasing pressure at any given temperature. Such a bundle of isopleths would presumably be bounded by the univariant curves for the pure Na- and K-end members. Owing to the high compressibility of phlogopite normal to (001), however, these same isopleths may well be encountered again at much higher pressures. This last conjecture is, in fact, reinforced by the experiments of Merrill and Wyllie (1975) on a natural kaersutite. At pressures less than 15 kbar the kaersutite decomposes, along a boundary of positive slope, to an assemblage that includes phlogopite and clinopyroxene. At pressures above 20 kbar the same phenomenon occurs along a boundary of negative slope. Similar results have been obtained with generalized mafic rock compositions by Merrill and Wyllie (1975) and others (Merrill and Wyllie, 1975, summarized earlier work; see Allen *et al.*, 1975; Allen and Boettcher, 1978; and Gilbert *et al.*, Chapter 9, Volume 9B, for more recent results). These studies imply, collectively, that isopleths on the compositions of amphiboles having filled A-sites, and that coexist with pyroxenes and trioctahedral micas, should have the general form as in curve D in Figure 9, as should the univariant curves for the limiting end-member reactions.

POLYTYPE STABILITY

Clinopyriboles of the simplest polytype (•) are overwhelmingly the most abundant. In these there is a large cation site designated as M2 in pyroxene, or M4 in amphibole (we shall here call it Mlc), that is occupied in the more common forms by Ca, less commonly by Na, Mg, Fe, or Mn. Ortho- (•×) and proto- (×) pyriboles, on the other hand, are virtually limited to forms in which the Mlc sites are occupied largely by the smaller species Mg and Fe^{2+}. If Mg-Fe^{2+} ortho- or protopyriboles coexist with an Mg-Fe clinopyribole, the clinopyribole is the richer in Fe. The tolerance of Mlc for Ca or Na in orthopyriboles is very limited, and in protopyriboles

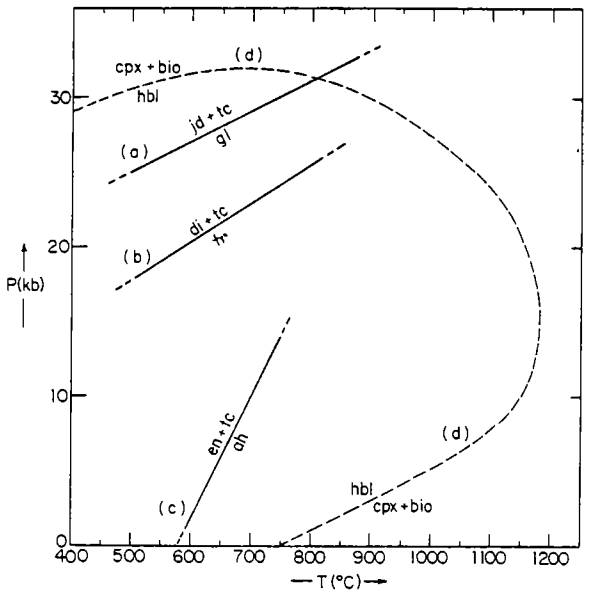

Figure 9. Association-dissociation reactions relating amphibole to mica and pyroxene. (a) and (b) are from Gilbert (Chapter 9, Volume 9B); (c) is from Day and Halbach (1979). The dotted curve (d) shows, schematically, a possible form for univariant curves for end-member amphiboles with occupied A-sites, or isopleths on amphibole compositions in generalized 3-phase assemblages. (d) is consistent with the observations of Merrill and Wyllie (1975), Hinrichsen and Schürmann (1977), and other experiments summarized by Gilbert (this volume); the high-temperature segment is probably metastable due to melting in most instances.

is even less (Longhi and Boudreau, 1980, Fig. 2). It is thus clear that cross-modules are strongly favored, other things equal, by small species (especially Mg) in Mlc, even though the crystallochemical reasons for this are complex (see Hawthorne, Chapter 1, this volume). Pyroxenes of the composition $MgSiO_3$ show all three forms, and those of composition $FeSiO_3$ show at least (•) and (•×). The experimental results on their relative stabilities have been summarized in Volume 7 of this series by Lindsley (1980, Figs. 2 and 3). The phase diagram for $MgSiO_3$ is consistent with the generalization that volume, enthalpy, and entropy all increase as the proportion of cross-modules increases, although the crystallochemical reasons for this are, again, complex. The diagram for $FeSiO_3$ is puzzling in that there is a second, high-temperature field for the clinopyroxene. This writer is inclined to believe that these clinopyroxenes, as suggested by Lindsley (1965), were protopyroxenes that inverted to clinopyroxenes on

quenching and agrees with Lindsley's later (1980) conclusion that the pyroxenoid Fs-III is not a quenching product.

Both clino- and ortho- forms appear among the Ca-poor Mg-Fe amphiboles, but the phase relations are still poorly known (Cameron and Papike, 1979). Only the Fe end member appears to have both forms occurring naturally.

Certain clinopyriboles, again those low in Ca or Na, have primitive ($P2_1/c$, pyroxene and $P2_1/m$, amphibole) rather than centered cells at low temperatures. The inversions to centered forms have many of the characteristics of lambda-transformations, though they are commonly interpreted as first-order. The primitive cell appears to be caused by a rotation of the tetrahedra that makes successive tetrahedral layers non-equivalent (Thompson, 1970; Papike *et al.*, 1973). This loss of symmetry can be shown by the addition of the symbols "O" and "S" (or "O" and "H," Thompson, 1981) to the polytype formula. The primitive forms would then have polytype formulas such as (O•O H•H), which is that of a D-D pyribole. Their primitive space groups are thus consistent with Table 1.

The primitive-to-centered transformation in Ca-poor clinopyroxenes has been studied in detail by Prewitt *et al.* (1971), Smyth and Burnham (1972), Brown *et al.* (1972), Ohashi and Burnham (1973), Smyth (1974), Ohashi *et al.* (1975), and Ohashi and Finger (1976). It is evident that the centered forms are favored by high temperatures and, from the volume effect, low pressure. Inversion temperatures are lowered by increasing iron content (from >1100°C to <500°C), and they are lowered drastically by even small amounts of calcium. The corresponding transformation in Ca-poor clinoamphiboles has been studied by Prewitt *et al.* (1970) and Sueno *et al.* (1972) and behaves much like that in the corresponding clinopyroxenes, but over a much lower range of temperatures (∿100°C).

THE CHEMICAL DESCRIPTION OF COMPLEX MINERALS

Mineralogists and petrologists have traditionally used additive or end-member components in the description of chemical variations in minerals. Where the composition space is one- or two-dimensional this rarely presents problems, but in more complex crystals, such as the biopyriboles, where the composition spaces are multidimensional, the end-member methods (see, for example, Perry, 1967, 1968, 1970; Cawthorn and Collerson, 1974), are

cumbersome and can be misleading unless used with great care.

A much neater method was suggested long ago by W. L. Bragg (1937; and partially reproduced in Bragg and Claringbull, 1965), who suggested that the departures from a composition be accounted for in terms of the substitutions by which the composition may be varied. With a few notable exceptions, as in a paper by J. V. Smith (1959), this suggestion has not been fully exploited until recently (Thompson, 1979; Thompson *et al.*, in press). Briefly, we describe chemical variations in terms of *exchange components* or *vectors* that represent displacement vectors in composition space. Formulas for such components may be written by the use of negative subscripts as, for example, KNa_{-1} or $Al_2Mg_{-1}Si_{-1}$, a positive subscript indicating "atom-in" and a negative one "atom out." These may be manipulated in stoichiometric equations in the same way as conventional additive components as, for example:

$$CaMgSi_2O_6 + Al_2Mg_{-1}Si_{-1} = CaAl_2SiO_6$$

or:

$$Al_2Mg_{-1}Si_{-1} = CaAl_2SiO_6 - CaMgSi_2O_6$$

An exchange vector may thus be expressed as a difference between two additive components. Because linear equations can be written between exchange vectors and additive components, the transformations to sets of components that include exchange vectors behave algebraically like all other transformations of components. Specifically, these are simple linear transformations, as in the classical calculation of a norm or in the recalculation of a mineral analysis. The new composition variables or advancements on the exchange vectors, X_{ex}, are simply the ratios of the numbers of formula units of the various vectors to the numbers of formula units of the additive components selected. Thus, if we select an additive amphibole component as $Ca_2Mg_5Si_8O_{22}(OH)_2$, then the compositions corresponding to $X_{Al_2Mg_{-1}Si_{-1}}$ having values of 1 and 2 are $Ca_2Mg_4Al_2Si_7O_{22}(OH)_2$ and $Ca_2Mg_3Al_4Si_6O_{22}(OH)_2$, respectively. A set of exchange vectors sufficient for the chemical description of most biopyriboles is given in Table 5, and a three-dimensional section of clinoamphibole space is shown in Figure 10.

Several aspects of Table 5 may puzzle the reader. One is that such components are concerned only with bulk chemistry, hence not with specific

TABLE 5. Exchange Components.

Exchange Component			Expressed as Oxides	Expressed in Other Ways
KNa_{-1}		=	$\frac{1}{2}K_2O$-$\frac{1}{2}Na_2O$	= $KAlSi_3O_8$-$NaAlSi_3O_8$
$NiFe_{-1}$		=	NiO-FeO	
$MnFe_{-1}$		=	MnO-FeO	= $\frac{1}{2}Mn_2O_3$-$\frac{1}{2}Fe_2O_3$
$FeMg_{-1}$		=	FeO-MgO	= $FeSiO_3$-$MgSiO_3$=$\frac{1}{2}Fe_2SiO_4$-$\frac{1}{2}Mg_2SiO_4$
$CrFe_{-1}$		=	$\frac{1}{2}Cr_2O_3$-$\frac{1}{2}Fe_2O_3$	
$TiFe_{-1}$		=	FeO+TiO_2-Fe_2O_3	
$FeAl_{-1}$		=	$\frac{1}{2}Fe_2O_3$-$\frac{1}{2}Al_2O_3$	
$MgCa_{-1}$	*(mc)*	=	MgO-CaO	
$Al_2Mg_{-1}Si_{-1}$	*(tk)*	=	Al_2O_3-MgO-SiO_2	
$NaSiCa_{-1}Al_{-1}$	*(pl)*	=	$\frac{1}{2}Na_2O$+SiO_2-CaO-$\frac{1}{2}Al_2O_3$	= $NaAlSi_3O_8$-$CaAl_2Si_2O_8$
$NaAlSi_{-1}$	*(ed)*	=	$\frac{1}{2}Na_2O$+$\frac{1}{2}Al_2O_3$-SiO_2	= $NaAlO_2$-SiO_2

1. All formulas refer to gram-formula or mol units.

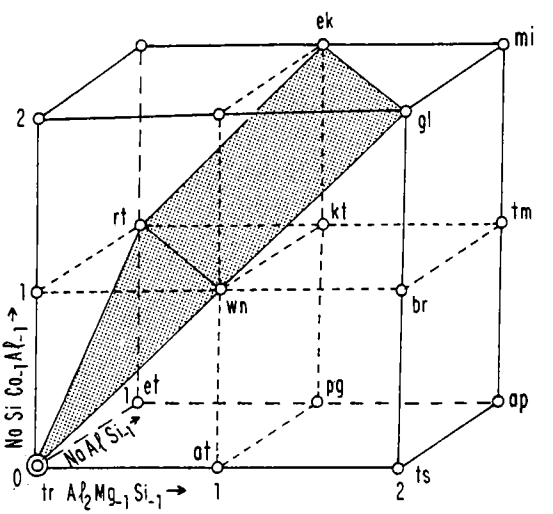

Figure 10. A part of the composition space for Na-Ca clinoamphiboles. The additive component is $Ca_2Mg_5Si_8O_{22}(OH)_2$ (tr), and the coordinate axes $Al_2Mg_{-1}Si_{-1}$, $NaAlSi_{-1}$, and $NaSiCa_{-1}Al_{-1}$ correspond to X_{tk}, X_{ed}, and X_{pl}, respectively (see text). The space corresponds to that of Figures 1 of Smith (1959), Phillips (1966) and Leake and Winchell (1978). The symbols correspond to idealized compositions for tremolite (tr), tschermakite (ts), winchite (wn), barroisite (br), glaucophane (gl), edenite (et), pargasite (pg), richterite (rt), katophorite (kt), taramite (tm), and eckermannite (ek), and also the compositions $Ca_2Mg_4Al_2Si_7O_{22}(OH)_2$ (at), $NaCa_2Mg_3Al_5Si_5O_{22}(OH)_2$ (ap), and $Na_3Mg_3Al_3Si_7O_{22}(OH)_2$ (mi). Compositions above the shaded plane are not accessible to clinoamphibole. (mi) corresponds to the "miyashiroite" of Phillips and Layton (1964).

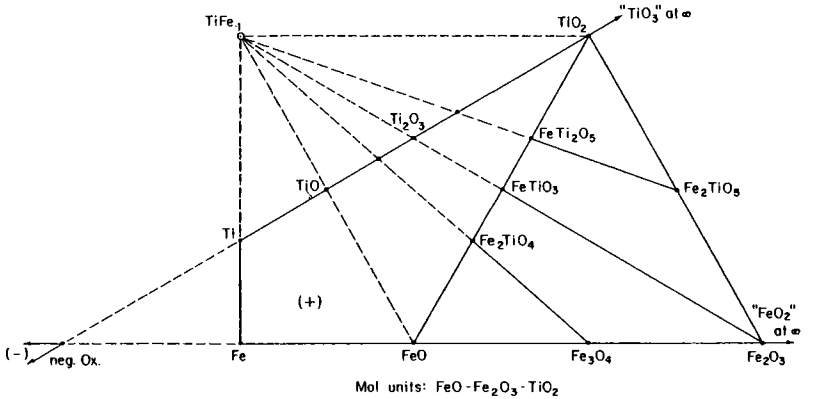

Figure 11. The system Fe-Ti-O based on the reference triangle $FeO-Fe_2O_3-TiO_2$ in mol units. The line "TiO_3-FeO_2" is at projective infinity, and more oxygen-rich compositions plot negatively. The point $TiFe_{-1}$ represents the exchange vector common to armalcolite-pseudobrookite, ilmenite-hematite, ülvospinel-magnetite, and Ti-Fe alloys. If weighted in oxygen equivalents rather than mol units, the line Fe-Ti-$TiFe_{-1}$ would be at projective infinity, and the lines radial to $TiFe_{-1}$ would be parallel.

structural sites nor with the valence states of the species involved. The vector $TiFe_{-1}$, for example, represents a variation possible in many phases in the system Fe-Ti-O, as shown in Figure 11. In most minerals the detailed substitution is $Fe^{2+}Ti^{4+}Fe^{3+}_{-2}$, but in an Fe-Ti alloy or in an armalcolite with Ti^{3+}, the details are obviously different. By the same token the vector $MnFe_{-1}$ includes either $Mn^{2+}Fe^{2+}_{-1}$ or $Mn^{3+}Fe^{3+}_{-1}$. Readers may also find that some expected vectors are missing. This is because the set in Table 5 has been pruned so that all are linearly independent (i.e., none can be expressed in terms of the others). Most of the "missing" ones are, in fact, effectively included by virtue of relations such as:

$$NaAlCa_{-1}Mg_{-1} = Al_2Mg_{-1}Si_{-1} + NaSiCa_{-1}Al_{-1}$$

$$KAlSi_{-1} = NaAlSi_{-1} + KNa_{-1}$$

$$CaAl_2Si_{-2} = NaAlSi_{-1} - NaSiCa_{-1}Al_{-1}$$

$$MgTiAl_{-2} = TiFe_{-1} - FeMg_{-1} + 2FeAl_{-1}$$

Thermodynamic calculations are also simplified by the use of exchange vectors. If the molar Gibbs energy is formulated in terms of P, T, and the various X_{ex}, then the chemical potential associated with an exchange

TABLE 6. Equations[1] for condensation into Na_2O-CaO-MgO-Al_2O_3-SiO_2-H_2O(NCMASH)

				"Old" components (all additive)
"New" additive Components	SiO_2	(S)	=	SiO_2
	Al_2O_3	(A)	=	$(Al_2O_3+Fe_2O_3+Cr_2O_3)$ + TiO_2
	MgO	(M)	=	(MgO+FeO+MnO+NiO) - TiO_2
	CaO	(C)	=	CaO
	Na_2O	(N)	=	(Na_2O+K_2O)
	H_2O	(H)	=	H_2O
"New" exchange Components	$FeAl_{-1}$		=	$2(Fe_2O_3+Cr_2O_3)$ + $2TiO_2$
	$CrFe_{-1}$		=	$2Cr_2O_3$
	$TiFe_{-1}$		=	TiO_2
	$FeMg_{-1}$		=	(FeO+MnO+NiO) - TiO_2
	$MnFe_{-1}$		=	MnO
	$NiFe_{-1}$		=	NiO
	KNa_{-1}		=	$2K_2O$

1. *Each formula represents here the number of molar units of the component in a given quantity of matter.*

vector (its *exchange potential*) is simply the first partial derivative of $\bar{G}$ with respect to the appropriate X_{ex} (Thompson *et al.*, in press; Laird in Robinson *et al.*, Chapter 8, Volume 9B). The equilibrium condition for a pure exchange reaction between two phases is then obtained simply by equating the two exchange potentials.

CONDENSED COMPOSITION SPACES, PYROXENES AND MICAS

Condensed composition spaces are obtained by transformation from a set of purely additive components to a mixed set of additive components and exchange vectors, and then projecting along the exchange vectors. These are not as unconventional as they may seem. Many of the familiar diagrams of petrology, such as those of Eskola (1939) and Niggli (1954), are essentially of this kind, inasmuch as they may be regarded as projections along vectors such as $FeMg_{-1}$ and KNa_{-1} into a space of fewer dimensions (see also Robinson *et al.*, Chapter 8, Volume 9B).

By retaining only the additive components SiO_2-Al_2O_3-MgO-CaO-Na_2O-H_2O and by replacing the remaining ones with the exchange vectors in Table 5 that involve other elements, we obtain the equations of Table 6, giving the formulas of the new components in terms of the old. The condensed composition space is then obtained by projecting along (i.e., neglecting) the exchange vectors and plotting mineral compositions in terms of the new additive components. Variations along the neglected vectors are invisible, but many revealing relationships remain. The full condensed space has six components and hence is five-dimensional, but pyroxenes, Figure 12, and trioctahedral micas, Figure 13, occupy only three-dimensional subspaces of it. Each of these spaces has been extended to its full physical limits; hence, only a part of each is accessible to pyroxene or mica. In each subspace there are three exchange vectors that can relate other compositions to a single additive component. The weighting in each diagram is in oxygen equivalents, so that displacements on a given exchange vector (oxygen-conserving) are on parallel lines.

In Figure 12 crystallochemically reasonable pyroxenes are limited to the pyramidal volume bounded by jd, di, ct, en and al-en. The more aluminous compositions, however, are stable relative to other phases or phase assemblages only at high pressures, and al-en ($MgAl_2SiO_6$) is probably always metastable relative to some combination involving garnet, corundum, cordierite, sapphirine or spinel. Garnets lie along the line gr-pr and are more dense than pyroxenes of the same compositions; hence, they are stabilized by increasing pressure, producing garnet or garnet-pyroxene pairs rather than pyroxenes alone.

Even if only pyroxene is present, the composition may be represented by two- or three-pyroxene assemblages such as augite-hypersthene-pigeonite or pairs of these three. Ortho- and protopyroxenes have little tolerance, as already noted, for Ca or Na. These are separated from each other and from the clinopyroxenes by first-order differences; hence, two-phase regions where the two pyroxenes are of different polytype are commonplace. Clinopyroxene-clinopyroxene pairs arise either through nonideality, as along the vector $MgCa_{-1}$ (*mc*), producing augite-pigeonite pairs, or through cation ordering, producing omphacite-diopside or omphacite-jadeite pairs. An ordered omphacite may be described polysomatically as an alternation of diopside-like and jadeite-like pyroxene modules along the *b*-axis (*c*-glides

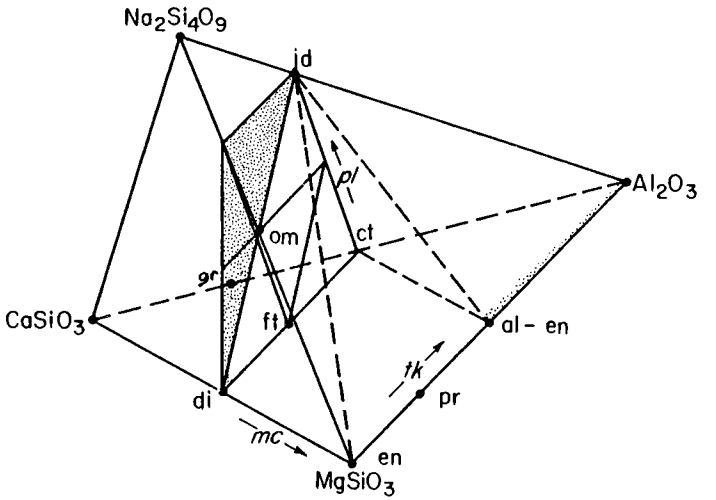

Figure 12. Condensed pyroxene space (see text). Vectors such as $FeMg_{-1}$, $FeAl_{-1}$, etc., are lines of projection into the simpler space here shown. The volume bounded by $NaAlSi_2O_6$ (jd), $CaMgSi_2O_6$ (di), $CaAl_2SiO_6$ (ct), $MgAl_2SiO_6$ (al-en), and $MgSiO_3$ (en) represents crystallochemically plausible pyroxene compositions, although some may be everywhere metastable relative to other phases. The line $Mg_3Al_2Si_3O_{12}$ (pr) - $Ca_3Al_2Si_3O_{12}$ (gr) is a condensed garnet space. (om) and (ft) represent idealized omphacite and fassaites, respectively.

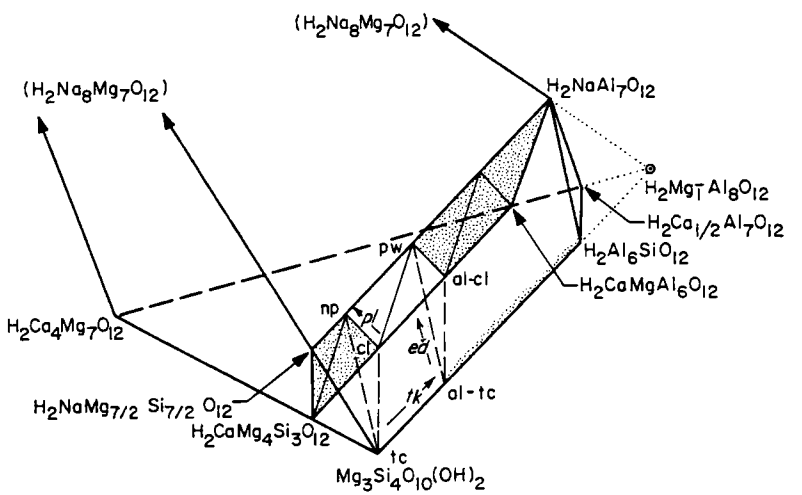

Figure 13. Condensed trioctahedral mica space (see text). The volume bounded by $Mg_3Si_4O_{10}(OH)_2$ (tc), $Mg_2Al_2Si_3O_{10}(OH)_2$ (al-tc), $NaMg_3AlSi_3O_{10}(OH)_2$ (np), $NaMg_2Al_3Si_2O_{10}(OH)_2$ (pw), $CaMg_3Al_2Si_2O_{10}(OH)_2$ (cl) and $CaMg_2Al_4SiO_{10}(OH)_2$ (al-cl) is accessible to mica. Owing to condensation on KNa_{-1}, the potassium micas plot with their Na analogs.

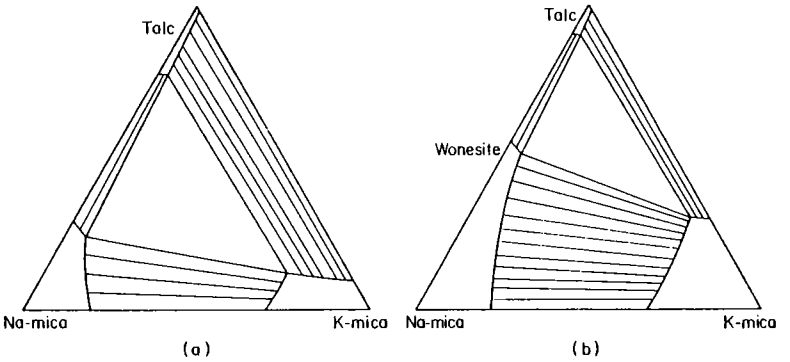

Figure 14. Schematic phase relations for talc and K-Na trioctahedral micas. (a) is consistent with observations of Schreyer *et al.* (1980). All phases are low in alumina. (b) is consistent with the observations of Spear *et al.* (1981). The alkali-rich micas are here considerably advanced on the vector $Al_2Mg_{-1}Si_{-1}$ (*tk*) compared to those in (a).

at the modular interfaces are therefore no longer possible). The polysome formula may then be written as (P_jP_d) which is that of a P-P clinopyroxene yielding the space group *P2/n* (or *P2/a* if the alternate choice of *a*-axis is taken).

In Figure 13 crystallochemically reasonable micas are limited to the wedge bounded by np, pw, cl, al-cl, tc, and al-tc, although al-tc is probably always metastable relative to other phases. There are also miscibility gaps, owing to nonideality along vectors such as KNa_{-1} (not shown owing to condensation along it) and $NaAlSi_{-1}$. Assemblages such as phlogopite, Na-phlogopite (or wonesite), and talc are now known (Schreyer *et al.*, 1980; Spear *et al.*, 1981). These are shown schematically in Figure 14. As in other systems, solid solution is more extensive from the side with the greater cell volume; the greater the volume difference, the more marked the asymmetry.

We may imagine the triangles of Figure 14 as expanded into triangular prisms by adding the vector $Al_2Mg_{-1}Si_{-1}$ (*tk*) as a third coordinate. It is of interest that when alkali micas coexist with talc, the micas show a notably greater advancement on $Al_2Mg_{-1}Si_{-1}$. Clintonites, furthermore, show a greater advancement on this vector than do coexisting phlogopites. A plausible explanation for this is that the local balance of valences about the shared oxygens of a tetrahedral sheet is improved by advancement on $Al_2Mg_{-1}Si_{-1}$ if the A-sites are occupied. The optimum values of X_{tk} are

nil if the A-site is empty, 1/3 if it is occupied by Na or K, and 2/3 if it is occupied by Ca. The optimum formula for an alkali mica would then be of the form $KMg_{8/3}Al_{5/3}Si_{8/3}O_{10}(OH)_2$ and that for a clintonite would be $CaMg_{7/3}Al_{7/3}Si_{7/3}O_{10}(OH)_2$. These formulas are approximated by a surprising number of natural occurrences, and it is also noteworthy that less aluminous clintonites are difficult or thus far impossible to synthesize (Olesch, 1975). The corresponding optimum formula for a chlorite would be $Mg_{14/3}Al_{8/3}Si_{8/3}O_{10}(OH)_8$ or 7:4:4 chlorite (see Albee, 1961). These considerations also imply a negative deviation from ideality along the vector $Al_2Mg_{-1}Si_{-1}$ in biopyriboles, and hence little chance of miscibility gaps related to it.

CONDENSED AMPHIBOLE SPACE

Amphiboles (and other hydrous pyriboles) can not be represented so simply as pyroxenes and micas, inasmuch as their subspaces in the six-oxide system are four-dimensional. By successively applying the constraints (i) A-site empty, (ii) A-site full, (iii) M4 wholly Ca and Na, and (iv) M4 wholly Mg, however, we obtain the four special sections of condensed amphibole space shown in Figures 15-18. Figures 15 and 16 are closely analogous to Figure 12, and Figure 18 is similar to Figure 13. The space of Figure 17 is essentially that of Figure 10, as extended to show its physically possible limits.

The amphibole spaces of Figure 10 and Figures 15-18 have been cut off arbitrarily at a value of 2 for X_{tk}, although more extensive substitution on this vector ($Al_2Mg_{-1}Si_{-1}$) is not crystallochemically unreasonable. The limits shown, however, encompass all known forms. Two-phase regions related to polytype differences and miscibility gaps related to the vector $MgCa_{-1}(mc)$ parallel directly the corresponding phenomena in pyroxenes, although observed solubilities are generally less in the amphiboles than in corresponding pyroxenes, owing to their lower temperatures of formation. There are also gaps along the vector $NaSiCa_{-1}Al_{-1}(pl)$, as in pyroxenes, but ordered amphiboles analogous to omphacites have not yet been identified. This would be expected in amphiboles such as winchites, barroisites, katophorites, and taramites, where the M4-site is approximately half Na and half Ca. Such amphiboles would have the polysome formula (MP_jMP_d),

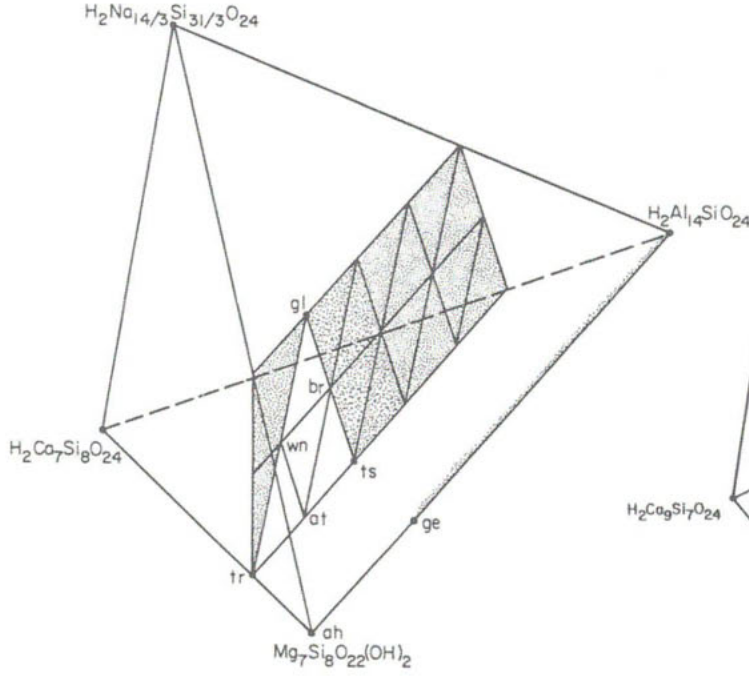

Figure 15. A condensed amphibole space for amphiboles with vacant A-sites. The volume accessible to amphibole is bounded by gl, tr, ts (see Fig. 10) and the points $Mg_7Si_8O_{22}(OH)_2$ (ah) and $Mg_5Al_4Si_6O_{22}(OH)_2$ (gd).

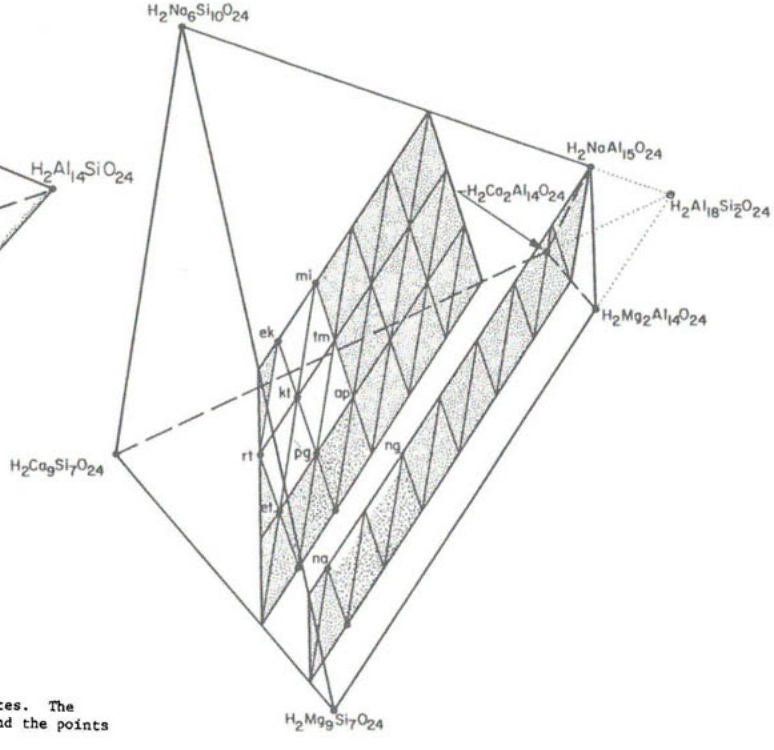

Figure 16. Condensed space for amphiboles with occupied A-sites. The points (na) and (ng) correspond to $NaMg_7AlSi_7O_{22}(OH)_2$ and $NaMg_5Al_5Si_5O_{22}(OH)_2$, respectively. Magnesiorichterite, $Na_2Mg_6Si_8O_{22}(OH)_2$ (mr), is not shown but plots between the two shaded planes in the left-hand face of the polyhedron.

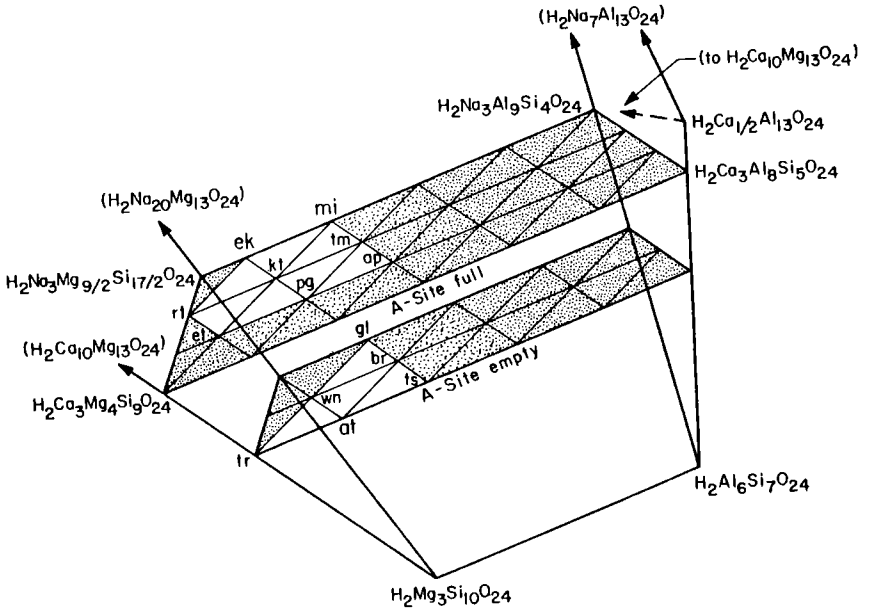

Figure 17. Condensed space for amphiboles with M4 occupied wholly by Ca or Na. This is the space of Figure 10 showing its extension to the physical limits.

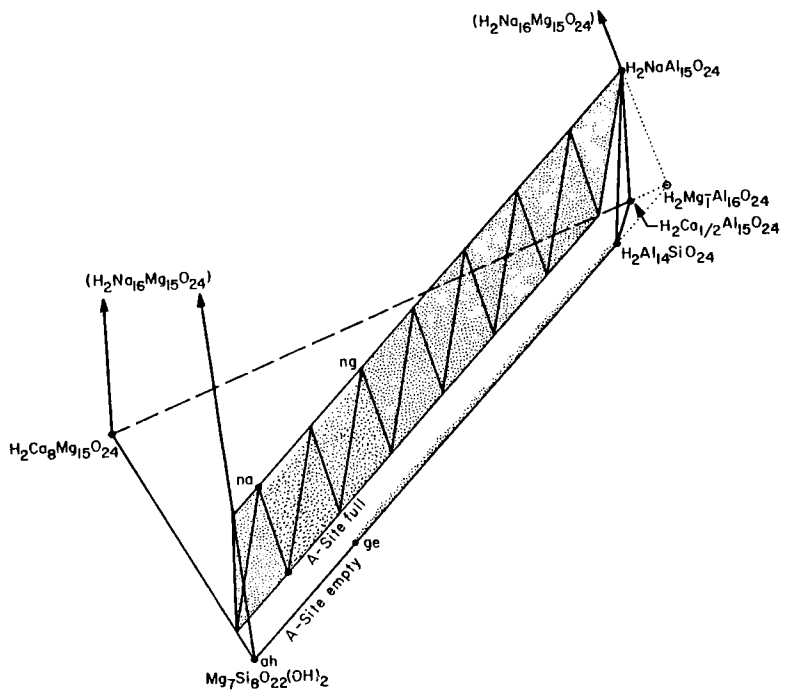

Figure 18. Condensed space for amphiboles with M4 occupied by Mg or Fe. Abbreviations are as in Figures 15 and 16.

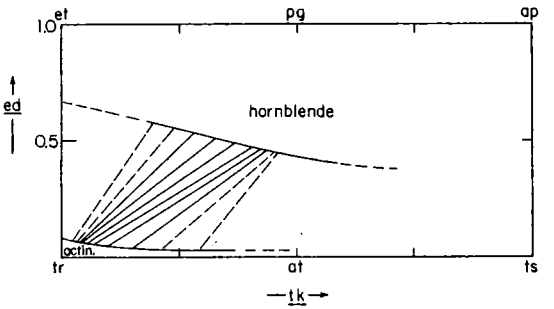

Figure 19. Schematic phase relations (condensed) for the actinolite-hornblende miscibility gap. Heavy tie-lines are consistent with observed occurrences (see references in text); dashed tie-lines are conjectural.

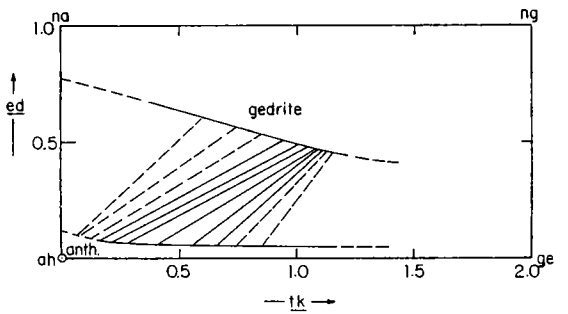

Figure 20. Schematic phase relations for the anthophyllite-gedrite miscibility gap. Heavy and dashed tie-lines as in Figure 19.

and hence would be P-P clinoamphiboles yielding the space group *P2/n* (or *P2/a* if the alternate choice of *a*-axis is taken).

Other miscibility gaps in amphiboles may be expected to parallel those in micas, although much more work needs to be done. Nonideality along the vector KNa_{-1} is probable, but the experiments of Huebner and Papike (1970) and of Hinrichsen and Schürmann (1977) are above the usual temperatures of critical mixing for K-Na solutions. Nonideality along the vector $NaAlSi_{-1}$ is strongly indicated by actinolite-hornblende (Compton, 1958; Shido and Miyashiro, 1959; Klein, 1969; Brady, 1974) and anthophyllite-gedrite pairs (Ross *et al.*, 1969; Robinson *et al.*, 1969, 1970, 1971; Stout, 1971; Spear, 1977, 1980), although continuous, supercritical variation along the vector $NaAlSi_{-1}(ed)$ is also known. As in the micas, the solvus appears to be highly asymmetric, and the phase with the higher A-site occupancy is the more advanced along the vector *tk*. The probable relations are shown schematically in Figures 19 and 20. If Figures 19 and 20 are essentially correct, as seems likely, the distinctions between "actinolite"

and "hornblende" and between "anthophyllite" and "gedrite" as recommended by the recent I.M.A. commission (Leake and Winchell, 1978) may prove awkward to maintain.

CONDENSED BIOPYRIBOLE SPACE

By applying constraints on A-site and M1c-site occupancy in pairs, as indicated, we obtain the interesting spaces of Figures 21-24. In these the various polysomes lie in parallel lines or planes. Only pyroxene, amphibole, and mica fields are shown; other polysomes lie in intermediate lines or planes parallel to these.

In Figures 12-24 it has been assumed that the vector $MgCa_{-1}$ does not represent a possible variation in mica, and that the vector $NaAlSi_{-1}$ (the only one in Table 5 that alters the metal-to-oxygen ratio) does not represent a possible variation in pyroxene. The latter, however, is probably not strictly true, as indicated by experimental work summarized by Robinson (1980, p. 431) in Volume 7 of this series, and by natural occurrences such as the pyroxenes from eclogite inclusions in kimberlites reported by Smyth (1980). In most crustal pyroxenes, however, the variation in metal-oxygen ratio is minor (if indeed outside analytical error) and hence is neglected here.

Many other sections of our condensed pyribole space can be constructed. Two of special interest are those of Figures 25 and 26. These show biopyribole spaces containing silica, feldspar, and feldspathoid components. In each of these the pyroxene and mica spaces are lines at opposite edges of a tetrahedron containing a central amphibole plane. Figure 27 combines some of the interesting features of both and has a triangular field for mica.

Further condensations are possible. By replacing the oxide Na_2O by the vector $NaSiCa_{-1}Al_{-1}$ and projecting along it, we may project biopyriboles into the simpler space SiO_2-Al_2O_3-MgO-CaO-H_2O. A projection of this space through SiO_2 and H_2O is shown in Figure 28, and the equations for the new additive components are given in Table 7a. Figure 28 has many features in common with the classical ACF projection of Eskola (1939). The principal difference is due to projection along $NaSiCa_{-1}Al_{-1}$ rather than through $NaAlSi_3O_8$. Glaucophane and tschermakite are thus coincident

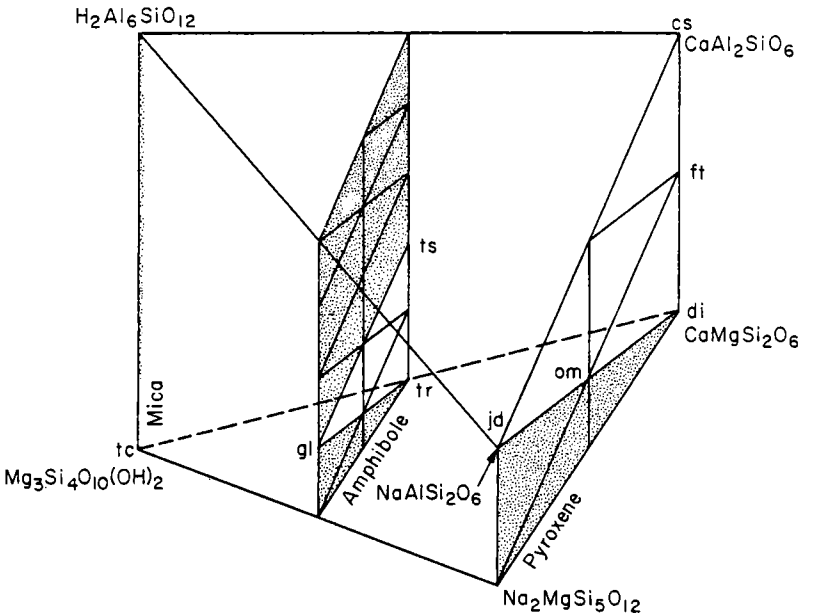

Figure 21. Condensed biopyribole space: A-sites empty and M1c-sites wholly occupied by Ca or Na. Abbreviations as in earlier figures.

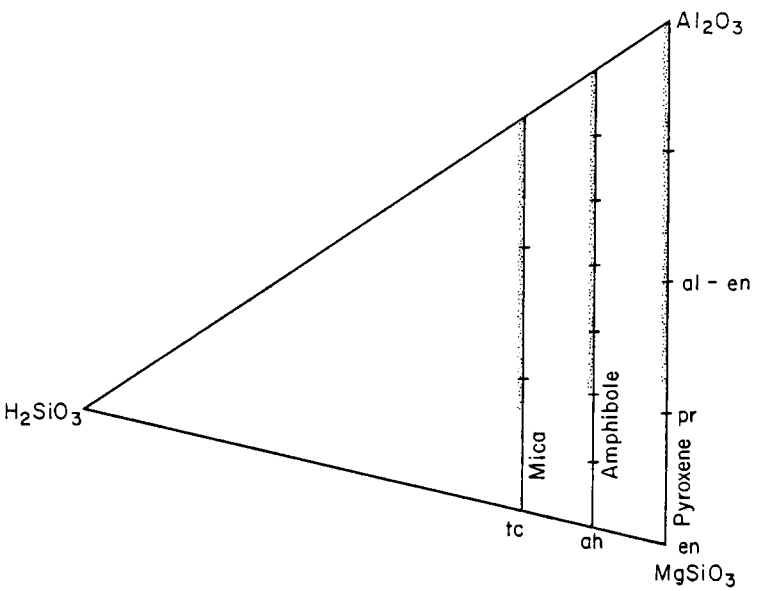

Figure 22. Condensed biopyribole space: A-sites empty and M1c-sites wholly occupied by Mg or Fe. Abbreviations as in earlier figures.

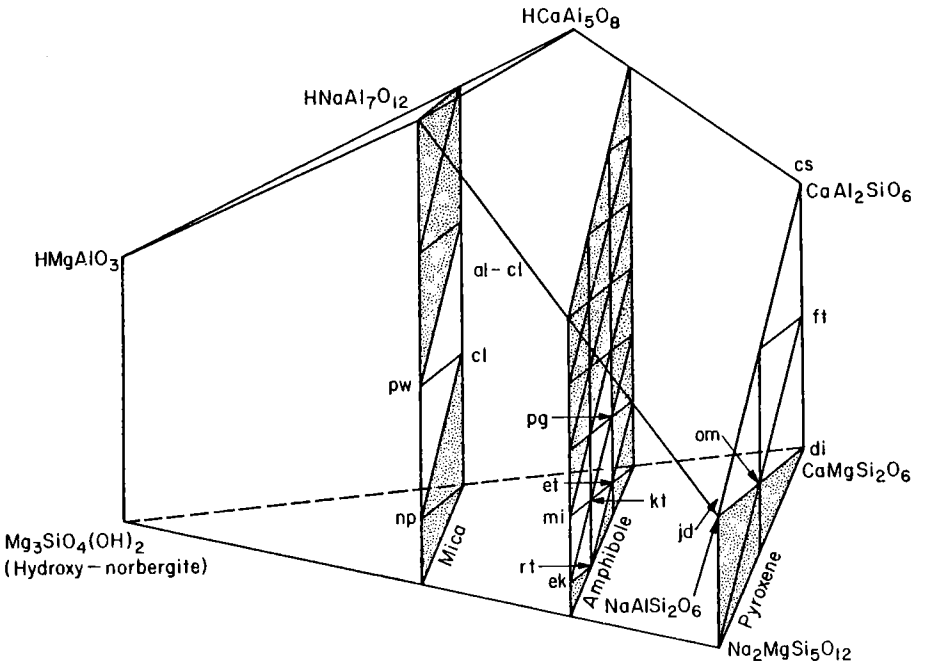

Figure 23. Condensed biopyribole space: A-sites full and Mlc-sites wholly occupied by Ca or Na. Abbreviations as in earlier figures.

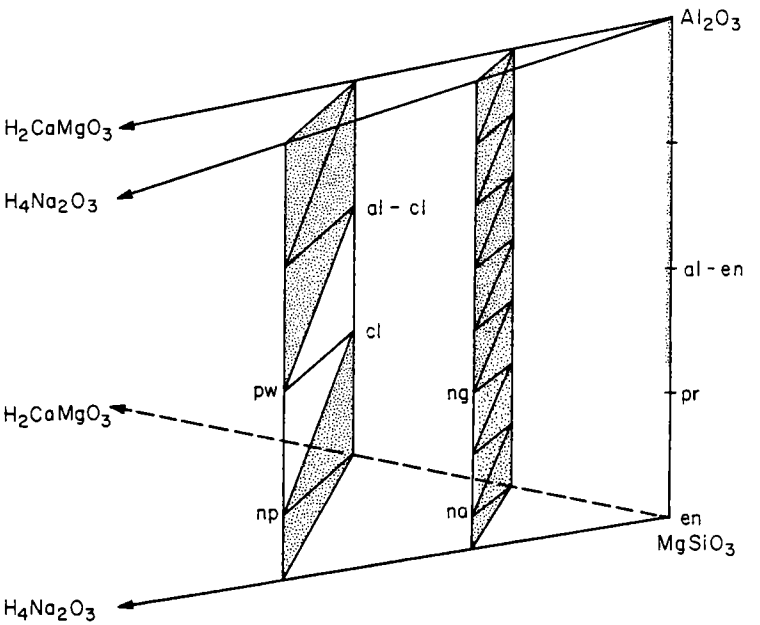

Figure 24. Condensed biopyribole space: A-sites full and Mlc-sites wholly occupied by Mg or Fe. Abbreviations as in earlier figures.

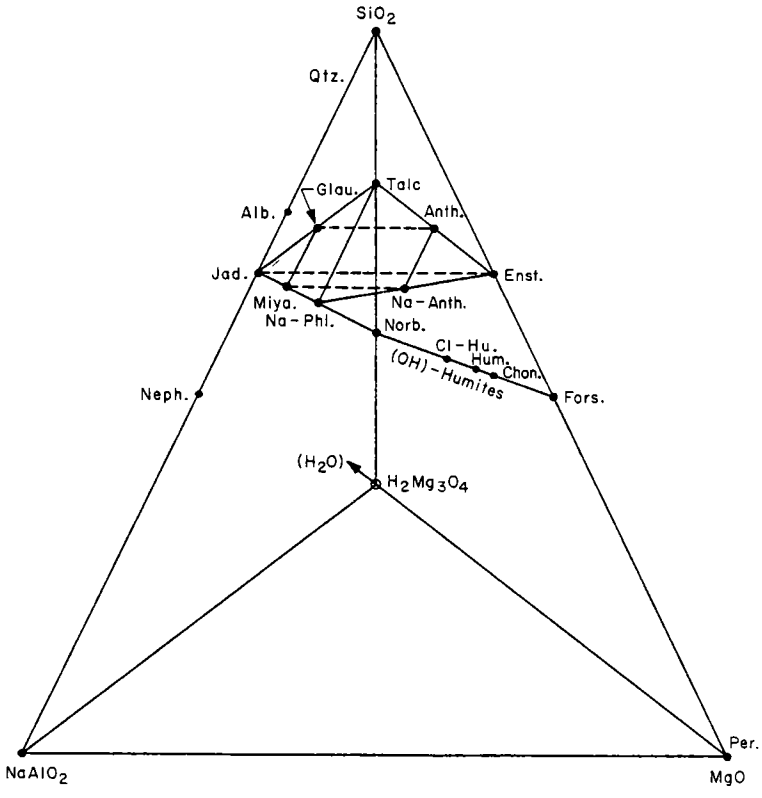

Figure 25. Biopyribole space as a tetrahedron embedded in SiO_2-$NaAlO_2$-MgO-H_2O. The right-hand face corresponds to Figure 8 of Thompson (1978).

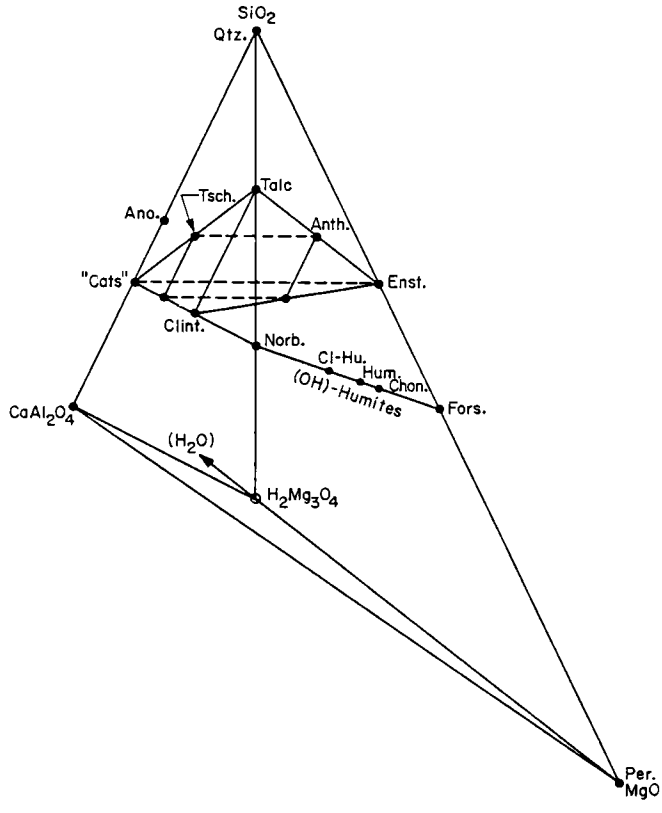

Figure 26. Biopyribole space as a tetrahedron embedded in SiO_2-$CaAl_2O_4$-MgO-H_2O. The right-hand face corresponds to Figure 8 of Thompson (1978).

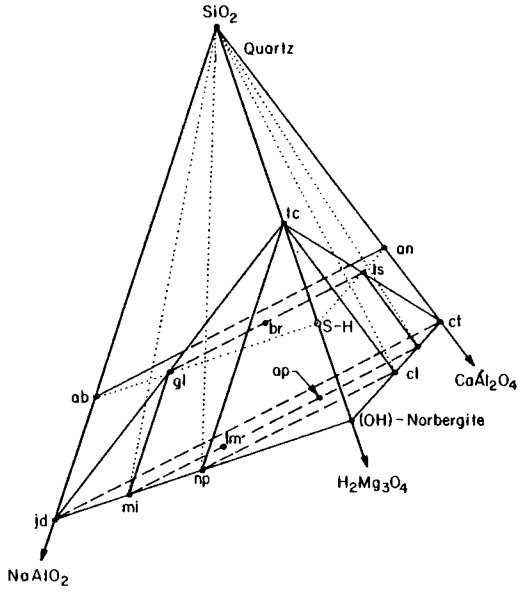

Figure 27. Biopyribole space as a pyramidal volume bounded by tc, np, cl, jd, and ct in SiO_2-$NaAlO_2$-$CaAl_2O_4$-$H_2Mg_3O_4$. The left and right faces are sections of Figures 25 and 26 respectively. The point S-H corresponds to a partially dehydrated lizardite or antigorite. Note that it is separated from feldspar (ab-an) by the pyribole volume, an important factor in the "blackwall" skarns that commonly appear between serpentinites and quartzofeldspathic country rocks.

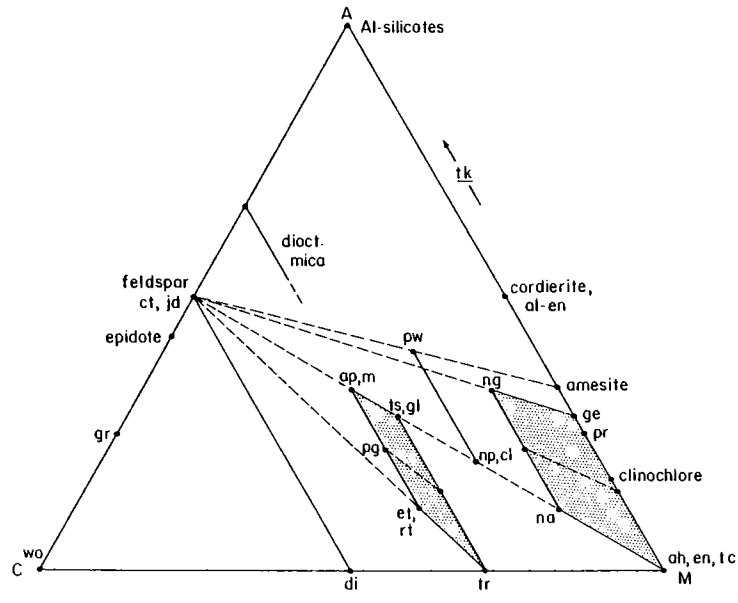

Figure 28. A further condensation of composition space including projection along the vector pl as in the projections of O'Hara (1968). The view shown here is also projected through SiO_2 and H_2O and has many features in common with the ACF diagram of Eskola (1939).

TABLE 7. Equations for condensation into CMASH and CMSH

a — Into CMASH[1]

SiO_2	(S)	=	$SiO_2 - 2(Na_2O+K_2O)$
Al_2O_3	(A)	=	$(Al_2O_3+Fe_2O_3+Cr_2O_3) + TiO_2 + (Na_2O+K_2O)$
MgO	(M)	=	$(MgO+FeO+MnO+NiO) - TiO_2$
CaO	(C)	=	$CaO + 2(Na_2O+K_2O)$
H_2O	(H)	=	H_2O
$NaSiCa_{-1}Al_{-1}$	(*pl*)	=	$2(Na_2O+K_2O)$

(Last seven equations as in Table 6)

b — Into CMSH

SiO_2	(S)	=	$SiO_2+(Al_2O_3+Fe_2O_3+Cr_2O_3) + TiO_2 - (Na_2O+K_2O)$
MgO	(M)	=	$(MgO+FeO+MnO+NiO) + (Al_2O_3+Fe_2O_3+Cr_2O_3) + (Na_2O+K_2O)$
CaO	(C)	=	$CaO + 2(Na_2O+K_2O)$
H_2O	(H)	=	H_2O
$NaSiCa_{-1}Al_{-1}$	(*pl*)	=	$2(Na_2O+K_2O)$
$Al_2Mg_{-1}Si_{-1}$	(*tk*)	=	$(Al_2O_3+Fe_2O_3+Cr_2O_3) + TiO_2 + (Na_2O+K_2O)$

(Last seven equations as in Table 6)

1. *Corresponds to condensation used by O'Hara, 1968.*

here, rather than widely separated. The transformation of components of Table 7a and the condensed space shown in projection in Figure 28 correspond in all essentials to the projection scheme devised by M. J. O'Hara (1968) for representation of the compositions of mafic rocks and magmas. The only difference is that we have omitted a phosphate component.

If we also replace the additive component Al_2O_3 by the vector $Al_2Mg_{-1}Si_{-1}$, as in the transformation of Table 7b, and condense into the space SiO_2-MgO-CaO-H_2O, we obtain the diagram of Figure 29. In this projection we can plot the compositions of nearly all rock minerals, as viewed from H_2O. The biopyriboles occupy a tetrahedral region. Pyroxenes and trioctahedral micas occupy the anhydrous and hydrous edges, spectively, and an amphibole plane lies midway between. The common clinopyriboles lie to the left, and the common orthopyriboles to the right, of the projected mica line. Yet another alternative would be to use the additive components SiO_2-$NaAlO_2$-$CaAl_2O_4$-$H_2Mg_3O_4$ with condensation on

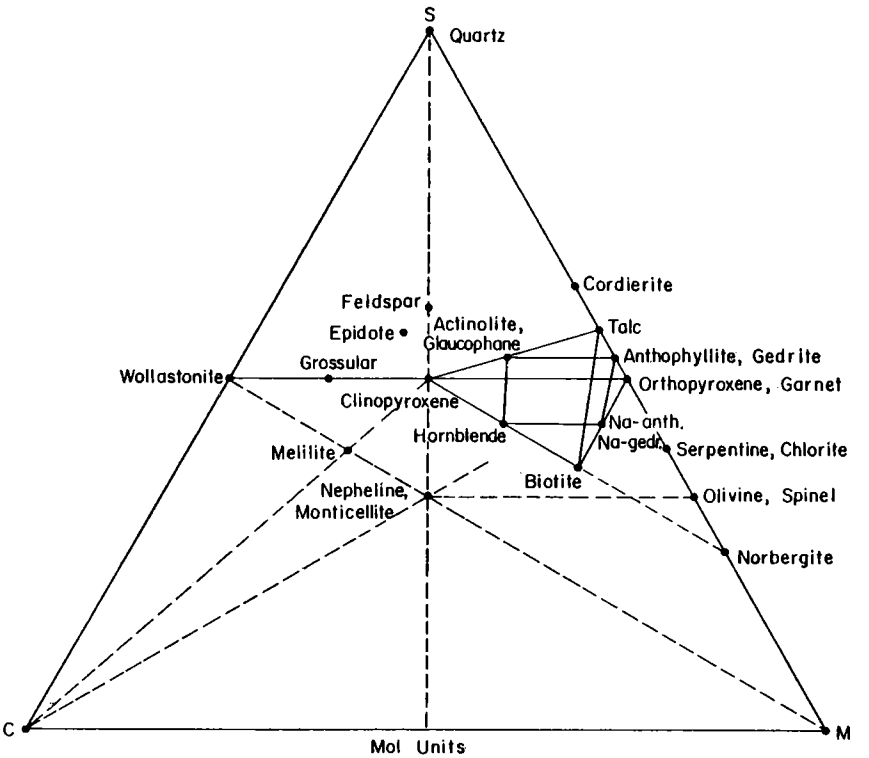

Figure 29. A further condensation of composition space that includes projection along *both pl* and *tk*. The view shown here is as viewed from H_2O. The biopyriboles occupy the tetrahedral volume bounded by clinopyroxene, orthopyroxene, talc, and biotite. The common clinopyriboles lie to the left and the common orthopyriboles to the right.

$Al_2Mg_{-1}Si_{-1}$ and $MgCa_{-1}$, but not on $NaAlSi_{-1}$ or $NaSiCa_{-1}Al_{-1}$. The geometry of the space defined by these last additive components would be essentially that of Figure 27, with all non-sodic pyroxene components projected at ct, all sodic ones at jd, and corresponding condensation of the amphiboles. (The transformation for such a projection is left as an exercise for the reader.)

BIOPYRIBOLES AND OTHER ROCK MINERALS

The number of independent closed system reactions possible in a mineral assemblage is found by determining the number of independently variable components, C_ϕ, in each phase ϕ, and summing these quantities. The number, N_R, of independent stoichiometric equations (possible reactions) that can be written is then the excess of this sum over the number

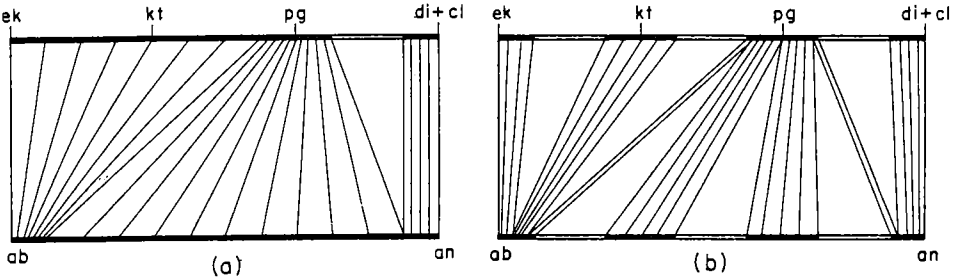

Figure 30. Schematic exchange relations between clinoamphiboles and plagioclase. Abbreviations as in earlier figures. Probable relations at high temperatures are shown in (a) and at lower temperatures, with possible miscibility gaps, in (b).

of independently variable components, C_s, of the system as a whole:

$$N_R = \sum_{\phi} C_{\phi} - C_s \ . \tag{1}$$

By the use of a single additive component for each phase, with variations therefrom shown by exchange vectors, it is possible to identify a great many of these possible reactions as pure *exchange reactions* between pairs of phases. Schematic relations between a line in amphibole space and the plagioclase feldspars are shown in Figure 30, with and without the possible complications arising from miscibility gaps in either series. Many other examples of exchange relations are possible. Most feldspars and feldspathoids have *pl* and KNa_{-1} exchange capacity, melilites have *tk* exchange capacity, some feldspathoids have *ed* exchange capacity, and garnets and carbonates have *mc* exchange capacity. $FeMg_{-1}$ exchange capacity is common to nearly all ferromagnesian minerals. The number of independent exchanges associated with a given vector is one less than the number of phases in which it operates; hence, those of the N_R reactions that are pure exchanges can be readily identified. Exchange reactions have a negligible effect on modal abundances. All remaining reactions must then involve a transfer from phase to phase of additive components and hence do affect modal abundances. The number N_T of such *net transfer reactions* is then given by:

$$N_T = \sum_{\phi} C_{\phi} - C_s - N_{ex} \tag{2}$$

where N_{ex} is the number of N_R reactions that are pure exchanges.

In open systems there is one additional net transfer reaction for each additive component (such as H_2O or CO_2) gained or lost. A formal

algebraic reduction scheme is presented elsewhere (Thompson *et al.*, in press), whereby all the unknowns in equations (1) and (2) may be determined and a sufficient and independent set of possible net transfer reactions obtained. We shall limit our examples here to a few of the simpler ones relating biopyriboles to other minerals.

Garnets, pyroxenoids, and many R_2O_3 oxides have composition spaces that are embedded in pyroxene space; hence, we may write many simple reactions of the form:

$$2CaMgSi_2O_6 + 2MgCa_{-1} + Al_2Mg_{-1}Si_{-1} = Mg_3Al_2Si_3O_{12} \qquad (3)$$

where the *mc* capacity may be provided by either pyroxene or garnet. Olivine and spinel may be related by the vector *tk* as in:

$$Mg_2SiO_4 + Al_2Mg_{-1}Si_{-1} = MgAl_2O_4 \qquad (4)$$

in which the necessary exchange capacity may be provided by any associated biopyribole (or by melilite). A more complicated relation can be found relating amphibole and quartz to epidote:

$$Ca_2Mg_5Si_8O_{22}(OH)_2 - 2MgCa_{-1} + 3Al_2Mg_{-1}Si_{-1} + SiO_2 = 2Ca_2Al_3Si_3O_{12}(OH) \qquad (5)$$

In this reaction the *mc* capacity can be provided by amphibole (at high T), or by associated garnet or carbonate.

Additive components along the join SiO_2-$NaAlO_2$ may be related, in pairs, by the vector *ed* as, for example:

$$NaAlSi_3O_8 = 4SiO_2 + NaAlSi_{-1} \qquad (6)$$

$$3SiO_2 + NaAlSi_{-1} = NaAlSi_2O_6 \qquad (7)$$

$$3NaAlSi_3O_8 + NaAlSi_{-1} = 4NaAlSi_2O_6 \qquad (8)$$

Any two of these three examples may be taken as independent in a quartz-plagioclase-jadeitic pyroxene assemblage. By elimination of *ed* between any two we have the familiar relation:

$$NaAlSi_3O_8 = NaAlSi_2O_6 + SiO_2 \ . \qquad (9)$$

Similar relations may be found for components on the joins SiO_2-$KAlO_2$ and SiO_2-$CaAl_2O_4$ by utilizing the vectors KNa_{-1} and $NaSiCa_{-1}Al_{-1}$. We have thus identified an important class of net transfer reactions relating biopyriboles to the silica minerals, feldspars, and feldspathoids.

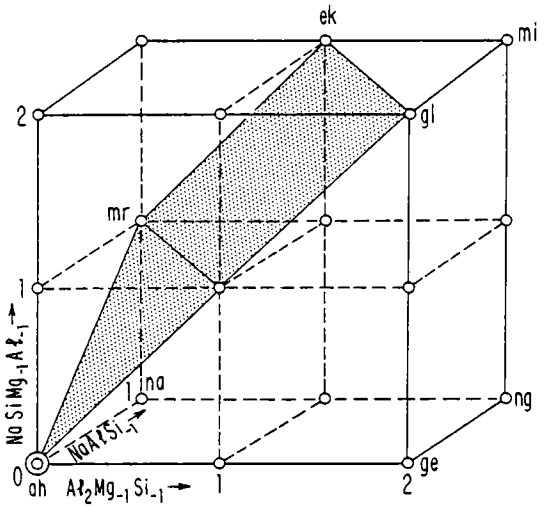

Figure 31. Amphibole space in the system SiO_2-Al_2O_3-MgO-Na_2O-H_2O. This is essentially the space of Figure 10 as transformed by the vector *mc*. The point mr is magnesiorichterite: $Na_2Mg_6Si_8O_{22}(OH)_2$.

An important consequence of relations (6), (7), and (8) is, other things being equal, that a low silica activity favors a high A-site occupancy in a mica or amphibole.

We may illustrate the above approach by considering, briefly, the occurrence of sodic amphiboles in the system SiO_2-Al_2O_3-MgO-Na_2O-H_2O (true, *not* condensed), and the problem of glaucophane stability. The amphibole space in this system is quaternary and has the form of Figure 31. This is essentially the space of Figure 10 transformed by the vector *mc*. The vector $NaSiMg_{-1}Al_{-1}$ in Figure 10 probably represents a strongly nonideal substitution; hence, glaucophane and other amphiboles in the upper face of the polyhedron would be unlikely to show significant solubility toward those lower down. The upper face contains the vectors *tr* and *ed*. These also relate talc and the sodic trioctahedral micas. With the vector $NaSiMg_{-1}Al_{-1}$ eliminated, we have the pyramidal composition space bounded by the quadrilateral $NaAlO_2$-Na_2MgO_2-$H_2Mg_3O_4$-HAl_3O_5 and the vertex SiO_2. The triangular section of this space that is bounded by SiO_2, $NaAlO_2$, and $H_2Mg_3O_4$ is also a section of Figure 25. In Figure 32 we see this section and some end-member compositions in it. We may also regard it as the full quaternary system as viewed along the vector *tk*. If the view is from the positive end of *tk*, then eckermannite, $Na_3Mg_4AlSi_8O_{22}(OH)_2$ (*ek*), lies behind "mi," $Na_3Mg_3Al_3Si_7O_{22}(OH)_2$, and preiswekite, $NaMg_2Al_3Si_2O_{10}(OH)_2$ (pw), lies toward the observer from Na-phlogopite. The only pyroxene component is $NaAlSi_2O_6$.

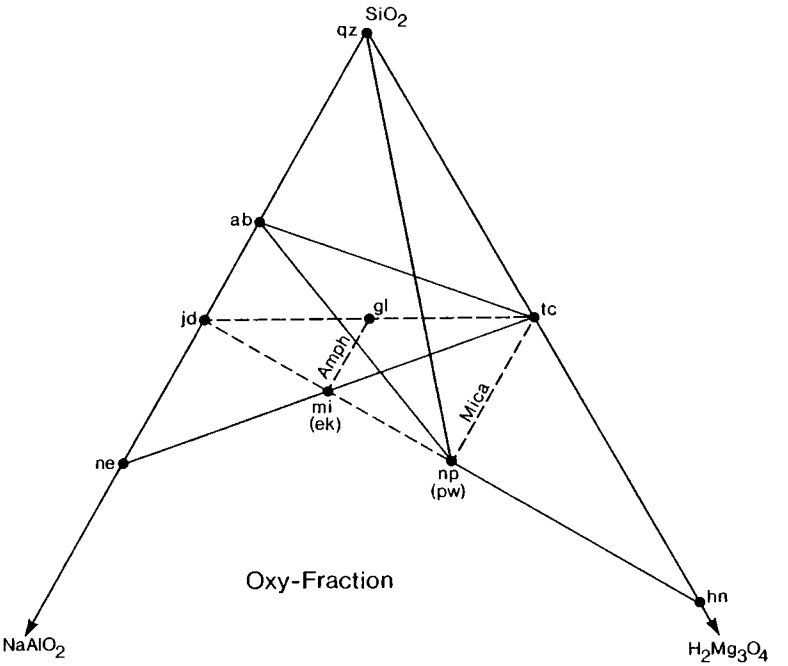

Figure 32. End-member compositions in the plane SiO_2-$NaAlO_2$-$H_2Mg_3O_4$. Mica-amphibole pairs may be quaternary. If the vector *tk* is added and directed toward the observer, there is a possible variation behind the plane from mi toward ek, and there are possible variations toward the observer from np toward pw and from tc toward al-tc. The pair ek + pw is chemically equivalent to mi + np; hence, tk exchange may take place normal to the projection.

Let us now consider a hypothetical assemblage containing quartz, albite, jadeite, talc, glaucophane, and an additional mica and amphibole, each with greater A-site occupancy than talc or glaucophane. Such an assemblage would, in this simple system, have a negative variance (seven phases, four components), but we may still obtain a sufficient set of possible reactions that must include those of its invariant, univariant, and other subassemblages. Micas and amphiboles are here ternary, and all other phases are of fixed composition. There are thus 15 minus four, or 11, independent reactions. Six of these may be taken as pure exchanges, three each on the vectors *ed* and *tk*. We are therefore left with five independent net transfer reactions. Two of these may be selected from equations (6) through (9). With $Mg_3Si_4O_{10}(OH)_2$ and $Na_2Mg_3Al_2Si_8O_{22}(OH)_2$ as the additive mica and amphibole components, respectively, the remaining three may be written as:

$$2NaAlSi_2O_6 + Mg_3Si_4O_{10}(OH)_2 = Na_2Mg_3Al_2Si_8O_{22}(OH)_2 \qquad (10)$$

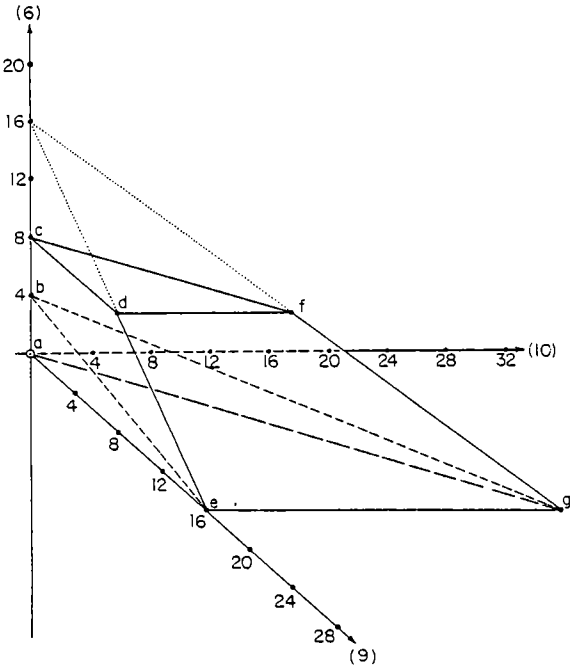

Figure 33. Net-transfer reaction space (a vector space) for assemblages in the system (SiO_2-$NaAlO_2$-$H_2Mg_3O_4$-$Al_2Mg_{-1}Si_{-1}$). Basis vectors are unit advancements, as defined in text, on reactions (6), (9), and (10). The truncated tetrahedron *a c d e f g* is the physically accessible region for the compositions of gl + $2SiO_2$, and the volume *b c d e f g* is that for the composition gl. See text for further explanations.

$$Mg_3Si_4O_{10}(OH)_2 \text{ [Mica A]} = Mg_3Si_4O_{10}(OH)_2 \text{ [Mica B]} \qquad (11)$$

and

$$Na_2Mg_3Al_2Si_8O_{22}(OH)_2 \text{ [Amph. A]} = Na_2Mg_3Al_2Si_8O_{22}(OH)_2 \text{ [Amph. B]} \ . \qquad (12)$$

It is also possible to construct a net-transfer *reaction space* (Thompson *et al.*, in press) by taking advancements on the reaction coordinates as a set of basis vectors. By considering only total mica and total amphibole (i.e., neglecting miscibility gaps) we may thus portray the above assemblage as modified by displacements in reactions (6), (9), and (10). Three-dimensional reaction spaces of this kind are presented by Thompson *et al.* (in press) and by Laird in Robinson *et al.* (Chapter 8, Volume 9B).

A net transfer reaction space defined by (6), (9), and (10) is shown in Figure 33. The unit advancement of each reaction is taken as that which transforms one oxygen equivalent from the additive components on

the left of each equation to the additive components on the right. The physically possible part of such a space is limited in any given direction either by loss of a reactant phase (i.e., loss of its additive component) or by loss of a necessary exchange capacity. The truncated tetrahedron in Figure 33 is that appropriate to matter containing 24 oxygen equivalents $Na_2Mg_3Al_2Si_8O_{22}(OH)_2$ and four oxygen equivalents of SiO_2 (i.e., the compositions of glaucophane plus quartz). The origin (*a*) is taken as the chemically equivalent assemblage albite plus talc. The plane *acde* represents amphibole-free assemblages. Planes parallel to it represent constant amounts of amphibole and of mica, both in oxygen equivalents, and the point *g* corresponds to 24 equivalents of amphibole, four of quartz, and none of mica. The plane *acfg* plays a similar role with respect to jadeite, as does *defg* with respect to albite. The upper and lower planes represent loss of *ed* exchange capacity, the upper plane requiring that all amphibole and mica A-sites are filled and the lower that all such sites are vacant. The albite-mica-quartz assemblage of Figure 34 is consistent with a point in the line *bc*. Vectors parallel to *de* and *be* correspond to reactions (7) and (8), respectively, both of which are linear combinations of (6) and (9), and the plane *beg* is one of constant quartz. Other special linear combinations of (6), (9), and (10) are:

$$2NaAlSi_3O_8 + Mg_3Si_4O_{10}(OH)_2 = 2SiO_2 + Na_2Mg_3Al_2Si_8O_{22}(OH)_2 \qquad (13)$$

corresponding to vectors parallel to *ag* and *cf*;

$$6SiO_2 + Mg_3Si_4O_{10}(OH)_2 + 2NaAlSi_{-1} = Na_2Mg_3Al_2Si_8O_{22}(OH)_2 \qquad (14)$$

corresponding to vectors parallel to *fg*; and

$$3NaAlSi_3O_8 + 2Mg_3Si_4O_{10}(OH)_2 + NaAlSi_{-1} = 2Na_2Mg_3Al_2Si_8O_{22}(OH)_2 \qquad (15)$$

corresponding to vectors parallel to *bg*. The amphibole-mica-quartz assemblage of Figure 35 corresponds to a point near *g* on *fg*.

Disequilibrium as well as equilibrium assemblages may be represented here. Points in the edges *ae* and *cd*, in the faces containing them, and in the interior of the polyhedron contain quartz-albite-jadeite as a subassemblage and hence can not have a variance greater than one and are constrained to a single univariant line in *P-T* space. If we accept the further probable constraint that glaucophane has no *tk* capacity in either

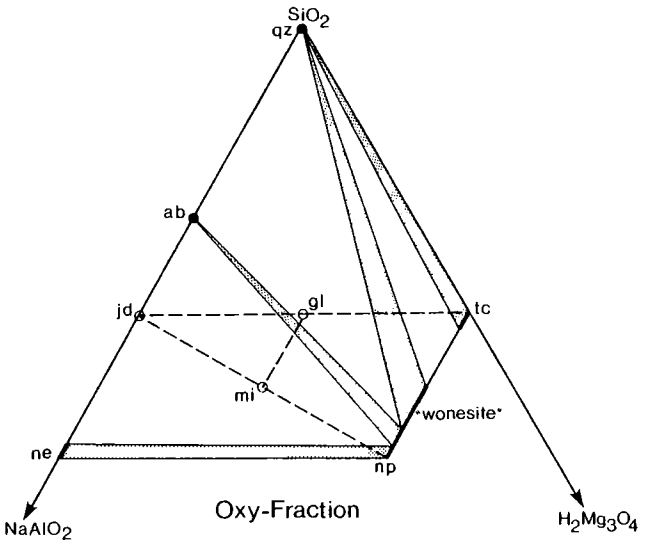

Figure 34. Schematic phase relations in the system of Figure 32 at low to moderate pressures. Relations are qualitatively consistent with the experimental results of Carman (1974b) and with the natural assemblages observed by Schreyer *et al.* (1980) and by Spear *et al.* (1981).

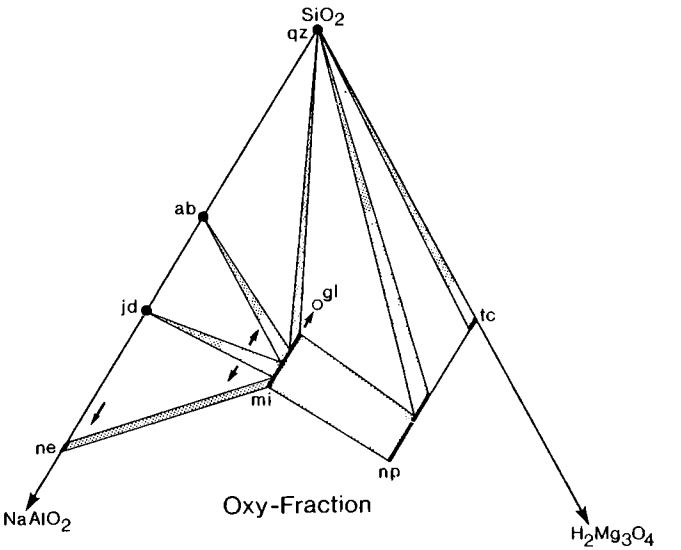

Figure 35. Schematic phase relations in the system of Figure 32 at high pressures. The variation of the amphibole coexisting with mica and quartz, as indicated by the arrow, would be consistent with the decrease in unit-cell volume recorded by Ernst (1963) and as interpreted by Maresch (1973, 1977). Arrows in other assemblages indicate effect of increasing pressure. There may be a miscibility gap in the amphiboles.

direction, then points in the lines *ag* and *eg* also represent assemblages that can not have a variance greater than one, and the plane *aeg* corresponds to assemblages that are invariant. Stable assemblages of variance two or more are thus restricted to the planes *acde* and *acfg* and lines and vertices bounding them *other than* the lines *ag and eg*. Examples of such assemblages are given in Figures 34 and 35, corresponding to points in the lines *bc* and *fg*, respectively.

If, on the other hand, we consider matter corresponding to 24 oxygen equivalents of end-member glaucophane composition, then the plane *bcg* is one of zero quartz and only points in or above it are physically possible. A consequence of this is that experiments on the glaucophane end-member composition can produce pure glaucophane only if neither quartz nor albite is present. Otherwise, as argued by Maresch (1973, 1977), any amphibole formed must have a non-zero A-site occupancy.

Figure 34 is also consistent with the low-to-moderate pressure assemblages reported by Schreyer *et al.* (1980) and by Spear *et al.* (1981), as well as with assemblages implied by the experiments of Carman (1974). Figure 35 is a possible configuration at higher pressure. The arrow in the assemblage quartz-mica-amphibole indicates a variation in the amphibole consistent with the decrease in cell volume with increasing pressure, as recorded by Ernst (1963) and as reinterpreted by Maresch (1973, 1977). It is thus likely that the "glaucophane I" of Ernst is an amphibole near mi or ek in Figure 31, although a magnesiorichterite (mr) component can not be ruled out entirely.

SUGGESTIONS FOR FURTHER WORK

The discerning reader will have realized, from the liberal use of qualifiers in the foregoing text, that much of what has been said is somewhat speculative. Each conjecture is thus a challenge to confirm or negate as the case may be. Two particularly urgent fields for study are the reactions relating mica, amphibole, and pyroxene, both in end-member and more complex systems, and a close examination of Na-Ca amphiboles to determine whether or not these show an ordering analogous to that in omphacite.

ACKNOWLEDGMENTS

I am grateful to Ernst Niggli and his colleagues at the University of Bern, Switzerland, for providing space and pleasant surroundings in 1971 when the groundwork for this paper was laid. Much of the draft writing and the preparation of many of the figures was done in 1976 when the writer held a Fairchild Fellowship at Caltech. Assistance has also been provided by the Higgins Fund of Harvard University. I have also benefited from discussions with C. W. Burnham, Jo Laird, Peter Robinson, J. H. Stout, A. B. Thompson, D. R. Veblen, and many others too numerous to mention and perhaps -- unfairly -- omitted. Also, my special thanks to Cynthia Rautio for able typing under stress.

Albee, A. L. (1961) Relationships between the mineral association, chemical composition, and physical properties of the chlorite series. Amer. Mineral. 47, 851-870.

Allen, J. C. and Boettcher, A. L. (1978) Amphiboles in andesite and basalt: II. Stability as a function of $\underline{P}$-$\underline{T}$-$\underline{f}_{H_2O}$-f_{O_2}. Amer. Mineral. 63, 1074-1087.

_____, _____ and Marland, G. (1975) Amphiboles in andesite and basalt: I. Stability as a function of $\underline{P}$-$\underline{T}$-$\underline{f}_{O_2}$. Amer. Mineral. 60, 1069-1085.

Borg, I. Y. (1967) Optical properties and cell parameters of the glaucophane-riebeckite series. Contrib. Mineral. Petrol. 15, 67-92.

Brady, J. B. (1974) Coexisting actinolite and hornblende from west-central New Hampshire. Amer. Mineral. 59, 529-535.

Bragg, W. L. (1937) *Atomic Structure of Minerals.* Cornell Univ. Press, Ithaca, New York.

_____ and Claringbull, G. F. (1965) *Crystal Structure of Minerals.* G. Bell and Sons, London.

Brown, G. E., Prewitt, C. T., Papike, J. J. and Sueno, S. (1972) A comparison of the structures of low and high pigeonite. J. Geophys. Res. 77, 5778-5789.

Buseck, P. R. and Iijima, S. (1975) High resolution electron microscopy of enstatite. II: Geological application. Amer. Mineral. 60, 771-784.

_____, Nord, G. L. and Veblen, D. R. (1980) Subsolidus phenomena in pyroxenes. *In* C. T. Prewitt, ed., *Pyroxenes,* Mineral. Soc. Amer. Rev. Mineral. 7, 117-211.

Bystrom, A. (1943) Rontgenuntersuchung des Systems MgO-Al_2O_3-SiO_2. Ber. Deutsch. Keram. Ges. 24, 2-12.

Cameron, M. and Papike, J. J. (1979) Amphibole crystal chemistry: A review. Fortschr. Mineral. 57, 28-67.

Carman, J. H. (1974a) Preliminary data on the $\underline{P}$-$\underline{T}$ stability of synthetic glaucophane (abstr.). Trans. Amer. Geophys. Union, 55, 481.

_____ (1974b) Synthetic sodium phlogopite and its two hydrates: stabilities, the properties and mineralogical implications. Amer. Mineral. 59, 261-273.

Cawthorn, R. G. and Collerson, K. D. (1974) The recalculation of pyroxene end-member parameters and the estimation of ferrous and ferric content from electron microprobe analysis. Amer. Mineral. 59, 1203-1208.

Chernosky, J. V., Jr. and Autio, L. K. (1979) The stability of anthophyllite in the presence of quartz. Amer. Mineral. 64, 294-303.

Colville, P., Ernst, W. G. and Gilbert, M. C. (1966) Relationships between cell parameters and chemical composition of monoclinic amphiboles. Amer. Mineral. 51, 1727-1754.

Compton, R. R. (1958) Significance of amphibole paragenesis in the Bidwell Bar region, California. Amer. Mineral. 43, 890-907.

Day, J. W. and Halbach, H. (1979) The stability field of anthophyllite: the effect of experimental uncertainty on permissible phase diagram topologies. Amer. Mineral. 64, 809-823.

Ernst, W. G. (1961) Stability relations of glaucophane. Amer. J. Sci. 259, 735-765.

_____ (1963) Polymorphism in alkali amphiboles. Amer. Mineral. 48, 241-260.

_____ (1968) *Amphiboles.* Springer-Verlag, New York.

Eskola, P. (1939) Die metamorphen Gestein. In: *Die Entstehung der Gesteine,* T. F. W. Barth, C. W. Correns, P. Eskola, eds. Springer-Verlag, Berlin, pp. 263-407.

Essene, E. J., Hensen, B. J. and Green, D. H. (1970) Experimental study of amphibolite and eclogite stability. Phys. Earth Planet. Interiors 3, 378-384.

Franz, G. and Althaus, E. (1976) Experimental investigation in the formation of solid solutions in sodium-aluminum-magnesium micas. N. Jahrb. Mineral. Abh. 126, 233-253.

Frondel, C. and Klein, C. (1965) Ureyite, $NaCrSi_2O_6$: A new meteorite pyroxene. Science 149, 742-744.

Gilbert, M. C. and Popp, R. K. (1973) Properties and stability of glaucophane at high pressure (abstr.). Trans. Amer. Geophys. Union 55, 464.

_____ and Troll, G. (1974) A comparison of the stabilities of OH- and F- tremolite (abstr.). Int'l. Mineral. Assoc., 9th Mtg., Germany, Coll. Abstracts, 84.

Greenwood, H. J. (1963) The synthesis and stability field of anthophyllite. J. Petrol. 4, 317-351.

_____ (1971) Anthophyllite: Corrections and comments on its stability. Amer. J. Sci. 270, 151-154.

_____ (1979) Thermodynamic properties of edenite. In Current Res. Pt.B., Geol. Surv. Canada, Paper 79-1B, 365-370.

Hazen, R. M. and Finger, L. W. (1978) The crystal structures and compressibilities of layer minerals at higher pressure. II. Phlogopite and chlorite. Amer. Mineral. 63, 293-296.

Hewitt, D. A. (1975) Stability of phlogopite-calcite-quartz. Amer. Mineral. 60, 391-397.

_____ and Wones, D. R. (1975) Physical properties of some synthetic Fe-Mg-Al trioctahedral biotites. Amer. Mineral. 60, 854-862.

Hinrichsen, Th. and Schürmann, K. (1977) Experimental investigations of the Na/K substitution in edenites and pargasites. N. Jahrb. Mineral. Abh. 130, 12-18.

Huebner, J. S. and Papike, J. J. (1970) Synthesis and crystal chemistry of sodium-potassium richterite $(Na,K)NaCaMg_5Si_8O_{22}(OH,F)_2$: a model for amphiboles. Amer. Mineral. 55, 1973-1992.

Jaffe, H. W., Robinson, P. and Klein, C. Jr. (1968) Exsolution lamellae and optic orientation of clinoamphiboles. Science 160, 776-778.

Keusen, H. R. (1972) Mineralogie und Petrographie des metamorphen Ultramafit Komplexes vom Geisspfad (Pennische Alpen). Schweiz. Mineral. Petrogr. Mitt. 52, 385-478.

_____ and Peters, T. (1980) Preiswerkite, an Al-rich trioctahedral sodium mica from the Geisspfad ultramafic complex (Penninic Alps). Amer. Mineral. 65, 1134-1137.

Klein, C. (1969) Two-amphibole assemblages in the system actinolite-hornblende-glaucophane. Amer. Mineral. 54, 212-237.

Kulke, H. G. (1976) Metamorphism of evaporitic carbonate rocks (N.W. Africa and Afganistan) and the formation of lapis lazuli (abstr.). 25th Int. Geol. Cong. Abstr. 1, 131.

Leake, B. E. and Winchell, H. (1978) Nomenclature of amphiboles. Amer. Mineral. 63, 1023-1052.

Lindsley, D. H. (1965) Ferrosilite. Carnegie Inst. Washington Yearbook 64, 148-149.

_____ (1980) Phase equilibria of pyroxenes at pressures > 1 atmosphere. *In* C. T. Prewitt, ed., *Pyroxenes*, Mineral. Soc. Amer. Rev. Mineral. 7, 289-307.

Longhi, J. and Boudreau, A. F. (1980) The orthoenstatite liquidus field in the system forsterite-diopside-silica at one atmosphere. Amer. Mineral. 65, 563-573.

Maresch, W. V. (1973) New data on the synthesis and stability relations of glaucophane. Earth Planet. Sci. Lett. 20, 385-390.

_____ (1977) Experimental studies on glaucophane: an analysis of present knowledge. Tectonophysics 43, 109-175.

Merrill, R. B. and Wyllie, P. J. (1975) Kaersutite and kaersutite eclogite from Kakanui, New Zealand--water-excess and water-deficient melting to 30 kilobars. Bull. Geol. Soc. Amer. 86, 555-570.

Moore, P. B. (1969) Joesmithite: a novel amphibole crystal chemistry. Mineral. Soc. Amer. Spec. Paper 2, 111-115.

Niggli, P. (1954) *Rocks and Mineral Deposits*. W. H. Freeman and Co., San Francisco.

O'Hara, M. J. (1968) The bearing of phase equilibria studies on synthetic and natural systems on the origin and evolution of basic and ultrabasic rocks. Earth Sci. Rev. 4, 69-133.

Ohashi, Y. and Burnham, C. W. (1973) Clinopyroxene lattice deformations: the roles of chemical substitution and temperature. Amer. Mineral. 58, 843-849.

_____, _____ and Finger, L. W. (1975) The effect of Ca-Fe substitution on the clinopyroxene crystal structure. Amer. Mineral. 60, 423-434.

_____ and Finger, L. W. (1976) The effect of Ca substitution on the structure of clinoenstatite. Carnegie Inst. Wash. Yearbook, 75, 743-746.

Olesch, M. (1975) Synthesis and solid solubility of trioctahedral micas in the system CaO-MgO-Al_2O_3-SiO_2-H_2O. Amer. Mineral. 60, 188-199.

Papike, J. J., Prewitt, C. T., Sueno, S. and Cameron, M. (1973) Pyroxenes: Comparisons of real and ideal structural topologies. Z. Kristallogr., 13, 254-273.

Perry, K. (1967) An application of linear algebra to petrologic problems: Part I. Mineral classification. Geochim. Cosmochim. Acta 31, 1043-1078.

_____ (1968) Representations of mineral chemical analyses in 11-dimensional space. Part II: Amphiboles. Lithos 1, 307-321.

_____ (1970) A general method for constructing the set of all end-members of a mineral group. (abstr.). Amer. Mineral. 55, 305.

Pëto, P. (1976) Synthesis and stability of edenitic hornblende. Prog. Expt'l. Petrol., Nat. Ener. Res. Council Publ. Ser. D., 1976, 6, 27-28.

Phillips, R. (1966) Amphibole compositional space. Mineral. Mag. 35, 945-952.

_____ and Layton, W. (1964) The calciferous and alkali amphiboles. Mineral. Mag. 275, 945-952.

Prewitt, C. T., Brown, G. E. and Papike, J. J. (1971) Apollo 12 clinopyroxenes: High temperature x-ray diffraction data. Proc. 2nd. Lunar Sci. Conf. 1, 59-68.

_____, Papike, J. J. and Ross, M. (1970) Cummingtonite: a reversible, unquenchable transition from $P2_1/m$ to C2/m symmetry.(abstr.). Amer. Mineral. 55, 305-306.

Robinson, P., Jaffe, H. W., Klein, C., and Ross, M. (1969) Equilibrium coexistence of three amphiboles. Contrib. Mineral. Petrol. 22, 248-258.

_____, Ross, M., and Jaffe, H. W. (1970) The composition field of anthophyllite and the anthophyllite miscibility gap. (abstr.). Amer. Mineral. 55, 307-309.

_____, _____, and _____ (1971) Composition of the anthophyllite-gedrite series, comparisons of gedrite and hornblende, and the anthophyllite-gedrite solvus. Amer. Mineral. 56, 1005-1041.

_____ (1980) The composition space of terrestrial pyroxenes-internal and external limits. *In* C. T. Prewitt, ed., *Pyroxenes,* Mineral. Soc. Amer. Rev. Mineral. 7, 419-494.

Ross, M., Papike, J. J. and Shaw, K. W. (1969) Exsolution textures in amphiboles as indicators of sub-solidus thermal histories. Mineral. Soc. Amer. Spec. Paper 2, 275-299.

Schreyer, W., Abraham, K. and Kulke, H. (1980) Natural sodium phlogopite coexisting with potassium phlogopite and sodian aluminian talc in a metamorphic evaporite sequence from Derrag, Tell Atlas, Algeria. Contrib. Mineral. Petrol. 74, 223-233.

Shido, F. and Miyashiro, A. (1959) Hornblendes of basic metamorphic rocks. J. Fac. Sci., Univ. Tokyo 12, 85-102.

Smith, J. V. (1959) Graphical representation of amphibole compositions. Amer. Mineral. 44, 437-440.

_____ and Yoder, H. S. (1956) Experimental and theoretical studies of the mica polymorphs. Mineral Mag. 31, 209-235.

Smyth, J. R. (1974) The high temperature crystal chemistry of clinohypersthene. Amer. Mineral. 59, 1069-1082.

_____ (1980) Cation vacancies and the crystal chemistry of breakdown reactions in kimberlitic omphacites. Amer. Mineral. 65, 1186-1191.

_____ and Burnham, C. W. (1972) The crystal structures of high and low clinohypersthene. Earth Planet. Sci. Lett., 14, 183-189.

Spear, F. S. (1977) Phase equilibria of amphibolites from the Post Pond Volcanics, Vermont. Carnegie Inst. Washington Yearbook 77, 808-812.

_____ (1980) The gedrite-anthophyllite solvus and the composition limits of orthoamphibole from the Post Pond Volcanics, Vermont. Amer. Mineral. 65, 1103-1118.

_____, Hazen, R. M. and Rumble, D. (1981) Wonesite: a new rock-forming silicate from the Post Pond Volcanics, Vermont. Amer. Mineral. 66, 100-105.

Stout, J. H. (1971) Four coexisting amphiboles from Telemark, Norway. Amer. Mineral. 56, 212-224.

Sueno, S., Papike, J. J., Prewitt, C. T. and Brown, G. E. (1972) Crystal structure of high cummingtonite. J. Geophys. Res. 77, 5767-5777.

Thompson, J. B., Jr. (1970) Geometrical possibilities for amphibole structures: model biopyriboles. Amer. Mineral. 55, 292-293.

_____ (1978) Biopyriboles and polysomatic series. Amer. Mineral. 63, 239-249.

_____ (1979) The Tschermak substitution and reaction in pelitic schists. In *Problems in Physicochemical Petrology,* V. A. Zharikov, V. I. Fonarev and S. P. Korikovskii, eds., Academy of Sciences, Moscow, pp. 146-159 (in Russian).

_____ (1981) Polytypism in complex crystals: contrasts between mica and classical polytypes. In *Structure and Bonding in Crystals,* M. O'Keefe and A. Navrotsky, eds. Academic Press, New York, pp. 167-196.

_____, Laird, J. and Thompson, A. B. (1982) Reactions in amphibolite, greenschist and blueschist. J. Petrol. (in press).

Turnock, A. C., Lindsley, D. H. and Grover, J. E. (1973) Synthesis and unit cell parameters of Ca-Mg-Fe pyroxenes. Amer. Mineral. 58, 50-59.

Veblen, D. R. and Burnham, C. W. (1978a) New biopyriboles from Chester, Vermont: I. Descriptive mineralogy. Amer. Mineral. 63, 1000-1009.

_____ and _____ (1978b) New biopyriboles from Chester, Vermont: II. The crystal chemistry of jimthompsonite, clinojimthompsonite, and chesterite, and the amphibole-mica reaction. Amer. Mineral. 63, 1053-1073.

_____ and Buseck, P. R. (1979) Chain-width order and disorder in biopyribles. Amer. Mineral 64, 687-700.

Whittaker, E. J. W. and Zussman, J. (1961) The choice of axes in amphiboles. Acta Crystallogr. 14, 54-55.

Widmark, E. T. (1974) An edenite-forming reaction: hydrothermal experiments. Neues Jahrb. Mineral. Monats. 1974, 7, 323-329.

Yoder, H. S. and Tilley, C. E. (1962) Origin of basalt magmas: an experimental study of natural and synthetic rock systems. J. Petrol. 3, 342-532.

Chapter 4

NON-CLASSICAL PYRIBOLES and POLYSOMATIC REACTIONS in BIOPYRIBOLES

David R. Veblen

INTRODUCTION

As shown by Thompson in Chapter 3, it is possible to visualize the amphibole structure as consisting of two types of slabs, parallel to (010), that have the structures of a pyroxene (P) and a mica or talc (M) (Thompson, 1970, 1978). The pyroxenes and micas consist of only one type

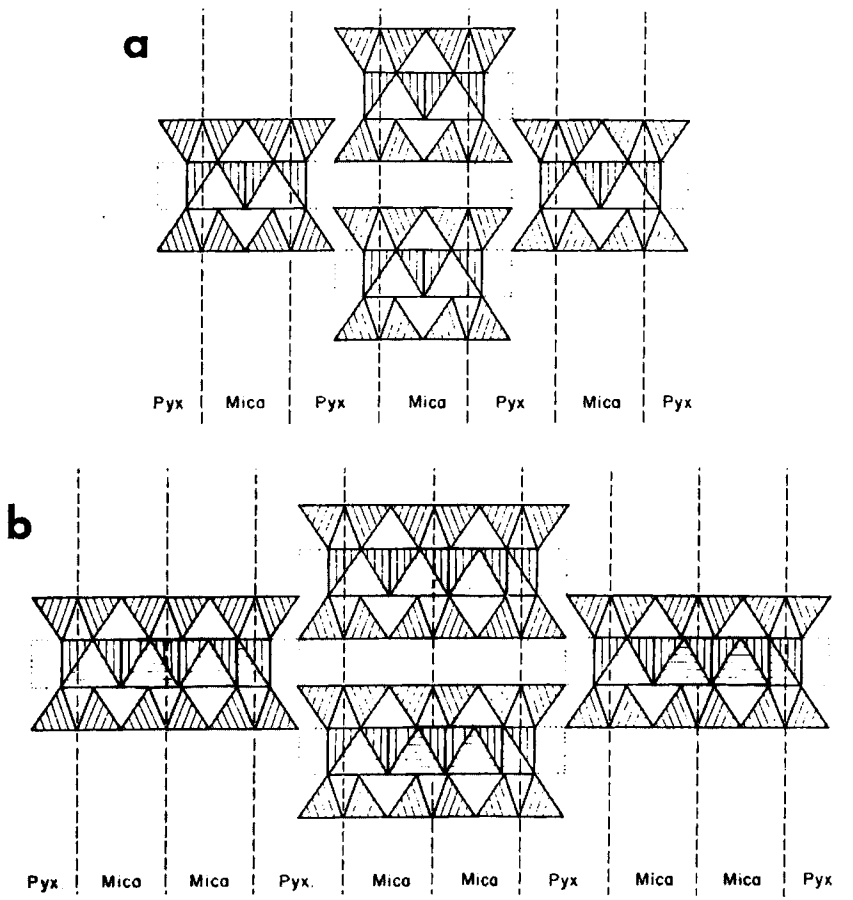

Figure 1. (a) The double-chain clinoamphibole structure, viewed parallel to the silicate chains, consists of (010) slabs having Mica and Pyroxene structures, arranged in the sequence ...MPMPMPMP...(after Thompson, 1978.) (b) The triple-chain clinojimthompsonite structure can be constructed from the same slabs, but in the sequence ...MMPMMPMMPMMP....

of slab (PPPPPP and MMMMMM), while in amphiboles, these M and P slabs coexist in rigorous alternation (MPMPMP; Fig. 1a). In fact, M and P slabs can fit together in any order, resulting potentially in an infinitely large family of structures that are collectively called biopyriboles. For example, if the M's and P's are assembled in the sequence MMPMMP, as shown in Figure 1b, the result is not a silicate with double chains (amphibole), but instead a structure containing triple chains. It is not even necessary to assemble the slabs in an ordered sequence; M's and P's theoretically can be put together in disordered sequences, even at random, resulting in biopyriboles with disordered chain widths.

Recently, there have been numerous reports, starting with Chisholm (1973) and Drits *et al.* (1974, 1976), of both ordered and disordered biopyriboles other than pyroxenes, amphiboles, and micas (including talc). It is the intent of this chapter to explore the range of these observed structures, reviewing x-ray, electron microscopic, and chemical results. Since these nonclassical biopyriboles are typically produced by solid-state replacement reactions from pyroxenes and amphiboles, we will also explore the reaction paths and the structural mechanisms by which replacement occurs.

BIOPYRIBOLE NOMENCLATURE

As with most evolutionary systems of nomenclature, confusion has occasionally arisen over certain aspects of biopyribole terminology. In this section, an attempt is made to clarify some of the potentially confusing terms. The term *biopyribole* was coined by Johannsen (1911) to collectively denote the micas (*bio*tite), *pyro*xenes, and amph*iboles* (*biopyribole* does *not* refer to a pyribole that has formed by a biological process!). Johannsen used *pyribole* to refer to the biopyriboles excluding the micas (i.e., the pyroxenes and amphiboles together). Thompson (1970, 1978) reinstituted Johannsen's terminology and extended it to include other minerals, at the time still hypothetical, that could be assembled from pyroxene and mica slabs. Thus, *biopyribole* now refers to any member of the homologous series extending from pyroxene to mica, whether structurally ordered or disordered, and *pyribole* refers to any member excluding the micas, talc, and pyrophyllite. In some cases, these terms have been interpreted to mean only the nonclassical

biopyriboles that have been discovered during the past few years; this is not the case, and proper use of the word biopyribole still denotes the group *including* pyroxene and amphibole.

Additional biopyribole nomenclature has evolved as the need for it has arisen, largely in papers by Veblen and coworkers. *Hydrous pyriboles* has been used to describe the pyriboles exclusive of pyroxenes, i.e., amphibole, jimthompsonite, etc. Though simple and descriptive, this term might be confusing because it is possible to replace the hydroxyl in pyriboles with fluorine and because natural pyroxenes commonly contain appreciable water (Martin and Donnay, 1972). As used, *hydrous pyribole* is meant to include fluorpyriboles but exclude even very wet pyroxenes. The term *wide-chain pyribole* has been used to denote pyriboles with triple chains or chains wider than triple, i.e., chesterite, jimthompsonite, disordered pyribole with predominantly triple or wider chains, etc. Some other authors have used *multiple chain* to denote chains wider than double, but this usage is not followed in the present paper. The terms *clinopyribole*, *orthopyribole*, and *protopyribole* have been used to describe collectively all pyriboles having the stacking sequences found in clinoenstatite, orthoenstatite, and protoenstatite, or cummingtonite, anthophyllite, and protoamphibole, respectively (see chapters by Hawthorne and Thompson, this volume).

Mixed-chain pyriboles are those that contain silicate chains of more than one width. Mixed-chain pyriboles that have a disordered sequence of silicate chain widths are said to be *structurally disordered*, to draw a distinction between this type of disorder and the cation site occupancy disorder that occurs in most biopyriboles; this type of disorder can be more specifically denoted as *chain-width disorder*. More-or-less isolated chains of anomalous width that occur in otherwise ordered pyribole can be referred to as *chain-width errors* or *chain-width defects*.

ORDERED NON-CLASSICAL BIOPYRIBOLES

The first wide-chain silicates to be recognized were synthetic barium silicates, which contain triple, quadruple and quintuple chains (Katcher and Liebau, 1965; Liebau, 1980). The silicate chains of these phases are topologically distinct from those of pyriboles, however,

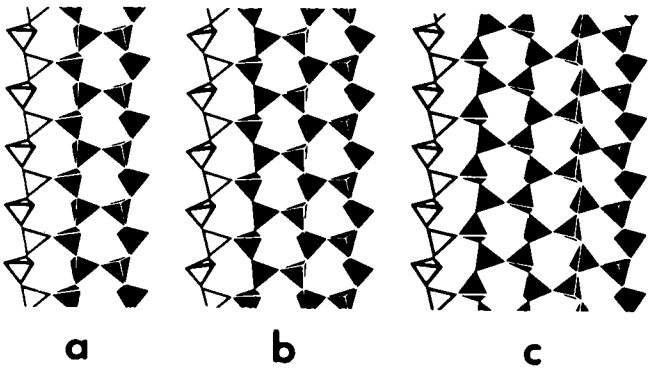

Figure 2. The silicate chains of barium silicates, which have their apical oxygens alternately pointing up and down. In each chain, one "subchain" was drawn white, while the others are black. (a) Triple chain. (b) Quadruple chain. (c) Quintuple chain. (After Liebau, 1980.)

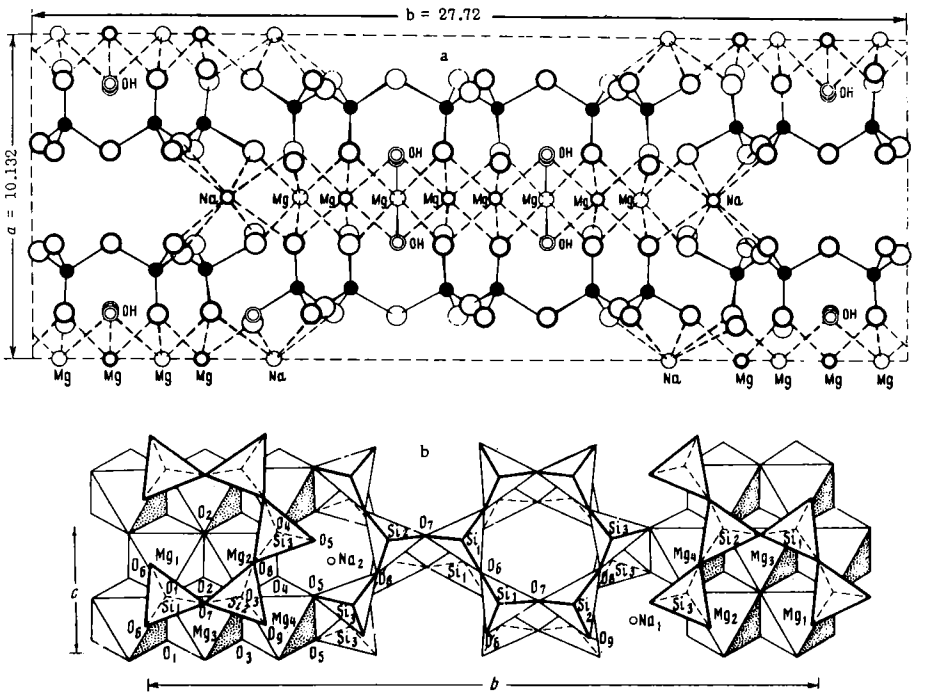

Figure 3. Structure of the triple-chain NaMg silicate synthesized by Drits *et al.* (1974). Topologically identical to the MMP clinopyribole shown in Figure 1b, this structure contains Mg in regular sites of a wide octahedral strip, with Na in the outermost, distorted sites of the strip. Articulation of the triple silicate chain to the octahedral strips is analogous to that in pyroxenes and amphiboles. (After Drits *et al.*, 1974.)

because the apical oxygens of the tetrahedra alternately point in opposite directions (Fig. 2). The first report of a structurally ordered wide-chain material that could be constructed from M and P slabs, and hence is a pyribole, was that of Drits *et al.* (1974). This synthetic phase was produced during experiments aimed at synthesizing amphibole asbestos, and the structure was solved using Fourier methods in conjunction with electron diffraction intensity data. The structure contains triple silicate chains, is monoclinic, and is an analog of the clinopyroxene and clinoamphibole structures. As shown in Figure 3, from Drits *et al.* (1974), the regular octahedra of the wide octahedral strips are occupied by Mg and the distorted, outermost sites of these strips, which are analogous to the M2 sites of pyroxenes and the M4 sites of amphiboles, are occupied by Na.

Based on bulk chemical analyses and the apparent absence of Na in the A-sites (which correspond to the A-sites of amphiboles and the interlayer sites of micas), Drits *et al.* concluded that the formula of their triple-chain silicate is $\square_2Na_2Mg_8[Si_{12}O_{30}(OH)_2](OH)_4$ (formula written on the basis of 36 oxygens to be consistent with amphibole formulas containing 24 oxygens). In this formula, two of the oxygens that are bonded to silicon are replaced by hydroxyl, suggesting that this material is the analog of a NaMg hydroamphibole having the composition $Na_2Mg_5[Si_8O_{20}(OH)_2](OH)_2$, or a NaMg hydropyroxene having the formula $NaMg[Si_2O_5(OH)]$. However, the inherent poor quality of electron diffraction intensity data casts some doubt on the ability of Drits *et al.* to ascertain the exact structural formula. A later synthesis by Tateyama *et al.* (1978) yielded a material with occupied A-sites, giving the formula $Na^A_2Na_2Mg_8[Si_{12}O_{32}](OH)_4$. The chemistry of these triple-chain silicates is discussed further in a later section.

Independently of the work by Drits and coworkers, Veblen and Burnham (1975, 1976) discovered four new minerals intergrown with anthophyllite and cummingtonite in the blackwall alteration zone of a metamorphosed ultramafic body near Chester, Vermont. Details of the occurrence, physical and optical properties, chemistry, and crystal structures of three of the minerals were subsequently reported by Veblen and Burnham (1978a,b). Structurally, the new minerals are chain silicates analogous to pyroxenes and amphiboles, but with either triple chains or

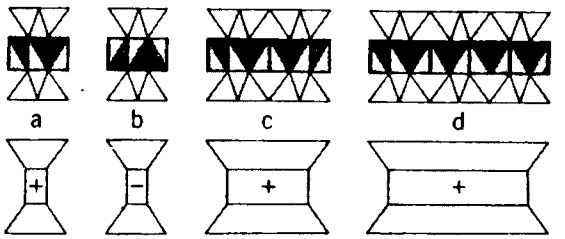

Figure 4. Pyribole I-beams (top) consist of two tetrahedral chains connected to an octahedral strip; also shown are the simplified representations of these I-beams (bottom). (a,b) Single-chain I-beams, as found in pyroxenes. (c) Double-chain I-beam, as in amphiboles. (d) Triple-chain I-beam. There are two distinct orientations for an I-beam, referred to as + and -, as shown in a and b. (After Veblen *et al.*, 1977.)

both double and triple chains occurring in regular alternation; one of them is isostructural with the triple-chain silicate of Drits *et al.* (1974). In this paper, the crystal structures and chemical properties of these nonclassical ordered pyriboles will be discussed, but the reader is referred to the earlier reports for other details.

Pyribole structures, unit cells, and symmetries

The crystal structures of pyribole minerals can be conveniently illustrated by using the I-beam representation (Thompson, 1970; Papike and Ross, 1970; Veblen *et al.*, 1977), in which the structures are viewed parallel to the direction of the silicate chains. As shown in Figure 4, each I-beam consists of a strip of octahedrally-coordinated cations sandwiched between two silicate chains. I-beams can be constructed with single chains (Fig. 4a,b), with double chains (Fig. 4c), with triple chains (Fig. 4d), or with chains wider than triple. I-beams may be oriented in two different ways with respect to the crystallographic axes, as shown for the single-chain I-beams in Figure 4a,b; these two orientations are commonly called + and -, as indicated.

Using the simplified representations of I-beams shown on the bottom of Figure 4, we can construct diagrams of the pyribole structures, Figure 5. These structures can be broken into two large groups based on the sequences in which I-beams in the + and - orientations are stacked. The four structures on the top of Figure 5 have the stacking sequence ...++--++--... in the *a* crystallographic direction; these structures are orthorhombic and are called *orthopyriboles*. The four structures

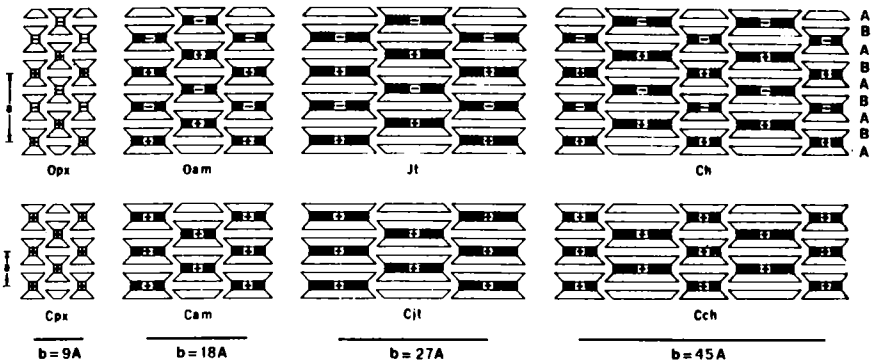

Figure 5. The orthopyriboles, top, all have the I-beam stacking sequence ++-- and a = 18A (Opx = orthopyroxene, Oam = orthoamphibole, Jt = jimthompsonite, Ch = chesterite). The clinopyriboles, bottom, have all of their I-beams oriented in the same way and a = 9A (Cpx = clinopyroxene, Cam = clinoamphibole, Cjt = clinojimthompsonite, Cch = monoclinic analog of chesterite). From left to right, the pyriboles are divided according to the widths of their silicate chains, which also determine the lengths of the b-axes, as shown: pyroxenes have single chains, amphiboles double chains, jimthompsonite triple chains, and chesterite alternating double and triple chains. (After Veblen *et al.*, 1977.)

on the bottom of Figure 5 have the stacking sequence ...++++++++... (which is equivalent to ...--------...); these structures are monoclinic and are called *clinopyriboles*. The ordered pyriboles are further divided according to the widths of the silicate chains. Thus, as shown in Figure 5, orthopyroxenes and clinopyroxenes have single chains, orthoamphiboles and clinoamphiboles have double chains, jimthompsonite and clinojimthompsonite have triple chains, and chesterite and its monoclinic analog have alternating double and triple chains.

The diagrams of Figure 5 can easily be related to the unit cell parameters of the various structures, as presented in Table 1. The c-axes of all pyriboles are parallel to the silicate chains; the length of c is determined by the chain periodicity and is about $5\frac{1}{4}$A for all of the structures. The a-axis is parallel to the stacking direction and is about 18A for orthopyriboles and about 9A for clinopyriboles, as shown in Table 1. Figure 5 and Table 1 also show that the lengths of the b-axes depend on the widths of the silicate chains and are approximate integral multiples of 9A: about 9A in pyroxenes, 18A in amphiboles, 27A in triple-chain pyriboles, and 45A in pyriboles with alternating

Table 1. Unit cell parameters and space groups of the major pyribole groups.

	Pyroxenes	Amphiboles	Triple-chain Silicates	Mixed-chain Silicates
Orthopyriboles (orthorhombic)	Enstatite	Anthophyllite	Jimthompsonite	Chesterite
Stacking sequence = ++--	Pbca ($Pbc2_1$) ***	Pnma	Pbca	$A2_1ma$
	a = 18.2A **	a = 18.6A	a = 18.6A	a = 18.6A
	b = 8.8	b = 18.1	b = 27.2	b = 45.3
	c = 5.2	c = 5.3	c = 5.3	c = 5.3
Clinopyriboles (monoclinic)	Diopside	Tremolite	Clinojimthompsonite and Drits synthetic	Unnamed mineral
Stacking sequence = ++++ or ----	C2/c ($P2_1/c$, P2/n, $P2^1$, C2)	I2/m * ($P2_1/m$, $P2/a$)	C2/c	A2/m
	a = 9.7A	a = 9.8A	a = 9.9A	a = 9.9A
	b = 8.9	b = 18.0	b = 27.2	b = 45.3
	c = 5.3	c = 5.3	c = 5.3	c = 5.3
	β = 105.6°	β = 104.7°	β = 109.5°	β = 109.7°
Protopyriboles (orthorhombic)	Protoenstatite	Protoamphibole	None reported	None reported
Stacking sequence = +-+-	Pbcn ($P2_1cn$)	Pnmn		
	a = 9.3A	a = 9.3A		
	b = 8.7	b = 17.9		
	c = 5.3	c = 5.3		

* The I-centered cell setting is analogous to the C-centered clinopyroxene cell (Thompson, 1978).

** Cell parameters in this table are from the following sources: Smith, 1969 (enstatite, protoenstatite); Clark et al., 1969 (diopside); Papike et al., 1969 (tremolite); Gibbs, 1969 (protoamphibole); Veblen and Burnham, 1978a (anthophyllite, jimthompsonite, clinojimthompsonite, chesterite, unnamed mineral).

*** Space groups in parentheses are subgroups of the space groups not in parentheses. The lower symmetry structures result from cation ordering or structural distortions of the maximum symmetry structures.

double and triple chains. Space group symmetries of the pyriboles also reflect both the stacking sequences and the chain widths (Veblen and Burnham, 1978b). For example, it can be seen in Table 1 that pyroxenes and triple-chain silicates, which have chains of odd width, have *c*-glide planes parallel to (010), while amphiboles, with chains of even width, have mirrors parallel to (010). Chesterite, which contains both double and triple chains, likewise contains both *c*-glides and mirrors. The cell parameters and space groups of all the ordered pyribole groups thus show many similarities that result from the structural similarities among them.

Crystal-chemical details of ordered nonclassical pyriboles

Most of what is known of the structural and chemical details of ordered pyriboles containing triple silicate chains is based on structure refinements and electron microprobe analyses of coexisting jimthompsonite, clinojimthompsonite, and chesterite from Chester, Vermont (Veblen and Burnham, 1978a,b). We will review briefly some of the details revealed by this work, comparing them with the details that are known from structure refinements of pyroxenes and amphiboles.

Polyhedral geometries. The polyhedral distortions found in ordered pyriboles with triple silicate chains are strikingly analogous to those encountered in pyroxenes and amphiboles; these similarities arise because analogous polyhedra in all of these structures reside in similar environments with respect to their neighboring coordination polyhedra.

To aid in discussion of the polyhedral distortions, three projections of the jimthompsonite structure and one of chesterite are shown in Figure 6. There are two symmetrically distinct triple silicate chains in the jimthompsonite structure, called the A- and B-chains; these are analogous to the A- and B-chains in orthopyroxenes (Cameron and Papike, 1980) and orthoamphiboles (Hawthorne, Chapter 1, this volume). In all these structures, the A-chains lie between (100) octahedral layers having opposite octahedral orientations (between + and -, or between - and +), while the B-chains lie between octahedral layers of like orientation (between + and +, and between - and -); the A- and B-chain layers are indicated in Figure 5. These triple chains each have three symmetrically distinct tetrahedra, which include two inner tetrahedra, Si1 and Si2,

Table 2. Ranges of O-Si-O angles in the inner and outermost tetrahedra of pyribole silicate chains.

	Inner Tetrahedra			Outermost Tetrahedra		
Structure	Polyhedron	O-Si-O Range	Difference	Polyhedron	O-Si-O Range	Difference
Jimthompsonite	Si1A	110.1-109.1°	1.0°	Si3A	117.0-100.7°	16.3°
	Si2A	111.6-108.1	3.5	Si3B	116.4-103.5	12.9
	Si1B	110.2-108.9	1.3			
	Si2B	112.0-108.4	3.6			
Clinojim-thompsonite	Si1	110.0-108.1	1.9	Si3	116.0-102.5	13.5
	Si2	111.6-107.5	4.1			
Chesterite	SiT1A	111.2-107.8	3.4	SiT3A	117.0-100.6	16.4
	SiT2A	111.3-107.7	3.6	SiT3B	117.2-103.4	13.8
	SiT1B	111.9-108.3	3.6	SiD2A	117.5-99.0	18.5
	SiT2B	113.3-107.1	6.2	SiD2B	116.4-103.7	12.7
	SiD1A	111.7-107.8	3.9			
	SiD1B	110.8-107.9	2.9			
Anthophyllite	T1A	110.8-108.4	2.4	T2A	116.7-100.1	16.6
	T1B	110.1-108.7	1.4	T2B	116.5-104.0	14.5
Cummingtonite	T1	110.5-108.6	1.9	T2	116.3-104.7	11.6
Orthoferrosilite				TA	116.7-101.0	15.7
				TB	116.6-105.4	11.1
Clinoferrosilite				TA	116.9-102.1	14.8
				TB	116.3-105.3	11.0
	Difference, Average Inner = 3.0°			Difference, Average Outermost = 14.2°		

Bond angles from Veblen and Burnham, 1978b; Finger, 1970; Ghose, 1961; Sueno et al., 1976; Burnham, 1967. All data refer to room temperature and pressure.

analogous to the inner tetrahedra (T1) of amphiboles and the tetrahedra of sheet silicates, and one outermost tetrahedron, Si3, which is analogous to the tetrahedron of a pyroxene chain or the outer tetrahedron (T2) of amphiboles. Using the range of tetrahedral O-Si-O angles as a simple measure of distortion, Table 2 shows that the outermost, pyroxene-like tetrahedra in all of these structures are rather distorted compared with the other, mica-like tetrahedra. These distortions arise primarily because the outermost tetrahedra share O···O edges, or nearly share edges, with the outermost M cation polyhedra of the octahedral strips of the structures (M5 in triple-chain silicates, M4 in amphiboles, and M2 in pyroxenes). Shortening of the shared edges and lengthening of other edges leads to more distorted tetrahedra.

Figure 6. The refined jimthompsonite and chesterite structures. (a) The almost unrotated A-chain and octahedral strip of jimthompsonite. (b) The more rotated B-chain of jimthompsonite. (c) Projection of jimthompsonite parallel to the silicate chains, showing the stacking of the I-beams. (d) Projection of chesterite parallel to the chains, showing how double and triple chains alternate parallel to *b*. The stacking sequence of octahedra is ++--, as in jimthompsonite. g_c = *c*-glide plane, g_b = *b*-glide, m = mirror. (After Veblen and Burnham, 1978b.)

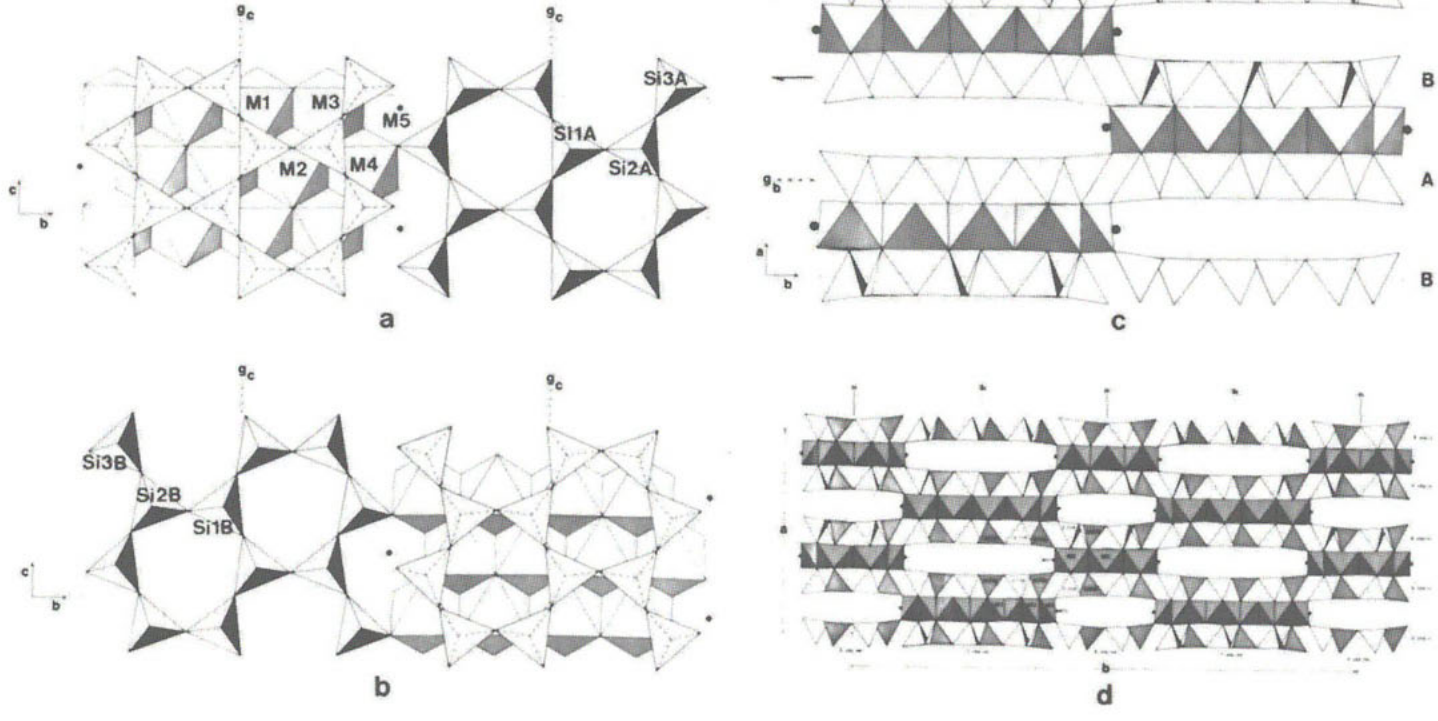

Table 3. Ranges of M-O distances in the inner and outermost polyhedra of pyribole octahedral strips.

Structure	Inner Octahedra			Outermost Octahedra		
	Polyhedron	M-O Range	Difference	Polyhedron	M-O Range	Difference
Jimthompsonite	M1	2.08-2.07A	0.01A	M5	2.80-2.00A	0.80A
	M2	2.10-2.07	0.03			
	M3	2.12-2.07	0.05			
	M4	2.15-2.03	0.12			
Clinojim-thompsonite	M1	2.08-2.06	0.02	M5	2.66-2.03	0.63
	M2	2.09-2.08	0.01			
	M3	2.10-2.07	0.03			
	M4	2.13-2.05	0.08			
Chesterite	MT1	2.12-2.02	0.10	MT5	2.82-2.04	0.78
	MT2	2.11-2.04	0.07	MD4	2.81-2.02	0.79
	MT3	2.16-2.05	0.11			
	MT4	2.16-2.00	0.16			
	MD3	2.10-2.04	0.06			
	MD1	2.16-2.03	0.13			
	MD2	2.12-2.06	0.06			
Anthophyllite	M3	2.08-2.06	0.02	M4	2.87-2.00	0.87
	M1	2.13-2.05	0.08			
	M2	2.14-2.01	0.13			
Cummingtonite	M3	2.10-2.07	0.03	M4	2.70-2.04	0.66
	M1	2.12-2.08	0.04			
	M2	2.13-2.03	0.10			
Orthoferrosilite	M1	2.20-2.09	0.11	M2	2.60-1.99	0.61
Clinoferrosilite	M1	2.20-2.08	0.12	M2	2.59-1.99	0.60
	Difference, Average Inner = 0.07A			Difference, Average Outermost = 0.72A		

Bond distances from Veblen and Burnham, 1978b; Finger, 1970; Ghose, 1961, as calculated by Papike et al., 1969; Sueno et al., 1976; Burnham, 1967. All data refer to room temperature and pressure.

Similarly, as can be seen in Figure 6, triple-chain structures contain wide strips of cation polyhedra. The coordination polyhedron of the outermost cation of the strip (M5) is quite distorted and is not even drawn in as a polyhedron in Figure 6. The inner polyhedra (M1, M2, M3, M4) are, however, much more regular octahedra. The distorted outermost polyhedra are analogous to the distorted outermost sites of amphiboles (M4) and pyroxenes (M2) (Hawthorne, Chapter 1, this volume; Cameron and Papike, 1980). Likewise, the regular inner octahedra of triple-chain pyriboles are analogous to the regular octahedra of amphiboles (M3, M1, M2) and pyroxenes (M1). The similarities in the degree of distortion

found in the M polyhedra of triple-chain pyriboles, amphiboles, and pyroxenes are shown in Table 3, which uses the largest difference in M-O distances within an octahedron as a simple measure of octahedral distortion. By this measure, the inner octahedra of all pyriboles are relatively regular; for those given in the table, the average range of M-O distances is only 0.07 A. For the distorted, outermost sites, however, the distance difference between the closest and farthest of the six nearest oxygens averages 0.72 A, indicating very distorted coordination.

As mentioned earlier, the striking similarities between octahedral distortions in all of the pyribole groups results because analogous polyhedra have very similar environments with respect to their nearest neighboring polyhedra. It is this local control of polyhedral geometry that permits the polysomatic M and P model of pyribole structures to predict not only ideal structures, but also to predict with some accuracy the distortions found in amphiboles and wide-chain pyriboles.

In addition to the tetrahedral and octahedral cation polyhedra, wide-chain pyriboles also possess A-sites, analogous to the A-sites of amphiboles (Hawthorne, Chapter 1, this volume) and the interlayer sites of micas and talc. As in the amphiboles, the precise geometries of the A-sites depend on the rotations of tetrahedra in the chains and the displacement parallel to c between six-membered tetrahedral rings in the two chains that coordinate the A-site. Unlike the A-sites of most amphiboles, however, those of triple-chain pyriboles do not have mirror symmetry. Difference Fourier syntheses of the A-sites of jimthompsonite and chesterite suggest the presence of small amounts of electron density, presumably from partial occupancy by sodium. As in some amphiboles, the sites appear to be split, but in a less symmetrical way than in amphibole (Veblen and Burnham, 1978b).

The geometries of coordination polyhedra in wide-chain pyriboles clearly bear very close resemblances to those found in pyroxenes, amphiboles, and micas. In addition to these similarities, there are also close analogies in the ways that the polyhedra, particularly the tetrahedra, are rotated in the different pyribole groups. These polyhedral rotations have been discussed in detail by several authors. It is not the intent of this paper to review them, but the reader is referred to Cameron and Papike

(1980), Veblen and Burnham (1978b), Sueno *et al.* (1976), Papike *et al.* (1973), Papike and Ross (1970), and Thompson (1970).

Structural control of chemistry. The stoichiometries of all biopyriboles are easily understood by noting that the stoichiometry of a P slab can be represented as $M_4T_4O_{12}$, while that of an M slab is $AM_3T_4O_{10}(OH)_2$, where A = A-site, M = octahedral sites, T = tetrahedral sites. It is very easy to find the structural formula for any pyribole, whether structurally ordered or disordered, simply by noting the number of M and P slabs in the structure and adding up the M and P formulas in the appropriate ratio. Thus, amphibole (MP) is

$$M_4T_4O_{12} + AM_3T_4O_{10}(OH)_2 = AM_7T_8O_{22}(OH)_2 .$$

Similarly, triple-chain silicate (MMP) is

$$M_4T_4O_{12} + 2AM_3T_4O_{10}(OH)_2 = AM_{10}T_{12}O_{32}(OH)_4$$

and so on. This method can be elaborated to include ratios of distorted and regular M sites, outermost and inner tetrahedral sites, etc.

Specific compositions can be derived by substituting appropriate cations for the A's, M's, and T's in the general formulas for the M and P slabs. Thus, a pure Mg jimthompsonite, $Mg_{10}Si_{12}O_{32}(OH)_4$, consists of an enstatite P slab, $Mg_4Si_4O_{12}$, and two talc M slabs, $Mg_3Si_4O_{10}(OH)_2$. However, the chemistry of the slabs becomes more complicated for the synthetic sodium triple-chain silicates. The composition of Drits *et al.* (1974), $Na_2^MMg_8[Si_{12}O_{30}(OH)_2](OH)_4$, can be made from a "hydropyroxene" P slab, $Na_2^MMg_2[Si_4O_{10}(OH)_2]$, in which part of the tetrahedral oxygen is replaced by hydroxyl, and two talc M slabs having the same composition and structure as those in clinojimthompsonite.

The triple-chain silicate of Tateyama *et al.* (1978) represents yet another case in which the M and P slabs are not electrostatically neutral. Their composition $Na_2^ANa_2^MMg_8[Si_{12}O_{32}](OH)_4$ can be assembled from one doubly-charged P unit, $\{Na_2^MMg_2[Si_4O_{12}]\}^{2-}$ and two singly-charged M slabs, $\{Na_1^AMg_3[Si_4O_{10}](OH)_2\}^{1+}$. It is interesting that an analogous amphibole, in which there are equal numbers of M and P slabs, cannot be made from these slabs, because it would not be charge balanced. As shown by Thompson (1978), it is, however, possible to combine M slabs of this composition with singly-charged P slabs, $\{Na_1^MCa_1Mg_2[Si_4O_{12}]\}^{1-}$, resulting

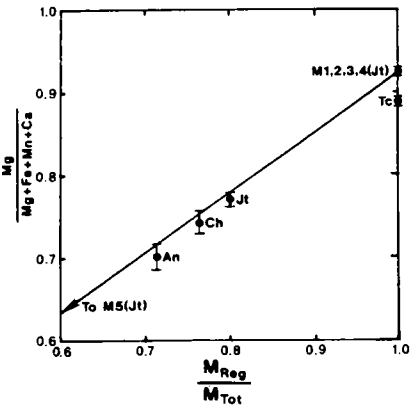

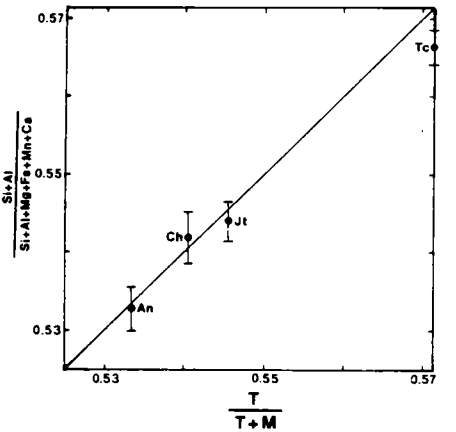

Figure 7 (left). The Mg/(Mg+Fe+Mn+Ca) ratios from electron microprobe analyses, plotted against the ratios of regular octahedral M sites to total M sites for coexisting anthophyllite, chesterite, jimthompsonite, and talc from Chester, Vermont. Error bars represent 1σ calculated from 17, 14, 14, and 5 analysis points for An, Ch, Jt, and Tc, respectively; analyses are from single crystals used for x-ray studies. The correlation between Mg content and number of regular M sites results because Mg partitions strongly into the regular M sites, while Fe partitions into the distorted sites, just as in MgFe pyroxenes and amphiboles (only minor Mn and Ca are present). The line in this diagram connects the refined occupancies of distorted (M5) and regular octahedral (M1, M2, M3, M4) sites in jimthompsonite; refined occupancies are thus in accord with the analytical data for jimthompsonite. (Data from Veblen and Burnham, 1978a,b.)

Figure 8 (right). Analyzed (Si+Al)/(Si+Al+Mg+Fe+Mn+Ca) plotted against the ratio of tetrahedral sites to tetrahedral plus M sites for anthophyllite, chesterite, jimthompsonite, and talc. Error bars are described in the caption of Figure 7. The analytical results are consistent with the stoichiometries. The overlapping analytical results also demonstrate the difficulty inherent in attempting to identify chesterite and jimthompsonite from microprobe data alone. (Data from Veblen and Burnham, 1978a.)

in richterite, $Na^{A}_{1}Na^{M}_{1}Ca_{1}Mg_{5}[Si_{8}O_{22}](OH)_{2}$. Thompson suggested that amphiboles of this sort might be less stable than some other compositions, because charge compensation is not purely local. In the triple-chain composition of Tateyama *et al.* (1978), however, the charge balancing takes place over an even longer range than in amphiboles consisting of charged M and P slabs.

The geometries and charge balance characteristics of the various polyhedra in wide-chain pyriboles can be expected to influence cation partitioning trends in much the same way as these factors affect the chemistry of pyroxenes and amphiboles. Thus, the distorted, outermost octahedral sites (M5) in triple-chain silicates should behave much as M2 of pyroxenes and M4 of amphiboles, accepting cations such as Na, Ca, Fe, Mn, and Mg. Likewise, the inner, regular octahedral sites should act like M1 of pyroxenes and M1, M2, and M3 of amphiboles; cations such as Mg, Al, and Fe should be able to reside in these regular octahedra. (For discussions of cation occupancies in pyroxenes and amphiboles see Cameron and Papike, 1980, and Hawthorne, Chapter 1, this volume.)

The only direct evidence on cation partitioning in wide-chain pyriboles is from the occupancy refinements of Veblen and Burnham (1978b) on jimthompsonite, clinojimthompsonite, and chesterite. As in low-calcium pyroxenes and amphiboles, these wide-chain silicates exhibit a marked preference for Fe in the distorted M sites and a preference for Mg in the regular octahedral sites. Microprobe analyses of coexisting anthophyllite, jimthompsonite, clinojimthompsonite, and chesterite support the results of the occupancy refinements. If Fe is, in fact, partitioned equally into the distorted sites of all these structures, then the Fe/Mg ratios should be correlated with the ratio of distorted to regular M sites. This is, in fact, the case, as shown in Figure 7. This analytical data is also consistent with the theoretical stoichiometry of these minerals, as shown in Figure 8. Thus, the ratios of tetrahedral cations to all cations also agree with the refined structures.

Electron microscopic observations of ordered wide-chain biopyriboles

Ordered wide-chain pyriboles have been observed in several high-resolution transmission electron microscopy (HRTEM) studies. These observations can be separated into those involving structure types already known from single-crystal x-ray studies and those involving ordered structures that have not been observed by other means.

Known structure types observed with HRTEM. Both the a-axis and c-axis have been used as viewing directions for observations of pyribole chain width in the TEM. Figures 9 and 10 illustrate the appearances of the anthophyllite, jimthompsonite, and chesterite structures in these two orientations, for the imaging conditions utilized by Veblen *et al.* (1977) and Veblen and Buseck (1979a). Clinopyriboles produce images similar to those of these orthopyriboles when viewed parallel to c, but a-axis images of clinopyriboles differ somewhat from those of Figure 9, because the stacking sequences parallel to a are different; experimental images of structurally ordered clinoamphibole have been shown by Buseck and Iijima (1974), and Mallinson *et al.* (1980) have calculated the image contrast expected for monoclinic amphibole and triple-chain silicates.

Specimens of the new ordered pyriboles from the type locality at Chester, Vermont, have been studied extensively with HRTEM. These investigations in part served to confirm that extensive areas of amphibole,

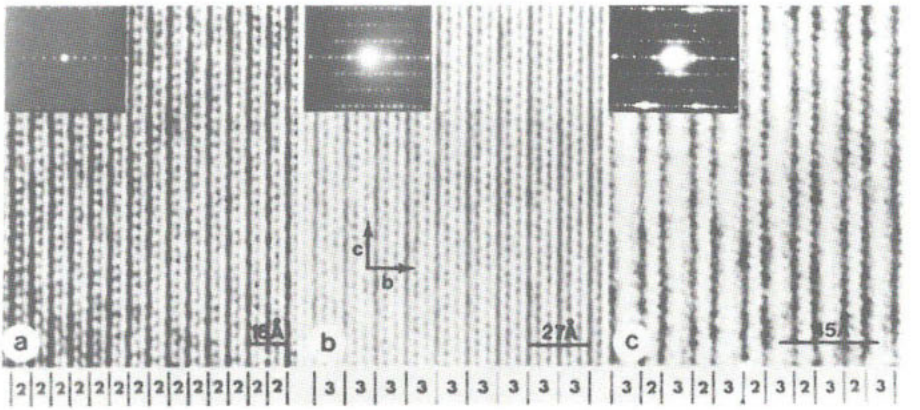

Figure 9. *a*-axis HRTEM images and electron diffraction patterns of anthophyllite, jimthompsonite, and chesterite. The positions and widths of the silicate chains are indicated. (After Veblen *et al.*, 1977.)

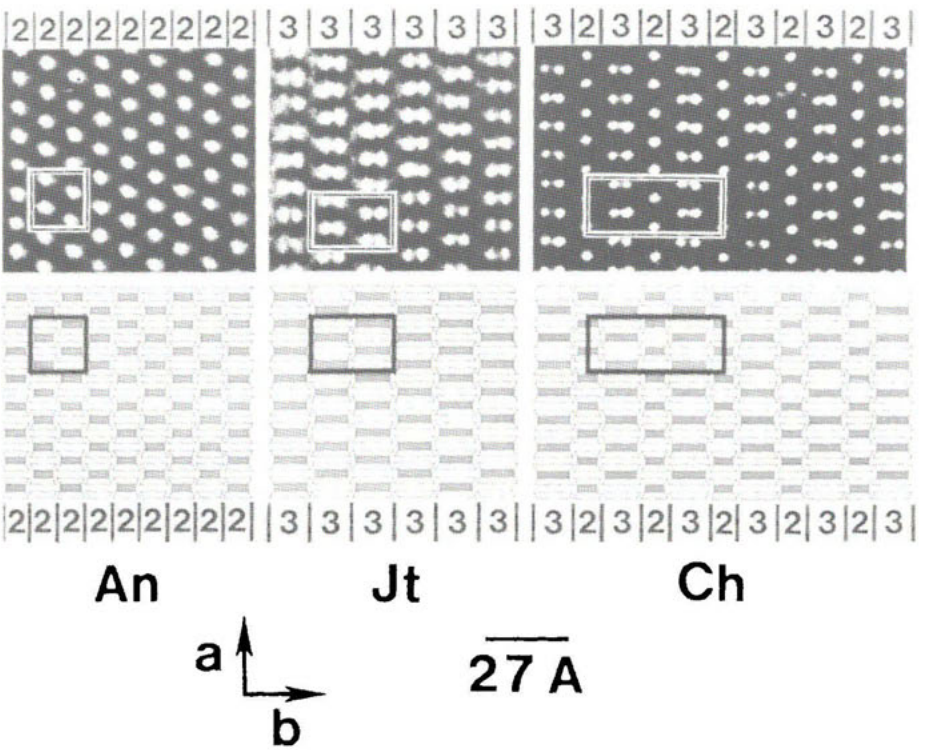

Figure 10. *a*-axis HRTEM images of anthophyllite, jimthompsonite, and chesterite. The widths of the silicate chains are indicated, as are the unit cells and correspondence between experimental images and I-beam representations. (After Veblen and Buseck, 1979a.)

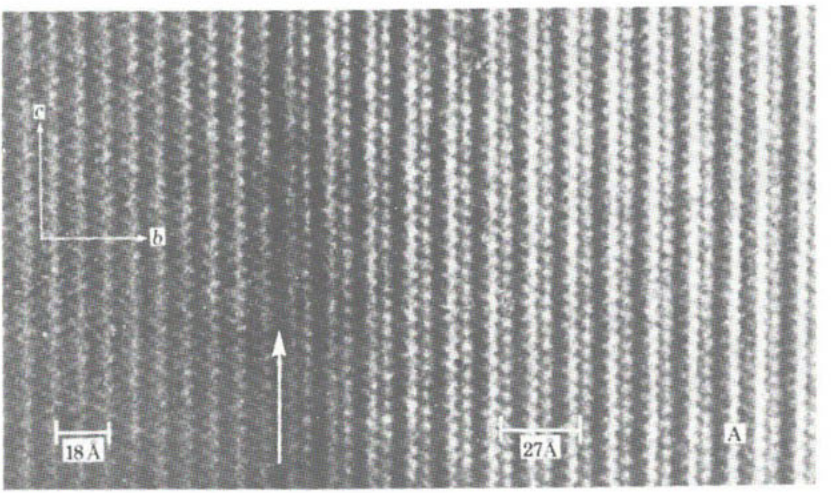

Figure 11. Ordered triple-chain silicate in a nephrite. An uninterrupted sequence of 11 triple chains occurs between the vertical arrow, an amphibole-triple chain interface, and the symbol "A." (After Mallinson *et al.*, 1980.)

triple-chain pyribole, and pyribole with alternating double and triple chains do, in fact, exist in a perfectly ordered state.

Of greater interest are observations of ordered wide-chain pyriboles in materials previously not known to contain them. Jefferson *et al.* (1978) and Mallinson *et al.* (1980) have shown domains consisting of as many as 11 uninterrupted triple chains existing in nephrite (actinolite) jade (Fig. 11). Although chemical analysis of this triple-chain structure has not yet been possible, it is likely that this material will prove to be the triple-chain analog of the calcic pyriboles diopside and tremolite, with the chemical composition $Ca_2(Mg,Fe)_8Si_{12}O_{32}(OH)_4$. This silicate could be assembled with P slabs of diopside composition and M slabs of talc composition (Thompson, 1978) and would be isostructural with clinojimthompsonite, although with a larger M5 site to accommodate the Ca atom.

Other reports of triple-chain silicate include that of Nissen *et al.* (1979), who found small domains of jimthompsonite in disordered materials intermediate in composition between anthophyllite and jimthompsonite; this specimen was from a hydrothermally altered olivine-bearing ultramafic rock. Nakajima and Ribbe (1980) found relatively large regions of clinojimthompsonite structure in altered augite (see Fig. 17 in the section "Chain-width disorder in pyroxenes"), as did Veblen and Buseck (1981) as noted in Buseck *et al.* (1980). As is the case with triple-chain silicate in

nephrites, the M cation chemistry of these materials is unknown; they could be clinojimthompsonite in the strict sense, since the final alteration products appear to contain talc, or they could be the triple-chain analogs of the calcic pyriboles diopside and tremolite, or augite and hornblende. In the future, microanalysis in the TEM should resolve these chemical questions.

In addition to naturally-occurring triple-chain silicates, another occurrence of chesterite has recently been reported. In a study of anthophyllite asbestos from Paakila, Finland, Cressey *et al.* (1981) found relatively abundant lamellae of chesterite; most of these lamellae are less than 10 unit cells wide, and the widest is 25 unit cells wide.

New pyribole structure types discovered with HRTEM. In the HRTEM studies of specimens from Chester, Vermont, several new ordered pyribole structures were discovered (Veblen and Buseck, 1979a). Like the macroscopically occurring chesterite structure, these materials contain silicate chains of two or three different chain widths, which are arranged in an ordered sequence. A test was utilized to separate statistically significant ordered mixed-chain structures from those that have a high probability of occurring simply by the random combination of chains of different widths. The sequences of double (2), triple (3), and quadruple (4) silicate chains found in a primitive unit cell of these new structures are (2233), (233), (232233), (222333), (2332323), (2333), (433323), (2234), and (43332343332423). HRTEM images of two of these structures are shown in Figure 12.

The complexity and stoichiometric coincidences of some of these structures suggest that they are probably not thermodynamically stable. Furthermore, some of the geometrical aspects of their occurrence suggest that they did not form by a simple spiral growth mechanism around a screw dislocation (see Verma and Kirshna, 1966, for a discussion of spiral growth). Therefore, Veblen and Buseck were unable to explain satisfactorily why these rare ordered mixed-chain structures occur, and the question of a mechanism for their formation remains open. In contrast, the mixed-chain silicate chesterite occurs abundantly enough to suggest that it represents a minimum in free energy compared to other configurations for the same chemical composition (Veblen and Buseck, 1979a, Fig. 8).

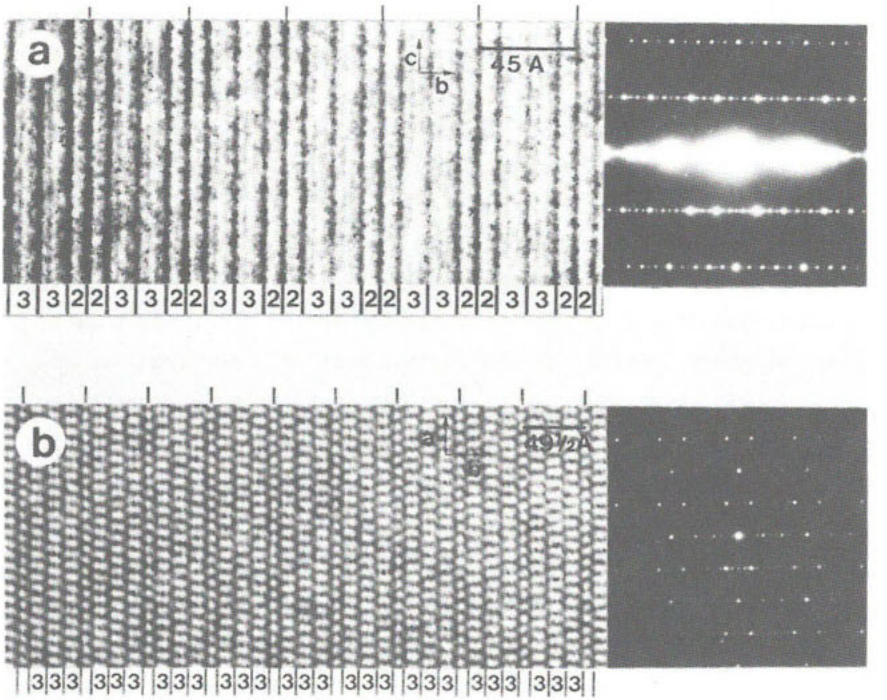

Figure 12. HRTEM images and electron diffraction patterns of rare, large-unit-cell ordered pyriboles from Chester, Vermont. (a) *a*-axis image of a structure with the chain sequence (2233). (b) *c*-axis image of a structure with the chain sequence (2333). (Veblen and Buseck, 1979a.)

CHAIN-WIDTH DISORDER IN PYRIBOLES

Up to this point, we have discussed only structurally ordered pyriboles, those that contain silicate chains of only one width or that contain chains of more than one width that are arranged in a regularly repeating sequence. In this section, we turn to pyribole crystals that are structurally disordered, in that they contain chains of mixed widths that are arranged in sequences that are *not* perfectly periodic. Because it involves a lack of order in the widths of the silicate chains, this type of disorder has been referred to as "chain-width disorder."

Chain-width disorder in amphiboles

Amphibole asbestos. The first report of chain-width defects in chain silicates was that of Chisholm (1973), who examined a number of

different amphibole asbestos specimens with electron diffraction and conventional TEM techniques. Chisholm noted that electron diffraction patterns were streaked parallel to a^* and b^* in three specimens of amosite (grunerite asbestos) and three specimens of crocidolite (riebeckite asbestos). The a^* streaking was attributed to stacking disorder, and the b^* streaking was attributed to the intercalation of pyroxene chains or silicate chains with widths wider than double, parallel to (010). In addition, planar defects were imaged parallel to (010) with conventional TEM methods.

Chisholm's results were confirmed and elaborated in a HRTEM study by Hutchison *et al.* (1975), and since this time most studies of chain-width disorder have relied on high-resolution methods. Hutchison *et al.* observed planar defects parallel to (010) in amosite, tremolite asbestos, and anthophyllite asbestos, and they argued that their images showed that these defects consisted of triple-chain structure in the host double-chain amphibole. More recent calculations of image contrast (Jefferson *et al.*, 1978; Veblen and Buseck, 1979a; Mallinson *et al.*, 1980) support this interpretation. More recent observations of triple-chain defects in asbestiform amphiboles include those of Chisholm (1975), Veblen *et al.* (1977), Alario Franco *et al.* (1977), Veblen and Buseck (1979a, 1980), Veblen (1980), Dorling and Zussman (1980), Whittaker *et al.* (1981), and Cressey *et al.* (1981).

Although the intercalation of triple-chain structure is the most common type of chain-width disorder in amphibole asbestos, chains of other widths have also been reported. Quadruple, quintuple, sectuple, and wider chains have been reported in the fibrous portions of anthophyllite from Chester, Vermont (Veblen *et al.*, 1977; Veblen and Buseck, 1979a). The widest chains observed in this material have widths greater than 300. Since very wide chains essentially have the talc structure, there is a semantic problem in whether to refer to such wide structures as chains or sheets; the existence of material with extremely wide chains demonstrates that there is a continuum of structures from the chain silicates to the sheet silicates. Figure 13 shows chains of several widths intergrown in anthophyllite. Chains wider than triple have also been reported in good-quality anthophyllite asbestos and amosite (Cressey *et al.*, 1981; Veblen, 1980) and in tremolite-actinolite asbestos (Dorling and Zussman, 1980).

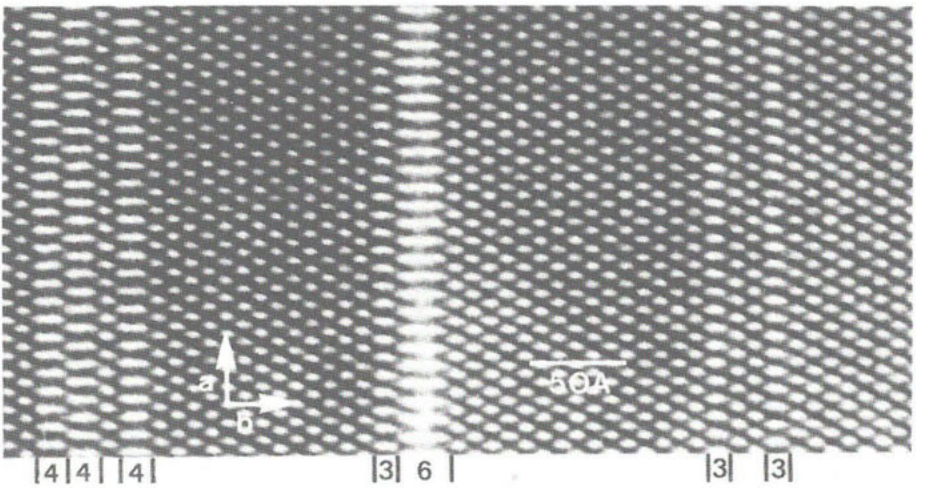

Figure 13. *c*-axis HRTEM image of anthophyllite from Chester, Vermont, containing triple, quadruple, and sextuple chain-width errors. Double-chain material is not labelled.

Nephrite (actinolite jade). The microstructures of nephrite have been extensively investigated with HRTEM techniques (Hutchison *et al.*, 1976; Jefferson *et al.*, 1978; Mallinson *et al.*, 1977; Mallinson, 1980; Dorling and Zussman, 1980). Much of this work has recently been summarized by Mallinson *et al.* (1980). In many respects, the microstructures found in nephrite are identical to those that occur in amphibole asbestos. There is generally at least some amount of chain-width disorder, with single, triple, quadruple, quintuple, and sextuple chains having been observed, and in some cases, the degree of disorder can be quite extreme. A variety of defects in which silicate chains of a given width transform along their lengths to chains of different width have been observed in nephrite (Mallinson *et al.*, 1980); such chain-terminating microstructures are discussed in the section on "Chain terminations."

Acicular and massive amphiboles. It has been noted by a number of workers that acicular or massive amphiboles typically possess far less chain width disorder than asbestiform amphiboles and nephrite (Chisholm, 1975, Veblen *et al.*, 1977; Veblen, 1980; Cressey *et al.*, 1981). Other electron microscopic studies of non-fibrous amphiboles in which chain-width disorder was not studied specifically (for example, Ghose *et al.*, 1974; Gittos *et al.*, 1976) further support this general conclusion, since extensive chain-width disorder probably would have been recognized had it

been present. Known exceptions to this correlation between acicular or massive habit and paucity of chain-width defects occur in anthophyllites and cummingtonites, in which substantial numbers of chain-width errors have been reported in a few specimens (Champness *et al.*, 1976; Veblen and Buseck, 1979b; Veblen, 1980; Cressey *et al.*, 1981). It is not known specifically what chemical and physical factors promote significant chain-width disorder in some acicular amphiboles, but it is likely that wider silicate chains tend to form during growth at relatively low temperatures, and HRTEM work with synthetic anthophyllites and ferroanthophyllites of various compositions has shown that the number of wide-chain defects in this system decreases with increasing Fe content (Veblen, 1982). Chain-width errors in acicular amphiboles can also form by alteration, as shown by the acicular portions of anthophyllite from Chester, Vermont (Veblen *et al.*, 1977).

Chain-width disorder in wide-chain pyriboles

Just as amphiboles exhibit a range of chain-width disorder phenomena, the wide-chain pyriboles jimthompsonite and chesterite and their monoclinic polymorphs can also occur in states ranging from perfect structural order to substantial disorder. The chain-width order and disorder phenomena in these minerals and in the anthophyllite that occurs with them has been detailed by Veblen *et al.* (1977) and Veblen and Buseck (1979a). Jimthompsonite and chesterite from Chester, Vermont, contain perfectly ordered regions up to at least a few tens of microns wide (in the *b* crystallographic direction). Some of the jimthompsonite contains scattered double-chain errors, as well as lamellae of chain width greater than triple (Fig. 14). Likewise, chesterite can contain isolated errors in the alternating sequence of double and triple chains; the most abundant chain width defects in chesterite, however, are coupled errors that preserve the chesterite stoichiometry. Three mistakes of this sort are shown in Figure 15.

In some regions of pyribole from Chester, there is extreme disorder, and it is not possible to apply a mineral name; material like this has been called "disordered pyribole." Figure 16 shows a small area from such a disordered region, in which double, triple, quadruple, and septuple chains occur together; another example is given by Zoltai, Figure 8,

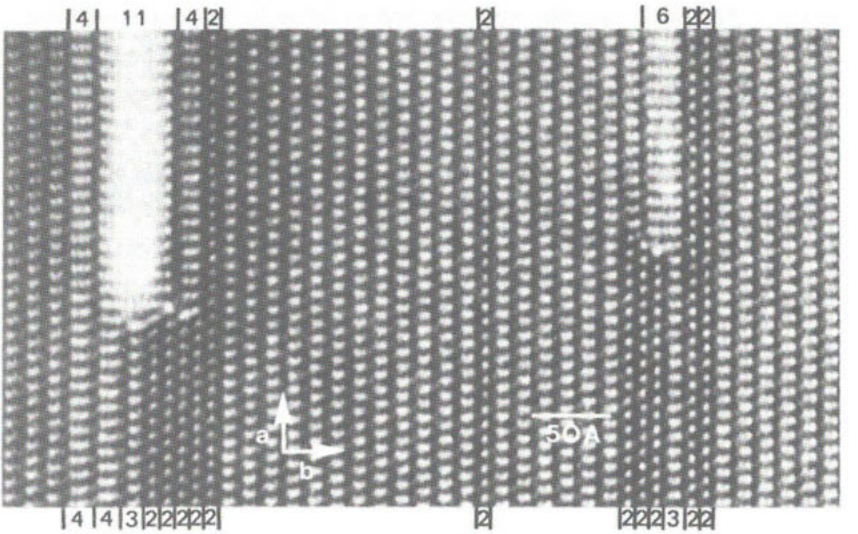

Figure 14. Chain-width errors in jimthompsonite from Chester, Vermont. Errors with chain widths of 2, 4, 6, and 11 are shown, with some of the errors terminating. Triple chains are not labeled. The slab of material with chain width 11 has become partially amorphous from rapid electron damage in the TEM, a characteristic of talc and wide-chain silicate.

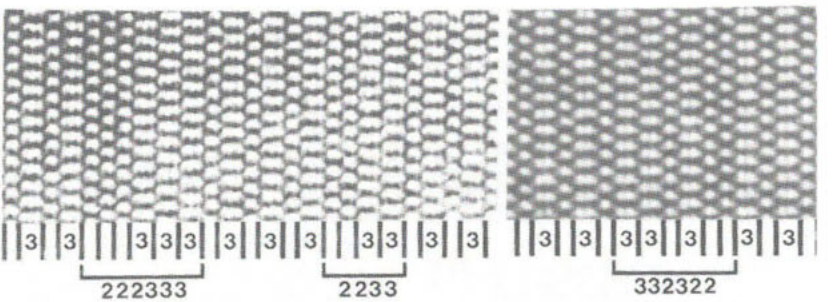

Figure 15. Chain width defects in chesterite that preserve the chesterite stoichiometry. Defects with chain sequences 222333, 2233, and 332322 are shown. (After Veblen and Buseck, 1979a.)

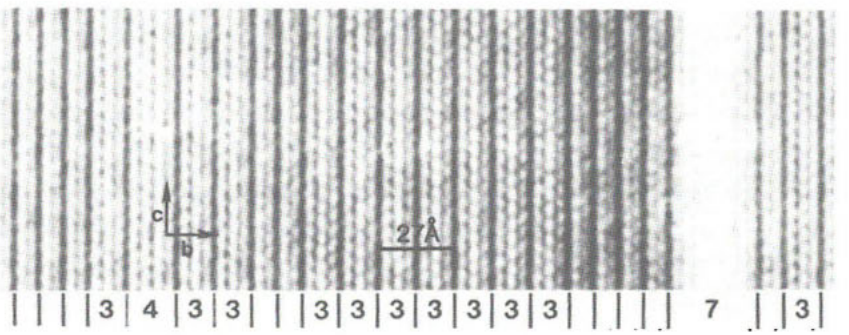

Figure 16. Disordered pyribole from Chester, Vermont, containing double, triple, quadruple, and septuple silicate chains. Double chains are not labeled. (After Veblen *et al.*, 1977.)

this volume. Nissen *et al.* (1979) have also reported low-calcium pyribole with extremely disordered chain widths in metamorphosed ultramafic rocks from the Alps. The stoichiometry of disordered regions generally does not conform to that of any of the known ordered pyriboles. In disordered material that does not contain pyroxene chains, the stoichiometry (as determined using the method described in the section "Structural control of chemistry") has been observed to vary from compositions near that of amphibole to compositions approaching that of talc. The latter regions consist of disordered mixtures of very wide chains.

Chain-width disorder in pyroxenes

The chain-width disorder that occurs in pyroxenes has recently been summarized by Buseck *et al.* (1980) in Volume 7 of this series, PYROXENES, (pages 187-194) and is discussed in more detail by Veblen and Buseck (1981); therefore, only a brief description of the observed phenomena will be presented here.

Most, if not all, observations of double and wider chains intergrown with pyroxene structure are consistent with mechanisms of formation for the hydrous pyribole involving alteration (hydration reaction), although it has also been proposed that narrow lamellae of amphibole in clinopyroxenes may form by exsolution (Smith, 1977; Yamaguchi *et al.*, 1978). The structural mechanisms of reactions that produce hydrous pyriboles in pyroxenes are discussed briefly in the section "Polysomatic reactions in pyriboles."

Lamellae of amphibole as narrow as one double chain have been observed with HRTEM, but such narrow lamellae typically contain an even number of amphibole chains, as a result of their growth mechanism. Blobs and rods of amphibole have likewise been reported. Lamellae of triple-chain pyribole have also been observed in pyroxenes, typically as narrow as one triple silicate chain. Larger regions of triple-chain pyribole have been observed in some cases. Figure 17, from Nakajima and Ribbe (1980), is an excellent example of the complex microstructures that can arise by the replacement of pyroxene. On the left of this figure, narrow lamellae of amphibole and triple-chain pyribole are intergrown with pyroxene. On the right are large areas of ordered and disordered clinojimthompsonite, as well as wider-chain silicate having

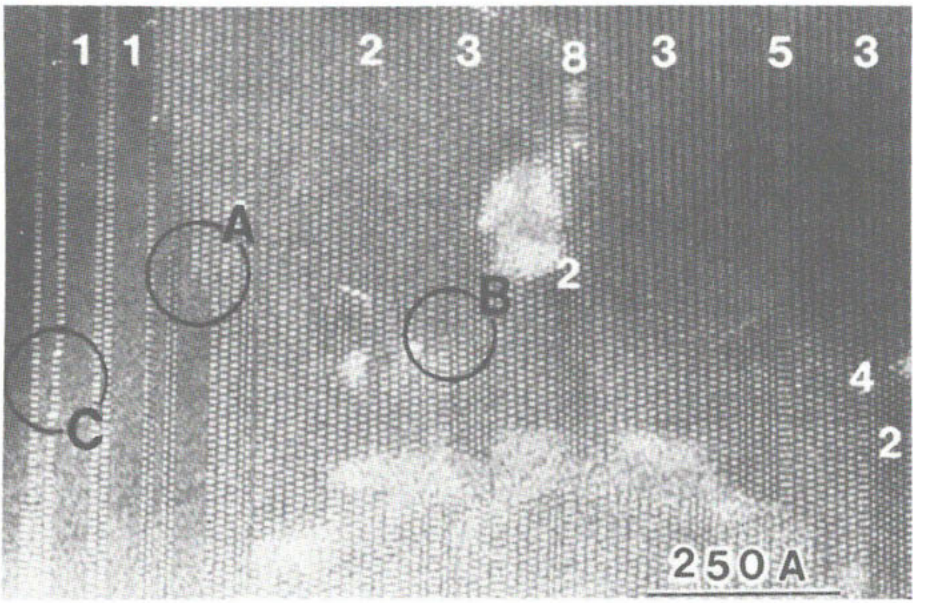

Figure 17. Altered augite that has largely been converted to clinojimthompsonite. Remnant pyroxene on the left contains narrow lamellae of amphibole and triple-chain material, and the clinojimthompsonite contains chain-width errors with widths 2, 4, 5, and 8. See Nakajima and Ribbe (1980) for further explanation of this complex microstructure. (After Nakajima and Ribbe, 1980.)

chain widths of 4, 5, and 8. Figure 17 also shows very clearly a variety of terminations of (010) lamellae having various chain widths. Such terminations will be considered in the next section.

TERMINATION DEFECTS

Chain terminations

A chain termination is a defect in which one or more silicate chains terminate completely or turn into silicate chains of a different width. Two types of chain terminations were recognized by Veblen *et al.* (1977). First, chains can terminate at low-angle grain boundaries, as shown in Figure 18. The crystal structure at such boundaries may be largely incoherent. In the case shown, double, triple, and quadruple chains all terminate along the defect, which was probably formed during natural deformation of the crystal. A second type of chain termination involves the cooperative termination of the chains in two or more (010) lamellae. Such terminations occur not only in low-calcium pyriboles, as shown in

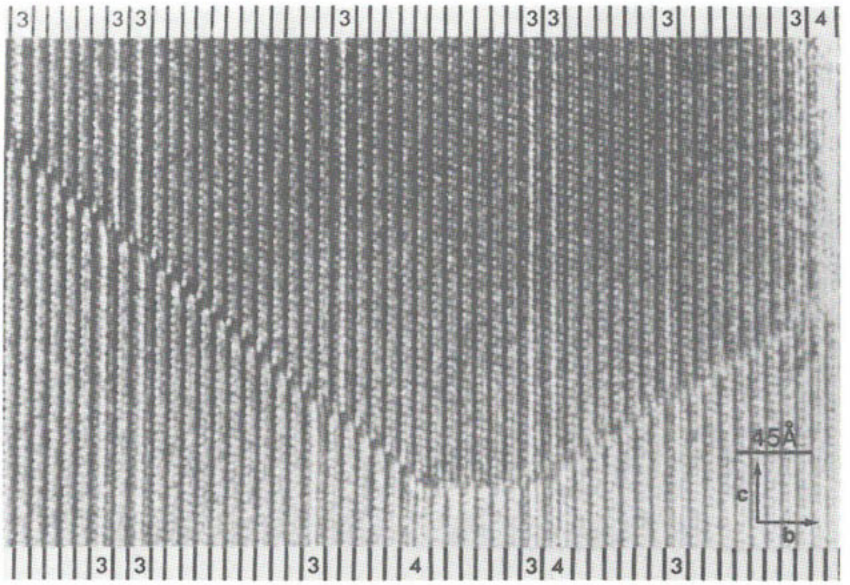

Figure 18. A low-angle grain boundary in disordered anthophyllite from Chester, Vermont, at which double, triple, and quadruple chains terminate. The rotation at the boundary of about 1° can be observed by viewing the figure at a low angle parallel to *c*. (After Veblen *et al.*, 1977.)

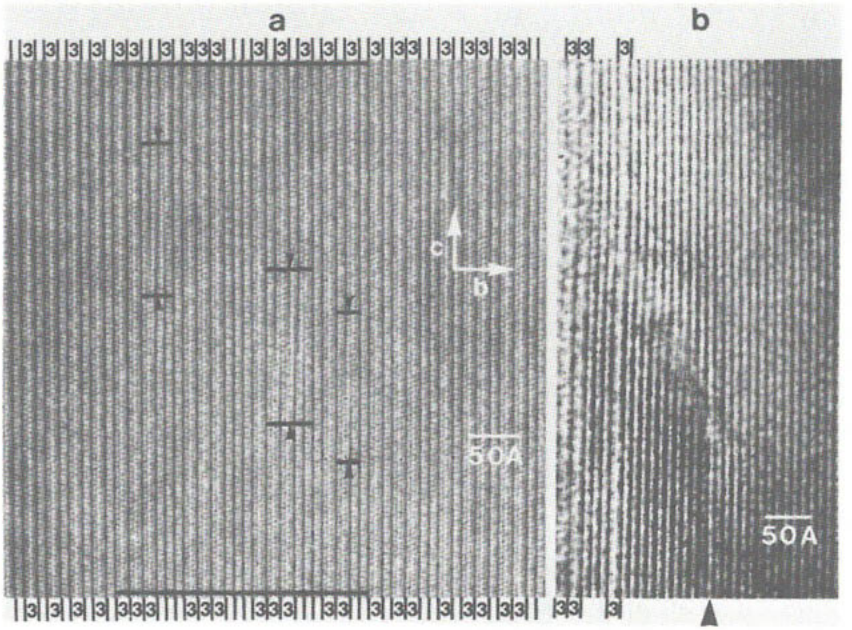

Figure 19. (a) Cooperative chain terminations, best viewed at a low angle parallel to *c*. From left to right, the three terminations involve changing the chain sequence 322 to 223, 3322 to 2323, and 32 to 23. (b) Termination of a double chain (arrowed) by a dislocation mechanism, best seen by viewing at a low angle parallel to *c*. The structure is distorted in the region of the termination. (After Veblen and Buseck, 1980.)

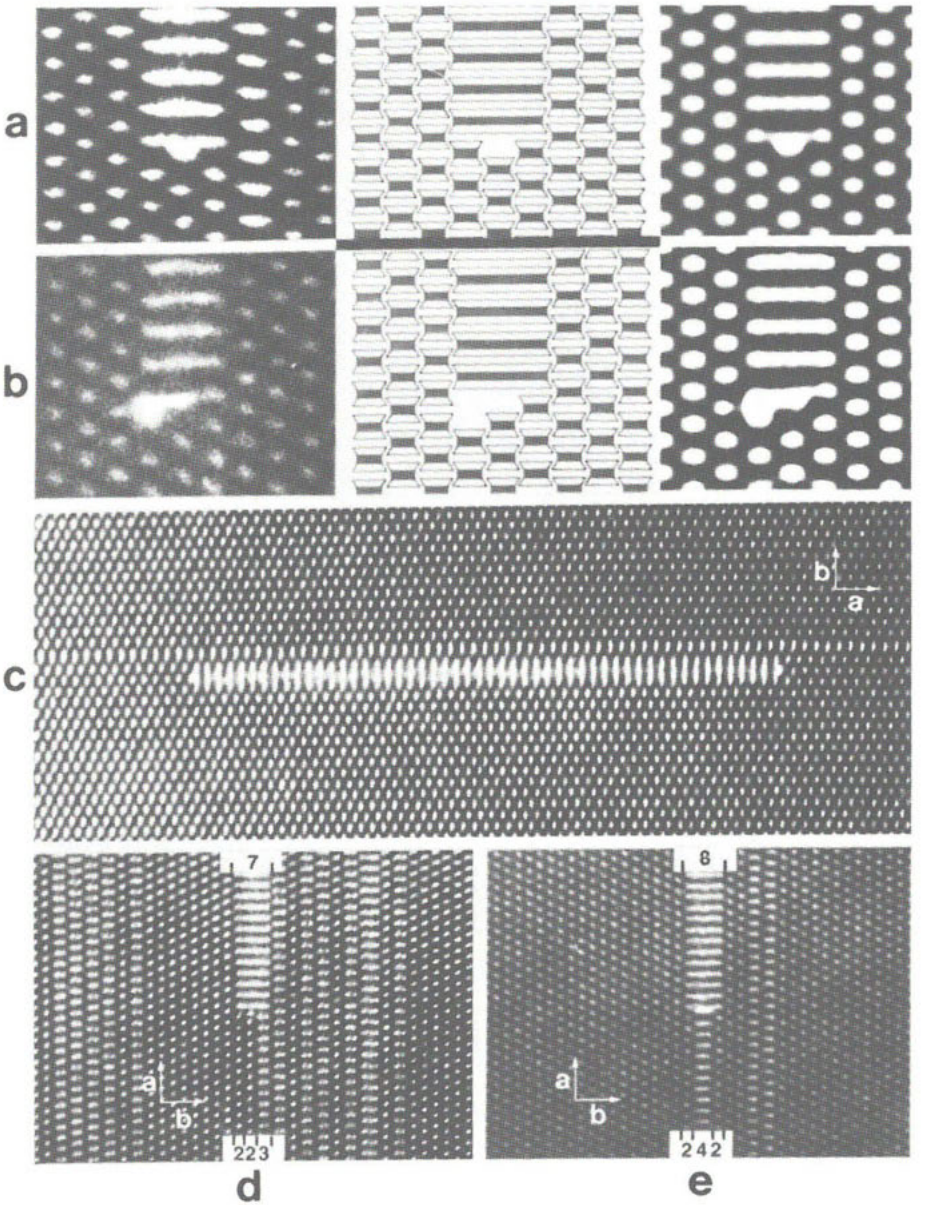

Figure 20. Simple coherent zipper terminations in pyribole from Chester, Vermont. (a,b) Two different termination types for sextuple-chain zippers in anthophyllite. From left to right are experimental HRTEM images, structural models of the terminations, and images calculated from the models to support the interpretation of the HRTEM results. The triple-chain slab immediately to the right of the sextuple zipper in *a* is ignored in the model. (c) A doubly-terminated sextuple-chain zipper. (d,e) The terminations of septuple and octuple zippers. (After Veblen and Buseck, 1980.)

Figure 19a, but have also been extensively studied in nephrites (Jefferson *et al.*, 1978; Mallinson *et al.*, 1980; Mallinson, 1980). An example of a cooperative chain termination in nephrite is shown in Figure 10 of Zoltai (this volume), where a slab of material containing a single and a triple chain separated by four amphibole chains turns into a slab of normal amphibole structure six chains wide. A schematic interpretation of the terminations is included in that figure.

A third, noncooperative type of chain termination has also been recognized but appears to be rare. This type involves the termination of a (010) slab at a dislocation, combined with structural readjustment parallel to a^*. An example of a double-chain termination is shown in Figure 19b.

Zipper terminations

In some cases, (010) slabs having a given chain width or combination of chain widths terminate along lines parallel to the c-axis. Such terminations do not cut across any of the silicate chains and hence are not chain terminations. When viewed down the c-axis in HRTEM images, wide-chain lamellae commonly resemble zippers (Fig. 20a,b), and hence the term "zipper termination" has been applied to these features. Many zipper terminations are coherent, which means that they do not involve disruption or distortion of the crystal structure except for the linear disruption parallel to c in the immediate neighborhood of the termination. Coherent terminations can be of two types: simple and cooperative. Figure 20 shows examples of the simple terminations of sextuple, septuple, and octuple zippers in anthophyllite and disordered pyribole; included is one example of a doubly-terminated zipper. Cooperative terminations occur when two or more zippers end together. Six different examples of such defects are shown in Figure 21 to give an idea of the variety of such features that is possible in pyribole structures.

In addition to the coherent types of zipper termination, there are two types of incoherent termination possible, again simple and cooperative. In simple incoherent terminations, a single zipper terminates, but in such a way that the surrounding structure is disrupted or distorted. Figure 22 shows two examples of this phenomenon, one in which a triple-chain slab terminates and becomes a double-chain slab by a dislocation mechanism, and one in which the termination of an octuple-chain zipper results in

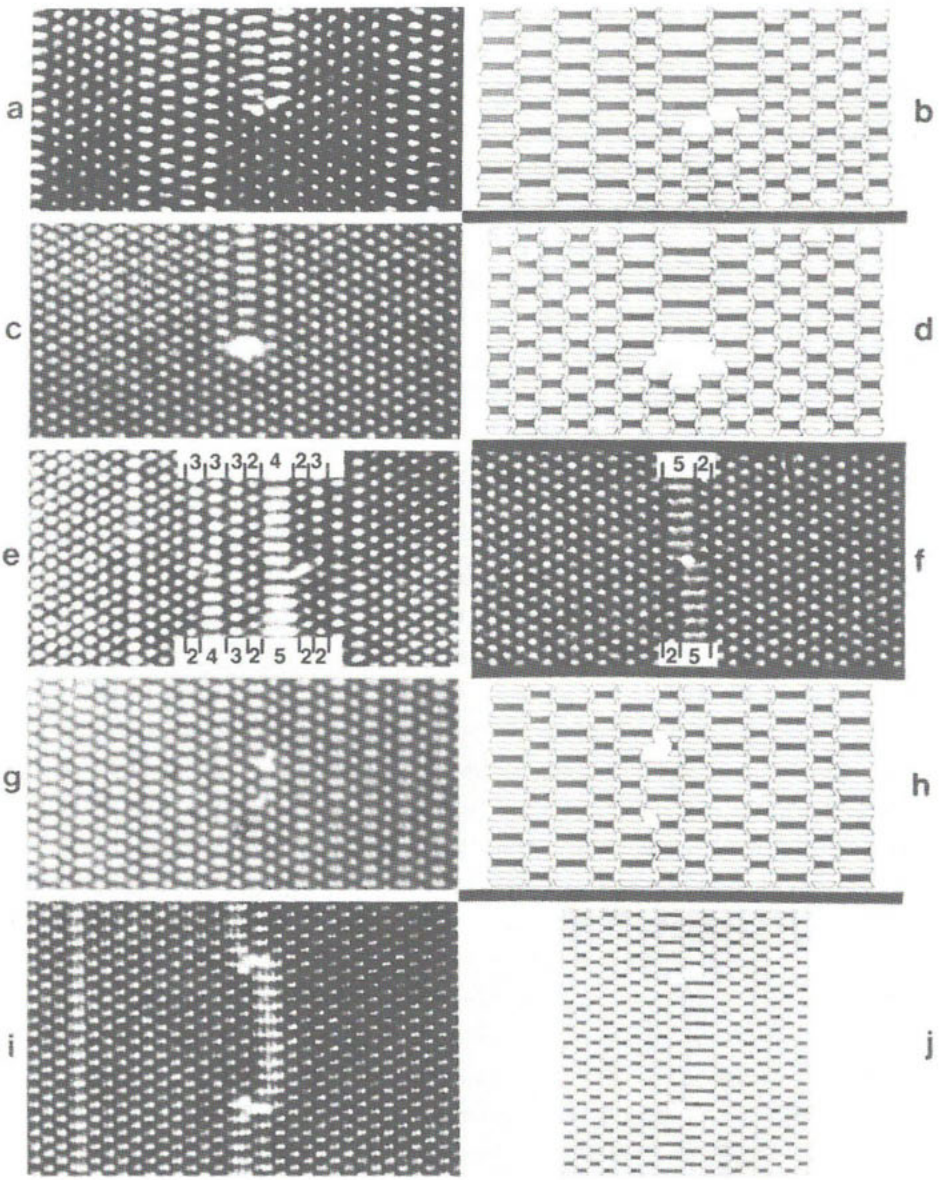

Figure 21. Cooperative coherent zipper terminations. (a,b) Two quadruple zippers terminating together in double-chain material. (c,d) Cooperative termination of two triple zippers and one quadruple zipper. (e) The chain sequence 2432522 turning into 3332423 by cooperative zipper termination. (f) "Derailment" of a quintuple zipper is equivalent to the replacement of the chain sequence 25 by the sequence 52. (g,h) Local switching of a double and a triple zipper along a chain-width error in chesterite. (i,j) Local replacement of double, triple, and quadruple zippers by two double and one quintuple zippers. (After Veblen and Buseck, 1980.)

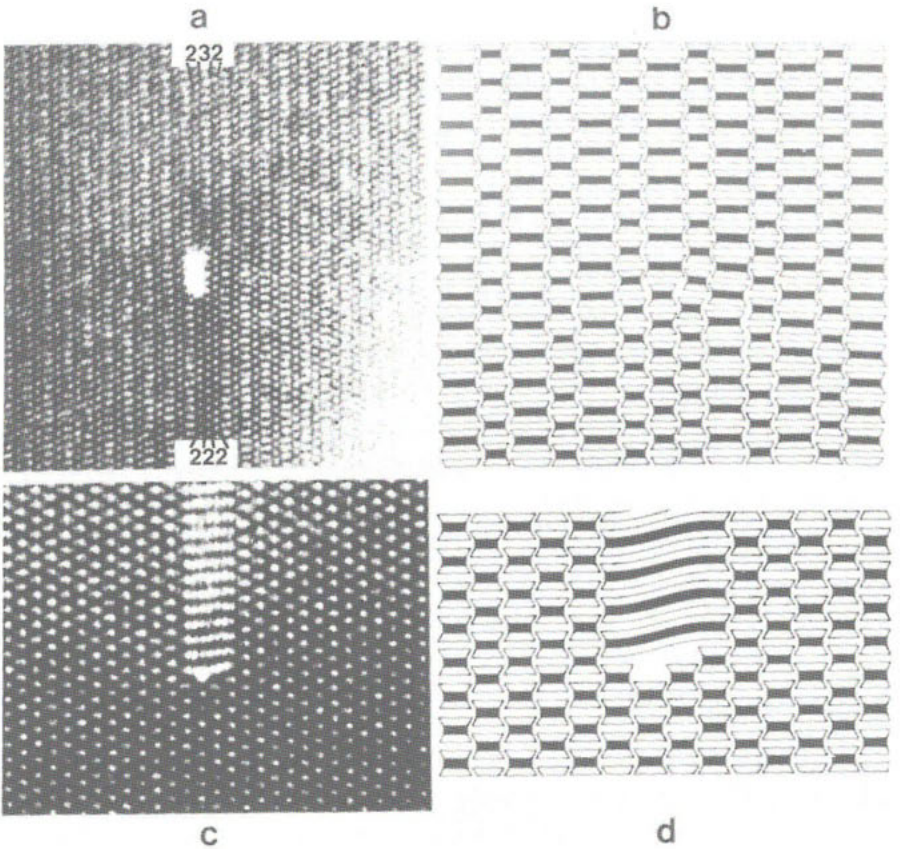

Figure 22. Simple incoherent zipper terminations, which result in structural distortion. (a,b) A double-chain zipper becomes a triple-chain zipper by a dislocation mechanism in chesterite. (c,d) An octuple-chain zipper terminating in anthophyllite. (After Veblen and Buseck, 1980.)

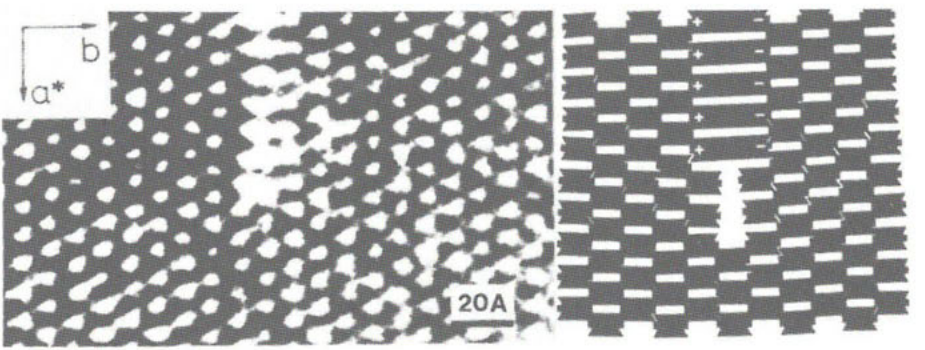

Figure 23. Experimental image and structural interpretation of a quintuple zipper turning into three double chains by a dislocation mechanism in grunerite asbestos. (After Whittaker *et al.*, 1981.)

bending of the silicate chains. Like noncooperative chain terminations, simple incoherent zipper terminations are rare in some pyriboles, compared to other termination types. Whittaker *et al.* (1981) have shown, however, that termination of (010) double-chain slabs can occur with some frequency in grunerite (Fig. 23), along with other dislocations having burgers vectors with components parallel to the *a*-axis, rather than the *b*-axis. Simple incoherent terminations also appear to be reasonably abundant in at least some uralites.

Cooperative incoherent zipper terminations involve two or more zippers, the terminations of which are connected by planar faults in the host structure. Figure 24 shows two examples of the cooperative termination of a pair of zippers; the type of planar fault is different for the two cases. The cooperative incoherent termination of three zippers is also illustrated (Fig. 24c,d). With the apparent exception of the grunerite asbestos described by Whittaker *et al.* (1981), most pyriboles with much chain-width disorder appear to contain more of these cooperative terminations than simple incoherent terminations, which necessarily require substantial structural distortion.

Termination rules

Two geometrical rules that can be used to determine whether a termination will be coherent or incoherent were derived by Veblen and Buseck (1980); an alternative derivation of these rules was presented by Whittaker *et al.* (1981). The two rules are as follows:

Rule #1 (the "subchain rule"). For structural coherence at a termination, there must be an equal number of subchains in a (010) pyribole slab and in the material it replaces. (A pyroxene chain contains one subchain, an amphibole chain has two, a triple chain three, and so on.) A violation of this rule is shown in Figure 25a, where a slab of double-chain pyribole (two subchains) replaces a slab that is three pyroxene chains wide (three subchains). There is a gap in the structure that would have to be taken up either by distortion around a partial dislocation or by the formation of a planar fault. In contrast, in Figure 25b, a triple-chain slab (three subchains) can coherently replace a slab of pyroxene three chains wide (also three subchains) with no structural distortion or planar faults.

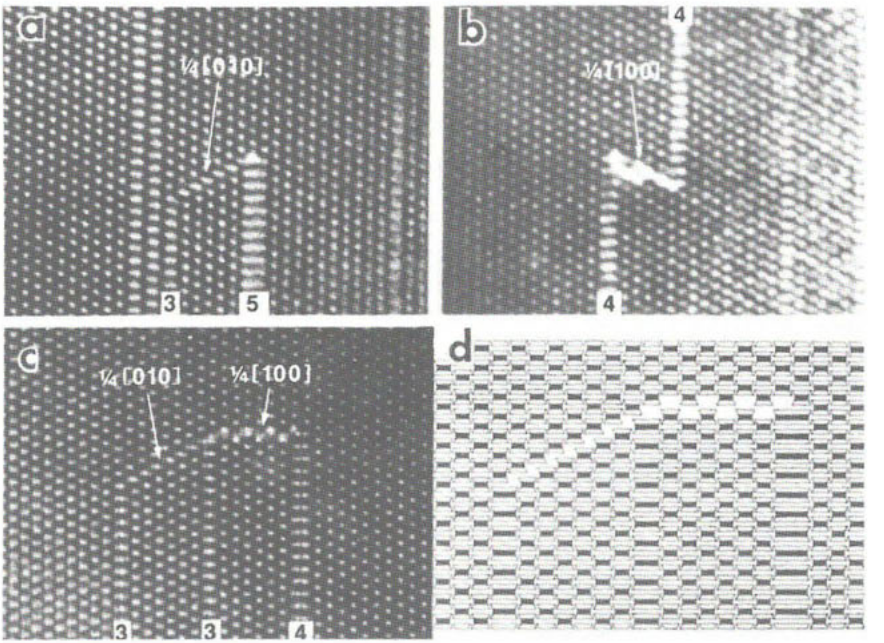

Figure 24. Cooperative incoherent zipper terminations and their associated planar faults. (a) A planar defect with projected displacement ½ [010] connecting the terminations of triple and quintuple zippers in anthophyllite. (b) A planar defect with projected displacement ½ [100] connecting the terminations of two quadruple zippers. (c,d) Both types of planar faults occurring together at the cooperative terminations of one quadruple and two triple zippers. (After Veblen and Buseck, 1980.)

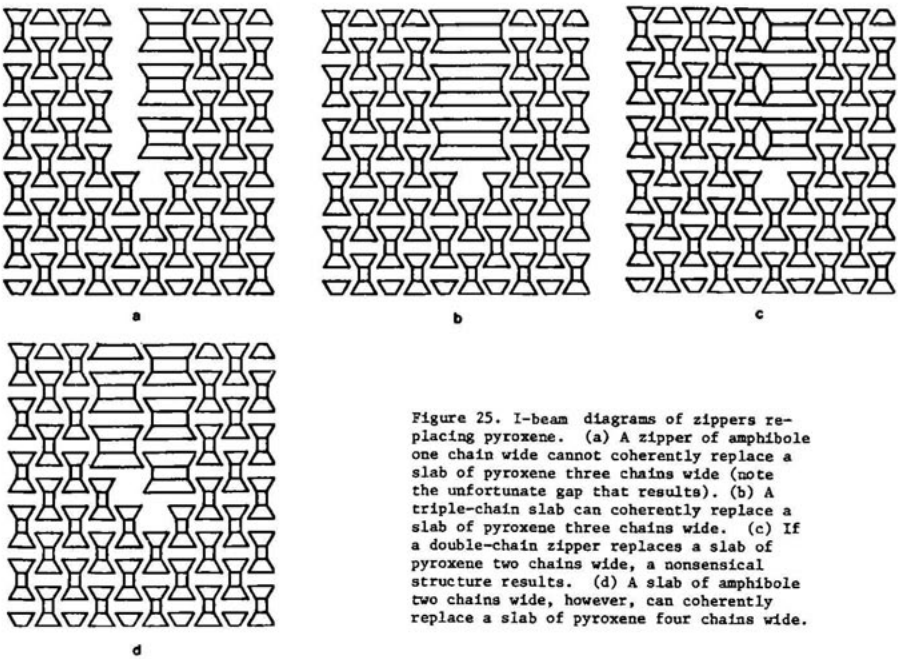

Figure 25. I-beam diagrams of zippers replacing pyroxene. (a) A zipper of amphibole one chain wide cannot coherently replace a slab of pyroxene three chains wide (note the unfortunate gap that results). (b) A triple-chain slab can coherently replace a slab of pyroxene three chains wide. (c) If a double-chain zipper replaces a slab of pyroxene two chains wide, a nonsensical structure results. (d) A slab of amphibole two chains wide, however, can coherently replace a slab of pyroxene four chains wide.

Rule #2 (the "odd-even rule"). For structural coherence at a termination, there must either be an even number of chains on both sides of the termination, or there must be an odd number on both sides. Figure 25c shows a violation of this rule where a slab containing a double chain and a single chain (two chains and hence an even number) turns into a slab three pyroxene chains wide (three chains and hence odd). Although the number of subchains is the same in both slabs (three), a nonsensical structure results. The termination in Figure 25d, on the other hand, is a "legal" coherent termination. Here, a slab two double chains wide (two chains = even) turns into a slab that is four single chains wide (four chains = even); since the number of chains is even in both cases, the odd-even rule is obeyed. Likewise, the termination in Figure 25b is also coherent, because an odd number of triple chains (one) turns into an odd number of pyroxene single chains (three).

The zipper terminations of Figures 20-24 can also be used to illustrate the termination rules. For example, in Figure 20a,b, a sextuple zipper one chain wide (six subchains, one chain = odd) replaces a slab of amphibole structure three chains wide (six subchains, three chains = odd); the reader can satisfy himself that the other simple terminations of Figure 20 obey the rules. The cooperative terminations of Figure 21 are also in compliance. A slab that is two quadruple chains wide (eight subchains, two chains = even) in Figure 21a turns into a slab of amphibole four chains wide (again eight subchains, four chains = even). A more complex case is shown in Figure 21e, where the chain sequence 3332423 (20 subchains, seven chains = odd) becomes the sequence 2432522 (also 20 subchains, seven chains = odd).

Similarly, observed incoherent terminations can be shown to violate the coherent termination rules. In Figure 22a,b, a slab with the chain sequence 232 turns into a slab of amphibole structure three chains wide; although there is an odd number of chains in both cases, the sequence 232 has seven subchains, compared to only six in the sequence 222, and structural distortion results because the subchain rule is broken. In Figure 22c,d, an octuple-chain zipper one chain wide (eight subchains, one chain = odd) turns into a slab of amphibole four chains wide (eight subchains, four chains = even), thus violating the odd-even rule and distorting the structure in the neighborhood of the termination.

The incoherent terminations of Figure 24, which are associated with planar displacive faults, likewise violate the rules for coherent termination. Thus, the observed structures of coherent and incoherent terminations are consistent with those that are predicted by the theoretically-derived rules for coherent zipper termination.

POLYSOMATIC REACTIONS IN BIOPYRIBOLES

Polysomatic reactions can be defined as reactions that turn one polysome into another. In biopyriboles, any reaction that changes the widths or sequences of the silicate chains, or that converts silicate chains into sheets, is thus a polysomatic reaction. Such reactions have long been recognized as important for pyribole mineralogy, starting with the observation of Goldschmidt (1911) that uralites are pseudomorphs of pyroxene that have been replaced by amphibole. Likewise, partial alteration of pyroxenes to amphiboles, micas, and talc, as well as similar alteration of amphibole, can commonly be observed in hand specimen or with a petrographic microscope. Recent work has shown that polysomatic reaction of pyriboles, generally in the direction of increasing hydration, is also a common feature on the scale observable with TEM methods. Much of the current attention has been focussed on the mechanisms of polysomatic reactions and on the question of how wide-chain pyriboles and pyriboles with chain-width disorder form (Veblen and Burnham, 1978b; Veblen and Buseck, 1980, 1981; Nakajima and Ribbe, 1980; Cressey *et al.*, 1981).

Mechanisms of polysomatic reactions

In the broadest sense, polysomatic reaction mechanisms can be separated into two categories: (1) bulk reaction mechanisms, in which transformation occurs along a broad reaction front; and (2) lamellar and ledge mechanisms, in which reaction proceeds by the growth of narrow lamellae of the product phase or by the migration of narrow ledges in the interface between two phases. Mechanisms of the first type are roughly analogous to the massive transformation mechanisms that have long been recognized by metallurgists (Christian, 1965), except that structural transformation must also be accompanied by diffusion in the case of polysomatic reactions. Mechanisms of the second type are in many

ways analogous to the mechanisms that operate in the nucleation and growth of exsolution lamellae in some silicates (Champness and Lorimer, 1976).

Replacement by a bulk reaction mechanism is apparently the primary mode of formation of uralites (Veblen and Buseck, 1981). Figure 26 shows the interface between amphibole and remnant pyroxene in such a specimen that is almost entirely replaced; such interfaces need not have any specific orientation with respect to the pyroxene and amphibole structures, but the two structures are topotactically related so that the pyroxene and amphibole crystallographic axes coincide, as initially noted by Goldschmidt (1911). This mechanism presumably involves nucleation of amphibole followed by migration of the interface, with diffusion of water into and octahedrally-coordinated cations out of the structure along the interface. The replacement of pyriboles by sheet silicates in some cases may also occur by a bulk mechanism (Fig. 27).

Although bulk mechanisms may operate in many cases of polysomatic reaction in biopyriboles, most electron microscopic observations have been made on materials that have been replaced at least in part by lamellar or ledge mechanisms. In the simplest form of lamellar reaction, a zipper of material having a different chain sequence from that of the host nucleates and grows. For example, sextuple-chain zippers, such as those shown in Figure 20, may nucleate and grow into the amphibole structure. Likewise, lamellae more than one chain wide can nucleate and grow cooperatively. In many of the partially-reacted pyriboles that have been studied, most of the nucleation events apparently obey the rules for coherent termination set forth in the last section, leading to lamellae that terminate coherently. It is, of course, possible for nucleation events that do not obey the rules to occur, leading to the growth of incoherently terminating zippers of either the simple (Fig. 22) or cooperative (Fig. 24) types. In the latter case, growth must involve not only the formation of the zippers, but also the dissolution and recrystallization of the material between them along the displacive planar faults. For example, the two triple zippers and quadruple zipper in Figure 24c,d could all grow cooperatively, but only by the reconstruction of the anthophyllite along the two planar faults connecting the zippers. The portion of the reaction taking place along these displacive faults could be classified as having a bulk mechanism that is analogous to the massive, non-diffusional

Figure 26 (to the left). Amphibole replacing pyroxene in a uralite by a bulk mechanism along a reaction front; this is a crystallographically oriented reaction. The amphibole-pyroxene interface in this case is inclined to the viewing direction (the *c*-axis), resulting in moiré constrast where the two structures overlap. (After Veblen and Buseck, 1981.)

Figure 27 (below). Anthophyllite that has been partially replaced by talc via a bulk mechanism. In this case, the reaction is oriented. (a) Overview of the talc-amphibole interface. (b,c,d) Detailed views of the talc-amphibole interfaces oriented parallel to (010), (210), and (100) of the anthophyllite, respectively. (After Veblen and Buseck, 1980.)

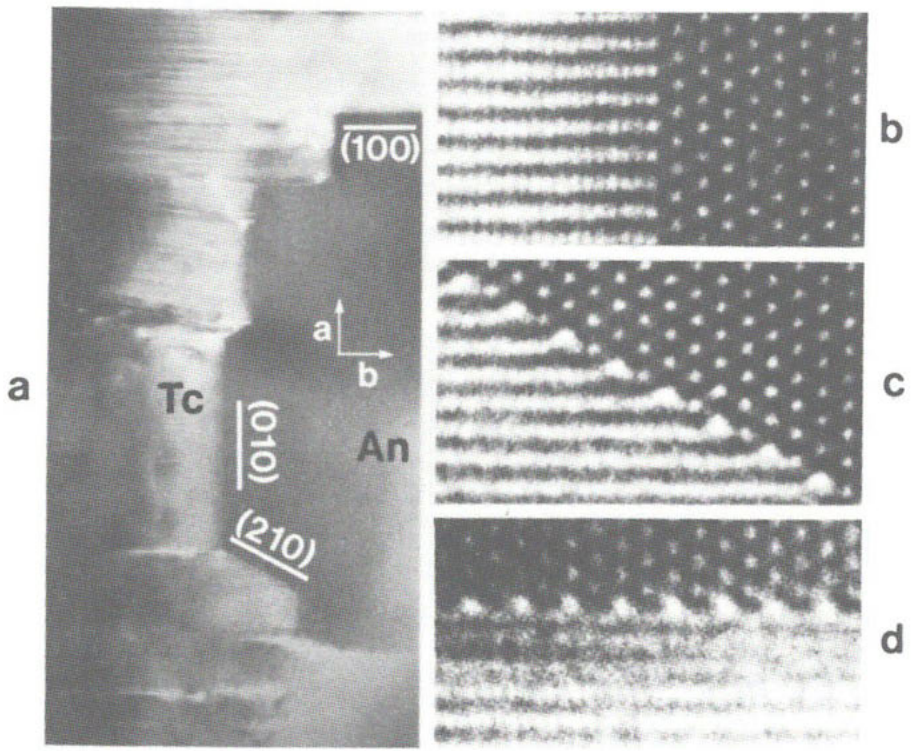

reactions that are common in metals (Christian, 1965), in that it requires complete reconstruction of the structure along a reaction front.

It is also possible that chain-width ordering and disordering reactions could occur by the migration of displacive planar faults, without any compositional changes occurring. A possible example of such a reaction is shown in Figure 28, where perfectly ordered chesterite on the top is separated from disordered pyribole on the bottom by an *en echelon* series of planar faults. Although it is disordered, the material on the right-hand two-thirds of the figure is stoichiometrically identical to chesterite. Migration of the planar faults toward the bottom of the figure would thus constitute an ordering reaction, since it would result in the replacement of disordered pyribole by ordered chesterite. It has been proposed that the replacement of amphibole by chesterite and jimthompsonite may take place by the nucleation and growth of wide-chain zippers, followed by such ordering reactions involving the migration of displacive planar faults (Veblen and Buseck, 1980).

Once a narrow lamella of pyribole having a different chain width from that of the host has formed, it is possible for the lamella to widen by the nucleation and migration of growth ledges. An example of such a ledge is shown in Figure 29, which is from an orthopyroxene that has been partially replaced by narrow amphibole lamellae. The amphibole ledge in this case is two chains wide, and migration of the ledge causes the replacement of a slab of pyroxene structure four chains wide. Because such ledges are simply a special case of zipper termination, in most cases they obey the termination rules outlined above, although amphibole ledges that are one chain wide and are combined with misfit dislocations have also been reported (Veblen and Buseck, 1981).

As noted above, the replacement of pyriboles by micas and talc in some cases may proceed by a bulk replacement mechanism, but in cases where there is a topotactic relationship between the two structures, reaction by ledge mechanisms can also occur. An example of ledges in the interface between talc and chesterite is shown in Figure 30. Migration of the ledges toward the bottom of the figure would result in replacement of part of the chain silicate by talc. In this case, c^* of the talc is approximately parallel to a^* of the pyribole, and the interface is parallel to pyribole (010), but growth ledges have also been observed

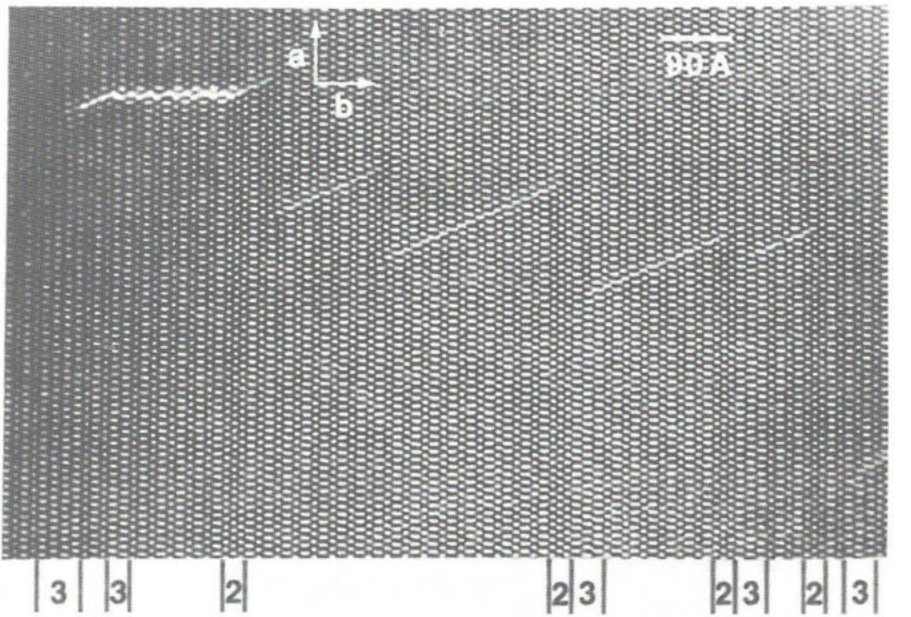

Figure 28. Structurally ordered chesterite, top, separated from chesterite having chain-width disorder (bottom) by a series of planar faults. Groups of double and triple chains are indicated by "2" and "3," respectively. (After Veblen and Buseck, 1980.)

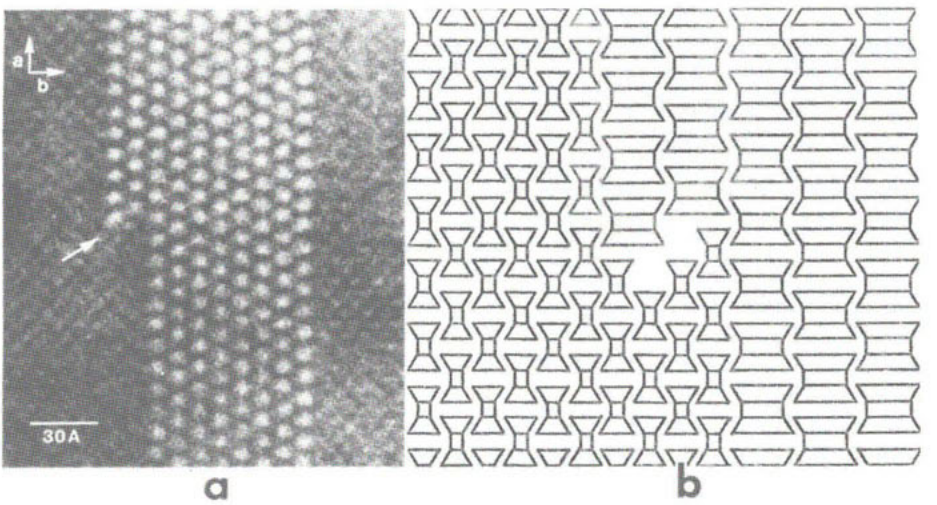

Figure 29. (a) HRTEM image of an amphibole lamella in an orthopyroxene. There is a growth ledge (arrowed) in the lamella that is two amphibole chains wide. The lamella is eight amphibole chains wide below the ledge and ten chains wide above it. (b) I-beam model of such a ledge, showing that a ledge two amphibole chains wide can coherently terminate and replace pyroxene structure four chains wide.

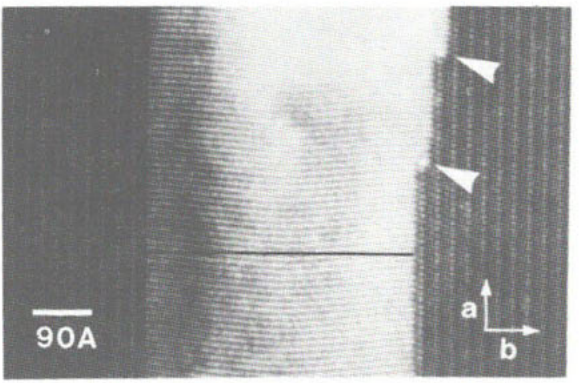

Figure 30. Growth ledges (arrowed) in an oriented interface between a talc lamella and chesterite. The straight, black line in the talc is for reference, showing that the talc layers are bent. (After Veblen and Buseck, 1980.)

for other orientation relationships and interface orientations between sheet and chain silicates (Veblen and Buseck, 1980).

Kinetics of polysomatic reactions

At the present time, experimental data that give some indication of the rates of polysomatic reactions in biopyriboles are extremely limited. TEM observations of experimental run products indicate that anthophyllite reacts to talc by a dissolution-precipitation mechanism, rather than a solid-state mechanism, when placed far enough into the talc stability field to achieve reasonable reaction rates (Veblen, 1982). Observations on natural anthophyllites suggest, in fact, that in the 600-700°C range, a slow metamorphic cooling rate is a prerequisite for an appreciable degree of reaction to chesterite, jimthompsonite, and talc via the lamellar mechanisms outlined above. On the other hand, the presence of amphibole lamellae in the pyroxenes of plutonic igneous rocks (Smith, 1977; Veblen and Buseck, 1981) indicates that at least limited lamellar reaction can occur at more rapid cooling rates under autometamorphic conditions. Similarly, the extensive degree of reaction from pyroxene to amphibole that is commonly exhibited by uralites in skarns and gabbros suggests that polysomatic reaction by bulk mechanisms can be a relatively rapid process under appropriate conditions.

Unlike polymorphic reactions, which require only reconstruction or distortion of the crystal structure, polysomatic reactions require chemical transport to occur together with reconstruction, because

polysomatic reactions involve a change in stoichiometry. This requirement for chemical diffusion in polysomatic reactions precludes the rapid reaction rates that are observed in many polymorphic reactions. Indeed, the extremely sluggish rates of diffusion in most silicates at metamorphic temperatures raise the question of how solid-state reaction involving chemical change occurs to the degree that is observed. The answer probably lies in the mechanisms of diffusion that operate in polysomatic reactions.

The diffusion coefficients that are usually used for solids, and the ones to which most geologists and mineralogists are accustomed, are measures of the average transport properties of a crystal structure; for most silicates, in which diffusion apparently occurs primarily by a vacancy-hopping mechanism, this average diffusion rate is very slow. In contrast to most silicates, some materials exhibit "ultrafast" or "pipe" diffusion, which occurs by the rapid motion of atoms or ions along structural tunnels (Peterson, 1968). Examples of such ultrafast diffusion include the transport of copper along tunnels in the tetragonal tin structure (Dyson *et al.*, 1967), the diffusion that occurs in some solid ionic conductors, and the diffusion of ions and molecules in zeolites. Such interstitial diffusion processes can occur on time scales of seconds. Similarly, it has recently been shown that there is very rapid diffusion of oxygen along dislocation cores in albite, with the pipe diffusion coefficient exceeding that for the non-defective feldspar structure by several orders of magnitude (Yund *et al.*, 1980).

It has been suggested that a similar case of localized ultrafast diffusion may operate during lamellar polysomatic reactions in pyriboles (Veblen and Buseck, 1980). As can be seen in Figures 20, 21, and 22, the local structures at the terminations of zippers probably involve tunnels where parts of I-beams are missing, owing to the mismatch of the two structures. These tunnels are very large compared to the sizes of the ions that must diffuse during polysomatic reactions in pyriboles, and they are also large compared to the tunnels of many zeolites that exhibit extremely rapid ion exchange properties even at room temperature. Likewise, as can be seen in Figures 25 and 29, the terminations of polysomatic lamellae in pyroxenes also involve relatively large structural tunnels. Diffusion along these tunnels presumably proceeds by an interstitial

mechanism and is therefore likely to be far more rapid than diffusion in more normal parts of the pyribole structures. Therefore, in the growth of polysomatic lamellae, there may be ultrafast diffusion localized along the line at which the reaction is actually taking place, and the necessity of transporting hydrogen and octahedral cations in and out of the reacting structure may not impose as great a kinetic barrier as would be implied by the diffusion coefficients of the bulk structures. Of course, transport of this sort is restricted to the *c* direction, and pyribole crystals tend to be elongated in this direction, suggesting that transport distances may be rather long; however, chemical communication with the crystal's environment would probably be facilitated by rapid chemical transport along fractures that cut the *c*-axis, which are commonly observed petrographically in pyroxenes and amphiboles and have also been observed with HRTEM (Fig. 18).

The cooperative growth of zippers that are connected by displacive planar faults is slightly more complicated than the growth of lamellae with no associated displacive faults. This can be seen by examining Figure 24c,d and noting that in order for the triple and quadruple zippers to grow into the amphibole structure, it is necessary to break up and recrystallize the amphibole that lies between the zippers. This recrystallization process takes place along the displacive faults and requires no long-range diffusion beyond that required for the formation of the wide-chain material. As noted above, the mechanism of recrystallization of the material between the zippers would be analogous to the massive transformations known from metallurgy, in that there is no compositional change of these regions, except that in this case the structure is replaced by itself, rather than a new structure. Under appropriate conditions, such massive transformations can occur very rapidly.

Also closely related to massive polymorphic transformations are the polysomatic reactions that take place by a bulk mechanism along a reaction front, as in the case of amphibole replacing pyroxene in uralites (Fig. 26). The difference between these mechanisms again lies in the requirement for diffusion of octahedral cations and hydrogen in pyribole polysomatic reactions. In this case, the diffusion presumably takes place along the structurally disordered interface between the two polysomes. The complete replacement of pyroxene by amphibole in many

uralites implies that this bulk mechanism, which combines diffusion and recrystallization, must be a very efficient process under certain conditions.

Distinguishing primary growth microstructures from reaction microstructures

It is clear from observations of triple and wider silicate chains in the products of anthophyllite synthesis experiments that chain-width errors in amphibole can form during primary growth of the crystals (Veblen, 1982). It is also quite obvious from textures observable in petrographic and electron microscopes that polysomatic reactions do occur in biopyriboles and that they can produce chain-width disorder in pyroxenes, amphiboles, and other pyriboles. It is therefore not a trivial matter to distinguish chain-width errors that form during primary growth from those that form subsequently by reaction.

In some cases, such as the nearly complete pseudomorphic replacement of pyroxene by amphibole in some uralites, it is clear simply from the extent of reaction that the replacing phase formed by polysomatic reaction (Veblen and Buseck, 1981). In most cases, however, more subtle textural relationships are the only basis for distinguishing between growth and reaction defects. In some cases, cross-cutting relationships among chain-width errors and fractures can be used to show that chain-width disorder arose after growth of the crystal (Veblen *et al.*, 1977; Veblen and Buseck, 1980; Cressey *et al.*, 1981). Some fractures simply offset recognizable sequences of chain-width errors, implying that the fractures and the deformation that caused them postdate the formation of the chain-width disorder (see Fig. 8 of Veblen and Buseck, 1980, for two obvious examples). In other cases, chain-width errors clearly terminate at fractures, as shown in Figure 31, demonstrating that the chain-width defects formed after the fracture and hence after growth of the crystal; this textural relationship constitutes clear evidence that chain-width errors can form by polysomatic reaction. Similarly, the proximity of terminating chain-width errors to grain boundaries and fractures can demonstrate an alteration reaction mechanism for their formation (Veblen, 1980; Veblen and Buseck, 1981).

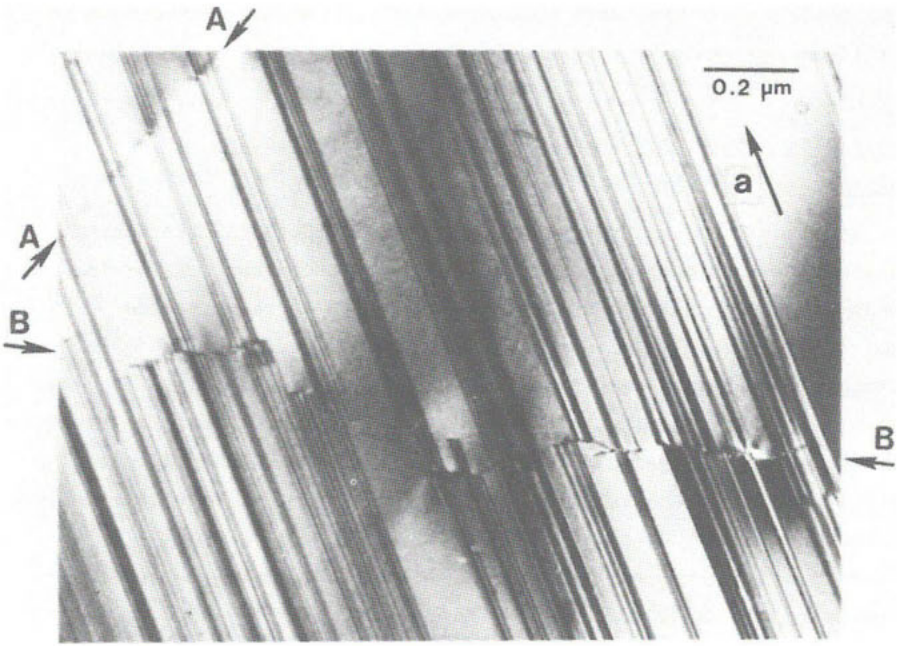

Figure 31. Conventional bright-field TEM micrograph of anthophyllite, showing the relationships between two fractures and numerous chain-width errors. The crystal was tilted out of perfect *c*-axis orientation to enhance the contrast of the chain-width errors, which are the dark lines running parallel to the trace of the *a*-axis ("a"). Fracture A merely displaces the chain-width errors by a small amount, indicating that the fracture formed after the chain-width defects. Fracture B, however, terminates most of these chain-width errors, indicating that the wide chains grew into the anthophyllite crystal after the formation of the fracture.

It has also been suggested by Cressey *et al.* (1981) that triple-chain defects in amphiboles do not form by reaction because they cannot terminate coherently within the amphibole structure; all triple-chain errors would thus be the result of primary growth. Cressey *et al.* and Whittaker (1981) discount the possibility of the cooperative growth of incoherently-terminating zippers that are connected by planar displacive faults because it requires the displacement of the amphibole structure lying between the zippers, as discussed in the last sections. This is probably not a valid argument, since this displacement can occur by a simple massive mechanism that is known to be kinetically rapid in other systems; the displacement of this material is also mechanistically little different from simple recrystallization processes, which obviously occur at geologically reasonable rates. Furthermore, there is textural evidence in some specimens that cooperative growth does occur and that triple-chain

defects can form subsequent to primary crystallization. For example, incoherent zippers terminating cooperatively in some cases are associated with alteration along fractures and grain boundaries (see Fig. 22b of Veblen and Buseck, 1980, and Fig. 1b of Veblen, 1980). In addition, triple-chain errors are commonly terminated by fractures, indicating that they have formed by polysomatic reaction (Fig. 17, for example). This does not mean that triple-chain errors do not form during primary growth in nature, but simply that they can form by either growth or reaction processes.

CONCLUSION AND SUGGESTIONS FOR FUTURE WORK

It has become clear during the last decade that the crystal chemistry of the pyribole minerals is far more complicated than previously recognized. In addition to the pyroxenes and amphiboles, there are other groups of ordered pyriboles, and in some cases structural disorder involving mixed silicate chain widths can be important. The range of behavior exhibited by pyriboles undergoing polysomatic reactions is quite varied and can give rise to an extraordinary variety of microstructures. Both x-ray and electron microscopic techniques have been applied to the study of polysomatic variations by biopyriboles, but the work to date is far from complete. The following are a few of the areas in which future work should prove fruitful:

1. Chemical characterization by TEM microanalysis of "clinojimthompsonite" occurring in nephrite and augite. These may prove to be the triple-chain analogs of actinolite and hornblende.

2. Synthesis and phase equilibrium experiments extending the work on Na-Mg compositions to other chemical systems. Careful work is needed to determine whether or not the clinojimthompsonite structure has a true field of stability at low temperatures in the Na-Mg system. Synthesis of this material as crystals suitable for x-ray structure refinement would also extend our understanding of pyribole crystal chemistry.

3. Kinetic experiments, particularly on pyroxenes, to determine rates of hydration reactions under different conditions of temperature and water pressure.

4. X-ray and TEM studies of many more specimens from a range of geological environments to determine how widespread polysomatic variations

are in pyroxenes and amphiboles. This is petrologically important, because polysomatic variations can significantly affect the geochemical behavior of pyriboles.

5. TEM examination of amphibole synthesis and phase equilibrium run products, especially those grown or equilibrated at relatively low temperatures, to determine whether such products really are amphiboles in all cases and to ascertain the state of chain-width order or disorder.

ACKNOWLEDGMENTS

I gratefully acknowledge Frank Hawthorne, Charles Burnham, and Paul H. Ribbe for constructive reviews. This work was supported by NSF grant EAR7927094.

Alario Franco, M. A., J. L. Hutchison and J. M. Thomas (1977) Structural imperfection and morphology of crocidolite (blue asbestos). Nature, 266, 520-521.

Burnham, C. W. (1967) Ferrosilite. Carnegie Inst. Wash. Year Book, 65, 285-290.

Buseck, P. R. and S. Iijima (1974) High resolution electron microscopy of silicates. Amer. Mineral., 59, 1-21.

_____, G. L. Nord, Jr., and D. R. Veblen (1980) Subsolidus phenomena in pyroxenes. *In* C. T. Prewitt, Ed., *Pyroxenes,* Mineral. Soc. Amer. Revs. in Mineral., 7, 117-211.

Cameron, M. and J. J. Papike (1980) Crystal chemistry of silicate pyroxenes. *In* C. T. Prewitt, Ed., *Pyroxenes,* Mineral. Soc. Amer. Revs. in Mineral., 7, 5-92.

Champness, P. E., G. Cliff and G. W. Lorimer (1976) The identification of asbestos. J. Microscopy, 108, 231-249.

_____ and G. W. Lorimer (1976) Exsolution in silicates. *In* H.-R. Wenk, P. E. Champness, J. M. Christie, J. M. Cowley, A. H. Heuer, G. Thomas and N. J. Tighe, Eds., *Electron Microscopy in Mineralogy*, p. 174-204. Springer-Verlag, Heidelberg.

Chisholm, J. E. (1973) Planar defects in fibrous amphiboles. J. Mater. Sci., 8, 475-483.

_____ (1975) Crystallographic shear in silicate structures. *In* M. W. Roberts and J. M. Thomas, Eds., *Surface and Defect Properties of Solids,* 4, 126-151.

Christian, J. W. (1965) *The Theory of Transformations in Metals and Alloys.* Pergamon Press, Oxford.

Clark, J. R., D. E. Appleman and J. J. Papike (1969) Crystal-chemical characterization of clinopyroxenes based on eight new structure refinements. Mineral. Soc. Amer. Spec. Pap., 2, 31-50.

Cressey, B. A., J. L. Hutchison and E. J. W. Whittaker (1981) Morphology and alteration of asbestiform grunerite and anthophyllite. Mineral. Mag., in press.

Dorling, M. and J. Zussman (1980) Comparitive studies of asbestiform and non-asbestiform calcium-rich amphiboles. Fourth Int'l Conf. on Asbestos, Torino, 317-333.

Drits, V. A., Y. I. Goncharov, V. A. Aleksandrova, V. E. Khadzhi and A. L. Dmitrik (1974) New type of strip silicate. Kristallografiya, 19, 1186-1193 (transl. Sov. Phys. Crystallogr., 19, 737-741).

_____, _____ and I. P. Khadzhi (1976) Formation conditions and physico-chemical constitution of triple chain silicate with (Si_6O_{16}) radical (in Russian). Izvestiya Akad. Nauk., Ser. Geol., 7, 32-41.

Dyson, B. F., T. Anthony and D. Turnbull (1967) Interstitial diffusion of copper in tin. J. Appl. Phys., 38, 3408.

Finger, L. W. (1970) Refinement of the crystal structure of an anthophyllite. Carnegie Inst. Wash. Year Book, 68, 283-288.

Ghose, S. (1961) The crystal structure of cummingtonite. Acta Crystallogr., 14, 622-627.

_____, W. C. Forbes and P. P. Phakey (1974) Unmixing of an alkali amphibole (tirodite) into magnesio-richterite and magnesio-riebeckite. Indian J. Earth Sci., 1, 37-42.

Gibbs, G. V. (1969) Crystal structure of protoamphibole. Mineral. Soc. Amer. Spec. Pap., 2, 101-109.

Gittos, M. F., G. W. Lorimer and P. E. Champness (1976) The phase distributions in some exsolved amphiboles. *In* H.-R. Wenk, P. E. Champness, J. M. Christie, J. M. Cowley, A. H. Heuer, G. Thomas and N. J. Tighe, Eds., *Electron Microscopy in Mineralogy*, p. 238-247, Springer-Verlag, Heidelberg.

Goldschmidt, V. M. (1911) Die Kontaktmetamorphose im Kristianiagebiet. Vidensk. Skrifter. I. Mat. - Naturv. K., No. 11.

Hutchison, J. L., M. C. Irusteta and E. J. W. Whittaker (1975) High resolution electron microscopy and diffraction studies of fibrous amphiboles. Acta Crystallogr., A31, 794-801.

_____, D. A. Jefferson, L. G. Mallinson and J. M. Thomas (1976) Structural irregularities in nephrite jade: an electron microscope study. Mater. Res. Bull., 11, 1557-1562.

Jefferson, D. A., L. G. Mallinson, J. L. Hutchison and J. M. Thomas (1978) Multiple-chain and other unusual faults in amphiboles. Contrib. Mineral. Petrol., 66, 1-4.

Johannsen, A. (1911) Petrographic terms for field use. J. Geol., 19, 317-322.

Katscher, H. and F. Liebau (1965) Über die kristallstruktur von $Ba_2Si_3O_8$, ein silikat mit dreifachketten. Naturwissenschaften, 18, 512-513.

Liebau, F. (1980) Classification of silicates. *In* P. H. Ribbe, Ed., *Orthosilicates*, Mineral. Soc. Amer. Revs. in Mineral., 5, 1-24.

Mallinson, L. G. (1980) Termination of planar defects in the amphibole mineral nephrite observed by high-resolution electron microscopy. Acta Crystallogr., A36, 378-381.

_____, J. L. Hutchison, D. A. Jefferson and J. M. Thomas (1977) Discovery of new types of chain silicates by high resolution electron microscopy. J. Chem. Soc. London Chem. Commun., 910-911.

_____, D. A. Jefferson, J. M. Thomas and J. L. Hutchison (1980) The internal structure of nephrite: experimental and computational evidence for the coexistence of multiple-chain silicates within an amphibole host. Phil. Trans. Royal Soc. London, 295, 537-552.

Martin, R. F. and G. Donnay (1972) Hydroxyl in the mantle. Amer. Mineral., 57, 554-570.

Nakajima, Y. and P. H. Ribbe (1980) Alteration of pyroxenes from Hokkaido, Japan, to amphibole, clays and other biopyriboles. N. Jb. Mineral. Mh., 6, 258-268.

Nissen, H.-U., R. Wessicken, C. F. Woensdregt and H. R. Pfeifer (1979) Disordered intermediates between jimthompsonite and anthophyllite from the Swiss Alps. *In* T. Mulvey, Ed., *Electron Microscopy and Analysis, 1979* (EMAG '79) Inst. of Physics (Bristol) Conf. Ser., 52, 99-100.

Papike, J. J., C. T. Prewitt, S. Sueno and M. Cameron (1973) Pyroxenes: comparisons of real and ideal topologies. Z. Kristallogr., 138, 254-273.

_____, and M. Ross (1970) Gedrites: crystal structures and intracrystalline cation distributions. Amer. Mineral. 55, 1945-1972.

_____, _____ and J. R. Clark (1969) Crystal-chemical characterization of clinoamphiboles based on five new structure refinements. Mineral. Soc. Amer. Spec. Pap., 2, 117-136.

Peterson, N. L. (1968) Diffusion in metals. *In* F. Seitz, D. Turnbull, and H. Ehrenreich, Eds., *Solid State Physics*, 22, p. 409-512. Academic Press, New York.

Smith, J. V. (1969) Crystal structure and stability of the $MgSiO_3$ polymorphs: physical properties and phase relations of Mg,Fe pyroxenes. Mineral. Soc. Amer. Spec. Pap., 2, 3-29.

Smith, P. P. K. (1977) An electron microscopic study of amphibole lamellae in augite. Contrib. Mineral. Petrol., 59, 317-322.

Sueno, S., M. Cameron and C. T. Prewitt (1976) Orthoferrosilite: high-temperature crystal chemistry. Amer. Mineral., 61, 38-53.

Tateyama, H., S. Shimoda and T. Sudo (1978) Synthesis and crystal structure of a triple chain silicate $Na_2Mg_4Si_6O_{16}(OH)_2$. Contrib. Mineral. Petrol., 66, 149-156.

Thompson, J. B., Jr. (1970) Geometrical possibilities for amphibole structures: Model biopyriboles (abstr.) Amer. Mineral., 55, 292-293.

_____ (1978) Biopyriboles and polysomatic series. Amer. Mineral., 63, 239-249.

Veblen, D. R. (1980) Anthophyllite asbestos: microstructures, intergrown sheet silicates, and mechanisms of fiber formation. Amer. Mineral., 65, 1075-1086.

_____ (1982) Structural disorder in synthetic anthophyllites. In preparation.

_____ and C. W. Burnham (1975) Triple-chain biopyriboles: Newly discovered intermediate products of the retrograde anthophyllite-talc transformation, Chester, VT. (abstr.) Trans. Amer. Geophys. Union (EOS), 56, 1076.

_____ and _____ (1976) Biopyriboles from Chester, Vermont: The first mixed-chain silicates (abstr.).Geol. Soc. Amer. Abstracts with Programs, 8, 1153.

_____ and _____ (1978a) New biopyriboles from Chester, Vermont: I. Descriptive mineralogy. Amer. Mineral., 63, 1000-1009.

_____ and _____ (1978b) New biopyriboles from Chester, Vermont: II. The crystal chemistry of jimthompsonite, clinojimthompsonite, and chesterite, and the amphibole-mica reaction. Amer. Mineral., 63, 1053-1073.

_____ and P. R. Buseck (1979a) Chain-width order and disorder in biopyriboles. Amer. Mineral., 64, 687-700.

_____ and _____ (1979b) Serpentine minerals: intergrowths and new combination structures. Science, 206, 1398-1400.

_____ and _____ (1980) Microstructures and reaction mechanisms in biopyriboles. Amer. Mineral., 65, 599-623.

_____ and _____ (1981) Hydrous pyriboles and sheet silicates in pyroxenes and uralites: intergrowth microstructures and reaction mechanisms. Amer. Mineral., 66, in press.

_____, _____ and C. W. Burnham (1977) Asbestiform chain silicates: New minerals and structural groups. Science, 198, 359-365.

Verma, A. R. and P. Krishna (1966) *Polymorphism and Polytypism in Crystals*. John Wiley and Sons, Inc., New York.

Whittaker, E. J. W., B. A. Cressey and J. L. Hutchison (1981) Terminations of multiple-chain lamellae in grunerite asbestos. Mineral. Mag., 44, 27-35.

Yamaguchi, Y., J. Akai and K. Tomita (1978) Clinoamphibole lamellae in diopside of garnet lherzolite from Alpe Arami, Bellinzona, Switzerland. Contrib. Mineral. Petrol., 66, 263-270.

Yund, R. A., B. M. Smith and J. Tullis (1980) Dislocation-assisted diffusion of oxygen in albite (abstr.). Geol. Soc. Amer. Abstracts with Programs, 12, 553.

Chapter 5
AMPHIBOLE ASBESTOS MINERALOGY

Tibor Zoltai

INTRODUCTION

Asbestos is one of the most desirable industrial minerals. This is because it possesses an unusual combination of exploitable properties, such as long fibrous shape, high strength and flexibility, low thermal and electric conductivity, high adsorbency, high chemical and mechanical durability, and relative incombustibility. Ironically, the industrially desirable physical properties of asbestos also appear to be responsible for a highly undesirable property, carcinogenicity.

Initially, asbestos was the name of a mineral (Zoltai, 1978). Today it is a *commercial term* applied to fibrous minerals utilized in industrial processes. The corresponding mineralogical term, *asbestiform habit*, specifies a unique crystallization habit. When minerals crystallize in this habit, they develop some or all of the industrially desirable properties of asbestos. Only a few minerals are known to both crystallize with this habit in large quantities and possess all the properties of commercial asbestos. There are also a significant number of other minerals which may crystallize in the asbestiform habit and possess all the properties of asbestos, but are not available in sufficient concentration or quantity for industrial exploitation. Some are available in sufficient quantity, possess all the properties of commercial asbestos, but exist only in shorter fibers which cannot be used commercially as asbestos. They may have other industrial applications, however. For example, palygorskite (also known as attapulgite) is one of the few minerals which is almost unknown in other than asbestiform habit (Marshall *et al.*, 1942; Huggins *et al.*, 1962). Palygorskite's property of high absorbance (ten times greater than that of kaolinite) makes it an excellent ingredient in cosmetics, dietary food supplements, and certain drugs (Walker *et al.*, 1981). The asbestiform fibers of palygorskite are not mineralogically different from the fibers of commercial asbestos.

It is most unfortunate, however, that health scientists and regulatory agencies have adopted the commercial definition of asbestos rather than the mineralogical one. Consequently, all particles of the five known commercial asbestos minerals are considered to be asbestos, pro-

vided that they have elongated shapes (with an aspect ratio of 3 to 1 or greater), regardless of their asbestiform crystallization. Due to this misconception, asbestiform fibers of other minerals are neglected, and their potential carcinogenic properties have not been investigated.

FIBROUS AND ASBESTIFORM HABITS

These terms, fibrous and asbestiform, are not synonymous: a mineral is said to have crystallized with a *fibrous* habit if it gives the appearance of being composed of fibers, whether the mineral actually contains separable fibers or not. On the other hand, the term *asbestiform* is more restricted: the mineral must resemble asbestos. Although this resemblance was limited to visual observation in the past, it implied the presence of asbestos properties by virtue of the fact that the characteristic appearance of asbestos is a consequence of its unique properties. These are (1) hair-like elongated shape resembling organic fibers. Their cross sections may be polygonal, circular, or irregular, and their faces are exceptionally smooth and may display unusual adamantine or silky luster. (2) The asbestiform fibers are stronger, more flexible and usually more durable than the same mineral crystallized in other habits. The development of these physical properties is gradational, but they are always well developed in high-quality commercial asbestos. The strength of well-developed asbestiform fibers may be as much as 50 times higher than that of single crystals of the same minerals. (3) The fibers usually crystallize in bundles of easily separable fibers and/or fibers which are composed of smaller diameter fibrils. Asbestiform fibers of various qualities may occur in different habits of crystal aggregation. The columnar habit is the most common.

The columnar growth habit

Most commercial asbestos crystallizes in columnar aggregation. Fibers are found in parallel, columnar arrangement in veins of differing widths. Fibers perpendicular to the wall of the veins are referred to as *cross fibers*. Inclined fibers are called *slip fibers*.

The common commercial asbestos minerals are chrysotile, anthophyllite, riebeckite, actinolite-tremolite, and cummingtonite-grunerite. Chrysotile is a serpentine in which the layered structure is curled up to form tubular or scroll-like patterns. Because of the unusual structural pattern, this asbestiform serpentine is considered a distinct mineral,

called chrysotile. The other commercial asbestos minerals are all amphiboles. The asbestiform variety of riebeckite has the varietal name crocidolite. Historically, crocidolite is the only asbestiform amphibole which has a valid varietal name, because it was known by that name before the parent mineral riebeckite was discovered. The identity of the two minerals was not firmly established until the crystal structure of crocidolite was determined by Whittaker (1949). The name *amosite* was introduced as a new mineral name (Hall, 1918) for a mineral occurring in major asbestos deposits in South Africa. Rabbitt (1948) demonstrated that "amosite" is not a distinct mineral but is a mixture of asbestiform varieties of actinolite-tremolite and cummingtonite-grunerite. He proposed that the name "amosite . . . should be restricted to commercial use," and thus "amosite" was promptly discredited as a valid mineral name (Fleischer, 1949).

In addition to the well-known commercial asbestos minerals, there are many other minerals known to crystallize in the columnar asbestiform habit on occasion, and possess comparable asbestos properties. Nuttal (1821) found some asbestiform *brucite* in New Jersey which he named nemalite. He claimed that nemalite is difficult to identify because of its "asbestos-like appearance." Many other occurrences of asbestiform brucite have since been found. Chester (1877) identified the asbestos he found in two-inch thick veins in Utah as copper-containing *sepiolite*. Kauffman (1943) also reported on the occurrence of sepiolite asbestos in Arizona. MacAdam (1886) gave the name of agalite to asbestiform *talc*. Although most asbestos-like talc was later determined to be pseudomorphic after chrysotile, some occurrences were confirmed to be primary talc asbestos. Some eight-inch long asbestos fibers found in Switzerland were identified as *tourmaline* by Dietrich *et al.* (1966). Ten years later Tarnovskii *et al.* (1976) also found some fine (1 μm diameter) and extremely flexible tourmaline asbestos in pegmatites. The chrysotile-like structure of tubular *halloysite* has long been known and has been repeatedly observed in electron micrographs (e.g., Kohyama *et al.*, 1978). *Imogolite* was also found to have similar tubular structure (Cradwick *et al.*, 1972). The good quality of *palygorskite* asbestos was described by Huggins *et al.* (1962); they concluded that asbestiform palygorskite would make good asbestos "if deposits of economic size could be found." Good quality potassium-*winchite* asbestos from Texas was described recently by Wylie and Huggins (1980).

A number of other minerals are also found in asbestiform habit. Some of these have limited asbestos properties and are more brittle than most commercial asbestos. Gruner (1946) makes references to asbestiform or fibrous *minnesotaite* and *stilpnomelane*. Fibrous *quartz* is rare, but not unknown (Braitsch, 1957; Frondel, 1978). Certain *micas* were also found to crystallize in fibers, and some of them display reasonably good asbestos properties (Rutstein, 1979; Zoltai, 1979; Güven *et al.*, 1980). Reutelspacher and van der Marel (1968) show several electron micrographs of fibrous crystals of minerals which are usually not considered to be fibrous. These include *calcite*, *nontronite*, *hydromagnesite*, and *amesite* (not to be mistaken for discredited "amosite").

The development of asbestos properties by fibers is a gradual process. Fibers in different stages of development possess different strengths and flexibilities. Poorly developed amphibole asbestos, for example, is usually referred to as "brittle asbestos" or "byssolite." The latter is the name introduced for poor-quality asbestos by Saussure in 1796. Similarly, the tubular or scroll-like structure of chrysotile may only be partially developed in some samples. This was illustrated by Veblen and Buseck (1979a) in electron micrographs (Fig. 1a). Some serpentine fibers have no obvious tubular or scroll-like structures and display low-quality asbestos properties. Such serpentine fibers are frequently referred to as picrolite. A special type of serpentine fibers, described by Cressey and Zussman (1976), is composed of segments of planar serpentine layers (Fig. 1b); it is called "polygonal serpentine" or "Povlen chrysotile."

The reticulated growth habit

In a reticulated growth habit, bundles of fibers of varying length are interlaced to produce a layer of limited thickness, resembling the texture of textiles. In these specimens asbestos is usually the only component, although occasionally some crystals may be "caught" in the lace. The layers of woven asbestos are strong and flexible, and go by varietal names, such as "matted chrysotile" or "mountain leather." In some cases the interlaced asbestos structure is extended in the third dimension. In such cases, it is called "mountain cork."

The fibers in the matted chrysotile of the Coalinga deposit, for example, are of high quality and provide commercial ore (Mumpton and

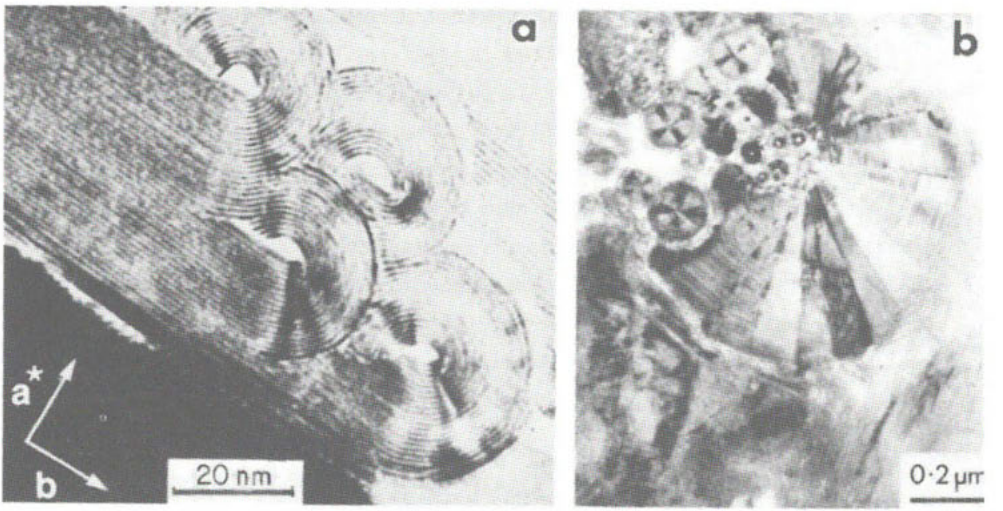

Figure 1. (a) Photograph taken by transmission electron microscope (TEM) of partially developed chrysotile fibers grading into planar serpentine. (After Veblen and Buseck, 1979a.) (b) Polygonal serpentine fibers. (After Cressey and Zussman, 1976.)

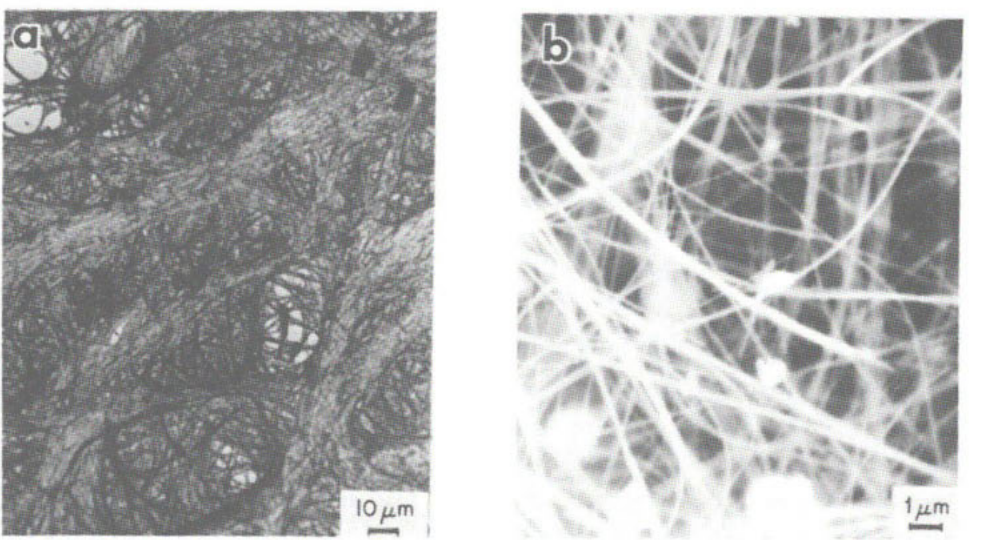

Figure 2. (a) Transmission electron micrograph of the replica of a chrysotile matt. (After Mumpton and Thompson, 1975.) (b) Scanning electron micrograph of palygorskite "mountain leather" from Templeton, Canada. (Photo by D. S. O'Hanley.)

Thompson, 1975). Figure 2a illustrates the attractive interlacing pattern of fibers in the Coalinga matted chrysotile. The most common asbestos mineral in mountain leather is palygorskite, as that which was first identified by Heddle in 1879 (he called this mineral pilolite -- it was later found to be identical with palygorskite). Sepiolite fibers in mountain leather are relatively rare but not unknown (Caillere, 1936). Actinolite-tremolite is more common (Fersmann, 1908), and according to Frondel (1980) most mountain leathers found in marble shear zones are actinolite-tremolite. Although chrysotile in the reticulated habit is currently referred to as matted chrysotile, it was previously called mountain leather (Fersmann, 1908; Caillere, 1936).

The radiated growth habit

In this habit acicular or fibrous crystals grow from what is apparently a central point along the radial directions of a sphere. Usually only a small segment of a sphere is represented by crystals, and only a few are actually joined at the center. Most of the crystals are shorter, start at a distance from the center, and fill the space between the longer crystals. This is a relatively common aggregation habit of minerals which have distinct chain structures. The crystals are acicular, fibrous or asbestiform. Radiated asbestiform fibers of cummingtonite-grunerite and of anthophyllite are relatively common. In most cases, however, their asbestos properties are poorly developed. Even the better developed fibers have low apparent tensile strength caused by the separation of fibers along the shorter fibrils.

The massive-fibrous growth habit

In most cases the massive-fibrous growth habit may be considered to be a special class of the radiated aggregation habit. This is because the fibers in this habit are frequently in radiated pattern. However, they may also contain fibers in straight and curved bundles. Both the radiating groups and the bundles have random orientation and there is some interlacing between the loose ends of fibers. The best example of the massive-fibrous habit is the amphibole jade, nephrite (actinolite). In macroscopic samples nephrite appears glassy and massive, but on a microscopic scale it is fibrous. The fibrous texture of nephrite has been observed by many investigators, and electron micrographs have been

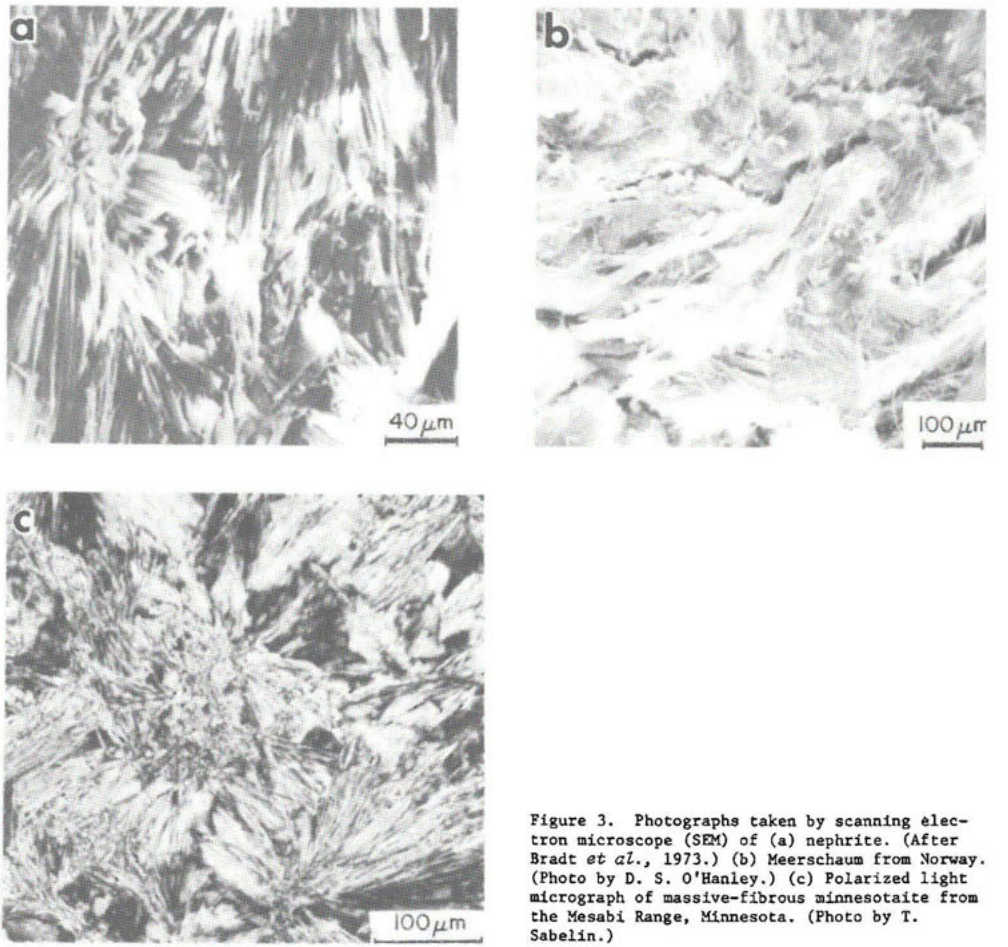

Figure 3. Photographs taken by scanning electron microscope (SEM) of (a) nephrite. (After Bradt *et al.*, 1973.) (b) Meerschaum from Norway. (Photo by D. S. O'Hanley.) (c) Polarized light micrograph of massive-fibrous minnesotaite from the Mesabi Range, Minnesota. (Photo by T. Sabelin.)

published (Bradt *et al.*, 1973; Rowcliffe and Fruhauf, 1977). While the fracture surface energies of silicates are on the order of 3,000-5,000 ergs/cm^2, Bradt *et al.* (1973) found that the fracture surface energy of high-quality nephrite is over 200,000 ergs/cm^2. Figure 3a is a reproduction of their scanning electron microscope (SEM) photograph of nephrite. (It should be noted that Bradt *et al.* found that the crystals in jadeite jade are not fibrous, and that its fracture surface energy is still over 100,000 ergs/cm^2. The possible reason for the toughness of the non-fibrous pyroxene jades will be discussed later in this paper.) The apparent differences in the mechanical properties of different nephrites

may be attributed to the differences in the texture and the quality of asbestos properties of the fibrous components. The possible asbestiform character of the fibers in nephrite is also supported by the observation of chain-width and other defects characteristic of amphibole asbestos fibers (Hutchison *et al.*, 1976a; Mallinson *et al.*, 1980).

The massive-fibrous habit is also found in other minerals, although their jade-like properties are, in general, less spectacular. The fibrous texture of meerschaum (sepiolite) has long been recognized because the fibers are usually large enough to be seen with a simple 10X loupe (see Fig. 3b). Some glassy, massive varieties of serpentine, known as "bowenite" or "precious serpentine," may also contain some fibrous crystals. The similarity between nephrite and bowenite was recognized by Bowen (1822), who referred to these minerals as "nephrite," but they were later identified and named bowenite by Dana (1950). Caillère (1936) made an extensive study of the serpentines and commented on the bowenite as having a "*texture compacte qui rappelle le jade, sans en avoir la durete.*" More recently, in an electron microscopic study, Huggins (1962) compared the fibers of chrysotile with those in a massive serpentine. He found that the major difference between the two is that in chrysotile the fibers are long and parallel, and in the massive serpentine they are shorter and the bundles are randomly oriented. The fibrous microstructure of some chalcedony (Braitsch, 1957; Frondel, 1962) is again similar to the characteristic texture of nephrite. The compact variety of minnesotaite (Fig. 3c) approaches the toughness of jade and is composed of both fibrous and curved platy crystals.

Isolated fiber growth habit

In the habits discussed thus far, the fibers are always small in diameter and usually occur in bundles. Some individual fibers, disseminated in rocks or grown in cavities, have comparable diameters. Most of them, however, are thicker. Some of these thicker crystals may be composed of smaller fibers or fibrils, but most are single crystals. Fibers which are larger diameter single crystals are usually referred to as "capillary" or "filamentary" crystals, instead of "fibers." Strictly speaking, these larger single crystals are not asbestiform.

Most of the isolated small diameter asbestiform fibers are composed of fibrils and possess the properties of commercial asbestos. Some

mineralogists prefer to describe these isolated fibers as "fibrous" instead of asbestiform because they do not constitute commercial ore (Trendall and Blockley, 1970). However, in some cases the concentration of isolated fibers may be sufficient to justify mining, and then the product is sold as asbestos (Mumpton and Thompson, 1976). Consequently, this distinction does not appear to be a valid mineralogical criterion. The term "fibrous" should be restricted to those fiber-sized crystals which do not possess asbestiform properties.

Many minerals can be found in isolated growth habit. They may be of fiber, capillary, or filamentary crystal dimensions. Their physical properties, except for not aggregating in bundles, resemble those of asbestos. Dana (1914), for example, described millerite as "brittle; capillary crystals elastic." Individual fine crystals of wollastonite were identified in a meteorite by Miyamoto *et al.* (1979). The diameter of these crystals ranged between 0.5 and 5.0 μm, and the authors referred to them as "whiskers."

Synthetic asbestos and whiskers

Most attempts to crystallize synthetic asbestos have involved amphiboles devoid of aluminum and with fluorine substituted for hydroxyl (e.g., Shell *et al.*, 1958; Nadgornyi *et al.*, 1965; Fedoseev *et al.*, 1970). These fibers were referred to as *synthetic asbestos*. Fibers of many other inorganic compounds have been synthesized, but only a few were labeled synthetic asbestos, e.g., the potassium-lead silicate fibers of Shell *et al.* (1957). Most others are called "needle-like," "filamentary," or "hair-like" crystals, or simple "whiskers." The difference between the terms "synthetic asbestos" and "whiskers" is strictly semantic and arbitrary. Most synthetic whiskers have mineral equivalents (wurtzite, sphalerite, halite, sylvite, fluorite, corundum, bromellite, zincite, periclase, quartz, forsterite, etc.). Some are also known to have asbestiform natural occurrences (e.g., wurtzite and brucite). It is interesting to note that the whisker possessing the highest strain rate (11%) is synthetic forsterite (Sears, 1962).

The basic physical properties of whiskers are identical to those of mineral asbestos fibers. Some whiskers may even grow in bundles. The natural-synthetic correlation between whiskers and asbestos usually is recognized by most investigators, inasmuch as they include asbestos

in the list of whiskers, under the heading of "cleaving whiskers." Several mineralogists have also accepted that relationship (Taber, 1916; Frondel, 1978) and a more extensive account of the comparison is given by Walker and Zoltai (1979).

THE UNIQUE STRUCTURE OF AMPHIBOLE ASBESTOS

The unique character of the physical properties of amphibole asbestos has long been recognized. Most evident is the conspicuous property of easy separation of bundles into increasingly smaller fibers and fibrils. This is in contrast to the higher stress required to cleave single crystals into acicular cleavage fragments. However, the individual asbestos fibers and acicular cleavage fragments are strikingly different. The fibers are extremely strong and flexible, while the acicular cleavage fragments are weak and brittle. Such conspicuous differences in properties obviously intrigued mineralogists.

Practically all amphibole asbestos, including monoclinic amphiboles, displays orthorhombic optical properties. Under crossed Nicols the extinction of the fibers is parallel to the fiber axis. Peacock (1928) in his classical study of amphibole asbestos described crocidolite, the asbestiform variety of riebeckite, as "a monoclinic amphibole in which the extinction angle is zero" and "amosite," the asbestos mineral named by Hall (1918), as an orthorhombic amphibole. (It was later in 1948 that Rabbitt demonstrated that "amosite" is a mixture of two monoclinic amphiboles.) This peculiar parallel extinction of the common monoclinic amphibole asbestos (riebeckite, actinolite-tremolite, and cummingtonite-grunerite) is a distinct property of these fibers and can be applied to discriminate between their asbestiform and nonasbestiform varieties (Wylie, 1979).

The apparent orthorhombic optics of the asbestiform varieties of monoclinic amphiboles imply that the fiber is composed of many crystals whose chain directions are parallel but differently rotated about [001]. Supporting observations were obtained from single-crystal diffraction patterns. Wylie (1979) found that the reciprocal lattice points in the [001] zone of thin actinolite asbestos fibers form a continuous line in Weissenberg patterns. Zoltai (1979) found the same effect in precession photographs of thin (10 μm diameter) fibers of grunerite asbestos.

The ((100)) twinning is not unknown in prismatic or acicular amphibole crystals. However, in monoclinic asbestos fibers, polysynthetic twinning on the ((100)) plane is frequent, and the twin lamellae may be very thin. In crocidolite and "amosite" the lamellae can be as thin as a few nanometers, while in some tremolite asbestos fibers twin planes are almost non-existent (Chisholm, 1973; Whittaker, 1979). Stacking faults on the (100) plane and planar faults on the (010) and (110) planes also appear to be common in fibrous amphibole crystals (Chisholm, 1973, 1975; Hutchison *et al.*, 1976). Twinning and stacking faults may account for the orthorhombic optical properties of monoclinic asbestos. A more satisfactory explanation was offered by electron microscope observations of the cross sections of brittle and flexible asbestos fibers. Apparently, the fibers contain differently oriented single-crystal fibrils. An excellent photograph taken by Alario Franco *et al.* (1977) is reproduced in Figure 4a. The different types of grain boundaries were studied by Veblen (1980). Figure 4b shows one of these low-angle (99°) boundaries observed in anthophyllite asbestos. A more complex boundary, containing different chain-width defects, was described by Crawford (1980) and is shown in Figure 4c. The presence of differently oriented fibrils and of different types of boundaries between fibrils can account fully for the observed optical and x-ray diffraction properties.

With the advent of the high-resolution electron microscope it became possible to observe some of the minute details of the crystal structures of minerals. Although some deviations from the known *average crystal structure* were already accepted (like domain structures), the high-resolution microscope offered unexpected variations (e.g., Buseck and Iijima, 1974; Czank and Liebau, 1980). One of the most exciting details was found in the crystal structures of pyroxenes, amphiboles and micas. It was known that the I-beam units of the pyroxenes and amphiboles were composed of similar chains of single and double tetrahedral width, and that both were derivable from the layer structures of the talcs and micas (or vice versa: see chapter by Veblen, this volume). It was not known, however, that intermediate-width tetrahedral chains also exist. Using x-ray diffraction followed by high-resolution electron microscopy, Veblen *et al.* (1977), for example, found two new minerals which are composed of triple tetrahedral chains (jimthompsonite) and of alternating double

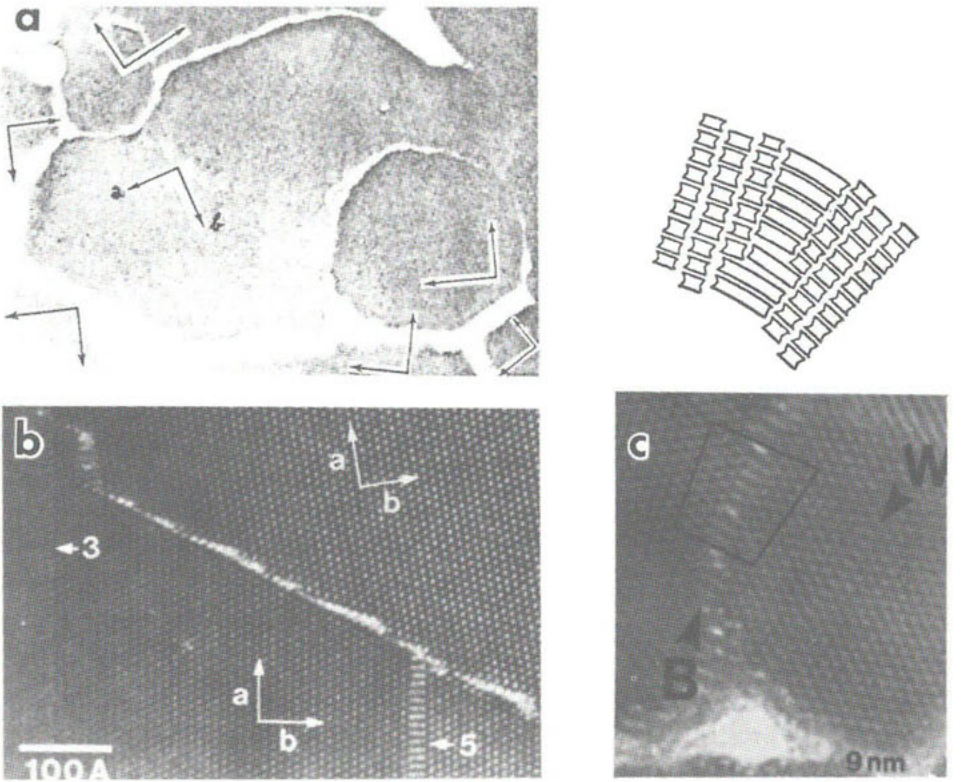

Figure 4. (a) Illustration of different crystallographic orientations of crocidolite fibers in a bundle. (After Alario Franco *et al.*, 1977.) (b) Low-angle boundary between anthophyllite fibers with triple and quintuple chain-width defects. (After Veblen, 1980.) (c) A complex boundary pattern between crocidolite fibers. (After Crawford, 1980.)

and triple chains (chesterite). The discovery of these minerals and observations on the intimate coexistence of micas, pyroxenes and amphiboles (Chisholm, 1975; Veblen and Buseck, 1979b, 1980) provided a strong impetus for the recognition of the mineral group name of *biopyriboles*. This name was introduced by Johannsen in 1911 and was revived by Thompson in 1970 to emphasize the similarities of the mica (*bio*tite), *pyro*xene, and amph*ibole* structures and their possible intermediates.

According to Thompson (1970), the structures of the minerals in this group can be visualized as being composed of *layer modules*, parallel to [010]; these structural relationships are described in the chapter by Thompson, this volume. A slightly different approach is followed here, using the mica modules of Thompson, which are the [010] single tetrahedral chain bands in the tetrahedral (*T*) - octahedral (*M*) - tetrahedral (*T*)

units in layered silicates. In line with the classification of layered silicates, which possess *di*- or *tri*-octahedral layers and *C* interlayer cations or vacancies, four types of layer modules can be recognized (Fig. 5): the *Di*, *Tri*, *DiC* and *TriC* modules. The width of these modules is one tetrahedral chain, and their height (t) is four times the height of an ideal polyhedral layer. These modules can be combined into complete crystal structures with a vertical displacement between the modules, $\tau = nt$; where n may be 0, 1/2, or 3/4. When n is equal to zero, the major layered silicates are produced. When n is equal to 1/2, the pyroxene structures occur, and when n alternatingly equals 0 and 1/2 between subsequent modules the amphibole structures are built. The sequence of n of 0 and 3/4 between modules produces palygorskite, and the sequence 0, 0, and 3/4 gives the sepiolite structure. The layer module constructions of the major biopyriboles are illustrated in Figure 6.

Structural defects in amphibole asbestos

The possible construction of the crystal structures of the biopyribole minerals from basic layer modules is more important than a simple descriptive scheme. It also illustrates a close genetic relationship among these minerals. Although each layer module construction pattern has a definite range of crystallization conditions, the differences between them may be relatively minor. Oversaturation, elevated temperature-pressure conditions, and instability of these and other parameters can cause structural faults, like the occasional incorporation of erroneous layer module combinations, in the same way that post-crystallization reactions can. Genetically, such "chain-width" errors are comparable to stacking errors in close-packed structures. Extremely rapid crystallization may also result in the development of similar errors. Whiskers under one-directional tension can grow almost instantaneously, and under some conditions asbestos fibers may grow rapidly. One of these reasons or a combination of some or all of them may be responsible for layer module defects in amphibole asbestos, as well as for the coexistence and structural continuity of different biopyribole minerals, such as those described by Veblen (1980) in the anthophyllite occurrence at Pelham, Massachusetts.

The existence of a certain type of planar defect in non-stoichiometric crystals was suggested by Wadsley (1955). These structural faults

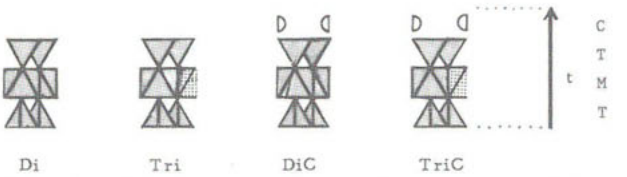

Figure 5. Illustration of the four basic layer modules of the biopyriboles. The tetrahedra are completely rotated so that the anions are in close-packed sheets. *Di* = dioctahedral, *Tri* = trioctahedral, *C* = interlayer cation. The second octahedra in Tri and TriC modules are dotted. (Intermediate layer module, not shown, is ½*Tri*, intermediate between *Di* and *Tri*; ½*C* indicates that one-half of the *C* sites are vacant.)

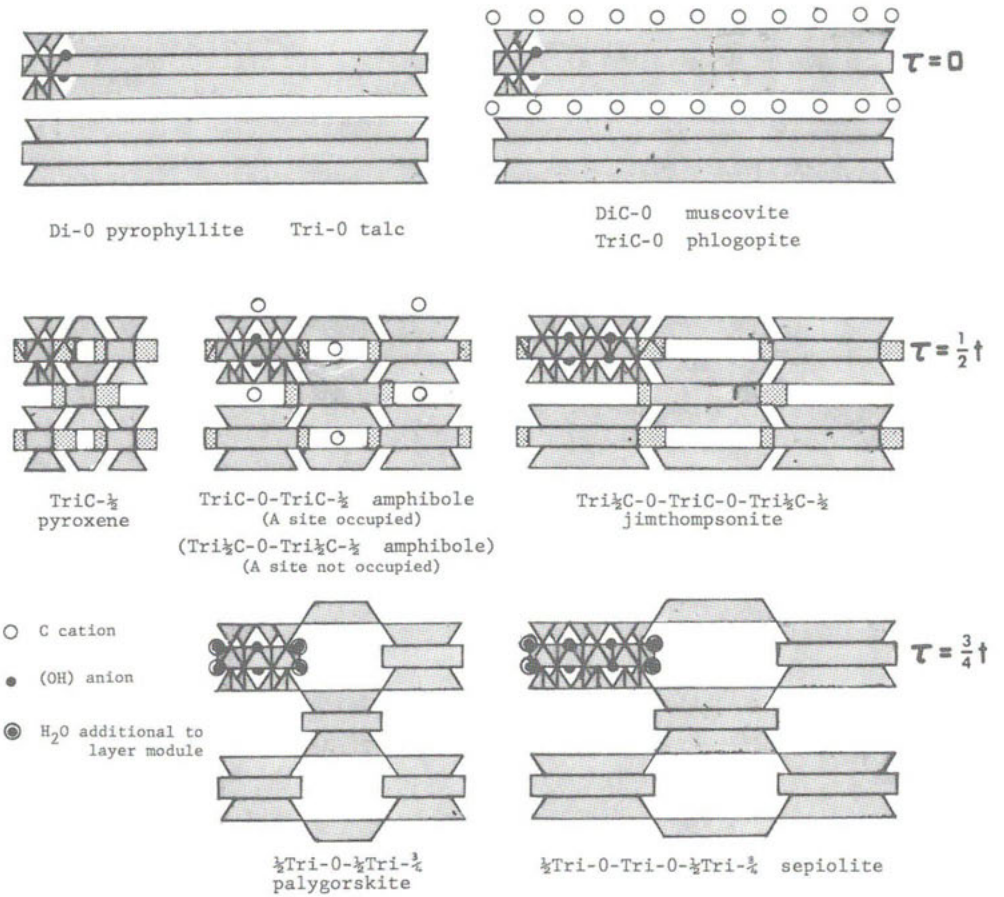

Figure 6. Illustration of the layer module construction of the major mineral groups of the biopyriboles. Note that in pyroxene a half *Tri* and a half *C* cation constitute the *M*-II octahedra, and in amphibole two ½*C* cations make up the *M*-IV cation.

are mistakes in the ordering of crystallographic shear planes and are usually referred to as Wadsley defects. Chisholm (1973) observed the streaking of the b^* diffractions in amphibole fibers and interpreted that as being due to the presence of faults in crystallographic shear planes, that is, Wadsley defects (Fig. 7). Hutchison *et al.* (1975, 1976b) published high-resolution electron microphotographs that clearly identify Wadsley defects as triple-chain layers in the (010) plane. Subsequently, the presence of triple-chain layer defects have been observed in all the major amphibole asbestos fibers (crocidolite, anthophyllite, actinolite-tremolite and cummingtonite-grunerite) as well as in the fibers of nephrite (Hutchison *et al.*, 1976a; Jefferson *et al.*, 1978; Mallinson *et al.*, 1980).

It has also been found that triple-chain defects may not be limited to layers, but rather may be isolated or form different patterns of grouping. Furthermore, quadruple-, quintuple- and sextuple-chains were found in different asbestiform amphibole fibers (Hutchison *et al.*, 1976a,b; Mallinson *et al.*, 1980). Even wider chains, up to more than 300 times the single chain width, were reported in the biopyriboles from Chester (Veblen *et al.*, 1977; Buseck and Veblen, 1978; Veblen and Buseck, 1979b, 1980). Figure 8 illustrates quadruple and quintuple chain defects in a matrix of a disordered double and triple chain structure (Veblen and Buseck, 1979b).

In c-axis orientation, slabs of chain defects resemble "zippers." The various types of zipper terminations were surveyed by Veblen and Buseck (1980). Most zippers appear to terminate coherently without other coordinated defects; other terminations are accompanied by displacive faults. Figure 9 shows a rather spectacular displacive termination. An interesting termination pattern, resembling coupled edge dislocations (Mallinson *et al.*, 1980), is shown in Figure 10.

The observation of these unusual structural details in amphibole asbestos fibers, combined with the apparent absence of the same features in most non-fibrous amphibole crystals strongly implicates that they may hold the secret to the unusual properties of amphibole asbestos. Chisholm (1975) postulated that "the (010) Wadsley defects inhibit the propagation of ((110)) cleavage cracks" and that they "may also play a part in accounting for the high strength ... the most important and

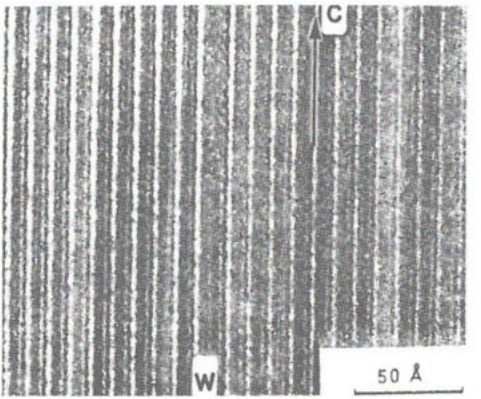

Figure 7. An early TEM photograph illustrating Wadsley defects (*W*) in "amosite". (After Hutchison *et al.*, 1974; as interpreted by Chisholm, 1975.)

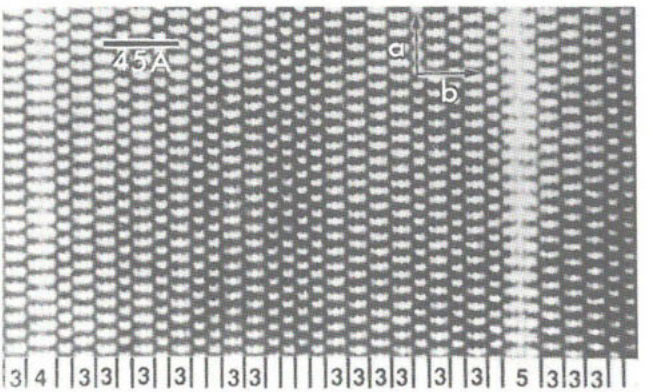

Figure 8. Illustration of triple, quadruple, and quintuple chain width defects in a TEM photograph of anthophyllite. (After Veblen and Buseck, 1979b.)

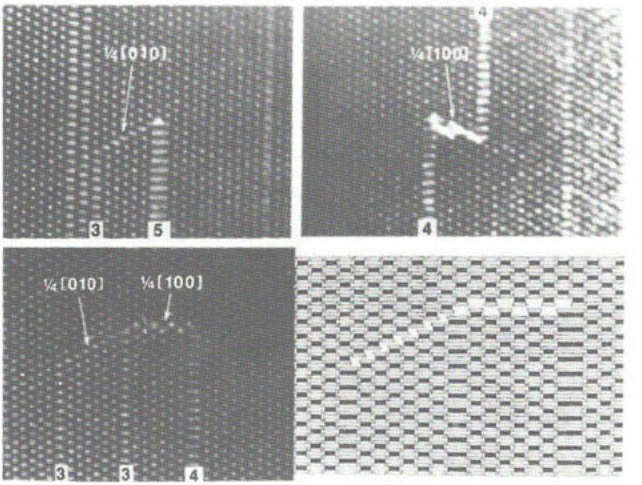

Figure 9. TEM photographs and the interpretation of a displacive fault termination of "zippers" in a *c*-axis orientation of anthophyllite. (After Veblen and Buseck, 1980.)

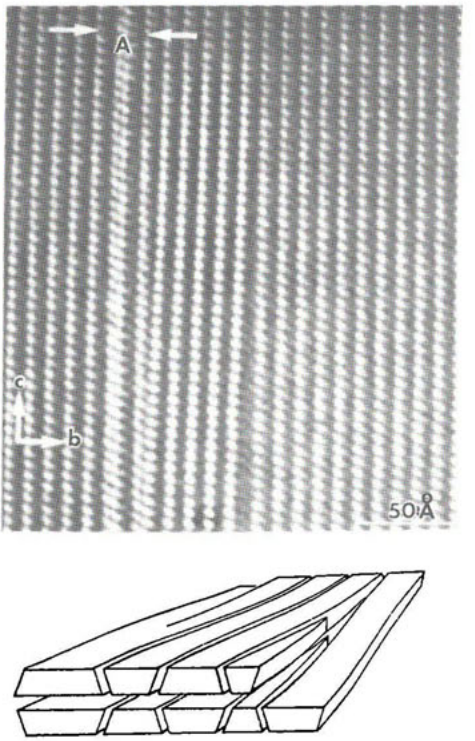

Figure 10. TEM photograph and the interpretation of longitudinal termination of chain-width defects in a fiber of nephrite. (After Mallinson *et al.*, 1980.)

remarkable properties of asbestos." Veblen (1980) took a different view. He states that "the primary mechanism for the formation of individual fibers must be the separation of the crystallites along grain boundaries." However, he also believes that in some asbestos fibers (from Chester, for example) "breakage along the (010) chain-width errors and the (100) exsolution lamellae and stacking faults" is the mechanism for the separation of fibers and fibrils; such breakage was observed with TEM. Crawford (1980) found no indication for such cleavage along (010). Instead, he observed cleavages along (100) faults in crocidolites and found that all cleavages propagated in the presence of (010) Wadsley defects without interference.

At this point it is not possible to connect chain-width defects with the development of the asbestos properties. The existence of wider chain defects would be expected to increase the surface energy and require more force to complete the fracture along the normal ((110)) cleavage plane. Conversely, it is also conceivable that there is a

significant concentration of stress around the misfit edges and longitudinal terminations of the chain-width defects. Such stress concentrations could enhance the cleavage of fibers. The same stress concentrations, however, would also decrease the strength of the crystals.

Whittaker (1979) has expressed skepticism about the possible explanation of the properties of asbestos fibers with the observed defects. Instead, he suggests that "The key to the problem is perhaps to be found in the work of Cook and Gordon (1964)" who have demonstrated that the strength of "cleaving whiskers" is increased through the longitudinal propagation of cracks along the cleavage planes. Whittaker proposes that an analogous situation may exist in fibers. The adhesion between fibers and fibrils is weaker than the bonds within the crystals. Initial cracks in the surface fibrils may be diverted to progress between and along fibrils before they break across the internal fibrils.

The spiral growth of many types of whiskers around a central screw dislocation has been demonstrated by Sears (1953) and by others, and has been suggested for quartz fibers by Frondel (1978). The possible growth of asbestos fibers around screw dislocations was raised by Walker and Zoltai (1979), and was proposed as a possible mechanism responsible for the unusual dissolution patterns observed in some amphibole asbestos (Walker, 1981). Whittaker *et al.* (1981) have interpreted structural irregularities in some grunerite asbestos ("amosite") fibers as screw dislocations with Burgers vectors having a $\frac{1}{2}c$ component.

It has been generally accepted that the exceptionally high strength of the whiskers is a consequence of their low surface defect density. In the following section it will be shown that the surface structure of a fiber must be different from its internal structure, that the surface structure by itself or through the low density of surface defects may be responsible for the strength and flexibility of the fibers, and that the strength of the surface structure appears to affect the strength of all fibers.

THE SURFACE STRUCTURE OF FIBERS

The bonding of atoms or ions on the surface *must be different* from that inside the crystal. The bonding pattern inside the crystal extends

in three dimensions. However, there are only two dimensions available for the termination of the structure on the surface, and thus a different structural scheme has to be developed. In the early 1930's crystallographers speculated on the possible patterns of surface structures. From their observation of the lower-than-theoretical strength of crystals arose a concentrated study on defective surface structures which could explain the weakness of the crystals. Mosaic, block, and lineage structure concepts and the relevance of dislocations to crystal strength were proposed. During the following decades, the importance of these concepts have been amply demonstrated, and modern material science is heavily dependent on their applications.

It is equally conceivable, however, that the surface structure is not weaker, but stronger than the internal structure of the crystal. In order to balance the incomplete bonds on the surface, some bond distances may become shorter and additional atoms or ions may be incorporated in the surface structure. Such modifications of bonding may produce a layer of exceptionally strong surface. Surface structures of asbestos or whisker fibers have not been investigated yet. However, the surface structures of other crystals have been studied by LEED (Low Energy Electron Diffraction) and Auger electron spectroscopy. Several features, such as shorter bond length, which may increase the strength of the surface structure, have been observed. The composition of the surface layer in small Al_2O_3 (corundum) crystals, for example, was found to contain higher cation-anion ratios. These ratios were found to be as high as 2:1, giving the formula of as Al_2O (French and Somorjai, 1970). Such an increase in the cation-anion ratio suggests stronger cation-anion bonds. The possible existence of strong surface structure was proposed by Griffith (1921), Orowan (1933), Weibull (1939), and others, in reference to the explanation of the strength of glass fibers and whiskers.

The increase in the strength of the surface structure can be augmented by decreased surface defect density. This, of course, constitutes an additional modification of the surface structure. The lower density of surface defects was observed in whiskers by a relatively large number of authors. More recently, Walker (1981) has shown that the density of surface defects, as illustrated by the density of etch

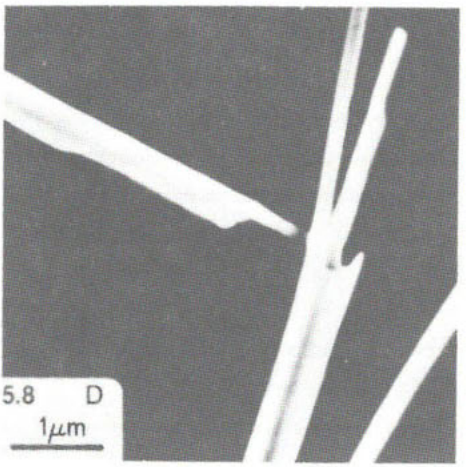

Figure 11. Illustration of the dissolution of a grunerite asbestos fiber ("amosite") in acids. This dissolution pattern indicates that the surface layer is more resistant to the acid than the fiber's internal structure. (After Walker, 1981.)

pits, is lower in amphibole asbestos than in cleavage fragments. He also found that the extended dissolution of cleavage fragments proceeds along cleavage planes and produces subsequently smaller acicular cleavage fragments before the complete dissolution of the mineral. By contrast, the dissolution of high quality asbestos fibers is initiated at the end of the fiber and proceeds inward before the surface layer is dissolved. This is illustrated by the initial development of inverted dissolution cups at the end of the fiber and by partially developed cylindrical structures, as shown in Figure 11.

The overall strength of an asbestos fiber is the composite of the strength of the surface and the internal structure of the fiber. The relative weight of the two strengths is proportional to the ratio of the surface area and the volume of the fiber. That ratio increases as the diameter of the fiber decreases.

The increasing strength of wires with decreasing diameter was first observed by Karmarsch in 1859. In the following 125 years, over a hundred similar observations were reported. Most of these studies were done on glass fibers and on whiskers. Only two investigations (Nadgornyi *et al.*, 1965; Aveston, 1969) involved natural (chrysotile, crocidolite, and anthophyllite) and synthetic (Mg-fluorichterite and Li-fluoramphibole) asbestos fibers. These experiments suggested that the role of the surface structure dominated the strength of both major types of asbestos, chrysotile and amphiboles (Fig. 12).

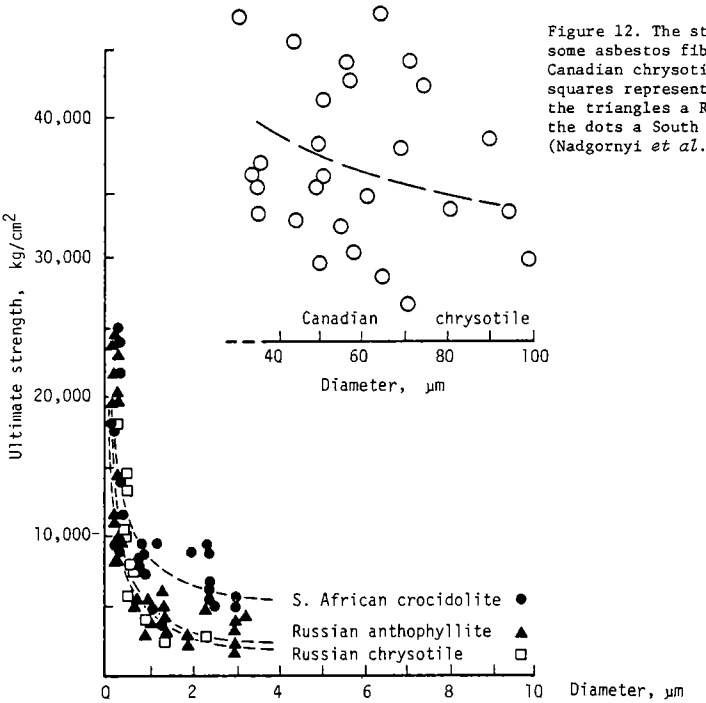

Figure 12. The strength-diameter graph of some asbestos fibers. The circles are of Canadian chrysotile (Aveston, 1969). The squares represent a Russian chrysotile, the triangles a Russian anthophyllite, and the dots a South African crocidolite (Nadgornyi *et al.*, 1965).

If we assume that the strong surface layer is only a couple of atoms deep and is uniform throughout the fiber, the proportional significance of the surface and the internal structure can be expressed by a simple equation:

$$\sigma_f = \sigma_i(1 + K\frac{As}{V}) \qquad (1)$$

where σ_f is the strength of the fiber, σ_i is the internal strength of the fiber, K is a constant expressing the increased strength of the surface structure, As is the surface area and V the volume of the fiber per unit length. It should be noted that the meaning of the internal strength in this equation is not necessarily the strength of the internal structure, but is a hypothetical value of strength where the internal and the surface structures are in balance and the ultimate fracture may be initiated anywhere in the fiber.

In the majority of the available strength-diameter measurements, the internal strength of the fibers, σ_i, is near the known "bulk" strength of the glass or the single crystal strength of the corresponding inorganic compound or mineral, within a range of expected experimental error. These fibers may be referred to as *type S* (*s*ingle crystal strength). In some

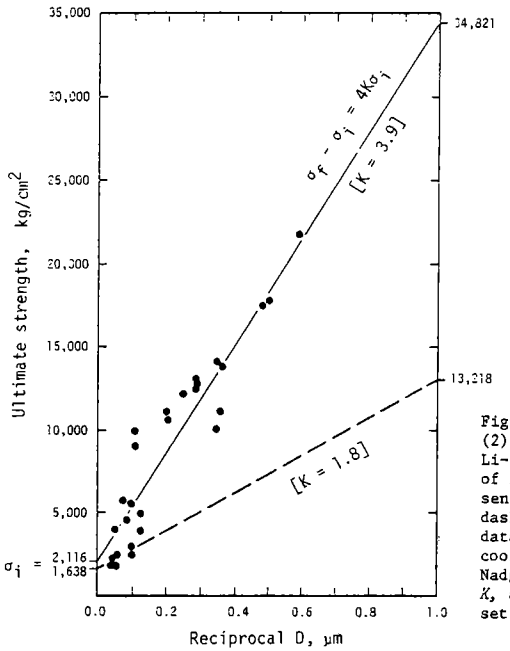

Figure 13. Graphical illustration of equation (2). The dots are the data from the synthetic Li-fluoramphibole asbestos cooled at the rate of 1.3°C per hour, and the solid line represents the linear regression of these points. The dashed line is the linear regression of similar data of the same Li-fluoramphibole asbestos cooled at the rate of 10°C per hour. (Data from Nadgornyi *et al.*, 1965.) The values of σ_i, of *K*, and of σ_f at 1 μm diameter are shown for each set of synthetic asbestos.

fibers the internal strength is significantly greater than the bulk or single crystal strength and may be referred to as *type X* (*e*xtra strong). As expected from their tubular or scroll-like structures, chrysotile asbestos and graphite whiskers are in this category. In some other fibers the internal strength is lower than the accepted bulk or single crystal strength. Yet, the fibers become stronger through the effect of the surface structure. These fibers may be classified as *type W* (*w*eak).

Most fibers are either circular, square, or hexagonal in cross section. They have the same surface area to volume ratio, provided that D is either the diameter of the circle, or is measured between parallel faces of square or hexagonal cross section fibers. Accordingly, for most fibers, equation (1) can be simplified to:

$$\sigma_f = \sigma_i(1 + K\frac{4}{D}) . \qquad (2)$$

The measurement of the ultimate strength of different diameter fibers can be plotted into a graph format, such as the one shown in Figure 13. The ordinate is the ultimate strength of the fiber (σ_f), and the reciprocal of the diameter (1/D) is the absissa. The Y intercept of the linear regression of the data points gives the value of the internal

Table 1. The parameters of the mechanical properties of natural and synthetic asbestos fibers.

Material	Type	σ_i kg/cm^2	K	k	Projected σ_f at D=1μm	Correlation coefficient	Number of points	Reference
Chrysotile (from Canada)	X	28,700	+2.1	+0.7	$>10^6$	0.68	30	Aveston (1969)
Chrysotile (from Bazhenovskii)	W	2,450	+1.0	+0.1	127,000	0.88	11	Nadgornyi et al. (196
Crocidolite (from Africa)	X	6,150	+0.6	-	22,100	0.77	28	Nadgornyi et al. (196
Anthophyllite (from Seysert)	X	3,000	+1.5	-	21,000	0.81	31	Nadgornyi et al. (196
Synthetic:								
Mg-fluor-richterite	S	2,950	+1.8	-	24,000	0.83	46	Nadgornyi et al. (196
Li-fluoramphibole (cooling 10°C/hour)	S	1,650	+1.8	-	13,200	0.92	27	Nadgornyi et al. (196
Li-fluoramphibole (cooling 1.3°C/hour)	S	2,150	+3.9	-	35,000	0.92	23	Nadgornyi et al. (196

strength (σ_i), and K can be calculated from the slope of linear regression line as:

$$K = \frac{D}{4}\left(\frac{\sigma_f}{\sigma_i} - 1\right) . \qquad (3)$$

Nadgornyi *et al.* (1965) measured the diameter dependent strength of crocidolite from South Africa and anthophyllite from Seysert, Russia, and synthetic asbestos, including Mg-fluor-richterite and an Li-fluor-amphibole. The fiber parameters (σ_i and K) as calculated from their data are given in Table 1. The correlation coefficients (Pearson Moments) of the regression lines are reasonably good. The internal strengths of the fibers are essentially within the range of the expected single-crystal strength of amphiboles. The only apparent exception is crocidolite, which has more than double the internal strength of the others. Although the number of strength-diameter measurements provided by Nadgornyi *et al.* are insufficient to justify firm conclusions, it is interesting to note that this high internal strength of crocidolite is in accord with the generally accepted opinion that crocidolite is the strongest amphibole asbestos. The higher internal strength of crocidolite also appears to be in accord with the observed lower density of chain-width defects in crocidolite than in anthophyllite and grunerite asbestos (Whittaker, 1979).

Equation (1) cannot be satisfactorily used for a large number of whiskers as the calculation gives negative internal strengths. Such is the

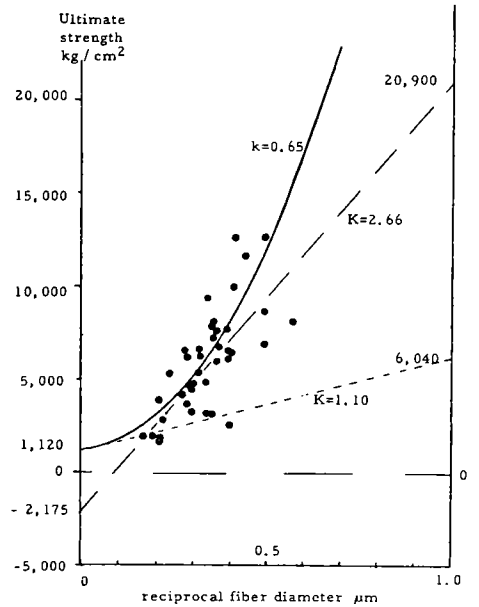

Figure 14. The strength-diameter graph of Cu_6Sn_5 whiskers (Davies, 1964). The dashed line is the linear regression of these points, giving a negative value for internal strength. The curved, solid line is the exponential fit of equation (4) giving a realistic value for the internal strength of these whiskers.

case of the Cu_6Sn_5 whiskers shown in Figure 14 (Davies, 1964). In these fibers the relative weight of the strength of the surface structure increases more rapidly with decreasing diameter than that allowed by the surface area to volume ratio at any value of K.

In the derivation of equation (1), the strong surface structure was assumed to have practically no depth. With that assumption, the relative weight of the surface strength was related to the surface area of the fiber, rather than to the volume of the surface layer. There are several other possibilities: (a) It is conceivable that the stronger bonds of the surface structure may extend deep into the fiber, through the decreased length of the more distant bonds. (b) It is also possible that the small growth steps on the longitudinal surfaces as observed in some fibers become shallower with decreasing fiber diameter, and the stress concentration around the steps diminishes. This theory was introduced by Friedel in 1962 and Marsh in 1963 in order to explain the diameter-strength effect. (c) The increased weight of the surface strength in some fibers may also be explained by an indirect effect of axial cleavage.

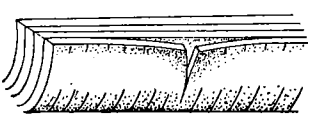

Figure 15. Illustration of the diversion of an initial crack by the axial cleavage of a "cleaving whisker".

Cook and Gordon proposed in 1964 that the propagation of surface cracks may be diverted by the axial cleavage in the so-called "cleaving whiskers." Figure 15 illustrates how an initial crack may be diverted after the first layer.

The nature and the geometric expression of these three possible causes for the increased effect of the surface structure are different. However, they are similar in the sense that their individual or combined effect on the fiber's strength can be expressed by an exponential factor, k. This exponential factor, still proportional to the surface area to volume ratio, can be added to equation (2):

$$\sigma_f = \sigma_i (1 + K\frac{4}{D})^{1+k\frac{4}{D}} \quad . \tag{4}$$

With this equation the calculated internal strength of the Cu_6Sn_5 whiskers becomes positive, with a magnitude that is comparable to the expected single-crystal strength of this sulfide (Fig. 14). Davies (1964) observed a relatively high density of surface steps in the Cu_6Sn_5 fibers, and the value of k may be an expression of the effect of these steps.

The increasing strength of the chrysotile fibers with decreasing diameter has long been known (Cosette and Delvaux, 1979). The strength-diameter data of the Russian chrysotile (Nadgornyi *et al.*, 1965) and the similar data of the Canadian chrysotile (Aveston, 1969) gave unrealistically low values for internal strength (e.g., 610 kg/cm^2 for the Russian chrysotile) when analyzed with equation (1). However, when equation (4) was used more realistic values were obtained (Table 1). In these fibers the constant k may be a consequence of the axial cleavage of the fibers. The two sets of chrysotile fibers appear to have significant differences in their mechanical properties. The internal strength of the Canadian chrysotile appears to be 10 times higher than that of the Russian. The higher internal strength of the Canadian chrysotile appears to be more realistic, as the rolled-up structure of the chrysotile is expected to increase the strength of the crystal. It is, of course, possible that the chrysotile of Nadgornyi *et al.* was of relatively poor quality. On the other hand, the scatter of the data points of the Canadian chrysotile (Fig. 12) is much broader than that of the Russian chrysotile. This may be due to differences in the

Table 2. The parameters of the mechanical properties of selected whiskers which have corresponding minerals.

Material	Type	σ_1 kg/cm^2	K	k	Projected σ_f at D=1μm	Correlation coefficient	Number of points	Reference
LiF	X	4,250	+0.4	+0.2	19,000	0.60	32	Fridman and Shpunt (1963)
KCl	S	120	+0.7	+0.3	2,250	0.71	22	Marsh (1963)
NaCl	S	90	+0.3	-	200	0.23	11	Ewald and Polanyi (1925)
NaCl	S	325	+0.6	+1.7	3,500	0.75	55	Gyulai (1954)
NaCl	S	450	+0.5	-	1,400	0.66	18	Marsh (1963)
NaCl (ceramic substrate)	S	250	+0.9	+0.7	7,600	0.84	42	Gyulai et al. (1961)
NaCl (foil substrate)	S	170	+1.5	+0.7	60,000	0.84	27	Gyulai et al. (1961)
NaCl (from alcohol solution)	W	100	+2.9	+1.0	949,000	0.74	46	Gyulai et al. (1961)
MgO	S	400	+6.1	+1.7	$>10^6$	0.76	6	Wolff and Cockren (1965)
ZnO	S	5,800	+0.6	+0.3	10,400	0.73	27	Evans et al. (1964)
SiO_2	X	5,000	+7.1	-	147,000	0.79	11	Reinkober (1931)
Al_2O_3	S	5,600	+4.1	+1.2	$>10^6$	0.76	36	Campbell (1970)
Al_2O_3 [100] fiber axis	X	13,000	+2.1	-	123,000	0.70	46	Bayer and Cooper (1967)
Al_2O_3	X	19,000	+2.1	-	178,000	0.61	27	Mehan et al. (1965)
Al_2O_3	X	21,000	+1.5	-	144,000	0.46	35	Mehan and Feingold (1965)
Al_2O_3 at 25°C	X	26,500	+2.3	-	266,000	0.78	15	Brenner (1962)
Al_2O_3 at 1,110°C	X	18,700	+2.5	-	205,000	0.66	28	Brenner (1962)
Al_2O_3 at 1,550°C	X	14,500	+0.7	-	57,000	0.66	12	Brenner (1962)
Al_2O_3 at 2,030°C	X	11,500	+0.5	-	36,000	0.20	10	Brenner (1962)
Al_2O_3	X	30,650	+2.5	-	341,000	0.62	32	Sutton (1970)
Al_2O_3 [001] fiber axis	X	35,000	+0.5	-	108,000	0.38	34	Bayer and Cooper (1967)
Al_2O_3	X	36,000	+0.2	-	100,000	0.39	40	Mehan and Feingold (1966)
Al_2O_3	X	38,000	+0.3	-	82,000	0.34	92	Mehan and Feingold (1967)
Al_2O_3	X	39,500	+0.6	-	139,000	0.60	33	Soltis (1967)
Al_2O_3	X	45,500	+0.5	-	130,000	0.39	26	Herzog (Mehan and Herzog, 1970)
Al_2O_3	X	49,500	+1.3	-	299,000	0.20	9	Cunningham (1960)
Al_2O_3	X	58,000	+0.5	-	150,000	0.63	33	Kelsey and Krock (1967)
Al_2O_3 [001] fiber axis	X	73,000	+0.3	-	166,000	0.66	29	Bokshtein et al. (1968)
Al_2O_3 [101] fiber axis	X	79,000	+0.2	-	146,000	0.49	62	Bokshtein et al. (1968)
Al_2O_3 [100] or [110] fiber axis	X	90,000	+0.2	-	164,000	0.47	38	Bokshtein et al. (1968)
Al_2O_3	X	16,000	+3.7	+1.2	$>10^6$	0.89	40	Regester et al. (1967)
C Grafil A	W	13,850	+0.9	-	64,000	0.31	11	Perry et al. (1971)
C Grafil HT (1,500°C)	W	7,150	+2.6	+0.9	$>10^6$	0.80	98	Lamotte and Perry (1970)
C Grafil A	S	24,000	-	-	24,000	0.31	96	Nicoll and Perry (1973)
C Grafil HT	S	23,000	+0.4	-	61,000	0.08	92	Nicoll and Perry (1973)
C Thornel 50	W	4,250	+2.4	+0.8	$>10^6$	0.40	36	Jones and Duncan (1971)
C PAN precursor	W	1,800	+4.6	+1.3	$>10^6$	0.41	36	Jones and Duncan (1971)
-same at 1,000-1,200°C	S	25,400	+0.2	+0.1	61,000	0.04	82	Jones (1971)

experimental techniques. For example, Aveston did not employ a rigid control on the length of the fibers. Further studies are needed before this puzzling question can be resolved.

Unfortunately, the quantity of information available on the strength-diameter relationships of asbestos fibers is limited to two publications. The publications on whiskers are more numerous, and many of the whiskers have mineralogical equivalents. The strength-diameter data of the latter category of whiskers is listed in Table 2. (For a more detailed development and discussion of the surface effect on the strength of fibers see Zoltai, 1981.)

Fiber length and strength

The decreasing strength of fibers with increasing length, at constant diameter, was also observed by many investigators. The first was Reinkober (1931). Figure 16 illustrates the same relationship observed in asbestos fibers (Zukowski and Gaze, 1959). These patterns are similar to those obtained for the diameter dependence of the strength. However, the strength-length relationship is not directly related to the diameter of the fiber.

Two somewhat related explanations have been offered for this phenomenon. One stipulates that longer fibers contain more short fibrils, and that premature fracture will occur by pulling the fiber apart along these shorter fibrils. The other explanation postulates that there are occasional high concentrations of strength-reducing defects in the fibers, and that they cause a rupture below the expected stress. These defect concentrations are expected to be more frequent as the length of the fiber increases. Both of these features act like "weak links" in the chain. If the distribution of shorter fibrils, defect concentrations, or both, are uniform, their effect on the strength of increasingly longer fibers can be statistically estimated (Tippett, 1925; Pierce, 1926; Weibull, 1939). Moreton (1969), for example, found an excellent match between the observed and calculated length-dependent strength pattern in some carbon whiskers.

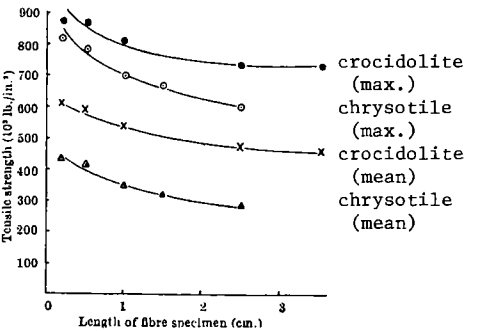

Figure 16. Illustration of the length dependence of the strength of some asbestos fibers. (After Zukowski and Gaze, 1959.)

Table 3. The mechanical properties of some polycrystalline materials expressed in terms of fiber parameters.

Material	Type	σ_i kg/cm^2	K	k	Projected σ_f at D=1um	Correlation coefficient	Number of points	Reference
Gold (2% Cu) wire	S	1,750	+121	-	780,000	0.93	3	Karmarsch (1859)
Silver wire	S	2,500	+79	-	800,000	0.95	5	Karmarsch (1859)
Steel wire	S	6,750	+122	-	over 10^6	0.96	5	Karmarsch (1859)
Zinc wire	S	1,250	+50	-	250,000	0.97	4	Karmarsch (1859)
Zinc wire	W	320	+47	-	60,000	0.91	9	Greenwood and Quarrell (1954)
Zinc wire	W	320	+14	-	18,000	0.91	29	Petch (1954)
René 41 wire	X	19,800	+5.9	-	500,000	0.98	7	Roberts (1961)
-same annealed	X	14,150	+1.7	-	110,000	0.94	6	Roberts (1961)
Steel wire (0.9% C)	X	32,000	+7.8	-	$>10^6$	0.99	4	Roberts (1961)
Tungsten wire	X	14,000	+3.6	-	210,000	0.96	27	Burwood-Smith (1970)
Molybdenum wire	X	7,300	+91	-	$>10^6$	0.99	5	Burwood-Smith (1970)
(0.5% Ti) Niobium wire	X	4,300	+400	-	$>10^6$	0.95	3	Burwood-Smith (1970)
Iron ignot	S	5,350	+3.3	-	76,000	0.97	26	Petch (1953)
Mild steel	S	5,800	+2.7	-	68,000	0.96	30	Petch (1953)
Cr-base alloy	S	2,400	+16	-	150,000	0.89	12	Havekotte et al. (1954)
Cr-base alloy	S	2,900	+28	-	325,000	0.99	10	Havekotte et al. (1954)
Martinsite 8650	X	15,000	+3.4	-	220,000	0.97	21	Grange (1966)
Martinsite 4340	X	13,500	+4.3	-	250,000	0.96	12	Grange (1966)
BeO	W	300	+26	+5.3	$>10^6$	0.97	5	Hyde et al. (1956)
Al_2O_3	S	1,650	+0.8	-	7,150	0.96	24	Spriggs and Vasilos (1963)
MgO (heat treated)	S	1,600	+0.7	-	7,550	0.86	13	Spriggs and Vasilos (1963)
MgO (machined)	S	1,000	+1.5	-	42,500	0.71	8	Spriggs and Vasilos (1963)

(Ultimate strength of wires is given as lower yield stress. The ceramic materials used are either nonporous or the data were corrected for porosity. Strength of ceramics usually measured as transverse bending strength.)

Fibers, crystals and fragments

In contrast to the strong surface structures of fibers, the surfaces of crystal fragments are expected to be weaker than the internal structure, as they are artificial surfaces and contain various types and sizes of defects introduced by the fracturing process. This argument holds for any fragment shape, including the acicular cleavage fragments of amphibole crystals. Consequently, cleavage fragments of amphibole crystals should yield the opposite strength-diameter effect than that observed in asbestos fibers. The strength of the fragments should decrease with decreasing fiber diameter and should yield negative values for K (and/or for k).

Unfortunately, there is no data available for the strength-diameter pattern of acicular amphibole cleavage fragments. (A project has been initiated at the University of Minnesota under the sponsorship of the U. S. Bureau of Mines, and some data are expected to be available by late 1981.) Some indirectly applicable data are available, however. Bartenev and Izmailova (1962) have investigated the mechanical properties of different diameter amorphous aluminoborosilicate fibers. They found that under normal conditions, the strength of the fibers increased with decreasing fiber diameter (K = +0.01 and σ_i = 21,500 kg/cm^2). After aging and exposing the fibers to stresses of thermal treatment, the diameter effect reversed its slope. The K value became negative (K = -0.01), while the internal strength remained the same (21,500 kg/cm^2). The surfaces of natural wool are also exposed to external abusement, and their surface structure is expected to become weaker. The reported strength-diameter data of wool (Mathews' Textile Fibers, 1947) provide such information. The calculated values of K are -2.0 and -0.7, for imported (Australian and British) and domestic wool, respectively.

Polycrystalline wires and aggregates

The strength-diameter effect observed in single-crystal fibers is demonstrated in polycrystalline wires as well. That is, most wires do not fracture along grain boundaries, but break across the grains. The effect of the strength of the surface structure of the grains appears to be comparable to that of single-crystal fibers.

Similar grain-size effects are observed in other polycrystalline materials, like martinsites and hot-pressed ceramics. The fracture of these materials also usually progresses across the grains, rather than along grain boundaries. Their tensile or bending strengths increase with decreasing grain size. That implies strongly that the surface structure and/or the intergranular bond is stronger than the internal strength of the single-crystal grains.

The cross sections of these polycrystalline substances resemble the cross sections of bundles of fibers, where the diameter of the grains corresponds to the diameter of the fibers. In this analogy the combined strength of the surface structure and the intergranular bond takes the role of the strength of the surface structure of fibers, and their strength can be approximated by the equations derived for fibers. Table 3 lists some of the available data on polycrystalline wires, plates and blocks, with the mechanical parameters derived by using equations (2) and (4). The validity of these calculations are, of course, functions of the validity of the assumption made in their comparison with bundles of fibers. Further studies are needed to test the merit of such comparison. Independent of the conclusions of such studies, the basic concept of a relationship between the strength of the surface and intergranular structure and the internal structure of the grains appears to be correct.

The unusual strength of the amphibole jade, nephrite, can be adequately explained by the strength of the fibers and their partial interlacing. The strength of the pyroxene jade (e.g., jadeite jade) cannot be explained by the same argument, because this jade does not contain fibers. It is composed of randomly-oriented prismatic or platy crystals (Fig. 17). Bradt *et al.* (1973) assume that the random orientation of the crystals and their cleavage planes may be responsible for the enhanced strength and toughness. It is also possible that the surface structures of the crystals and/or the intercrystalline bonds between the crystals may produce a strengthening effect. Strength measurements on pyroxene jades having different grain sizes could clarify the relative role of the two proposed causes of increased strength. The enhanced mechanical properties of nonfibrous, platy bowenites and quartzites, for example, may also have similar causes.

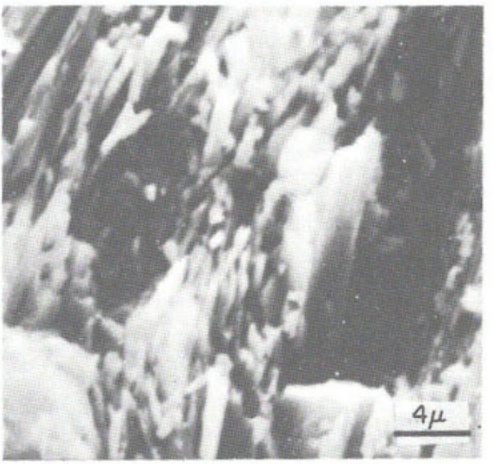

Figure 17. SEM photograph of the fracture surface of a jadeite jade. (After Bradt *et al.*, 1973.)

ORIGIN OF ASBESTOS AND WHISKER FIBERS

The natural-synthetic identity of asbestos and whisker fibers can be further enlightened by the comparison of the geological origin of asbestos fibers and the laboratory conditions maintained in the crystallization of whiskers. In the following, the respective origins of the two types of fibers will be briefly described, discussed and compared.

Whisker growth

The various methods of whisker growth are all characterized by the restrictive, one-directional growth of the crystals. This one-dimensional growth is achieved by crystallization conditions which either (1) forbid growth in other directions or (2) promote growth in only one crystallographic direction, or both. In the first case, the conditions can be produced by dense nucleation in one plane and free growth in a direction perpendicular or inclined to that plane. Such conditions for crystallization or recrystallization can exist in rocks, caused by strain relaxation and consequent one-dimensional tension. The laboratory design of such settings is rather difficult, however. It is simpler to design conditions which promote growth in one direction. Consequently, most whisker growth methods follow the second route of synthesis.

Whiskers can be crystallized both from solutions and from vapor, provided that the conditions allow growth in one direction only. One simple way to create such conditions is through restricted directional

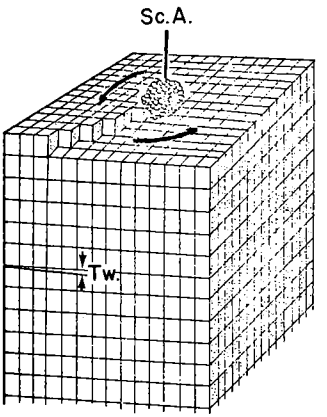

Figure 18. Illustration of the ever-present growth step (and kinks) of a central screw dislocation (*Sc.A.*). The direction of the growth is illustrated by arrows. One effect of this spiral growth, a twist in the fiber (*Tw*), can sometimes be observed.

supply of the material needed for growth. If a porous ceramic plate is partially submerged in a saturated solution, for example, whiskers will grow on the surface of the plate (Taber, 1916). This occurs by adding new material to the base of the crystal from the supply coming through the porous ceramic plate. Through capillary mechanisms the growth material is transported to the tip of the whisker, where it can evaporate. Whiskers may also be grown within a solution, provided, for example, that the crystal is structurally anisotropic and the level of saturation, temperature, and pressure conditions permit growth on one crystal face but are below the level required for growth on other faces. The one-dimensional growth of crystals from solution may also be caused by the existence of a central screw dislocation that provides ever-present growth steps and kinks on the face perpendicular to the screw axis (Fig. 18); fibrous crystals can develop through spiral growth. Screw dislocations are common in some types of whiskers (e.g., Eshelby, 1953; Sears, 1953; Webb *et al.*, 1957; Hamilton, 1960), and in some cases they are believed to be the exclusive cause of whisker growth (Evans, 1972).

Whiskers are commonly grown by vapor-condensation methods. Substances which will not decompose upon heating and can produce appreciable vapor pressure below the melting temperature can grow as whiskers by a direct evaporation-condensation process. The transportation of the source material to the cooler growth zone in the container is achieved by effusion. In the case of other materials, a chemical reaction is involved to lower the temperature of the process and to provide suitable transportation

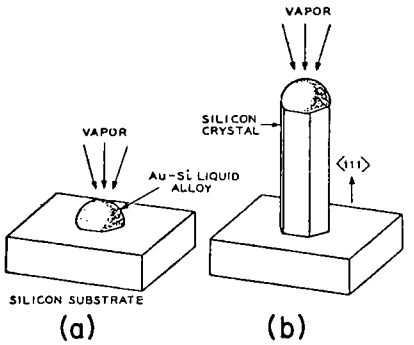

Figure 19. Illustration of the uni-directional growth of a fiber by the *VLS* mechanism. (After Wagner and Eillis, 1965.) The vapor condenses on a gold seed (*a*) in the cooler portion of the tube and initiates the crystallization of the fiber. The continuous condensation of the vapor on the tip of the fiber (*b*) provides the necessary material for the growth of the crystal.

agents (usually volatile oxides). Most refractory whiskers are grown by this process, including aluminum oxides, silicon carbides and nitrides. The chemical reaction provides a stable gaseous phase which can be transported to the growing whisker and supplies the material needed for growth. Although the theoretical understanding of this process is still developing, the so-called *VLS* (*V*apor-*L*iquid-*S*olid) mechanism of Wagner and Ellis (1965) is generally accepted. According to this theory, the vapor condenses on a suitable substrate or around nucleation seeds (usually gold). The impurities evaporate from this initial drop of liquid as crystallization proceeds (Fig. 19a). The subsequent crystallization of the whisker is assured by the continuous condensation of the vapor at the tip of the fiber (Fig. 19b). Whiskers grown by the *VLS* method usually do not have a central screw dislocation, except when such dislocations are continuations of the substrate surface (Evans, 1972).

Growth of fibers from solutions and by vapor-condensation requires special conditions, a balanced coexistence of a number of factors. It is conceivable that such conditions may exist in smaller, partially enclosed geologic units. However, neither of these growth processes or other less common whisker growth processes (like electrolysis) appear to be applicable to the explanation of the origin of the major asbestos deposits.

Origin of asbestos

The method of whisker growth which seems to offer the most reasonable comparison with the crystallization of major asbestos deposits is where the unidirectional growth is caused by unidimensional tension. A brief review of the geological environments of asbestos deposits indicates that

all major asbestos deposits are closely associated with structural activity which could produce unidirectional tension.

The overwhelming majority of commercial asbestos deposits contain columnar cross and slip fiber veins. As early as 1895 Merrill recognized ". . .the efficacy of pressure in the production of fibrous serpentine. . . ." He proposed that the presence of shearing stress is responsible for the crystallization of cross and slip fiber veins. Taber (1916) postulated that ". . .the fibrous structure must [therefore] be attributed to the circumstance that the material for growth was accessible only in one direction. . . ." Because of the columnar aggregation of the fibers, ". . .crystal growth may be limited to the direction of least pressure. . ." from whence the material for growth was available. According to Taber, the direction of "least pressure" was not related to the strain in the rocks, but was caused by the unidimensional source of growing materials. In fact, he states that the one-dimensional growth of fibers in the veins made ". . .room for themselves by pushing apart the enclosing walls." The force needed for "pushing the walls apart" was, accordingly, provided by the expansion of the crystallizing material. On the other hand, Graham (1917) believes that the decrease in the volume of the initial peridotite due to thermal contraction is greater than the increase in the volume due to later serpentinization. Thus, conditions of "differential pressure" develop in the rock. Therefore, the conditions are set for ". . .an expansive strain in one direction, which will determine the direction of elongation of the fibers." Peacock (1928) recognizes the possible importance of the "relief of pressure" as the cause of fibrous crystallization. However, he maintains that the primary cause of the fibrous growth is the ". . .control which boundary surfaces exert on the orientation of the structure of fibrous minerals crystallizing from solutions and gels."

Following these early studies, the relationship between unusual stress conditions and asbestos crystallization became broadly accepted. Vermaas (1952) concluded from his extensive studies of the South African amphibole asbestos deposits that the asbestiform varieties, "amosite" and crocidolite, are the stress habits of the corresponding minerals. Trendall and Blockley (1970) surveyed the northwest Australian banded iron formations and the associated amphibole asbestos deposits. They concluded

that the crystallization of crocidolite is limited almost exclusively to those locations in the folded rocks which were subjected to a "stress reversal" process. In his review, Anhauser (1976) refers to chrysotile as a "stress controlled" mineral and states: "Systematic structural studies in many asbestos deposits throughout the world have shown that cross-fiber asbestos seams require tensional conditions, whereas slip fibers are localized in planes along which shearing has taken place." Dreyer and Robinson (1978) make comparable statements concerning the crystallization of amphibole asbestos. They observed that "the greatest development of fiber occurs where two sets of folds intersect to form domes or basins." There does not seem to be any doubt among geologists that the development of vein-type asbestos deposits require certain stress-related structural conditions.

Although the majority of commercial asbestos deposits contain the fibers in veins, there are a few exceptions. Most of these deposits are relatively insignificant. The chrysotile deposit at Coalinga, California, however, is one of the important sources of asbestos in the United States (Mumpton and Thompson, 1975). The fibers are found in various aggregates and are of variable length and quality. They believe that the chrysotile was transformed from nonasbestiform antigorite and lizardite as "a result of intensive shearing that it [the rock] underwent during or after emplacement." The rocks in the commercially important anthophyllite deposits in Finland are also intensely deformed. [For a more detailed description of the geology of the major asbestos deposits, see the chapter by M. Ross (this volume) on the geological occurrence of amphibole asbestos.]

CONCLUSIONS

The crystal structures of amphibole asbestos fibers contain a variety of structural aberrations which are either unique to this crystallization habit, or that occur more frequently in fibers than in other crystals. It is conceivable that further studies will relate a few of these structural defects with some of the properties of asbestos fibers. However, the structural features observed so far fail to explain their total physical properties.

A comparison of the properties of asbestos, whisker, and glass fibers indicate that there is a basic similarity between their properties and

that there may be a fundamental structural character common to all fibers. This common character of fibers appears to be the exceptional strength of their surface structures. The surface structure of a crystal must be different from the internal structure of the crystal, as one dimension of bonding is not available at the surface. It is conceivable that the bonding of atoms in the surface layer of some crystals may be significantly stronger than that of the basic internal structure of the crystal. The unusual unidirectional growth of the fibers produces continuous and consistent parallel surfaces, and this may represent the conditions needed for the development of strong surface structures. The possible validity of this theory is supported by the observation that the strength of fibers increases with decreasing diameter, in proportion to the ratio of the surface area (or the volume of the surface layer) to the volume of the fiber. This observation appears to be valid even for fibers which contain tubular or scroll-like structures. The stronger surface structure theory is further supported by the apparently better quality of the surfaces of fibers than of other crystals. This is demonstrated by the smoother and shinier appearance of the fiber surfaces.

The hair-like shape and the strong surface structure of the fibers develop during the unidirectional growth of the crystal. The conditions for unidirectional growth can be provided by various methods. For the development of major asbestos deposits the conditions are set by one-dimensional tension. As the quality and the magnitude of the conditions can be variable, the quality of the asbestos properties of the fibers can also vary. Fine (cc. < 15 μm in diameter) and well-developed (strong and flexible) fibers, when crystallized in bundles, are referred to as asbestiform. Larger elongated crystals are called capillary, filamentary, or acicular, instead of fiber.

In different deposits the conditions of crystallization may be different, and asbestiform fibers of the same mineral may exhibit different degrees of asbestos properties (strength and flexibility). They may also have different biological activities. Pott *et al.* (1974, 1976) and Palekar *et al.* (1979) have demonstrated that cleavage fragments and asbestos fibers of different qualities appear to have differences in the level of their biological properties, including hemolitic activity, cytotoxicity, and possibly carcinogenecity. Stanton and Layard (1979) concluded that "the

carcinogenecity of asbestos is greatly reduced if asbestos is heated sufficiently to increase its fragility," i.e., to destroy its asbestos properties.

Abrahamson, E. P., II (1968) The influence of grain refinement on some mechanical properties. In *Surfaces and Interfaces II*. J. L. Burke, N. O. Reed and V. Weiss, eds. Syracuse Univ. Press, 262-269.

Alario Franco, M. A., Hutchison, J. L., Jefferson, D. A., and Thomas, J. M. (1977) Structural imperfections and morphology of crocidolites (blue asbestos). Nature 266, 520-521.

Anhauser, C. A. (1976) The nature of chrysotile asbestos occurrences in Southern Africa: A review. Econ. Geol. 71, 96-116.

Aveston, J. (1969) The mechanical properties of asbestos. J. Materials Sci. 4, 625-633.

Bartenev, G. M., and Izmailova, L. K. (1962) Defect-free glass fibers. Akad. Nauk. SSSR, Chem. Techn. Sec. 146, 196-198.

Bayer, P. D., and Cooper, R. E. (1967) Size-strength effects in sapphire and silicon nitride whiskers at 20°C. J. Materials Sci. 2, 233-237.

Bokshtein, S. Z., Koshkin, S. T., and Svotkov, I. L. (1963) Tensile testing of filament crystals of copper, nickel and cobalt to failure. Sovj. Phys. Solid State 4, 1271-1277.

_____, Koshkin, S. T., Nazarrova, M. P., and Svetlov, I. I. (1968) Size effect and anisotropy in the strength of sapphire crystal whiskers at room temperature. Sovj. Phys. Solid State 9, 1488-1494.

Bowen, G. T. (1822) Analysis of a variety of nephrite from Smithfield. Amer. J. Sci. Arts 5, 346-348.

Braitsch, O. (1957) Über die natürlichen Fäser und Aggregationstypen beim SiO_2, ihre Verwachsungsformen, Richtungstatistik und Doppelbrechung. Heidelberg. Beitr. Mineral. Petrogr. 5, 331-372.

Bradt, R. C., Newnham, R. E., and Biggers, J. V. (1973) The toughness of jade. Amer. Mineral. 58, 727-732.

Brenner, S. S. (1962) Mechanical behavior of sapphire whiskers at elevated temperatures. J. Appl. Phys. 33, 33-39.

Burwood-Smith, A. (1970) Mechanical properties of refractory metal wires for high temperature reinforcement. Fibre Sci. Technol. 3, 105-117.

Buseck, P.R., and Iijima, S. (1974) High resolution electron microscopy of silicates. Amer. Mineral. 59, 1-21.

_____, and Veblen, D. R. (1978) Trace elements, crystal defects and high-resolution electron microscopy. Geochim. Cosmochim. Acta 42, 669-678.

Caillère, S. (1936) Contribution a l'etude des minereaux de serpentines, *and* Etude de quelques silicates magnesiensa facies asbestiform ou papyrace n'appartentant pas au groupe de l'antigorite. Bull. Soc. Franc. Mineral. 59, 163-326 and 353-374.

Campbell, W. B. (1970) Growth of whiskers by vapor-phase reactions. Chapter 1 in *Whisker Technology*, A. P. Levitt, ed., Wiley Intersci., New York.

Chester, A. H. (1877) On a fibrous variety of sepiolite from Utah. Amer. J. Sci. 8, 475-483.

Chisholm, J. E. (1973) Planar defects in fibrous amphiboles. J. Material Sci. 8, 475-483.

_____, (1975) Crystallographic shear in silicate structures. Chapter 5 in *Surface and Defect Properties of Solids*, Chem. Soc. London, 4.

Cook, J. E., and Gordon, J. E. (1964) A mechanism for the control of crack propagation in all-brittle systems. Proc. Royal Soc. London 282 A, 508-518.

Cosette, M., and Delvaux, P. (1979) Technical evaluation of chrysotile asbestos ore bodies. Mineral Assoc. Canada Short Course Handbook 4, 79-110.

Cradwick, P. D. G., Farmer, V. C., Russel, J. D., Masson, C. R., Wada, K., and Yoshinaga, N. (1972) Imogolite, a hydrated aluminium silicate of tubular structure. Nature Phys. Sci. 240, 187-189.

Crawford, D. (1980) Electron microscopy applied to studies of biological significance of defects in crocidolite asbestos. J. Microscopy 120, 181-192.

Cressey, B. A., and Zussman, J. (1976) Electron microscopic study of serpentines. Canadian Mineral. 14, 307-313.

Cunningham, A. L. (1960) Mechanism of growth and physical properties of refractory oxide fibers. Horizons Contr. NOnr-2619(00).

Czank, M., and Liebau, F. (1980) Periodicity faults in chain silicates: a new type of planar lattice fault observed with high resolution electron microscopy. Phys. Chem. Mineral 6, 85-93.

Dana, J. D. (1950) *A System of Mineralogy*, 3rd edition, John Wiley & Sons, New York.

Dana, E. S. (1914) *The system of Mineralogy of James Dwight Dana: Descriptive Mineralogy*, John Wiley & Sons, New York.

Davies, G. J. (1964) On the strength and fracture characteristics of intermetallic fibres. Phil. Mag. Ser. 8, 9, 953-964.

Dietrich, V., de Quervain, F., and Nissen, H. U. (1966) Tourmalinasbest aus alpinen Mineralkluften. Min. Pet. Mitt. 46, 695-697.

Dreyer, C. J. B., and Robinson, H. A. (1978) The occurrence and exploitation of amphibole asbestos in South Africa. Soc. Mining Eng. of AIME, Preprint No. 78-H-64.

Eshelby, J. D. (1953) Screw dislocations in thin rods. J. Appl. Phys. 24, 176-179.

Evans, C. C., (1972) *Whiskers*. M and B Monograph ME/8. Mills and Boon Ltd., London.

_____, Gordon, J. E., and Marsh, D. M. (1964) The strength of whiskers of silicon, zinc oxide and phthalocyanine. Proc. Royal Soc. London 282 A, 218-220.

Ewald, W., and Polanyi, M. (1925) Plastizitat und Festigkeit von Steinsalz unter Wasser. Z. Physik. 31, 29-50.

Fedoseev, A. D., Grigoreva, L. F., Chigareva, O. G., and Romanov, D. P. (1970) Synthetic fibrous fluoramphiboles and their properties. Amer. Mineral. 55, 854-863.

Fersmann, A. (1908) Ueber die Palygorskitgruppe. Bull. Acad. Imper. Sci. St. Petersbourg, 2, 255-274.

Fleischer, M. (1949) Discredited minerals. Amer. Mineral. 34, 339.

French, T. M., and Somorjai, G. A. (1970) Composition and surface structure of the (0001) face of α-alumina by low energy electron diffraction. J. Phys. Chem. 74, 2489-2495.

Fridman, V. Y., and Shpunt, A. A. (1963) Investigation of the strength of lithium fluoride crystal fragments. Sovj. Phys. Solid State 5, 575-579.

Friedel, J. (1962) *Electron Microscopy and the Strength of Crystals*. John Wiley & Sons, New York, 605 pp.

Frondel, C. (1962) *The System of Mineralogy. Silica Minerals. Vol. III*. John Wiley & Sons, New York.

_____. (1978) Characters of quartz fibers. Amer. Mineral. 63, 17-27.

_____. (1980) Personal communication.

Graham, R. P. D. (1917) Origin of massive serpentine and chrysotile-asbestos, Black Lake, Thetford area, Quebec. Econ. Geol. 12, 154-202.

Grange, R. A. (1966) Strengthening steel by grain austenite refinement. Trans. A.S.M. 59, 26-48.

Greenwood, G. W., and Quarrell, A. G. (1954) Cleavage fracture of pure polycrystalline zinc in tension. J. Inst. Metals 82, 551-560.

Griffith, A. R. (1921) The phenomena of rupture and flow in solids. Phil. Trans. Royal Soc. London, Ser. A., 221, 163-198.

Gruner, J. W. (1946) The mineralogy and geology of the taconites and iron ores of the Mesabi Range, Minnesota. Comm. Iron Range Res. Rehab., Minn. Geol. Survey, 127 pp.

Güven, N., Hower, W. F., and Davies, D. K. (1980) Nature of authigenic illites in sandstone reservoirs. J. Sed. Petrol. 50, 761-766.

Gyulai, Z. (1954) Festigkeits- un Plastizitätseiegenschaften von NaCl-Nadelkristallen. Z. Phys. 138, 317-321.

_____, Hartman, E., and Jeszenszky, B. (1961) Zerreissfestigkeitsmessungen an NaCl-Nadelkristallen (Whiskers). Phys. Status Solidi 1, 726-729.

Hall, A. L. (1918) On the mode of occurrence and distribution of asbestos in the Transvaal. Trans. Geol. Soc. So. Africa 21, 1-36.

Hamilton, D. R. (1960) Interferonmetric determination of twist and polytype in silicon carbide whiskers. J. Appl. Phys. 31, 112-116.

Havekotte, W. L., Greenidge, C. T., and Cross, H. C. (1954) Chromium-base alloys. Proc. Amer. Soc. Test. Materials 50, 1101-1130.

Heddle, F. (1979) Pilolite, an unrecognized species. Mineral. Mag. 2, 206-219.

Huggins, C. W. (1962) Electron micrographs of some unusual inorganic fibers. U.S. Bur. Mines Rep. Invest. No. 6020, 27 pp.

_____, Denny, M. V., and Shell, H. R. (1962) Properties of palygorskite, an asbestiform mineral. U.S. Bur. Mines, Rep. Ivest. No. 6071, pp. 17.

Hutchison, J. L., Irusteta, M. C., and Whittaker, E. J. W. (1974) 8th Int. Congr. Electron Micros. 1, 492.

_____, _____, and _____ (1975) High-resolution electron microscopy and diffraction studies of fibrous amphiboles. Acta Crystallogr. A31, 794-801.

_____, Jefferson, D. A., Mallinson, L. G., and Thomas, J. M. (1976a) Structural irregularities in nephrite jade: an electron microscope study. Mat. Res. Bull. 11, 1557-1562.

_____, _____, and Thomas, J. M. (1976b) The ultrastructure of minerals are revealed by high resolution electron microscopy. Chapter 8 in *Surface and Defect Properties of Solids,* Chem. Soc. London, 6.

Hyde, C., Quirk, J. F., and Duckworth, W. H. (1956) Preparation of dense beryllium oxide. Chem. Eng. Prog. Nucl. Eng. Sympos. Ser. Part IV, 52, 105-112.

Jefferson, D. A., Mallinson, L. G., Hutchison, J. L., and Thomas, J. M. (1978) Multiple-chain and other unusual faults in amphiboles. Contrib. Mineral. Petrol. 66, 1-4.

Johannsen, A. (1911) Petrographic terms for field use. J. Geology 19, 317-322.

Jones, B. F. (1971) Further observations concerning the effect of diameter on the fracture strength and Young's Modulus of carbon and graphite fibers made from polyacrylonitrile. J. Mat. Sci. 6, 1225-1227.

_____, and Duncan, R. G. (1971) The effect of fiber diameter on the mechanical properties of graphite fibers manufactured from polyacrylonitrile and rayon. J. Mat. Sci. 6, 289-293.

Karmarsch, K. (1859) Ueber die absolute Festigkeit der Metalldrähte. Mitt. gew. Ver. Hannover, 137-156.

Kauffman, A. J. (1943) Fibrous sepiolite from Yavapai County, Arizona. Amer. Mineral. 22, 512-520.

Kelsey, R. H., and Krock, R. H. (1967) Tension testing alumina whiskers. J. Materials 2, 146-159.

Kohyama,N., Fukushima, K., and Fukami, A. (1978) Observations of the hydrated form of tubular halloysite by an electron microscope equipped with an environmental cell. Clays and Clay Minerals 26, 25-40.

de Lamotte, E., and Perry, A. J. (1970) Diameter and strain rate dependence of the ultimate strength and Young's Modulus of carbon fibres. Fibre Sci. Technol. 3, 157-166.

MacAdam, W. I. (1886) On the analysis of talc used in papermaking. Mineral. Soc. London 7, 75.

Mallinson, L. G., Jefferson, D. A., Thomas, J. M., and Hutchison, J. L. (1980) The internal structure of nephrite. Royal Soc. London, Phil. Trans. A 295, 537-551.

Marsh, D. M. (1963) Stress concentrations at steps on crystal surfaces and their role in fracture. Fracture of Solids Metall. Soc. Conf., 20, Intersci. Publ., New York.

Marshall, E. C., Hubert, R. P., Shaw, B. T., and Caldwell, O. G. (1942) Studies of clay particles with electron microscope: II. The fractionation of beidellite, nontronite, magnesium bentonite and attapulgite. Soil Sci. 54, 149-158.

Mathews' Textile Fibers (1947) H. R. Mauersberger, ed., John Wiley and Sons, London.

Mehan, R. L., and Feingold, E. (1966) Strength and structure of very fine sapphire whiskers. Chapter 15 in *Strengthening Mechanisms,* J. H. Burke, N. L. Reed, and V. Weiss, eds., Syracuse Univ. Press.

_____, and _____ (1967) Room and elevated temperature strength of Al_2O_3 whiskers and their structural characteristics. J. Materials 2, 239-270.

_____, _____, and Gatti, E. (1965) Techn. Report AFML-TR 65, 275.

_____, and Herzog, J. A. (1970) Mechanical properties of whiskers. Chapter 6 in *Whisker Technology,* A. P. Levitt, ed., Wiley Intersci. Publ., New York.

_____, Sutton, W. J., and Herzog, J. A. (1966) A review of measuring the strength of whiskers and their role in reinforcing ductile metal matrices, A. Inst. Aero. Astro. J. 4, 1889-1898.

Merrill, G. P. (1895) Notes on asbestos and asbestiform minerals. Proc. Nat'l Mus. 18, 281-292.

Miyamoto, M., Onuma, N., and Takeda, H. (1979) Wollastonite whiskers in the Allende meteorite and their bearing on a possible post-condensation process. Geochim. J. 13, 1-5.

Moreton, R. (1969) The effect of gauge length on the tensile strength of R.A.E. carbon fibres. Fibre Sci. Technol. 2, 273-284.

Morrison, W. B. (1966) The effect of grain size on the stress-strain relationship in low-carbon steel. Trans. Ouotwr. Amer. Soc. Metals 59, 824-846.

Mumpton, F. A., and Thompson, C. S. (1975) Mineralogy and origin of the Coalinga asbestos deposit. Clays and Clay Minerals 23, 131-143.

Nadgornyi, L. F., Grigoreva, L. F., and Ivanov, A. P. (1965) The mechanical properties of synthetic fluoramphiboles and certain forms of natural asbestos. Izvest. Akad. Nauk. SSSR Noerg. Mt. 1, 1117-1123.

Nicoll, A. R., and Perry, A. J. (1973) Diameter dependence of carbon fibre mechanical properties. Fibre Sci. Technol. 6, 135-139.

Nuttal, T. (1821) Observations on the serpentine rocks of Hoboken, New Jersey, and on the minerals which they contain. Amer. J. Sci. Arts 4, 16-23.

Orowan, E. (1933) Die erhöhte Festigkeit dünner Fäden, der Joffé-Effekt und verwandte Erscheinungen von Standpunkt der Griffitschen Bruchtheorie. Z. Physik. 86, 194-213.

Palekar, L. D., Spooner, C. M., and Coffin, D. L. (1979) Influence of crystallization habit of minerals on in vitro cytotoxicity. Annals N. Y. Acad. Sci. 330, 673-686.

Peacock, M. A. (1928) The nature and origin of the amphibole asbestos of South Africa. Amer. Mineral. 13, 241-285.

Perry, A. J., Phillips, K., and de Lamotte, E. (1971) The mechanical properties of carbon fibres. Fibre. Sci. Technol. 3, 317-319.

Petch, N. J. (1953) Cleavage strength of polycrystals. J. Iron Steel Inst. (London) 174, 25-28.

_____, (1954) Fracture of metals. Chapter 1 in *Progress in Metal Physics*, B. Chalmers, ed., Wiley Intersci. Publ., New York, 5.

Pierce, F. T. (1926) Tensile tests for cotton yarns - "The weakest link" theorems on the strength of long and of composite specimens. J. Te t. Inst. 17, 355-368.

Pott, F., Huth, F., and Friedrich, K. H. (1974) Tumorigenic effect of fibrous dust in experimental animals. Envir. Health Persp. 9, 313-315.

Rabbit, J. C. (1948) A new study of the anthophyllite series. Amer. Mineral., 33, 263-323.

Regester, R. F., Goesuch, P. D., and Girifalco, L. (1967) Structure and properties of aluminum oxide whiskers. Mat. Res. Std. 7, 203-206.

Reinkober, O. (1931) Die Zerreiszfestigkeit dunner Quarzfaden. Physik. Zeitschr., 32, 243-250.

Reutelspacher, H. and van der Marel, H. W. (1968) *Atlas of Electron Microscopy of Clay Minerals and their Admixtures*. Elsevier Publ., Amsterdam.

Roberts, D. A. (1961) Physical and mechanical properties of some high-strength fine wires. Batelle Mem. Inst. DMIC Memorandum 80.

Rowcliffe, D. J., and Fruhauf, V. (1977) The fracture of jade. J. Materials Sci. 12, 35-42.

Rutstein, M. S. (1979) Fibrous intergrowth of cross muscovite and cross chlorite from shear zones of Pennsylvanian carbonaceous rocks in Rhode Island. Amer. Mineral. 64, 151-155.

Saussure, H. B. (1796) *De Voyages dans les alpes*. Neuchatel.

Sears, G. W. (1953) Screw dislocation theory of whisker growth. Acta Metal. 1, 457-459.

_____, (1962) Ultimate strength of crystals. J. Chem. Phys. 36, 862.

Shell, H. R., Comeforo, J. E., and Eitel, W. (1958) Synthetic asbestos investigations: Synthesis of fluormphiboles from melts. U.S. Bur. Mines, Rept. Invest., No. 5417. 35 pp.

_____, Hatch, R. A., and Brown, D. L. (1957) Synthetic asbestos investigations. III Synthesis and properties of fibrous potassium-lead silicate. U.S. Bur. Mines, Rep. Invest. No. 5293, 20 pp.

Soltis, P. J. (1967) A new method and technique for tension testing whiskers. J. Materials 2, 300-324.

Spriggs, R. M., and Vasilos, T. (1963) Effect of grain size on transverse bend strength of alumina and magnesia. J. Am. Ceram. Soc. 46, 224-228.

Stanton, M. F., and Layard, M. (1979) The carcinogenicity of fibrous minerals. Nat. Bur. Std. Spec. Paper 506, 143-151.

Sutton, W. H. (1970) Principles and methods for fabricating whisker-reinforced composites. Chapter 9 in *Whisker Technology*, A. P. Levitt, ed., Wiley Intersci., New York.

Taber, S. (1916) The origin of veins of the asbestiform minerals. Proc. Nat. Acad. Sci. 2, 659-664.

Tarnovskii, G. N., Kashaeva, G. M., Shirgaeva, V. A., and Afonina, G. G. (1976) First discovery of tourmaline asbestos in pegmatites of the USSR. Vopr. Mineral. Geokhim. Pegmatitov. Vost. Sib., 54-64.

Thompson, J. B. (1970) Geometrical possibilities for amphibole structures: Model biopyriboles. Amer. Mineral. 55, 292-293.

Tippett, L. H. C. (1925) On the extreme individuals and the range of sample taken from a normal population. Biometrika 17, 364-387.

Trendall, A. F., and Blockley, J. G. (1970) The iron formations of the Precambrian Hamersley Group, Western Australia. Geol. Soc. W. Austral. Bull. 119, 366 pp.

Veblen, D. R. (1980) Anthophyllite asbestos: microstructures, intergrown sheet silicates, and mechanisms of fiber formation. Amer. Mineral. 65, 1075-1086.

_____, Buseck, P. R., and Burnham, C. W. (1977) Asbestiform chain silicates: New minerals and structural groups. Science 198, 359-365.

_____, and _____ (1979a) Serpentine minerals: intergrowths and new combination structures. Science 206, 1398-1400.

_____, and _____ (1979b) Chain-width order and disorder in biopyriboles. Amer. Mineral. 64, 687-700.

_____, and _____ (1980) Microstructures and reaction mechanisms in biopyriboles. Amer. Mineral. 65, 599-623.

Vermaas, F. H. S. (1952) The amphibole asbestos of South Africa. Trans. Proc. Geol. Soc. South Africa 55, 199-229.

Wadsley, A. D. (1955) The crystal chemistry of non-stoichiometric compounds. Rev. Pure Appl. Chem. 5, 165-193.

Wagner, R. S. and Ellis, W. E. (1965) The VLS mechanism of whisker growth. Trans. Met. Soc. AIME, 233, 1054-1064.

Walker, J. S. (1981) Asbestos and the asbestiform habit of minerals. M. S. thesis, University of Minnesota.

_____, Ring, S. J., and Zoltai, T. (1981) Asbestiform varieties of palygorskite and sepiolite. Science, in press.

_____, and Zoltai, T. (1979) A comparison of asbestos fibers with synthetic crystals known as "whiskers". Annals N.Y. Acad. Sci. 330, 687-704.

Webb, W. W., Dragsdorf, R. D., and Forgeng, W. D. (1957) Dislocations of whiskers. Phys. Rev. 108, 498-499.

Weibull, W. (1939) A statistical theory of the strength of materials. Proc. 151, Ingen. Vetensk. Akad. Stockholm.

Whittaker, E. J. W. (1949) The structure of Bolivian crocidolite. Acta Crystallogr. 2, 312-317.

_____, (1979) Mineralogy, chemistry and crystallography of amphibole asbestos. Mineral. Assoc. Canada Short Course Handbook 4, 1-34.

_____, Cressey, B. A., and Hutchison, J. L. (1981) Terminations of multiple-chain lamellae in grunerite asbestos. Mineral. Mag. 44, 27-35.

Wolff, E. G., and Cockren, T. D. (1965) Growth and morphology of magnesium oxide whiskers. J. Amer. Ceram. Soc. 48, 279-285.

Wylie, A. G. (1979) Optical properties of fibrous amphiboles. Annals N. Y. Akad. Sci. 330, 611-619.

_____, and Huggins, C. W. (1980) Characteristics of a potassium winchite - asbestos from the alamoore talc district, Texas. Canadian Mineral. 18, 101-107.

Zoltai, T. (1978) History of asbestos-related mineralogical terminology. Nat'l Bur. Standards Spec. Paper 506, 1-18.

_____, (1979) Asbestiform and acicular mineral fragments. Annals N. Y. Acad. Sci. 330, 687-704.

_____, (1981) Surface structure and strength of fibers and strong polycrystalline materials. Unpublished manuscript.

Zukowski, R. and Gaze, R. (1959) Tensile strength of asbestos. Nature 183, 35-37.

Chapter 6

The GEOLOGIC OCCURRENCES and HEALTH HAZARDS of AMPHIBOLE and SERPENTINE ASBESTOS

Malcolm Ross

INTRODUCTION

The problem

The widespread use of amphibole and serpentine asbestos[1] by industrial society has contributed greatly to human safety and convenience by service in brake and clutch facings, electrical and heat insulation, fire-proofing materials, cement water pipe, tiles, filters, packings, construction materials, and many other products. Yet, while these very tangible benefits were accruing to our society, some asbestos workers were dying of asbestosis, lung cancer, and mesothelioma.

The hazards of certain forms of asbestos under certain conditions have been so great that several countries have taken extraordinary actions to greatly reduce or even ban their use. Recent experiments with animals demonstrate that the commercial asbestos minerals as well as other fibrous materials can cause tumors to form when the fibrous particles are implanted within the pleura.[2] These experiments have convinced some health specialists that asbestos-related diseases can be caused by many types of elongate particles; the mineral type, according to these health specialists, is not the important factor in the etiology of

---

[1]At present, the most widely used definition of asbestos by various groups concerned with environmental health problems is from the notice of proposed rule-making for "Occupational Exposure to Asbestos" published in the *Federal Register* (Oct. 9, 1975, p. 47652, 47660) by the U.S. Occupational Safety and Health Administration (OSHA). In this notice, the naturally occurring amphibole minerals amosite, crocidolite, anthophyllite, tremolite, and actinolite and the serpentine mineral chrysotile are classified as asbestos if the individual crystallites or crystal fragments have the following dimensions: length greater than 5 micrometers, maximum diameter less than 5 micrometers, and a length to diameter ratio of 3 or greater. Any product containing *any* of these minerals in this size range is also defined as asbestos.

[2]The lungs are invested by a double membrane, the two layers of which form the closed pleural sac. For discussion of these animal experiments see Stanton and Layard (1978) and Pott (1978).

disease, but rather the size and shape of the particles which enter the human body.

The question now before the United States health and regulatory establishment is whether the hazards of asbestos outweigh the benefits. Should the asbestos minerals and perhaps other asbestos-like minerals be banned from use? Minerals belonging to the amphibole group are particularly important in this regard, for they are ubiquitous and commonly have crystalline habits which are considered by some to be asbestos-like.

The dilemma

The concern for human health, the great usefulness of many asbestos products, the appearance of asbestos minerals or asbestos-like minerals in the natural background and in many kinds of mining operations, and the uncertainty of the exact health effects of different kinds of minerals, different mineral particle sizes, and different mineral dust concentrations combine to present a formidable problem to minerals scientists, the minerals industries, and legal and health professionals. Must the use of all commercial asbestos be stopped? Must all mine dusts containing such particles be controlled to the lowest feasible levels and wastes from those mines be considered toxic and thus isolated from surrounding air and water?

To obtain an insight so that we might intelligently address these questions, I will review the role of asbestos in the world economy, past and present, the important geological occurrences of commercial amphibole and chrysotile asbestos, and the health hazards of asbestos use. As we will see, the six asbestos minerals utilized in commerce are not identical in crystal structure, chemical composition, abundance, and geologic occurrence; nor do the different asbestos dusts have the same impact on human health. Evidence will be presented to indicate that many of the benefits obtainable from asbestos may be retained with minimal health risk through utilization of the common chrysotile form of asbestos, provided that dust emissions are controlled to levels presently in force at the mines and mills of Quebec. It would appear that, instead of treating all asbestos minerals and other fibrous industrial and gangue minerals as equally potent carcinogens, each mineral should be examined on its own merits with regard to its usefulness to society and its potential to cause disease.

Standard references published over the past 50 years usually list six forms of asbestos; the amphibole varieties are amosite, crocidolite, anthophyllite, tremolite, and actinolite, and the serpentine variety is chrysotile. A detailed understanding of the chemistry and crystal structures of these asbestos minerals postdates their discoveries; thus, some of the older literature can be confusing with regard to mineral identifications.

The commercial deposits of asbestos contain one of the following minerals: chrysotile, $Mg_3Si_2O_5(OH)_4$; amosite, $(Fe^{2+},Mg)_7Si_8O_{22}(OH)_2$ (a variety of grunerite); crocidolite, $Na_2(Fe^{2+},Mg)_3Fe^{3+}_2Si_8O_{22}(OH)_2$ (a variety of riebeckite); "fibrous" anthophyllite, $(Mg,Fe)_7Si_8O_{22}(OH_2)$; and "fibrous" tremolite and actinolite, $Ca_2(Mg,Fe)_5Si_8O_{22}(OH)_2$. Tremolite and actinolite are now, as they were in the past, of little economic importance; anthophyllite is of little economic importance now. About 95 percent of the commercial asbestos now used in the United States is chrysotile, of which about 90 percent is imported from Canada.

Amphibole asbestos

The crystal structures of the amphibole asbestos minerals are composed of strips or ribbons of linked polyhedra, which join together to form the three-dimensional crystal. The individual strips are composed of three elements -- two double chains of linked $(Si,Al)O_4$ tetrahedra that form a "sandwich" with a strip of linked MgO_6, FeO_6, or AlO_6 octahedra. The structural relationship of the upper double tetrahedral chain to the octahedral part of the strip is shown in Figure 1. The three-dimensional arrangements of these strips or "I-beams" in orthoamphibole (anthophyllite) and in clinoamphibole (tremolite, amosite, actinolite, and crocidolite) are shown in Figure 2. Complete reviews of the amphibole crystal structures are given by Cameron and Papike (1979) and Hawthorne, Chapter 1, this volume.

Amosite is the very rare asbestiform variety of grunerite, $(Fe,Mg)_7Si_8O_{22}(OH)_2$; the name is derived from the word *Amosa* -- an acronym for the company "Asbestos Mines of South Africa" (Hall, 1918, p. 13-14). This valuable commercial asbestos, mined only in the Transvaal Province of South Africa, was first discovered in 1907 in

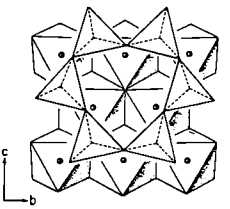

Figure 1. Structural relationship between the upper double chain of linked $(Si,Al)O_4$ tetrahedra and the octahedral part of the amphibole strip or "I-beam." The circles represent Mg, Fe, or Al atoms in octahedral coordination; at the apices of the polyhedra are oxygen atoms. Tetrahedral Si and Al atoms are not shown. The "I-beams" extend infinitely in a direction parallel to the *c*-axis (the fiber axis). The width of the "I-beam" in the *b*-direction is three octahedra. Modified from Papike and Ross (1970).

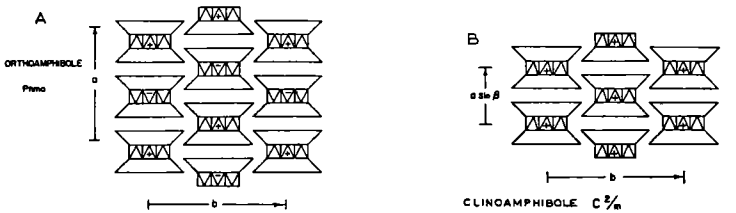

Figure 2. Arrangement of the amphibole strips or "I-beams" in (A) orthoamphibole (space group *Pnma*) and (B) clinoamphibole (space group *C2/m*). The "I-beams" are viewed end-on (parallel to the fiber *c*-axis). The central portion of the "I-beam" is composed of $(Mg,Fe,Al)O_6$ octahedra; the upper and lower portions are composed of double chains of $(Si,Al)O_4$ tetrahedra. The I-beams are stacked in two ways: (1) +++... (clinoamphibole), and (2) +-+-... (orthoamphibole). Modified from Papike and Ross (1970).

Table 1. Chemical analyses and formulas of amphibole asbestos.

	Amosite			Crocidolite				Anthophyllite
	1.	2.	3.	4.	5.	6.	7.	8.
SiO_2	49.70	51.30	50.90	50.70	52.00	55.65	52.85	57.20
Al_2O_3	0.40	nil	nil	0.70	nil	4.00	0.18	--
Fe_2O_3	0.03	0.90	16.85	18.30	16.05	13.01	18.55	0.13
FeO	39.70	35.50	20.50	17.50	17.65	3.84	14.94	10.12
MnO	0.22	1.76	0.05	0.06	trace	trace	trace	--
MgO	6.44	6.90	1.06	3.05	4.28	13.09	4.64	29.21
CaO	1.04	0.95	1.45	1.30	1.20	1.45	1.07	1.02
K_2O	0.63	0.51	0.20	trace	0.06	0.39	0.05	--
Na_2O	0.09	0.05	6.20	5.30	6.21	6.91	5.97	--
H_2O^+	1.83	2.31	2.37	2.53	2.43	1.78	2.77	2.18
H_2O^-	0.09	0.05	0.22	0.29	0.26	trace	0.22	0.28
CO_2	0.09	0.25	0.20	0.45	0.09	trace	0.23	--
	100.26	100.48	100.00	100.18	100.23	100.12	101.47	100.14
	NUMBER OF IONS ON BASIS OF O=22, OH=2							
Si	7.898	8.055	7.949	7.823	7.942	7.791	7.927	7.848
Al	0.075	--	--	0.127	--	0.209	0.032	--
	7.973	8.055	7.949	7.950	7.942	8.000	7.959	7.848
Al	--	--	--	--	--	0.451	--	--
Fe^{3+}	0.004	0.106	1.980	2.125	1.844	1.371	2.094	0.013
Fe^{2+}	5.277	4.662	2.678	2.259	2.254	0.450	1.874	1.161
Mn	0.030	0.234	0.007	0.008	--	--	--	--
Mg	1.525	1.615	0.247	0.701	0.974	2.731	1.037	5.972
Ca	0.177	0.160	0.243	0.215	0.196	0.218	0.172	0.150
K	0.128	0.102	0.040	--	0.012	0.070	0.010	--
Na	0.028	0.015	1.877	1.585	1.839	1.875	1.736	--
	7.165	6.894	7.072	6.893	7.119	7.166	6.923	7.296

1. Amosite, Penge, Transvaal, South Africa (Hodgson, 1979)
2. Amosite, Weltevreden, Transvaal, South Africa (Hodgson, 1979)
3. Crocidolite, Koegs, Cape Province, South Africa (Hodgson, 1979)
4. Crocidolite, Kuruman, Cape Province, South Africa (Hodgson, 1979)
5. Crocidolite, Pomfret, Cape Province, South Africa (Hodgson, 1979)
6. Crocidolite, Cochabamba, Bolivia (Hodgson, 1979)
7. Crocidolite, Hammersley Range, W. Australia (Hodgson, 1979; see also Trendall and Blockley, 1970)
8. Anthophyllite, Paakkila, Finland (Hodgson, 1979, see also Haapala, 1936)

Sekukuniland. Until relatively recently, its true relationship to grunerite was not known. It is now clear (Hutchison *et al.*, 1975; Champness *et al.*, 1976) that amosite and grunerite are the same mineral species, having identical crystal structures and similar chemical compositions. The chemical compositions of samples of amosite from the important Penge and Weltevreden mining areas are given in Table 1.

Crocidolite is the asbestiform variety of riebeckite, ideally $Na_2(Fe^{2+},Mg)_3Fe^{3+}_2Si_8O_{22}(OH)_2$, and has been mined in only four localities: in the Transvaal and Cape Provinces of South Africa, in the Hammersley Range area of Western Australia, and in the Cochabamba area of Bolivia. Only the South African mines are still active. Five chemical analyses of crocidolite from three of these areas are given in Table 1.

The only other form of amphibole asbestos that has been mined commercially on a significant scale is anthophyllite, $(Mg,Fe)_7Si_8O_{22}(OH)_2$, from the Paakkila area of East Finland, a chemical analysis of which is given in Table 1.

There are numerous reports of minor occurrences of tremolite asbestos, $Ca_2Mg_5Si_8O_{22}(OH)_2$, and relatively few reports of actinolite asbestos, $Ca_2(Mg,Fe)_5Si_8O_{22}(OH)_2$, occurrences. No mining of these asbestos minerals on a significant scale has occurred, save perhaps some of the early mining of tremolite asbestos in the Alps of northern Italy. Much of the reported "tremolite asbestos" from this area may have actually been chrysotile. Asbestiform hornblende has been reported (for example, Shannon, 1926, p. 56-57; Hall, 1918, p. 97) but has not apparently been used in commerce.

Chrysotile asbestos

Chrysotile, one of the three common polymorphs of serpentine (lizardite, antigorite, and chrysotile), is generally fibrous, although non-fibrous massive varieties are known. The structure of chrysotile asbestos consists of double sheets, each double sheet being composed of a layer of linked SiO_4 tetrahedra that is coordinated to a second layer of linked $MgO_2(OH)_4$ octahedra through the sharing of oxygen atoms. This composite double sheet, due to a misfit between the SiO_4 and $MgO_2(OH)_4$ layers, rolls up like a window shade to form long hollow tubes. The diameters of the individual tubes are approximately 25 nm; the lengths

vary from a few hundred to a few million nanometers. Chemical analyses of chrysotile asbestos from four important mining localities are given in Table 2.

ASBESTOS IN THE WORLD ECONOMY

Early beginnings

While the general use of asbestos in international commerce dates only to the late 19th century, its utility in human culture goes back to at least 2500 B.C. Archeological studies (Europaeus-Äyräpää, 1930) show that the inhabitants of the Lake Juojärvi region of East Finland knew how to strengthen earthenware pots and cooking utensils with anthophyllite asbestos. This asbestos probably came from the same areas where it was commercially exploited in recent times. According to Huuskonen (1980; see also Europaeus Äyräpää, 1930; Noro, 1968), the use of asbestos-strengthened ceramic wares began during the Stone Age and continued throughout the Bronze Age and into the Iron Age. The use of such utensils spread over a wide area of Finland, Scandinavia, and Russia. The most important modern use of asbestos, to strengthen materials, was apparently also the first use -- dating back several thousand years.

Until recently, however, most other uses of asbestos were trivial; its fabrication into such curiosities as cremation cloth (Pliny refers to this as a rare and costly cloth -- linum vivum -- the funeral dress of kings), tablecloths (reputedly, Charlemagne, or according to some writers, Charles V, astonished guests by throwing the cloth into fire and later withdrawing it cleansed, but unconsumed), and lamp wicks (Plutarch recorded that the vestal virgins used "perpetual" lamps). The fabrication of lamp wicks may have been a cottage industry during certain times in history; Herodotus clearly documented use of such asbestos wicks in the earlier Greek civilization. Even well into the last century, asbestos could not be regarded as a product of commerce unless one includes such endeavors as the small industry developed in Russia during the rule of Peter the Great, where chrysotile asbestos from the Urals was used for a short period in the production of textiles.

In the 1860's and 1870's the market for asbestos products rapidly

Table 2: Chemical analyses and formulas of commercial chrysotile asbestos (Hodgson, 1979)

	1.	2.	3.	4.
SiO_2	38.75	39.00	39.70	39.93
Al_2O_3	3.09	4.66	3.17	3.92
Fe_2O_3	1.59	0.54	0.27	0.10
FeO	2.03	1.53	0.70	0.45
MnO	0.08	0.11	0.26	0.05
MgO	39.78	38.22	40.30	40.25
CaO	0.89	2.03	1.08	1.02
K_2O	0.18	0.07	0.05	0.09
Na_2O	0.10	0.07	0.04	0.09
H_2O^+	12.22	11.37	12.17	12.36
H_2O^-	0.60	0.77	0.64	0.92
CO_2	0.48	1.83	2.13	1.04
	99.79	100.20	100.51	100.22

NUMBER OF IONS ON BASIS OF O=5, OH=4

Si	1.845	2.000	1.851	2.000	1.885	2.000	1.882	2.000
Al	0.155		0.149		0.115		0.118	
Al	0.018	3.047	0.112	3.013	0.062	3.025	0.100	3.016
Fe^{3}_{+}	0.057		0.019		0.010		0.004	
Fe^{2+}	0.081		0.061		0.028		0.018	
Mn	0.003		0.004		0.010		0.002	
Mg	2.823		2.704		2.853		2.827	
Ca	0.045		0.103		0.055		0.052	
K	0.011		0.004		0.003		0.005	
Na	0.009		0.006		0.004		0.008	

1. Chrysotile, King Beaver Mine, Thetford Mines, Quebec
2. Chrysotile, Asbest, Urals, U.S.S.R.
3. Chrysotile, Shahani Mines, Zimbabwe
4. Chrysotile, Havelock Mine, Swaziland

Table 3. World asbestos production in 1978 (Clifton, 1979)

Fiber Locality	Production (in thousands of metric tonnes)
Chrysotile	
North America	
Canada	1620
United States	93
South America	
Argentina	1
Brazil	100
Europe	
Bulgaria	21
Italy	162
U.S.S.R.	2582
Yugoslavia	10
Africa	
Zimbabwe	210
South Africa	118
Swaziland	48
other	1
Asia	
China	210
Cyprus	37
India	21
Japan	7
Korea	7
Taiwan	1
Turkey	10
Oceania	
Australia	58
(World chrysotile total)	5317
Crocidolite	
South Africa	210
Amosite	
South Africa	71

changed, probably for three reasons: the need for insulation for the new steam technology, the formation of an international trading company of Italian and English entrepreneurs, and the reopening of the chrysotile asbestos deposits of northern Italy and simultaneous exploitation of the vast chrysotile resources in Quebec. The supply for the first time was ample, and the market was ready.

The modern industry

The reopening of the asbestos deposits of northern Italy, deposits which had previously been worked as far back as Roman times, serves to mark the beginning of the modern asbestos industry. The Italian asbestos was unusually silky and long fibered[3] and thus readily woven into textiles. The shrouds and cloths of antiquity may have been made from this asbestos.

By 1890 the modern asbestos industry was full blown, with hundreds of applications being introduced (Jones, 1890); by the turn of the century the large South African crocidolite deposits had been opened up, and the Russian deposits in the Urals were once again producing in large quantity. Within a few years, the amosite deposits of the Transvaal would be exploited.

From the time of the first recorded use of asbestos by Stone Age man to 1900, the total world production of all types of fiber was probably about 200,000 metric tonnes, certainly no more than 300,000 tonnes. Of this, 150,000 tonnes came from Quebec. By 1980 over 100 million tonnes of asbestos had been mined throughout the world; of this over 90 percent was chrysotile and over 5 percent crocidolite and amosite. Total production of anthophyllite asbestos to date is probably no more than 400,000 tonnes, 350,000 tonnes being produced by Finland alone. Production of tremolite asbestos has been sporadic; it was mined in various parts of the world for short periods of time. Total production to date for this

[3]Two samples of Italian asbestos on deposit at the U.S. National Museum are both chrysotile. One, U.S.N.M. No. 73539, is from "Piedmonte," Italy, and was acquired by the museum in 1900 from the Isaac Lea Collection. The fibers in this sample are up to 120 cm long! The second sample, U.S.N.M. No. R3172 (Roebling Collection) is from Val Malenco, Sondrio, Lombardia, Italy. Fibers are up to 15 cm long in this specimen.

form of asbestos is probably no more than a few thousand tonnes. Commercial exploitation of actinolite asbestos is practically unknown.

The world asbestos production for 1978 is given in Table 3. Russia leads with 46.1 percent and Canada is second with 28.9 percent of the world output. Both countries mine only chrysotile asbestos, and most of the fiber comes from the Urals and Quebec. The third leading asbestos producer is the Republic of South Africa (7.1 percent); the asbestos ore consists of amosite, crocidolite, and chrysotile. These three countries furnished 82.1 percent of the world's asbestos in 1978. The other countries listed in Table 3 produce mostly chrysotile.

Modern asbestos uses

As alluded to before, heat insulation was one of the most important uses of asbestos during the early beginnings of the modern industry; apparently the first application for this purpose was in 1866 (Bowles, 1937, p. 9). The principal uses of asbestos in the United States in 1978 in order of importance were as follows: in cement pipe (145,800 metric tonnes), in flooring products (122,400), in friction materials (81,600), in roofing products (58,300), in asbestos cement sheet (29,200), in coatings and compounds (29,100), in paper (29,100), in packings and gaskets (23,300), and in insulation (14,300) (Clifton, 1979).

MAJOR GEOLOGICAL OCCURRENCES OF AMPHIBOLE ASBESTOS

There are many minerals, including the amphiboles and chrysotile, that are described variously as fibrous, asbestiform, acicular, filiform, and prismatic, terms which suggest an elongate habit. Although such minerals are extremely common, in only relatively few places do they obtain suitable physical and chemical properties to be valuable as commercial asbestos. Locally, amphibole minerals may show an asbestiform habit, for example in vein fillings and in areas of secondary alteration, but usually they do not appear in sufficient quantity to be profitably exploited.

Deposits of commercial asbestos are found in four types of rocks: (1) banded ironstones (amosite and crocidolite), (2) alpine-type ultramafic rocks, including ophiolites (anthophyllite, tremolite, and chrysotile), (3) stratiform ultramafic intrusions (tremolite and chrysotile),

and (4) serpentinized limestone (chrysotile). Of these, the banded ironstones of South Africa and Western Australia and the alpine-type ultramafic rocks of East Finland are or were the only major sources of amphibole asbestos.

Amosite and crocidolite in ironstones of South Africa

The mining of amphibole asbestos is now essentially confined to South Africa.[4] The amosite and crocidolite asbestos occur in the banded ironstones of the Transvaal Supergroup, a thick succession of Precambrian sediments (∿ 2200 m.y., Truswell, 1977, p. 42) with widespread outcrops in the Transvaal and Cape Provinces and in southeastern Botswana. The two asbestos producing localities are the *Transvaal Asbestos Field* in the north-central part of the Transvaal Province and the *Cape Asbestos Field* in the northern Cape. At present about 200,000 tonnes of amphibole asbestos are produced yearly from these two fields.

Transvaal Asbestos Field. This field stretches from Chuniespoort easterly to beyond Penge, Transvaal Province, a distance of about 100 km (Fig. 3). Most of the amosite presently mined is derived from the Penge area, about 80 km north of Lydenburg. Minor amounts of amosite and crocidolite are mined intermittently in the Chuniespoort-Malips Drift area to the west of Penge (Dreyer and Robinson, 1978). The Penge area is sometimes referred to as the "Lydenburg asbestos field" and the Chuniespoort-Malips Drift area as the "Pietersburg asbestos field."

In the Transvaal the rock members of the Transvaal Supergroup consist essentially of quartzite, shale, dolomite, and conglomerate at the base (Wolkberg Formation, Black Reef Series), dolomite, banded ironstone, and shale in the center zone (Dolomite Series); and quartzite, shale and hornfelses at the top (Pretoria Series). The asbestos-bearing rocks lie within the Banded Ironstone Stage of the Dolomite Series (Fig. 3). These rocks have been intensely folded along two major fold axes (Dreyer and Robinson, 1978), the folding predating the deposition of the Pretoria Series. The banding within the ironstones is fine and regular; the

[4]Small amounts of anthophyllite and tremolite asbestos come into the international market sporadically, at most a few thousand tonnes a year. These types of fiber are generally from small, marginally profitable, deposits.

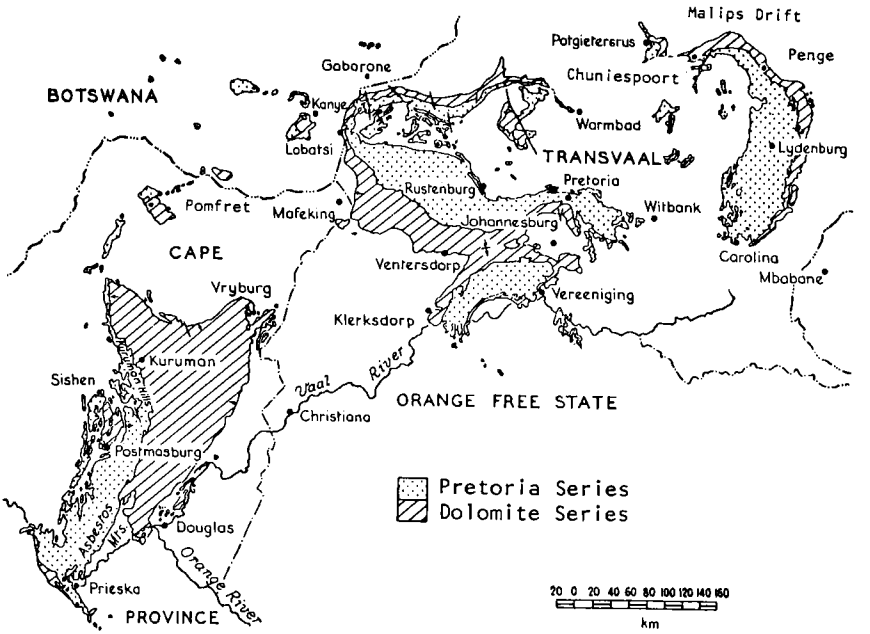

Figure 3. Index map of the crocidolite and amosite asbestos-bearing iron formations of the Transvaal and Cape Provinces of South Africa. After Truswell (1977).

light colored bands consist of chert with some siderite, the dark bands of magnetite and grunerite. Within the banded ironstone sequences the asbestos-bearing seams occupy definite stratigraphic horizons, generally known as the Lower Zone, the Main Zone, the Short Fibre Zone, and the Upper Zone. Some intermediate zones are developed locally. Each zone consists of a large number of individual fiber seams or groups of seams which are given local names (Coetzee *et al.*, 1976). In the Pietersburg asbestos field amosite and crocidolite are sometimes observed occurring in adjacent seams (Hall, 1930, Fig. 38, p. 212). East of the Mohlapitse River, crocidolite decreases rapidly, so that only amosite is found in the Lydenburg asbestos field near Penge.

Within the Transvaal Province there is evidence of thermal metamorphism of the Transvaal Supergroup rocks as a result of the intrusion of the Bushveld Igneous Complex. For example, the shales of the Pretoria Series overlying the banded ironstones were recrystallized to hornfelses, scapolite appears in the dolomites underlying the ironstones, and amphibolization took place throughout most of the banded ironstone sequence. Crystallization of the amphibole asbestos, however, took place after

emplacement of the diabasic sills (considered forerunners of the main Bushveld intrusion) and before cooling of the main body of the Complex (Cilliers, 1964).

Cape Asbestos Field. This field is in Griqualand West, Cape Province, 700 km to the west of the asbestos mining areas of the Transvaal. It lies along a line of low hills (Asbestos Mountains, Kuruman Hills) that stretches from 40 km south of Prieska, northward past Kuruman to Pomfret near the Botswana Border, a distance of 480 km (Fig. 3). The crocidolite asbestos-bearing ironstones of this area are included within the Pretoria Series of the Transvaal Supergroup and are suggested to be correlated with the Pretoria Series rocks to the east in the Transvaal (Cilliers, 1964, p. 581). Stratigraphic correlations between the Transvaal and Cape regions are subject to somewhat different interpretation (Cilliers, 1964; Cilliers and Genis, 1964; Beukes, 1973, 1980). New nomenclature proposals by Beukes (1980) place the crocidolite-bearing banded ironstones of the Cape within the Griquatown and Kuruman Iron Formations of the Asbesheuwels Subgroup. Cilliers (1964, p. 5881) states that it may be accepted that the banded ironstones in the Cape Province and in the Transvaal were formed contemporaneously and under similar conditions. The asbestos deposits of the Cape are generally located in the monoclinal folds. Metamorphism is generally absent.

Formation of banded ironstones. The origin of the Precambrian banded ironstones of South Africa is still the subject of much debate, but it is possible to summarize some of the main ideas on their paragenesis. The deposition of the sediments probably occurred in relatively shallow water, in some places in saline basins. Iron and silica were derived from normal weathering processes. Primary precipitates such as silica and hydrous iron oxides and silicates may have been the precursors to the later-formed stilpnomelane , minnesotaite, and riebeckite. Biochemical actions of organic matter also probably had an important influence on the mineral chemistry. The change of amphibole mineralogy from amosite in the Penge area, mixed amosite-crocidolite in the Chuniespoort-Malips Drift area, to crocidolite in the Cape suggests that there was a gradual change of conditions of sediment formation: deposition in a predominantly fresh water environment in the Transvaal to a

predominantly saline environment in the Cape (Cilliers, 1964).

The reason why the amphiboles crystallized in an asbestiform habit rather than the typical prismatic form is a subject of some interest. It is pertinent to note the comments of Dreyer and Robinson (1978), who state (p. 3-4) "the greatest development of fibre occurs where two sets of folds intersect to form domes or basins. It is firmly believed that the development of fibre deposits could only have taken place in a favourable stress environment." For further comments on crystal growth of asbestos minerals in stress fields, see Zoltai (Chapter 5, this volume).

Crocidolite in ironstones of Western Australia

Crocidolite asbestos is also found in the banded ironstones of the Hamersley Iron Province, Western Australia (Fig. 4). These formations are remarkably similar to those of the Cape Province of South Africa and are included among the great iron formations of the world which formed under very similar conditions and during a single geologic epoch approximately 1900 to 2500 m.y. ago (James and Sims, 1973).

The banded ironstones are widely distributed in the Marra Mamba, Brockman, and Boolgeeda Iron Formations of the Hamersley Group, Mount Bruce Supergroup. The ironstones are approximately 2000 m.y. old (Trendall, 1973). Although riebeckite is widely distributed in these three iron formations, it is only abundant in fibrous form (crocidolite) in four narrow zones.

The Hamersley ironstones are thought to have formed in much the same way as those of South Africa, by precipitation of volcanically derived iron and silica in a shallow basin. Massive riebeckite developed during diagenesis from previously existing minerals, with crocidolite asbestos crystallizing later in a stress environment. The major asbestos deposits are confined to the northern limb of the broad syncline of the Hamersley Range (Trendall and Blockley, 1970). These authors propose a "stress-reversal" for asbestos growth; they state (p. 18) "Crocidolite grew later by splitting and dialation of magnetite mesobands in banded iron formation as a relief from balanced compression from two sides in particular structural situations, where gravitational sliding opposed 'tectonic' stress."

Crocidolite mining in Western Australia began on a very small scale

in 1933, but it was not until 1944 that significant production started. By 1966, the year of the final closing of the mines, 138,000 tonnes of crocidolite had been shipped. Ninety-eight percent of this fiber came from two mines in the Wittenoom Gorge (Fig. 4), the Colonial Mine and the Wittenoom Mine. Here mining was entirely within the Dales Gorge Member of the Brockman Iron Formation (Trendall and Blockley, 1970).

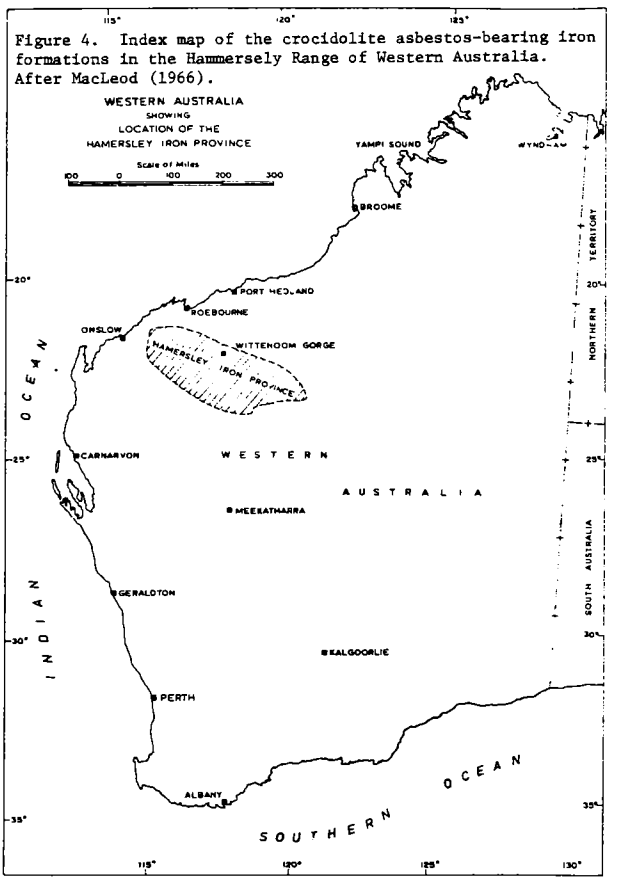

Figure 4. Index map of the crocidolite asbestos-bearing iron formations in the Hammersely Range of Western Australia. After MacLeod (1966).

Anthophyllite in Alpine-type ultramafic rocks of East Finland

In the Karelian Mountains of East Finland there occur a number of ultramafic bodies in the form of pods or lenses which were originally dunite or enstatite-bearing peridotites. These alpine-type serpentinized ultramafic masses are thought to have been once a part of much larger

slabs of oceanic or continental mantle material, which during the mountain building episode broke up into smaller volumes of rock and were injected upwards into overlying rocks of the Karelidic schist belt. The Karelide metasediments are thought to range in age from ∿2200 to ∿2000 m.y. (Simonen, 1980). Late Karelian granites (∿1900 m.y.) were injected into the schist belt rocks, and where they make contact with the serpentinized periotites, commercial quality anthophyllite asbestos is developed -- at Paakkila, located on the northern shore of Lake Juojärvi, East Savo, and at Maljasalmi, 10 km to the southeast.

The main asbestos producing area at Paakkila is comprised of biotite gneiss with numerous pods or lenses of ultramafic rock cut by Maarianvaava granite (Fig. 5). These pods typically contain relict olivine surrounded by serpentine aggregates and bundles of anthophyllite needles. Commonly the anthophyllite needles penetrate poikiloblastically the relict olivine (Wiik, 1953). Talc sometimes has replaced anthophyllite and olivine; there is not much serpentinization (Haapala, 1936).

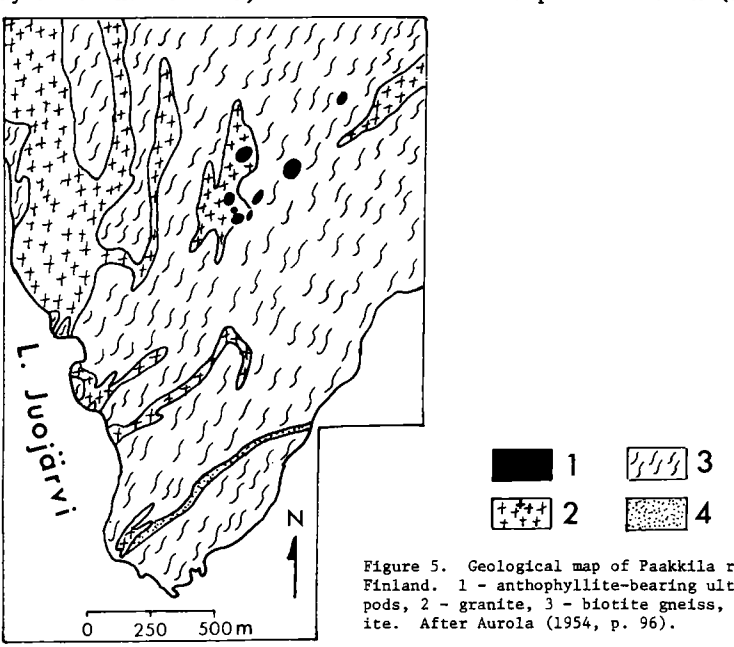

Figure 5. Geological map of Paakkila region, East Finland. 1 - anthophyllite-bearing ultramafic pods, 2 - granite, 3 - biotite gneiss, 4 - quartzite. After Aurola (1954, p. 96).

The country rocks in the Maljasalmi area, the secondary anthophyllite asbestos producing locality, are Karelian mica schist cut by granite pegmatite dikes. The serpentinized peridotites within the schists are

similar to those of Paakkila, with the exception that anthophyllite has clearly replaced enstatite. Relict enstatite is still present, penetrated by needles of anthophyllite; in addition, olivine-bearing serpentine, talc, and chlorite have been observed (Aurola, 1954).

The anthophyllite asbestos deposits at Paakkila were first leased in 1907 but not worked to any degree until 1918, when they were taken over by Suomen Mineraali Oy and operated continuously until production stopped for economic reasons in 1975. Paakkila produced in total 350,000 tonnes of asbestos, of which 230,000 tonnes was exported (Huuskonen *et al.*, 1980). The asbestos mine and mill at Maljasalmi was operated contemporaneously by the same company, but the ore was inferior to that from Paakkila.

MINOR GEOLOGICAL OCCURRENCES OF AMPHIBOLE ASBESTOS

Anthophyllite asbestos

Small deposits of anthophyllite asbestos have been worked in many localities, but none approached the Paakkila output of 350,000 tonnes. In the United States anthophyllite has been mined in a number of localities, particularly in Georgia, North Carolina, Idaho, Maryland, and Massachusetts. Some of the more active mines were the Sall Mountain and Calhoun mines, Sall Mountain, Georgia; the Hollywood mine, Habersham County, Georgia; the Kamiah mine, Idaho County, Idaho; the Bok Asbestos mine and Alberton mine, Baltimore County, Maryland; and the Pelham quarry, Hampshire County, Massachusetts. The mode of occurrence of anthophyllite asbestos in these localities is very similar to that in Paakkila and Maljasalmi, East Finland. Typically these anthophyllite deposits are found in metamorphosed ultramafic bodies, generally serpentinized and amphibolized dunites and harzburgites caught up as inclusions within the country rock schists and gneisses. In localities within the Appalachian Orgenic belt, metamorphism is regional and repeated; in Kamiah, Idaho, much of the metamorphism was accomplished by the intrusion of the Idaho batholith. Granitic intrusions are noted in some localities and may have contributed to the metamorphism, particularly in regard to supply of heat, SiO_2, and H_2O.

The Kamiah deposit (Anderson, 1931) is particularly interesting in

its similarity to the Finnish deposits. Here also the ultramafic lenses (dunites and harzburgites) are included within mica schists and gneisses. Anthophyllite clearly replaced olivine and enstatite, for needles grew into the relict grains. In addition, anthophyllite replaces antigorite, the antigorite having previously replaced olivine. Talc is a minor constituent in the Kamiah deposit but replaces anthophyllite, antigorite, and olivine. The various assemblages observed at Kamiah, Paakkila, and Maljasalmi can be explained with the phase diagrams suggested by Hemley *et al.* (1977), three of which are shown in Figure 6.

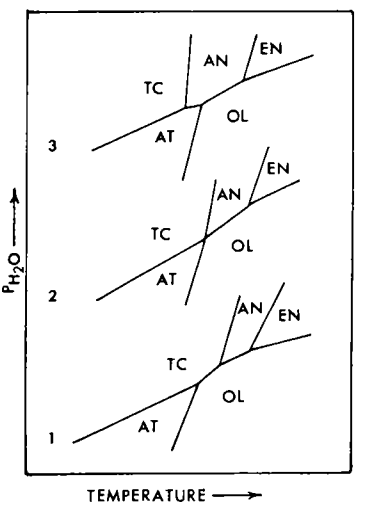

Figure 6. Proposed phase relations in the system $MgO-SiO_2-H_2O$ (Hemley *et al.*, 1977). EN - enstatite, AN - anthophyllite, AT - antigorite (serpentine), OL - olivine, TC - talc. Suggested reactions which could occur at lower or higher P_{H_2O} (1, 2, or 3) are: EN → AN (M,K), OL → AN(P,K), OL → AT (P,K), AT → TC (K), AN → TC (P,K). Reaction at lower P_{H_2O} only: OL → TC (P,K). Reaction at higher P_{H_2O} only: AT → AN (K). M - Maljasalmi, Finland; P - Paakkila, Finland; K - Kamiah, Idaho.

Tremolite asbestos

Although there are numerous references to tremolite asbestos in the literature, relatively little of this fiber entered the world market. Probably the most famous reference to tremolite asbestos is to that from the Italian Alps, reportedly the asbestos of the Romans. Inquiry into this, however, leads one to believe that most of the asbestos fiber from the Alps was chrysotile, not tremolite.[3] Fibrous tremolite has not been reported in the recent and extensive literature on metamorphosed ultramafic rocks from north Italy, whereas chrysotile is often mentioned. Also, in a letter to Oliver Bowles, asbestos commodity specialist, U.S. Bureau of Mines (Bowles, 1937, p. 6), the chief mineral inspector in Rome stated in part:

"For a long time it was believed that the Italian 'amianti' were all the tremolite type because the first examinations of the material were based on samples of tremolite. It was only in recent years that, after further studies, the producers recognized that their products were for the most part chrysotile with a long, flexible fiber."

Tremolite asbestos has been mined in the Natal, South Africa, where it occurs in green talcose rocks -- probably altered ultramafic rocks similar to those of the Jamestown Series in the Barberton district of South Africa (Hall, 1918, p. 109). In the United States tremolite asbestos has been mined in small quantities near Powhatan and Pylesville, Maryland, where it occurs in amphibolized ultramafic rocks. Anthophyllite asbestos also occurs in these same rocks.

Actinolite, amosite, and crocidolite asbestos

Commercial mining of actinolite asbestos is practically unknown. No mining of amosite asbestos occurs outside the Transvaal. In the past crocidolite was mined in the Cochabamba, Bolivia, from rocks of igneous origin.

MAJOR OCCURRENCES OF CHRYSOTILE ASBESTOS

The commercially most important form of asbestos, chrysotile, is found in three distinct types of deposits: (Type I) alpine-type ultramafic rocks, including ophiolites, (Type II) stratiform ultramafic intrusions, and (Type III) serpentinized limestones. Type I deposits are by far the most important, furnishing at least 85 percent of the world's chrysotile fiber. Type III deposits are relatively unimportant but do furnish some high quality fiber.

Type I deposits

One example of a Type I deposit has already been discussed, the Paakkila and Maljasalmi fields of East Finland. In these deposits, however, the valuable asbestos mineral is anthophyllite, not chrysotile.

The two most important asbestos producing localities in terms of production, past and present, are the serpentinized ultramafic rocks of the central and southern Urals and of the Appalachian Mountains in

southeast Quebec and northern Vermont. The Russian and North American occurrences are similar; the serpentinites are of the alpine-type and part of ophiolite sequences (Coleman, 1977).

The chrysotile asbestos deposits of Quebec, and their extension into northern Vermont, occur in altered peridotites, which form part of an ophiolite suite of rock types. Included in this suite, in addition to the peridotites (dunites and harzburgites), are gabbro cumulates, diabase sills, tholeiitic pillow lavas, and red argillites. These units were emplaced tectonically into the country rocks in early Ordovician time. The peridotites, regarded as fragments of oceanic crust and mantle, are suggested to have undergone the following sequence of events: (1) the formation of peridotites in an oceanic environment through lithosphere accretions and sea-floor spreading; (2) the fragmentation and tectonic emplacement; and (3) deformation of the ultramafic rocks within the Cambro-Ordovician country rocks (Laurent and Hébert, 1979). These same authors propose that serpentinization occurred in two stages: (1) early serpentinization in an oceanic environment at low temperatures, where lizardite was the principal serpentine mineral, and (2) late serpentinization in a dynamic regime of tectonic transport and emplacement, where fracturing of the peridotite masses took place. Chrysotile asbestos formed in these late-stage fractures, probably in a stress environment.

Chrysotile-bearing serpentinites form a part of a discontinuous belt of ultramafic bodies and associated rocks extending for almost the entire length of the Appalachian Mountain chain. The major and active chrysotile deposits are, however, centered in Quebec in the towns of Black Lake, East Broughton, Thetford Mines, and Asbestos; smaller active deposits are at Baie Verte, Newfoundland, and Eden Mills, north-central Vermont. Further south in the Appalachian Chain, the ultramafic bodies generally contain only small amounts of chrysotile; thus, only minor production of this fiber, with the exception of the Vermont Asbestos Group operation at Eden Mills, has occurred in the eastern United States. As already alluded to, these ultramafic rocks in Maryland, Virginia, North Carolina, and Georgia have been the sources of minor amounts of anthophyllite and tremolite asbestos.

The Quebec chrysotile deposits were first discovered in 1877 in the

serpentine hills of Thetford and Coleraine. By 1900 this area had already produced 150,000 tonnes of chrysotile fiber; by 1980 nearly 40 million tonnes had been mined -- approximately 40 percent of the world's total asbestos production to that date. At present Quebec is the second leading producer of asbestos, approximately 1.4 million tonnes per annum, and is led only by the Ural areas of Russia, where the annual production is approximately 2.4 million tonnes.

The serpentinites associated with ophiolites within the Ural Mountain belt of the Soviet Union account for about 95 percent of the Russian production, all of which is chrysotile fiber. The two principal centers of production in the Urals are the Uralasbest complex, 90 km northeast of Sverdlovsk, and near Dzhetygara, in the southern Urals.

Other major Type I chrysotile asbestos deposits are found in the Italian Alps, the Troodos Mountains of Cyprus, and the Coalinga area of California. The classic asbestos deposits of north Italy are located in the Susa, Lanzo, Aosta, and Val Malenco areas of the Alps. These are areas underlain by metamorphosed ultramafic rocks of the alpine-type. At present the Balangero mine, located 30 km northwest of Turin in the Lanzo area, is the only operating asbestos mine in western Europe of any significance. The mine opened in 1916 and its present production is about 160,000 tonnes of chrysotile fiber per year.

The occurrence of asbestos on Cyprus may have been known many centuries ago, but significant production of chrysotile fiber began only in the 1920's. Production is now about 40,000 tonnes per annum. The deposits are in the Mt. Troodos Ophiolite Complex, one of the best studied ophiolite sequences in the world.

Near Coalinga, California, and located in the southern extension of the Diablo Range is a serpentinite dome exposed to the surface in an area 19.2x6.4 km and extending in depth to perhaps 4.5 km. This serpentine diapir consists of highly sheared serpentine minerals, which replaced the original olivine-orthopyroxene assemblage. The diapir probably formed by dismemberment of an ophiolite peridotite by tectonic forces, the sheared mélange moving upwards diapirically during subsequent orogenic events (Coleman, 1977, 1980; Mumpton and Thompson, 1975). The chrysotile asbestos is mined by several companies at Coalinga, but mining is sporadic and production is limited. Even though the ore runs up to 50 percent

chrysotile (Quebec ore usually runs 3 to 6 percent), mining has lagged because of environmental controls and the shortness of the fibers (grades nos. 6 and 7). The reserves at Coalinga are tremendous; perhaps tens of millions of tonnes of short fiber are available near the surface, making Coalinga a vast resource for a type of asbestos which will be useful to strengthen plastics, tiles, etc.

Type II deposits of southern Africa

Whereas most of the chrysotile mined in the two major asbestos producing countries, Canada and the U.S.S.R., is from serpentinized ultramafic rocks within ophiolite sequences, almost all of the southern African production comes from Archean ultramafic stratiform complexes. These are generally associated with the ancient greenstone belts on the Rhodesian and Kaapvaal Cratons (Anhaeusser, 1976). Within the African greenstone belt, and particularly in the Lower Ultramafic Unit, a number of layered differentiated ultramafic pods and sills are developed which contain chrysotile fiber of economic importance. While age, stratigraphic, and genetic relationships of these Archean ultramafics are quite different from those of the ophiolites, both contain peridotite assemblages, including dunites, which have altered to chrysotile-bearing serpentinite.

South Africa and Swaziland. Here the two largest producers of chrysotile asbestos are the Msauli and Havelock mines, situated approximately 30 km southeast of Barberton, South Africa. The Havelock mine is situated just over the Transvaal border in Swaziland. These deposits are included within the Swartkoppie Formation, which straddles the Swaziland-Transvaal border. This formation includes green and gray schists, banded cherts, and a number of serpentine pods or lenses positioned in the same stratigraphic horizon. The serpentinized ultramafic inclusions are considered to represent parts of a once continuous or nearly continuous differentiated sill emplaced penecontemporaneously with the remaining Swartkoppie rocks and conformable with the latter (Anhaeusser, 1976). The other active chrysotile mines in South Africa occur in ultramafic bodies similar to those in the Msauli-Havelock area. Deposits located in Barberton Mountain Land of South Africa occur in the Stolzburg, Koedoe, Handsup-Mundt's Concession, Kaapsehoop, Kalkkloof, and

Rosentuin ultramafic bodies. Three small deposits are situated within the Muldersdrif ultramafic body about 25 km north of Johannesburg.

Chrysotile production in Swaziland for the year 1978 was 48,000 tonnes -- mainly from the Havelock mine. South African production of this fiber for 1978 was 113,000 tonnes and came from the Type II ultramafic deposits described above, as well as from Type III sedimentary deposits of the Carolina district.

Zimbabwe. The two principal chrysotile producing mines in Zimbabwe are located within the Mashaba and Shabani igneous complexes. The Mashaba complex occurs at the western end of the Fort Victoria greenstone belt in southern Zimbabwe. It is a layered ultramafic intrusion which includes pyroxenites and serpentinized dunites and harzburgites. The Shabani ultramafic body, located approximately 100 km west of Fort Victoria and immediately east of the Great Dyke, is a lenticular ultramafic sill and is suggested to have intruded into the Archean gneisses at the northeast margin of the Belingwe schist belt (Anhaeusser, 1976).

Small chrysotile deposits are found in the Filabusi ultramafic complexes located about 50 km west of the Shabani deposits and at the Ethyl deposit at the north end of the Great Dyke. The Great Dyke is an elongate mass of mafic and ultramafic rocks extending nearly 500 km across the Rhodesian Craton. It is not a true dike but rather the remains of four lopolithic intrusions. Chrysotile asbestos is found in the vicinity of faults where serpentinization apparently was promoted.

In 1978 the Zimbabwean chrysotile production was 210,000 tonnes, of which about 60 percent came from the Shabani and 35 percent from the Mashaba deposits.

Type III deposits

Commercially less important, yet geologically very interesting chrysotile deposits occur in serpentinized limestones; two notable localities are in the Globe area of central Arizona and in the Carolina area of the Transvaal.

The Arizona asbestos-bearing strata occur in the Precambrian Mescal limestone formations of the Apache Group, where diabase sills a few centimeters to a few meters thick have intruded. The commercial asbestos is developed by replacement of the limestones by serpentine, usually occurring

within 40 meters of the diabase intrusion (Bateman, 1923; Stewart, 1961). Although only about 50,000 tonnes of chrysotile asbestos has been produced from Arizona from the time the deposits were opened early in this century to the present, the fiber is of very high quality and much sought after for applications in advanced technology.

An occurrence very similar to that in Arizona is found in the Transvaal Basin, where dikes and sills of diabase have intruded and altered the Malmani Dolomite. The principal asbestos deposits are located in eastern Transvaal west of Barberton Mountain Land and east of Carolina. The sills commonly produced a metamorphosed assemblage in the dolomite extending for a meter or more above the upper chilled contacts with the diabase. The controls on serpentine mineralization involve dedolomitization to calcite to furnish magnesium, solution of chert to furnish silica, and the presence of the diabase sill to furnish H_2O and heat (Anhaeusser, 1976). Fiber is not developed in chert-free dolomite but is seen replacing chert where present immediately above the sill.

As with the formation of amphibole asbestos discussed previously, it appears that in addition to the necessary chemical controls, a stress environment resulting from folding, faulting, or differential heating is required to promote the growth of chrysotile fiber. Anhaeusser (1976) suggests that the dominant regional controlling factor for asbestos development is folding.

HEALTH HAZARDS OF ASBESTOS

Diseases related to asbestos exposure

There are three principal diseases which are related to exposure to one or more of the commercial asbestos minerals. These are: (1) lung cancer, which includes cancer of the trachea, bronchus, and lung proper; (2) mesothelioma, a cancer of the pleural and peritoneal membranes which invest the lung and abdominal cavities, respectively; and (3) asbestosis, a diffuse interstitial fibrosis of the lung tissue often leading after long exposure to severe loss of lung function and respiratory failure. The lung cancer of asbestos workers is also associated with cigarette smoking, which leads to considerable difficulty in assigning relative risks of asbestos exposure to smokers. Mesothelioma, a disease which is

usually fatal in one to two years after diagnosis, is rare, accounting for about 280 deaths per year in the United States and Canada. Of these deaths, there was a definite or a probable exposure to some form of asbestos in about 50 percent of the cases. Exposure to asbestos was unlikely in about 30 percent of the cases (McDonald and McDonald, 1980).

There are some epidemiological studies which suggest that asbestos workers may suffer excess cancer of the digestive tract (Selikoff and Lee, 1978); other studies do not support this conclusion (McDonald and McDonald, 1980; Meurman *et al.*, 1974; Rubino *et al.*, 1979; Nicholson *et al.*, 1979). There is still some question, then, as to the role played by asbestos in the etiology of digestive tract cancers. Becklake (1976), Selikoff and Lee (1978), and Simpson (1979) give complete reviews of the subject of asbestos and disease.

Although there seems to be no question that the residency of asbestos fibers within the lung and pleura for long periods of time can cause lung cancer, asbestosis, and mesothelioma, the exact mechanisms of disease production and the relative potencies of the different asbestos minerals are subjects of much study and many differences of opinion. By reviewing in the next section the health of miners exposed to specific minerals dusts and asbestos trades workers exposed to a variety of dusts, perhaps we can become more enlightened on this subject.

Particle size and shape appear to be the controlling factors with regard to whether mineral particles enter the lung and remain in the lung or are removed from the lung after entering. Particles such as asbestos fibers which have diameters greater than approximately 5 μm can not enter the bronchial airways[5]; those with smaller diameters do. Particles with diameters < 3 μm can penetrate to the smaller bronchioles and even to the alveolar sacs, the critical gas exchange portions of the lung. Most particles which enter the upper respiratory tract (the mainstem, bronchi, and bronchioles) are quickly and effectively removed by the mucocilliary

[5]The airways of the lung form the bronchial tree, which is subdivided into the main stem and then into 22 additional branchings. The first several branchings constitute the bronchi, the last several the bronchioles. The terminal bronchioles lead to the respiratory bronchioles, which are lined with alveoli; the latter constitute the lower respiratory tract.

escalator; this is a system of mucous membranes and cilia lining the airways of the upper respiratory tract, which moves foreign particles upward to the pharynx, where they are unconsciously swallowed or spit out. A second lung clearance mechanism operates in the lower respiratory tract (the respiratory bronchioles and alveoli). Here pulmonary macrophages, or scavenger cells, engulf the foreign particles (phagocytosis) and then (1) move to the upper respiratory tract, where the mucociliary escalator is operative, or (2) move through the alveolar wall into the interstitium and eventually to the lymph channels.

Asbestos fibers which are longer than approximately 5 μm are not readily phagocytized by the macrophage cells and thus tend to remain in the lower respiratory tract, or they may penetrate the pleural membrane and enter the interpleural space. It is thought that when such fibers remain in the lung for lengthy periods of time, various biochemical reactions take place which promote the growth of interstitial collagen within the lung tissue, causing it to become fibrous with ensuing asbestosis. Long term residency of fibers in the lung and pleura also causes lung cancer and mesothelioma; the mechanisms by which this occurs are far from being understood.

Pleural cancer as we will see seems to be caused by crocidolite asbestos but not by chrysotile or anthophyllite asbestos. Lung cancer is caused by chrysotile, anthophyllite, amosite, and crocidolite asbestos in asbestos workers who smoke cigarettes. Evidence for excess lung cancer in non-smoking asbestos workers is weak. Two completely different substances, asbestos and cigarette smoke, combine to produce a very significant risk to many asbestos workers, particularly those who were heavily exposed to asbestos dusts.

Generally, asbestos-related diseases appear in asbestos workers only after many years have elapsed since first exposure. A significant increase in the lung cancer death rate appears 10 to 14 years after first exposure and peaks at 30 to 35 years. The mesothelioma death rate becomes significant 20 years after first exposure but continues to climb even after 45 years have elapsed. The asbestosis death rate becomes significant 15 to 20 years after first exposure and apparently peaks at 40 to 45 years (Selikoff *et al.*, 1980a).

Epidemiology

Before considering the mortality studies of the various occupational groups exposed to asbestos, it is useful to briefly consider the roles the three important types of asbestos (amosite, crocidolite, and chrysotile) have played in the commerce of North America and Europe, the areas where the major epidemiological studies of asbestos workers were made.

In North America, chrysotile entered the market in large quantities early in this century. Crocidolite was apparently first used in the United States in 1912 when 9 tonnes was imported, but it was not until World War I that its use for high temperature insulation became established -- particularly in the ship building industry. By 1930 nearly 32,000 tonnes of crude crocidolite fiber had been imported into the United States (*Mineral Resources of the United States*, 1907...1929, U.S. Dept. Interior, Washington, D.C.). It was not until the mid 1930's that amosite asbestos gained a market in North America when it began to replace crocidolite for high temperature insulation. Crocidolite was milled in Bound Brook, New Jersey, in 1920, and in 1924 the operation moved to larger facilities in Millington, New Jersey. The many advertisements in the trade journal *Asbestos* during the period 1920 to 1945 indicate that crocidolite was used in many products and particularly for insulation of steam boilers, locomotives, and pipes. As an example, a product containing crocidolite asbestos and called "85% Magnesian Sectional Pipe Covering" was advertised monthly in *Asbestos* from 1920 to 1945 (see also McCullagh, 1980). Amosite, crocidolite, and chrysotile were almost universally used aboard ships during World War II, amosite for high temperature boilers and pipes, crocidolite for packings exposed to acids or salt water, and chrysotile for low temperature and electric insulation.

The use of asbestos in Europe paralleled that in North America, with one notable exception -- the extensive use in Europe of crocidolite asbestos as a sprayed-on coating to fireproof ships[6], railroad cars,

[6]Mesothelioma is prevalent in the shipyard workers of Europe; at Walcheren, Wilhelmshaven, Plymouth, Trieste, Hamburg, Nantes, Rotterdam, and Malmö (McDonald and McDonald, 1977). The extensive use of crocidolite aboard European ships prior to and during World War II is suggested to be an important factor in the etiology of this disease.

buildings, etc. Sprayed-on coatings were also used in the United States after World War II, but the coatings contained, with few exceptions, chrysotile rather than crocidolite. Sprayed-on asbestos coatings were not used on U.S. ships, the principal use being to fireproof steel building girders and as acoustical coatings in schools and offices.

Asbestos trades workers. A very significant increased incidence, relative to the general male population, of lung cancer, asbestosis, and mesothelioma is found in men who were employed in the "asbestos trades" -- the insulation of steam locomotives, boilers, ships, and buildings; and the fabrication and installation of asbestos-containing textiles, roofing materials, cement products, tiles, wallboards, brake linings, clutch facings, filters, packings, gaskets, etc. Those in the "trades" generally used several types of asbestos minerals during their working careers; most commonly these were chrysotile, crocidolite, and amosite, and rarely anthophyllite. Significant exposures of any group of workers, at least for the past fifty years, to tremolite or actinolite asbestos dusts has probably not occurred.

Thirteen major mortality studies of asbestos trades workers are presented in Table 4; five of these are of workers engaged in the asbestos insulation trades, and eight are of workers in the factory and textile trades. Most of the workers are male, a few are female. In all, 38,904 individuals were followed; of these, 5,450 have died, including 998 (18.3 percent) who died of lung cancer and 327 (6.0 percent) who died of mesothelioma. In the thirteen studies the lung cancer mortality varied from 6.1 to 24.5 percent of all deaths; mesothelioma mortality varied from 0 to 9.5 percent of all deaths. The workers involved in studies nos. 1 through 12 worked with more than one form of asbestos; those in study no. 13 worked only with chrysotile asbestos.

Estimates of expected cancer mortality are very difficult to predict, because cancer rates are modified by the individual's "lifestyle," as well as by occupation. The major "lifestyle" contribution to lung cancer is cigarette use. To better assess the significance of these health studies, it is necessary to examine the cancer mortality patterns of cigarette smokers who were not exposed to asbestos dusts. Unless prevalence of smoking within the study group is carefully evaluated, it

is impossible to predict accurately the health effects of occupational exposure to carcinogens such as asbestos, radon gas, and arsenic. Unfortunately, in only a few of the studies listed in Table 4 have adequate assessments been made of the proportion of workers who smoke cigarettes.

The contribution of cigarette smoking to the increased incidence of disease has been evaluated in several studies and has led to a concensus that this habit produces a very significant increase in risk of dying of lung cancer, as well as of the various cardiovascular diseases. The largest study of cigarette smokers is that of E. Cuyler Hammond and colleagues under the auspices of the American Cancer Society. This study is based on questionnaires and mortality follow-up accomplished between July 1960 and June 1971 for approximately 51,000 men (Hammond *et al.*, 1978). The proportional mortality of lung cancer (percent lung cancer deaths relative to deaths by all causes), based on the Hammond study, is shown graphically in Figure 7. For a group of men who all smoke cigarettes (cohort of 100 percent smokers) lung cancer mortality is approximately 7 percent at age 45, reaches a maximum of approximately 10 percent at age 70, then decreases slightly at older ages. For a cohort of male non-smokers, lung cancer mortality is 2 percent at age 45 and then decreases continuously to approximately 1 percent at age 95.

Smoking is most prevalent in blue-collar occupations relative to professional and managerial occupations (Sterling and Weinkam , 1978). This prevalence also holds true for the asbestos trades, mining, and milling occupations. In a group of 13,722 asbestos insulation workers whose smoking habits were recorded, 70 percent had a history of cigarette smoking (Selikoff and Hammond, 1975; Saracci, 1977). In a group of 1,015 chrysotile asbestos miners and millers, 85 percent were smokers (McDonald *et al.*, 1974). Data given in Figure 7 predicts that the lung cancer mortality for a cohort composed of 75 percent smokers would be at least 6 to 7.5 percent, regardless of occupation. In Table 4 we see that the lung cancer mortality for the total of 13 cohorts of asbestos "trades" workers was 18.3 percent -- approximately three times that expected if mortality predictions were based only on the apparent smoking habits.

The increased risk of lung cancer due to asbestos exposure in non-smokers is very low (Saracci, 1977). There appears to be no relationship

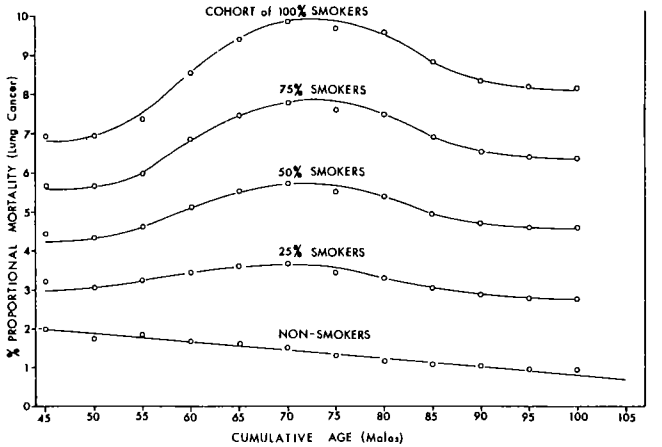

Figure 7. Percent of lung cancer deaths in males relative to deaths by all causes (proportional mortality - lung cancer) plotted with respect to age for four groups (cohorts) with different cigarette smoking characteristics and for a cohort of non-smokers. For example, for a cohort of 70-year old males which is composed of 75 percent cigarette smokers, 7.8 percent of all deaths at age 70 are predicted to be from lung cancer. Graphical presentation based on data from Hammond *et al.* (1978).

Table 4. Cancer mortality for men working in the asbestos "trades"

Study No.	Ref.[1]	Occupation	No. in cohort	No. deaths	Lung cancer No.	Lung cancer (%)[3]	Mesothelioma No.	Mesothelioma (%)[3]
1	(A)	Insulators, NY-NJ (1943-74)	632	451	89	(19.7)	35	(7.8)
2	(B)	Insulators, U.S., Canada (1967-76)	17800	2270	485	(21.4)	175	(7.7)
3	(A)	Factory, N.J. (1941-74)	933	483	83	(17.2)	10	(2.1)
4	(C)	Insulators, U.S. (1967-71)	7289	446	79	(17.7)	23	(5.2)
5	(B)	Factory, U.S. (1959-75)	689	274	35	(12.8)	26	(9.5)
6	(D)	Factory, England (1931-74)	1106[2]	317	51	(16.1)	10	(3.2)
7	(E)	Insulators, N.Y. (1945-65)	152	46	10	(21.7)	3	(6.5)
8	(F)	Insulators, Belfast (1940-66)	170	98	24	(24.5)	7	(7.1)
9	(G)	Textiles, London (1931-70)	6760	350	63	(18.0)	24	(6.9)
10	(H)	Factory, Cardiff (1936-62)	1165	133	11	(8.3)	1	(0.8)
11	(I)	Factory, Penn. (1938-64)	1265	330	35	(10.6)	8	(2.4)
12	(J)	Textiles (1933-74)	679	186	29	(15.6)	5	(2.7)
13	(K)	Factory, U.S.A.[4] (1945-74)	264	66	4	(6.1)	0	0
Total of cohorts			38904	5450	998	(18.3)	327	(6.0)

[1] References: (A) Selikoff, 1977; (B) Nicholson et al., 1978; (C) Selikoff et al., 1973; (D) Peto et al., 1977; (E) Kleinfeld et al., 1967; (F) Elmes and Simpson, 1971; (G) Newhouse, 1973; (H) Elwood and Cochrane, 1964; (I) Mancuso and El Attar, 1967; (J) Peto, 1978; (K) Weiss, 1977.

[2] includes 284 women

[3] percent of all deaths (proportional mortality)

[4] workers were exposed only to chrysotile asbestos

between smoking habits and the incidence of mesothelioma; this disease is equally prevalent in smokers and non-smokers alike. Of the studies listed in Table 4, only Study no. 13 of chrysotile factory workers shows a lung cancer mortality that would be expected from the smoking habits alone.

Asbestos miners and millers. Men working in the mining and milling of asbestos ore are generally exposed to only one form of fiber. A few exceptions occur in the mining regions of South Africa, where some workers have been employed in crocidolite, amosite, and chrysotile mines. Anthophyllite and tremolite asbestos miners may have been exposed to some chrysotile asbestos, because these minerals can coexist in metamorphosed ultramafic rocks, for example those of Paakkila, Finland, and Kamiah, Idaho.

Epidemiological studies of asbestos miners and millers who were exposed to only one form of asbestos are useful for understanding how the different asbestos minerals affect human health. In Table 5 are given the mortality data for the five major epidemiological studies of asbestos miners and millers. In addition, three studies are given of miners exposed to cummingtonite and grunerite amphibole dusts and one study of tunnel workers exposed to hornblende amphibole dust. Some classify these amphiboles as asbestos, even though they do not possess the physical properties requisite to be valuable commercially. Such a classification has been made in the case of taconite mining by the courts (United States District Court for Minnesota, 380 F. Supp. 11) and by the U.S. Environmental Protection Agency (Reserve Mining *vs* EPA, U.S. Court of Appeals Eighth Circuit, March 14, 1975), which has sued to prevent the Reserve Mining Company from dumping taconite tailings into Lake Superior because of the perception that these tailings contain "amosite asbestos" and thus constitute a threat to public health. For a complete review of the case, see 514 Federal Reporter, 2d Series, 492-542, 1975; 256 North Western Reporter, 2nd Series, 808-852, 1977. Of interest regarding this suit are the health studies accomplished on the Reserve iron ore miners exposed to cummingtonite and grunerite in the taconite rock (Table 5, Study II) and on the Homestake gold miners exposed to

Table 5. Mortality from selected causes in the principal epidemiological studies of commercial asbestos miners and millers and other hard rock miners and tunnel workers exposed to rock dust containing minerals sometimes defined as asbestos[1/]

Cause of Death[2/]	Number of Deaths	Study I	II	III	IV	V	VI	VII	VIII	IX	Totals
		900 men 1936-1967	5751 men 1952-1976	932 men 1955-1972	440 men 1960-1973	1321 men 1937-1973	-- 1943-1977	933 men 1946-1975	544 men 1961-1977	10939 men 1910-1975	(excluding Study VI)
All causes (000-999)	Observed	216	298	294	71	631	519	332	178	4463	6483
	Expected		344	225	52.9	549.7	600.3	214.4	159.9		
	Obs./Exp.		0.87	1.30	1.34	1.15	0.86	1.55	1.11		
Respiratory cancer (162)	Obs.	21	15	21	10	16	60	10	28	250	371
	% all deaths	9.7	5.0	7.1	14.1[3/]	2.5	11.6	3.0	15.7	5.6	5.7
	Exp.	12.6	17.9	13.15	2.7	16.5	38.9	10.4	11.1		
	Obs./Exp.	1.67	0.84	1.60	3.0	0.97	1.54	0.96	2.5		
Mesothelioma, peritoneum, pleura (58,163)	Obs.	0	0		0	17	17	17	1	10[5/]	11 + 2?
	% all deaths	0	0		0	0.16?	3.3	0.30?	0.56	0.22	0.17+0.03?
Gastro-intestinal cancer (150-154) or (150-159)	Obs.	7	20	10		39		19	10	168	273
	% all deaths	3.2	6.7	3.4		6.2		5.7	5.6	3.8	4.2
	Exp.	14.9	17.6	11.13		35.1		19.3	9.5		
	Obs./Exp.	0.47	1.14	0.90		1.11		0.98	1.05		
Pneumoconiosis (500-519)	Obs.		4[4/]	20	5	37	21[1/]	20	30	46[6/]	
	% all deaths		1.3	6.8	7.0	5.9	4.0	6.0	16.9	1.0	
Asbestosis (501)	Obs.	13						9	26		
Silicosis (502)	Obs.					35					
Respiratory tuberculosis (011-012)	Obs.	36		11		39	4	18		248	
	% all deaths	16.7		3.7		6.2	0.77	5.4		5.6	

Locality	North Savo, Finland	Minnesota, U.S.A.	Manhatten I. N.Y., U.S.A.	Lead, ND, U.S.A.	Lead, ND, U.S.A.	Wittenoom, W. Australia	Balangero, Italy	Quebec, Canada	Quebec, Canada
Type of Mining	ashestos	iron ore	tunneling	gold	gold	asbestos	asbestos	asbestos	asbestos
Type of Rock	ultramafic	taconite	schist,gneiss, amphibolite	qtz-cumming-tonite schist	qtz-cumming-tonite schist	banded ironstone	serpentinite	serpentinite	serpentinite
Suspected mineral pathogen	anthophyllite asbestos	cummingtonite, grunerite, quartz	hornblende, quartz	cummingtonite, hornblende, quartz	cummingtonite, hornblende, quartz	crocidolite asbestos, quartz	chrysotile asbestos	chrysotile asbestos	chrysotile asbestos
Source	Meurman et al., 1974	Higgins, 1981	Selikoff, 1978	Gillam et al. 1976	McDonald et al., 1978	Hobbs et al., 1980	Rubino et al., 1979	Nicholson et al., 1979	McDonald et al., 1980

1/ Cummingtonite, grunerite,and hornblende (Studies II, III, IV, V) may he defined as "ashestos" in U.S. Federal Regulations.
2/ International Classification of Diseases, 9th revision (ICD-9-CM), January 1, 1979.
3/ Includes one carcinoma of the maxillary sinus and one mediastinal carcinoma (unspecified). See footnote 7/ in text.
4/ Pneumoconiosis Board Records (Western Australia) show pneumoconiosis of mixed type, ashestosis, silico-ashestosis, and silicosis.
5/ Two mesothelioma victims worked with crocidolite in addition to chrysotile.
6/ Pneumoconiosis is probably predominantly ashestosis since rock dust contains little crystalline silica (quartz, etc.)
7/ "Selected respiratory disease"

cummingtonite in the gold-bearing schists (Table 5, Study IV, V).[7] Studies II and V show no evidence of asbestos-related diseases appearing in the study groups.

Mortality comparisons, trades vs. mines. The cancer mortality pattern for those in the asbestos trades and mining occupations is graphically presented in Figure 8, where lung cancer mortality is plotted with respect to mortality due to mesothelioma. The studies of the

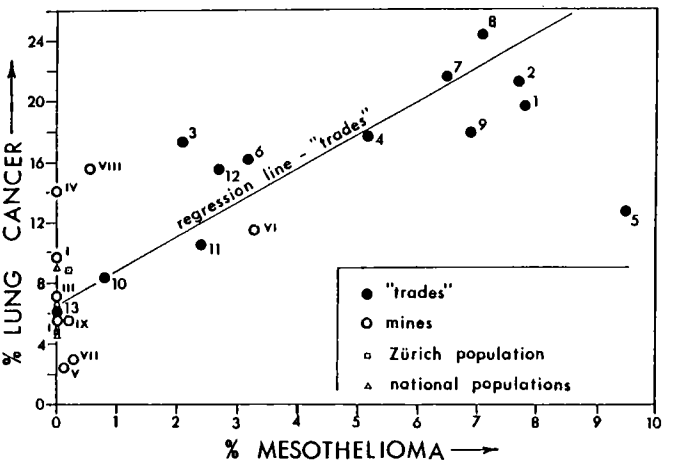

Figure 8. Graphical comparison of the proportional mortality due to lung cancer and mesothelioma for the asbestos trades workers ("trades," Table 4, Studies 1-13), the asbestos miners and millers ("mines," Table 5, Studies I-IX), the male population of the Zürich area of Switzerland, and the male populations of five nations (Table 6). Regression analysis of the mortality of the asbestos trades workers (Studies 1-4, 6-13) shows a positive correlation between the two diseases; 78 percent of the variance ($\bar{r}^2$) of lung cancer is accounted for by mesothelioma. The regression line is of the form: y(mesothelioma) = -2.94 + 0.446x (lung cancer). The intercept at y = 0 is 6.6 percent lung cancer, a reasonable estimate of mortality for this disease if the asbestos trade workers had never worked with asbestos but had retained their smoking habits.

[7] Study V (McDonald *et al.*, 1978) discredits Study IV (Gillam *et al.*, 1976). Study IV was accomplished on a sub-cohort of the Study V cohort. The latter study is much more complete; statistically it is based on 631 deaths, whereas Study IV is based on 71 deaths. In addition, Study IV presents an implausible mortality pattern: (1) No deaths due to silicosis, tuberculosis, or silico-tuberculosis were reported, despite the fact that the mining company has been coping with a quartz dust problem for a century, and (2) a 14·1 percent respiratory cancer mortality (incorrectly included as respiratory cancer were a sinus and a mediastinal carcinoma) was attributed to "cummingtonite asbestos," yet no mortality due to asbestosis was reported. The cummingtonite found in the quartz-cummingtonite schist host rock is not asbestos, but rather garden-variety, rock-forming amphibole.

asbestos trades workers (Table 4; Fig. 8, solid circles) show a very significant excess of mortality due to mesothelioma relative to that found in the miners (Table 5, Fig. 8, open circles) -- with one exception, the crocidolite miners of Western Australia (Study VI). For the asbestos trades workers a disease correlation is evident. Neglecting Study 5 (Table 4, Fig. 8), which is somewhat anomalous, regression analysis of the twelve trades data points (Studies 1-4, 6-13, Table 4, Fig. 8) shows a positive correlation between lung cancer and mesothelioma mortality; 78 percent of the variance $(\bar{r}^2)$ of lung cancer is accounted for by mesothelioma. Part of the remaining variance (22%) can be accounted for by inter-cohort differences in prevalence of cigarette smoking. This is because the smoking habits of asbestos workers seem to greatly influence the lung cancer incidence but not mesothelioma incidence.

In regard to high mesothelioma mortality, it is important to note the health studies of two groups of specialized factory workers who, during World War II, were employed at the task of placing crocidolite filter pads into gas mask canisters. One group working in Canada, composed of 109 men and 90 women, suffered 12.5 and 16.1 percent lung cancer and mesothelioma mortality, respectively (McDonald and McDonald, 1978). A second group of 1600 people, mostly women, were employed at this same task at a factory in Nottingham, England. Jones *et al.* (1976) reported that 26 mesothelioma deaths have occurred in this group; 25 were women. A large number of workers in these two groups were exposed to asbestos only during this brief World War II work period. The high proportion of women with their more moderate smoking habits in the gas mask worker cohorts would suggest that the ratio of mesothelioma to lung cancer (1.3 for the Canadian group) would be higher than that observed in the more typical "trades" cohorts (Table 4), where the ratio averages 0.44 (Fig. 8).

With the exception of the crocidolite miners (Study VI), the mortality patterns of the hardrock miners (Studies II, V), the tunnel workers (Study III), the asbestos miners (Studies I, VII-IX), and the chrysotile factory workers (Study 13) is quite different from that of the "trades" (Studies 1-12). The most apparent difference between the "trades" cohorts and these miners, tunnel workers, and chrysotile factory workers is the relative incidence of mesothelioma. The latter groups,

composed of individuals who did not come into contact with crocidolite, have very low mesothelioma mortality.

To make further comparisons it is useful to examine the mortality with respect to lung cancer and mesothelioma in national populations. In Table 6 are given the lung cancer and mesothelioma mortality of all males over 24 years of age in five nations. These data are plotted in Figure 8. We find that the average lung cancer mortality of these five national populations is 5.7 percent, a figure identical to the 5.7 percent average mortality of the miners and tunnel workers (Table 5, excluding crocidolite miners). The mesothelioma mortality of the five national populations is 0.03 percent (Table 6) and is probably significantly underreported because of (1) the great difficulty in diagnosing this disease, even after autopsy (McDonald and McDonald, 1977, 1980; Vejlsted and Hansen, 1980; Kannerstein and Churg, 1980; Legha and Muggia, 1977) and (2) complications arising in properly and consistently coding this disease for later information retrieval.

Table 6. Cancer mortality in men over 24 years of age for 5 nations (McDonald and McDonald, 1977)

Nation	Deaths (year)	Lung cancer No.(%)[1/]	Mesothelioma No.(%)[1/]
England-Wales	278,617 (1970)	24913 (8.9)	154 (0.06)
Finland	22,332 (1970)	1586 (7.1)	8 (0.04)
Italy	272,795 (1970)	11867 (4.7)	not reported
U.S.A.	988,620 (1969)	50481 (5.1)	250 (0.03)
Canada	82,052 (1970)	4312 (5.3)	25 (0.03)
Totals	1,624,416	93159 (5.7)	437 (0.03)

[1/] percent of all deaths (proportional mortality)

It is more meaningful to compare mesothelioma mortality among asbestos workers and miners in whom this disease is looked for to the mortality in a population where the causes of death are based on a large number of autopsies and where asbestos exposure is minimal. A review has been made by Rüttner (1978) of the deaths in the Zürich area of Switzerland, where there are no asbestos mines, mills, or industries and where the

cause of death is often based on autopsy. Among the 28,110 male deaths (all autopsied) over the period 1961 to 1976, 51 deaths were due to mesothelioma (0.18 percent) and 2466 were due to lung cancer (8.8 percent). Among women (22,583 deaths) 23 were caused by mesothelioma (0.10 percent) and 368 caused by lung cancer (1.6 percent). The proportional mesothelioma mortality for hard-rock miners, tunnel workers, and asbestos miners (other than crocidolite) is 0.17 to 0.20 percent (Table 5). The asbestos trades workers, by contrast, have an average mesothelioma mortality of 6.0 percent (Table 4).

Among the asbestos miners and millers there is no question that those exposed to heavy concentrations of chrysotile and anthophyllite dust over long periods of time have suffered a significant excess mortality due to lung cancer and asbestosis -- but not to mesothelioma (Studies I, VIII, Table 5). The most detailed health study of asbestos miners to date is that of the chrysotile asbestos miners of Quebec (Table 5, Study IX). Here McDonald *et al.* (1980) have carefully documented the relationship between lung cancer incidence and cumulative dust exposure. The average dust concentrations that the miners and millers experienced during the working day were divided into four categories depending on the work tasks performed during their careers in the mines: low level 2.5 to 4.2 mpcf[8], medium level 4.3 to 9.4, high level 14.4 to 23.6, and very high level 46.8 to 82.6 mpcf. The mean within these four categories in terms of chrysotile fibers per cm^3 is: low 10 fibers/cm^3, medium 21 fibers/cm^3, high 95 fibers/cm^3, and very high 194 fibers/cm^3. For the men exposed for over 20 years in the low and medium dust categories (averaging 6.6 mpcf or approximately 20 fibers/cm^3), total mortality was less than expected (SMR = 0.94).[9] For

[8] mpcf = millions of particles of rock dust per cubic foot. Conversions of this figure into asbestos fibers per cubic centimeter, the usual measurement for industrial hygiene monitoring, is difficult, but an approximate and conservative figure is: 1 mpcf = 3 fibers/cm^3 (McDonald *et al.*, 1980, p. 21, 23; see also McDonald *et al.*, 1976).

[9] SMR (standard mortality ratio) = number of deaths expected in a cohort at risk divided by the number of deaths in a cohort not at risk (control cohort). "Standard" implies that the control cohort does not differ in a way from the cohort at risk other than exposure to a

these men there was a slight excess risk of lung cancer (SMR = 1.15) and respiratory tuberculosis (SMR = 1.14). Since exposures of 20 fibers/cm^3 are an order of magnitude higher than that experienced now (dust levels for the past few years have been maintained at less than 2 fibers/cm^3), miners working a lifetime under the present dust levels are not expected to present any significant health problems relative to those in other mining industries.

McDonald *et al.* (1980) have also studied the health statistics of a cohort of 440 women who also worked in the Quebec chrysotile asbestos mines and mills. Of the 84 who have died, there was one death due to lung cancer and one due to mesothelioma.

Crocidolite exposure. There is persuasive data, much already surveyed, which shows that crocidolite asbestos is much more hazardous than chrysotile, anthophyllite, and amosite. Of the mining populations of the world only those in the crocidolite mining area of the Cape Province of South Africa and at Wittenoon Gorge, Western Australia, have a statistically significant increase in mortality due to mesothelioma. Also, mesothelioma deaths have been reported among the residents of these areas who are not employed in the mines or mills. For example, Webster (1978) reports that the South African Asbestos Tumour Reference Panel placed 712 cases of mesothelioma on the register, which included all the known cases since 1956. Of these, occupational and environmental background was established for 420 cases. Actual mining exposure accounted for 139 of the 420 cases, of which 120 were in connection with Cape crocidolite mining and two with Transvaal crocidolite mining. There were only four mesothelioma cases in those associated with amosite mining, and two of these had been exposed to Cape crocidolite as well. In the chrysotile mining industry there was only one case -- a miner from Rhodesia. Of the 100 environmental cases (those not employed in any occupation where asbestos is used), 93 had been exposed to Cape crocidolite, two to Transvaal crocidolite, and one possibly to amosite.

Additional prevalence studies in the Cape Province (Talent *et al.*,

---

particular occupational or lifestyle hazard. SMR's are useful to compare total mortality as well as mortality related to a particular disease or accident *provided* a proper control cohort can be chosen.

1981) discovered 65 active cases of mesothelioma in people who had presented themselves for medical examination. Fifteen of these cases appeared in two groups, numbering 755 and 947 individuals, who were once employed in the crocidolite mines. An additional thirty-eight mesothelioma cases appeared in a survey of certain patients at the St. Michael's Hospital in Kuruman, Cape Province, who were not responding to treatment for suspected pulmonary tuberculosis. Fourteen of these mesothelioma patients were known to have worked in the crocidolite asbestos mines. Lastly, 12 of the 65 cases appeared in a medical survey of 53 females who, in the past, had hand-cobbed crocidolite asbestos.

In contrast to the prevalence of mesothelioma in the Cape Province, this disease is very rare in the Transvaal, where all of the world's amosite is mined. Wagner *et al.* (1960), in regard to their initial discovery of the association of crocidolite asbestos with mesothelioma, state (p. 260) "the tumour (referring to mesothelioma) is rarely encountered elsewhere in South Africa. During the past five years, with the exception of the present series (in Cape Province), no neoplasm of this nature has been diagnosed amongst 10,000 lungs examined at the Pneumoconiosis Bureau in Johannesburg, or in the Pathology Department of the South African Institute for Medical Research. Higginson and Oettle (1957) did not observe a single case in their survey of malignant tumours occurring in the Bantu and Cape Coloured population of Johannesburg and the North Eastern Transvaal."

The incidence of mesothelioma in Zimbabwe (Rhodesia), a country which is a major producer of chrysotile but mines no other form of asbestos, is very low. In a communication to Mostert and Meintjes (1979), the Secretary of the Rhodesia Pneumoconiosis Board stated that no cases of mesothelioma were reported in the mining industry. It is of interest to note that two cases of mesothelioma were reported in the Rhodesian railway industry, a locomotive engineer and a storeman. The locomotives were insulated with crocidolite asbestos to which these two men were exposed (Mostert and Meintjes, 1979). Cochrane and Webster (1978) report 12 cases of mesothelioma in men employed as insulators in the locomotive workshops of the South African Railways.

The prevalence of mesothelioma among the miners of Wittenoon Gorge has been discussed (Table 5, Study VI). The town of Wittenoon, the

center of crocidolite mining in Western Australia, reached a peak population of about 1,000 in the 1960's. At present the population is down to about 200 and the West Australian State Government has suggested the closing of the town and evacuation of the residents because of continuing risks of airborne asbestos dust (*Chemical Week*, December 8, 1978, p. 25). The risk of mesothelioma among the residents of the town who were not employed by mines is demonstrated by the case of a 27-year-old woman who had an environmental childhood exposure to crocidolite (Langlois *et al.*, 1978).

SUMMARY

Production

Of the six forms of asbestos, only four have been used to any significant degree in commerce. These are amosite, crocidolite, anthophyllite, and chrysotile. Although asbestos was used by Stone Age man, it was not until the latter part of the 19th century that it came into widespread use in the industrialized world. The modern industry began in Italy and England after 1860, with Quebec being the main supplier of the crude fiber. By 1900 two to three hundred thousand metric tonnes had been mined, mostly in Quebec. By 1980 over 100 million tonnes had been mined worldwide of which about 90 percent was of the chrysotile variety. Approximately 75 percent of all asbestos ever mined has come from just three chrysotile mining localities, Quebec, Canada, and the central and southern Urals of the Soviet Union. The chrysotile producing countries in order of importance are the Soviet Union (46.1 percent of the world's total asbestos production in 1978), Canada (28.9%), Zimbabwe (3.8%), China (3.8%), Italy (2.9%), South Africa (2.1%), Brazil (1.8%), U.S.A. (1.7%), and Australia (1.0%).

Two to three percent of the world's asbestos production has been the crocidolite variety, most of which came from South Africa. Western Australia was a minor producer of crocidolite between 1944 and 1966. All amosite has been mined in the Transvaal Province of South Africa and accounts for about two to three percent of all asbestos ever produced. The only significant anthophyllite production came from Finland, where 350,000 tonnes was mined between 1918 and 1966. Total production of

anthophyllite asbestos probably accounts for no more than 0.5 percent of the world's total asbestos production to date.

Geology

Deposits of commercial asbestos are found in four types of rocks: (I) alpine-type ultramafic rocks, including ophiolites (chrysotile, anthophyllite, and tremolite); (II) stratiform ultramafic intrusions (chrysotile and tremolite); (III) serpentinized limestone (chrysotile); and (IV) banded ironstones (amosite and crocidolite). Type I deposits are by far the most important and probably account for over 85 percent of the asbestos ever mined. The most important Type I deposits are those of Quebec and the Urals.

Type II deposits are found mostly in South Africa, Swaziland, and Zimbabwe. These furnish mostly chrysotile asbestos. Type III deposits are small in size; the most notable of these are located in Globe, Arizona, and in the Carolina area of the Transvaal Province of South Africa. Type IV deposits are found only in the Precambrian banded ironstones of the Transvaal and Cape Provinces of South Africa and of Western Australia. Only the South African deposits are still in production.

There is considerable geologic evidence that commercial asbestos deposits form only where there is a favorable stress environment, such as where folding or faulting occurs.

Asbestos and health

The three principal diseases which are related to asbestos exposure are (1) lung cancer, (2) cancer of the pleural and peritoneal membranes (mesothelioma), and (3) asbestosis, a condition in which the lung tissue becomes fibrous and thus loses its ability to function. Lung cancer can be caused by exposure to chrysotile, anthophyllite, amosite, and crocidolite asbestos; however, increased risk of this disease is probably found only in those who also smoke cigarettes. Asbestosis is also caused by heavy and prolonged exposure to all four forms of asbestos. Mesothelioma is caused principally by exposure to crocidolite asbestos. There is good evidence that anthophyllite and chrysotile asbestos do not cause any significant increase in mesothelioma mortality, even after heavy

exposure for many years. Thus far only about 10 or 12 deaths among anthophyllite and chrysotile miners have been attributed to this disease.

There is some question as to the relationship between exposure to amosite asbestos and incidence of mesothelioma. Transvaal amosite miners seem not to show this disease, whereas, according to I.J. Selikoff and coworkers, fourteen men exposed to amosite during World War II at a Patterson, New Jersey, factory have died of pleural or peritoneal mesothelioma (Selikoff *et al.*, 1980b). It should be noted, however, that only one mesothelioma case was noted on the death certificates. The thirteen other deaths were recorded by Selikoff from a postmortem "best estimate." Such "adjustments" of death certificate data make it impossible to compare different epidemiological studies or to compare to "control" groups. In addition, there are two other observations relating to amosite asbestos that Selikoff does not address: (1) the very low mesothelioma rates in the Transvaal amosite miners and (2) the strong possibility that many of the Patterson factory amosite workers had previous work experience in New Jersey factories that processed crocidolite asbestos. McCullagh (1980) in a review of the Patterson workforce suggests that "something like one-third, or some 300 members, of the Patterson cohort may have been occupationally exposed to asbestos before entering the cohort."

Chrysotile asbestos, which accounts for about 95 percent of the asbestos in the present market, is much less harmful to miners than is crocidolite and probably amosite. McDonald *et al.* (1980) found that for men exposed for over 20 years to chrysotile dust averaging 20 fibers/cm^3, the total mortality was less than expected (620 observed deaths, 659 expected deaths). Risk of lung cancer was slightly increased: 48 deaths observed, 42 deaths expected. Exposures to 20 fibers/cm^3 are an order of magnitude greater than those experienced now (generally less than 2 fibers/cm^3); thus, chrysotile miners working a lifetime under these present dust levels should not be expected to suffer any measureable excess cancer.[10]

[10]If there is no threshhold below which there is a zero risk of developing cancer from exposure to a carcinogen (many believe such a threshhold exists, many do not), then even exposures to chrysotile

Epidemiological evidence does not exist to assess the health effects of tremolite or actinolite asbestos. The minerals cummingtonite, grunerite, and hornblende, which are sometimes considered to be asbestos-like, have been shown not to cause asbestos diseases in miners.

ACKNOWLEDGMENTS

I thank David B. Stewart for a helpful review of this paper.

---

asbestos as low as two fibers per cubic centimeter could cause a few cancers to develop within a significantly large work force. Yet, the same also can be said of the human cost of operating heavy mining and manufacturing machinery; there will be some accidents resulting in injury and loss of life no matter how carefully the safety procedures are designed and followed. If, as some propose, society is to abandon the use of chrysotile asbestos despite the optimistic health picture for the present Quebec asbestos miners and millers, we should first be able to answer these questions:
(1) What will the health risk be to those exposed to the asbestos substitutes?
(2) Will the substitutes be less effective for fire protection, for braking efficiency, and for strengthening materials, resulting in increased injury and loss of life?
(3) Will the costs of the substitutes prevent their use, for example, as replacement material for asbestos in cement water pipe and reinforced construction cement?

Anderson, A.L. (1931) Genesis of the anthophyllite deposits near Kamiah, Idaho. J. Geol., 39, 68-81.

Anhaeusser, C.R. (1976) The nature of chrysotile asbestos occurrences in southern Africa: A review. Econ. Geol., 71, 96-116.

Aurola, E. (1954) The mines and quarries of Finland. Geologinen Tufkimuslaitos Geoteknillisiäulkaisuja, No. 55, 123 pp.

Bateman, A.M. (1923) An Arizona asbestos deposit. Econ. Geol., 18, 663-683.

Becklake, M.R. (1976) Asbestos-related diseases of the lung and other organs: Their epidemiology and implications for clinical practice. Amer. Rev. Resp. Disease, 114, 187-227.

Beukes, N.J. (1973) Precambrian iron-formation of southern Africa. Econ. Geol., 68, 960-1004.

Beukes, N.J. (1980) Lithofacies and stratigraphy of the Kuruman and Griquatown iron-formations, northern Cape Province, South Africa. Trans. Geol. Soc. South Africa, 83, 69-86.

Bowles, O. (1937) Asbestos. U.S. Bureau of Mines, Bull. 403, 92 pp.

Cameron, M., and Papike, J.J. (1979) Amphibole crystal chemistry: A review. Fortschr. Miner., 57, 28-67.

Champness, P.E., Cliff, G., and Lorimer, G.W. (1976) The identification of asbestos. J. Microscopy, 108, 231-249.

Cilliers, J.J. le R. (1964) Amosite at the Penge Asbestos Mine. In *The Geology of Some Ore Deposits in Southern Africa, Vol. II*, S.H. Haughton, ed., Geol. Soc. of South Africa, Johannesburg, 579-591.

Cilliers, J.J. le R., and Genis, J.H. (1964) Crocidolite asbestos in the Cape Province. In *The Geology of Some Ore Deposits in Southern Africa, Vol. II*, S.H. Haughton, ed., Geol. Soc. South Africa, Johannesburg, 543-570.

Clifton, R.A. (1979) *Asbestos*. MCP mineral commodity profiles, U.S. Bureau of Mines, July 1979, 19 pp.

Cochrane, J.C., and Webster, I. (1978) Mesothelioma in relation to asbestos fibre exposure - a review of 70 serial cases. S. African Med. J., 54, 279-281.

Coetzee, C.B., Brabers, A.J.M., Malherle, S.J., and van Biljon, W.J. (1976) Asbestos. In *Mineral Resources of the Republic of South Africa*, C.B. Coetzee, ed., Department of Mines, Geological Survey, South Africa, 261-268.

Coleman, R.G. (1977) *Ophiolites*. Springer-Verlag, Berlin, 229 pp.

Coleman, R.G. (1980) Tectonic inclusions in serpentinites. Arch. Sc., 33, 89-102.

Dreyer, C.J.B., and Robinson, H.A. (1978) The occurrence and exploitation of amphibole asbestos in South Africa. Preprint No. 78-H-64, Soc. Mining Eng. AIME, Salt Lake City, Utah, 1-21.

Elmes, P.C., and Simpson, M.J.C. (1971) Insulation workers in Belfast. 3. Mortality 1940-66. Brit. J. Ind. Med., 28, 226-236.

Elwood, P.C., and Cochrane, A.L. (1964) A follow-up of workers from an asbestos factory. Brit. J. Ind. Med., 21, 304-307.

Europaeus-Äyräpää, A. (1930) Die relative Chronologie der steinzeitlichen Keramik in Finland. Acta Archaeol., 1, 169-190.

Gillam, J.D., Dement, J.M., Lemen, R.A., Wagoner, J.K., Archer, V.E., and Blejer, H.P. (1976) Mortality among hard rock gold miners exposed to an asbestiform mineral. Annals N.Y. Acad. Sci., 271, 336-344.

Haapala, P. (1936) On serpentine rocks in northern Karelia. Bull. Commission Géologique Finland, No. 114, 1-88.

Hall, A.L. (1918) *Asbestos in the Union of South Africa*. Mem. No. 12, Geol. Survey of South Africa, 152 pp.

Hall, A.L. (1930) *Asbestos in the Union of South Africa*. Mem. No. 12, 2nd Ed., Geol. Survey of South Africa, 324 pp.

Hammond, E.C., Garfinkel, L., and Lew, E.A. (1978) Longevity, selective mortality, and competitive risks in relation to chemical carcinogenesis. Env. Res., 16, 153-173.

Hemley, J.J., Montoya, J.W., Shaw, D.R., and Luce, R.W. (1977) Mineral equilibria in the $MgO-SiO_2-H_2O$ system: II. Talc-antigorite-forsterite-anthophyllite-enstatite stability relations and some geologic implications in the system. Amer. J. Sci., 277, 353-383.

Higgins, I. (1981) Mortality study of employees of the Reserve Mining Company. Pers. comm., May 12, 1981, from Ian T.T. Higgins, M.D., Professor of Epidemiology, School of Public Health, The University of Michigan.

Higginson, J., and Oettle, A.C. (1957) Acta Un. Int. Cancer, 13, 949.

Hobbs, M.S.T., Woodward, S., Murphy, B., Musk, A.W., and Elder, J.E. (1980) The incidence of pneumoconiosis, mesothelioma and other respiratory cancer in men engaged in mining and milling crocidolite in western Australia. In *Biological Effects of Mineral Fibres:* Proceedings of a symposium organized by IARC, the French National Institute of Health and Medical Research and the Medical Research Council, Penarth, UK, held at the International Agency for Research on Cancer, Lyon, France, 25-27 September, 1979, J.C. Wagner, ed., IARC Scientific Publication No. 30, Lyon: IARC 2, 615-625.

Hodgson, A.A. (1979) Chemistry and physics of asbestos. In *Asbestos, vol. 1, Properties, Applications and Hazards*, L. Michaels and S.S. Chissick, eds., John Wiley and Sons, New York, 67-114.

Hutchison, J.L., Irusteta, M.C., and Whittaker, E.J.W. (1975) High-resolution electron microscopy and diffraction studies of fibrous amphiboles. Acta Crystallogr., A31, 794-801.

Huuskonen, M.S. (1980) Asbestos and cancer in Finland. J. Tox. Env. Health, 6, 1261-1265.

Huuskonen, M.S., Ahlman, K., Mattsson, T., and Tossauainen, A. (1980) Asbestos disease in Finland. J. Occupantional Med., 22, 751-754.

James, H.L., and Sims, P.K. (1973) Precambrian iron-formations of the World. Econ. Geol., 68, 913-914.

Jones, J.S.P., Pooley, F.D., and Smith, P.G. (1976) Factory populations exposed to crocidolite asbestos - a continuing survey. IARC Scientific Publications, INSERM, 52, 117-120.

Jones, R.H. (1890) *Asbestos, its Properties, Occurrence and Uses*. Crosby, Lockwood and Son, London, 236 pp.

Kannerstein, M., and Churg, J. (1980) Mesothelioma in man and experimental animals. Env. Health Perspect., 34, 31-36.

Kleinfeld, M., Messite, J., and Kooyman, O. (1967) Mortality experience in a group of asbestos workers. Arch. Environ. Health, 15, 177-180.

Langlois, S. Le P., Glancy, J.J., and Henderson, D.W. (1978) The radiology of malignant pleural mesothelioma in Western Australia. Aust. Radiology, 232, 305-314.

Laurent, R., and Hébert, Y. (1979) Paragenesis of serpentine assemblages in harzburgite tectonite and dunite cumulate from the Québec Appalachians. Canadian Mineral., 17, 857-869.

Legha, S.S., and Muggia, F.M. (1977) Pleural mesothelioma: Clinical features and therapeutic applications. Ann. International Med., 87, 613-621.

Liddell, D. (1981) Asbestos and public health. Thorax, 36, 241-244.

MacLeod, W.N. (1966) *The Geology and Iron Deposits of the Hamersley Range Area, Western Australia*. Geol. Surv. W. Australia Bull. No. 117, 170 pp.

Mancuso, T.F., and El Attar, A. (1967) Mortality pattern in a cohort of asbestos workers. J. Occup. Med., 9, 147-162.

McCullagh, S.F. (1980) Amosite as a cause of lung cancer and mesothelioma in humans. J. Soc. Occup. Med., 30, 153-156.

McDonald, A.D., and McDonald, J.C. (1978) Mesothelioma after crocidolite exposure during gas mask manufacture. Environ. Res., 17, 340-346.

McDonald, A.D., and McDonald, J.C. (1980) Malignant mesothelioma in North America. Cancer, 46, 1650-1656.

McDonald, J.C., Becklake, M.R., Gibbs, G.W., McDonald, A.D., and Rossiter, C.E. (1974) The health of chrysotile asbestos mine and mill workers of Quebec. Arch. Environ. Health, 28, 61-68.

McDonald, J.C., and Becklake, M.R. (1976) Asbestos-related disease in Canada. Hefte z. Unfallheilkunde, 126, 2. Deutsch-Österreichisch-Schweizeisch, Unfalltagung in Berlin 1976, Springer-Verlag, Berlin, 521-535.

McDonald, J.C., and McDonald, A.D. (1977) Epidemiology of mesothelioma from estimated incidence. Preventive Med., 6, 426-446.

McDonald, J.C., Gibbs, G.W., Liddell, F.D.K., and McDonald, A.D. (1978) Mortality after long exposure to cummingtonite-grunerite. Amer. Rev. Resp. Disease, 118, 271-277.

McDonald, J.C., Liddell, F.D.K., Gibbs, G.W., Eyseen, G.E., and McDonald, A.D. (1980) Dust exposure and mortality in chrysotile mining, 1910-1975. Brit. J. Ind. Med., 37, 11-24.

Meurman, L.O., Kiviluoto, R., and Hakama, M. (1974) Mortality and morbidity among the working population of anthophyllite asbestos miners in Finland. Brit. J. Ind. Med., 31, 105-112.

Mostert, C., and Meintjes, R. (1979) Asbestos and mesothelioma on the Rhodesia railways. Central African J. Med., 25, 72-74.

Mumpton, F.A., and Thompson, C.S. (1975) Mineralogy and origin of the Coalinga asbestos deposit. Clays & Clay Minerals, 23, 131-143.

Newhouse, M.L. (1973) Cancer among workers in the asbestos textile industry, biological effects of asbestos. IARC Scientific Publications No. 8, 203-208. WHO, Lyon.

Nicholson, W.J., Langer, A.M., and Selikoff, I.J. (1978) Epidemiological evidence on asbestos. In *Proc. Workshop on Asbestos: Definitions and Measurement Methods*, C.C. Gravatt, P.D. Lafleur, and K.F.J. Heinrich, eds., Nat. Bur. Standards Spec. Pub. 506, 71-93.

Nicholson, W.J., Selikoff, I.J., Seidman, H., Lilis, R., and Formby, P. (1979) Long-term mortality experience of chrysotile miners and millers in Thetford Mines, Quebec. Annals New York Acad Sci., 330, 11-21.

Noro, L. (1968) Occupa tional and "non-occupational" asbestosis in Finland. Amer. Ind. Hyg. Assoc. J., 29, 53-59.

Papike, J.J., and Ross, M. (1970) Gedrites: Crystal structures and intracrystalline cation distributions. Amer. Mineral., 55, 1945-1972.

Peto, J., Doll, R., Howard, S.V., Kinlen, L.G., and Lewinsohn, H.C. (1977) A mortality study among workers in an English asbestos factory. Brit. J. Ind. Med., 34, 169-173.

Peto, J. (1978) The hygiene standard for chrysotile asbestos. Lancet, 4 March, 1978, 484-489.

Pott, F. (1978) Some aspects on the dosimetry of the carcinogenic potency of asbestos and other fibrous dusts. Staub-Reinhalt Luft, 38, 486-490.

Rubino, G.F., Piolatto, G., Newhouse, M.L., Scansetti, G., Aresini, G.A., and Murray, R. (1979) Mortality of chrysotile asbestos workers at the Balangero mine, northern Italy. Brit. J. Ind. Med., 36, 187-194.

Rüttner,J.R. (1978) Comments. In *Proceedings of Asbestos Symposium, Johannesburg, South Africa*, H.H. Glen, ed., Dept. of Mines, S. Africa, October 3-7, 1977, p. 86-89.

Saracci, R. (1977) Asbestos and lung cancer: An analysis of the epidemiological evidence on the asbestos-smoking interaction. Int. J. Cancer, 20, 323-331.

Selikoff, I.J., Hammond, E.C., and Seidman, H. (1973) Cancer risk of insulation workers in the United States. *Biological Effects of Asbestos*. IARC Scientific Publications No. 8, WHO, Lyon, 209-216.

Selikoff, I.J., and Hammond, E.D. (1975) *Multiple Risk Factors in Environmental Cancer*, J. Fraumeni, ed., Academic Press, New York.

Selikoff, I.J. (1977) Cancer risk of asbestos exposure. Origins of Human Cancer, Cold Spring Laboratory, 1765-1784.

Selikoff, I.J. (1978) Carcinogenic potential of silica compounds. In *Biochemistry of Silicon and Related Problems*, G. Bendz, and I. Lindquist, eds., Plenum Pub. Corp., New York, 311-335.

Selikoff, I.J., and Lee, D.H.K. (1978) *Asbestos and Disease*. Academic Press, New York, 549 pp.

Selikoff, I.J., Hammond, E.C., and Seidman, H. (1980a) Latency of asbestos disease among insulation workers in the United States and Canada. Cancer, 46, 2736-2740.

Selikoff, I.J., Seidman, H., and Hammond, E.C. (1980b) Mortality effects of cigarette smoking among amosite asbestos factory workers. J. Nat. Cancer Inst., 65, 507-513.

Shannon, E.V. (1926) The mineralogy and petrology of intrusive Triassic diabase at Goose Creek, Loudoun County, Virginia. Proc. U.S. Nat. Mus., 66, No. 2539, Art. 2, 1-86.

Simonen, A. (1980) *The Precambrian in Finland*. Geol. Surv. Finland Bull. 304, 58 pp.

Simpson, W. (1979) *Asbestos:* Vol. 1, Final report of the advisory committee; Vol. 2, Papers commissioned by the committee. Health and Safety Commission, Great Britain.

Stanton, M.F., and Layard, M. (1978) The carcinogenicity of fibrous minerals. In *Proc. Workshop on Asbestos: Definitions and Measurement Methods*, C.C. Gravatt, P.D. Lafleur, and K.F.J. Heinrich, eds., Nat. Bur. Standards Spec. Pub. 506, 143-151.

Sterling, T.D., and Weinkam, J.J. (1978) Smoking patterns by occupation, industry, sex, and race. Arch. Environ. Health, Nov./Dec., 313-317.

Stewart, L.A. (1961) Mining methods and costs, Regal Asbestos Mine JAGUAYS Mining Corp., Gila County, Ariz. U.S. Bur. Mines Information Circular 7981.

Talent, J.M., Harrison, W.O., Solomon, A., and Webster, I. (1981) A survey of black mine workers of the Cape crocidolite mines. Unpubl. manuscript, National Centre for Occupational Health, Johannesburg, South Africa.

Trendall, A.F., and Blockley, J.G. (1970) *The Iron Formations of the Precambrian Hammersley Group, Western Australia*. Geol. Surv. W. Australia Bull. 119, 366 pp.

Trendall, A.F. (1973) Varve cycles in the Weeli Formation of the Precambrian Hammersley Group, Western Australia. Econ. Geol., 68, 1089-1097.

Truswell, J.F. (1977) *The Geological Evolution of South Africa.* Purnell and Sons, Cape Town, 218 pp.

Vejlsted, H., and Hansen, B.F. (1980) Pleural mesothelioma. Scand. J. Thor. Cardiovasc. Surg., 14, 119-122.

Wagner, J.C., Sleggs, C.A., and Marchand, P. (1960) Diffuse pleural mesothelioma and asbestos exposure in the northwestern Cape Province. Brit. J. Ind. Med., 17, 260-271.

Webster, I. (1978) Discussion. In *Proceedings of Asbestos Symposium, Johannesburg, South Africa*, H.H. Glen, ed., Dept. of Mines, S. Africa, October 3-7, 1977, p. 79.

Weiss, W. (1977) Mortality of a cohort exposed to chrysotile asbestos. J. Occup. Med., 19, 737-740.

Wiik, H.B. (1953) *Composition and Origins of Soapstone.* Bull. Commission Geologique Finlande, No. 165, 57 pp.

Zoltai, T. (1981) Amphibole asbestos. In *Reviews in Mineralogy*, Vol. 9A, *Amphiboles and Other Hydrous Pyriboles - Mineralogy*, D.R. Veblen, ed. [this volume].

Chapter 7

SUBSOLIDUS REACTIONS and MICROSTRUCTURES in AMPHIBOLES

Subrata Ghose

INTRODUCTION

In this chapter we describe the subsolidus phenomena in amphiboles, which include four different topics: (1) the thermodynamics and kinetics of Mg-Fe^{2+} order-disorder in ferromagnesian and sodic amphiboles, (2) miscibility gaps and exsolution, (3) phase transitions in ferromagnesian amphiboles, and (4) thermal decomposition of amphiboles. The first two phenomena can be regarded as two different expressions of the cation ordering process. In contrast with pyroxenes, our knowledge of the subsolidus phenomena in amphiboles is relatively meager for several reasons. First, the stability limits of many amphiboles are much lower in temperature than the pyroxenes; hence, the subsolidus reactions take place at relatively lower temperatures, where reaction kinetics are slower, giving rise to microscopic exsolution textures which may go unnoticed. Secondly, experimentation at these lower temperatures ($\sim$700°C or below) under controlled partial water and oxygen pressures is difficult. In spite of these problems, significant progress has been made since 1960 through the application of single-crystal X-ray and electron diffraction and electron microscopy, as well as spectroscopic techniques. Experimental determination of solvus gaps in amphiboles has been made in two cases; however, considerable work remains to be done in this field. Nonetheless, the crystal-chemical principles guiding the subsolidus phenomena are fairly clear, and in spite of the tremendous chemical complexity of the amphiboles, a comprehensible general picture is emerging. Hopefully, in the next decade most of the details of the subsolidus phenomena in amphiboles will be clarified through a concerted effort of petrologists and mineralogists working both in the field and in the laboratory.

THERMODYNAMICS AND KINETICS OF THE Fe^{2+}-Mg^{2+} ORDER-DISORDER REACTION IN FERROMAGNESIAN AMPHIBOLES

Mg-Fe in cummingtonite and actinolite

Anthophyllite and cummingtonite-grunerite belong to an essentially binary solid solution series, $Mg_7Si_8O_{22}(OH)_2$-$Fe_7Si_8O_{22}(OH)_2$, with minor

amounts of Al in anthophyllite and Ca,Mn in cummingtonite. In spite of the difference in symmetry, the natures of the four crystallographically different octahedral sites in both mineral series are closely comparable: the M1 and M3 sites are nearly regular with 4(O) and 2(OH) as ligands, M2 is quite regular with 6(O) as ligands, and M4 is very highly distorted from the octahedral symmetry. In grunerite, the M4 site is coordinated by four near-oxygen atoms, two at 2.135A and two at 1.988A, and by two more oxygens at a distance of 2.757A (Finger, 1969). In anthophyllite, the M4 site is effectively five-coordinated, with four oxygen atoms at an average distance of 2.081±0.057A, a fifth oxygen at 2.387A, and two further ones at 2.865 and 2.867A (Finger, 1970). The M4 site plays a very special role in all amphibole structures regardless of symmetry, since it holds adjacent T-O-T slabs ("I-beams") together.

Because of the intrinsic differences in the chemical and structural environments among the different octahedral cation sites in ferromagnesian amphiboles, it was expected that Fe^{2+} and Mg^{2+} would be distributed unequally among these sites (see discussions by Hawthorne in Chapter 1 of this volume). From single-crystal X-ray refinements of a grunerite (Ghose and Hellner, 1959) and a cummingtonite (Ghose, 1961), it was found that Fe^{2+} has a strong preference for the M4 site, Mg^{2+} for the M2 site, and that Fe^{2+} and Mg^{2+} are nearly equally distributed in M1 and M3. Subsequent X-ray refinements of cummingtonite and grunerite by Fischer (1966) and Finger (1969) confirmed this trend. Based on the cummingtonite results, Ghose (1962, 1965) predicted that anthophyllite would show a similar ordering trend, subsequently confirmed by infrared and Mössbauer spectroscopy (Bancroft *et al.*, 1966) and crystal structure analysis (Finger, 1970).

Mueller (1960) considered the Fe^{2+}-Mg^{2+} distribution in coexisting actinolite and cummingtonite from a metamorphosed iron formation near Bloom Lake, Quebec, Canada. From the smooth variation of the Fe-Mg distribution coefficient between coexisting mineral pairs, he concluded that the minerals closely attained local equilibrium. The ion-exchange reaction between coexisting actinolite and cummingtonite is the following:

$$\tfrac{1}{5}\ Ca_2^{V}Fe_5^{W}Si_8O_{22}(OH)_2 + \tfrac{1}{7}\ Mg_2^{V}Mg_5^{W}Si_8O_{22}(OH)_2 \rightleftarrows$$

$$\tfrac{1}{5}\ Ca_2^{V}Mg_5^{W}Si_8O_{22}(OH)_2 + \tfrac{1}{7}\ Fe_2^{V}Fe_5^{W}Si_8O_{22}(OH)_2 \qquad (a)$$

where superscripts V and W denote sublattices M4 and (M1,M2,M3), respectively. The equilibrium relation for reaction (a) is given by Mueller (1962):

$$K_a = \frac{X^{Mg}_{act}(1 - X^{Mg}_{cum})}{X^{Mg}_{cum}(1 - X^{Mg}_{act})} \exp 0.40\ (1 - 2X^{Mg}_{cum}) ,$$

where X^{Mg}_{act} and X^{Mg}_{cum} are the mole fractions Mg/(Mg+Fe) in actinolite and cummingtonite, respectively. The value of the equilibrium constant K_a was found to be 1.80. The observed intercrystalline cation distribution was explained by Mueller (1961) on the basis of the assumption that actinolite behaves as an ideal solution, whereas cummingtonite behaves as a regular solution (Guggenheim, 1952). The deviation of cummingtonite from ideal behavior was considered to be due to the strong site preference of Fe^{2+} for the M4 site in cummingtonite, whereas this site is occupied by Ca in actinolite. Mueller (1962) reasoned that since the configurations of the M1, M2 and M3 sites are not very different in either actinolite or cummingtonite, to a first approximation, the intracrystalline Fe-Mg distribution in cummingtonite can be considered to be between the M4 site ("V sublattice") on the one hand, and M1,M2,M3 sites taken together ("W sublattice") on the other. Indeed, subsequent Mössbauer spectroscopy of cummingtonite (Whitfield and Freeman, 1967; Bancroft *et al.*, 1967; Hafner and Ghose, 1971) has failed to distinguish the Fe^{2+} occupancies of the M1, M2 and M3 sites. Following Dienes (1955), Mueller (1962) proposed a treatment of the Fe^{2+}-Mg^{2+} order-disorder in cummingtonite as an ion exchange reaction between the V and W sublattices, which we will denote as M4 and M1,2,3, respectively:

$$Fe^{2+}(M4) + Mg^{2+}(M1,2,3) \rightleftarrows Mg^{2+}(M4) + Fe^{2+}(M1,2,3) . \qquad (b)$$

Assuming ideal solution behavior at each set of sites, the equilibrium constant K_b for reaction (b) can be written as

$$K_b = \frac{X^{Fe}_{M1,2,3}(1 - X^{Fe}_{M4})}{X^{Fe}_{M4}(1 - X^{Fe}_{M1,2,3})}$$

where $X^{Fe}_{M1,2,3}$ and X^{Fe}_{M4} are the mole fractions Fe/(Fe+Mg) in the (M1,M2,M3) and (M4) sites, respectively, as determined by single-crystal X-ray diffraction studies or Mössbauer spectroscopy. However, to explain the

observed intercrystalline partitioning data, Mueller (1962) postulated a partially regular solution model for cummingtonite, where the mixing of Fe and Mg in the W sublattice is ideal, and all the excess free energy of mixing is associated with the V sublattice (M4). Matsui and Banno (1965), on the other hand, used the ideal site model to explain the Fe-Mg partitioning between coexisting actinolite and cummingtonite. For the most general case, where the mixing of Fe and Mg at the M4 and the M1,2,3 sites deviates from ideal solution behavior, the equilibrium constant K_b can be written as

$$K_b = \frac{X^{Fe}_{M1,2,3}(1 - X^{Fe}_{M4})}{X^{Fe}_{M4}(1 - X^{Fe}_{M1,2,3})} \cdot \frac{f^{Fe}_{M1,2,3} f^{Mg}_{M4}}{f^{Mg}_{M1,2,3} f^{Fe}_{M4}},$$

where the f values are the partial activity coefficients for Fe or Mg in M1,2,3 or M4.

We now have to define the partial activity coefficients. Mueller (1964) has considered two coexisting phases in equilibrium, α and β, each of which behaves as a *regular* solution. For an exchange reaction involving two ions A and B between the two phases, the equilibrium constant K can be written as

$$K = \frac{(1-X^{\beta}_A)X^{\alpha}_A \; exp\; [(1-2X^{\alpha}_A)W^{\alpha}_A/RT]}{(1-X^{\alpha}_A)X^{\beta}_A \; exp\; [(1-2X^{\beta}_A)W^{\beta}_A/RT]},$$

where X^{α}_A is the ionic mole fraction A/(A+B) in phase α and X^{β}_A the corresponding mole fraction in phase β. W_{α} and W_{β} are exchange energies associated with phases α and β, respectively.

If we consider the "V" and "W" sublattices to be coexisting subphases in ion-exchange equilibrium within the cummingtonite phase, the above equation can be recast in the following form:

$$K = \frac{X^{Fe}_{M1,2,3}(1 - X^{Fe}_{M4}) \; exp\; [(1-2X^{Fe}_{M1,2,3})W^{M1,2,3}/RT]}{(1 - X^{Fe}_{M1,2,3})X^{Fe}_{M4} \; exp\; [(1-2X^{Fe}_{M4})W^{M4}/RT]}$$

where $X^{Fe}_{M1,2,3}$ and X^{Fe}_{M4} are mole fractions Fe/(Fe+Mg) at the M1,2,3 sites and the M4 site respectively; $W^{M1,2,3}$ and W^{M4} are ion exchange energies associated with these sites, respectively. The partial activity coefficients can be defined now in the form

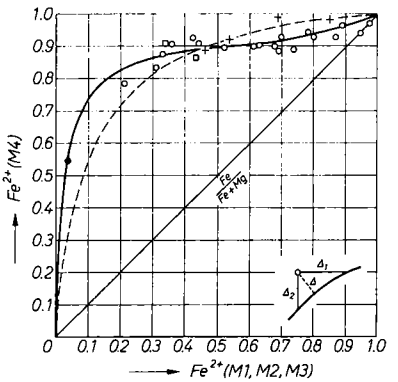

Figure 1. Fe^{2+}-Mg^{2+} distribution in the M4 site and the set of sites M1, M2, M3 in cummingtonites. Squares are samples from Butler, crosses samples of Klein, open circles samples of Mueller, and solid circle sample of Kisch. The solid curve is the least-squares fit to the data based on a regular solution model; the dashed line is an ideal solution model. From Hafner and Ghose (1971).

$$ln\ f^{Fe}_{M1,2,3} = \frac{W^{M1,2,3}}{RT}\ (1 - X^{Fe}_{M1,2,3})^2 .$$

This is the regular solution model of Hildebrand (1929) and Guggenheim (1952), which implies that the entropy of mixing at each site is that of an ideal solution and that the partial molar heat of mixing varies with the square of the concentration, but is independent of temperature. The two heat constants $W^{M1,2,3}/RT$ and W^{M4}/RT are associated with (M1,2,3) and (M4) sites, respectively. The magnitudes of these constants serve as a measure of the deviation of Fe-Mg mixing at each set of sites from ideal behavior.

Although Bancroft *et al.* (1967) determined Fe-Mg distributions in a number of cummingtonites by infrared and Mössbauer spectroscopy, the observed distributions showed a large scatter, and a test of these thermodynamic models was not possible. Subsequently, Hafner and Ghose (1971) determined the Fe-Mg distribution in 26 cummingtonite-grunerite specimens ranging in composition from 0.96 to 0.18 Fe/(Fe+Mg), all except one being derived from the metamorphosed iron formations of Quebec (Mueller, 1960; Klein, 1966; Butler, 1969). Since these specimens came from well-equilibrated amphibolite facies granulite rocks, it was expected that the observed Fe-Mg distribution data would show a smooth trend, which would allow testing of the postulated thermodynamic models. Figure 1 shows the Fe-Mg distribution data, which can be approximated by a *regular* solution model.

If we consider the Mueller (1960) samples only, the equilibrium constant is 0.19, and W^{M4}/RT and $W^{M1,2,3}/RT$ have values of 1.58 and 0.54, respectively (Hafner and Ghose, 1971). In rocks studied by Mueller

(1960), the oxygen isotope ratios O^{16}/O^{18} between coexisting quartz and magnetite indicate a "quench-in" temperature for ion exchange of 600±20°C (Sharma *et al.*, 1965). This represents a lower limit for the temperature of formation of these rocks. It is expected that the Fe-Mg ion exchange within the crystals will continue to lower temperatures, as a function of reasonably slow cooling of a regionally metamorphosed rock. If we assume 425°C to be the effective "quench-in" temperature for the intracrystalline Fe-Mg exchange for cummingtonites from the metamorphosed iron formation (see below), then $\Delta G°$, the Gibbs free energy of the ion exchange, can be calculated from the relationship $\Delta G° = -RT \ln K$ as 2.32 Kcal/mole.

The rocks from Klein's (1966) and Butler's (1969) areas crystallized at a higher temperature than the rocks from Mueller's (1960) area, since they contain orthopyroxene as a thermodynamically stable phase coexisting with cummingtonite, actinolite and clinopyroxene. If we consider Klein's (1966) samples only, a good fit is obtained using an ideal solution model with the distribution coefficient K = 0.092.

Ghose and Weidner (1971b) have determined the Mg-Fe distribution isotherms in natural cummingtonites at 600 and 700°C. Cummingtonites, ranging in composition from 38 to 84 mole percent $Fe_7Si_8O_{22}(OH)_2$, were sealed with 3 wt % H_2O in silver capsules and were equilibrated under 2 kbar total pressure (90% Ar, 10% H_2). The Mg-Fe distribution at M4 and (M1,M2,M3) sites was determined by Mössbauer spectroscopy. At 600°C the mixing of Mg and Fe is regular at each set of sites. The equilibrium constants, K, W^{M4} and $W^{M1,2,3}$ at this temperature are 0.26, 1.09 and 1.23, respectively (Fig. 2). The Gibbs free energy change at 600°C is 2.35 Kcal/mole. On the other hand, if we assume an ideal distribution model to be valid at each set of sites, the equilibrium constant, K, and the Gibbs free energy change, $\Delta G°$, obtained from Ghose and Weidner's data (Fig. 3) are:

T(°C)	K	$\Delta G°$(Kcal/mole)
600	0.106	3.9
700	0.153	3.6

The enthalpy change, ΔH, is estimated to be ∿3.6 Kcal/mole, indicating a small contribution of the configurational entropy to free energy. In view

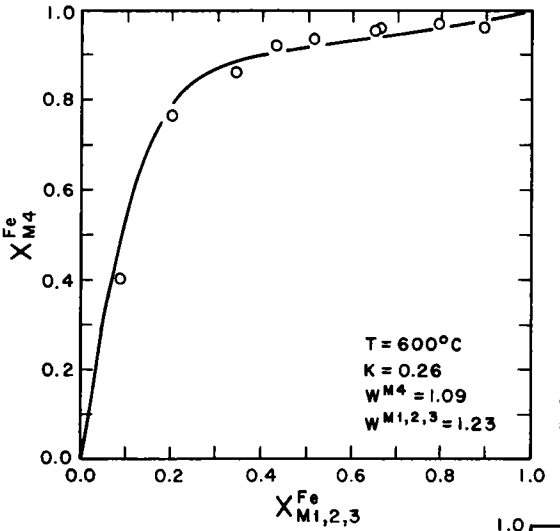

Figure 2. Fe^{2+}-Mg^{2+} distribution isotherm in heat-treated cummingtonites at 600°C. The solid curve is based on the regular solution model. From Ghose and Weidner (1971b).

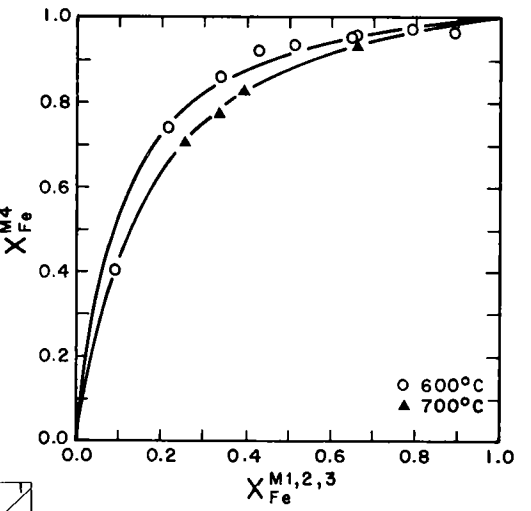

Figure 3. Fe^{2+}-Mg^{2+} distribution isotherms in cummingtonites at 600° and 700°C. The solid curves are fits to the ideal solution model at each set of sites. From Ghose and Weidner (1971b).

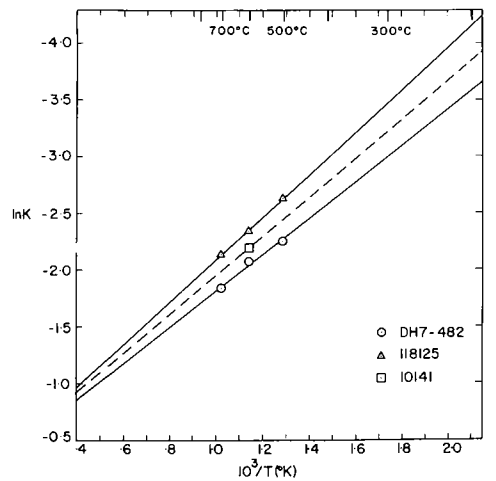

Figure 4. Plot of $\ln K$ versus 1/T for heated cummingtonite samples. Slopes of the curves yield $-\Delta H°/R$. From Ghose and Weidner (1972).

of these results, it would appear that Klein's (1966) samples were equilibrated in terms of intracrystalline Mg-Fe distribution at a temperature slightly less than 600°C.

To be able to use the Fe-Mg order-disorder in cummingtonite as a geothermometer, Ghose and Weidner (1972) heat treated three magnesium-rich cummingtonites at various temperatures. These results are plotted in Figure 4. From extrapolation, the "quench-in" equilibration temperatures of the cummingtonites were as follows:

Table 1. Estimated crystallization and/or equilibration temperatures of cummingtonites

Rock type [sample no.]	Fe/(Fe+Mg)	T(°C)
Metamorphosed iron-formation -- (amphibolite facies) [DH7-482]	0.38	425±20
Chlorite-amphibolite schist, Baltimore, Maryland [118125]	0.36	290±20
Chlorite-amphibolite, Cooma Complex, Australia [10141]	0.18	265±30

The cummingtonite sample [118125] was heated at 398°C for 672 hours, and showed no cation migration at this temperature. On the basis of this result and the observed equilibration temperature (425°C) of the sample DH7-482 from the metamorphosed iron formation (Mueller, 1960), which crystallized at or above 600°C, Ghose and Weidner (1972) concluded that the temperature T_c below which no cation migration takes place is 425°C. The observed low temperatures of cation equilibration for the other two samples were believed to reflect their crystallization temperatures, which were below T_c. Although this possibility cannot be completely ruled out, in view of the kinetic data on Mg-Fe order-disorder in anthophyllite subsequently reported by Seifert and Virgo (1974, 1975), the above interpretation needs revision.

Mg-Fe in anthophyllite and the cooling rate of rocks

Seifert and Virgo (1974, 1975) have studied the kinetics of Mg^{2+}-Fe^{2+} order-disorder between M4 and M1,2,3 sites in an anthophyllite from Montana with the chemical composition $Na_{0.05}Ca_{0.09}Mg_{5.79}Fe_{1.17}(Si_{7.81}Al_{0.18})O_{22}(OH)_2$, using Mössbauer spectroscopy at 77°K. They carried out a series of heating experiments in the temperature range 400-720°C at 2 kbar in standard cold-seal bombs and with controlled oxygen fugacity (quartz-fayalite-magnetite buffer). At temperatures of 600°C and above, an equilibrium distribution is attained within a few days. The exchange reaction can be written as:

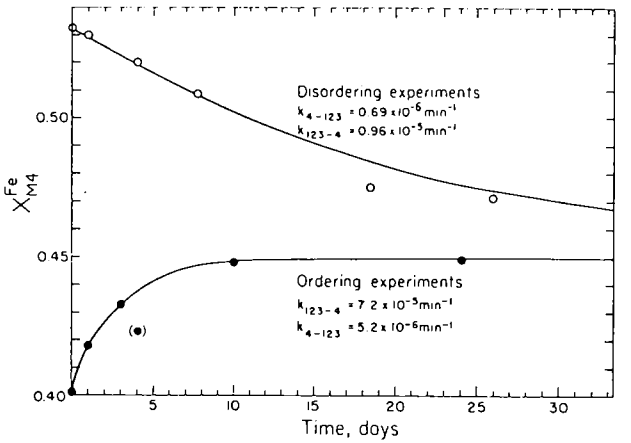

Figure 5. Changes in the Fe^{2+} occupancy of the M4 site, X^{Fe}_{M4}, in an anthophyllite as a function of run duration at 550°C, 2 kbar. Open circles, starting material is natural unheated anthophyllite; closed circles, starting material is anthophyllite previously disordered at 720°C, 2 kbar for 1 day. From Seifert and Virgo (1974).

$$Mg(M1,2,3) + Fe^{2+}(M4) \rightleftarrows Fe^{2+}(M1,2,3) + Mg(M4)$$

The equilibrium distribution coefficients K_D found at 600, 670 and 720°C define a straight line on a K_D versus $1/T_k$ diagram, indicating a constant exchange reaction Gibbs free energy $\Delta G° = 4247 \pm 54$ cal/mole. Assuming the ideal distribution of Mg and Fe at each set of sites and assuming the $\Delta G°$ to be constant and the same at lower temperatures, the cation distribution of the unheated anthophyllite corresponds to a temperature of cation equilibration of about 270°C. Detailed rate experiments were made at 500 and 550°C, starting from unheated and previously partially disordered material (720°C, 1 day). The results presented in Figure 5 can be fitted by the rate equation for a second-order competing rate process (Mueller, 1967):

$$-\frac{dX_i}{dt} = C_o \sum_{j=1}^{n-1} \nu_{ji} k_{ji} \phi_{ji} X_j (1-X_i) - C_o \sum_{j=1}^{n-1} \nu_{ij} k_{ij} \phi_{ij} X_i (1-X_j) ,$$

where X_i = mole fraction of Fe^{2+} in site i,

ν_{ij} and ν_{ji} = stoichiometric coefficients,

k_{ij} and k_{ji} = rate constants for competing ordering and disordering processes,

ϕ_{ij} and ϕ_{ji} = activity coefficients for the intracrystalline exchange, and

C_o = total Fe^{2+} concentration of all sites per unit cell volume.

In anthophyllite there are two M4 and a total of five M1, M2 and M3 sites per formula unit. Hence, assuming anthophyllite to be a Mg-Fe^{2+} binary solid solution, the above equation becomes:

$$-\frac{dX_4}{dt} = C_o \tfrac{5}{7}\ \phi_{4-123} k_{4-123} X_4 (1-X_{123}) - C_o \tfrac{5}{7}\ \phi_{123-4} k_{123-4} X_{123} (1-X_4)$$

where X_4 and X_{123} are mole fractions $Fe^{2+}/(Fe^{2+}+Mg)$ at M4 and M1,2,3 sites, respectively. This equation can be reduced to a logarithmic decay for one site occupancy with time (Mueller, 1969) by substituting in the equilibrium constant K°_{123-4} and the bulk X^{Fe} value and by assuming ideal mixing at the sites, namely $\phi_{123-4} = \phi_{4-123} = 1$.

$$K^{\circ}_{123-4} = \frac{X_4(1-X_{123})}{X_{123}(1-X_4)} = \frac{k_{123-4}}{k_{4-123}} \quad [\text{Note that } X_{123} = \tfrac{7}{5} X^{Fe} - \tfrac{2}{5} X_4.]$$

The rate equation now becomes

$$-\frac{dX_4}{dt} = k_{4-123}(aX_4^2 + bX^4 + a)\ ,$$

where $a = K^{\circ}_{123-4} X^{Fe}$,

$b = K^{\circ}_{123-4} X^{Fe} - X^{Fe} + \tfrac{2}{7} K^{\circ}_{123-4} + \tfrac{5}{7}$, and

$c = \tfrac{2}{7} (1-K^{\circ}_{123-4})$.

Mueller (1969) has provided a solution for this differential equation. The disordering rate constants k_{4-123} and activation energies determined by Seifert and Virgo (1975) at 550°C and 500°C are given in Table 2. The activation energy of the disordering process (∿55 Kcal) and the temperature dependence of the rate constants in anthophyllite are much higher than those reported for orthopyroxenes (E = 20 Kcal) by Virgo and Hafner (1969). The rate constants are expected to drop very rapidly at lower temperatures, the rate constant for disordering decreasing more rapidly than that for ordering. The calculated rate constant for disordering at 400°C indicates that a change of X^{Fe}_{M4} by 0.001 would require a heating run of four years. From these kinetic results, there is no evidence of a high temperature thermal barrier for ordering in anthophyllite, as was previously suggested for orthopyroxene (Virgo and Hafner, 1969) and cummingtonite (Ghose and Weidner, 1972). Hence, the degree of ordering in natural

Table 2. Disordering rate constants $k_{4\text{-}123}$, where $K^{\circ}_{123\text{-}4} = k_{123\text{-}4}/k_{4\text{-}123}$, determined for a natural anthophyllite at 500° and 550°C, and calculated activation energies for disordering, E_{aD}. From Seifert and Virgo (1975).

Experiments	$k_{4\text{-}123}$ (year^{-1})		E_{aD}
	550°C	500°C	(kcal)
Ordering	37.8432	3.3112	61.6
Disordering	5.0458	0.57816	54.8

anthophyllite can be quantitatively interpreted in terms of measured rate constants. At very low temperatures, the ordering process will cease, due to slow reaction kinetics. Provided the X^{Fe}_{M4} of a natural (unheated) anthophyllite is known, from these rate constants the X^{Fe}_{M4} values that are attained after a given time interval at a given temperature can be calculated. Seifert and Virgo (1975) and Seifert (1977) have presented a time-temperature-(percentage) transformation (T-T-T) diagram (Fig. 6) plotted on a logarithmic time scale, which can be used to derive the cooling history of a rock in terms of temperature and time. Assuming that the anthophyllite of Seifert and Virgo crystallized at 720°C, a linear cooling rate of 2.5×10^{-5}°C/yr for the rock can be derived.

In view of the kinetic results on anthophyllite, it now appears very likely that the low temperatures indicated by the cation distribution in two cummingtonites derived from metamorphosed ultrabasic rocks (290° and 265°C) and one from a metamorphosed iron formation (425°C) studied by Ghose and Weidner (1972) are indeed cation equilibration temperatures and not crystallization temperatures of the rocks. However, if one assumes no high-temperature thermal barrier to cation order to be present in cummingtonites, the relatively high temperature of equilibration (425°C) for the iron formation cummingtonite cannot be explained on the basis of available results. In fact, all of the samples from the metamorphosed iron formation of Quebec studied by Hafner and Ghose (1971) indicate an apparent equilibration temperature of 425°C or higher. One must either assume that the cooling rate for these cummingtonites was unusually fast or that the rate constants of cummingtonites are considerably different from those of anthophyllites. The latter possibility is rather unlikely in view of the fact that samples 118125 and DH7-482 (Table 1) have very similar X^{Fe} values (0.364 and 0.378) and yet indicate very different temperatures of cation equilibration (290 and 425°C).

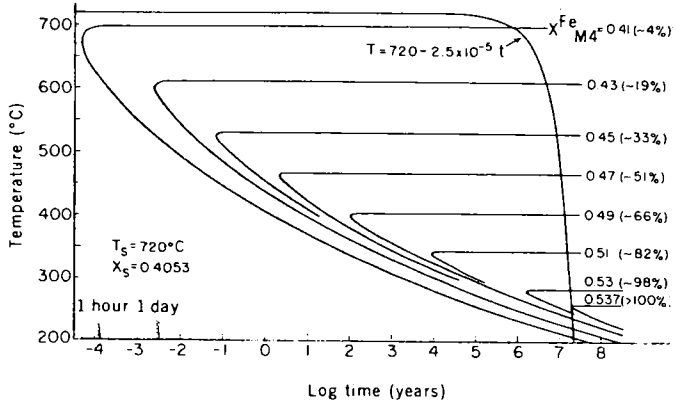

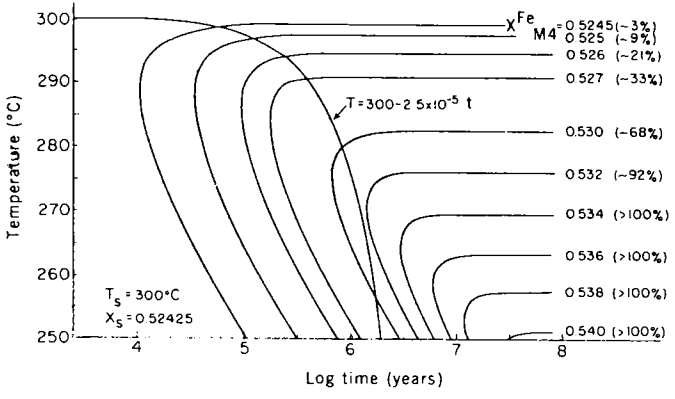

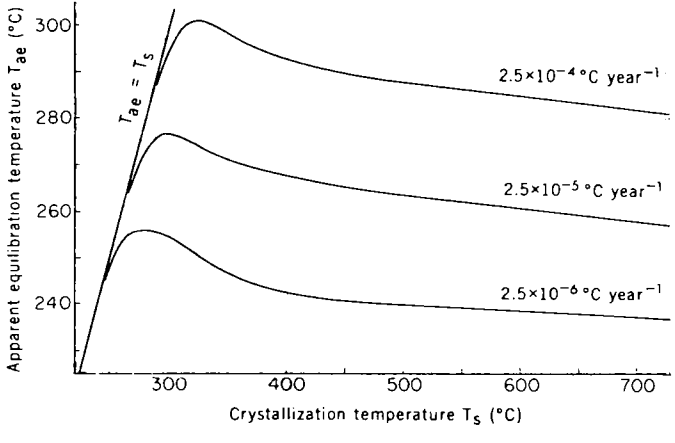

Figure 6. (a - upper left). Time-temperature-percentage transformation plot for anthophyllite crystallized at 720°C (starting $x^{Fe}_{M4} = x_S = 0.4053$). Also plotted is a model cooling of a rock taken as T (°C) = 720-2.5 × 10^{-5}t. The equilibration temperature of the natural sample of Seifert and Virgo (1975) is 270°C (x^{Fe}_{M4} = 0.533). Numbers in parentheses refer to the percentage of ordering, from x_S = 0.4053 (0 per cent) to 0.5327 (100 per cent natural sample). The horizontal portion of each percentage transformation curve refers to the time in excess of that required to achieve equilibrium at a given temperature.
(b - upper right). Time-temperature-percentage transformation plot for anthophyllite crystallized at 300°C (x_S = 0.52425).
(c - left). Plot of the apparent equilibration temperature T_{ae} as a function of the crystallization temperature T_S for three distinct linear cooling rates of the rock. The straight line corresponds to a model where $T_{ae} = T_S$. From Seifert and Virgo (1975).

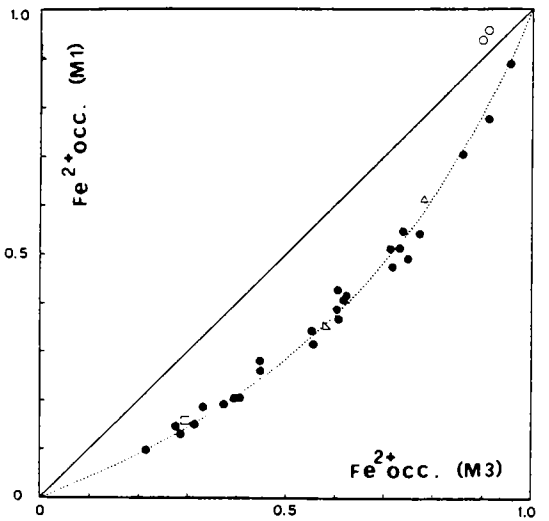

Figure 7. Distribution of Fe^{2+} and Mg in M1 and M3 sites of 28 blue sodic amphiboles; the dotted line corresponds to the ideal solution model at each site, where $K_D = X_{M1}^{Fe}(1-X_{M3}^{Fe})/X_{M3}^{Fe}(1-X_{M1}^{Fe}) = 0.403$. From Ungaretti (1980).

We urgently need kinetic studies on cummingtonites to clarify these anomalies so that eventually they can be used to determine cooling rates of rocks. Ganguly and Ghose (1982) are currently studying this problem.

Mg-Fe in sodic amphiboles

In the sodic amphiboles, where the M4 site is occupied by Na^+, the M2 site is occupied by trivalent ions such as Al and Fe (Whittaker, 1949; Ghose, 1965). The Fe^{2+} and Mg^{2+} ions are concentrated in the M1 and M3 sites. Fe^{2+} shows a preference for M3 in glaucophane, as indicated by crystal structure refinement and Mössbauer spectroscopy (Papike and Clark, 1968; Bancroft and Burns, 1969). In the glaucophane-crossite-riebeckite series, the Mössbauer and infrared spectra indicate a change in the relative enrichment of Fe^{2+} ions from M3 to M1 with increasing Fe^{3+} content (Bancroft and Burns, 1969). Ungaretti *et al.* (1978) and Ungaretti (1980) have determined cation distributions in 26 blue sodic amphiboles that are relatively poor in ferric iron. The Fe^{2+} in these amphiboles shows a relatively strong preference for the M3 site; in addition, the Fe^{2+}-Mg^{2+} distribution between M1 and M3 sites shows a smooth hyperbolic pattern, indicating an ideal distribution of Fe^{2+} and Mg at each site (Fig. 7). The equilibrium constant,

$$K_D = \frac{X_{M1}^{Fe} \cdot (1 - X_{M3}^{Fe})}{X_{M3}^{Fe} \cdot (1 - X_{M1}^{Fe})} = 0.403 \ .$$

If we assume the temperature of crystallization and the temperature of equilibration of these sodic amphiboles to be about the same (∿300°C), we obtain an estimate of the Gibbs free energy, ΔG°, of the ion-exchange reaction to be about 1.09 Kcal/mole.

PHASE TRANSITIONS IN FERROMAGNESIAN AMPHIBOLES

The $P2_1/m \rightarrow C2/m$ phase transition in magnesium-rich cummingtonite

Nature of the structural changes. It was Bown (1965) who first showed that the exsolved lamellae of magnesium-rich cummingtonite in tremolite possess $P2_1/m$ symmetry, rather than the usual $C2/m$ symmetry shown by other clinoamphiboles. Such "primitive" cummingtonite has since been identified in many metamorphosed ultrabasic rocks (Ross *et al.*, 1969; Kisch, 1969; Rice *et al.*, 1974). The crystal structure of a primitive manganoan cummingtonite with the chemical composition $(Ca_{0.36}Na_{0.06}Mn_{0.96}Mg_{5.57}Fe_{0.01}Al_{0.01})Si_8O_{22}(OH)_2$ has been determined by Papike *et al.* (1969); it is characterized by two crystallographically distinct double silicate chains with different degrees of kinking. However, because of the high Mn occupancy of the M4 site (0.49 Mn, 0.28 Mg, 0.19 Ca, 0.03 Na, 0.01 Fe), the configuration of this site is comparable to that found in other, *C*-centered (Mg,Fe) cummingtonites, i.e., four short oxygen bonds at an average distance of 2.154A and two further ones at 2.511 and 2.650A. High-temperature X-ray studies indicated that this primitive manganoan cummingtonite transforms reversibly to *C*-centered cummingtonite above 40°C (Prewitt *et al.*, 1970). The crystal structure of the high-temperature form at 100°C is very similar to another manganoan cummingtonite that is *C*-centered at room temperature (Sueno *et al.*, 1972). In both forms, the configurations of the M1, M2, M3 and M4 octahedra are similar. The principal structural changes due to temperature or differences in chemical composition are brought about by the rotation of tetrahedra in the silicate chains, so that above the transition temperature, both chains become crystallographically identical. In contrast to the pigeonite $P2_1/c \rightarrow C2/c$ transition, in the $P2_1/m \rightarrow C2/m$ transition in magnesiocummingtonite, no chemical bonds are broken, the transition being purely displacive (Sueno *et al.*, 1972). Apparently, the $P2_1/m$ cummingtonite is a metastable phase, which forms instead of the more stable

orthorhombic (anthophyllite) phase, due to the sluggishness of the clino → ortho transformation, which is reconstructive and involves considerable breakage and reformation of M-O bonds.

The chemical composition range of the $P2_1/m$ (Mg,Fe) cummingtonite is known to extend from 77 mole % of the Mg component (Ghose, 1974, unpublished) to more magnesian compositions. The crystal structure determination of a primitive (Mg,Fe) cummingtonite with 86 mole % of the Mg component (specimen #31B, Ticino, Switzerland, Rice *et al.*, 1974) indicates that the configuration of the M4 site (highly enriched in Fe^{2+}) is close to that found in anthophyllite (Finger, 1970), i.e., it is five-coordinated with four oxygen atoms at an average distance of 2.070A, with a fifth oxygen atom at 2.415A; the sixth and seventh oxygen atoms are at distances of 2.868 and 2.889A (Ghose and Wan, 1981; in preparation). These new data further support the idea that the $P2_1/m$ cummingtonite is a metastable phase.

Possible anti-phase domains in cummingtonite. When *C*-centered cummingtonite transforms into primitive cummingtonite, it is expected that domains of *P*-cummingtonite will form which will have anti-phase relationships with one another (*cf.* pigeonite; for a review of anti-phase domains in pigeonite, see Morimoto, 1974). The formation of the primitive phase is expressed in X-ray diffraction photographs by the appearance of extra reflections ($h + k = 2n + 1$), which violate the *C*-centering. In principle, it is possible to view the anti-phase domains directly, when the crystal is imaged through these reflections in the electron microscope, using the dark-field technique. The reflections ($h + k = 2n + 1$) on the $h0l$ net of primitive cummingtonite from Ruby Mountain, Montana, are usually sharp but in some cases may be weak and diffuse (Ross *et al.*, 1969). By analogy with pigeonite, we postulate that the degree of sharpness of these reflections indicates the size of the anti-phase domains which are present in primitive cummingtonite (*cf.* Hamil *et al.*, 1973, and Ghose *et al.*, 1972).

Although anti-phase domains probably exist in primitive cummingtonite, attempts to image the anti-phase domain boundaries directly by transmission electron microscopy have failed so far (Lally and Ghose, 1972, unpublished; G. L. Nord, Jr., 1973, unpublished results). The reason for the failure may lie in the low transition temperature (∿100°C) for

$P \rightarrow C$ cummingtonite; presumably the sample heats up under the electron beam to a temperature higher than T_c, thus obliterating the anti-phase domains. However, if this explanation is true, according to Nord (1981, private communication), one would expect to see some $h + k \neq 2n$ spots disappearing from the electron diffraction pattern while moving about the thin foil, since only the position of the specimen under observation is heated. As a matter of fact, no $h + k \neq 2n$ spots can be found in the diffraction pattern, except a diffuse streak in the overexposed pattern. Hence, heating up of the specimen may not be a satisfactory explanation. Whether anti-phase domains exist in primitive cummingtonite is still uncertain.

Anthophyllite-cummingtonite phase relations

By analogy with pyroxene phase relations and on the basis of the observed exsolution phenomena in cummingtonites and the primitive to *C*-centered inversion in magnesium-rich cummingtonites, Ross *et al.* (1969) and Prewitt *et al.* (1970) postulated the following phase relations among primitive and *C*-centered cummingtonite and anthophyllite: "A *C2/m* amphibole containing Ca and Mg (or Fe^{2+}) in the M4 site, which is stable at high temperature with respect to anthophyllite, on cooling unmixes sufficient calcic clinoamphibole to place its composition in the stability field of anthophyllite. Recrystallization to anthophyllite should occur but since this would require a complete reconstruction of the crystal structure, inversion is prevented and a displacive transformation to $P2_1/m$ cummingtonite proceeds"; the primitive cummingtonite may persist as a metastable phase. "The cummingtonites from the Gouverneur, New York area, which are very magnesium rich, may show part of the reaction sequence described above, but the reaction has stopped well before complete unmixing of the Ca-component and inversion to anthophyllite."

The rest of the sequence in this scheme has now been found in the primitive cummingtonite from Ticino, Switzerland (Evans *et al.*, 1974). The amphibole is primarily Mg-rich primitive cummingtonite (86 mole % Mg), with fine lamellae of anthophyllite parallel to the (010) and (100) planes. Single-crystal precession photographs of the $h0l$ net indicate three oriented intergrown phases: (1) the bulk of the crystal consists of cummingtonite (space group $P2_1/m$); (2) a small amount of anthophyllite (space group *Pnma*)

sharing the a^* axis with the cummingtonite; and (3) a very small amount (∿5%) of tremolite (space group $C2/m$) sharing the c^* axis with the cummingtonite. Hence, the anthophyllite and tremolite phases have respectively (100) and ($\bar{1}01$) planes in common with the cummingtonite. This situation is completely analogous to the inversion of a lunar pigeonite studied by Ghose *et al.* (1973), in which the pigeonite exsolved augite lamellae parallel to (001) and subsequently inverted to orthopyroxene sharing the (100) plane with the host pigeonite. By analogy with this situation, we conclude that the Ticino cummingtonite first exsolved tremolite, and then inverted to the orthorhombic anthophyllite phase. Strictly from the orientation relationship of these three phases, of course, it is not possible to determine the direction of this reaction and determine which is the low-temperature phase. However, the indirect evidence indicates that the anthophyllite is the low-temperature phase. The indirect evidence includes the fact that the anthophyllite has diffuse X-ray spots elongated parallel to a^*, indicating the presence of very fine anthophyllite lamellae parallel to (100), which are at the most only a few hundred Ångströms thick. Secondly, it is well known that the cummingtonite, which is monoclinic, can accommodate more calcium in the structure than anthophyllite, which is orthorhombic. Hence, the reaction we are observing is retrograde. In this case, from other geological evidence one concludes that a fluid phase was present, which may have made the inversion possible.

MISCIBILITY GAPS AND EXSOLUTION TEXTURES IN AMPHIBOLES

Introduction

Many compositionally complex amphiboles are expected to break down under equilibrium conditions into two or more compositionally simpler phases. The attainment of thermodynamic equilibrium at temperatures below 800°C is hindered considerably, however, by the slow diffusion rates of the exchanging cations. As a result, even if an amphibole that has equilibrated at low temperatures is effectively a two-phase assemblage, detection of exsolution may be very difficult optically, because the exsolution lamellae are commonly extremely fine and submicroscopic. Hence, application of techniques that are capable of a resolution better than

that possible with optical microscopy, such as single-crystal X-ray diffraction or electron diffraction and microscopy combined with chemical analysis using energy dispersive detection, may be necessary to observe exsolution. Fine-scale oriented lamellar intergrowth of two amphiboles is the most reliable proof of exsolution in amphiboles. These results should be corroborated by the determination of subsolidus phase relations between appropriate amphibole pairs. Again, because of slow reaction kinetics, attainment of equilibrium within a reasonable time period in the laboratory is hampered; unless reversed reactions have been achieved, such experimental results may be suspect.

In spite of these difficulties, a number of miscibility gaps between amphibole pairs have been confirmed from observed exsolution phenomena, two of which have been further confirmed by experimental determinations of the subsolidus phase relations in the laboratory. These pairs include: anthophyllite-gedrite, cummingtonite-actinolite, cummingtonite-hornblende, actinolite-hornblende, tremolite (actinolite)-riebeckite, arfvedsonite-cummingtonite, and richterite-riebeckite. In addition, although not yet confirmed, miscibility gaps between actinolite-glaucophane, hornblende-glaucophane and cummingtonite-riebeckite are very likely on crystal-chemical grounds.

Analogy of the amphibole pairs with corresponding pyroxenes allows us to draw some general crystal-chemical rules with respect to exsolution in amphiboles. Immiscibility is to be expected between two amphiboles under the following conditions:

Rule (1): where the M4 site is filled with large cations such as Ca^{2+} in one amphibole and small cations such as Fe^{2+} and Mg^{2+} in the other (hornblende-cummingtonite, actinolite-cummingtonite);

Rule (2): where the A-site is fully or partially occupied in one and empty in the other (hornblende-actinolite, hornblende-cummingtonite, gedrite-anthophyllite, richterite-riebeckite);

Rule (3): where the M4 site is occupied by Ca in one and by Na in the other (actinolite-riebeckite).

Hence, the size and the charge of the cations occupying the M4 and the A-sites play critical roles. On the other hand, between two amphiboles such as glaucophane and riebeckite, no miscibility gap is to be

expected except under very low-temperature conditions (below perhaps 300°C), since the exchanging cations involved (Al^{3+} and Fe^{3+} in the M2 site) have similar charges and ionic radii. In spite of the perplexing chemical complexity of the amphiboles, a generally consistent picture is emerging in terms of miscibility gaps, many of which can be experimentally confirmed in judiciously chosen systems. Obviously, much work is still needed both on natural assemblages and synthetic systems to clarify the subsolidus phase relations in amphiboles.

On the basis of a large number of analyses for members of the anthophyllite-gedrite, cummingtonite-grunerite and tremolite-actinolite series, Sundius (1933) was able to outline the miscibility gaps among these series. Non-existence of amphibole compositions between these three series was taken as the indirect proof of the existence of miscibility gaps. Since then, a considerable number of analyzed amphibole pairs have been reported in the literature (see Klein, 1968). Provided it can be shown that chemical equilibrium has been established, such pairs prove the existence of miscibility gaps. However, establishing chemical equilibrium can be difficult, since such pairs often appear as intergrowths, which can be (a) primary intergrowths of two amphibole phases, (b) replacement of one amphibole by another, (c) overgrowth of one amphibole on another, and (d) exsolution or unmixing of two amphiboles from a homogeneous primary phase. Replacement of one amphibole by another and overgrowth can be sometimes recognized. Distinction between primary intergrowth and exsolution cannot be made without detailed single-crystal X-ray investigation. In clinoamphiboles, the host and the exsolved phases usually share the ($\bar{1}01$) and (100) planes in the space group *C2/m*. In the *I2/m* orientation, which corresponds to the *C2/c* orientation of clinopyroxenes, these lamellae are parallel to the (001) and (100) planes (Fig. 8--refer to Fig. 26 in chapter by Robinson *et al.*, p. 56, Vol. 9B). For further discussion we will exclusively use the *C2/m* orientation for clinoamphiboles. Very fine-scale exsolution, as observed through single-crystal X-ray diffraction and electron microscopy, is a clear proof of miscibility gaps in amphiboles.

Unmixing of two amphiboles from a primary homogeneous phase can proceed by two mechanisms: (1) nucleation and growth; or (2) spinodal decomposition. In the latter mechanism, compositional waves are set up

within the homogeneous phase in the initial stages of exsolution. These compositional modulations subsequently develop as regularly spaced exsolution lamellae. Nucleation and growth appears to be the most common mechanism, but the spinodal mechanism seems to operate in some cases (e.g., gedrite-anthophyllite).

Actinolite-hornblende

Shidô and Miyashiro (1959) reported a miscibility gap between actinolite and blue-green hornblende from metamorphosed basic rocks from the Central Abukuma Plateau, Japan, which crystallized in the lowest temperature range of the amphibolite facies. The two amphiboles with sharp boundaries in discontinuously zoned crystals, actinolite grains with hornblende patches, and fibrous intergrowths of two amphiboles were considered to indicate an equilibrium assemblage. Numerous actinolite-hornblende occurrences from metamorphic rocks have since been described (see Klein, 1969) where subhedral grains show irregular zones and patches of hornblende in actinolite and vice versa. From the textural evidence, these two amphiboles are most likely not in equilibrium, but represent arrested stages of reaction during recrystallization (Grapes, 1975; Grapes and Graham, 1978). Actinolite and hornblende in apparent chemical equilibrium occur as separate grains in amphibolites at Hanover, New Hampshire (Brady, 1974). Klein (1969) described a rock from Tsintobolovolo, Madagascar, where equidimensional grains of the two amphiboles are interwoven. The green hornblende shows abundant exsolution lamellae 0.25 μm in thickness parallel to ($\bar{1}01$) and (100), which are most likely actinolite in composition. Cooper and Lovering (1970) observed exsolution lamellae of hornblende in actinolite and vice versa from metamorphosed basic rocks of southern New Zealand. Tagiri (1977) suggested that the lamellar intergrowths of actinolite and hornblende in some metamorphosed igneous rocks represent an equilibrium assemblage which may indicate a miscibility gap. A miscibility gap is also suggested by the compositional gap between analyses of tremolites and aluminous hornblendes from the lower medium range of the amphibolite facies rocks from the North Cascades, Washington (Misch and Rice, 1975).

Oba (1980) has experimentally determined the phase relations on the tremolite-pargasite join in the temperature range 750-1150°C under water

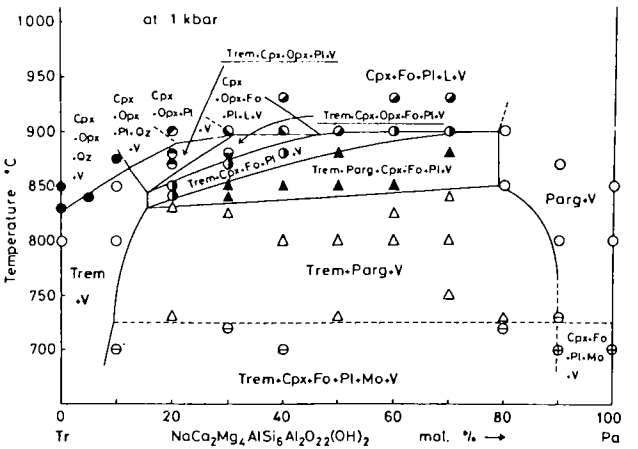

Figure 9. Solvus between tremolite and pargasite at 1 kbar. From Oba (1980).

vapor pressures of 1 and 5 kbar. At 850°C and 5 kbar, there is a continuous solid solution between the composition $Tr_{85}Pa_{15}$ and $Tr_{0}Pa_{100}$. At 800°C and 1 kbar, there is a solvus between tremolite and pargasite (Fig. 9). Under these conditions between $Tr_{90}Pa_{10}$ and $Tr_{10}Pa_{90}$ tremolitic and pargasitic amphiboles coexist with vapor. These results seem to be in agreement with field relations. Plots of amphibole compositions from skarns and marbles (low pressure and high temperature) within the Tr-Ts-Ha (Tr = tremolite, Ts = tschermakite, Ha = hastingsite) ternary system show the existence of a compositional gap, whereas amphiboles from igneous rocks formed at high temperature and high pressure (above 1 kbar) do not show the compositional gap (Oba, 1980).

Hornblende-anthophyllite

Sundius (1933) postulated a miscibility gap between hornblende and anthophyllite, i.e., a monoclinic and an orthorhombic amphibole. However, exsolution in such systems is always of a second amphibole of the same crystal system. For example, in a hornblende-anthophyllite assemblage from New Hampshire, the hornblende exsolves primitive cummingtonite parallel to $(\bar{1}01)$ and (100), and the anthophyllite exsolves gedrite (Robinson and Jaffe, 1969; Ross *et al.*, 1969). These phenomena can be explained on the basis of crystal structural control exerted by the host on the nucleated phases. The comparable analog in pyroxenes is augite-orthopyroxene, where augite may exsolve metastable pigeonite along (001).

The hornblendes coexisting with anthophyllite have less iron than those coexisting with cummingtonite (Robinson and Jaffe, 1969). Furthermore, hornblendes coexisting with anthophyllite generally exsolve primitive cummingtonite, whereas hornblendes coexisting with cummingtonite exsolve *C*-centered cummingtonite.

Actinolite (tremolite)-anthophyllite

Klein (1968) has analyzed the coexisting tremolite-actinolite and anthophyllite (+ talc) from Balmat, New York. This pair has a distinctly higher Mg/(Mg+Fe) ratio than the hornblende-anthophyllite pair described above. Kamineni *et al.* (1980) have described an equilibrium assemblage of actinolite-cummingtonite-anthophyllite from metamorphosed ultramafic rocks of Baffin Island, Arctic Canada. All three amphiboles occur as independent grains and with all three in mutual contact. All three amphiboles are homogeneous and devoid of any microscopic exsolution features. From the metamorphosed ultramafic body at Chester, Vermont, Veblen and Buseck (1980) describe composite amphibole crystals consisting of low calcium amphibole (anthophyllite) at one end and actinolite at the other. The intermediate parts of such composite crystals consist of a fine intergrowth of anthophyllite and actinolite on planes (100). The actinolite contains cummingtonite lamellae exsolved on $(\bar{1}01)$.

The calcic amphiboles (hornblende or actinolite) have higher Mg/(Mg+Fe) ratios than anthophyllite that coexists with them (Klein, 1968). A similar Mg-Fe distribution is found in igneous and metamorphic orthopyroxene-calcic pyroxene pairs (Kretz, 1963). These observations can be explained by the fact that the M4 site in anthophyllite and the M2 site in orthopyroxene strongly prefer Fe^{2+}, whereas these sites in calcic amphiboles and pyroxenes are occupied by Ca^{2+}.

Hornblende-cummingtonite

Although Eskola (1914) first noticed hornblende-cummingtonite intergrowths which may have been due to unmixing, he interpreted them to be due to replacement of hornblende by cummingtonite. Asklund (1923) first suggested an exsolution origin of the hornblende-cummingtonite intergrowth and proposed that a miscibility gap exists between these two amphiboles. This suggestion was subsequently verified by detailed optical microscopy and single-crystal X-ray diffraction studies of coexisting hornblende and

cummingtonite from amphibolite rocks at Sköthagen, Sweden, which revealed fine ($\bar{1}01$) lamellae of cummingtonite in the hornblende and vice versa (Asklund *et al.*, 1962). Similar exsolution lamellae in coexisting hornblende and cummingtonite observed through optical microscopy were reported from amphibolite rocks in Perniö, Finland (Seitasaari, 1952), Queensland, Australia (Vernon, 1962), Orange, Massachusetts, and New Hampshire (Robinson, 1963), New South Wales, Australia (Binns, 1965), Novarra, Italy (Boriano and Minutti, 1965), and Adamello, Italy (Calleghari, 1966), and other areas.

In addition to the ($\bar{1}01$) lamellae, fine (100) lamellae in hornblende and cummingtonite were noticed through optical microscopy and X-ray diffraction (Robinson, 1963; Binns, 1965; Calleghari, 1966; Jaffe *et al.*, 1968; Robinson *et al.*, 1969).

Hornblende-cummingtonite, hornblende-anthophyllite and actinolite-cummingtonite intergrowths have been extensively studied using optical microscopy, microprobe analysis and X-ray diffraction by Ross *et al.* (1969) and Robinson and Jaffe (1969). These papers should be consulted for details. We summarize here some of their results. Table 3 shows unit-cell dimensions of 10 hornblende and cummingtonite specimens that show exsolution phenomena. The hornblende coexisting with *C*-cummingtonite contains exsolution lamellae of *C*-cummingtonite, but when it is coexisting with anthophyllite, the exsolution lamellae in hornblende are *P*-cummingtonite, indicating the structural control of the host and the metastable nature of the *P*-cummingtonite. The ($\bar{1}01$) lamellae are usually thicker than the (100) lamellae. The exsolution lamellae may subsequently be obliterated by intergranular recrystallization. Hornblendes coexisting with anthophyllite contain less iron than those associated with cummingtonite; furthermore, the coexisting anthophyllite shows exsolution lamellae of gedrite (Robinson and Jaffe, 1969).

Gittos *et al.* (1974, 1976) have studied exsolution intergrowths of hornblende and grunerite with transmission electron microscopy. The hornblende contains coherent lamellae of grunerite approximately parallel to (100) and ($\bar{1}01$), which nucleated heterogeneously. In turn, the grunerite also contains heterogeneously nucleated lamellae of hornblende approximately parallel to (100) and ($\bar{1}01$). Figure 10 shows hornblende lamellae that have nucleated at a (100) twin boundary of grunerite. The semi-coherent

Table 3. Crystallographic data for amphiboles showing exsolution, from metamorphosed volcanics from Massachusetts and New Hampshire (Ross *et al.*, 1969).

No.	Crystal No.	Amphibole Intergrowths	% of grain	a(Å)	b(Å)	c(Å)	β	Space Group	V(Å^3)
6A9X	1	hornblende host	90	9.80	18.00	5.32	105°0′	$C2/m$	906.5
		P-cummingtonite on (100)	7	9.51	18.00	5.31	102°15′	$P2_1/m$	888.3
		P-cummingtonite on ($\bar{1}$01)	3	9.50	18.00	5.31	102°0′	$P2_1/m$	888.2
	2	anthophyllite host	70	18.57	18.05	5.29	—	$Pnma$	1773.1
		gedrite	30	18.57	17.88	5.29	—	$Pnma$	1756.4
N30X	1	anthophyllite host	50	18.58	18.04	5.29	—	$Pnma$	1753.5
		gedrite	50	18.58	17.84	5.29	—	$Pnma$	1773.1
	2	hornblende host	90	9.81	18.02	5.31	105°0′	$C2/m$	906.7
		P-cummingtonite on ($\bar{1}$01)	5	9.49	18.02	5.30	101°55′	$P2_1/m$	886.8
		P-cummingtonite on (100)	5	9.49	18.02	5.30	102°5′	$P2_1/m$	886.3
7E8BX	1	C-cummingtonite	100	9.50	18.18	5.31	101°55′	$C2/m$	897.3
	2	hornblende host	99	9.77	18.02	5.32	104°40′	$C2/m$	906.1
		C-cummingtonite on (100)	1	9.51	18.02	5.30	102°5′	$C2/m$	888.1
7A8BX	1	C-cummingtonite host	92					$C2/m$	
		hornblende on (100)	4					$C2/m$	
		hornblende on ($\bar{1}$01)	4					$C2/m$	
	2	C-cummingtonite host	88	9.51	18.15	5.31	102°5′	$C2/m$	896.2
		hornblende on ($\bar{1}$01)	10	9.82	18.15	5.33	104°50′	$C2/m$	918.3
		hornblende on (100)	2					$C2/m$	
	3	hornblende host	90					$C2/m$	
		C-cummingtonite on ($\bar{1}$01)	10					$C2/m$	
	4	hornblende host	94	9.82	18.12	5.31	104°55′	$C2/m$	913.0
		C-cummingtonite on (100)	3	9.51	18.12	5.33	102°10′	$C2/m$	897.8
		C-cummingtonite on ($\bar{1}$01)	3					$C2/m$	
I34JX	1	gedrite host	>99	18.55	17.81	5.29	—	$Pnma$	1746.8
		rutile	<1	4.58	—	—	—	—	—
I34-I	1	gedrite	100	18.601(4)[a]	17.839(3)	5.284(2)	—	$Pnma$	1753.2(5)
I38DX	1	gedrite host	80	18.56	17.87	5.29	—	$Pnma$	1754.5
		anthophyllite	20	18.56	18.11	5.29	—	$Pnma$	1778.1
W95JX	1	gedrite host	80	18.54	17.76	5.27	—	$Pnma$	1735.2
		anthophyllite	20	18.54	17.98	5.27	—	$Pnma$	1756.8
I38A	A	C-cummingtonite host	90	9.49	18.13	5.30	102°5′	$C2/m$	891.7
		hornblende on (100)	6	9.80	18.13	5.30	104°45′	$C2/m$	910.6
		hornblende on ($\bar{1}$01)	4						
	C-A	C-cummingtonite host	98					$C2/m$	
		hornblende on (100)	2					$C2/m$	
	1	hornblende host	85	9.80	18.08	5.31	104°45′	$C2/m$	909.8
		C-cummingtonite on (100)	10	9.52	18.08	5.31	102°10′	$C2/m$	893.4
		cummingtonite on ($\bar{1}$01)	5					$C2/m$?	
	2	anthophyllite host	55	18.58	18.11	5.28	—	$Pnma$	1776.6
		gedrite	45	18.58	17.85	5.28	—	$Pnma$	1751.1
QB27C	1-H	hornblende host	75	9.79	18.02	5.31	104°57′	$C2/m$	905.2
		P-cummingtonite on (100)	25	9.48	18.02	5.31	102°5′	$P2_1/m$	887.0
	1-P	P-cummingtonite host	85	9.45	18.00	5.30	102°5′	$P2_1/m$	881.6
		hornblende on (100)	15	9.75	18.00	5.30	104°55′	$C2/m$	898.8
	2-A	anthophyllite host	80	18.57	18.00	5.30	—	$Pnma$	1771.6
		gedrite	20	18.57	17.81	5.30	—	$Pnma$	1752.9

[a] Unit-cell parameters obtained by least-squares refinement of X-ray diffraction powder data.

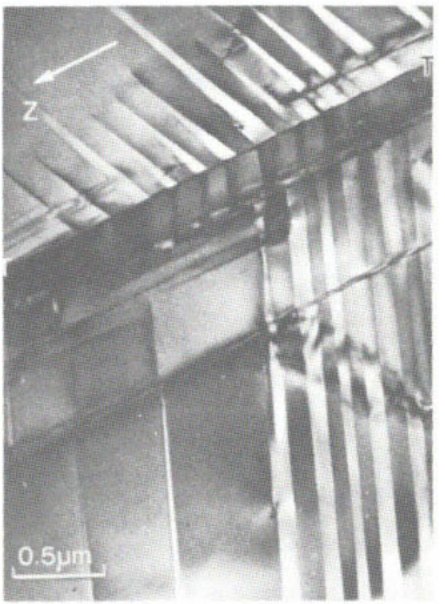

Figure 10. Nucleation of ($\bar{1}01$) hornblende lamellae at a (100) twin boundary T-T in grunerite. From Gittos *et al.* (1976).

Figure 11. Grunerite lamellae in hornblende showing growth ledges. From Gittos *et al.* (1974).

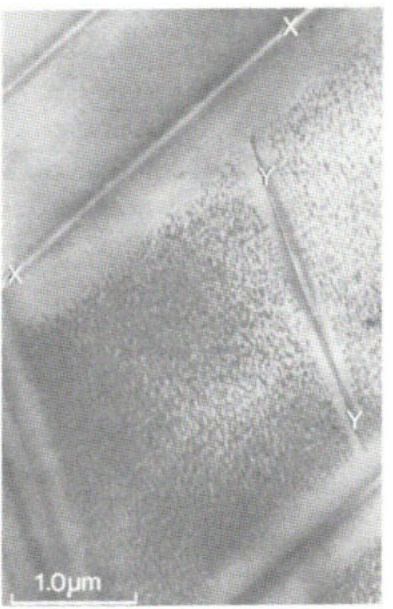

Figure 12. Homogenous precipitation of (100) platelets (Guinier Preston Zones) between heterogeneous ($\bar{1}01$), X-X and (100), Y-Y lamellae in grunerite. From Gittos *et al.* (1976).

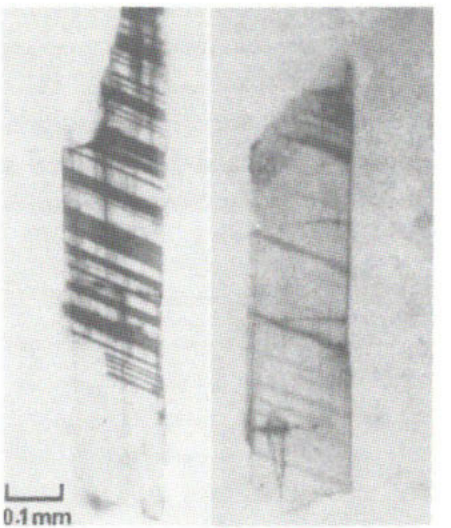

Figure 13. Composite photomicrograph showing actinolite host and cummingtonite host that coexist in the same rock sample. The grain on the left is actinolite (dark areas) containing about 55% primitive cummingtonite lamellae oriented parallel to ($\bar{1}01$). The grain on the right is primitive cummingtonite containing about 10% actinolite lamellae (darker areas) oriented parallel to ($\bar{1}01$) of the host. Oil mount, uncrossed polarizers. From Ross *et al.* (1969).

interface between integrown grunerite and hornblende may also act as a nucleation site for additional lamellae; these exsolution lamellae are completely coherent with the host (i.e., the lattice planes of the precipitate and matrix are continuous across the interface), even for lamellae up to 0.5 μm thick. The exsolution lamellae often pinch out, and sometimes irregularly-spaced steps or ledges are observed at the interfaces of the (100) lamellae (Fig. 11). Similar ledges have been observed at the interfaces of (100) lamellae of augite in orthopyroxene. These ledges have been interpreted as growth features, and the motion of these ledges along the interfaces provides the thickening mechanism for the exsolution lamellae. "If such ledges are arranged in a systematic manner on each side of a lamella they could explain the fact that although the (100) or ($\bar{1}$01) lattice planes are always nearly parallel in the matrix and precipitate for a lamella approximately parallel to (100) and ($\bar{1}$01), the interface may lie at a small to moderate angle to these planes. However, the rarity of this phenomenon suggests it is an unlikely explanation for the angular relations observed by Robinson *et al.* (1971a)" (Gittos *et al.*, 1976).

The cummingtonite and grunerite examined by Gittos *et al.* (1976) also contain a homogeneous distribution of fine (100) platelets between the (100) and ($\bar{1}$01) hornblende lamellae (Fig. 12). "A precipitate-free zone occurs adjacent to the lamellae and indicates that the platelets formed after the lamellae in areas where the calcium supersaturation was high enough to overcome the energy barrier for homogeneous nucleation" (Gittos *et al.*, 1976).

(Tremolite) actinolite-cummingtonite

Coexisting actinolite and cummingtonite from amphibolites and metamorphosed iron formation rocks most commonly show fine ($\bar{1}$01) exsolution lamellae through optical microscopy. Such intergrowths have been extensively studied by Ross *et al.* (1969). We report some of their results here. Figure 13 shows fine ($\bar{1}$01) exsolution lamellae of primitive manganoan cummingtonite in tremolite and vice versa from Gouverneur, New York. X-ray precession photographs of these amphiboles reveal common b^* and c^* axes and separate a^* axes of the two amphiboles (Fig. 14). An electron microscopic study of the primitive cummingtonite by G. L. Nord, Jr. (unpublished) revealed fine-scale ($\bar{1}$01) lamellae of tremolite (Fig. 15).

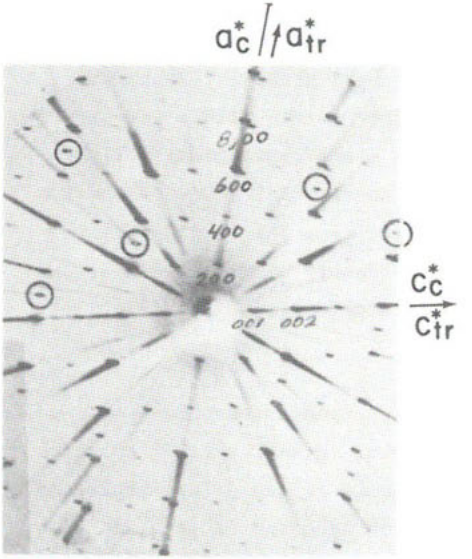

Figure 14 (to the left). Precession photograph of a primitive manganoan cummingtonite grain. The strong set of reflections marked by axes a^*_c and c^*_c are due to cummingtonite host. Some of the stronger reflections violating the $C2/m$ space group symmetry are circled (i.e., 502, 304, $30\bar{2}$, $10\bar{4}$ and $70\bar{4}$). The weaker set of reflections marked by axes a^*_{tr} and c^*_{tr} are due to the tremolite lamellae. MoKα radiation. From Ross *et al.* (1969).

Figure 15 (to the right). Exsolution lamellae of tremolite along ($\bar{1}01$) of primitive manganoan cummingtonite host, Talcville, New York (sp. no. 115046; Ross *et al.*, 1968). A narrow stacking fault along (010) cuts across both host and lamellae. Bright-field electron micrograph, g = $\bar{1}01$, 200 keV. Courtesy of G.L. Nord, Jr.

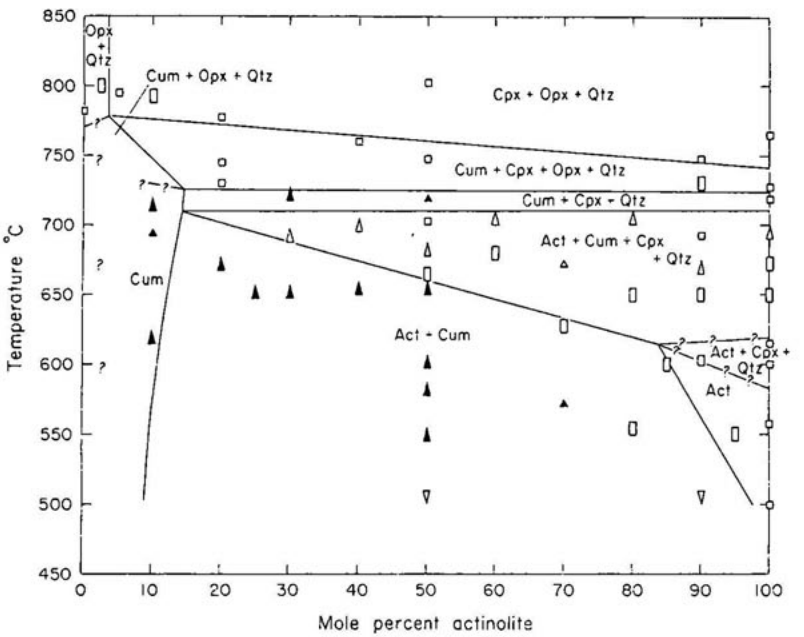

Figure 16. The actinolite-cummingtonite solvus in the pseudo-binary join $Mg_{3.5}Fe_{3.5}Si_8O_{22}(OH)_2$-$Ca_2Mg_{2.5}Fe_{2.5}Si_8O_{22}(OH)_2$ + excess H_2O at P fluid = 2 kbar and oxygen fugacities defined by the fayalite-magnetite-quartz buffer. From Cameron (1975).

Similar orientation relationships are shown by actinolite exsolving primitive cummingtonite and vice versa from Ruby Mountain, Montana. Ross *et al.* (1969) have proposed an asymmetric solvus within the pseudobinary join actinolite-cummingtonite with a steep cummingtonite limb. This suggestion has been confirmed by the experimental study of Cameron (1975), who studied the pseudobinary join $Mg_{3.5}Fe_{3.5}Si_8O_{22}(OH)_2$-$Ca_2Mg_{2.5}Fe_{2.5}Si_8O_{22}(OH)_2$ with excess H_2O at fluid pressure of 2 kbar and at oxygen fugacity defined by the fayalite-magnetite-quartz buffer (Fig. 16).

Tremolite (actinolite)-riebeckite

A miscibility gap at lower metamorphic temperatures (500°C or less) between tremolite and riebeckite is postulated on the basis of the lack of complete solid solution in lower metamorphic grades. The exsolution between these two end members involves cation exchange of the type $Na^+Fe^{3+} \rightleftarrows Ca^{2+}Mg^{2+}$. Immega and Klein (1976) described an amphibole paragenesis from the Carter Creek area of southwestern Montana, which "consists of a pale green sodic tremolite, which shows patchy anomalous extinction and rims of finer grained blue magnesioriebeckite. Boundaries between the Na-tremolite and the rimming riebeckite within a grain are optically sharp; there is no visible exsolution within either amphibole.... Precession photographs of single crystals of Na-tremolite with no optically visible riebeckite usually have riebeckite reflections," both phases sharing a common *b* axis and both possessing the space group *C2/m*. The unit-cell dimensions of the Na-tremolite are a = 9.80, b = 18.01, c = 5.24A, β = 104°40', and those of the riebeckite, a = 9.79, b = 18.01, c = 5.28A, β = 103°. Similar observations on the Na-tremolite have been made by the author and S. Varadarajan (1977, unpublished).

Actinolite-glaucophane

Klein (1969) has assembled reports of coexisting actinolite-glaucophane assemblages. Because of zoning which is commonly present, it is not always possible to determine if these phases are in equilibrium. However, as in tremolite-riebeckite, a miscibility gap is expected at lower metamorphic temperatures on crystal-chemical grounds. From the glaucophane schists from Marin County, California, and the Cazadero area, Sonoma County, California, Dudley (1967) and Lee *et al.* (1966) have described the coexistence of actinolite and glaucophane, which are present

in distinct individual grains in apparent chemical equilibrium. Often a single amphibole grain may consist of both actinolite and glaucophane. This observation, which is common in other amphibole pairs as well, does not contradict chemical equilibrium but reflects the kinetic ease with which one amphibole may act as a nucleation center for the second amphibole. Similar coexisting actinolite-glaucophane has been reported by Ernst *et al.* (1970).

Iwasaki (1963) describes zoned amphiboles from the Kôtu Bizan area of Eastern Shikoku, Japan, where actinolite cores are rimmed by glaucophane and vice versa. The boundaries of the cores and rims are sharp. This occurrence may also indicate chemical equilibrium and can be explained on the basis of the ease of nucleation of one amphibole phase on the other. Single-crystal X-ray photographs usually show a common orientation of the *b* axes of the lattices in such cases. Electron microscopic examination of the boundary regions of two amphiboles would be of interest.

Hornblende-glaucophane

Hornblende-glaucophane schists from Marin County, California, show textures similar to the actinolite-glaucophane pairs (Dudley, 1967). No exsolution lamellae have been found in these coexisting amphiboles. Due to the patchy texture, a replacement origin cannot be ruled out, although optically and chemically sharp boundaries may indicate a miscibility gap (Klein, 1969).

Glaucophane-riebeckite

A complete solid solution series between glaucophane and riebeckite has been found in alkali amphiboles from the blueschists of the Cazadero area, California (Coleman and Papike, 1968). Since immiscibility would require Al^{3+}-Fe^{3+} unmixing, the complete solid solution in this series is not surprising. Koslowski and Hinrichsen (1979) synthesized a glaucophane-riebeckite mixed crystal (crossite) at 700°C and 4 kbar H_2O pressure. The upper stability limit is near 800°C at 1-2 kbar H_2O pressure.

Table 4 (after Ghose *et al.*, 1974).

ELECTRON MICROPROBE ANALYSES OF CLEAR PATCHES AND HOST-LAMELLA PAIR IN TIRODITE, TIRODI MINE, MADHYA PRADESH, INDIA

	(1)		(2)		(3)		(4)	
SiO_2	56.0		55.2		55.6		56.7	
Al_2O_3	0.8		0.8		1.2		0.9	
FeO	14.7		14.9		6.3		14.5	
MnO	1.0		8.4		6.1		4.2	
MgO	14.6		14.3		17.3		16.7	
CaO	0.2		1.1		3.1		1.6	
Na_2O	7.1		6.7		5.3		6.7	
K_2O	0.2		0.3		1.4		0.2	
Si	8.00		8.00		8.00		8.00	
Al	0.14		0.14		0.19		0.14	
Fe	1.76	5.14	1.80	6.04	0.75	5.39	1.71	5.86
Mn	0.12		1.02		0.74		0.50	
Mg	3.12		3.08		3.71		3.51	
Ca	0.03		0.17		0.48		0.24	
Na	1.98	2.06	1.88	2.10	1.47	2.19	1.83	2.10
K	0.03		0.05		0.24		0.03	
(O,OH,F)	24		24		24		24	

(1) Ca-poor phase : Magnesio-riebeckite, extremal composition in a clear patch in tirodite. Analyst, E. Olsen.
(2) Ca-rich phase : Magnesio-richterite, extremal composition in a clear patch in tirodite. Analyst, W. C. Forbes.
(3) Host in tirodite. Analyst, W. C. Forbes.
(4) Lamella in tirodite. Analyst, W. C. Forbes.

Table 5 (after Ghose *et al.*, 1974).

CELL DIMENSIONS OF MAGNESIO-RIEBECKITE, MAGNESIO-RICHTERITE AND EXSOLVED AMPHIBOLE PHASES IN TIRODITE (SPACE GROUP $C2/m$)

	Magnesio-riebeckite $Na_4Mg_3Fe_2^{3+}$ $Si_8O_{22}(OH)_2$ (Ernst 1968)	Magnesio-richterite $Na_2Mg_5Si_8$ $O_{22}(OH)_2$ (Witte *et al* 1969)	Exsolved amphibole phases in tirodite					
			Crystal no. 1		Crystal no. 2		Crystal no. 3	
			Phase 1	Phase 2	Phase 1	Phase 2	Phase 1	Phase 2
a_0(Å)	9.73	9.73	9.77	9.56	9.75	9.67	9.82	9.56
b_0(Å)	17.95	17.91	17.99	17.99	17.92	17.92	17.98	17.98
c_0(Å)	5.30	5.28	5.33	5.30	5.34	5.34	5.28	5.28
β(°)	103.3	102.6	104.0	102.9	103.7	102.8	104.3	102.5

Richterite-magnesio-riebeckite

The straw-yellow alkali amphibole from Tirodi, Madhya Predesh, India, originally described as tirodite* by Dunn and Roy (1938), occurs as coarse bladed prisms associated with braunite, spessertite, rhodonite and quartz. In terms of the bulk chemical composition, it is a manganoan magnesio-richterite-arfvedsonite. Ghose *et al.* (1974) made a detailed optical, X-ray, electron microprobe and electron microscopic examination of this amphibole, which turned out to be a lamellar intergrowth of two amphiboles.

*The type tirodite is a manganoan alkali amphibole. Segeler (1961) mistakenly used this name for a manganoan cummingtonite. This mistake seems to have received the blessing of the I.M.A. commission on amphibole nomenclature (Leake, 1978). However, it is strongly recommended that this mistake not be perpetuated. [See Chapter 1, this volume, for discussion of nomenclature.]

Optically, the bulk of this material consists of very fine lamellae of two different kinds parallel to ($\bar{1}01$), with occasional clear patches. The submicron lamellae are discontinuous and are themselves variable in composition. The electron microprobe analyses of the clear patches also show variable composition. Two of the extreme compositions, as well as an attempt to determine the chemical differences of two adjacent lamellae, are listed in Table 4.

X-ray precession photographs of single crystals of the Tirodi amphibole show the presence of two clinoamphibole phases with common b and c axes. The unit-cell dimensions, particularly β angles (Table 5), indicate a variability of chemical composition of the two exsolved phases. In one case, the (h00)-type X-ray diffraction spots from the two phases are connected by diffuse streaks running parallel to c^*, indicating a rather early stage of exsolution (*cf.* lunar pigeonite-augite: Ghose *et al.*, 1972).

Under dark field conditions in the transmission electron microscope, the exsolution lamellae can be very clearly observed (Fig. 17). The lamellae are apparently coherent and run parallel to ($\bar{1}01$). The most interesting feature observed with the electron microscope is the presence of dark round patches distributed throughout a lamella which also shows fine exsolution lamellae. In a different part of the crystal, these dark patches coalesce and form irregular domains of the second phase, which coexists with areas showing fine-scale exsolution (Fig. 17). From the similarity of the diffraction contrast, it appears that one set of exsolution lamellae and the irregular domains are similar in chemical composition. Subsequent electron microscopic examination revealed a second set of extremely fine-scale irregular exsolution lamellae parallel to (100) cutting through the ($\bar{1}01$) lamellae (Fig. 18). "There are no interfacial dislocations between the lamellae, and the electron diffraction patterns do not show any extra spots apart from a slight splitting. The very slight strain at the interface of the lamellae can only be seen when they cross a bend contour. The two phases are therefore nearly coherent. In Figure 19, the 8.4A lattice fringes due to the (110) planes are seen to run through both ($\bar{1}01$) and (100) lamellae without any interruption or deviation at the boundaries between the two phases" (Phakey and Ghose, 1974). This evidence suggests spinodal decomposition in this amphibole, in contrast to the case of the nucleation and growth mechanism found to operate in actinolite-grunerite

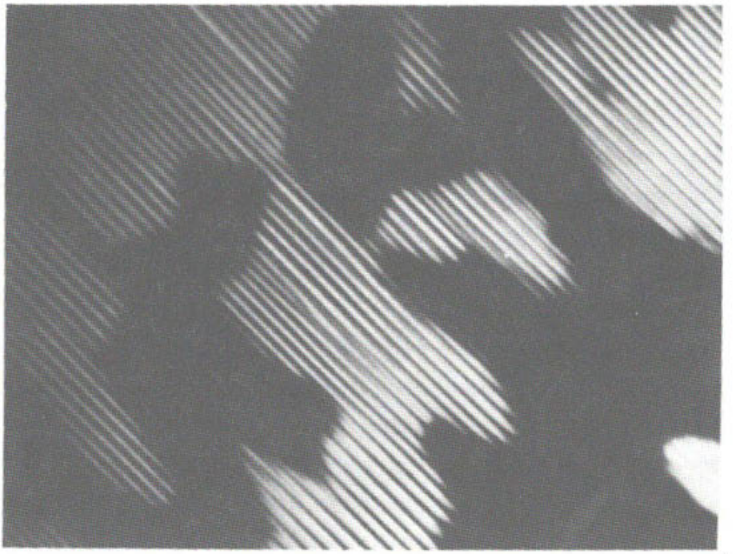

Figure 17. Dark-field transmission electron micrograph of exsolution lamellae in the alkali amphibole tirodite from Tirodi Mine. The regular exsolution lamellae are approximately 500 Å wide. Note that one set of exsolution lamellae (darker contrast) in places has coalesced into irregular patches. After Ghose *et al.* (1974).

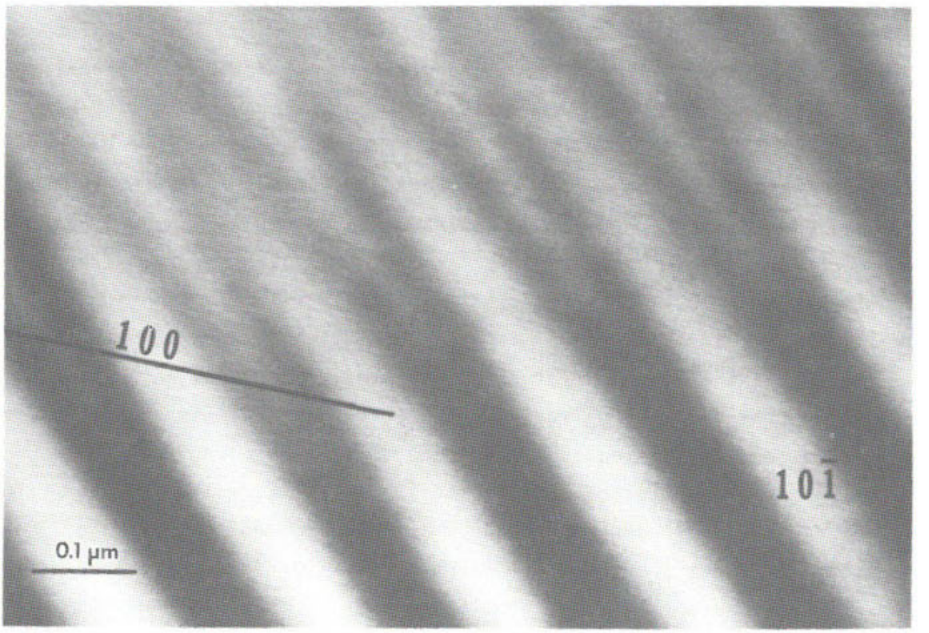

Figure 18. Higher magnification of the same area in tirodite showing another set of extremely fine-scale and not so regular exsolution lamellae (trace 100) approximately parallel to (100) cutting through the ($\bar{1}$01) lamellae. From Phakey and Ghose (1974).

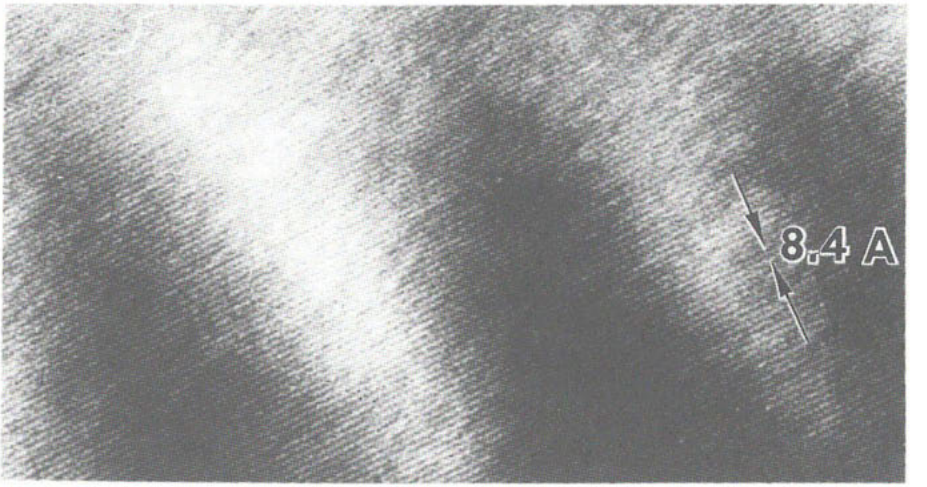

Figure 19. High resolution electron micrograph of the same area showing the 8.4 Å lattice fringes due to (110) planes running through both ($\bar{1}01$) and (100) lamellae without any interruption or deviation at the phase boundaries. After Phakey and Ghose (1974).

(Phakey and Ghose, 1974). Another sample revealed exsolution of ($\bar{1}01$) and (100) lamellae in nearly equal amounts (Fig. 20).

Single-crystal photographs of another sample of tirodite from the same locality indicated the absence of exsolution. This indirect evidence corroborates the suggestion that the exsolution observed in the other sample is in the beginning stages.

Anthophyllite-gedrite

Anthophyllite and gedrite are both essentially ferromagnesian amphiboles and are orthorhombic in symmetry (space group *Pnma*). Chemically, gedrite can be distinguished from anthophyllite by a much higher content of Al and Na in the former (Robinson and Jaffe, 1969). The sodium ions in gedrite partially fill the A-site (Papike and Ross, 1970).

The solvus between anthophyllite and gedrite was first discovered through single-crystal X-ray photographs of these minerals, which showed doubled reflections, indicating that they are actually oriented intergrowths of two orthorhombic amphiboles (both with space group *Pnma*). The orientation of the a, b and c axes were common to both phases, and only the b dimensions differed, indicating that the two sets of lamellae were gedrite and anthophyllite (Robinson and Jaffe, 1969; Ross *et al.*,

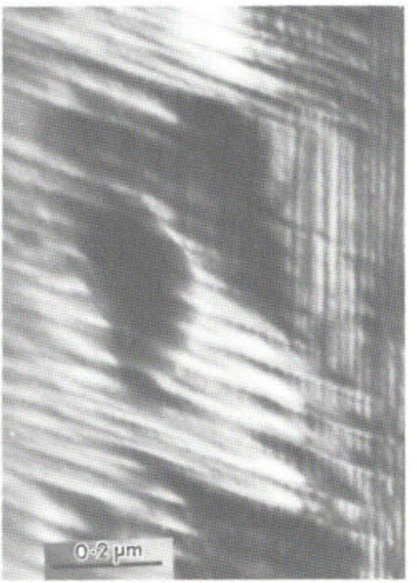

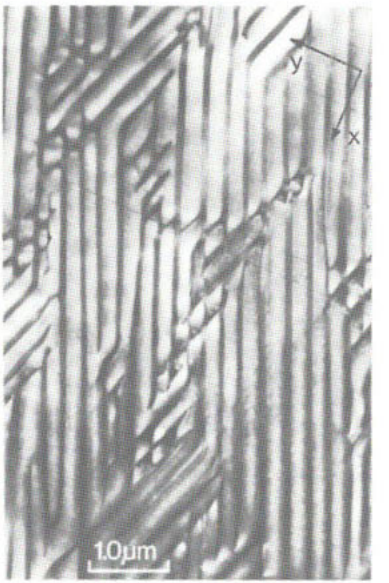

Figure 20 (above, left). Coexisting ($\bar{1}01$) and (100) exsolution lamellae in tirodite. The (100) lamellae are vertical. (Phakey and Ghose, 1974, unpublished electron micrograph)

Figure 21 (above, right). Interlinked exsolution lamellae approximately parallel to {120} in anthophyllite. Note also the (100) linear features.

Figure 22 (above, left). Exsolution in anthophyllite. In localized areas the precipitates are isolated, "wavy" particles. Between them are smaller (010) platelets, some of which have nucleated on the (100) faults (shown by arrows).

Figure 23 (above, right). (010) exsolution lamellae of gedrite in anthophyllite.

Figures 21, 22 and 23 from Gittos et al. *(1976, Figs. 3, 4 and 6).*

1969; Robinson *et al.*, 1971b). Optical examination revealed pervasive fine (010) lamellae in two very aluminous gedrites, 0.2 and 0.8 μm thick. Anthophyllites show no optically observable exsolution lamellae although in hand specimen in some cases they show strong schiller effect with variable blue, green and yellow colors, indicating the presence of fine-scale exsolution lamellae (as in peristerites and labradorites). Exsolved anthophyllite and gedrite lamellae in the intergrowths from New Hampshire and Massachusetts typically contain approximately 0.2 and 1.6 tetrahedral Al per formula unit, respectively (Robinson *et al.*, 1971). Coexisting anthophyllite and gedrite from Telemark, Norway, also suggest a solvus between these two amphiboles (Stout, 1970, 1971, 1972).

Coexisting high Na-Al gedrites and low Al-Na anthophyllites from the Post Pond volcanics, Vermont, described by Spear (1980), exhibit a variety of equilibrium growth textures, including discrete grains, bladed intergrowths, patchy intergrowths, overgrowths and lamellar intergrowths with lamellae parallel to (120). Coexisting orthoamphiboles show optically visible exsolution lamellae parallel to (010). Exsolution is much more pronounced in the gedrite than in the anthophyllite, which suggests that the solvus is steeper on the anthophyllite limb. The crest of the solvus is estimated by Spear (1980) to be about 600°C.

An electron microscopic examination of one gedrite and two anthophyllite specimens was made by Gittos *et al.* (1976). Interlinked lamellae lying on irrational matrix planes close to {120} were found in an anthophyllite with 34% gedrite component (Fig. 21). "Localized areas of the matrix are depleted in aluminium. Here the volume fraction of the second phase decreases and the structure degenerates into a series of 'wavy' precipitates straddling the (010) plane or, in regions very low in aluminium, into isolated particles, some of which are surrounded by a second generation of small (010) precipitates" (Fig. 22; Gittos *et al.*, 1976). A set of very fine planar features only a few unit cells thick were also found to lie parallel to (100); these have acted as nucleation sites for some of the (010) platelets.

In the second specimen of anthophyllite (with 41% gedrite) examined by Gittos *et al.* (1976), periodic, coherent lamellae of gedrite were seen whose interfaces were not strictly planar but on the average parallel to (010) (Fig. 23). A similar microstructure in an orthoamphibole with 60%

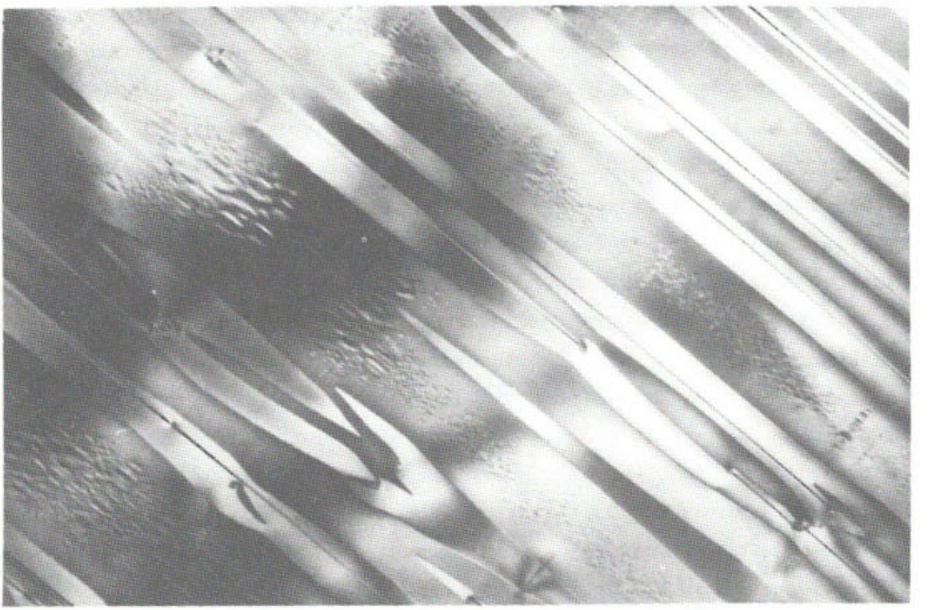

Figure 24. The microstructure of gedrite showing (010) lamellae of anthophyllite with a complicated morphology and small (010) platelets between them. Some of these platelets have nucleated on planar faults parallel to (100). × 24,000. From Gittos *et al.* (1976).

gedrite component has been observed by Christie and Olsen (1974). The homogeneous distribution of the lamellae with a periodicity of about 0.16 μm indicates that the exsolution may have occurred by spinodal decomposition followed by coarsening.

The specimen with ∿60% gedrite component examined by Gittos *et al.* (1976) reveals a complex texture consisting of (010) lamellae of anthophyllite with a complicated morphology and small (010) platelets between them (Fig. 24). Some of the platelets have nucleated on thin (100) "faults." The anthophyllite lamellae also contain planar features parallel to (010). A three-stage exsolution sequence has been proposed by Gittos *et al.* (1976): "heterogeneous nucleation and growth of the large lamellae at a high temperature followed by the heterogeneous nucleation of the platelets on the (100) 'fault' at a lower temperature and, finally, homogeneous nucleation of the platelets at an even lower temperature."

Arfvedsonite-cummingtonite

Klein (1966, 1968) described the equilibrium occurrence of the amphibole pair manganoan magnesioarfvedsonite-manganoan cummingtonite from the

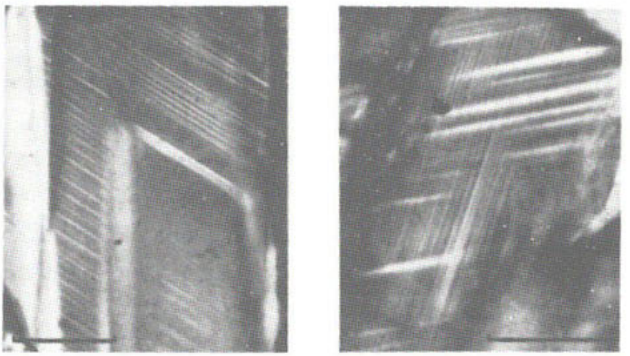

(A) (B)

Figure 25. Photomicrographs of magnesioarfvedsonite and manganoan cummingtonite from the Wabush Iron Formation, Labrador, under crossed nicols. A) Composite grain of cummingtonite and magnesioarfvedsonite (lower right corner) showing abundant thicker lamellae and a few thin lamellae (left side). B) Magnesioarfvedsonite grain at extinction showing two illuminated sets of cummingtonite exsolution lamellae. The thinner lamellae lie in the obtuse angle between the thicker lamellae and the *c* crystallographic axis. Length of scale bars: 50 μm. From Robinson *et al.* (1971a).

Table 6. Optical and x-ray parameters for manganoan magnesio-arfvedsonite and manganoan cummingtonite (Robinson *et al.*, 1971a).

	Magnesioarfvedsonite	*Manganoan Cummingtonite*
Optical Properties		
γ	1.650 ± .001	1.650 ± .001
β	1.643 ± .001	1.644 ± .001
α	1.638 ± .001	1.628 ± .001
$\gamma - \alpha$	0.012	0.022
$Z \wedge c$	39° ± 1°	22° ± 1°
2V (calc)	80°+	63°−
$c \wedge$ thicker exsolution lamellae	123° ± 1°	125° ± 1°
$c \wedge$ thinner exsolution lamellae	6° ± 1°	6° ± 1°
Angle between thinner and thicker lamellae	117° ± 1°	119° ± 1°
Color	very pale yellow; not pleochroic; anomalous blue and brown interference colors.	colorless
Unit Cell Parameters[1]		
Space Group *C2/m*		
a	9.885 ± .005 Å	9.620 ± .002 Å
b	18.006 ± .006 Å	18.062 ± .002 Å
c	5.295 ± .004 Å	5.314 ± .002 Å
β	104.04° ± .05°	102.78° ± .02°
V	914.23 ± .83 Å^3	900.51 ± .33 Å^3
Space Group *I2/m* (calculated)		
a	10.018 Å	9.907 Å
β	106°49′	108°45′

[1] Based on slow scan X-ray diffractometer powder patterns (goniometer speed $\frac{1}{4}$° per minute, chart speed $\frac{1}{2}$ inch per minute) in ascending and descending modes, using high purity silicon as an internal standard. Parameters calculated using a least squares refinement program (Burnham, 1962) from 15–17 unambiguously indexed diffraction lines between 20° and 80° 2θ (CuKα).

metamorphosed Wabush Iron Formation, southwestern Labrador, Canada. The sodic amphibole was incorrectly identified then as riebeckite. Further investigation of these two amphiboles by Robinson *et al.* (1971a) revealed that they most commonly occur as closely intergrown, independent subhedral grains, both exhibiting numerous fine exsolution lamellae, observable under crossed nicols at high magnification. The magnesioarfvedsonite is light yellow in color, whereas the cummingtonite is colorless. A set of lamellae (∿1 μm) occur at angles of 123° and 125° to the *c* axis in magnesioarfvedsonite and manganoan cummingtonite, respectively, and a thinner set of lamellae (<1 μm) occurs at an angle of 6° to the *c* axis (Fig. 25). On the other hand, single-crystal X-ray precession photographs of the two amphiboles show that the lattices of the host and the lamellae are oriented very closely along ($\bar{1}01$) and (100). This difference between the lattice orientation and the spatial orientation of the lamellae in the host has been explained by the theory of optimal phase boundaries (Robinson *et al.*, 1971a). The lattice dimensions of the lamellae match closely those of the other coexisting host amphibole (Table 6). Careful microprobe analyses of the host and qualitative probe scans across the lamellae confirm the identification that the lamellae in magnesioarfvedsonite are those of manganoan cummingtonite and vice versa (Table 7). The fractionation of MnO, CaO, Na_2O and K_2O is very pronounced in the two amphiboles. The lamellae in cummingtonite are more Fe poor and Mn rich than the host, whereas the Mg content is about the same.

Tremolite-richterite

Aoki *et al.* (1972) have described an amphibole intermediate in composition between tremolite and richterite (tremolite 57 mol %, richterite 31%, pargasite 6.3%, cummingtonite 5.4%, eckermannite 0.6%) occurring in kimberlite from Buell Park, Arizona. Single-crystal photographs indicate no exsolution, with unit-cell dimensions a = 9.876, b = 18.065, c = 5.281A, β = 104°40' (space group *C2/m*). On crystal-chemical grounds (see Rule 2) one would expect this amphibole to break down into two amphiboles at temperatures below ∿600°C under appropriate geologic or laboratory conditions.

Table 7. Chemical analyses and ionic ratios for magnesio-arfvedsonite and manganoan cummingtonite (Robinson *et al.*, 1971a).

(1) Wet chemical analysis of bulk sample of approximately 80 percent magnesioarfvedsonite and 20 percent cummingtonite. Analyst: Jun Ito. FeO not detected; if present probably less than 0.5 weight per cent.
(2) Electron probe determination of individual magnesioarfvedsonite. n.d. = not detected. Total Fe recalculated as Fe_2O_3 only.
(3) Electron probe determination of individual manganoan cummingtonite. n.d. = not detected. Total Fe recalculated as Fe_2O_3 only.

	(1)	(2)	(3)	Recalculated on basis of 23 oxygens		
SiO_2	55.32	54.9	55.8		(2)	(3)
TiO_2	0.00	n.d.	n.d.	Si	7.890	8.000
Al_2O_3	0.10	0.1	0.1	Al	.016	—
Fe_2O_3	6.86	8.3	2.3	Fe^{3+}	.094	—
				Σ (tet.)	8.000	8.000
FeO	n.d.	0	0			
MnO	7.65	6.0	15.3	Si	—	.010
MgO	18.18	17.6	20.8	Al	—	.016
CaO	2.11	2.3	0.7	Fe^{3+}	.804	.252
Na_2O	4.65	5.7	1.1	Mg	3.770	4.450
K_2O	1.97	2.2	0.1	Mn^{2+}	.426	.272
				Σ [*M*(1-3)]	5.000	5.000
$H_2O(+)$	2.98					
$H_2O(-)$	.50			Mn^{2+}	.305	1.589
F	.15			Ca	.354	.108
	100.47	97.1	96.2	Na	1.341	.303
				Σ [*M*(4)]	2.000	2.000
−O=F	0.06					
	100.41			Na	.246	.002
				K	.404	.017
				Σ (*A*)	.650	.019
				100 Mg/Mg+Fe+Mn	69.8	67.8
				100 Mn/Mn+Fe+Mg	13.5	28.4
				100 Na/Na+K+Ca	67.7	70.7

Conclusions

It is clear that although exsolution has been observed in a number of amphiboles, the details of the exsolution process are far from clearly understood. Nucleation and growth seems to be the mechanism operating in cummingtonite-actinolite (hornblende) exsolution, whereas the spinodal mechanism is likely in some of the anthophyllite-gedrite and richterite-riebeckite pairs that have been examined. The study of exsolution in amphiboles through transmission electron microscopy and microanalysis will be highly rewarding in the next decade.

THE THERMAL DECOMPOSITION OF AMPHIBOLES INTO PYROXENES AND OTHER PHASES

Crocidolite and sodic amphiboles

The thermal decomposition of crocidolite (fibrous riebeckite, approximately $Na_2Fe^{3+}_2Fe^{2+}_{2.6}Mg_{0.4}Si_8O_{22}(OH)_2$) has been studied by a number of workers (Addison *et al.*, 1962a,b; Addison and Sharp, 1962; Hodgson *et al.*, 1965; Patterson, 1965; Patterson and O'Connor, 1966; O'Connor and Patterson, 1966; Clark and Freeman, 1967; Freeman and Frazer, 1968). When crocidolite is heated in argon or nitrogen, the uncombined water is lost between 50-400°C. At 500-700°C an endothermic dehydroxylation takes place, yielding an anhydrous amphibole with a crystal structure similar to the original material. At about 800°C, the anhydride decomposes endothermally into acmite, cristobalite, spinel and a liquid. By contrast, when crocidolite is heated in oxygen or air, at 300-450°C hydrogen ions and electrons are lost to yield an oxyamphibole $Na_2Fe^{3+}_4Fe^{2+}_{0.6}Mg_{0.4}Si_8O_{24}$. The process is exothermic and probably occurs by proton and electron migration (Hodgson *et al.*, 1965a; Addison *et al.*, 1962a). At 600-950°C the oxyamphibole decomposes endothermically, during which most of the Fe^{2+} is oxidized, giving acmite, hematite, cristobalite and spinel. The pyroxene formed under both oxidizing and reducing conditions, as well as the oxyamphibole and the amphibole anhydride, maintain a strong axial orientation relationship with the original amphibole (Hodgson *et al.*, 1965a; Patterson, 1965; Freeman and Frazer, 1968). Small structural rearrangements take place during oxidation and dehydroxylation, as indicated by the broadening and shifting of the main infrared absorption bands; decomposition of the structure produces marked changes in the spectra (Patterson and O'Connor, 1966). The kinetic data on the dehydroxylation of crocidolite *in vacuo* have been interpreted by Clark and Freeman (1967) in terms of a diffusion-controlled reaction based on radial diffusion out of a cylinder. The activation energy of the dehydroxylation process is 49 kcal/mole.

Thermal behavior of 12 natural sodic amphiboles within the field of magnesio-riebeckite, riebeckite, glaucophane and ferroglaucophane has been studied using Mössbauer, infrared, X-ray and optical methods by Ernst and Wai (1970). Heat treatment of iron-bearing sodic amphiboles

in air at 705°C results in rapid loss of hydrogen and concomittant increase in Fe^{3+}/Fe^{2+} ratio. When Fe^{2+} ions are available in the M1 and M3 sites, electrons are transferred to the adjacent (OH) groups, resulting in neutralization and expulsion of hydrogen atoms. Subsequent to the fairly rapid loss of hydrogen, oxydation takes place slowly, presumably involving electron and/or ionic diffusion. Simultaneously, considerable cation disordering occurs. The resulting sodic amphiboles have shorter *a*, *b* and *c* axes and higher indices of refraction and birefringence compared to the original material.

The crystal structure of a riebeckite with the chemical composition $Li_{0.04}Na_{1.96}Mg_{1.21}Fe^{2+}_{1.79}Fe^{3+}_{1.54}Al_{0.46}Si_8O_{22}(OH)_2$ was determined before and after heating in air at 650°C for four days (Ungaretti, 1980). The unit-cell volume decreased by about 2.5%, and the crystal changed color as a result of heating. The M1-O3 and M3-O3 distances decreased from 2.111 and 2.087A respectively to 1.954 and 1.988A. The average M1-O and M3-O bond lengths also decreased from 2.099 and 2.112A respectively in the unheated crystal to 2.028 and 2.049A in the heated crystal. The Si-O, M4-O and M2-O bond distances remained relatively unchanged. Considerable rearrangement of the cations as a result of the heat treatment was also confirmed.

Tremolite

Freeman and Taylor (1960) have investigated the dehydroxylation of tremolite by single-crystal methods. Crystals of tremolite heated between 700 and 900°C show X-ray reflections from both unreacted tremolite and pyroxene. Those heated above 1000 or 1100°C show only pyroxene reflections. The *c*-axis oscillation and *hk*0 Weissenberg photographs show that the resulting pyroxene is a good single crystal, which retains the axial orientation of the tremolite (in *I2/m* orientation). The unit-cell dimensions of the tremolite are $a = 9.91$, $b = 18.04$, $c = 5.3$A, $\beta = 107.2°$, and those of the pyroxene, which has the composition $Ca_2Mg_5Si_7O_{21}$, are: $a = 9.73$, $b = 8.87$, $c = 5.3$A, $\beta = 107.2°$. The pyroxene X-ray photograph contains weak reflections which violate the *C*-centering. The space group probably is $P2_1/c$. The sequence of oxygen, silicon and cation layers parallel to (100) are the same in both tremolite and the pyroxene; furthermore, both have 12 oxygens and eight silicons in the oxygen and silicon layers, respectively. In the cation layer, tremolite has seven

(Ca+Mg), whereas the pyroxene has eight (Ca+Mg). Freeman and Taylor (1960) postulated a *donor* region (1/8 of the tremolite) which provides the (Ca+Mg) cations necessary to form the pyroxene within the *acceptor* region (7/8 of the tremolite). Through small atomic movements parallel to the (100) plane, tremolite can transform into a Ca-Mg pyroxene (Fig. 26). The reactions taking place within the *donor* and *acceptor* regions are shown below:

$$Ca_2Mg_5Si_8O_{24}H_2 + 14H^+ \rightarrow 2Ca^{2+} + 5Mg^{2+} + 8SiO_2 + 8H_2O$$

$$7(Ca_2Mg_5Si_8O_{24}H_2) + 2Ca^{2+} + 5Mg^{2+} \rightarrow 7(Ca_{2\frac{2}{7}}Mg_{5\frac{5}{7}}Si_8O_{24}) + 14H^+ .$$

A determination of the resulting pyroxene structure would be worthwhile.

Grunerite (and amosite)

Ghose and Weidner (1971a) have observed two different phenomena that occur as a result of heating grunerite at 500 bars argon pressure: (a) decomposition under relatively oxidizing conditions to form a second amphibole phase ("oxygrunerite"), accompanied by dehydrogenation and the formation of trace amounts of magnetite; (b) breakdown under reducing conditions to form a pyroxene phase, silica and water.

In the first reaction the oxyamphibole that forms retains the *a*, *b* and *c* axes of the original grunerite, but the cell dimensions are slightly smaller. A similar relationship between amosite and the oxyamphibole produced by heating has been observed by Hodgson *et al.* (1965b). The oxyamphibole forms as a result of loss of hydrogen, which combines with oxygen molecules to form water. If the oxyamphibole product is completely anhydrous, the reaction can be written as a partial oxidation of Fe^{2+} to Fe^{3+} and dehydroxylation (Hodgson *et al.*, 1965b): $Fe_7^{2+}Si_8O_{24}H_2 + 1/2O_2 \rightarrow Fe_5^{2+}Fe_2^{3+}Si_8O_{24} + H_2O$.

The breakdown of grunerite into clinoferrosilite under reducing conditions involves no oxidation of Fe^{2+} ions. The reaction takes place fairly quickly (∿1 hour) at about 775°C, resulting in an oriented intergrowth where the *a*, *b* and *c* axes of the pyroxene are parallel to the *a*, *b* and *c* axes of the amphibole in the *I2/m* orientation (Fig. 27). The grunerite utilized by Ghose and Weidner (1971a) had the chemical composition $(Ca_{0.110}Mn_{0.142}Fe_{6.685}Mg_{0.096})(Si_{7.968}Al_{0.016})O_{22}(OH)_2$ and the

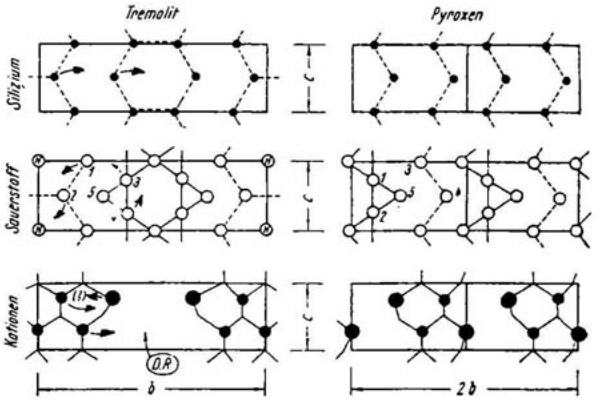

Figure 26. Idealized atomic arrangement of silicon, oxygen and cation layers parallel to (100) in tremolite and Ca-Mg pyroxene. Silicon (*Silizium*) layer: dashed lines connect the atoms which belong to the same silicate chain. Oxygen (*Sauerstoff*) layer: full lines connect the atoms which form the bases of SiO_4 tetrahedra in a chain. The dashed lines connect the apices of the tetrahedra of the same layer. Cation (*Kationen*) layer: lines indicate the cation-oxygen bonds. Only bonds on one side of the layer are shown. Arrows show the possible atomic movements during the phase transformation. D.R. = movement of atoms out of the *donor* region. From Freeman and Taylor (1960)

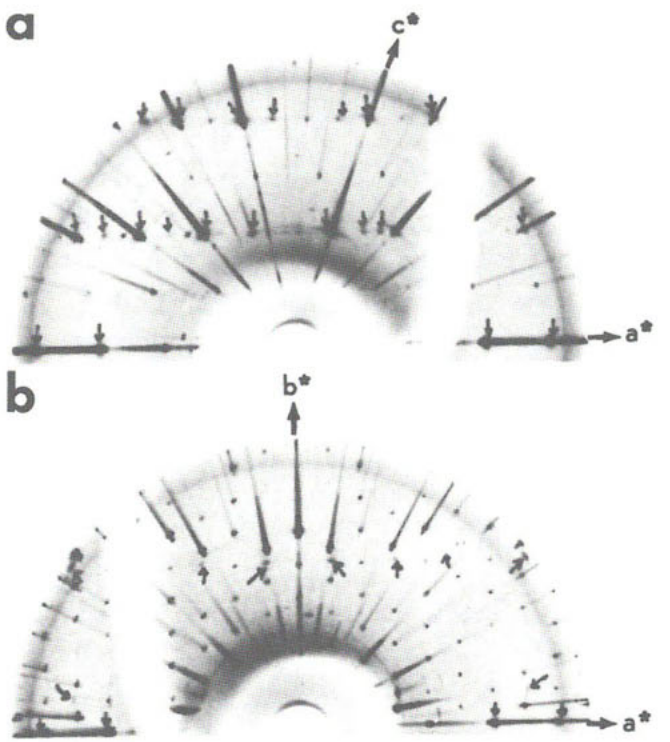

Figure 27. Upper halves of (a) a^*c^* and (b) a^*b^* precession photographs of a grunerite crystal heated at 775°C for 30 min. Arrows indicate clinoferrosilite spots. Mo$K\alpha$ radiation. From Ghose and Weidner (1971).

following unit-cell dimensions: a = 9.964, b = 18.453 and c = 5.343A and β = 109.65° in the *I2/m* orientation. The unit-cell dimensions of the resulting clinoferrosilite are a = 9.77, b = 9.08 and c = 5.30A and β = 109.5° (space group $P2_1/c$). The identity of the clinoferrosilite was confirmed by Mössbauer spectroscopy, which indicated a quadrupole splitting of 2.56 mm/sec and an isomer shift of 1.92 mm/sec (with respect to Fe) at room temperature. The area ratio of the two quadrupole split doublets from Fe^{2+} at M1 and M2 was one-to-one, indicating the chemical composition to be very close to $Fe_2Si_2O_6$. Following Freeman and Taylor (1960), a similar model of *donor* and *acceptor* regions has been proposed to explain the oriented transformation of grunerite into clinoferrosilite. The chemical reactions taking place within the *donor* and *acceptor* regions are:

$$Fe_7Si_8O_{24}H_2 + 14H^+ \rightarrow 7Fe^{2+} + 8SiO_2 + 8H_2O$$

$$7[Fe_7Si_8O_{24}H_2 + Fe^{2+}] \rightarrow 7[4(Fe_2^{2+}Si_2O_6) + 2H^+] \ .$$

This postulate of *donor* and *acceptor* regions seems to be substantiated by long exposure $h0l$ and $0kl$ precession photographs showing sharp spots from the pyroxene phase and weak powder rings (Fig. 27). The sharp spots originate from the pyroxene formed within the *acceptor* region, whereas powder rings are formed from partial breakdown of the *donor* regions of grunerite. An electron microscopic examination of such pyroxene-amphibole intergrowths would yield a more exact picture of the reaction mechanism (*cf.* Veblen and Buseck, 1980).

ACKNOWLEDGMENTS

I am greatly indebted to Drs. P. E. Champness, G. L. Nord, Jr., and P. P. Phakey for providing me with the original electron micrographs. I would also like to express my deep appreciation to Prof. E. F. Bertaut and M. Marezio, C.N.R.S., Laboratoire de Cristallographie, Grenoble, France, and Prof. K. Langer, Institut für Mineralogie und Kristallographie, Technische Universität Berlin, where this paper was written, for their kind hospitality. Support from the National Science Foundation (grants EAR 76-13373 and EAR 79-04868) is also gratefully acknowledged.

Addison, C.C., Addison, W.E., Neal, G.H., and Sharp, J.H. (1962a) Amphiboles Part I. The oxidation of crocidolite. J. Chem. Soc., 278, 1468-1471.

Addison, C.C., Neal, G.H., and Sharp, J.H. (1962b) Amphiboles Part II. The kinetics of the oxidation of crocidolite. J. Chem. Soc., 279, 1472-1475.

Addison, W.E., and Sharp, J.H. (1962) Amphiboles Part III. The reduction of crocidolite. J. Chem. Soc., 716, 3693-3698.

Aoki, K., Fodor, R.V., Keil, K., and Dowty, E. (1972) Tremolite with high richterite molecule content in kimberlite from Buell Park, Arizona. Amer. Mineral., 57, 1889-1893.

Asklund, B. (1923) Petrological studies in the neighborhood of Stavsjö at Kilmärten. Sverigs Geol. Unders. Arsb., 17, no. 6, 122 pp.

Asklund, B., Brown, W.L., and Smith, J.V. (1962) Hornblende-cummingtonite intergrowths. Amer. Mineral., 47, 160-163.

Bancroft, G.M., and Burns, R.G.(1969) Mössbauer and absorption spectral study of alkali amphiboles. Mineral. Soc. Amer. Spec. Paper, 2, 137-148.

Bancroft, G.M., Burns, R.G., and Maddock, A.G. (1967) Determination of cation distribution in the cummingtonite-grunerite series by Mössbauer spectra. Amer. Mineral., 52, 1009-1026.

Bancroft, G.M., Burns, R.G., Maddock, A.G., and Strens, R.G.J. (1966) Cation distribution in anthophyllite from Mössbauer and infrared spectroscopy. Nature, 212, 913-915.

Binns, R.A. (1965) The mineralogy of metamorphosed basic rocks from Willyama Complex, Broken Hill District, New South Wales, Part I. Hornblendes. Mineral. Mag., 35, 306-326.

Boriani, A., and Minutti, L. (1965) La cummingtonite di Ornavasso. Rend. Inst. Lombardo Sci. Lett., 99, 412-424.

Bown, M.G. (1965) A new amphibole polymorph in intergrowth with tremolite: clino-anthophyllite? (abstr.) Amer. Mineral., 51, 259-260.

Brady, J.B. (1974) Coexisting actinolite and hornblende from West Central New Hampshire. Amer. Mineral., 59, 529-535.

Butler, P., Jr. (1969) Mineral compositions and equilibria in the metamorphosed iron formation of the Gagnon region, Quebec, Canada. J. Petrol., 10, 56-100.

Callegharí, E. (1965-66) Osservazioni su alcune cummingtonite del massiccio dell'Adamello. Mem. Accad. Patavina, Cl. Sci. Mat.-Nat., 78, 273-310.

Cameron, K.L. (1975) An experimental study of actinolite-cummingtonite phase relations with notes on the synthesis of Fe-rich anthophyllite. Amer. Mineral., 60, 375-390.

Choudhuri, A. (1972) Hornblende-actinolite and hornblende-cummingtonite associations of Cuyuni River, Guyana, South America. Amer. Mineral., 57, 1540-1546.

Christie, O.H.J., and Olsen, A. (1974) Spinodal precipitation in minerals: Review and some new observations. Bull. Soc. Franc. Mineral. Cristallogr., 97, 386-392.

Clark, M.W., and Freeman, A.G. (1967) Kinetics and mechanism of dehydroxylation of crocidolite. Trans. Faraday Soc., No. 536, v. 63, 2051-2056.

Coleman, R.G., and Papike, J.J. (1968) Alkali amphiboles from the blueschists of Cazadero, California. J. Petrol., 9, 105-122.

Cooper, A.F., and Lovering, J.F. (1970) Greenschist amphiboles from Haast River, New Zealand. Contrib. Mineral. Petrol., 27, 11-24.

Dienes, G.J. (1955) Kinetics of order-disorder transformations. Acta Metal., 3, 549-557.

Dudley, P.P. (1967) *Glaucophane Schists and Associated Rocks of the Tiburon Penninsula, Marin County, California.* Ph.D. Dissertation, University of California, Berkeley.

Dunn, J.A., and Roy, P.C. (1938) Tirodite, a manganese amphibole from Tirodi, Central Provinces. Rec. Geol. Surv. India, 73, 295-298.

Ernst, W.G. (1968) *Amphiboles.* Springer Verlag, New York, 125 pp.

Ernst, W.G., Seki, Y., Onuki, H., and Gilbert, M.C. (1970) *Comparative Study of Low-Grade Metamorphism in the California Coast Ranges and the Outer Metamorphic Belt of Japan.* Geol. Soc. Amer. Memoir, 124, 276 pp.

Ernst, W.G., and Wai, C.M. (1970) Infrared, X-ray and optical study of cation ordering and dehydrogenation in natural and heat-treated sodic amphiboles. Amer. Mineral., 55, 1226-1258.

Eskola, P. (1914) On the petrology of the Orijärvi region in South Western Finland. Bull. Comm. Geol. Finlande, 40.

Evans, B.W., Ghose, S., Rice, J.M., and Trommsdorff, V. (1974) Cummingtonite-anthophyllite phase transformation in metamorphosed ultramafic rocks, Ticino, Switzerland (abstr.). Trans. Amer. Geophys. Union, 55, 469.

Finger, L.W. (1969) The crystal structure and cation distribution of a grunerite. Mineral. Soc. Amer. Spec. Paper, 2, 95-100.

Finger, L.W. (1970) Refinement of the crystal structure of an anthophyllite. Carnegie Inst. Wash. Year Book, 68, 283-288.

Fischer, K.F. (1966) A further refinement of the crystal structure of cummingtonite $(Mg,Fe)_7(Si_4O_{11})_2(OH)_2$. Amer. Mineral., 51, 814-818.

Freeman, A.G., and Frazer, F.W. (1968) A pseudo-polymorphic transition: the amphibole → pyroxene reaction. Nature, 220, 67-68.

Freeman, A.G., and Taylor, H.F.W. (1960) Die Entwässerung von Tremolit. Silikat. Tech., 11, 390-392.

Ghose, S. (1961) The crystal structure of a cummingtonite. Acta Crystallogr., 14, 622-627.

Ghose, S. (1962) The nature of Mg^{2+}-Fe^{2+} distribution in some ferromagnesian silicate minerals. Amer. Mineral., 47, 388-399.

Ghose, S. (1965) A scheme of cation distribution in the amphiboles. Mineral. Mag., 35, 46-54.

Ghose, S., Forbes, W.C., and Phakey, P.P. (1974) Unmixing of an alkali amphibole (tirodite) into magnesio-richterite and magnesio-riebeckite. Indian J. Earth Sci., 1, 37-42.

Ghose, S., and Hellner, E. (1959) The crystal structure of grunerite and observations on the Mg-Fe distribution. J. Geol., 67, 691-701.

Ghose, S., McCallum, I.S., and Tidy, E. (1973) Luna 20 pyroxenes: exsolution and phase transformation as indicators of petrologic history. Geochim. Cosmochim. Acta, 37, 831-839.

Ghose, S., Ng, G., and Walter, L.G. (1972) Clinopyroxenes from Apollo 12 and 14: exsolution, domain structure and cation order. Proc. 3rd Lunar Sci. Conf. (suppl. 3, Geochim. Cosmochim. Acta), 1, 507-531, M.I.T. Press.

Ghose, S., and Weidner, J.R. (1971a) Oriented transformation of grunerite to clinoferrosilite at 775°C and 500 bars argon pressure. Contrib. Mineral. Petrol., 30, 64-71.

Ghose, S., and Weidner, J.R. (1971b) Mg^{2+}-Fe^{2+} distribution isotherms in cummingtonites at 600° and 700°C (abstr.). Trans. Amer. Geophys. Union, 52, 381.

Ghose, S., and Weidner, J.R. (1972) Mg^{2+}-Fe^{2+} order-disorder in cummingtonite, $(Mg,Fe)_7Si_8O_{22}(OH)_2$: A new geothermometer. Earth Planet. Sci. Lett., 16, 346-354.

Gittos, M.F., Lorimer, G.W., and Champness, P.E. (1974) Precipitation (exsolution) in an amphibole (the hornblende-grunerite system). J. Mater. Sci., 9, 184-192.

Gittos, M.F., Lorimer, G.W., and Champness, P.E. (1976) The phase distributions in some exsolved amphiboles. In *Electron Microscopy in Mineralogy*, H.R. Wenk, ed., Springer Verlag, New York, pp. 238-247.

Grapes, R.H. (1975) Actinolite-hornblende pairs in metamorphic gabbros, Hidaka Mountains, Hokkaido. Contrib. Mineral. Petrol., 49, 125-140.

Grapes, R.H., and Graham, C.R. (1978) The actinolite-hornblende series in metabasites and the so-called miscibility gap: A review. Lithos, 11, 85-97.

Guggenheim, E.A. (1952) *Mixtures*. Clarendon Press, Oxford.

Hafner, S.S., and Ghose, S. (1971) Iron and magnesium distribution in cummingtonites $(Fe,Mg)_7Si_8O_{22}(OH)_2$. Z. Kristallogr., 133, 301-326.

Hamil, M.H., Ghose, S., and Sparks, R.A. (1975) Antiphase domains in a lunar pigeonite: determination of the average shape, size and orientation from a measurement of three-dimensional intensity profiles of diffuse ($h+k$ = odd) reflections. Acta Crystallogr., A31, 126-130.

Hildebrand, J.H. (1929) Solubility-XII. Regular solutions. J. Amer. Chem. Soc., 51, 66-80.

Hodgson, A.A., Freeman, A.G., and Taylor, H.F.W. (1965a) The thermal decomposition of crocidolite from Koegas, South Africa. Mineral. Mag., 35, 5-30.

Hodgson, A.A., Freeman, A.G., and Taylor, H.F.W. (1965b) The thermal decomposition of amosite. Mineral. Mag., 35, 445-463.

Immega, I.P., and Klein, C., Jr. (1976) Mineralogy and petrology of some metamorphic Precambrian iron-formations in southwestern Montana. Amer. Mineral., 61, 1117-1144.

Iwasaki, M. (1963) Metamorphic rocks of the Kôtu-Bizan area, Eastern Shikoku. J. Fac. Sci. Tokyo Univ. Sec. 2, 15, pt. 1, 1-90.

Jaffe, H.W., Robinson, P., and Klein, C., Jr. (1968) Exsolution lamellae and optic orientation of clino-amphiboles. Science, 160, 776-778.

Kamineni, D.C., Jackson, G.D., and Bonnardi, M. (1979) Coexisting magnesian and calcic amphiboles in meta-ultramafics from Baffin Island (Arctic Canada). N. Jb. Miner. Mh., 1979, 542-555.

Kisch, H.J. (1969) Magnesio-cummingtonite - $P2_1/m$: A Ca- and Mn-poor clinoamphibole from New South Wales. Contrib. Mineral. Petrol., 21, 319-331.

Klein, C., Jr. (1966) Mineralogy and petrology of the metamorphosed Wabush Iron Formation, southwestern Labrador. J. Petrol., 7, 246-305.

Klein, C., Jr. (1968) Coexisting amphiboles. J. Petrol., 9, 281-330.

Klein, C., Jr. (1969) Two-amphibole assemblages in the system actinolite-hornblende-glaucophane. Amer. Mineral., 54, 212-237.

Koslowski, T., and Hinrichsen, Th. (1979) Synthesis, properties and upper thermal stability of a glaucophane-riebeckite mixed crystal. N. Jb. Mineral. Mh., 1979, 357-362.

Kretz, R. (1963) Distribution of magnesium and iron between orthopyroxene and calcic pyroxene in natural mineral assemblages. J. Geol., 71, 773-785.

Leake, B.E. (1978) Nomenclature of amphiboles. Amer. Mineral., 63, 1023-1052.

Lee, D.E., Coleman, R.G., Bastron, H., and Smith, V.C. (1966) A two amphibole glaucophane schist in the Franciscan Formation, Cazadero area, Sonoma County, California. Prof. Paper U.S. Geol. Surv., 550c, 148-157.

Matsui, Y., and Banno, S. (1965) Intracrystalline exchange equilibrium in silicate solid solutions. Proc. Jap. Acad., 41, 461-466.

Misch, P., and Rice, J.M. (1975) Miscibility of tremolite and hornblende in progressive Skagit metamorphic suite, North Cascades, Washington. J. Petrol., 16, 1-21.

Morimoto, N. (1974) Crystal structures and fine texture of pyroxenes. Fortschritte. Mineral., 52, 52-80.

Mueller, R.F. (1960) Compositional characteristics and equilibrium relations in mineral assemblages of a metamorphosed "iron" formation. Amer. J. Sci., 258, 449-497.

Mueller, R.F. (1961) Analysis of relations among Mg, Fe and Mn in certain metamorphic minerals. Geochim. Cosmochim. Acta, 25, 267-296.

Mueller, R.F. (1962) Energetics of certain silicate solid solutions. Geochim. Cosmochim. Acta, 26, 581-598.

Mueller, R.F. (1964) Theory of immiscibility in mineral systems. Mineral. Mag., 33, 1015-1023.

Mueller, R.F. (1967) Model for order-disorder kinetics in certain quasibinary crystals of continuously variable composition. J. Phys. Chem. Solids, 28, 2239-2243.

Mueller, R.F. (1969) Kinetics and thermodynamics of intracrystalline distributions. Mineral. Soc. Amer. Spec. Paper, 2, 83-94.

Oba, T. (1980) Phase relations in the tremolite-pargasite join. Contrib. Mineral. Petrol., 71, 247-256.

O'Connor, D.J., and Patterson, J.H. (1966) The solid state reaction of the thermal decomposition of Australian crocidolite in vacuum. 8th Conf. on the Silicate Industry (1965). Akadéiai Kiadó, Budapest.

Papike, J.J., and Clark, J.R. (1968) The crystal structure and cation distribution of glaucophane. Amer. Mineral., 53, 1156-1173.

Papike, J.J., and Ross, M. (1970) Gedrites: crystal structures and intracrystalline cation distributions. Amer. Mineral., 55, 1945-1972.

Papike, J.J., Ross, M., and Clark, J.R. (1969) Crystal-chemical characterization of clino-amphiboles based on five new structure refinements. Mineral. Soc. Amer. Spec. Paper, 2, 117-136.

Patterson, J.H. (1965) The thermal disintegration of crocidolite in air and in vacuum. Mineral. Mag., 35, 31-37.

Patterson, J.H., and O'Connor, D.J. (1966) Chemical studies of amphibole asbestos I. Structural changes of heat-treated crocidolite, amosite and tremolite from infrared absorption studies. Australian J. Chem., 19, 1155-1164.

Phakey, P.P., and Ghose, S. (1974) Study of unmixing of an alkali amphibole. In *Diffraction Studies of Real Atoms and Real Crystals*. Australian Acad. Sci., 11, E-2, 171.

Prewitt, C.T., Papike, J.J., and Ross, M. (1970) Cummingtonite: a reversible, nonquenchable transition from $P2_1/m$ to $C2/m$ symmetry. Earth Planet. Sci. Lett., 8, 448-450.

Rice, J.M., Evans, B.W., and Trommsdorff, V. (1974) Widespread occurrence of magnesiocummingtonite in ultramafic schists, Cima di Gagnone, Ticino, Switzerland. Contrib. Mineral. Petrol., 43, 245-251.

Robinson, P. (1963) *Gneiss Domes of the Orange Area, Mass. and N.H.* Ph.D. Dissertation, Harvard University.

Robinson, P., and Jaffe, H.W. (1969) Chemographic exploration of amphibole assemblages from central Massachusetts and southwestern New Hampshire. Mineral. Soc. Amer. Spec. Paper, 2, 251-274.

Robinson, P., Jaffe, H.W., Klein, C., Jr., and Ross, M. (1969) Equilibrium coexistence of three amphiboles. Contrib. Mineral. Petrol., 22, 248-258.

Robinson, P., Jaffe, H.W., Ross, M., and Klein, C., Jr. (1971a) Orientation of exsolution lamellae in clinopyroxenes and clinoamphiboles: consideration of optimal phase boundaries. Amer. Mineral., 56, 909-939.

Robinson, P., Ross, M., and Jaffe, H.W. (1971b) Composition of the anthophyllite-gedrite series, comparisons of gedrite and hornblende, and the anthophyllite-gedrite solvus. Amer. Mineral., 56, 1005-1041.

Ross, M., Papike, J.J., and Shaw, K.W. (1969) Exsolution textures in amphiboles as indicators of sub-solidus thermal histories. Mineral. Soc. Amer. Spec. Paper, 2, 275-299.

Ross, M., Papike, J.J., and Weiblen, P.W. (1968) Exsolution in clinoamphiboles. Science, 159, 1099-1104.

Segeler, C.G. (1961) First U.S. occurrence of manganoan cummingtonite, tirodite. Amer. Mineral., 46, 637-641.

Seifert, F.A. (1977) Reconstruction of rock cooling paths from kinetic data on the Fe^{2+}-Mg exchange reaction in anthophyllite. Phil. Trans. Roy. Soc. London, A 286, 303-311.

Seifert, F.A., and Virgo, D. (1974) Temperature dependence of intracrystalline Fe^{2+}-Mg distribution in a natural anthophyllite. Carnegie Inst. Wash. Year Book, 73, 405-411.

Seifert, F.A., and Virgo, D. (1975) Kinetics of the Fe^{2+}-Mg order-disorder reaction in anthophyllites: quantitative cooling rates. Science, 188, 1107-1109.

Seitasaari, J. (1952) An association of cummingtonite and hornblende. Ann. Acad. Sci. Fennicae Ser. A., III, Geol. Geogr., 30, 5-20.

Sharma, T., Mueller, R.F., and Clayton, R.N. (1965) O^{18}/O^{16} ratios of minerals from the iron formations of Quebec. J. Geol., 73, 664-667.

Shido, F., and Miyashiro, A. (1959) Hornblendes of basic metamorphic rocks. J. Pac. Sci. Univ. Tokyo, 12, 85-102.

Spear, F.S. (1980) The gedrite-anthophyllite solvus and the compositional limits of orthoamphibole from the Post Pond volcanics, Vermont. Amer. Mineral., 65, 1103-1118.

Stout, J.H. (1970) Three-amphibole assemblages and their bearing on the anthophyllite-gedrite miscibility gap (abstr.). Amer. Mineral., 55, 312-313.

Stout, J.H. (1971) Four coexisting amphiboles from Telemark, Norway. Amer. Mineral., 56, 212-224.

Stout, J.H. (1972) Phase petrology and mineral chemistry of coexisting amphiboles from Telemark, Norway. J. Petrol., 13, 99-145.

Sueno, S., Papike, J.J., Prewitt, C.T., and Brown, G.E. (1972) Crystal structure of high cummingtonite. J. Geophys. Res., 77, 5767-5777.

Sundius, N. (1933) Über die Mischungslücken zwischen Anthophyllit-Gedrit, Cummingtonit-Grünerit, und Tremolit-Aktinolith. Tschermaks Min. Pet. Mitt., 43, 422-440.

Tagiri, M. (1977) Fe-Mg partition and miscibility gap between coexisting calcic amphiboles from the Southern Abukuma Plateau, Japan. Contrib. Mineral. Petrol., 62, 271-281.

Ungaretti, L. (1980) Recent developments in x-ray single crystal diffractometry applied to the crystal-chemical study of amphiboles. Proc. 15th Conf. Yugoslav Center of Crystallogr., Bor. (in press).

Ungaretti, L., Mazzi, F., Rossi, G., and Dal Negro, A. (1978) Crystal-chemical characterization of blue amphiboles. Proc. 11th IMA General Mtg., Novosibirsk (in press).

Veblen, D.R., and Buseck, P.R. (1980) Microstructures and reaction mechanisms in biopyriboles. Amer. Mineral., 65, 599-623.

Vernon, R.H. (1962) Co-existing cummingtonite and hornblende in an amphibolite from Duchess, Queensland, Australia. Amer. Mineral., 47, 360-370.

Virgo, D., and Hafner, S.S. (1969) Fe^{2+}, Mg order-disorder in heated orthopyroxenes. Mineral. Soc. Amer. Spec. Paper, 2, 67-81.

Whitfield, J.J., and Freeman, A.G. (1967) Mössbauer study of amphiboles. J. Inorg. Nucl. Chem., 29, 903-914.

Whittaker, E.J.W. (1949) The structure of Bolivian crocidolite. Acta Crystallogr., 2, 312-317.

Witte, P., Langer, K., Seifert, F., and Schreyer, W. (1969) Synthetische Amphibole mit OH-Überschuss im System Na_2O-MgO-SiO_2-H_2O. Naturwissenschaften, 56, 414-415.